ORNL-6816
Distribution—UC-404

SOLID STATE DIVISION PROGRESS REPORT for Period Ending September 30, 1993

J. B. Roberto, Director
R. M. Moon, Associate Director
L. A. Boatner, Section Head
J. F. Cooke, Section Head
B. C. Larson, Section Head
H. A. Mook, Section Head
D. M. Zehner, Section Head

Edited by:
P. H. Green
L. W. Hinton

Date Published – August 1994

Prepared for the
Division of Materials Sciences

Prepared by the
OAK RIDGE NATIONAL LABORATORY
Oak Ridge, Tennessee 37831
managed by
MARTIN MARIETTA ENERGY SYSTEMS, INC.
for the
DEPARTMENT OF ENERGY
UNDER CONTRACT NO. DE-AC05-84OR21400

Reports previously issued in this series are as follows:

ORNL-1095	Period Ending April 30, 1951
ORNL-1128	Period Ending July 31, 1951
ORNL-1214	Period Ending October 31, 1951
ORNL-1261	Period Ending January 31, 1952
ORNL-1301	Period Ending May 10, 1952
ORNL-1359	Period Ending August 10, 1952
ORNL-1429	Period Ending November 10, 1952
ORNL-1506	Period Ending February 10, 1953
ORNL-1606	Period Ending August 30, 1953
ORNL-1677	Period Ending February 28, 1954
ORNL-1762	Period Ending August 31, 1954
ORNL-1851	Period Ending February 28, 1955
ORNL-1852	Period Ending February 28, 1955
ORNL-1944	Period Ending August 31, 1955
ORNL-1945	Period Ending August 31, 1955
ORNL-2051	Period Ending February 29, 1956
ORNL-2052	Period Ending February 29, 1956
ORNL-2188	Period Ending August 31, 1956
ORNL-2189	Period Ending August 31, 1956
ORNL-2413	Period Ending August 31, 1957
ORNL-2414	Period Ending August 31, 1957
ORNL-2614	Period Ending August 31, 1958
ORNL-2829	Period Ending August 31, 1959
ORNL-3017	Period Ending August 31, 1960
ORNL-3213	Period Ending August 31, 1961
ORNL-3364	Period Ending August 31, 1962
ORNL-3480	Period Ending May 31, 1963
ORNL-3676	Period Ending May 31, 1964
ORNL-3841	Period Ending May 31, 1965
ORNL-3935	Period Ending December 31, 1965
ORNL-4098	Period Ending December 31, 1966
ORNL-4250	Period Ending December 31, 1967
ORNL-4408	Period Ending December 31, 1968
ORNL-4526	Period Ending December 31, 1969
ORNL-4669	Period Ending December 31, 1970
ORNL-4779	Period Ending December 31, 1971
ORNL-4861	Period Ending December 31, 1972
ORNL-4952	Period Ending December 31, 1973
ORNL-5028	Period Ending December 31, 1974
ORNL-5135	Period Ending December 31, 1975
ORNL-5328	Period Ending April 30, 1977
ORNL-5486	Period Ending September 30, 1978
ORNL-5640	Period Ending February 29, 1980
ORNL-5850	Period Ending September 30, 1981
ORNL-5975	Period Ending March 31, 1983
ORNL-6128	Period Ending September 30, 1984
ORNL-6306	Period Ending March 31, 1986
ORNL-6453	Period Ending September 30, 1987
ORNL-6571	Period Ending March 31, 1989
ORNL-6664	Period Ending September 30, 1990
ORNL-6722	Period Ending March 31, 1992

DISCLAIMER

DISCLAIMER

Portions of this document may be illegible in electronic image products. Images are produced from the best available original document.

Contents

MAGNETIC PROPERTIES

MANY-BODY THEORY, PHOTOVOLTAICS, AND SUCH

2. *Neutron Scattering*

SMALL-ANGLE SCATTERING AND NEUTRON REFLECTOMETRY

NEUTRON DIFFRACTION

INELASTIC NEUTRON SCATTERING

3. *Synthesis, Processing, and Characterization of Materials*

SUPERCONDUCTIVITY

THIN-FILM BATTERIES AND SOLID ELECTROLYTES

FERROELECTRICS AND PEROVSKITE-STRUCTURE OXIDES

MATERIALS PROPERTIES

OPTICAL CHARACTERIZATION OF MATERIALS

4. *Ion Beam and Laser Processing*

ION BEAM PROCESSING

ION IMPLANTATION AND ANALYSIS

LASER AND MOLECULAR BEAM PROCESSING OF THIN FILMS

5. *Structure of Solids and Surfaces*

SURFACE PHYSICS

ELECTRON MICROSCOPY

X-RAY DIFFRACTION

Acronyms

AES – auger electron spectroscopy
ANS – Advanced Neutron Source
APS – Advanced Photon Source
APECS – Auger-photoelectron coincidence spectroscopy
BCA – binary collision approximation
CHESS – Cornell High-Energy Synchrotron Source
CPA – constant-phase angle
CVD – chemical vapor deposition
DSC – differential scanning calorimetry
ECR – electron cyclotron resonance
EDX – energy dispersive x-ray
EELS – electron energy loss spectroscopy
EPR – electron paramagnetic resonance
FWHM – full width at half maximum
HFIR – High Flux Isotope Reactor
HPLC – high-performance liquid chromatography
HREM – high-resolution electron microscopy
HREELS – high-resolution electron energy loss spectroscopy
HRLEED – high-resolution low-energy electron diffraction
HRTEM – high-resolution transmission electron microscopy
HTSc – high-temperature superconductors
IBD – ion beam deposition
IPNS – Intense Pulsed Neutron Source
LDA – local density approximation
LEED – low-energy electron diffraction
MBE – molecular beam epitaxy
MOCVD – metallo-organic chemical vapor deposition
NSLS – National Synchrotron Light Source
ORISE – Oak Ridge Institute of Science and Engineering
PIGE – proton-induced gamma emission
PIXE – particle-induced x-ray emission
PLA – pulsed-laser ablation
PLD – pulsed-laser deposition
QMS – quadrupole mass spectrometer
RBS – Rutherford backscattering spectroscopy
RHEED – reflection high-energy electron diffraction
SANS – small-angle neutron scattering
SAXS – small angle x-ray scattering
SEM – scanning electron microscopy
SPEG – solid-phase-epitaxial growth
STEM – scanning transmission electron microscopy
STM – scanning tunneling microscopy
TCR – thermochemical reduction
TDS – thermal desorption spectroscopy
TEM – transmission electron microscopy
TRR – time-resolved reflectivity
UHV – ultrahigh vacuum
UIUC – University of Illinois at Urbana-Champaign
WAND – wide-angle neutron diffractometer
WAXD – wide-angle x-ray diffraction
XDCD – x-ray double-crystal diffraction
XPS – x-ray photoemission spectroscopy
YSZ – yttria-stabilized zirconia

Introduction

This report covers research progress in the Solid State Division from April 1, 1992, to September 30, 1993. During this period, the division conducted a broad, interdisciplinary materials research program with emphasis on theoretical solid state physics, neutron scattering, synthesis and characterization of materials, ion beam and laser processing, and the structure of solids and surfaces. This research effort was enhanced by new capabilities in atomic-scale materials characterization, new emphasis on the synthesis and processing of materials, and increased partnering with industry and universities.

The theoretical effort included a broad range of analytical studies, as well as a new emphasis on numerical simulation stimulated by advances in high-performance computing and by strong interest in related division experimental programs. Superconductivity research continued to advance on a broad front from fundamental mechanisms of high-temperature superconductivity to the development of new materials and processing techniques. The Neutron Scattering Program was characterized by a strong scientific user program and growing diversity represented by new initiatives in complex fluids and residual stress.

The national emphasis on materials synthesis and processing was mirrored in division research programs in thin-film processing, surface modification, and crystal growth. Research on advanced processing techniques such as laser ablation, ion implantation, and plasma processing was complemented by strong programs in the characterization of materials and surfaces including ultrahigh resolution scanning transmission electron microscopy, atomic-resolution chemical analysis, synchrotron x-ray research, and scanning tunneling microscopy. The materials processing research spanned the continuum from basic studies to applications and included more than a dozen cooperative research agreements with industry in areas such as superconductivity, thin-film battery materials, plasma processing, thermoelectric materials, crystal growth, and photovoltaic materials.

In addition to the research progress summarized in the report, the division continued a tradition of service and leadership in the scientific community. During this period, 18 division staff members chaired or co-chaired national conferences and workshops, 5 served as national officers or executive committee members for professional societies, 14 served on national or international review committees, 12 served on editorial boards for technical journals, and 7 edited or co-edited books and proceedings.

1. *Theoretical Solid State Physics*

During the period of time covered by this report, the scope of the Theory of Condensed Matter Program has continued to expand into new areas of fundamental research. Much of this new activity is motivated by participation in Laboratory Director's Research and Development, Cooperative Research and Development Agreement, and DOE/Division of Materials Sciences 2% initiative programs. Significant progress has also been made in ongoing research programs. A comprehensive overview of these research accomplishments is given in this chapter which is organized into four sections—Superconductivity, Numerical Simulation and Band Structure, Magnetic Properties, and Many-Body Theory, Photovoltaics, and Such.

The recent availability of the INTEL Paragon, a massively parallel computer located at ORNL, has opened up new opportunities for research. Six projects are currently being pursued; three of these are incorporated in this chapter. This work includes the prediction of a new extended point defect in diamond cubic crystals, first-principles study of a Ge atom adsorbed on a Si surface, and computer modeling of the laser ablation process for producing thin films.

Work on high-temperature superconductors has established the important role played by band structure effects, both for theoretical predictions and interpretation of experiments. An analysis of the resistivity of superlattices composed of superconducting and barrier layer materials has revealed the roles played by a number of effects (e.g., charge transfer, dimensionality). Predictions based on specific pairing models have also helped define their possible role in real systems.

Research on magnetism has led to an explanation of why small transition-metal impurities have such a profound effect on the magnetic properties of chromium, predictions of the impact electron screening has in transition-metal ferromagnets, and predictions about longitudinal and transverse spin modes in the sinusoidal phase of rare-earth magnets.

The contributions explicitly mentioned in this introduction constitute less than half of the research covered in this chapter. Other contributions are, however, equally important and help reflect the versatility, breadth, and capabilities of the overall theory program.

SUPERCONDUCTIVITY

ENERGY GAP STRUCTURE OF LAYERED SUPERCONDUCTORS[1]

S. H. Liu and R. A. Klemm[2]

All copper-oxide-based high-T_c superconductors have a stratified crystal structure. The charge carriers move freely within the CuO_2 layers, but hop weakly between the layers. The effects of the crystal structure on the superconducting properties have been studied using a simple model consisting of one superconducting layer and one normal layer within a unit cell. In general, the critical temperature T_c decreases with increasing hopping, as shown in Fig. 1.1. This prediction is in qualitative agreement with the observation that higher T_c is correlated with a higher degree of c-axis to ab-plane anisotropy.

One surprising result of the calculation is that the density-of-states curves (Fig. 1.2) show double-peaked structures for hopping strengths comparable to T_c although there is only one

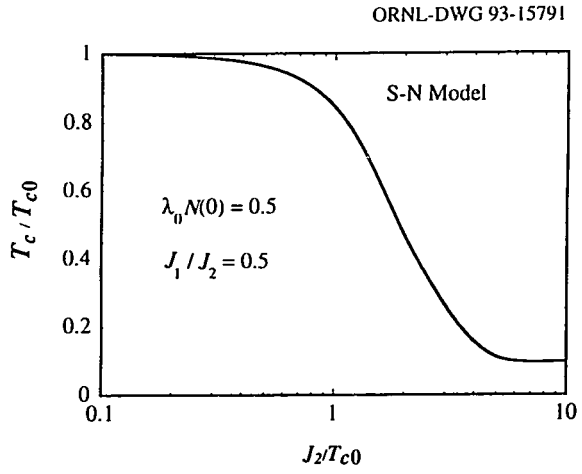

Fig. 1.1. The dependence of the critical temperature T_c on the hopping strengths for the two-layer model, showing the monotonic decrease of T_c with increasing hopping.

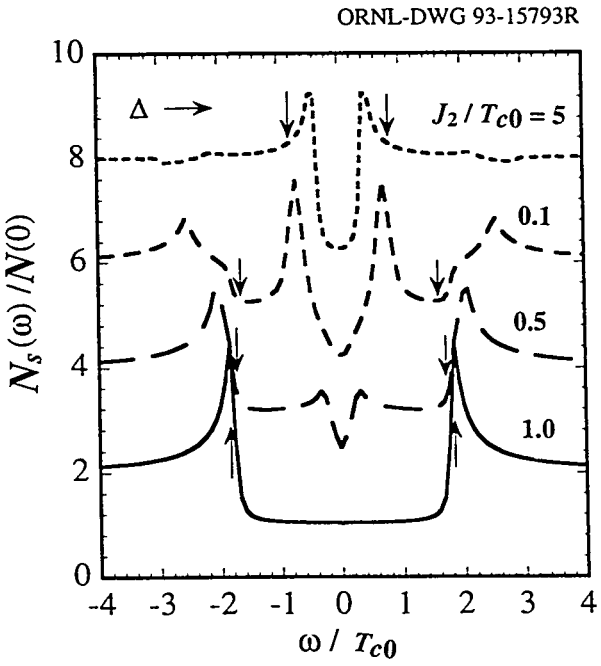

Fig. 1.2. A set of density-of-states curves at zero temperature for the two-layer model. The curves are displaced vertically by 2 units successively.

energy gap. Neither set of peaks corresponds to the energy gap, which is marked by arrows. This contradicts a commonly accepted explanation of tunneling data on high-T_c materials (i.e., that the peaks correspond to the energy gaps in two different layers). It has been shown that the two sets of peaks represent the order parameters of intra- and interband pairing, respectively. Also, in this range of parameter space, the density-of-states curves are gapless with V-shaped bottoms, as seen in many tunneling experiments. It is concluded that the tunneling data can be understood on the basis of singlet pairing without any need to invoke exotic pairing mechanisms or electronic properties.

---

1. Summary of paper to be published.
2. Argonne National Laboratory, Argonne Ill.

HIGH-T_c SUPERCONDUCTING SUPERLATTICES[1]

R. F. Wood

Superlattices composed of $YBa_2Cu_3O_7$ and various barrier layer materials have been studied extensively experimentally, and several theoretical attempts to correlate the resistivity as a function of temperature with the superlattice structure have appeared in the literature. Theoretical interest in such structures comes about primarily because of the insight they provide into dimensionality effects, interlayer coupling, and interlayer charge redistribution in the high-T_c superconductors. On the experimental side, there are possibilities for device applications that are just now beginning to be explored. In the work reported here, resistivity, $R(T)$, data up to T = 300 K have been analyzed for 17 superlattices consisting of $YBa_2Cu_3O_7$ and barrier layers of $PrBa_2Cu_3O_7$, $PrY_{03}Ba_2Cu_3O_7$, and $PrY_{0.5}Ca_{0.5}Ba_2Cu_3O_7$. The results show that both charge transfer and barrier-layer conductivity must be taken into account in order to explain the unusual normal-state $R(T)$ behavior in some superlattices. These effects also contribute in the resistive transition region where Kosterlitz-Thouless vortex-antivortex unbinding and Aslamozov-Larkin fluctuation effects play major roles. The calculations indicate that normal-state conductivity in the barrier layers takes place by a two-dimensional variable range hopping mechanism. The charge transfer effects extracted from fitting the experimental data are compared with those obtained from a charge transfer calculation reported earlier, and good agreement is found. The difficulty in disentangling charge transfer and dimensionality effects in determining the nominal transition temperature is emphasized, and other mechanisms that influence the width of the resistive transition are considered.

---

1. Summary of paper to be published.

SPIN-POLARON THEORY OF HIGH-T_c SUPERCONDUCTIVITY[1]

R. F. Wood

The concept of a spin polaron is introduced and contrasted with the more familiar ionic polaron picture. A brief review of aspects of ionic bipolaronic superconductivity is given with particular emphasis on the real-space pairing and true Bose condensation characteristics. The formation energy of spin polarons is then calculated in analogy with ionic polarons. The spin-flip energy of a Cu spin in an antiferromagnetically (AF) aligned CuO_2 plane is discussed. It is shown that the introduction of holes into the CuO_2 planes will always lead to the destruction of long-range AF ordering because of the formation of spin polarons. The pairing of two spin polarons can be expected because of the reestablishment of local (short-range) AF ordering; the magnitude of the pairing energy is estimated using a simplified model. The paper closes with a brief discussion of the formal theory of spin polarons.

After an introductory discussion of electronic structure calculations for the CuO_2 planes in the copper-oxide based high-T_c superconductors, the method suggested by Slater for

studying AF metals is described. In this method, as applied here, the chemical unit cell is doubled to form a magnetic unit cell which contains one Cu ion with predominantly up spin and one with predominantly down spin. Down spins are kept off up-spin sites and, conversely, by the introduction of a Hubbard U term. As a result, the band structure obtained is typical of that for a Mott-Hubbard (M-H) or, more generally, a charge transfer insulator. Conductivity in the a-b plane results when holes are introduced into the M-H valence band. The band structure as a function of the parameters in Koster-Slater type calculations is discussed, and the Fermi surface is described. A calculation of the delocalization energy for spin-polaron formation is carried out within the context of the band calculations.

Results from previous papers in this series are used for the gap and T_c within the framework of a Cooper-pairing approach. The possible symmetry types of the gap are discussed. It is shown how the proximity of the Fermi level to the M-H band edge and the interplay of O $2p\sigma$ and $2p\pi$ bands and/or localization effects can provide good fits to the variation of T_c with x in $La_{2-x}Sr_xCuO_4$ and $YBa_2Cu_3O_{7-x}$. It is concluded that the in-plane gap is either s- or d-like but anisotropic in either case. Other aspects and implications of the model and of the calculations are given, and comparisons with Mott's spin-bipolaron model are made.

---

1. Summary of three papers: in *Proceedings of the International Symposium on High-T_c Superconductivity and Its Applications*, Cairo, Egypt, April 4–16, 1993 (in press).

ELECTRON-PHONON INTERACTION NEAR VAN HOVE SINGULARITIES[1]

G. D. Mahan[2]

Superconductivity occurs when electrons bind in pairs in a solid. High-temperature superconductors are composed of planes of copper oxide, and the motion of superconducting electrons are confined to these planes. In two dimensions, the density of energy states for electrons always have a logarithmic singularity at some energy E_s, which is called the van Hove singularity. There have been numerous suggestions that this singularity in the density of states is the cause of high-temperature superconductivity.

The Eliashberg equations describe the pairing of electrons. These equations were solved for the case where the interaction between electrons was caused by the electron-phonon interaction. It was desirable to see whether the van Hove singularity increased the transition temperature of the superconductor, and it was found that it did increase T_c significantly when the chemical potential μ was very near E_s. However, whenever $|\mu - E_s|$ was more than 10% of the bandwidth, the singularity had no effect on T_c. Because actual superconductors are obtained by impurity doping, they have a chemical potential which is far from E_s; therefore, the van Hove singularity does not cause high-temperature superconductivity.

Another calculation was made on the increase in T_c because of an anisotropic energy gap. It is assumed that the energy gap of the superconductor was s-wave, but anisotropic; the variation of the energy gap with angle around

the Fermi line is $\Delta(\phi) = \Delta_0 + \Delta_4 \cos(4\phi)$ which maintains *s*-wave symmetry. It was also shown that in addition to the normal electron-phonon coupling constant λ_0, there is another coupling constant λ_4 which is associated with an anisotropic interaction. If λ_4 is large, then T_c is increased significantly.

---

1. Summary of paper: *Physical Review B* (in press).
2. ORNL/UT Distinguished Scientist.

RESISTIVITY AND SUPERCONDUCTIVITY FROM ANHARMONIC PHONONS[1]

G. D. Mahan[2] *and J. O. Sofo*[3]

The electrical resistivity is calculated for electron scattering from anharmonic phonons. Phonon potential energies of the form $\sim Q^n$, as well as double-well potentials $\sim Q^4 - \alpha Q^2$, were considered. For phonon potential energies with a power law $\sim Q^n$, the resistivity at high temperatures is proportional to T^2/n. At low temperatures, the resistivity rises rapidly and then flattens, thereby forming a knee shape. This behavior explains the resistivity of cuprate superconductors in the normal state.

A question that appears immediately is are these anharmonic phonons the gluing bosons of the superconducting state. To answer this question, the Eliashberg theory was applied to calculate the critical temperature, using the anharmonic phonons, to see if the same set of parameters used to explain the resistivity measurements can explain the high critical temperature of the cuprates. These results show that it is impossible to find a proper set of parameters to match the results of the resistivity and the critical temperature.

Quite reasonable values explain the electrical resistivity. However, much larger values of the electron phonon coupling constant are needed for higher values of T_c. These large values would predict a much larger resistivity than is observed. The situation is different in the A-15 compounds. They have large values of resistivity, and smaller values of T_c. It is more likely that the anharmonic phonons are pairing the electrons in the superconducting state.

---

1. Summary of paper: *Phys. Rev. B* **47**, 8050 (1993).
2. ORNL/UT Distinguished Scientist.
3. ORNL/ORISE postdoctoral research associate.

FRUSTRATION-INDUCED DISORDER OF FLUX LINES IN LAYERED SUPERCONDUCTORS[1]

G. I. Watson[2] *and G. S. Canright*[3]

A "frustrated" system is one whose Hamiltonian is a sum of terms which cannot all be minimized simultaneously. For such systems, it is often a nontrivial task to deduce the ground state; furthermore, there may be many metastable states which are strongly competitive with the global minimum of the free energy. All these low-energy states are, in general, quite complex and not easily studied.

A standard technique for frustrating a system is to introduce random disorder into the Hamiltonian. However, this widely studied

idea neatly circumvents one-half of the problem, because the disorder presumably came from some underlying frustration in a simple Hamiltonian without disorder (e.g., the Hamiltonian of a set of impurities interacting with a host material).

A model which lacks disorder in the Hamiltonian, but nevertheless is highly frustrated, has been chosen for study. This model may be physically realized[4] by flux lines in layered superconductors. It also may be mapped to a one-dimensional *XY* model with long-range antiferromagnetic coupling—hence, the frustration. (The purely antiferromagnetic, long-range coupling arises from the pure repulsion among the flux lines.) Some interesting but highly structured metastable states were found by Levitov.[4] Prior to our work, however, there was no systematic way to study the enormously many complex metastable states which may, in fact, compete with the ground state for a frustrated system. Pursuing Levitov's analogy of this problem with plant growth (phyllotaxis), flux-line lattices were numerically "grown" using an algorithm which should give energetically favorable configurations as attractors. Both periodic (of many different periods) and aperiodic (chaotic) attractors for the algorithm, representing long-period and disordered flux-line lattices, respectively, were found. It was also shown that all of these structures are competitive in energy with the lowest state, which is still (so far) a simple period-one (Bravais) lattice. This method is the only one, to our knowledge, which allows the systematic generation of complex (including disordered) metastable states. The method will be exploited further with a number of frustrated one-dimensional models, such as the Frenkel-Kontorova model (representing lattice mismatch between substrate and overlayer) and the ANNNI model (relevant to stacking polytypism in metals and semiconductors).

---

1. Summary of paper to be published.
2. Guest scientist from the ORNL/UT Distinguished Scientist Program.
3. Guest scientist from The University of Tennessee, Knoxville, Tenn.
4. L. S. Levitov, *Phys. Rev. Lett.* **66**, 224 (1991).

NUMERICAL SIMULATION AND BAND STRUCTURE

A NEW EXTENDED POINT DEFECT STRUCTURE IN DIAMOND CUBIC CRYSTALS[1]

Mark Mostoller, Theodore Kaplan, and M. F. Chisholm

In the course of atomistic simulations of the dislocation array at the Ge/Si(001) interface, a new closed symmetric defect structure comprising 18 atoms has been generated that may be found in a variety of circumstances, including dislocations and grain boundaries. The structure maintains tetrahedral bonding with reasonable changes in bond lengths and angles and may have interesting electronic properties. This new structure is called a "dreidl" after the child's top that it resembles.[2]

In a perfect diamond cubic structure, the atoms form sixfold rings viewed along [1,±1,0]. Commonly observed defect structures are alternating fivefold and sevenfold rings, joined to form a figure of 10 atoms with 2 shared by the pentagon and the heptagon. These occur, for example, in the core of the $(a/2)[1,1,0]$ edge dislocation, in the 90° partial dislocation, and in the S9 twin boundary.

There is almost precisely a 4% mismatch between the lattice constants of Ge and Si. When a film of Ge is grown epitaxially on an Si(001) substrate, the misfit strain can result in the formation at the interface of a regular two-dimensional array of edge dislocations with Burgers' vectors $(a/2)[1,\pm1,0]$. Classical molecular dynamics simulations have been made of this dislocation array for rather large microcrystals (~20,000 atoms). The minimum energy structure of the dislocation grid was obtained by a sequence of simulated annealing runs followed by conjugate gradient minimization using the Stillinger-Weber and Tersoff potentials.

The simulations yield orthogonal edge dislocations, each with the five- plus sevenfold core structure, with the core of one displaced above the other by one layer $a/4$ along [0,0,1]. At their intersection, they form the closed symmetric structure shown in Fig. 1.3, the dreidl. The fivefold rings join at the bottom; the sevenfold rings at the top. While tetrahedral bonding is maintained, changes in bond lengths and angles are somewhat larger than those at the core of a single-edge dislocation, raising the possibility that electronic states localized at the dreidl may penetrate deeper into the band gap and make

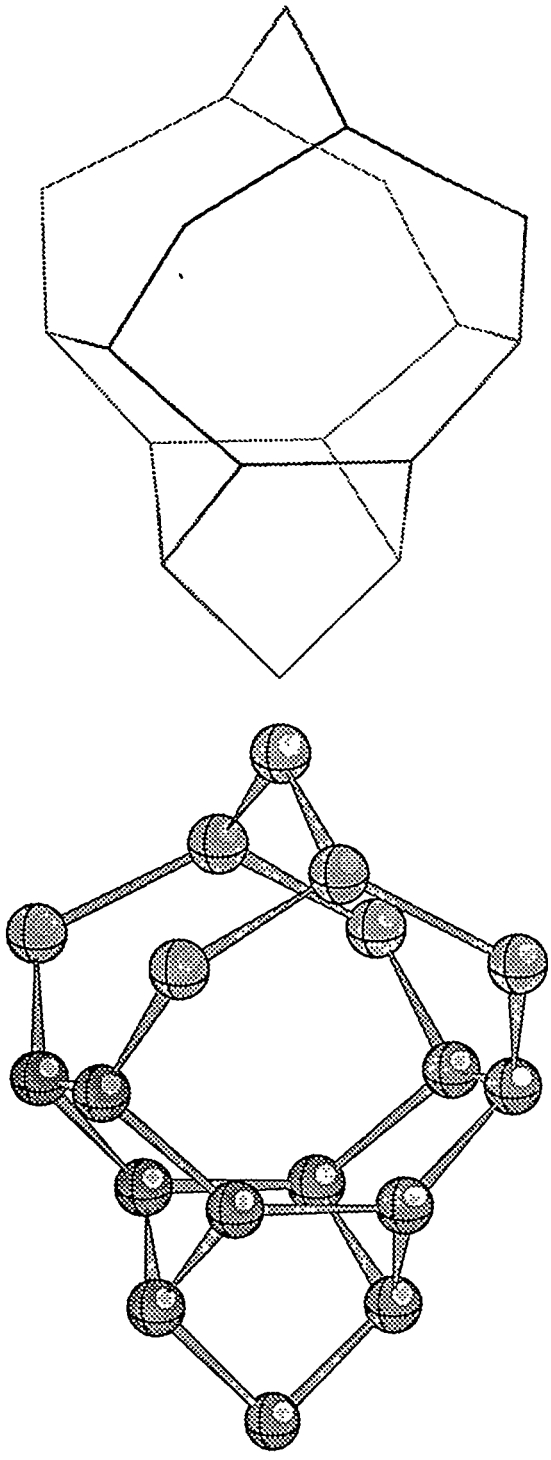

Fig. 1.3. The dreidl, a closed symmetric structure of 18 atoms predicted by simulations to occur at the intersection of $(a/2)[1,1,0]$ dislocations in Ge/Si. The [0,0,1] direction connects the bottom Si atom and the top Ge atom.

the defect electrically active. At the Ge-Si interface, these new defects may reach a very high planar concentration of ~$10^{12}/cm^2$.

---

1. Summary of paper to be published.
2. **dreidl** \rhymes with cradle\1: a 4-sided toy marked with Hebrew letters and spun like a top in a game of chance, *Webster's Ninth New Collegiate Dictionary*.

A NEW EMPIRICAL POTENTIAL FOR Si AND Ge

Mark Mostoller, Benjamin Liu,[1] *and Theodore Kaplan*

Several empirical potential models, notably those of Stillinger and Weber[2] and of Tersoff,[3] have been widely used in classical simulations of bulk Si and Ge, of their surface structure and dynamics, and of various defects and interfaces. These models combine central pair potentials with three-body angular terms that penalize variations away from tetrahedral bonding. Despite some successes, these potentials suffer from some well-known shortcomings. They are both very short range, with the pair potential contributions extending only to first nearest neighbors (1NNs), so that, for example, a stacking fault introduces no change in total energy. They predict symmetric dimers at the Si(001) surface, where buckled asymmetric dimers are observed. They do a poor job of fitting the bulk lattice vibrations, particularly the elastic constants, which are crucial to simulations of dislocation properties.

A new empirical potential model that includes four-body as well as two- and three-body interactions in a fashion demanded by the bulk lattice dynamics has been formulated. A family of numerically specified potentials has been found, extending from the 1NN separation on out, that matches the experimental values for the lattice constant and cohesive energy and that gives a good fit to the bulk phonon dispersion curves. The pair potentials for this family do not exhibit a single well, but rather a minimum near the 1NN separation, then a rise to a shoulder or actually oscillatory behavior at greater distances. As yet, however, it has not been possible to construct a simple functional form for the pair potential that extends to shorter distances than 1NN in a way that retains diamond cubic as the equilibrium structure.

---

1. Graduate student from the University of Pennsylvania, Philadelphia, Pa.
2. F. H. Stillinger and T. A. Weber, *Phys. Rev. B* **31**, 5262 (1985).
3. J. Tersoff, *Phys. Rev. B* **39**, 5566 (1989).

NUMERICAL SIMULATION OF He^+ AND Li^+ COLLISIONS WITH C_{60}[1]

T. Kaplan, M. Rasolt,[2] *M. Karimi,*[3] *and Mark Mostoller*

Since the recent discovery of an efficient process for the synthesis of fullerenes, there has been a dramatic increase in interest in these compounds. Recent research efforts have focused on developing new fullerene-based materials. One method that has been investigated is the incorporation of dopants into the hollow cage structure of C_{60} through high-energy collisions. Numerical simulations of

high-energy collisions of He^+ and Li^+ with C_{60} in free space and on the surface of an Fe substrate have been carried out. These calculations were undertaken with the aims of interpreting and serving as a rough complementary guide to ongoing experiments by R. A. Zuhr and collaborators.

Classical molecular dynamics is used to simulate the collision process. The implantation of He^+ has been observed to form endohedral $He^+@C_{60}$ at various energies in the energy range 35–90 eV. Figure 1.4 shows a few frames for a 45-eV He^+ collision at normal incidence on a six-member ring of the C_{60} molecule on an Fe substrate. Li^+ collisions with C_{60} do not form $Li^+@C_{60}$. Instead, insertion and fragmentation were found to form $Li^+@C_{54}$ and $Li^+@C_{56}$ in the energy range 115–200 eV. The yield of any particular collision depends strongly not only on the incident energy but also on the incident

SSDN-4669

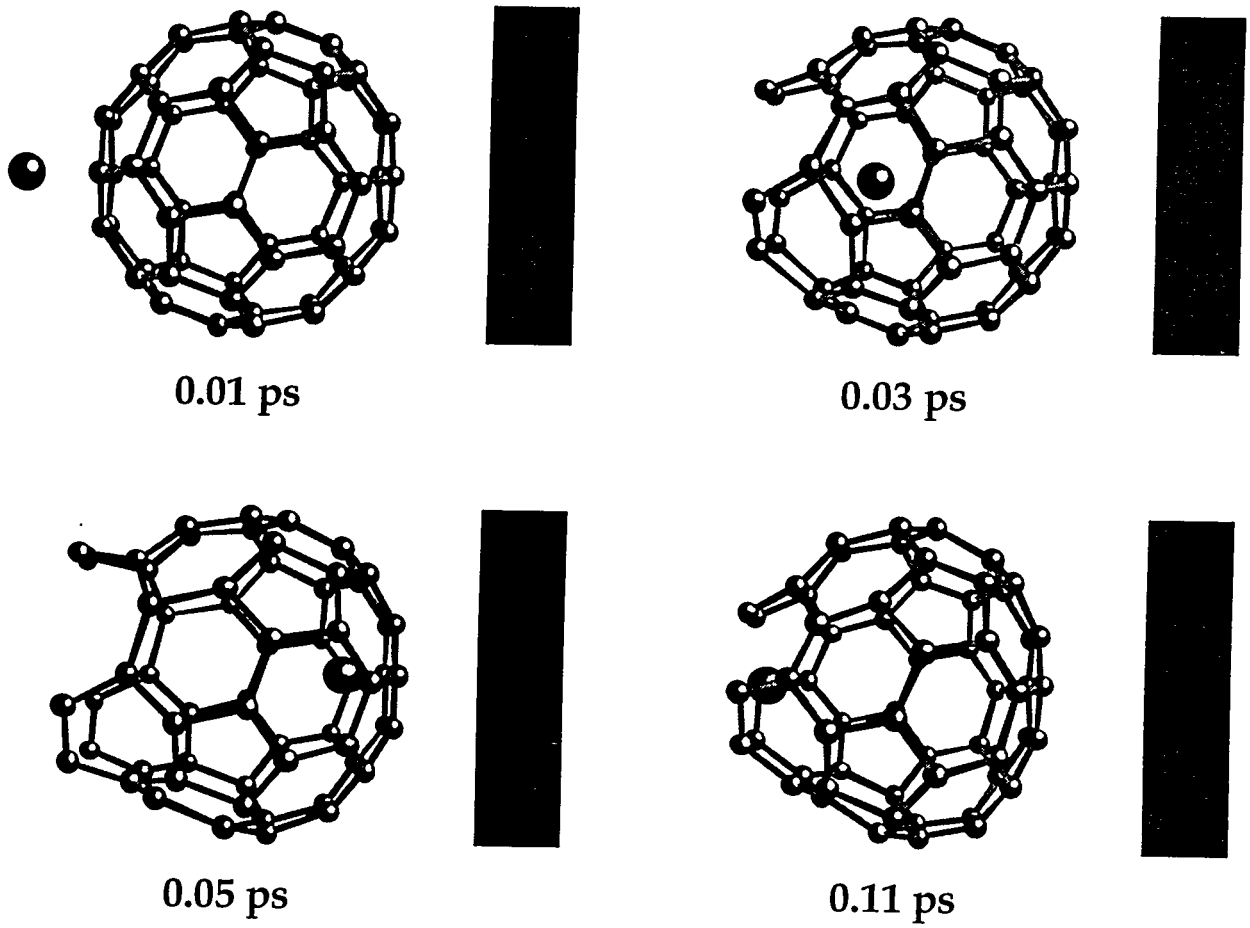

Fig. 1.4. The 45-eV He^+ collision at normal incidence with the six-member ring of a C_{60} molecule on an Fe substrate at 0.01, 0.03, 0.05, and 0.11 ps. The He^+ ion is indicated by the larger ball and the position of the substrate by the solid bar. The He^+ is trapped in the endohedral cavity of the C_{60}.

angle and the point of impact and has a weak dependence on whether or not the C_{60} is on the substrate or in free space.

---

1. Summary of paper: *J. Phys. Chem.* **97**, 6124 (1993).
2. Deceased.
3. ORISE faculty research participant from Indiana University of Pennsylvania, Indiana, Pa.

THE STATISTICS OF SPUTTERING[1]

Mark T. Robinson

The sputtering of crystalline solids by energetic ions has well-known dependences on the kinetic energy and direction of the incident ions and on the crystallographic orientation of the target surface, as well as on the nature of the atoms and other variables. The sputtering yield is the number of atoms ejected by a single ion, averaged over the asymmetric mesh on the target surface. Unlike currently feasible experiments, computer simulations allow the study of fluctuations in the yield from one ion to another. Several studies report distributions of single ion yields, without discussing the origin of the fluctuations (for a review, see ref. 2). At low ion energies, these show a moderately broad distribution with a mode somewhat near the mean. At higher energies, however, a significant fraction of the ions, increasing with energy, produces no sputtering at all, the distribution extends to yields much higher than the mean, and there is often no well-defined mode near the mean.

The MARLOWE program was used to study the statistics of sputtering, on the example of 1–100-keV Au atoms, normally incident on static {001} and {111} Au crystals. The yield of sputtered target atoms was examined as a function of the impact point of the incident atoms on the target surfaces. At a given energy, yields varied over a wide range: for 20-keV Au on {001}, for example, yields ranged from 0 to 104 in a sample of 1225 events, with a mean of 25.6 ± 0.6; at 100 keV, where the mean is 25.6 ± 1.4, individual values ranged from 0 to 328. Spatial structure was observed in the yield on two different scales. The effects of axial and planar channeling could be traced, with the details depending on the target orientation and the ion energy. Channeling is clearly responsible for broad regions of low yield. Locally, however, the yield was very sensitive to the impact point, small changes in position often producing large changes in yield. The results indicate strongly that the sputtering yield is a random ("chaotic") function of the impact point, superimposed on a structural variation because of channeling.

---

1. Summary of paper: *Nuclear Instruments and Methods in Physics Research Section B* (in press).
2. M. T. Robinson, *K. Dan. Vidensk. Selsk. Mat. Fys. Medd.* **43**, 27 (1993).

SIMULATION OF PLASMA-BASED MATERIALS PROCESSING TECHNIQUES

C.-L. Liu,[1] D. B. Geohegan, J.-N. G. Leboeuf,[2] and R. F. Wood

Progress has been made in this first year toward all three original goals of this project; namely, development of plasma formation and transport modules, module integration, and

module optimization. In the laser ablation area, integration of laser materials interactions and plasma plume transport modules has been achieved. A one-dimensional (1D) version of Laser8 has been extended to handle not only the melting of the material by the laser but also its vaporization, as well as the plasma formation phase. Output from Laser8 now provides input density and temperature profiles to a 1D, gas dynamics, plasma plume transport module. This module provides for absorption of the laser energy by way of several plasma processes (e.g., electron-neutral and election-ion inverse bremsstrahlung and plasma resonance.) As the temperature of the plasma increases, charged species of Si are assumed to be generated in concentrations predicted by the Saha equation. Even before vaporization of the surface, electrons and ions can be generated by thermionic emission, and these also may contribute to plasma ignition. The integrated model shows formation of shock and ionization fronts in the early stages of plume expansion and yields velocities in the experimentally measured range. Moreover, a novel 2D particle-in-cell hydrodynamic plume transport model with appropriate boundary conditions has been devised. Expansion and transport of the plasma from point of formation to the substrate, including reflections therefrom, have been simulated successfully. Modeling of laser ablation is leading to the consideration of otherwise neglected ionization and absorption mechanisms and motivating more detailed experiments in silicon.

---

1. ORNL/ORISE postdoctoral research associate.
2. Physics Division, ORNL.

QUANTUM MONTE CARLO WITH COMPLEX WEIGHTS[1]

Lizeng Zhang,[2] *G. S. Canright,*[2] *and T. Barnes*[3]

Quantum Monte Carlo techniques are widely used for problems for which standard analytical techniques, such as mean-field and perturbation theory, are not reliable. Previously, such techniques were applied to two types of many-particle problems: bosons—which are relatively tractable even at low temperatures because their ground state is nodeless—and fermions. Given the importance of electrons in condensed matter, the fermion problem has always been a very high priority, but unfortunately much more difficult to treat by Monte Carlo sampling, because of the presence of alternating signs in the wave function—the "sign problem."

An algorithm (previously used almost exclusively for bosons) has been adapted to allow for a continuous variation of the statistics parameter (i.e., the exchange phase θ) from the Bose to the fermi limit. In between, the particles

are anyons, and the Hamiltonian and ground state are necessarily complex. It has been shown that anyons can be successfully simulated by this technique; this represents the first application of quantum Monte Carlo to the anyon problem. It has also been shown that fermions can be represented in a "complex gauge" as anyons with $\theta = \pi$. By treating fermions in this "anyon representation," it has been possible to explore the many possible "gauge choices" for the statistical "flux." In fact, the sampling error (and therefore the computing time needed) for fermions can be greatly reduced by an appropriate choice of gauge. However, it remains to be seen whether this (improved) method can be a practical method for treating many fermions, because the improvement gained is with respect to a starting point which was not practical and other methods exist. Further work will be needed to optimize the current method and assess its ultimate efficiency.

Particles in an external magnetic field—another "complex" problem—have been investigated. This is another first for our method. It has been shown that the noise arising from the "statistical" flux and from the external flux can *cancel* to a large extent. Hence, fermions can be treated in a large external field much more easily than zero-field fermions. Plans are being considered to exploit this possibility to simulate the quantum Hall effect in future work.

---

1. Summary of papers: p. 199 in *Computer Simulation Studies in Condensed-Matter Physics VI*, ed. by D. P. Landau, K. K. Mon, and H.-B. Schüttler, Springer-Verlag, Berlin, 1993; to be published.

2. Guest scientist from The University of Tennessee, Knoxville, Tenn.
3. The University of Tennessee, Knoxville, Tenn., and Physics Division, ORNL.

LARGE-SCALE *AB INITIO* STUDY OF THE BINDING AND DIFFUSION OF A Ge ADATOM ON THE Si(100) SURFACE[1]

V. Milman,[2] D. E. Jesson, S. J Pennycook, M. C Payne,[3] M. H. Lee,[3] and I. Stich[3]

The study of fundamental atomistic processes that govern the surface kinetics of the epitaxial growth of Si-Ge materials is of considerable scientific and technological interest.[4,5] Scanning tunneling microscopy (STM) experiments cannot establish the exact nature of the adsorption site or the migration path for an individual Ge adatom. These important issues can be resolved by a theoretical study of Ge adsorption and diffusion on the Si surface from first principles. Using the pseudopotential total energy method, it was possible to resolve the controversy regarding the binding geometry and migration path for the adatom and to investigate its influence on the buckling of Si dimers. The supercell that was of a sufficient size for this purpose contained 194 atoms, and the study was made possible only by using massively parallel computers.[6]

The energy surface was mapped out by calculating the total energy for fixed (x,y) positions of the adatom with the total energy minimization in the space of ionic coordinates and wavefunction expansion coefficients. The global minimum is found on top of the second layer atom (Fig. 1.5), while the pedestal site on top of the

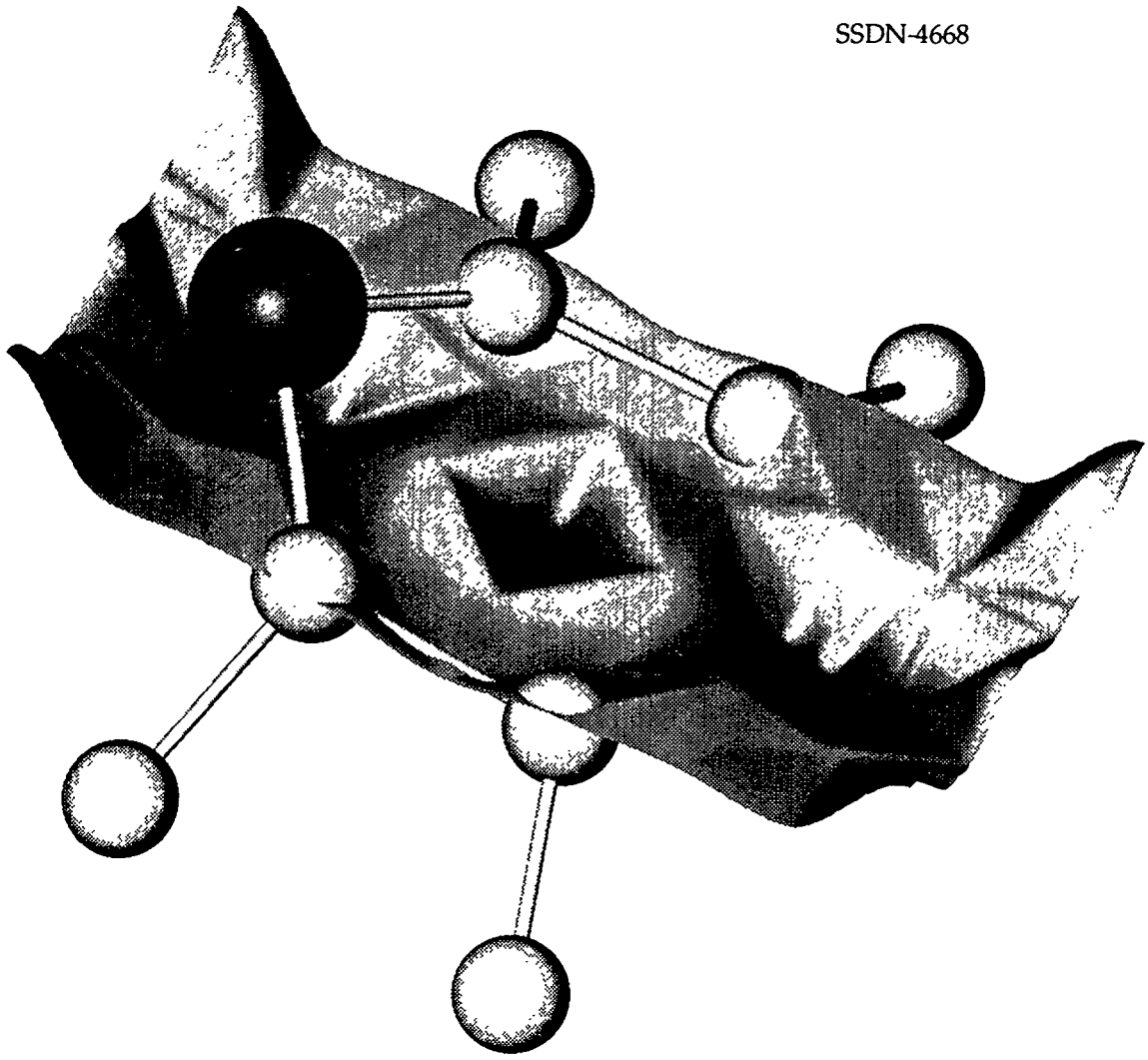

Fig. 1.5. The energy surface for a Ge adatom. The first- and second-layer Si atoms from the p(2 × 1) cell are shown. Two equivalent side minima correspond to the equilibrium binding site; the central minimum corresponds to the metastable pedestal site.

row of dimers is only 0.06 eV higher in energy. No binding site was found in the channel between the dimer rows. The diffusion path in the direction along the dimer rows is a zig-zag, and the barrier height is 0.62 eV, which is in excellent agreement with the experimental estimate. The cross-channel hopping is characterized by a barrier of 0.95 eV which corresponds to a diffusion anisotropy of 2000:1 at 500 K in agreement with the STM observations. The adatom causes maximum strain on the dimer bond when it is located at the saddle point for the hopping across the trough. The bond stretching is so pronounced that this configuration can be considered as a broken dimer.

The most striking effect of the adatom on dimer buckling is seen with the adatom in its equilibrium position. It induces strong in-phase buckling of the two dimers in the next row. The

resulting configuration of two adjacent dimers buckled in the same direction has indeed been observed experimentally, and it is suggested that the observed buckle-inducing defects might correspond to single Si adatoms. Their imaging gives the only experimental information available on the binding site of the adatom.

---

1. Summary of paper to be published.
2. ORNL/ORISE postdoctoral research associate.
3. University of Cambridge, Cambridge, United Kingdom.
4. D. E. Jesson, S. J. Pennycook, and J.-M. Baribeau, *Phys. Rev. Lett.* **66**, 750 (1991).
5. D. E. Jesson et al., *Phys. Rev. Lett.* **68**, 2062 (1992).
6. This research is part of the Grand Challenge Project on "First-Principles Simulation of Materials Properties," funded by the High-Performance Computing and Communications Initiative.

HYDRATION OF Mg-CORDIERITE INVESTIGATED BY *AB INITIO* TOTAL ENERGY CALCULATIONS [1]

B. Winkler,[2] *V. Milman,*[3] *and M. C. Payne*[4]

Ab initio total energy calculations based on the local density approximation (LPA) have been performed for hydrated Mg-cordierite to elucidate the location, orientation, and total energy of hydration in the ground state. The orientation and dynamics of the water molecule in cordierite, $Mg_2Al_4Si_5O_{18} \cdot nH_20$, have been the subject of several contradicting spectroscopic and structural studies. In view of experimental difficulties, quantum mechanical calculations present a unique tool for the atomistic modeling of this system. This is especially true for the hydrogen-containing materials, as these are difficult to simulate using empirical potentials. Modeling of hydrated cordierite required a supercell containing 61 atoms of 5 different species, which represents the most complicated inorganic compound ever studied using the first-principles LDA method.

In contrast to structural studies, but consistent with the interpretation of infrared experiments, the calculations demonstrate that the stable configuration of the water molecule in alkali-free Mg-cordierite has a proton-proton vector aligned parallel to the (001) direction. The water molecule is found to be nearly undistorted, and there is only a weak hydrogen bonding. This result confirms an interpretation of the existing spectroscopic and quasielastic neutron scattering data. Furthermore, the *ab initio* calculation predicts that the water molecule is displaced with respect to the center of the cavity by 0.04 Å along (001), which is consistent with the results of quasielastic neutron scattering experiments. The calculated internal structure opens the way to correct interpretation of the recent contradictory structural and calorimetric studies.

The total energy of hydration for cordierite with one water molecule per primitive unit cell has been calculated to be 0.4 eV. The local distortions caused by the hydration are very small, thus indicating an ideal mixing behavior. The results related to the water molecule docking in the cavity are expected to be applicable to a number of water-bearing minerals.

---

1. Summary of paper to be published.

2. Kiel University, Kiel, Germany.
3. ORNL/ORISE postdoctoral research associate.
4. University of Cambridge, Cambridge, United Kingdom.

MAGNETIC PROPERTIES

MAGNETIC STRUCTURE AND SPIN DYNAMICS OF CHROMIUM ALLOYS[1]

R. S. Fishman[2] and S. H. Liu

It has been known for many years that the antiferromagnetic ordering properties of chromium are profoundly influenced by adding a small amount of transition-metal impurities. For instance, while 4% of vanadium impurity can suppress magnetic ordering entirely, the same percentage of manganese impurity doubles the Néel temperature T_N. Also, the ordered state of pure chromium is a spin-density wave with a periodicity incommensurate with the lattice; as little as 1% of manganese impurity renders the magnetic structure commensurate.

A consistent model, which has answered a number of puzzles, for the impurity effects has been constructed. There are three factors involved. Impurities on the right-hand side of chromium on the periodic table add electrons to the systems, which improve Fermi surface nesting and raise T_N. Conversely, impurities on the left-hand side of chromium on the periodic table lower T_N. Impurity sites also provide scattering centers for the band electrons, and these cause T_N to decrease. The third factor is that the nesting model is only approximately correct. The spin-density wave state with minimum free energy has a wave vector slightly shifted from the nesting position. The combined effects of these three factors give an excellent account of the observed magnetic ordering properties of chromium alloys.

The same model has been used to predict the nature of paramagnetic spin fluctuations above T_N. In general, the constant-energy neutron scattering cross section shows two peaks at positions corresponding to the wave vectors of magnetic ordering below T_N. The two peaks can be shifted by adding impurities in the same way as the magnetic ordering wave vector. The temperature provides an additional parameter which modifies the linewidths and peak positions. Detailed predictions have been made and are being tested experimentally at the Brookhaven National Laboratory.

---

1. Summary of papers: *Phys. Rev. B* **47**, 11870 (1993); ibid **48**, 3820 (1993).
2. ORISE faculty research participant from North Dakota State University, Fargo, N. Dak.

ROLE OF ELECTRONIC SCREENING IN ITINERANT-ELECTRON MAGNETS[1]

J. F. Cooke, J. M. Bass,[2] and J. A. Blackman[2]

Results from previous calculations of the static and dynamic properties of itinerant-electron magnets have been shown to be in excellent agreement with corresponding experimental results for nickel, iron, and cobalt at low

temperatures. Such results have been found to be sensitive to screened coulomb matrix elements which appear in the theory. In the past, symmetry arguments have been used to reduce the number of these matrix elements to a relatively small subset. Under certain approximations, some of these could be estimated from static properties (e.g., magnetic moment and form factor data). Ideally, it would be best to calculate all of the matrix elements from a first-principles approach. Unfortunately, results of such calculations based on the local density approximation lead to incorrect results from both a qualitative and quantitative perspective.

As the first step in an alternate approach, the possibility of calculating all of the relevant matrix elements from a Thomas-Fermi screened Coulomb potential has been investigated. This has the advantage of reducing the number of independent parameters to one (i.e., the screening length). This parameter is fixed so as to produce the experimentally measured magnetic moment. This procedure has been found to work well for cobalt. For nickel, however, even though the overall bandwidth was predicted accurately, the multi-branch character of the spin-wave dispersion curve along 100 was not reproduced as shown in Fig, 1.6. In both cases, the value of the screening length which gave the correct moment also gave good overall agreement with spin-wave data. As the result of the somewhat unexpected success of this approach, various ways of generalizing the theory are being pursued.

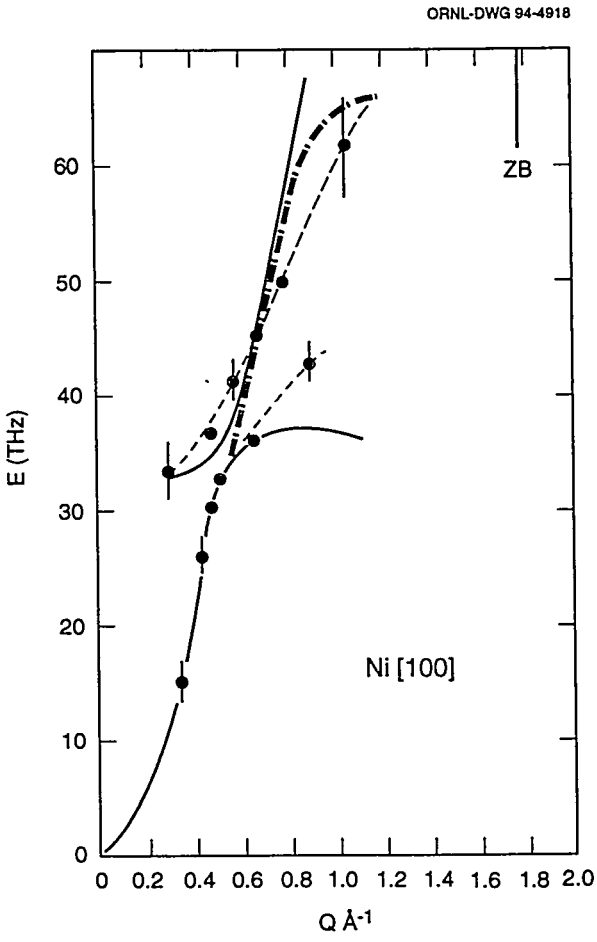

Fig. 1.6. Spin-wave dispersion curve along 100 for nickel; solid line is previous theory, dash-dot line is Thomas-Fermi result, dots are experiment.

---

1. Summary of paper: *J. Phys., Condens. Matter* **4**, L275 (1992).
2. University of Reading, Reading, United Kingdom.

ELECTRONIC THEORY AND THE MAGNETIC MOMENT OF ITINERANT-ELECTRON SYSTEMS[1]

J. F. Cooke

The magnetic moment of itinerant-electron systems can be determined directly from the correlation function $<c^{\dagger}_{nk\sigma}c_{nk\sigma}>$ where n is the energy band index, k is the wave vector, and σ is the spin. One of the most straightforward ways of determining this correlation function is to use the Green's function formalism. The relevant Green's function which must be calculated is the single-particle propagator. By using diagrammatic expansions, functional derivative, or equation of motion methods, an equation can be derived for the single-particle propagator in terms of the electronic self-energy. This approach establishes a direct link between the electronic self-energy, the electronic band structure, and the magnetic moment of itinerant-electron systems. The simplest application of this theory is based on the random phase approximation (RPA). This leads to predictions that the magnetic moment per site decreases with increasing temperature, eventually going to zero at a Curie temperature, which is well above experimental values for transition-metal systems.

There are, of course, many factors which could account for this discrepancy. Perhaps the most obvious is that the RPA calculation does not include spin-wave contributions. In principle, creation of spin waves reduces the moment of the system. This is obvious for local moment systems where the zero temperature moment is directly reduced by the number of spin waves. For itinerant systems, such contributions must be included in the electron self-energy expression. Phenomenological approaches of including spin-wave contributions lead to minimal corrections. In order to assess the importance of terms in the self-energy beyond RPA, formal expressions have been derived using the functional derivative technique. The terms can be divided into contributions from ladder, bubble, and exchange diagrams. Work on obtaining numerical estimates of the size of these various terms is currently under way. In addition, numerical investigation of the temperature dependence of relevant coulomb matrix elements, which result from the spin dependence of the radial part of the electronic wave function, indicates that this effect may also be important.

---

1. Summary of paper to be published.

LONGITUDINAL AND TRANSVERSE SPIN DYNAMICS IN THE SINUSOIDAL PHASE OF ERBIUM AND THULIUM[1]

S. H. Liu and J. F. Cooke

Spin dynamics in the sinusoidal phase of erbium and thulium have been studied experimentally for some time. Unlike the low-temperature phases, data for the sinusoidal phase are difficult to interpret because the inelastic neutron scattering lines are broad and a reliable theory has not been developed. This deficiency has been addressed by formulating a theory using a radically different approach from the conventional spin-wave theory.

All theories of spin dynamics rely on some form of mean-field decoupling approximation. The conventional spin-wave theory treats the ordered moment as an approximate constant of motion. In the sinusoidal phase where the ordered moment is small and spatially varying, this procedure becomes questionable. This new method calculates the moments of the frequency, treating both the ordered moments and the two-spin correlation functions as constants of motion. As a result, the theory should be reliable from the well-ordered phase up to the paramagnetic phase. A drawback is that it does not give a formula for the line shape directly. With enough moments, however, one can fit the results to a sum of Gaussian lines and obtain a theoretical line shape that can be compared with experiments. In the sinusoidal phase, calculations up to the fourth moment of the frequency have been made, and the results have been fit to two Gaussian functions. It is found that both transverse and longitudinal modes are broad lines, but for different physical reasons. There has been one report on narrow longitudinal modes in Er, but it is concluded that the observation may be spurious. Only broad longitudinal lines are seen in Tm, which is in agreement with our theory.

---

1. Summary of paper to be published.

SPONTANEOUS MAGNETIZATION OF ANYONS WITH LONG-RANGE REPULSION[1]

Jaichul Yi[2] *and G. S. Canright*[2]

One of the controversial tests of the "anyon superconductor" model for the high-temperature superconductors (HTSc) has been the search for spontaneous magnetic moments[3] arising from the broken time-reversal symmetry of the anyons. The controversy arises from the theoretical side, because there are a variety of estimates[4,5] for the spontaneous magnetization, ranging from zero to much larger than the experimental threshold of resolution. One of the main problems in this area is the use of mean-field theory for the fractional statistics; it is not clear whether estimates of physical properties which are derived from mean-field theory are reliable.

This question has been examined previously[4] for noninteracting anyons, using the virial expansion, which is a high-temperature, low-density expansion which avoids the use of mean-field theory. In the present work, it was found that the second virial coefficient for anyons interacts with a long-range repulsion ($\propto 1/r^2$). It was also found that the spontaneous magnetization, derived in this limit from the second virial coefficient, is drastically reduced by the repulsive interaction. This result, coupled with our earlier estimate[3] from exact numerical results at $T = 0$, implies that the spontaneous magnetization of interacting anyons is small or zero over a wide range of temperatures. Hence,

it is believed that measurements of the local magnetization in the HTSc are not a good test for the anyon hypothesis.

---

1. Summary of paper: *Phys. Rev. B* **47**, 273, 1993.
2. Guest scientist from The University of Tennessee, Knoxville, Tenn.
3. B. I. Halperin, J. March-Russell, and F. Wilczek, *Phys. Rev. B* **40**, 8726, 1989.
4. G. S. Canright and M. D. Johnson, *Phys. Rev. B* **42**, 7931 (1990).
5. Y. Kitazawa, *Phys. Rev. Lett.* **65**, 1275 (1990).

MAGNETOPLASMA EDGE MODES OF TWO-DIMENSIONAL ELECTRON GAS SYSTEMS[1]

J. J. Quinn[2] *and X. Xia*[2]

A two-dimensional (2D) electron gas in which the electron concentration drops abruptly from its bulk value to zero supports an edge plasmon whose frequency is about 10% lower than the frequency of a bulk 2D plasmon of the same wavelength. For an edge electron density profile which does not drop abruptly to zero, a sequence of higher multipole edge modes occur below the bulk 2D plasma frequency. These modes have been studied for several model edge density profiles, and the results are consistent with picturing them as bulk modes of the low-density surface region which cannot propagate into the bulk. In the presence of a dc magnetic field B normal to the 2D layer, a number of new low-frequency modes are found for one direction of propagation along the edge. For a double-step profile, these low-frequency modes appear to be coupled inter- and regular-edge magnetoplasma modes. For smooth profiles, many low-frequency magnetoplasma edge modes are found. The nature of these modes and their potential use in VLSI circuits are being investigated.

---

1. Summary of paper to be published.
2. Guest scientist from The University of Tennessee, Knoxville, Tenn.

NUMERICAL STUDIES OF TWO-DIMENSIONAL ELECTRON-HOLE SYSTEMS IN A STRONG MAGNETIC FIELD[1]

J. J. Quinn[2] *and Ximing Chen*[2]

The eigenstates of a two-dimensional system containing a finite number (N_e = 6, 7, 8) of electrons interacting with one or more valence band holes are obtained by numerical diagonalization within the subspace of the lowest Landau level. The valence band holes are located on a plane separated by a distance d from the electron layer, and the holes can be free or localized on defects. Studies of the energy spectrum as a function of Landau level degeneracy $2S + 1$ and layer separation d help to illuminate the nature of the low-lying excitations of the quantum Hall states. Strong evidence for the existence of stable "anyonic ions" or "anyonic excitons," bound states of the valence band hole and one or more Laughlin quasielectrons, is found. The luminescence spectrum is studied as a function of s, d, and temperature T. This spectrum can contain one, two, or three peaks and can be understood

in terms of processes involving the annihilation and creation of Laughlin quasiparticles and the "band" structure of the initial and final state energy spectra.

---

1. Summary of paper to be published.
2. Guest scientist from The University of Tennessee, Knoxville, Tenn.

MANY-BODY THEORY, PHOTOVOLTAICS, AND SUCH

ADVANCED DEPOSITION AND SUBSTRATE TECHNOLOGIES FOR THIN-FILM POLYCRYSTALLINE SILICON PHOTOVOLTAICS

R. F. Wood, G. E. Jellison, Jr., D. Eres, S. M. Gorbatkin, R. D. Westbrook,[1] *A. J. Moorhead,*[2] *and P. A. Menchhofer*[2]

Research under this Cooperative Research and Development Agreement (CRADA) with the Electric Power Research Institute seeks to demonstrate the feasibility of a photovoltaic technology that uses films ($\lesssim 50\ \mu m$) of polycrystalline silicon (p-Si) deposited on low-cost ceramic substrates. The work has three general research tasks.

Task 1. Development of Low-Cost Substrates. Substrate materials must have thermal properties compatible with those of Si from room temperature to the melting point of Si (1410°C). Several ceramics meet the requirement, but mullite and SiC have proved particularly interesting and probably can be made to satisfy the low-cost criteria. It is important that molten Si wet the substrate and that large-grained films result from the coating process. In addition, certain impurities must not diffuse from the substrate into the Si on which the solar cells will be made. Other conditions also must be met, but space precludes discussing them here. Suffice it to say that considerable progress has been made in developing the type of substrate needed.

Task 2. Recrystallization of Deposited Films. The p-Si on which the cells are to be made must have large grain sizes in order to prevent excessive carrier recombination at grain boundaries. This will probably involve some type of melting and recrystallization. Large-grained material has been obtained by directional solidification in crystal growth furnaces. A zone-melting recrystallization apparatus was built, and zone melting was demonstrated. In this method, a narrow molten zone is swept through the deposited coating in much the same way as in float-zone crystal growth. A flat heater on which the substrate is held is used to heat the sample to ~1200°C, while a strip of graphite serves as a top heater to supply the incremental heating needed to create the molten zone. The substrate can be translated beneath the graphite strip to move the molten zone through the silicon.

Task 3. Advanced Film Deposition Technologies. Different Si film deposition techniques have been investigated, including pulling from the melt, e-beam evaporation, plasma spray, sputtering, molecular-jet chemical vapor deposition (MJ-CVD), and liquid-phase epitaxy (LPE). The last two are of particular interest because they

can provide epitaxial growth on a p-Si substrate at temperatures well below 1410°C. For example, a 20-μm thick layer of large-grained p-Si has been grown epitaxially on a Si-coated SiC substrate by MJ-CVD at 800°C. Similar results can be obtained by LPE at ~1000°C. A suggested approach is first to obtain a highly doped, "dirty" layer of Si by pulling from the melt and then to deposit a "clean" layer of Si by MJ-CVD or LPE. The dirty layer serves as the back contact while the clean layer provides the active material for solar cell fabrication. This approach is now under active investigation.

---

1. Consultant representing self.
2. Metals and Ceramics Division, ORNL.

FRACTAL VERTEX FOR ELECTRON-ELECTRON INTERACTIONS[1]

G. D. Mahan[2]

Electron-electron interactions cause the motions of electrons to be mutually correlated. The lowest level of an approximate theory is called the random phase approximation. Higher levels of theoretical approximation include adding vertex corrections to evaluations of the correlation functions. The most common approximation is to add a set of ladder diagrams.

An exact expression which included all ladder diagrams was derived. It was shown that this approximation has a fractal character, in that the diagrams can be reduced to hierarchical sets. Each ladder diagram has a vertex correction on each end. These corrections are also ladders, which have their own vertex corrections. The numerical implications of this theory are still being developed.

---

1. Summary of paper: *Mod. Phys. Lett. B* 7, 13 (1993).
2. ORNL/UT Distinguished Scientist.

RESTRICTED APPLICABILITY OF ONSAGER'S RECIPROCITY RELATIONS TO MODELS OF INTERFACE MOTION[1]

Theodore Kaplan, M. J. Aziz,[2] *and L. J. Gray*[3]

Rapid solidification experiments in binary alloys have demonstrated that there is a breakdown of local equilibrium at the crystal-melt interface and a kinetic coupling between the motions of the two atomic species across the interface during rapid interface motion. A number of models for interface motion have been developed to account for this behavior, as well as for similar behavior in other growth processes. A common goal of this work is a prediction of the interface velocity and the composition of the growing phase in terms of the temperature and composition of the parent phase at the interface. Because of the experimental difficulties involved in measuring the relevant quantities at a rapidly moving interface, only partial tests of some of these models have been possible to date.

Onsager's theorem for irreversible processes, deduced from time-reversal symmetry of the microscopic fluctuations that comprise steady-state behavior, identifies certain symmetries that hold for the coefficients of the linear

flow equations near equilibrium. These symmetries are referred to as Onsager's reciprocity relations. For theories of phase transformations in alloys, Onsager's theorem can provide an important test of their validity near equilibrium and potentially reduce the number of theories that need to be tested experimentally. In an earlier paper,[4] Onsager's relations were applied to a phase transformation at a moving planar interface in a two-component system. Appropriate pairs of thermodynamic forces and conjugate fluxes were determined and then used to test two proposed models for binary alloy solidification, the continuous growth model "with solute drag" and "without solute drag" of Aziz and Kaplan.[5] It is shown that these two models and several others are members of a class of models for which Onsager's relations do not apply, because of a dependency in the thermodynamic driving forces near equilibrium.

---

1. Summary of paper: *J. Chem. Phys.* **99**, 8031 (1993).
2. Harvard University, Cambridge, Mass.
3. Engineering Physics and Mathematics Division, ORNL.
4. T. Kaplan, M. J. Aziz, and L. J. Gray, *J. Chem. Phys.* **90**, 1133 (1989).
5. M. J. Aziz and T. Kaplan, *Acta Metall.* **36**, 2335 (1988).

SCREENING AND MOBILITY OF *n*-SILICON[1]

B. A. Sanborn,[2] P. B. Allen,[2] and G. D. Mahan,[3]

The electron mobility of *n*-silicon was calculated at room temperature as a function of the concentration of donors. Because the chemical potential is near the band edge, the integrals over particle distributions must be done numerically. Silicon is the most well-studied of any material, and all parameters are known. Prior calculations of the mobility, done without adjusting any parameters, gave results which disagreed with experiments by a factor of 4.

The present calculation was done in order to improve the agreement between theory and experiment. Great care was exercised in the calculation of the scattering of electrons from the ionized donors. All scattering was characterized by energy-dependent phase shifts which were calculated numerically. Screening by the electrons of the donor potential was calculated using both the random phase approximation (RPA) or the Singwi-Tosi-Land-Sjölander (STLS) theories. The screening was calculated at an appropriate nonzero temperature, and the mobility was calculated by solving Boltzmann's transport equation using Rode's method which is numerically exact. Elastic scattering was included from impurities and acoustic phonons, and the inelastic scattering was included from optical phonons.

The theoretical mobilities agreed well with experimental results for donor concentrations exceeding 10^{19} cm^{-3} at both T = 77 and 300 K. The agreement was poor for donor concentrations less than this value. Little difference was found between RPA and STLS results.

An unexpected result of the calculation was the value of the compressibility of the electron gas that was found. At T = 77 K, it was found to be negative over a wide range of donor concentrations. This theoretical result had not been

published previously and was a major new result of the calculation.

---

1. Summary of paper: *Phys. Rev. B* **46**, 15123 (1992).
2. State University of New York, Stony Brook, N.Y.
3. ORNL/UT Distinguished Scientist.

NONLINEAR POLARIZABILITY OF CORRELATED ONE-DIMENSIONAL SYSTEMS[1]

A. G. Rojo[2] and G. D. Mahan[3]

Conducting polymers are very nonlinear optical materials. Because they are relatively inexpensive to manufacture, they are very promising as optical materials. The third-order polarizability γ, called the hyperpolarizability, increases rapidly with the number N of monomers according to the empirical power law $\gamma = A + B N^n$, where A is the contribution of end-effects on the polymer chain and B and n characterize the monomer.

Free-electron theories predict that the exponent $n = 5$. Electron-electron interactions usually suppress charge fluctuations and are expected to reduce polarizabilities. Electron-electron interactions were introduced using the Hubbard model, which includes only the largest interaction, that occurs when two electrons of opposite spinS occupy the same π-orbital. Using Lanczos methods, the one-dimensional Hubbard model with an electric field was solved exactly. Results were obtained for chains of length N up to $N = 10$.

These results were totally surprising. Contrary to all expectations, it was found that the hyperpolarizability increased for moderate values of U/t, where U is the Hubbard on-site interaction and t is the bandwidth in the tight-binding model. Secondly, it was found that the exponent n increased to $n = 6$ for $U \approx t$. It is, therefore, concluded that electron-electron interactions increase the hyperpolarizability of conducting polymers.

---

1. Summary of paper: *Phys. Rev. B* **47**, 1794 (1993).
2. Guest scientist from the ORNL/UT Distinguished Scientist Program.
3. ORNL/UT Distinguished Scientist.

MEAN-FIELD THEORY OF ELASTIC DIPOLES ON A FCC LATTICE[1]

R. S. Pfeiffer[2] and G. D. Mahan[3]

Long-range interactions between atoms in solids can occur through either coulomb or elastic forces. For neutral atoms, the elastic interactions dominate. Molecular solids composed of diatomics such as N_2 or CO have an ordering transition. At low temperatures, the molecules are orientationally ordered, while at higher temperatures they are disordered. Because the molecules are neutral, their ordering must occur through interactions between elastic dipoles.

The general form of the short- and long-range interactions from elastic dipoles for cubic lattices was calculated. These interactions were

used to construct interaction potentials between near- and far-neighboring molecules. Mean-field theory was used to calculate the temperature for orientational ordering.

---

1. Summary of paper: *Phys. Rev. B* **48**, 669 (1993).
2. Auburn University, Auburn, Ala.
3. ORNL/UT Distinguished Scientist.

2. *Neutron Scattering*

The High-Flux Isotope Reactor (HFIR) operated normally through this period with an availability of about 64%. The user program operated well with the number of users in the Neutron Scattering and Small-Angle X-Ray programs increasing to 152.

The Neutron Scattering Program has been growing strongly in the area of structural determinations of important materials. Fascinating new structures have been observed in complex fluids under shear as a result of the Structures of Anistropic Colloidal Materials Program, in collaboration with The University of Tennessee and Los Alamos. Residual stress has been determined for industrially important materials, and a new Center for Residual Stress has been developed in collaboration with the ORNL Metals and Ceramics Division. Measurements continued on the fluxoid lattice in high-temperature superconductors, and two-dimensional melting was measured for the first time. The powder diffractometer worked well, and a number of new structures were determined. Measurements were started on biological materials with the new full-circle diffractometer that was built in collaboration with the ORNL Biology Division.

The HFIR, operated at 85 MW, is still the world's highest flux reactor. The neutron instrumentation is being upgraded to take full advantage of the reactor. The second and third axes of the three main triple-axis spectrometers are being completely rebuilt with the most modern equipment available. These spectrometers will be unsurpassed worldwide in neutron flux and performance, particularly in the area of polarization analysis. The powder diffractometer will be modified to utilize a new collimator system and will achieve a large take-off angle for high resolution and intensity. Two new small-angle scattering spectrometers are being installed. One will use multiple-bounce Si reflections to obtain very high resolution. The other will use spherically bent Si crystals to obtain very high intensities at moderate resolution. The neutron reflectometer will also be improved by moving it to a much more intense beam. Residual stress measurements have been so productive that a dedicated spectrometer will be built for these measurements.

The U.S.-Japan Cooperative Program on Neutron Scattering continues to produce important results. Funds have been provided from the Japan Atomic Energy Institute for a major upgrade of the wide-angle diffractometer that will include a new computer and data interface and a new position-sensitive detector which will utilize the latest electronic developments to accommodate very high data rates and obtain high angular resolution.

SMALL-ANGLE SCATTERING AND NEUTRON REFLECTOMETRY

COMPATIBILITY OF BLENDS OF POLYETHYLENE IN THE MELT AND SOLID STATES BY SMALL-ANGLE NEUTRON SCATTERING (SANS)[1]

G. D. Wignall, R. G. Alamo,[2] L. Mandelkern,[2] J. D. Londono,[3] and F. C. Stehling[4]

Polyethylene (PE) can be classified as high density (HD), low density (LD), or linear low density (LLD), depending on the chain structure and branch content. Blends of HDPE, LDPE, and LLDPE have attained widespread commercial applications, although understanding the mechanical and melt-flow properties of the blends is handicapped by the absence of a consensus at the most fundamental level (i.e., the degree of mixing of the components both in the melt and in the solid state). Despite the fact that PEs have been used since the 1930s, widely different views continue to be expressed in the literature, ranging from liquid-liquid phase segregation[5] to complete homogeneity in the melt[6] for HDPE/LDPE mixtures.

An obvious way to distinguish between these options is to perform SANS experiments. These were attempted over a decade ago using the scattering contrast obtained by deuterium labeling one of the components, and the results were interpreted in terms of miscibility for HDPE/LDPE in the melt.[6] However, the analysis was inconclusive because of some puzzling features that were not understood at the time. For example, SANS from 50/50 mixtures indicated that the components were compatible in the melt when only part of the HDPE was D-labeled. However, if all of the HDPE was deuterated, the system apparently phase separated. As a result of recent studies[7] of isotope effects in D-labeled PEs, this behavior can now be understood as resulting from a small enthalpic interaction parameter (χ_{HD}) between labeled and unlabeled segments, because the number of units on the chains (N) was large enough to exceed the critical condition for demixing ($N\chi_{HD} = 2$). Thus, phase segregation at higher labeling levels was an artifact caused by isotope effects rather than a basic incompatibility between the species. Recent experiments[7] with components of lower molecular weight (and hence lower N) ensure that $N\chi < 2$ and demonstrate that HDPE/LDPE mixtures are compatible in the melt for all compositions. This is illustrated in Fig. 2.1 which shows a fit to the SANS data from a blend of

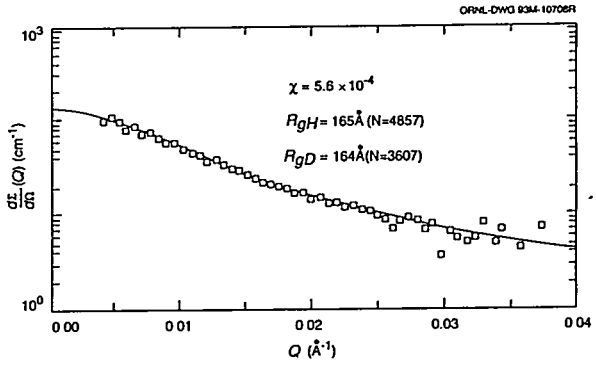

Fig. 2.1. Fit to random phase approximation for blend of branched LDPE ($\phi_H = 0.91$) and deuterated linear HDPE ($\phi_D = 0.09$) at 143°C.

deuterated linear HDPE-D and unlabeled branched LDPE. For high volume fractions (ϕ) of branched material, a phase-separated melt had been proposed previously,[5] based on indirect measurements of the solid state after quenching (e.g., melting points). Direct SANS measurements in the melt state indicate that the blend is homogenous, and a fit to the random phase approximation gives an interaction parameter close to the isotopic interaction measured in linear/linear blends.[7] This research is relevant to determining phase structures, to interpreting observed property changes on mixing, and to guiding strategies to improve blend properties.

---

1. Summary of paper: *Macromolecules* (in press).
2. Florida State University, Tallahassee, Fla.
3. ORNL/ORISE postdoctoral research associate.
4. Exxon Chemical Company, Baytown, Tex.
5. M. J. Hill, P. H. Barham, and A. Keller, *Polymer* **33**, 2530 (1992).
6. F. S. Stehling and G. D. Wignall, *Am. Chem. Soc. Div. Polym. Chem. Prepr.* **24**, 211 (1983).
7. J. D. Londono et al., *Macromolecules* (submitted for publication).

MISCIBILITY AND COCRYSTALLIZATION IN HOMOPOLYMER SEGMENTED BLOCK COPOLYMER BLENDS[1]

K. P. Gallagher,[2] X. Zhang,[2] J. P. Runt,[2] G. Huynh-ba,[3] and J. S. Lin

In the development of poly(ester-ether) (PEE) segmented block copolymers, it became apparent that the mechanical properties of blends of the copolymers with poly(butylene terephthalate) (PBT) were, in general, grossly different from pure copolymers containing the same overall hard segment concentration. Since PBT is the homopolymer analog of the crystallizing copolymer segments and preliminary experiments suggest that some PBT/PEE blends are miscible, it was postulated previously that PBT and certain PEE copolymers are capable of cocrystallization (i.e., crystallization into the same lamellar crystal).[4]

In this investigation, it was found that the amorphous phase behavior of blends of PBT and PEE varied from completely immiscible to miscible, depending on the copolymer composition. The predictions of the Flory-Huggins relationship are in general agreement with the observed behavior when the interaction parameters are estimated from solubility parameters. The result of thermal analysis (e.g., differential scanning calorimetry) and small-angle x-ray scattering experiments strongly suggest that the PBT and PEE copolymers are capable of cocrystallization in the miscible blends under all conditions. The cocrystalline microstructure results from the complete miscibility and the blocky nature of the copolymer (i.e., the identical chemical and crystalline structures of PEE hard segments and PBT). The crystallization rate of the copolymer in the miscible blends was found to be enhanced significantly because of the presence of PBT, and the resulting crystal thickness was found to be the same as that observed for PBT. Partially miscible blends of PBT with copolymers

containing intermediate hard segment concentrations formed distinguishable crystal populations, but the crystallization rate of the copolymer in these blends was also strongly influenced by the presence of PBT.

---

1. Summary of paper: *Macromol.* **26**, 588 (1993).
2. Pennsylvania State University, University Park, Pa.
3. E. I. duPont de Nemours Company, Wilmington, Del.
4. J. Runt et al., *Macromol.* **22**, 3908 (1989).

STATISTICAL SEGMENT LENGTH MISMATCH ON POLYMER BLEND MISCIBILITY[1]

G. D. Wignall, M. D. Gehlsen,[2] and F. S. Bates[2]

Saturated hydrocarbon polymers (polyolefins) represent the single largest segment of the synthetic polymer market. Their phase behavior is governed by van der Waals interactions, though the absence of a single dominant thermodynamic factor renders these mixtures susceptible to subtle variations in molecular architecture. In particular, the hypothesis[3] that the difference in the magnitude of the statistical segment lengths (Δa) of the blend components produces an additional additive term to the Flory-Huggins interaction parameter, χ, which decreases miscibility may provide fundamental insights into a long-standing question of why polyolefins do not mix. Conversely, if this mismatch can be shown to be the dominant term governing mixing, it should be possible to design polyolefins that are more miscible by minimizing Δa. Recent SANS experiments on two specifically tailored polyolefins (PEP29 and PEE70), whose structures are shown in Fig. 2.2, indicate that this

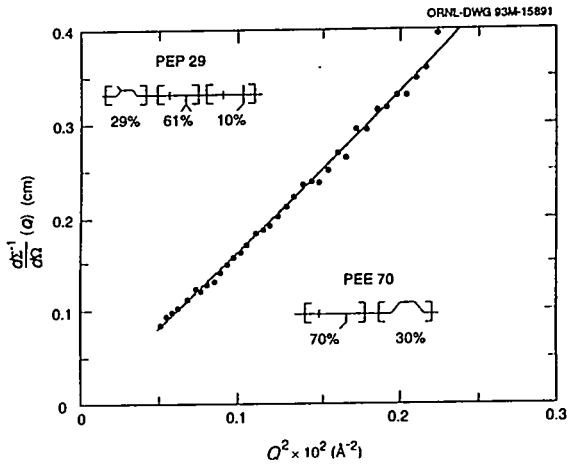

Fig. 2.2. Ornstein-Zernike plot of the reciprocal cross section vs Q^2 for 50:50 blend of PEE70 and PEP29 at 25°C.

methodology constitutes a very promising contribution to understanding polyolefin blend miscibility. The Ornstein-Zernike plot of the small-angle neutron scattering cross section (Fig. 2.2) has a positive intercept that is characteristic of a homogenous mixture. The measured interaction parameter ($\chi \approx 3 \times 10^{-3}$) is below the critical value, which again is consistent with miscibility. The segment lengths of the components (a = 5.7 Å for PEP29; a = 6.5 Å for PEE70) are close to that of polypropylene (a = 6.1 Å), and in future investigations, the mutual miscibility of these components will be explored. To the authors' knowledge, no polyolefins are miscible with PP; and if these results show PP is miscible with PEP29 and PEE70, this will have an

enormous impact on polymer blend theory and on new PP blend opportunities.

---

1. Summary of paper to be published.
2. University of Minnesota, Minneapolis, Minn.
3. F. S. Bates et al., *Macromol.* **25**, 5547 (1992).

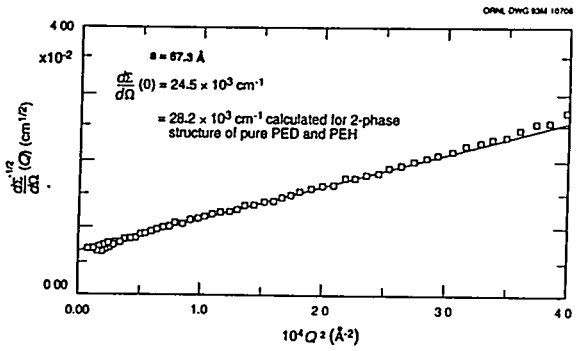

Fig. 2.3. Debye-Bueche plot for phase-separated blend of deuterated HDPE and protonated LDPE slow cooled from the melt at 0.75°C/min.

THE MORPHOLOGY OF BLENDS OF LINEAR AND BRANCHED POLYETHYLENES IN SOLID STATE BY SMALL-ANGLE NEUTRON SCATTERING (SANS)[1]

G. D. Wignall, R. G. Alamo,[2] L. Mandelkern,[2] J. D. Londono,[3] and F. C. Stehling[4]

Blends of high-density (HD) and low-density (LD) polyethylenes (PE) have recently been shown to be homogenous in the melt via SANS.[5] However, in the solid state, the HDPE/LDPE system shows extensive segregation because of the differences in melting points for HDPE (T_m ~ 134°C) and LDPE (T_m ~ 111°C). The domain sizes are ~10^2 Å in size after slow cooling from the melt, and this implies that the two components form separate lamellae. Two-peak melting curves obtained for such mixtures are consistent with this conclusion. Thus, even if the blends are homogenous in the melt, they may subsequently separate, depending on thermal treatment, as the higher melting component crystallizes first. Figure 2.3 shows a Debye-Bueche[6] (DB) plot of the data for a "50/50" blend of deuterated (HDPE-D) and protonated (LDPE-H) after cooling from the melt at 0.75°C/min. The extrapolated cross section [$d\Sigma/d\Omega(0) = 24.5 \times 10^3$ cm^{-1}] is well over an order of magnitude higher than in the melt, and assuming complete separation of the deuterated and protonated components, the calculated cross section is 28.2×10^3 cm^{-1}. In view of the fact that the experiments are independently calibrated with no arbitrary fitting factors in the intensity scale, agreement with the absolute cross sections calculated from the DB theory is excellent.

The sizes of the domains may be estimated from the mean-chord intercept lengths[7] ($L_1 \simeq L_2 \simeq 175$ Å). There are "peaks" or modulations at $Q \sim 0.02$ Å and $Q \sim 0.055$ Å in the small-angle x-ray scattering data from this sample, which correspond to length scales of $D \simeq 2\pi/Q^* \sim 275$ and 115 Å. Therefore, it seems reasonable to associate the phase-separated domains with individual lamellae.

These studies are relevant for evaluating the potential for recycling polyethylenes, which constitute approximately 50% of plastic wastes. Determining the degree of compatibility of the various components has important implications for designing strategies for recycling,

reprocessing, and evaluating the usefulness of the resulting blend material.

---

1. Summary of paper: *Macromolecules* (in press).
2. Florida State University, Tallahassee, Fla.
3. ORNL/ORISE postdoctoral research associate.
4. Exxon Chemical Company, Baytown, Tex.
5. G. D. Wignall et al., "Compatibility of Blends of Polyethylenes in the Melt and Solid States by Small-Angle Neutron Scattering," this report.
6. P. Debye and A. M. Bueche, *J. Appl. Phys*. **20**, 518 (1949); P. Debye, H. R. Anderson, and H. Brumberger, *J. Appl. Phys.* **28**, 679 (1957).
7. R. A. Alamo et al., *Macromolecules* (in press).

MICRODOMAIN CONTRACTION IN MICROPHASE-SEPARATED MULTIBLOCK COPOLYMERS[1]

S. D. Smith,[2] R. J. Spontak,[3] M. M. Satkowski,[2] A. Ashraf,[2] and J. S. Lin

When chemically dissimilar contiguous sequences (blocks) of an AB diblock copolymer are sufficiently incompatible, the copolymer undergoes microphase separation and self-organizes into periodic microdomains which measure on the order of the gyration radius (R_g) of the domain forming block. For a symmetric (50/50 vol %) copolymer, the transition from a disordered state to one possessing long-range order occurs when $\chi N = (\chi N)_c \approx 10.5$ (χ is the Flory-Huggins interaction parameter, and N is the number of monomers along the copolymer backbone) in the absence of critical fluctuations.[4] When $\chi N >> (\chi N)_c$, a strongly segregated symmetric copolymer orders into a lamellar morphology of alternating A and B blocks.

Linear multiblock copolymers, like their diblock analogs, also undergo order-disorder transitions. To explore the conformations of such materials, four symmetric poly(styrene-b-isoprene)$_n$ copolymers with $2n$ ($1 \leq n \leq 4$) perfectly alternating blocks of nearly equal mass have been synthesized. Small-angle x-ray scattering reveals that the microdomain periodicity decreases with n along the lamellar normal, thereby confirming theoretical predictions[5,6] and providing direct evidence for bridging among the $2(n - 1)$ middle blocks.

---

1. Summary of paper: *Phys. Rev. B* **47**, 14555 (1993).
2. The Procter and Gamble Co., Cincinnati, Ohio.
3. North Carolina State University, Raleigh, N.C.
4. G. H. Fredrickson and E. Helfand, *J. Chem. Phys.* **87**, 697 (1987).
5. H. Benoit and G. Hadziioannou, *Macromol.* **21**, 1449 (1988).
6. T. Kavassalis and M. D. Whitmore, *Macromol.* **24**, 5340 (1991).

TEMPERATURE COEFFICIENTS FOR THE CHAIN DIMENSIONS OF POLYSTYRENE AND POLYMETHYLMETHACRYLATE[1]

G. D. Wignall, A. J. Boothroyd,[2] and A. R. Rennie[3]

The temperature dependence of the unperturbed dimensions of a polymer relates to the variation in thermal population of the different rotational configurations of adjacent bonds and is represented by the parameter κ =

$d \ln\langle S^2\rangle_0/dT$, where $\langle S^2\rangle_0$ is the unperturbed, square radius of gyration. A reliable knowledge of κ for different polymers is essential to the development of microscopic models of polymers in bulk and in solution because many physical properties depend crucially on chain size. Traditional methods for measuring κ (from the intrinsic viscosity in a series of theta solvents, or by viscoelastic measurements on cross-linked networks) are indirect and so depend upon the assumptions of the model used. Small-angle neutron scattering (SANS), on the other hand, measures the change in dimensions directly, and for polyethylene, the SANS value for κ agrees well with that obtained by the old techniques. With other polymers, however, the situation is much less clear. Polystyrene, for instance, was thought for many years to have a κ value of 0.4×10^{-3}, but more recently a variety of conflicting results have been obtained by rheological and viscoelastic methods that vary both in magnitude and in sign. A similar confusion exists with polymethylmethacrylate (PMMA). These two polymers are common materials of great commercial interest, and definitive measurements of them have been performed to facilitate a comparison of values of κ obtained by SANS, viscometric, and rheological measurements which may point toward defects in theory that cause the latter two techniques to produce errant results.

Contrary to most previous reports based on rheological measurements, it was found that neither polymer exhibits a significant change in dimensions with temperature. Coefficients of $\kappa = (0.0 \pm 0.1) \times 10^{-3}\ K^{-1}$ for polystyrene and $(0.1 \pm 0.1) \times 10^{-3}\ K^{-1}$ for PMMA were deduced. These values are close to those given by thermoelastic measurements but are difficult to reconcile with theoretical predictions of the rotational isomeric state model. In order to resolve this apparent contradiction further, SANS measurements in dilute solutions are currently being performed to explore whether the unperturbed dimensions are the same in the molten state as in an ideal solvent, and whether the dimensions obtained by intrinsic viscosity and SANS are identical.

---

1. Summary of paper: *Journal of Physical Chemistry* (in press).
2. Oxford University, Oxford, United Kingdom.
3. Cambridge University, Cambridge, United Kingdom.

STRUCTURAL CHARACTERIZATION OF C_{60} AND C_{70} FULLERENES BY SMALL-ANGLE NEUTRON SCATTERING (SANS)[1]

K. A. Affholter,[2] G. D. Wignall,
S. J. Henderson,[3] G. J. Bunick,[3]
R. E. Haufler,[4] and R. N. Compton[4]

The discovery that C_{60} and C_{70} molecules can be produced in quantity with high purity has generated significant interest in the basic and applied research communities. Potential applications are being considered in many areas (tribology, photoconductivity, nuclear medicine, superconductivity, etc.). Although the research and resulting publications have increased exponentially, a nondestructive technique to study fullerenes in solution had not

been successfully accomplished until this work. SANS is a proven tool for examining the structure and interactions of particles in solution, though the dimensions of fullerenes are close to the lower resolution limit of the technique. Deuterated solvents have virtually no SANS contrast with carbon, and the high incoherent cross section of protonated solvents limits the path length. These difficulties have been circumvented by using CS_2 as a solvent which has good contrast with carbon and a low incoherent cross section, which allows the use of long path lengths. The radii of gyration of both C_{60} ($R_g = 3.82 \pm 0.05$ Å) and C_{70} ($R_g = 4.13 \pm 0.05$ Å) have been measured, and these dimensions are close to those calculated from the atomic coordinates. Figure 2.4 shows the Guinier plots for C_{60} and C_{70} fullerenes in CS_2. Excellent agreement was achieved between the measured absolute scattering cross sections and the values estimated from the particle and solvent scattering length densities. The second virial coefficient is close to that calculated from the particle volume/mass, without invoking particle-particle or particle-solvent interactions. To our knowledge, this represents the first successful application of small-angle scattering for the characterization of fullerenes. SANS makes it possible to study the sizes and shapes of modified buckyballs and the locations of light atoms (e.g., H^1). Complementary small-angle x-ray scattering data should prove useful in locating heavy atoms (e.g., in metal-carbon clusters).

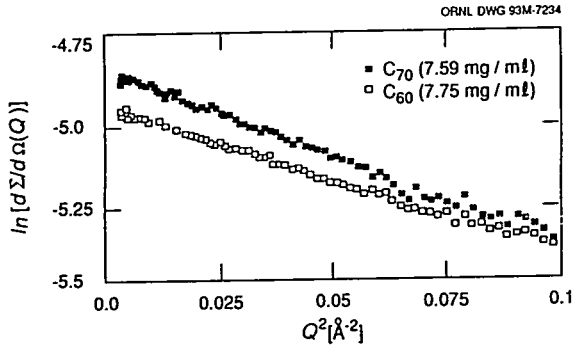

Fig. 2.4. Guinier plot of SANS data from C_{60} and C_{70} fullerenes in CS_2.

---

1. Summary of paper: *J. Chem. Phys.* **99**, 11 (1993).
2. Consultant representing self.
3. Biology Division, ORNL.
3. Health Sciences Research Division, ORNL.

EVALUATION OF PRECIPITATE EVOLUTION IN 6XXX ALLOYS USING SMALL-ANGLE NEUTRON SCATTERING TECHNIQUES

C. W. Bartges[1] *and Steve Spooner*

Aluminum-based 6XXX alloys are an important class of commercial aluminum alloys. However, the aging response of these Al-Mg-Si-(Cu) alloys is not as well-known as in 2XXX and 7XXX alloys. Although there is a general understanding of the aging response, industrial experience with 6XXX alloys makes it clear that the aging reactions are very sensitive to processing conditions. Small-angle neutron scattering (SANS) experiments were used to evaluate the potential for studying aging reactions in these materials. It was found that very small particles are present in the naturally aged condition and are replaced by distinctly larger particles at 177°C. The amount of precipitate increases with increasing solute levels. The greatest change in hardness occurred during the

first 8 h at 177°C which parallels the most obvious changes in the precipitate scattering. The results show SANS to be very sensitive to precipitate evolution. The present findings will be used as a foundation for more quantitative evaluations of the aging response of 6XXX alloys.

---

1. Alcoa Technology Center, Alcoa, Pa.

MATRIX PRECIPITATE EVOLUTION DURING DECOMPOSITION OF ALUMINUM ALLOY 7075[1]

C. W. Bartges,[2] L. H. Edelson,[3] S. Y. Tzeng,[2] and J. S. Lin

Many important properties of aluminum alloys are developed during artificial aging. This process involves decomposition of a supersaturated solid solution to yield a homogeneous distribution of matrix precipitates. The primary objective of this study was to develop a quantitative understanding of matrix precipitate microstructural evolution of one particular Al alloy (7075) containing 5.8 wt% Zn, 2.7 wt% Mg, 1.5 wt% Cu, plus trace amounts of Si, Fe, Cr, Ti, etc. Electrical conductivity, wide-angle x-ray diffraction, differential scanning calorimetry, and transmission electron microscopy can provide a qualitative description of the decomposition process. Small-angle x-ray scattering (SAXS) can better quantify the matrix precipitate characteristics in the process.

Analysis of SAXS results from alloy 7075 annealed at 121°C from 6 to 192 h concluded that: (1) The Guinier-Preston zones are the primary strengthening precipitates in the naturally aged specimen, but they play a minor role in artificial aging. (2) The volume fraction and number density of matrix precipitates, η' and η, increase dramatically in the first 24 h at 121°C, and the coarsening occurs after 24 h. (3) Throughout the decomposition process, the particles grew according to a $t^{1/9}$ law. (4) Particle size distribution of matrix precipitate was obtained via the method of Fedorova and Schmidt.[4]

---

1. Summary of paper to be published.
2. ALCOA Technical Center, Alcoa, Pa.
3. Xerox Corporation, Rochester, N.Y.
4. I. S. Fedorova and P. W. Schmidt, *J. Appl. Crystallogr.* **11**, 406 (1978).

CHARACTERIZATION OF POROSITY IN CERAMIC MATERIALS BY SMALL-ANGLE SCATTERING[1]

D. W. Schaefer,[2] R. K. Brow,[2] B. J. Olivier,[2] T. Rieker,[2] G. Beaucage,[2] L. Hrubesh,[3] and J. S. Lin

Porosity is a dominant factor affecting the performance of ceramic materials. Failure of structural ceramics, for example, offer results from flaws that originate at voids present in green compacts. Ceramists employ the tools of colloid chemistry to prepare powders that sinter in such a way as to eliminate such troublesome voids.

Equally important are ceramic materials that depend on engineered porosity to fulfill their intended role. Membranes and filters are prime examples. Particulate filters require porosity in the micron-size range, whereas gas separation

membranes require tightly controlled pores below 10 Å. Porous ceramics also serve as catalyst supports and high-temperature insulators. An emerging class of selective adsorbents use crystalline silicotitanates with lattice constants in the range 5–15 Å. In all cases, porosity with specific morphology and topology is required.

Small-angle x-ray scattering (SAXS) and small-angle neutron scattering are powerful tools for the characterization of porosity in ceramic materials. The chord lengths, internal surface area, pore volume, and size distribution can be determined from scattering data. A series of aerogels from acid-catalyzed and base-catalyzed hydrolysis of $Si(OCH_3)_4$ has been studied to determine how the structure of solution-derived silica aerogels depends on density. Recent results on Vycor (a commercial leached borosilicate) glass have illustrated the value of SAXS in distinguishing competing models for the origin of porosity.

---

1. Summary of paper: in *Modern Aspects of Small-Angle Scattering*, Kluwer Academic Publisher, Boston, Mass., in press.
2. Sandia National Laboratories, Albuquerque, New Mex.
3. Lawrence Livermore National Laboratory, Livermore, Calif.

SHEAR-INDUCED "CRYSTALLIZATION" OF RODLIKE MICELLES[1]

W. A. Hamilton, P. D. Butler,[2] S. M. Baker,[3] G. S. Smith,[3] J. B. Hayter, L. J. Magid,[4] and R. Pynn[3]

Aqueous solutions of certain cationic surfactants can be made strongly viscoelastic by the introduction of an appropriate counterion. The micellar structure in these fluids has been shown in some cases to involve highly extended, threadlike micelles which entangle, producing solutions with polymer-like properties. Small-angle neutron scattering (SANS) measurements which revealed the existence of a new type of shear-induced anisotropic colloidal phase occurring in the near-surface region when such a fluid flows past a solid interface were performed recently.

Our measurements were made using the ORNL 30-m SANS camera at the High-Flux Isotope Reactor. The sample was a dilute (20-mM) viscoelastic solution of the surfactant hexadecyltrimethylammonium 3,5-dichlorobenzoate (CTA3,5ClBz) in D_2O. In a specially developed reflection geometry shear cell,[5] the solution is pumped in a closed cycle through a shallow channel beneath a polished slab of crystalline quartz. Neutrons are incident through the slab, passing into the solution at low angle to the solid-liquid interface, along the direction of flow. Some are reflected at the interface, but most enter and are scattered in the solution. The absorption in the fluid is such that coherent scattering is only seen for neutrons which scatter back through the quartz slab from the first 30 μm below the interface. This coincides with the fluid flow boundary layer, a region of dramatic shear strain (dv/dz ~100/s). A difference in scattering pattern for shear-on vs no flow is shown in Fig. 2.5. The scattering indicates that under shear the solution's rodlike micelles (5-nm diam × 200 nm in length) have not only aligned with the flow, but are also ordered in a hexagonal array across the flow

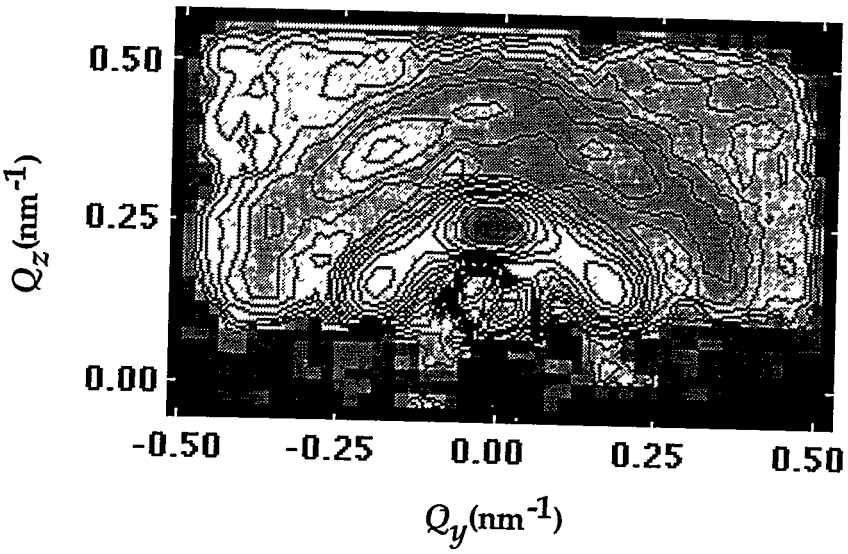

Fig. 2.5. Shear-on vs shear-off small-angle Bragg diffraction pattern for 20-mM CTA3,5ClBz.

direction with a nearest neighbor separation of about 36 nm. This near-surface phase appears to be condensed, since this spacing is about 10% less than would be calculated from the bulk surfactant concentration. It is interesting to note that the shear which induces this ordering also means that the rodlike components in a layer at some depth in this "crystal" are passing by the next layer 32 nm toward the interface at several 100 nm/s.

---

1. Summary of paper to be published.
2. The University of Tennessee, Knoxville, Tenn.
3. Los Alamos National Laboratory, Los Alamos, N. Mex.
4. University of Kentucky, Lexington, Ky.
5. S. M. Baker et al., *Review of Scientific Instrumentation* (in press).

NEUTRON DIFFRACTION

NEUTRON SCATTERING MEASUREMENTS OF RESIDUAL STRESS IN AUSTENITIC AND FERRITIC PLATES

Steve Spooner, C. R. Hubbard,[1] *Xun-Li Wang,*[1] *and S. A. David*[1]

The welding of ferritic and austenitic steels differs because of the austenite-to-ferrite phase transformation that occurs below 900°C in ferritic steels. This transformation is accompanied by a density change and shear which acts as a source for residual stresses in addition to the differential shrinkage involved in weld metal solidification. A mapping of residual stresses in

multipass welds in 1/2-in. plates of 304-type austenitic stainless steel and 2-1/4 Cr-1 Mo ferritic steel gives evidence of the transformation effect. Three orthogonal strain components are graphed in Fig. 2.6, where it can be seen that the longitudinal component is dominant in both cases. The curve for the longitudinal strain component shows a higher strain at the center of the weld. A shoulder in the same curve at about 22 mm from the weld center is highlighted by an arrow. Independent residual strain measurements done in test bars which were heated without melting indicate the same tendency to give a strain peak because of the austenite/ferrite transformation effects. The heating and cooling history for a multipass weld represents the superposition of several heating and cooling cycles and probably accounts for the smearing out of transformation effects as seen in the curve.

---

1. Metals and Ceramics Division, ORNL.

WELD METAL CHEMISTRY MEASURED WITH NEUTRON POWDER DIFFRACTION

S. Spooner and J A. Fernandez-Baca

The solidification and consequent heat rejection of weld metal in a multipass weld are complex processes. Large differential thermal contractions in the vicinity of the weld, as well as solid state transformations if present, result in a distribution of residual strains in the weld. These strains can be characterized by the variation of the lattice parameters of the various

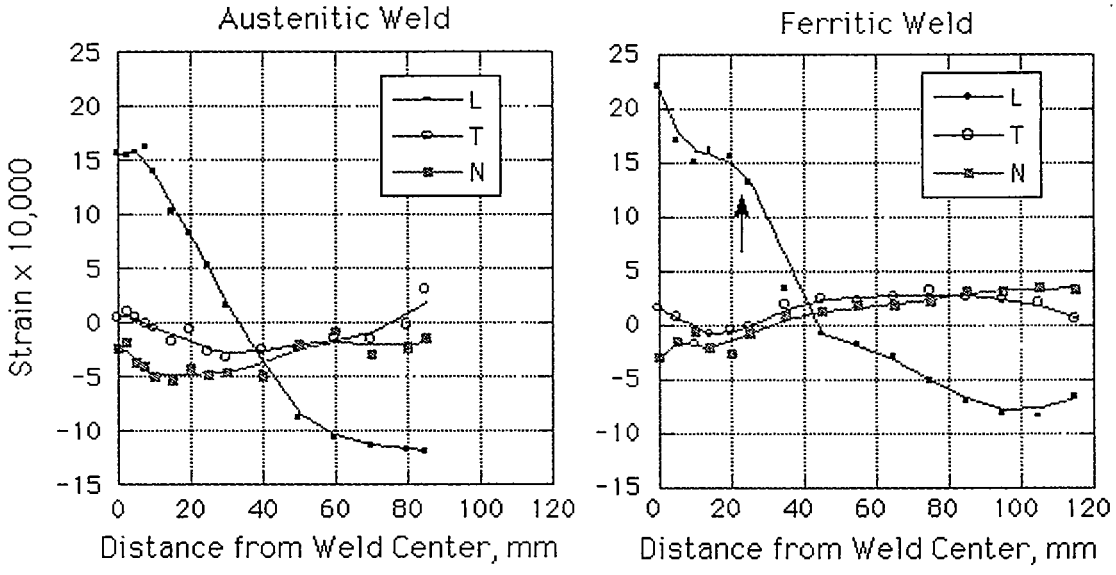

Fig. 2.6. The main difference between the two welds is that the longitudinal (L) strain curve exhibits a shoulder (indicated by the arrow) at about 22 mm from the weld center in the ferritic weld. The transverse and normal components are small and nearly equal.

phases of the weld with respect to the strain-free material. It is important, however, to be able to separate the lattice parameter changes because of these strains from those changes introduced by the chemistry of the welding materials. In an effort to isolate the effects of the chemistry of a multipass weld in a 1-in.-thick stainless steel plate, a 1-in. section of the weld zone was cut into 5 × 5 × 25-mm pillars with the long axis parallel to the weld line. By this means the individual pillars are in a "strain free" condition where the residual stresses have been released by the removal of the surrounding material. These samples were characterized using the high-resolution neutron powder diffraction facility at HB-4. A diffraction pattern covering Bragg peaks from 35° to 130° 2θ with a wavelength of 1.4165 Å was collected from each of the pillars and analyzed with a Rietveld refinement routine which yielded the lattice parameters and fractions of the principal phase (fcc, austenite) and the minor phase (bcc, ferrite). The variation in the austenite lattice parameter is indicated by the column height in Fig. 2.7. These results will be used to furnish corrected residual stresses in the weld in the 1-in. plate.

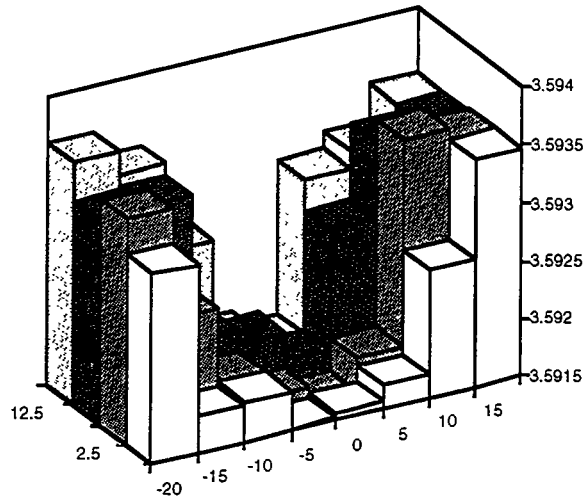

Fig. 2.7. Variation of the lattice parameters because of the chemical composition in the weld metal are given by column heights. The diffraction specimen size is indicated by dimensions of the column bases.

MARTENSITIC PHASE TRANSITION IN $In_{0.77}Tl_{0.23}$

J. L. Robertson[1] *and H. G. Smith*

InTl binary solid solutions with Tl concentrations between 15.5 and 31.0 at. % are known to undergo a martensitic phase transition from face-centered cubic (fcc) to face-centered tetragonal (fct) upon cooling below the transformation temperature T_m.[2]

The intent of the present study is to examine more closely the structural changes which take place when the alloy transforms. A 2-mm-thick plate of polycrystalline $In_{0.77}Tl_{0.23}$ was formed into a cylinder with an outer diam of 11 mm and a length of 60 mm. High-resolution neutron diffraction patterns were collected at several temperatures starting at 300 K and decreasing to 9 K. The martensitic transformation was observed to begin around 250 K when the peaks associated with the fcc phase develop small shoulders. The powder patterns were analyzed using the computer program RIETAN,[3] which uses the Reitveld method. Although the diffraction data were collected several times at 250 K over a 46-h period, the transformation did

not progress far enough for the Reitveld program to separate the two phases.

At 240 K, the shoulders on the face-centered peaks could be resolved as separate peaks and the two phases, fcc and fct, analyzed. The structure continued to change continuously as the temperature was decreased to 9 K, even though the sample had completely transformed to the fct phase at around 200 K. The lattice parameters are shown as a function of temperature in Fig. 2.8. The volume fraction of the fct phase increased somewhat in the time between the first and second scan, but the lattice parameters remained essentially constant. Another interesting result is that the structural transformation is nearly volume conserving. If one plots the cell volume as a function of temperature, it decreases at a constant rate through the transition with only a 0.05% difference in cell volume between the two phases in the region where they coexist.

---

1. ORNL/ORISE postdoctoral research associate.

2. H. L. Luo, J. Hagen, and M. F. Merriam, *Acta Metall.* **13**, 1012 (1965).

3. Y. Morii et al., *Reitveld Analysis System Reitan*, JAERI-M 91-162, Japan Atomic Energy Research Institute (1991).

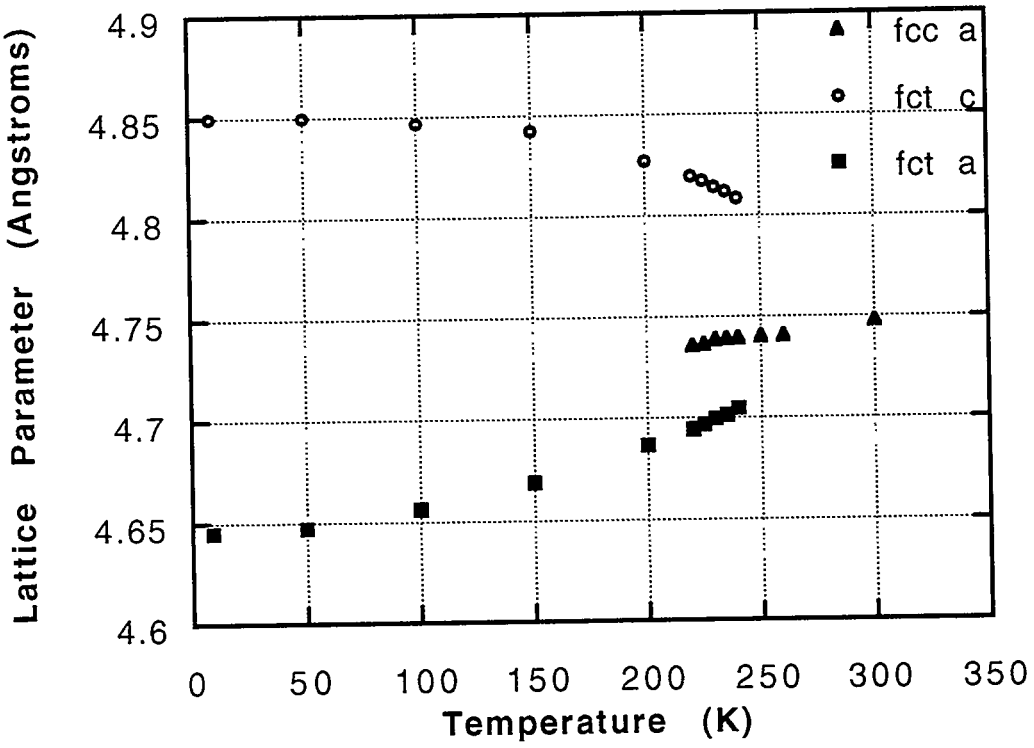

Fig. 2.8. Lattice parameter, a, for the fcc phase and a and c for the fct phase as a function of temperature.

NEUTRON SCATTERING STUDY OF THE $t \rightarrow m$ PHASE TRANSITION IN Al_2O_3-ZrO_2 (12 mol % CeO_2) CERAMIC COMPOSITES

Xun-Li Wang,[1] *J. A. Fernandez-Baca, C. R. Hubbard,*[1] *K. B. Alexander,*[1] *and P. F. Becher*[1]

The introduction of tetragonal (t)-ZrO_2 particles into a ceramic matrix can result in a significant increase in the ceramic fracture toughness of the ceramic. This improved toughness is achieved when the t-ZrO_2 grains at a crack tip transform to monoclinic (m) ZrO_2 during the fracture process. Thus an understanding of the $t \rightarrow m$ phase transition in this type of materials is of considerable interest in the field of ceramics engineering. For this reason, a neutron diffraction study of the temperature dependence of the $t \rightarrow m$ transformation in Al_2O_3-ZrO_2 (12 mol % CeO_2) ceramic composites containing 40 and 10 vol % ZrO_2 has been performed. This type of study is a valuable complement to conventional transport measurements because the diffraction technique provides a direct observation of the phase transformation, as well as a quantitative measure of the volume fraction of the transformed phases. These measurements were performed using the high-resolution neutron powder diffractometer (HB-4) at the HFIR. This study confirmed that the sharp increase in the thermal expansion upon cooling, typically observed in composites with a high content (e.g., 40 vol %) of ZrO_2, corresponds to the onset of the $t \rightarrow m$ phase transformation in these materials. The neutron diffraction patterns were refined using the Rietveld analysis technique to determine the volume fraction of the m-ZrO_2 phase as a function of temperature. Below the onset transformation temperature, the amount of the m-ZrO_2 phase increased progressively until it reached a maximum at lower temperatures. This maximum indicated that only a fraction of the t-ZrO_2 phase (e.g., 23% in the sample containing 40 vol % ZrO_2) transformed into m-ZrO_2. The observed temperature dependence of the transformation can be explained in terms of the size distribution of t-ZrO_2 grains. The lattice parameters of the Al_2O_3 matrix and the remaining t-ZrO_2 phases exhibited dramatic changes related to the stress changes resulting from the transformation. The refined cell parameters were used to calculate the bulk thermal expansion of the composite. The calculated thermal expansion was in excellent agreement with the dilatometry measurements.

---

1. Metals and Ceramics Division, ORNL.

Sr_2IrO_4: A TWO-DIMENSIONAL SPIN-1/2 HEISENBERG ANTIFERROMAGNET[1]

M. K. Crawford,[2] *M. A. Subramanian,*[2] *R. L. Harlow,*[2] *J. A. Fernandez-Baca, Z. R. Wang,*[3] *and D. C. Johnston*[3]

The discovery of high-temperature superconductivity in doped copper oxides, which in their insulating (undoped) forms are nearly ideal two-dimensional (2D) spin-1/2 Heisenberg antiferromagnets, has stimulated great interest in finding new examples of such magnetic systems. It is of particular interest to find new oxides, other than cuprates, which exhibit this spin-1/2

2D antiferromagnetic behavior and may be candidates for high-temperature superconductivity. The Sr_2IrO_4 oxide has a K_2NiF_4 structure in which the Ir^{4+} ions are octahedrally coordinated. The ground state of these Ir^{4+} ions is a (spin-1/2) Kramers doublet, the same as found in Cu^{2+}. In this study, x-ray and neutron powder diffraction, as well as magnetic susceptibility measurements, were performed. The x-ray measurements were performed at the National Synchrotron Light Source at Brookhaven National Laboratory. The neutron measurements were performed using the high-resolution powder diffractometer (HB-4) at the HFIR. The magnetic susceptibility measurements were performed at Ames. The x-ray data at T = 20 K showed weak superlattice peaks that indicated a distortion from the *I4/mmm* structure. In order to resolve if this distortion involved the displacement of oxygen atoms, the neutron diffraction experiment was performed at the HFIR. From this analysis on the neutron data at T = 13 K, it is proposed that the IrO_6 octahedra are rotated about the crystallographic c axis by about 11°, reducing the space group symmetry of this system from *I4/mmm* to *I4/acd*. The magnetic susceptibility measurements showed a distinctive magnetic transition at $T \approx 250$ K. Magnetic hysteresis measurements at $T = 5$ K showed that the magnetic structure has a ferromagnetic component, although this component is too small ($10^{-2}\mu_B$ per Ir ion) to attribute it to ferromagnetically aligned Ir^{4+} spins. Instead, it seems more reasonable to attribute this magnetic response to canted antiferromagnetism, the origin of the canting being the structural distortion described above. Preliminary attempts to observe the magnetic reflections of this structure by neutron diffraction have failed. It is presumed that this failure might be due to the combination of the small ordered moment, the appreciable neutron absorption cross section of Ir, and the large incoherent scattering cross section of the vanadium holder. Efforts to improve these measurements are in progress.

---

1. Summary of paper to be published.
2. Dupont, Wilmington, Del.
3. Ames Laboratory, Iowa State University, Ames, Iowa.

SPIN DENSITY WAVES IN DILUTE CuMn ALLOYS

J. W. Cable and Y. Tsunoda[1]

Neutron polarization analysis measurements[2] on CuMn alloys show the presence of incommensurate magnetic modulations that have now been identified[3] as spin density waves (SDW). The SDW model, as originally proposed by Overhauser[4] to explain the peculiar thermal and magnetic properties of CuMn alloys, is a collective, deformed state of the conduction electron gas that can be stabilized for particular wave vectors. The localized solute spins interact with the SDW, and this leads to helical ordering of the localized spins with an ordering wave vector characteristic of the SDW and, therefore, incommensurate with the lattice. The interaction with the localized solute spins also contributes to the SDW stability, so there may well be a critical Mn concentration below which the

static SDW are no longer stable. There is no such cutoff in the Overhauser SDW model where the transition temperature is simply linear with concentration, but it has been established[5] that the SDW are absent in pure Cu, and this suggests a critical concentration for SDW stability. Furthermore, a recent calculation by Ioffe and Feigel´man[6] for a random array of localized spins subject to a modified RKKY interaction gives magnetic order that depends on the interaction range and the density of spins on the lattice. For CuMn alloys, they obtain spin-glass behavior at low concentration and a crossover to short-range helical order near 10% Mn. This does not agree with previous results[2] on annealed CuMn alloys, which showed short-range SDW ordering down to 5% Mn. Even so, the interaction range is not well established, so a crossover at some lower concentration remains a possibility. It was decided to extend these measurements to lower Mn concentrations to determine which of these two models provides the best description of magnetic order in CuMn alloys.

Neutron scattering measurements were made on single crystals of CuMn alloys containing 1.4 and 3.0% Mn. Elastic scans along $\langle 1\zeta 0\rangle$ at temperatures well below T_f yield the same type of intensity distribution as that previously observed for the more concentrated alloys and show the existence of static SDW at dilutions down to 1.4% Mn. Inelastic scans in the same Q region for the Cu-3% Mn alloy clearly show the presence of dynamic SDW at temperatures up to $T/T_f = 7.5$. These results favor the SDW model of Overhauser as the best description of magnetic order in dilute CuMn alloys.

---

1. Guest scientist from Osaka University, Osaka, Japan.
2. J. W. Cable et al., *Phys. Rev. Lett.* **49**, 829 (1982); *Phys. Rev. B* **29**, 1268 (1984).
3. S. A. Werner, J. J. Rhyne, and J. A. Gotaas, *Solid State Commun.* **56**, 457 (1985).
4. A. W. Overhauser, *Phys. Rev. Lett.* **3**, 414 (1959); *J. Phys. Chem. Solids* **13**, 71 (1960).
5. S. A. Werner, *Comments Condens. Matter Phys*. **15**, 55 (1990).
6. L. B. Ioffe and M. V. Feigel´man, *Sov. Phys. JETP* **61(2)**, 354 (1985).

STRUCTURE OF THE MODULATED MAGNETIC PHASE OF Mn_3Sn

J. W. Cable, N. Wakabayashi,[1] and P. Radhakrishna[2]

The intermetallic compound Mn_3Sn has a hexagonal DO_{19} crystal structure with six Mn and two Sn atoms per unit cell. Below 420 K, triangular antiferromagnetic order develops by which the three spins within each layer assume 120° relative orientations and the interlayer Mn atoms connected through a center of inversion are aligned parallel.[3] Below 270 K, this triangular order remains within each layer, but the parallel interlayer coupling is replaced by a long-period modulation along the c axis. This has generally been described as a helical modulation with temperature-independent periods ranging from about 10 c_0 to about 12 c_0. In a recent study[2] of the magnetic excitations of Mn_3Sn, an energy gap of about 4 meV for both the triangular and the modulated phases was

observed. For the triangular phase, this gap was attributed to the energy required for a uniform fluctuation of spins away from the easy-axis directions within the basal plane. The energy gap is not so readily explained for the modulated phase where a gap can occur only if the modulation period is commensurate with the lattice and if a uniform fluctuation of spins forces an appreciable fraction of the spins to move away from the easy axes. This does not seem possible for such a long-period helical modulation since the rotation angle per layer becomes so small that spins are just as likely to approach hard axes as easy axes. This inconsistency called into question the helical model and prompted a reexamination of the magnetic structure of the modulated phase.

Two distinct modulations, both propagating along the c axis and both with periods that are commensurate with the lattice below about 120 K, were found. The satellite reflections associated with these two modulations have quite different intensities and temperature dependences suggesting coexistent modulated phases. For the dominant 11 c_0 phase, a third harmonic with an intensity that is 4% of the first harmonic was observed, but no fifth or seventh harmonic to a sensitivity of about 10^{-4} was found. The presence of this third harmonic shows a significant distortion of the helical modulation wave. The observed harmonic intensity distribution was compared with magnetic structure factor calculations for configurational models with moment directions bunched around the easy axes in the basal plane. The results suggest a model for which the moments are bunched around the 6-fold axes in a (7·2·2·7·2·2) sequence.

---

1. Consultant from Keio University, Yokohama, Japan.
2. Consultant from Jawaharlal Nehru Centre for Advanced Scientific Research, Bangalore, India.
3. J. S. Kouvel and J. S. Kasper, p. 169 in *Proceedings of Conference on Magnetism*, Nottingham, 1964.

NEUTRON DIFFRACTION STUDY OF THE MAGNETIC ORDERING OF $BaCuO_{2+x}$

Xun-Li Wang,[1] *J. A. Fernandez-Baca, Z. R. Wang,*[2] *D. Vaknin,*[2] *and D. C. Johnston*[2]

The study of the magnetism of $BaCuO_{2+x}$ is of practical and fundamental interest. This system is a common impurity in $RBa_2Cu_3O_{7-x}$ superconducting materials,[3] and the characterization of its magnetic properties is of importance in interpreting magnetic measurements on $RBa_2Cu_3O_{7-x}$-type systems. The fundamental aspect of this study derives from the fact that, despite its simple chemical formula, $BaCuO_{2+x}$ has a rather complicated crystal structure. This compound has a large body-centered-cubic unit cell (space group $Im3m$, a = 18.25 Å) with 90 formula units per unit cell. Each cell contains eight Cu_6O_{12} ring clusters, two $Cu_{18}O_{24}$ sphere clusters, and six incomplete Cu_2O_{12} clusters. A study of the magnetic properties of $BaCuO_{2+x}$ should provide valuable insights on the nature of the magnetic interactions (intracluster and intercluster) in this rather complex system. For this reason, neutron diffraction experiments

have been performed utilizing unpolarized neutrons and polarized neutrons with full polarization analysis at the HFIR. From these experiments, it was found that $BaCuO_{2+x}$ orders antiferromagnetically below $T_N = 15.0 \pm 0.5$ K with a magnetic propagating vector k = [1 1 1]. This structure is commonly referred to as a [π π π] or a *G* structure. The Cu atoms in the Cu_6O_{12} ring clusters, located at the (1/4, 1/4, 1/4) positions, order ferromagnetically within these clusters while the clusters themselves order antiferromagnetically. The ordered magnetic moment of each of these Cu atoms is 0.89 $\pm$ 0.05 μ_B at T = 4.2 K. No evidence of long-range magnetic ordering of the Cu atoms in the $Cu_{18}O_{24}$ clusters, located at the (0, 0, 0) and (1/2, 1/2, 1/2) positions, was found down to a temperature T = 2.5 K. These results are in agreement with recent magnetization measurements by Wang et al.,[4] which revealed that the magnetic moments in the $Cu_{18}O_{24}$ clusters remain paramagnetic down to T = 2 K.

---

1. Metals and Ceramics Division, ORNL.
2. Iowa State University, Ames, Iowa.
3. D. C. Vier et al., *Phys. Rev. B* **36**, 8888 (1987).
4. Z. R. Wang et al. (unpublished).

CRYSTAL STRUCTURE AND SUPERCONDUCTIVITY OF $La_{2-x}Ba_xCuO_4$[1]

S. Katano,[2] J. A. Fernandez-Baca, S. Funahashi,[2] N. Mori,[3] and K. Koga[3]

The study of the relationship between the crystal and electronic structures of high-T_c superconductors is of considerable interest. A recent investigation of $YBa_2Cu_3O_{7-y}$, for example, indicated that the Cu (planar)-O (apical) bond lengths are a sensitive measure of the hole density in the CuO_2 planes and are thus related to the superconductivity of this system. An experiment to study the systematic changes in the structural parameters of $La_{2-x}Ba_xCuO_4$ for $0.03 < x < 0.24$ has been carried out. Neutron measurements were made using the high-resolution powder diffractometer (HB-4) at the HFIR, and magnetic susceptibility measurements were performed at the Institute for Solid State Physics (Tokyo). Neutron data (for $15 < T < 300$ K) were refined using the Rietveld analysis technique (Fig. 2.9). At 115 K, the Cu-O

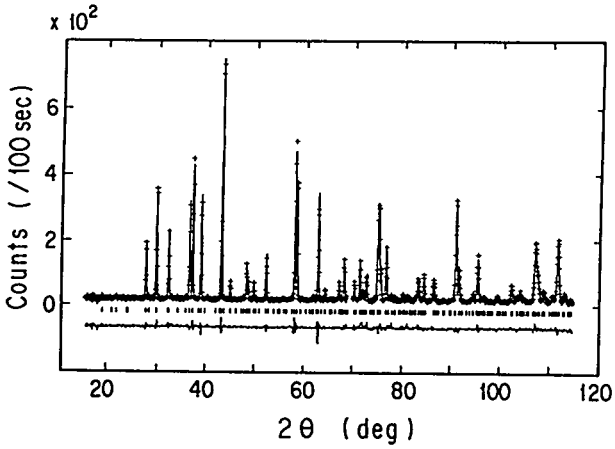

Fig. 2.9. Neutron diffraction data (+) for $La_{2-x}Ba_xCuO_4$ with x = 0.125 at 15 K (space group *P4/ncm*). The solid line is the refined profile. The tick marks show the positions of the calculated reflections.

(planar) bond length decreases with increasing x at a rate of 0.008 Å per 1/10 of x, indicating that the overlap of planar Cu and O atoms in the CuO_2 planes increases with x. The length of the Cu-O (apical) bonds decreases with x at a rate of about one half that of the Cu-O (planar) bonds,

suggesting that the apical O atoms in the CuO_6 octahedra also play an important role in the charge transfer process. These results have been discussed in terms of their implication to the electronic structure and superconductivity of this system.

---

1. Summary of paper: *Physica C* **214**, 64 (1993).
2. Guest scientist from Japan Atomic Energy Research Institute, Tokai, Japan.
3. Guest scientist from the Institute for Solid State Physics, Tokyo, Japan.

OBSERVATION OF THE FLUX LATTICE IN $Bi_{2.15}Ba_{1.95}CaCu_2O_{8+x}$

M. Yethiraj,[1] H. A. Mook, E. M. Forgan,[2] R. Cubitt,[2] M. Wylie,[2] D. Mck. Paul,[3] S. L. Lee,[4] P. H. Kes,[5] T. W. Li,[5] and K. Mortensen[6]

Measurements were made of the flux-line lattice in $Bi_{2.15}Ba_{1.95}CaCu_2O_{8+x}$ (BSCCO) as a function of temperature from 1.5 up to 60 K using small-angle neutron scattering techniques. The highly layered structure of this compound tends to confine supercurrents in the Cu-O planes. Hence, the flux lines tend to dissociate into two-dimensional (2d) "pancake" vortices when the applied field is increased beyond a point. For this reason, previous attempts at observing the flux lattice in BSCCO had failed. It has also become clear that the difference between BSCCO and $YBa_2Cu_3O_7$ is a very large anisotropy of the Bi compound. This large anisotropy also increases the instability of the flux lattice with respect to thermal fluctuations. This has led to suggestions of flux-lattice melting well below the superconducting transition temperature T_c.

The current set of measurements were done at applied fields as low as 20 mT. It showed clearly the existence of a flux-line lattice at low fields and low temperatures, as shown in Fig. 2.10. The diffracted intensity goes to zero at low temperatures as the magnetic field is increased. It is presumed that this is due to the decomposition of the flux lines into "pancakes" as has been suggested. Further, it was found that this 3d–2d transition occurred at the same field, largely independent of the temperature of the sample.

The temperature (T) dependence of the lattice shows that the signal disappears well below T_c. The actual T at which the signal disappears

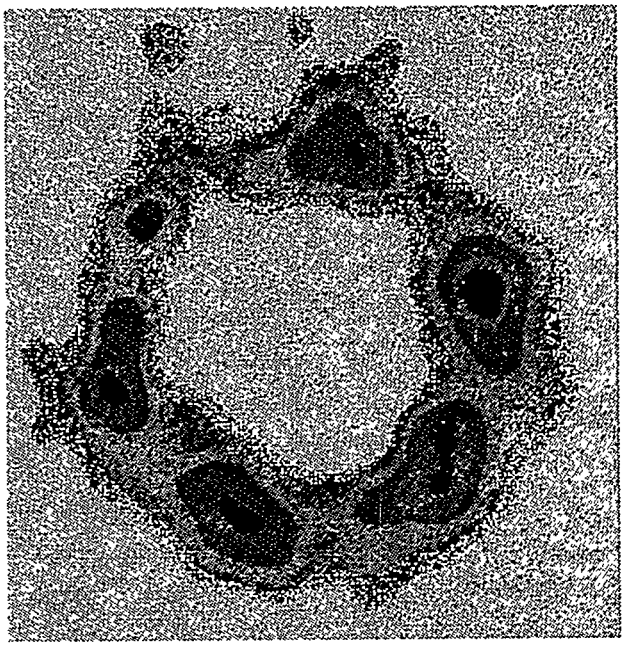

Fig. 2.10. The flux lattice observed in BSCCO at $T = 1.5$ K with an applied field of 500 Oe. The measurements were made at Risø National Laboratory.

decreases as the applied magnetic field is increased. This melting occurs at the position of the irreversibility line determined for the sample.

The FLL Bragg intensity is inversely proportional to the fourth power of the London penetration depth, l_L, which is an order parameter for the superconducting system. Hence, the *T* dependence of the intensity is very important information and contributes to an understanding of the driving mechanism for the transition. The *T* dependence in BSCCO is very different from conventional BCS theory; more work is in progress.

---

1. ORNL/ORISE postdoctoral research associate.
2. University of Birmingham, United Kingdom.
3. University of Warwick, United Kingdom.
4. ETH-Zürich, Switzerland.
5. Kammerlingh Onnes Laboratorium, the Netherlands.
6. Risø National Laboratory, Roskilde, Denmark.

ANISOTROPIC FLUX LATTICE IN $YBa_2Cu_3O_7$

M. Yethiraj,[1] *H. A. Mook, R. Cubitt,*[2] *E. M. Forgan,*[2] *S. L. Lee,*[3] *and D. Mck. Paul*[4]

Small-angle neutron scattering (SANS) has been used to observe an anisotropic flux-line lattice (FLL) in a single crystal of $YBa_2Cu_3O_7$ (YBCO). In general, these compounds are nominally uniaxial systems since the *a-b* (basal plane) anisotropy is fairly small and the c axis is considerably different. In $YBa_2Cu_3O_7$, the crystal structure is nearly tetragonal with $c \approx 3a$, and the *a/b* ratio is approximately 0.99. There has been much discussion about the role this anisotropy plays in the superconductivity in these materials. Clearly, information regarding the behavior of vortex lattices in low-symmetry geometries is extremely important.

This is the first study of anisotropy in YBCO which measures the vortex lattice in a bulk sample directly. SANS studies yield information about the structure of the lattice that can be used to determine accurately the anisotropy ratio *g*. A difference in *g* is seen directly in the ratio of lengths of the basis vectors of the lattice, and the uncertainty is substantially smaller by this technique than by many other methods.

The properties of the flux-line lattice in $YBa_2Cu_3O_7$ with the applied field along the c axis and for the case where the field was 30° from the c axis has been reported previously. These studies have been extended in order to probe the mass anisotropy ratio, m_3/m_1; and measurements were made as a function of angle, *Q*, between the 8-kOe applied field and the crystallographic (001) axis at a series of angles with $0° \le Q \le 80°$. (Note: m_3 and m_1 are the effective masses of the electron in the basal plane and along the c axis, respectively.)

Irrespective of the actual crystallography of the lattice, all diffracted spots can be shown to fall on an ellipse whose axial ratio is given by $\sqrt{m_{zz} / m_3}$. This measure is independent of the structure details. The scattering when the applied field was 60° from the c axis is shown in Fig. 2.11. Two symmetry-related sixfold lattices

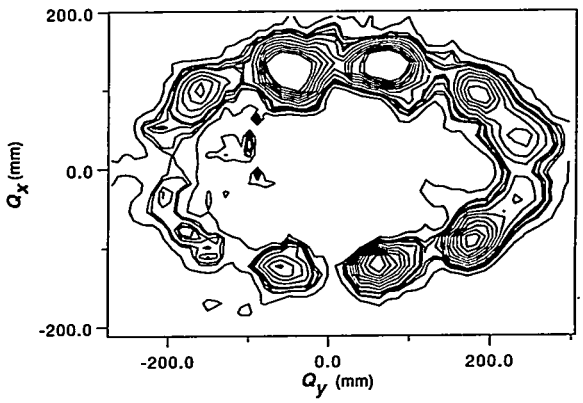

Fig. 2.11. Bragg scattering due to flux lines in $YBa_2Cu_3O_7$ when the applied field is 60° from the *c* axis.

are evident in the scattering. The orientation of the lattices may be related to the twin planes.

In this experiment, the axial ratio of the ellipse is more accurately measured than the a_1/a_2 ratio or the angle between a_1 and a_2, which can also be used to deduce γ^2. The position of the Bragg peak is changed slightly by not positioning the flux-line crystal on the Bragg condition. Corrections for this positional shift have been made. The square of the (corrected) ratio of the minor to major axis of the ellipse plotted against $\sin^2\Theta$ fits a straight line which gave a slope of -0.9503 ± 0.003. The value of the γ^2 obtained from the axial ratio of the ellipse as a function of Θ is 20 ± 2. ($\gamma = 4.6 \pm 0.2$). Values of γ^2 in the literature are rather variable, with the most common value being approximately 25.

The observed temperature dependence of the intensity was measured. The intensity drop for the anisotropic lattice is slower than for the *B//c* data at the same applied field, where the intensity fell much more precipitously. The dependence for $0 < T < 50$ K can be estimated adequately by a straight line; however, it is not possible to extract an analytical form for the temperature dependence for the order parameter from these data.

---

1. ORNL/ORISE postdoctoral research associate.
2. University of Birmingham, United Kingdom.
3. ETH-Zürich, Switzerland.
4. University of Warwick, United Kingdom.

INELASTIC NEUTRON SCATTERING

MAGNETIC EXCITATIONS IN THE TRIANGULAR ANTIFERROMAGNETS Mn_3Sn AND Mn_3Ge

J. W. Cable, N. Wakabayashi,[1] and P. Radhakrishna[2]

Inelastic neutron scattering was used to study magnetic excitations of the triangular antiferromagnets Mn_3Sn and Mn_3Ge. These compounds have itinerant *d* electrons and large magnetic moments localized at the Mn sites and may be regarded as materials that lie in the intermediate regime between local moment and itinerant-electron systems. The spin-wave spectra exhibit steep dispersion and strong damping, which are characteristic behavior for itinerant-electron systems. Nevertheless, it is useful to analyze the data in terms of a local moment model with anisotropy. It was found that the data were remarkably well-described by this model with exchange parameters extending to

fifth nearest neighbors and with both axial- and basal-plane anisotropy. The axial anisotropy parameters were determined from the uniform out-of-plane spin fluctuation, and the signs show that the spins were confined to the basal plane. The second-order basal-plane anisotropy constants were determined by satisfying both the magnitude of the weak basal-plane ferromagnetic moments and the observed splitting of a doubly degenerate acoustic spin-wave branch. The sixth-order basal-plane anisotropy was determined by adjusting to the observed energy gap associated with spin fluctuations within the basal plane. The exchange parameters have the correct signs to stabilize the triangular antiferromagnetic structure but yield Néel temperatures that are higher than those observed by a factor of 3 or 4. This overestimation of the Néel temperature is not an uncommon result when a local moment model is applied to an itinerant-electron system.

---

1. Consultant from Keio University, Yokohama, Japan.
2. Consultant from Jawaharlal Nehru Centre for Advanced Scientific Research, Bangalore, India.

TRANSVERSE SPIN EXCITATIONS IN THE SINUSOIDAL MAGNETIC PHASE OF ERBIUM

R. M. Nicklow and N. Wakabayashi[1]

Erbium is a heavy rare-earth (hcp) metal with a variety of unusual magnetic structures.[2] Between ~52 K and T_N (~87 K), the ordered component of the Er moment is parallel to the c axis, and its magnitude varies sinusoidally as one moves along the c direction. In this c-axis amplitude-modulated phase (CAM), the modulation wave vector **q** is not commensurate with the crystal lattice periodicity, although it is within 2% of $(2/7)c^*$. Previous neutron scattering measurements of the excitations in this phase showed a rather featureless, broad intensity distribution in energy which showed some dependence on Q. While the broad distribution was qualitatively consistent with expectations, the data were not quantitatively analyzed because of a lack of appropriate theoretical models.

Recently, quite different theoretical treatments of the transverse excitations of a sinusoidally modulated spin structure have been put forward by Lovesey[3] and McEwen et al.[4] Lovesey has produced an exact mathematical formulation, based on linear spin-wave theory, for the excitation spectrum at $T = 0$ K for a model system having small magnetic anisotropy. The main features of Lovesey's results include a broad continuum of excitation energies with a finite neutron scattering cross section at $E = 0$, which is independent of wave vector, and a sharp peak at the top of the continuum which may be broadened by interactions. The theory of McEwen et al. is an RPA theory based on a numerical diagonalization of the molecular-field Hamiltonian. It explicitly includes magnetoelastic interactions, crystal-field anisotropy of arbitrarily large magnitude and finite temperatures. However, it involves a difficult iterative numerical calculation of a two-site Green's function, and it has only been applied to thulium.

In view of this recent theoretical work, new and more extensive neutron scattering experiments on Er in the CAM phase have been carried out with better energy resolution than that used in our previous work. The new measurements bear no resemblance to the linear spin-wave theory of Lovesey as applied to Er by Lantwin.[5] Therefore, calculations have been made for Er based on McEwen's theory and the known crystal-field interactions together with the exchange interactions that had been determined previously by Lindgard[6] from our measurements[7] of the spin-wave dispersion in the conical phase of Er at 5 K. In these calculations, magnetoelastic interactions have been neglected, and it has been assumed that the spin structure is commensurate with the crystal [i.e., $\mathbf{q} = (2/7)\mathbf{c}^*$]. These assumptions lead to a significant simplification in the model since no iterative calculations are required, although a numerical diagonalization of the Hamiltonian is still required. The results of these calculations are in fairly good agreement (Fig. 2.12) with our measurements, which show two features—a peak at $E = 0$ with a Q-dependent intensity and structure in the form of peaks or shoulders at finite energies which are also Q-dependent. The main disagreement is that the calculated intensity at $E = 0$ shows a much stronger decrease with increasing Q than do the data.

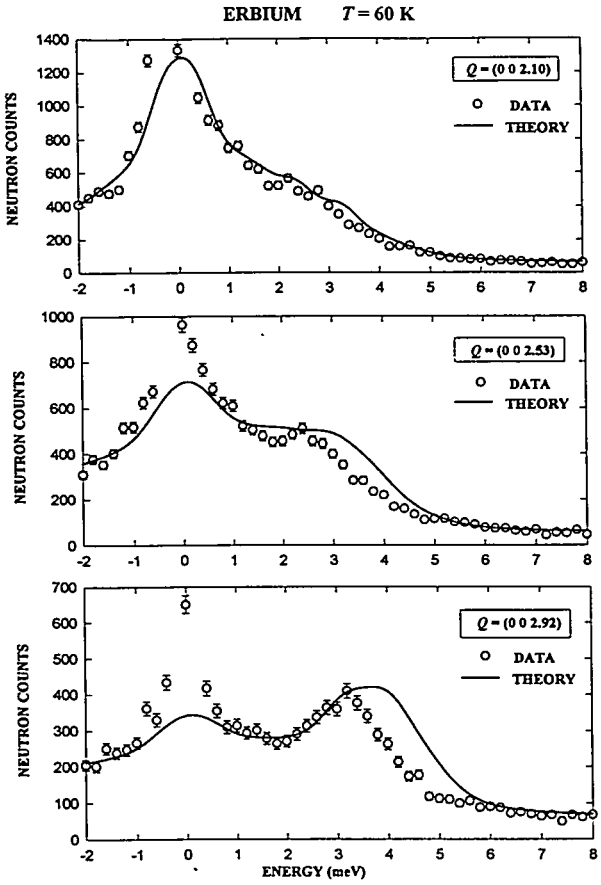

Fig. 2.12. Comparison of neutron scattering data and theory for erbium at $T = 60$ K.

4. K. A. McEwen et al., *Phys. Rev.* **43**, 3298 (1991).
5. C. J. Lantwin, *J. Phys. B* **79**, 47 (1990).
6. P. Lindgard, *Phys. Rev. B* **17**, 2348 (1978).
7. R. M. Nicklow et al., *Phys. Rev. Lett.* **27**, 334 (1971).

FRACTON EXCITATIONS IN A DILUTED HEISENBERG ANTIFERROMAGNET NEAR THE PERCOLATION THRESHOLD[1]

H. Ikeda,[2] J. A. Fernandez-Baca, R. M. Nicklow, M. Takahashi,[2] and K. Iwasa[3]

In recent years, considerable attention has been directed toward the dynamical properties of highly ramified percolating networks that

---

1. Consultant from Keio University, Yokohama, Japan.
2. M. Habenschuss et al., *Phys. Rev.* **10**, 1020 (1974).
3. S. W. Lovesey, *J. Phys. C: Solid State Phys.* **21**, 2805 & 4967 (1988).

exhibit fractal geometry. Recent theories[4] and computer simulations[5] of these systems predict the existence of highly localized fracton excitations. The ideal system to probe the existence of these excitations is a random site-diluted Heisenberg antiferromagnet, where a fractal geometry is realized at length scales shorter than the geometrical correlation length ξ_G. Thus an inelastic neutron scattering experiment has been performed to study the spin dynamics of $RbMn_xMg_{1-x}F_3$ ($x = 0.39$), where x is close to the percolation concentration, $c_p = 0.312$.

This system is better suited for the study of fracton excitations than $Mn_{0.5}Zn_{0.5}F_2$, studied by Uemura and Birgeneau,[6] because $RbMn_xMg_{1-x}F_3$ exhibits negligible anisotropy and is considerably closer to the percolation concentration ($c_p = 0.245$ for the MnF_2 structure). It is believed that this study constitutes the first quantitative measurement of fracton excitations in a near-percolating system. The experiments were performed at triple-axis spectrometers at the HFIR. At $T = 4.5$ K, no evidence of propagating spin waves in this system was observed, but instead energy spectra consisting of a broad peak superimposed on narrow peaks because of Ising cluster excitations were observed. This broad peak exhibits the following characteristics: (1) the linewidth is much larger than the instrumental energy resolution and increases with increasing wave vector, (2) the energy also increases with increasing wave vector, (3) the integrated intensity decreases with increasing wave vector, (4) the integrated intensity is much higher than that of the Ising cluster excitations, and (5) it persists even at $T = 100$ K, while the Ising-cluster excitations disappear above $T_N = 18$ K. This magnetic response is attributed to the excitation of fractons in a percolating network. This broad magnetic response was fitted to a damped harmonic oscillator (DHO) form, and it was found that the fitted values of the energy $E(q)$ and width $\Gamma(q)$ satisfy a power-law relationship with the same exponent [i.e., $E(q) \propto \Gamma(q) \propto q^{1.1\pm0.2}$]. This result, based on an analysis using the DHO form, is in qualitative agreement with the single-length scale postulate,[5] although recent calculations by Yakubo et al.[7] using a Lorentzian form yielded an exponent of 2.5 instead of 1.1.

---

1. Summary of paper to be published.
2. Guest scientist from National Laboratory for High-Energy Physics, Tsukuba, Japan.
3. Guest scientist from Keio University, Yokohama, Japan.
4. R. Orbach, *Science* **251**, 814 (1986).
5. T. Nakayama, K. Yakubo, and R. Orbach, *Reviews of Modern Physics* (in press).
6. Y. J. Uemura and R. J. Birgeneau, *Phys. Rev. Lett.* **57**, 1947 (1986).
7. K. Yakubo, T. Terao, and T. Nakayama, private communication.

LOW-ENERGY EXCITATIONS IN SUPERCONDUCTING $LA_{1.86}Sr_{0.14}CuO_4$[1]

T. E. Mason,[2] G. Aeppli,[3] S. M. Hayden,[4] A. P. Ramirez,[3] and H. A. Mook

One signature of unconventional superconductivity is a gap function with nodes on the Fermi surface. In a clean BCS superconductor, such nodes do not occur, and the low-energy quasiparticle excitations are absent for energies

less than the gap energies. Another way to generate a superconductor with a vanishing gap is to introduce magnetic impurities, in which case low-energy excitations exist everywhere on the Fermi surface. It was found that neutron scattering done with good energy and momentum resolution is a good bulk probe of the wave-vector dependence of the superconducting gap function.

Neutron measurements on $La_{1.86}Sr_{0.14}CuO_4$ show that the magnetic excitations at low temperatures consist of incommensurate peaks found at $(\Pi,\Pi) \pm \delta\,(\Pi,0)$ and $(\Pi,\Pi) \pm \delta\,(0,\Pi)$. As the sample is cooled below the superconducting transition (T_c) at 35 K, the peaks diminish in intensity. Heat capacity measurements on a crystal grown in the same way as the one used in the neutron measurements showed that magnetic impurities were present in the sample corresponding to spin 1/2 with a concentration of 0.7×10^{-3} per Cu. The neutron measurements showed that the intensity reduction found below T_c was independent of the momentum transfer direction, and thus no new anisotropy was introduced as a result of the superconductivity.

The scattering results were consistent with an isotropic suppression of intensity with the remaining scattering resulting from the magnetic impurities found in the specific heat measurements. The measured magnetic response is thus incompatible with currently available predictions for a clean superconductor with *d*-wave pairing.

---

1. Summary of paper: *Phys. Rev. Lett.* **71**, 919 (1993).

2. Risø National Laboratory, Roskilde, Denmark.
3. AT&T Bell Laboratories, Murray Hill, N.J.
4. University of Bristol, United Kingdom.

MAGNETIC EXCITATIONS IN $YBa_2Cu_3O_7$[1]

H. A. Mook, M. Yethiraj,[2] G. Aeppli,[3] T. E. Mason,[4] and T. Armstrong[5]

Magnetic inelastic neutron scattering is a powerful technique which gives direct information about the behavior of electrons in materials. This information is of particular value for high-temperature superconductors where electron correlations may be responsible for some of the unusual physical properties of the material. However, the measurements are particularly difficult for $YBa_2Cu_3O_7$ because the intensity of the magnetic excitations on the energy scale of the superconducting gap is smaller than the scattering by phonons. Polarized beam measurements which give the magnetic scattering directly, free of phonon contamination, have been performed. Results for the measurements made for the normal state at 100 K and well below the superconducting transition of 92 K are shown in Fig. 2.13.

The magnetic response was found to be centered at (π,π) in the reciprocal lattice, and for the normal state [Fig. 2.13(a)], it consists of a small peak at 41 meV and a continuum of scattering at lower energies. There is an energy region near 25 meV that is inaccessible because of parasitic elastic scattering from the (006) reflection. At 10 K in the superconducting state, the 41-meV scattering has increased considerably while the

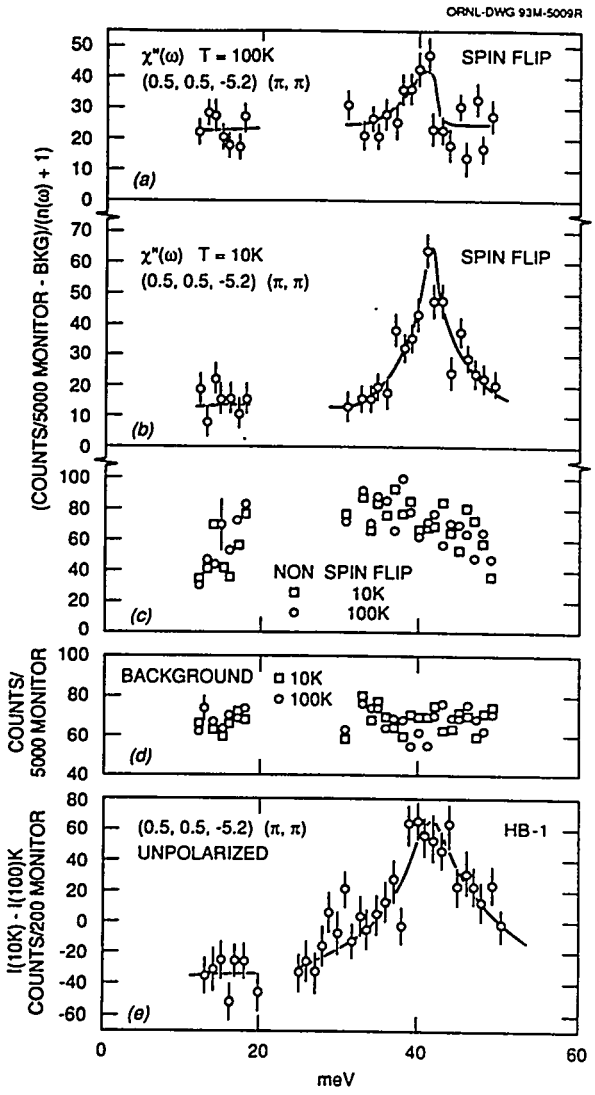

Fig. 2.13. Neutron scattering measurements showing the scattering at (π,π) reciprocal lattice position for $YBa_2Cu_3O_7$.

scattering at lower energies has greatly diminished [Fig. 2.13(b)]. The nonspin flip or phonon scattering is shown in Fig. 2.13(c) while Fig. 2.13(d) shows the background. Since neither the phonon scattering nor the background change between 100 and 10 K, unpolarized measurements can be used to show a difference in the scattering [Fig. 2.13(e)].

The reduction of the intensity at low energies can be attributed to the establishment of a gap in the spin fluctuation spectrum. In this case, the gap energy would correspond to the zero crossing shown in Fig. 2.13(e), or about 35 meV. The origin of the large peak at 41 meV is not understood. It may correspond to a singlet-triplet transition of pairs formed between neighboring spins in adjacent layers.

---

1. Summary of paper: *Phys. Rev. Lett.* **70**, 3490 (1993).
2. ORNL/ORISE postdoctoral research associate.
3. AT&T Bell Laboratories, Murray Hill, N.J.
4. Risø National Laboratory, Roskilde, Denmark.
5. Allied Signal Research Laboratories, Torrance, Calif.

GROUND-STATE WAVE FUNCTIONS OF Tb^{3+} IONS IN PARAMAGNETIC $TbPO_4$: A NEUTRON SCATTERING STUDY[1]

C.-K. Loong,[2] L. Soderholm,[2] G. L. Goodman,[2] M. M. Abraham, and L. A. Boatner

A number of investigations, both experimental and theoretical, have been undertaken previously in attempts to understand the intriguing physical properties of $TbPO_4$. At low temperatures, this compound exhibits two magnetic phase transitions—an antiferromagnetic ordering of the Tb moments along the crystallographic c axis of the tetragonal zircon structure at 2.28 K and a tilting of the magnetic moments away from the c axis in the (100) planes below 2.15 K. The latter transition is accompanied by a cooperative Jahn-Teller effect

involving Tb ion-lattice coupling that induces a tetragonal-to-monoclinic distortion of the crystal lattice. The crystal-field states and spin dynamics of the Tb^{3+} ions have important consequences for the magnetic and luminescence properties of $TbPO_4$, which are manifested in the magnetic susceptibility, magnetization, specific heat, magnetic phase transitions, and optical-adsorption/emission spectra. A characterization of the electronic wave functions of the crystal-field states and the nature of the spin-spin and spin-lattice interactions are useful for understanding both the bulk and microscopic properties of the material.

Magnetic neutron scattering probes the low-lying electronic states via magnetic-dipole transitions as opposed to the electric-dipole transitions between the ground state and the significantly higher energy states normally observed in an optical study. Therefore, these two techniques provide complementary information regarding the energy-level structure of magnetic ions.

In the present investigations, the paramagnetic-excitation spectrum of $TbPO_4$ has been investigated by means of inelastic neutron scattering techniques, and the observed crystal-field transitions were analyzed using a Hamiltonian that included the atomic free-ion and crystal-field interactions for an f^8 configuration. The resulting crystal-field level scheme for the Tb^{3+} $^7F_6$ ground multiplet is shown schematically in Fig. 2.14. Five parameters for the crystal-field potential that provided a satisfactory description of the neutron data collected at

SSDN-4688

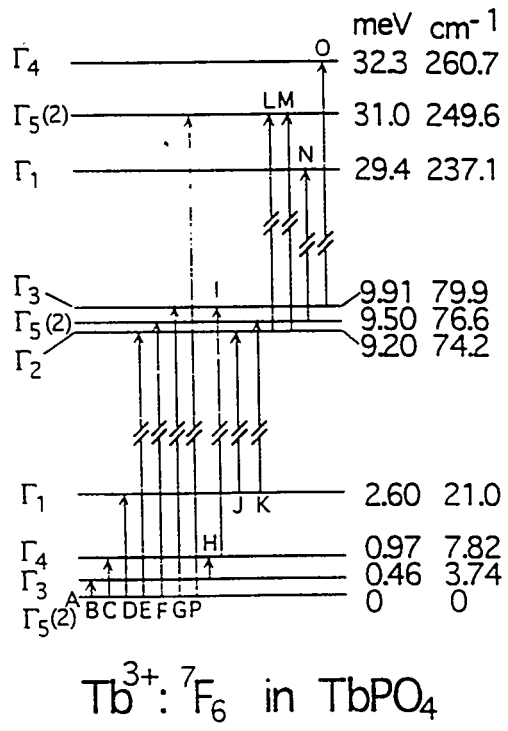

Fig. 2.14. Schematic diagram of the splitting of the Tb^{3+} ground multiplet by the crystal field into seven singlets $2\Gamma_1 + \Gamma_2 + 2\Gamma_3 + 2\Gamma_4$ + and three doublets, $3\Gamma_3$.

temperatures between 4.2 and 150 K were obtained. The calculated crystal-field contribution to the specific heat in the 4–10-K temperature range and the paramagnetic susceptibility agree well with the experimental results. The large anisotropy of the magnetic ground-state doublet of the Tb ions with respect to the crystallographic c axis has important consequences for the spin structure in the antiferromagnetic phases at low temperatures. The effective internal magnetic field in antiferromagnetic $TbPO_4$ was estimated based on the crystal-field level scheme, and a molecular-field approximation

and was found to be in good agreement with the values reported from other measurements.

---

1. Summary of paper: *Phys. Rev. B* 48, 6124 (1993).
2. Argonne National Laboratory, Argonne, Ill.

RARE-EARTH ENERGY LEVELS AND MAGNETIC PROPERTIES OF $DyPO_4$[1]

C.-K. Loong,[2] *L. Soderholm,*[2] *J. S. Xue,*[2] *M. M. Abraham, and L. A. Boatner*

Crystal-field (CF) states and spin dynamics of Dy^{3+} ions have important consequences for the magnetic properties of $DyPO_4$. In spite of numerous prior studies, information regarding the CF-split ground-multiplet wave functions of the Dy^{3+} ions in $DyPO_4$ is still incomplete. From neutron diffraction, optical absorption, and Mössbauer effect studies, the ground state is known to have large $|15/2 \pm 15/2\rangle$ components and spectroscopic splitting g factors parallel and perpendicular to the c-axis given by $g_{\parallel} = 19$ and $g_{\perp} = 0$, respectively. The energies and symmetries of all other states, however, are not known. Consequently, the magnetic behavior has been interpreted by Ising-like interactions of magnetic ions with effective spins of 1/2. Since the excited states are ignored in this approach, only the low-temperature data can be analyzed quantitatively.

In the present work, inelastic neutron scattering and magnetic-susceptibility measurements are performed, along with a corresponding determination of the crystal-field parameters for the orthophosphate $DyPO_4$. $DyPO_4$ exhibits a number of intriguing magnetic properties at low temperatures. In the absence of an applied magnetic field, $DyPO_4$ orders antiferromagnetically with the Dy moments oriented parallel and antiparallel to the crystallographic c-axis at temperatures $T < T_N$ = 3.4 K. Below T_N, an antiferromagnetic-to-paramagnetic phase transition can be induced by a magnetic field applied along the c-axis. The nature of the spin structure and phase transitions in the region of mixed metamagnetic phases ($T < T_T$, $0.5 < H < 1$ T), however, is not yet understood.

In the present investigation, the dynamic and static paramagnetic responses of $DyPO_4$ were studied by neutron inelastic scattering and single-crystal magnetic susceptibility measurements. The observed energies and intensities of the magnetic transitions at 15 and 100 K were used to refine the parameters of the crystal-field potential for Dy^{3+} ions in $DyPO_4$. The resulting crystal-field level scheme for the Dy^{3+} $^6H_{15/2}$ ground multiplet is shown schematically in Fig. 2.15, and the derived crystal-field level structure provides a basis for explaining the low-temperature magnetic properties of this compound.

---

1. Summary of paper: *Journal of Alloys and Compounds* (in press).
2. Argonne National Laboratory, Argonne, Ill.

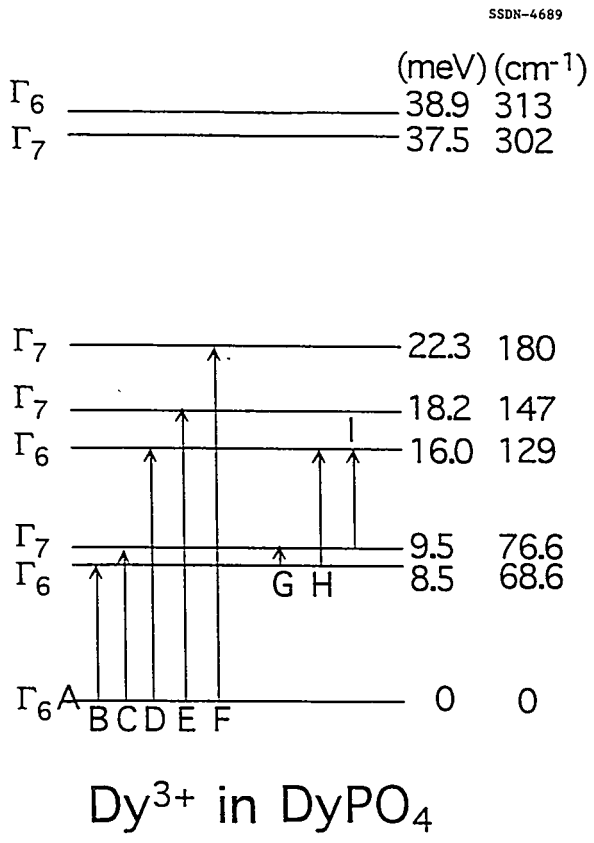

Fig. 2.15. Schematic diagram of the splitting of the Dy^{3+} $^6H_{15/2}$ ground multiplet by the crystal field into $4\Gamma_6 + 4\Gamma_7$ Kramers doublets. The transition labels refer to the experimentally observed transitions.

CRYSTAL-FIELD EXCITATIONS AND MAGNETIC PROPERTIES OF $TmPO_4$[1]

C.-K. Loong,[2] L. Soderholm,[2] M. M. Abraham, L. A. Boatner, and N. M. Edelstein[3]

Rare-earth orthophosphates (*RE*PO_4, *RE* = rare earth) exhibit a variety of properties that are of interest in many subfields of physics and chemistry. For example, *RE*-activated luminescence in lanthanide orthophosphates makes these materials of interest for possible applications as phosphors and lasers. The structural stability and long-term corrosion resistance of *RE*PO_4 compounds in the form of synthetic polycrystalline ceramics have led to the concept of their application as a storage medium for nuclear wastes.[4,5] The low-temperature magnetic properties of the *RE*PO_4 compounds (e.g., the close approximation of $DyPO_4$ to a model three-dimensional Ising antiferromagnet) have also prompted a number of fundamental experimental and theoretical investigations. Obviously, achieving a characterization of the RE levels and wave functions in *RE*PO_4 is a prerequisite for understanding these relatively complex physical phenomena.

In the present work, the magnetic-excitation spectrum of $TmPO_4$ has been studied using inelastic neutron scattering techniques. Pure $TmPO_4$ crystallizes in the tetragonal zircon structure (space group $I4_1/amd$),[15] which is the crystal structure common to the second half of the *RE*PO_4 series (*RE* = Tb–Lu, Y, and Sc). The Tm ions are located at sites of D_{2d} point-group symmetry. The Tm^{3+}:$^3H_6$ ground multiplet is split by the crystal field into 7 singlets, $2\Gamma_1 + \Gamma_2 + 2\Gamma_3$ Γ_4, and 3 doublets, $3\Gamma_5$; and the next higher multiplet $^3F_4$ lies at energies above 5000 cm^{-1}.

Sharp crystal-field transitions were observed in the spectra obtained at 15 and 100 K, yielding new information regarding the energy-level structure of the Tm^{3+} ground-multiplet splitting. The data were analyzed using a Hamiltonian that included the atomic free-ion and crystal-field interactions for an f^{12} configuration. Using the Tm free-ion parameters derived from optical spectroscopy of Tm^{3+} diluted in a $LuPO_4$ host, a set of crystal-field parameters were obtained for

Tm^{3+} in pure $TmPO_4$. The calculated magnetic spectra of $TmPO_4$ agree very well with the results of neutron and Raman measurements. The calculated bulk magnetic susceptibility of $TmPO_4$ exhibited a large anisotropy at low temperatures and is in good agreement with the experimental data. A significant contribution to the specific heat from Tm^{3+} crystal-field states was found at temperatures below 100 K. The present analysis provides an estimate of the contributions from the Tm^{3+} low-lying crystal-field states to both the bulk magnetic susceptibility and the specific heat in $TmPO_4$.

---

1. Summary of paper: *J. Chem. Phys.* 98, 4214 (1993).
2. Argonne National Laboratory, Argonne, Ill.
3. Lawrence Berkeley Laboratory, Berkeley, Calif.
4. L. A. Boatner et al., p. 411 in *Management of Alpha-Contaminated Wastes*, IAEA-SM-246/73, IAEA, Vienna, Austria, 1981.
5. L. A. Boatner, p. 289 in *Scientific Basis for Nuclear Waste Management*, ed. by C. J. Northrup, Vol. II, Plenum Press, New York, 1980.

RARE-EARTH ENERGY LEVELS AND MAGNETIC PROPERTIES OF $HoPO_4$ AND $ErPO_4$[1]

C.-K. Loong,[2] *L. Soderholm,*[2]
J. P. Hammonds,[2] *M. M. Abraham,*
L. A. Boatner, and N. M. Edelstein[3]

Mixed natural rare-earth orthophosphates, $REPO_4$ (RE = rare earths), form the minerals monazite (RE = La–Gd) and xenotime (RE = Tb–Lu). The high melting temperatures (about 2000°C), structural and chemical stability, and long-term corrosion resistance of the $REPO_4$ compounds make these substances attractive for applications as high-temperature components and nuclear waste storage media.[4,5]

The optical and magnetic properties of the RE ions in RPO_4 hosts, including their RE-activated luminescence, magnetic phase transitions, and Jahn-Teller effects, have also prompted numerous fundamental experimental and theoretical investigations. Increasing our knowledge of the RE energy levels and wave functions in $REPO_4$ compounds is, of course, essential to understanding both the bulk and microscopic properties of these materials.

A systematic study of magnetic excitations in the stoichiometric $REPO_4$ series using neutron spectroscopy has recently been initiated. In the present work, the static and dynamic magnetic responses of $HoPO_4$ and $ErPO_4$ have been studied by means of neutron spectroscopy and magnetic susceptibility measurements. The inelastic neutron scattering spectra exhibit well-defined transitions characteristic of crystal-field excitations of the RE ions. The data were analyzed using a Hamiltonian that included atomic free-ion and crystal-field interactions for an f^N configuration (N = 10 and 11 for Ho^{3+} and Er^{3+}, respectively). Using the free-ion parameters derived from optical spectroscopy of the corresponding RE ions diluted in a YPO_4 host, crystal-field parameters for both $HoPO_4$ and $ErPO_4$ were obtained. The derived crystal-field level structure provides a basis for explaining the low-temperature magnetic properties of both compounds. The calculated and measured paramagnetic susceptibilities agree well for $HoPO_4$ and $ErPO_4$ in the tem-

perature range 5–300 K. The highly anisotropic, saturated magnetization of the ground doublet in $HoPO_4$ may act as a "bootstrap" for long-range magnetic ordering of the moments parallel to the c-axis at low temperatures. The nearly spherically symmetric moments of the low-lying Kramers doublets of $ErPO_4$, however, tend to couple less effectively via exchange interactions. The effective exchange field in antiferromagnetic $HoPO_4$, as estimated based on the crystal-field level scheme and a molecular-field approximation, is found to be in good agreement with that reported from a specific-heat analysis. The paramagnetic specific-heat, spectroscopic splitting g factors of the low-lying doublet states and saturated moments for $HoPO_4$ and $ErPO_4$ obtained from the present study are applicable to interpreting specific heat, hyperfine interaction, electron paramagnetic resonance, and neutron diffraction measurements.

---

1. Summary of paper: *J. Phys. Condens. Matter* **5**, 5121 (1993); *J. Appl. Phys.* **73**, 6069 (1993).
2. Argonne National Laboratory, Argonne, Ill.
3. Lawrence Berkeley Laboratory, Berkeley, Calif.
4. L. A. Boatner et al., p. 411 in *1981 Management of Alpha-Contaminated Wastes*, IAEA-SM-246/73, Vienna, Austria, 1981.
5. L. A. Boatner et al., p. 289 in *1980 Scientific Basis for Nuclear Waste Management II*, ed. by C. J. Northrup, Plenum Press, New York, 1980.

3. *Synthesis, Processing, and Characterization of Materials*

Breakthroughs in the related fields of solid state physics and materials sciences often depend on the synthesis and subsequent characterization of new materials. Research in the Solid State Division has a strong tradition of emphasizing a broad range of material synthesis activities which include superconductors, glasses, insulating crystals, metal alloys and crystals, nanophase solids, and solid electrolytes. The selection of materials to be synthesized are carefully coordinated with other research activities in the division and are designed to answer fundamental or applied questions concerning energy-related problems. Many of the materials that are produced are unique or rare research samples which naturally lead to collaborative activities involving university laboratories, other divisions at ORNL, other national laboratories, and industrial research centers.

This chapter is divided into the following five sections: *Superconductivity*, which reports some striking fundamental results on the role of both extrinsic and intrinsic defects on flux pinning and flux motion; *Thin-Film Batteries and Solid Electrolytes*, which describes a dynamic blend of applied and basic research projects aimed at understanding and producing new types of solid state electrolytes and thin-film rechargeable batteries; *Ferroelectric and Perovskite-Structure Oxides*, which describes interesting research activities dealing with an important class of ferroelectric materials for electro-optic, photorefractive, and thin-film substrate applications; *Materials Properties*, which reports some new characterization and processing techniques that have led to a better understanding of the initial stages of sintering, a more complete structural model of an important class of amorphous phosphates, and production of a remarkable theoretical model that can accurately reproduce the microstructure of welded single crystals; and *Optical Characterization of Materials*, which reports on a new promising scintillator material and on fundamental studies of optically active ions and defects in single-crystal hosts.

SUPERCONDUCTIVITY

EFFECTS OF COLUMNAR DEFECTS ON THE SUPERCONDUCTING PROPERTIES OF $YBa_2Cu_3O_{7-\delta}$: LIMITS TO THE IRREVERSIBILITY LINE[1]

D. K. Christen, S. Zhu,[2] C. E. Klabunde, H. R. Kerchner, J. R. Thompson,[3] R. Feenstra, L. Civale,[4] and J. M. Phillips[5]

Systematic studies of flux pinning and critical-current enhancement by columnar defects have provided an experimental perspective on the projected operating limits of several classes of the high-temperature superconducting (HTSc) materials. The flux pinning provided by these defects is nearly optimal, and the observed improvements in the irreversibility fields $B^*(T)$ are near the upper limits. Recently, a comparison has been made of the irreversibility lines for a number of optimal YBCO materials with the proposed "vortex-melting line" that has been determined by others on nearly defect-free single crystals. The melting line should represent an intrinsic breakdown in vortex correlations because of thermal fluctuations. The more anisotropic superconductors are most strongly affected, because of the proposed thermally induced decoupling of vortex segments. Flux pinning is observed to increase the irreversibility lines of all HTSc, until an apparent upper limit is reached. Figure 3.1 shows that for several optimized YBCO samples, the enhanced irreversibility fields nearly coincide with the previously determined melting lines. Thus, the results suggest the achievement of an *intrinsic* limit to loss-free behavior. These observations are qualitatively consistent with recent theoretical models that consider mechanisms for vortex depinning from columnar defects. These mechanisms are related to the same vortex elastic properties that determine the melting line.

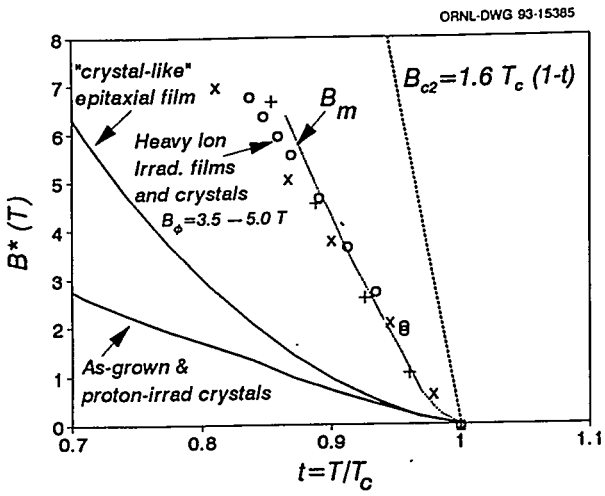

Fig. 3.1. The irreversibility field B^* for several YBCO materials, compared with published vortex melting curves B_m The upper critical field B_{c2} is represented by the dashed line. The results indicate that B_m is the upper limit to the achievable field and temperature range for useful critical currents in YBCO.

---

1. Summary of paper: *Physica B* (in press).
2. Graduate student from The University of Tennessee, Knoxville, Tenn.
3. Adjunct research and development participant from The University of Tennessee, Knoxville, Tenn.
4. Consultant from IBM Thomas J. Watson Research Center, Yorktown Heights, N. Y.
5. AT&T Bell Laboratories, Murray Hill, N.J.

LIMITS TO CRITICAL CURRENTS IN HIGH-TEMPERATURE SUPERCONDUCTORS: WHAT WE CAN LEARN FROM TAILORED DEFECTS[1]

D. K. Christen, J. R. Thompson,[2] H. R. Kerchner, B. C. Sales, B. C. Chakoumakos, L. Civale,[3] A. D. Marwick,[3] and F. Holtzberg[3]

Factors that limit the loss-free conduction of electric current in the vortex state of HTSc have been considered. Simple arguments lead to an estimate of the maximum possible critical-current densities arising from optimally sized linear defects that pin each vortex core over its entire length. In a series of model experiments, such linear-defect structures have been tailored at controlled densities in several HTSc materials by irradiation with high-energy heavy ions. Results from these studies have been compared with estimated zero-temperature theoretical limits. At higher temperatures, the irradiated materials provide unique systems for evaluation of the current theories of flux motion that account for both the intrinsic, anisotropic material properties and the unique defect structures. In particular, from measurements that relate the pinning to the angle between the vortex and defect lines, direct information can be obtained about the influence of material anisotropy on the vortex structure. Results have been compared for different classes of HTSc materials. Figure 3.2 compares the irreversibility fields $B_{irr}(T)$ for $YBa_2Cu_3O_{7-\delta}$ and $Bi_2Sr_2CaCu_2O_8$ in the as-formed and optimized states.

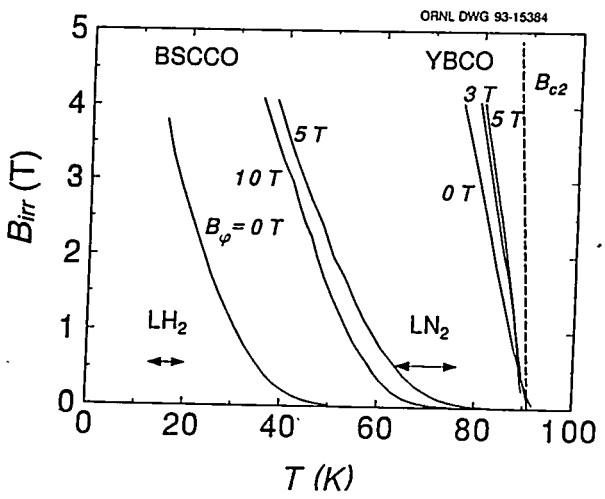

Fig. 3.2. Irreversibility lines $B_{irr}(T)$ of single-crystal YBCO and Bi2212 that have been irradiated parallel to the c axis with 580-MeV Sn ions, where irradiation fluences are indicated by the effective matching flux density B_Φ. The upper critical field line $B_{c2}(T)$ is a reasonable representation for both unirradiated materials, where the initial T_c values were 92 and 89 K for YBCO and Bi2212, respectively. The temperature ranges of pumped liquid hydrogen (LH_2) and liquid nitrogen (LN_2) are indicated.

1. Summary of paper: p. 24 in *Superconductivity and Its Applications*, ed. by H. S. Kwok, D. T. Shaw, and M. J. Naughton, American Institute of Physics, New York, 1993.

2. Adjunct research and development participant from The University of Tennessee, Knoxville, Tenn.

3. Consultant from IBM Thomas J. Watson Research Center, Yorktown Heights, N.Y.

SYSTEMATICS OF FLUX PINNING VS OXYGEN DEFICIENCY δ IN ALIGNED $YBa_2Cu_3O_{7-\delta}$ MATERIALS[1]

J. R. Thompson,[2] J. G. Ossandon,[3] D. K. Christen, Y. R. Sun,[4] B. C. Sales, H. R. Kerchner, J. E. Tkaczyk,[5] and K. W. Lay[5]

Magnetization studies were made on a series of oxygen-deficient $YBa_2Cu_3O_{7-\delta}$ materials to determine the role of oxygen deficiency $\delta \leq 0.20$ on intragrain superconductive properties. As oxygen was removed, the critical-current density J_c decreased steadily, even

where T_c was nearly constant. Flux-creep studies were analyzed to obtain the effective vortex-pinning energy $U_{eff}(J)$, which depends on the instantaneous current density J. The results were well-described by the vortex glass/collective-pinning relation $U_{eff}(J) = (U_o/\mu)[(J_{c0}/J)^{\mu-1}]$, with $\mu \approx 0.9$ for all oxygen compositions studied. Experimental values for the pinning energy scale U_o are compared with predictions from collective-pinning theory. The resulting interpretation within a collective-pinning/collective-creep framework gives a picture that is internally consistent. Specifically, similar values for the characteristic exponent μ are obtained from direct analysis of $M(t)$ and analysis of the vortex-pinning energy $U(J)$. These values lie between the respective theoretical values, 1/7 and 3/2. In magnitude and compositional dependence, the calculated energy scales are consistent with this interpretation. Finally, the experimental values for the energy scale U_o and μ are similar to those used to model $J_c(T)$ in comparable single crystals.

1. Summary of papers: *Cryogenics* **32,** 982 (1992); *Applied Superconductivity* **1,** 371 (1993).
2. Adjunct research and development participant from The University of Tennessee, Knoxville, Tenn.
3. Guest scientist from University of Talca, Talca, Chile.
4. Graduate student from The University of Tennessee, Knoxville, Tenn.
5. General Electric Corporate R&D Laboratory, Schenectady N.Y.

ENHANCED VORTEX-PINNING STRENGTH AND MAGNETIC IRREVERSIBILITY VIA COLUMNAR DEFECTS IN SINGLE-CRYSTAL $Bi_2Sr_2CaCu_2O_8$[1]

H. R. Kerchner, J. R. Thompson,[2] Y. R. Sun,[3]
D. K. Christen, J. O. Thomson,[4]
B. C. Sales, B. Chakoumakos,
L. Civale,[5] and A. D. Marwick[6]

To enhance vortex pinning in the high-T_c superconductor $Bi_2Sr_2CaCu_2O_8$, single crystals were irradiated with energetic heavy ions to create columnar defects. Ions impinged samples at various angles with respect to the c axis. Quasistatic magnetization measurements showed magnetic hysteresis (and critical-current density), which approaches zero as shown in Fig. 3.3 at a line of irreversibility, $T_{irr}(B)$.[6] Dynamic ac susceptibility measurements showed shielding currents that approached zero at a somewhat higher temperature T^*. Thermally assisted flux-flow resistivity ρ_{TAFF} was deduced in the regime between T_{irr} and T^*, and the pinning energy U_0 was determined from the Arrhenius temperature dependence of ρ_{TAFF}. Irradiation-induced defects showed U_0 values larger than observed in unirradiated samples by a factor of ~3, relatively independent of the ion beam exposure, which increased both J_c and the irreversible B-T regime. Independence of J_c and U_0 from the magnetic-field orientation suggests the predominance of strong pins interacting with two-dimensional pancake vortices.

1. Summary of paper: *Physica B* (in press).
2. Adjunct research and development participant from The University of Tennessee, Knoxville, Tenn.

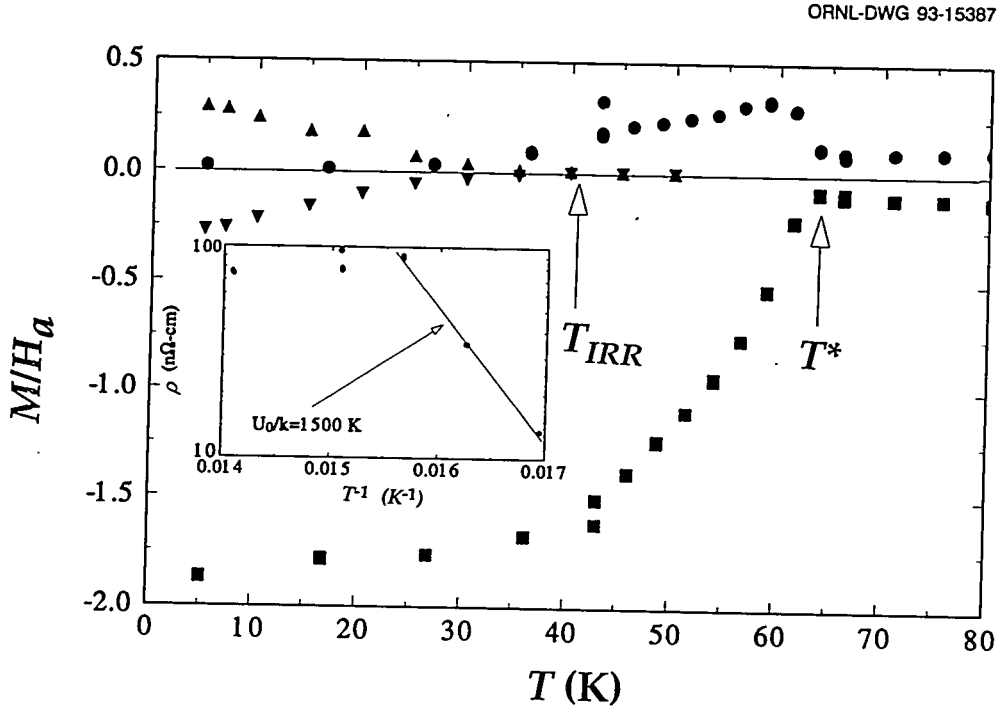

Fig. 3.3. ac susceptibility, χ' (■) and χ'' (●), in the presence of a static magnetic field B_{dc} = 10 kG and dc magnetization in increasing (▲) and decreasing (▼) fields for a BSCCO crystal exposed to 575-MeV Ag ions. Inset shows that the resistivity, ρ_{TAFF}, deduced at temperatures near T^*, obeys Arrhenius' law, $\rho = \rho_0 exp(-U_0/kT)$.

3. Graduate student from The University of Tennessee, Knoxville, Tenn.

4. Consultant from The University of Tennessee, Knoxville, Tenn.

5. Consultant from IBM Thomas J. Watson Research Center, Yorktown Heights, N. Y.

6. J. R. Thompson et al., *Appl. Phys. Lett.* 60 2306 (1992); p. 48 in *Solid State Division Progress Report for Period Ending September 30, 1992*, ORNL-6722 (September 1992).

VORTEX PINNING, SUPERCURRENT DECAY, AND WEAK LINKS IN THE Hg-BASED HIGH-T_c MATERIAL $HgBa_2CuO_{4+\delta}$[1]

J. R. Thompson,[2] *D. K. Christen, Y. R. Sun,*[3] *M. Paranthaman,*[4] *and J. Brynestad*[4]

Random polycrystalline samples of the Hg-based cupric-oxide superconductor $HgBa_2CuO_{4+\delta}$ were synthesized using a one-step reaction of powdered precursor materials. X-ray diffractometry revealed tetragonally structured Hg-1201 with little evidence for extraneous phases. A SQUID-based magnetometer was used in magnetic characterization to study magnetization $M(H,T,t)$ vs magnetic field H, temperature T, and time t. Low-field studies (H = 4–20 G), with both zero-field and field cooling, gave a diamagnetic onset T_c = 95 K, complete shielding, and Meissner signal of ~30% of $(-1/4\pi)$. Most importantly, clear evidence was found for weak coupling between the randomly oriented superconducting grains. Further measurements in large magnetic fields, strong enough to decouple the grains, showed that M was hysteretic. The hysteresis ΔM (proportional to the intragrain supercurrent

density in a Bean model) diminished rapidly with increasing field and temperature, following a quasi-exponential temperature dependence $\Delta M \sim \exp(-T/T_0)$. For $H = 10$ kG, the characteristic temperature $T_0 = 7$ K lies intermediate to values for single crystals of $YBa_2Cu_3O_{7-\delta}$ ($T_0 \sim$ 20 K) and $Bi_2Sr_2CaCu_2O_8$ ($T_0 \sim$ 5 K), as illustrated in Fig. 3.4. These decreases in the supercurrent density are attributed to substantial flux creep, which routinely leads to such a temperature dependence. Furthermore, thermally activated motion of magnetic flux is clearly evident in studies of M vs t.

---

1. Summary of papers: *Nature* **364**, 98 (1993) and *Physica C* **213**, 271 (1993).

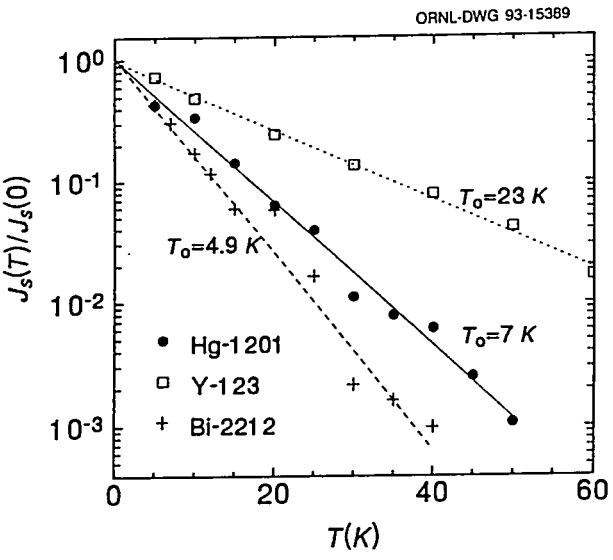

Fig. 3.4. The capability to conduct electrical current deteriorates rapidly with T. The persistent supercurrent density $J_s(T)$, relative to its value at 0 K, decreases quasi-exponentially as $\exp(-T/T_0)$, because of flux creep. With a 1-T magnetic field, intragrain results for polycrystalline Hg-1201 are compared with data for single crystals of Y-123 and Bi-2212, with magnetic field $H \perp$ Cu-O planes.

2. Adjunct research and development participant from The University of Tennessee, Knoxville, Tenn.
3. Graduate student from The University of Tennessee, Knoxville, Tenn.
4. Chemistry Division, ORNL.

ENHANCED TRANSPORT CRITICAL CURRENT AT HIGH FIELDS AFTER HEAVY ION IRRADIATION OF TEXTURED $TlBa_2Ca_2Cu_3O_x$ THICK FILMS[1]

J. E. Tkaczyk,[2] J. A. DeLuca,[2] P. L. Karas,[2] P. J. Bednarczyk,[2] D. K. Christen, C. E. Klabunde, and H. R. Kerchner

Spray-pyrolyzed $TlBa_2Ca_2Cu_3O_x$ films (~3-μm thickness) were deposited on polycrystalline YSZ substrates, and the electrical-transport properties were measured before and after irradiation with energetic heavy ions (Ag^{29+} at 575 MeV). The resulting columnar defects, created parallel to the c axis, were found to decrease the zero-field critical current by a factor of 2, but produced large enhancements at high fields. The irreversibility line at a field level of 5 T is shifted to higher temperatures by ~20 K, demonstrating a potential for operation in substantial magnetic fields in the liquid-nitrogen temperature range.

---

1. Summary of paper: *Appl. Phys. Lett.* **62**, 3031 (1993).
2. General Electric Corporate Research and Development, Schenectady, N.Y.

VORTEX FLUCTUATIONS, MAGNETIC PENETRATION DEPTH, AND UPPER CRITICAL MAGNETIC FIELD H_{C2} IN Hg- AND Tl-BASED HIGH-T_c SUPERCONDUCTORS[1]

J. R. Thompson,[2] J. G. Ossandon,[3] D. K. Christen, B. C. Chakoumakos, Y. R. Sun,[4] M. Paranthaman,[5] and J. Brynestad[5]

The presence of strong vortex fluctuation effects in two families of layered high-temperature superconductors [$HgBa_2CuO_{4+\delta}$ and $Tl_2Ca_2Ba_2Cu_3O_{10+\delta}$] has been established. From experimental studies of the equilibrium magnetization in the mixed state, detailed information was obtained on the London penetration depth λ_{ab}, upper critical field H_{c2}, and Ginzburg-Landau parameter κ_{ab} (with magnetic field $\perp$ Cu-oxide planes) of these materials. This experimental study gives the first clear evidence for vortex-fluctuation effects in the recently discovered Hg-based family of high-T_c superconductors and equally strong evidence of fluctuations in the Tl-2223 superconductor. As predicted theoretically, the magnetization is field independent and diamagnetic at a characteristic temperature $T^* < T_c$; the mixed-state magnetization M persists at temperatures above the low-field onset T_c; and M follows the theoretical lnH dependence from T^* to much lower temperatures. With fluctuations included, both $(1/\lambda)^2$ and H_{c2} are well behaved and extrapolate to a mean field T_{co} that lies several K above T_c, as predicted. Figure 3.5 shows the temperature dependence of these quantities for Tl-2223 and also that κ is almost constant, as it should be. This work clearly supports the recent theory of vortex fluctuations, giving strong evidence for their presence in these Hg- and Tl-based high-T_c superconductors.

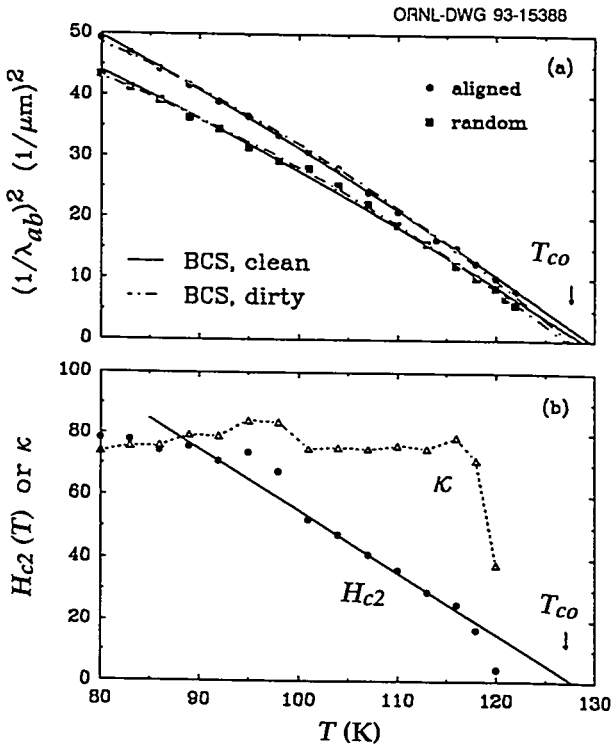

Fig. 3.5. For a polycrystalline Tl-2223 superconductor, the temperature dependence of (a) the London penetration depth λ_{ab} and (b) the upper critical field H_{c2} and κ are shown. Lines (fits to BCS and WHH theory, respectively) extrapolate to the mean-field transition temperature T_{co}.

---

1. Summary of paper: *Phys. Rev. B* 48, 14031 (1993).
2. Adjunct research and development participant from The University of Tennessee.
3. Guest scientist from University of Talca, Talca, Chile.
4. Graduate student from The University of Tennessee, Knoxville, Tenn.
5. Chemistry Division, ORNL.

EFFECT OF FLUX CREEP ON THE TEMPERATURE DEPENDENCE OF THE CURRENT DENSITY IN YBaCuO CRYSTALS[1]

J. R. Thompson,[2] *Y. R. Sun,*[3] *L. Civale,*[4] *A. P. Malozemoff,*[5] *M. W. McElfresh,*[6] *A. D. Marwick,*[7] *and F. Holtzberg*[7]

The temperature-dependent persistent-current density and normalized flux-creep rate, together with the current dependence of the vortex-pinning energy, were studied in as-grown and proton-irradiated YBaCuO crystals. A consistent interpretation of these features has been found within the collective-pinning or vortex-glass models. It is noteworthy that the same theoretical treatment gives a good description of both unirradiated and irradiated crystals, with similar and physically reasonable parameter values. Only the overall scale of current density differs significantly. These features are consistent with the idea that the increased critical-current density in proton-irradiated YBaCuO crystals arises primarily from an increased density of point-like defects. Thus, we can conclude that among existing theories, vortex glass and/or collective pinning theories provide the first successful phenomenological interpretation of the quasi-exponential dependence on temperature for the persistent current density, the normalized flux-creep rate $S(T)$, and the current dependence of the vortex-pinning energy $U(J)$.

---

1. Summary of paper: *Phys. Rev. B* 47, 14440 (1993).
2. Adjunct research and development participant from The University of Tennessee, Knoxville, Tenn.
3. Graduate student from The University of Tennessee, Knoxville, Tenn.
4. Consultant from Centro Atomico Bariloche, Bariloche, Argentina.
5. American Superconductor Corporation, Watertown, Mass.
6. Purdue University, West Lafayette, Ind.
7. IBM T. J. Watson Research Center, Yorktown Heights, N. Y.

OBSERVATION OF FREE-FLUX FLOW AT HIGH DISSIPATION LEVELS IN $YBa_2Cu_3O_7$ EPITAXIAL FILMS[1]

M. N. Kunchur,[2] *D. K. Christen, and J. M. Phillips*[3]

Highly controlled pulsed currents were used to investigate superconducting transport properties at exceptionally high power dissipation levels (approaching 10^9 W/cm^3!). Although the phenomenon of superconductivity is often associated with a state of vanishing resistance, this is neither a necessary nor sufficient condition for characterizing the superconducting state. At current densities beyond the critical value, $J > J_c$, dissipation sets in—although superconductivity itself persists up to $J = J_d$, the pair-breaking current. Novel and interesting physics is expected to occur between J_c and J_d, and some of these effects have been investigated.

In the mixed state of a superconductor, the material is permeated by quantized flux vortices. The motion of these vortices leads to dissipation and thus finite resistivity. For the idealized case of unhindered free-flux motion, the variation of resistivity with field is described by the well-known Bardeen-Stephen model[4] ($\rho/\rho_n = B/H_{c2}$). Because ordinarily flux motion is hindered by various crystalline defects, this behavior had until now not been observed in any

superconductor—high- or low-T_c. Our measurements on $YBa_2Cu_3O_7$ provided the first verification of this very basic phenomenon. The use of enormous current densities provided sufficiently large driving forces on the vortices so that their motion was relatively unaffected by defect-generated pinning forces. As can be seen in Fig. 3.6, the data follow the Bardeen-Stephen behavior over three decades.

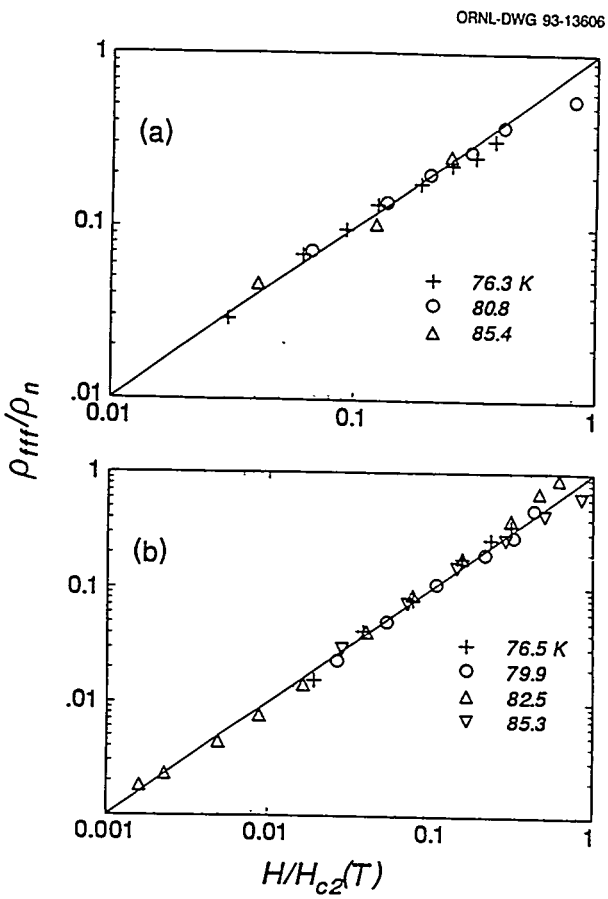

Fig. 3.6. Normalized free-flux-flow resistivity plotted vs normalized field for (a) specimen I and (b) specimen II. The data for all fields and temperatures fall roughly on the line $\rho/\rho_n = B/H_{c2}(T)$.

---

1. Summary of paper: *Phys. Rev. Lett.* **70**, 998 (1993).
2. ORNL/ORISE postdoctoral research associate.
3. AT&T Bell Laboratories, Murray Hill, N. J.
4. J. Bardeen and M. J. Stephen, *Phys. Rev.* **140**, A1197 (1965).

MAGNETIC RELAXATION STUDIES IN $YBa_2Cu_3O_{7-\delta}$ SUPERCONDUCTORS[1]

Y. R Sun,[2] J. R. Thompson,[3] D. K. Christen, Y. J. Chen,[2] and A. Goyal[4]

The effects of field sweep rate $K = \partial H/\partial t$ on magnetization-hysteresis loops $M(H)$ and on flux-creep studies $M(t)$ in high-temperature superconductors have been investigated both theoretically and experimentally. The basic relation between M and K is, to first order, the following:

$$M = const - [(dM/dln(t)) \bullet ln(K)] - [Kt_{eff}/10],$$

where $dM/dln(t) = aC/30$ is the flux-creep rate in a cylindrical sample of radius a, and t_{eff} is an effective attempt time for vortex hopping. The largest possible M, which corresponds to the critical-current density J_{c0} in the absence of thermal activation, develops when $K \geq K_{max} = aC/[(1+a\alpha)t_{eff}]$ with $\alpha = \partial J/\partial H$. The time origin of flux creep, which is essential in studying the initial stages of relaxation, is given by $t^* = aC/K(1 + a\alpha)$. The model agrees well with experiments on a melt-textured growth sample of $YBa_2Cu_3O_{7-\delta}$.

An analysis of magnetization hysteresis loops with this method was used to study flux creep in the high-temperature superconductors.

By combining field creep studies with conventional flux creep experiments, it is possible to detect magnetic decay in both the middle and the very beginning stages and thereby expand the time window up to 5–6 decades. Among the four models tested, only the vortex glass/corrective pinning theory gives a consistent description for both stages. The analyzed value of μ (exponent) showed a strong temperature and field dependence. The effective hopping time of vortices, t_{eff}, is ~0.1 s.

---

1. Summary of papers: *Phys. Rev. B* **46**, 8480 (1992); *Phys. Rev. B* **47**, 14 481 (1993).
2. Graduate student from The University of Tennessee, Knoxville, Tenn.
3. Adjunct research and development participant from The University of Tennessee, Knoxville, Tenn.
4. Metals and Ceramics Division, ORNL.

CORRELATIONS BETWEEN THE HALL COEFFICIENT AND THE SUPERCONDUCTING TRANSPORT PROPERTIES OF OXYGEN-DEFICIENT $YBa_2Cu_3O_{7-\delta}$ EPITAXIAL THIN FILMS[1]

E. C. Jones,[2] D. K. Christen, J. R. Thompson,[3] R. Feenstra, S. Zhu,[2] D. H. Lowndes, J. M. Phillips,[4] M. P. Siegal,[4] and J. D Budai

Strong correlations between the Hall coefficient R_H, the transition temperature T_c, and the critical-current density J_c were established in a series of epitaxial $YBa_2Cu_3O_{7-\delta}$ thin films as a function of oxygen deficiency δ. Steady increases in R_H with δ suggest that deoxygenation reduces the density of states which, according to BCS theory, should lead to corresponding decreases in T_c. In contrast, two well-known plateaus occurring at 90 and 60 K were observed in T_c vs δ. Others have ascribed these plateaus to either electronic phenomena or phase separations. At ORNL it was found that in the 90-K plateau, the critical-current density $J_c(\delta, H = 0)$ decreases with δ and extrapolates toward zero at the edge of the plateau, as illustrated in Fig. 3.7. This observation suggests a rapid decline in flux pinning with removal of charge carriers. However, measurements in magnetic fields show that the relative field dependence of $J_c(\delta, H)$ and the flux creep pinning energies are independent of δ in the plateau. These observations suggest that a phase separation scenario occurs on the 90-K plateau. However, electronic origins cannot be

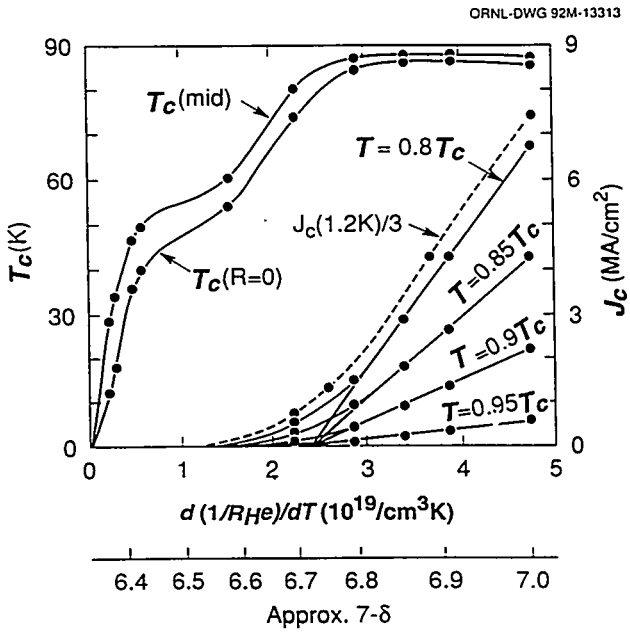

Fig. 3.7. Transition temperature T_c, and critical-current density J_c evaluated at fixed reduced temperatures, as a function of either the oxygen deficiency d or the "apparent carrier density" $d(1/R_H)/dT$ from Luttinger liquid theory.

ruled out at present because of difficulties in determining the equilibrium superconducting properties of oxygen-deficient $YBa_2Cu_3O_{7-\delta}$ films.

---

1. Summary of paper: *Phys. Rev. B* 47, 8986 (1993).
2. Graduate student from The University of Tennessee, Knoxville, Tenn.
3. Adjunct research and development participant from The University of Tennessee, Knoxville, Tenn.
4. AT&T Bell Laboratories, Murray Hill, N.J.

UPPER CRITICAL FIELDS OF $YBa_2Cu_3O_{7-\delta}$ EPITAXIAL THIN FILMS WITH VARIABLE OXYGEN DEFICIENCY δ[1]

E. C. Jones,[2] D. K. Christen, J. R. Thompson,[3] J. G. Ossandon,[2] R.Feenstra, J. M. Phillips,[4] and M. P. Siegal[4]

Through low-temperature heat treatments, the oxygen deficiencies of three epitaxial thin films of $YBa_2Cu_3O_{7-\delta}$ were systematically varied in the range $\delta < 0.3$. Electrical resistivities in the magnetic-field-dependent superconducting transition were analyzed using recent fluctuation theories in the limit of high magnetic fields. For oxygen contents corresponding to the 90-K "T_c plateau," the three-dimensional (3D) theory yielded an upper critical field slope at T_c, $dH_{c2}(T)/dT = -1.7$ T/K for $H \| c$, consistent with previous observations of transport and magnetic properties on single crystals. Moreover, the 3D scaling showed better convergence than the two-dimensional scaling, which gave relatively low values of H_{c2}. In contrast, the transitions were not described adequately by either scaling for δ values where $T_c < 90$ K, off the 90-K plateau. It is speculated that this arises from an extrinsic broadening of the transitions, possibly because of the lack of a complete percolation path of the ortho–I phase ($\delta = 0$).

---

1. Summary of paper: *Phys. Rev. B* 49, 572 (1994).
2. Graduate student from The University of Tennessee, Knoxville, Tenn.
3. Adjunct research and development participant from The University of Tennessee, Knoxville, Tenn.
4. AT&T Bell Laboratories, Murray Hill, N.J.

ELECTRON-DOPED AND HOLE-DOPED INFINITE-LAYER $Sr_{1-x}CuO_{2-\delta}$ FILMS GROWN BY LASER MOLECULAR BEAM EPITAXY[1,2]

R. Feenstra, X. Li,[3] M.Kanai,[3] T. Kawai,[3] S. Kawai,[3] J. D. Budai, E. C. Jones,[4] Y. R. Sun,[4] J. R. Thompson,[5] S. J. Pennycook, and D. K. Christen

Comprising a simple oxygen-deficient perovskite unit cell, the so-called "infinite-layer" $ACuO_2$ structure is the simplest structure containing the CuO_2 sheets necessary for high-temperature superconductivity. Basically, all the presently known superconducting cuprates may be structurally derived from the infinite-layer structure by the insertion of chemically distinct metal-oxide lattice planes parallel to the CuO_2 sheets. Because of the intimate relation between the charge carriers injected into the CuO_2 sheets because of these intermediate oxide layers and the onset of high-T_c superconductivity, there is great interest in the intrinsic

electrical properties of the infinite-layer structure.

Thin films of the infinite-layer cuprate $Sr_{1-x}CuO_{2-\delta}$ were epitaxially grown on (100) $SrTiO_3$ substrates using a novel laser molecular beam epitaxy technique developed at Osaka University, Osaka, Japan, by the successive excimer-laser ablation of Sr(O) and CuO_{1-x} monolayers from Sr and CuO targets, respectively. Different SrCuO deposition schemes were employed to produce distinct defect structures in the as-grown films. Subsequently, the doping mechanism was evaluated from the electrical response to reversible low-temperature oxygen exchange. The results, illustrated for a number of films in Fig. 3.8, indicate that the infinite-layer $Sr_{1-x}CuO_{2-\delta}$ films exhibit a natural tendency for electron doping but that this trend may be reversed toward hole doping by the insertion of SrO_{1-x} defect layers. This apparently different doping behavior provides important information for future layer-by-layer growth attempts of this material aimed at producing high-T_c superconductivity.

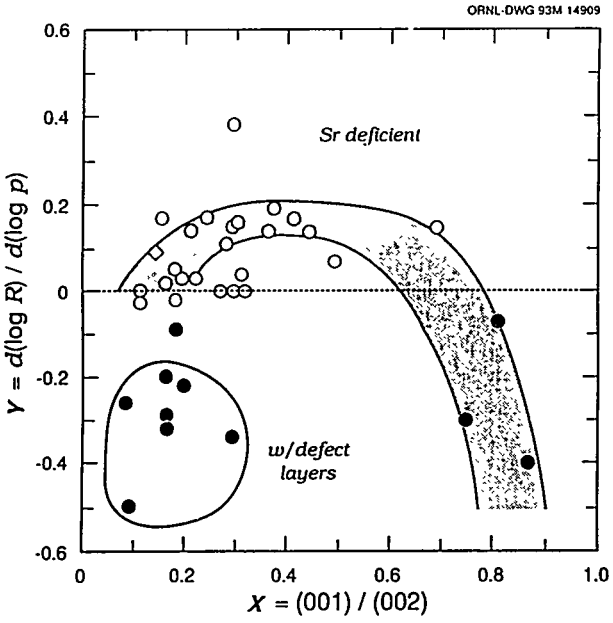

Fig. 3.8. Rate of change, Y, of the room-temperature resistivity of $Sr_{1-x}CuO_{2-\delta}$ thin films with oxygen pressure during successive anneals at 300° C vs the ratio, X, of the intensities of (001) and (002) x-ray diffraction peaks. X increases with increasing Sr deficiency of the films.

---

1. Summary of paper: *Physica C* (to be published).
2. Research performed while the first author was on foreign assignment at Osaka University, October 1992–April 1993. Partial funding for the assignment was received from the Japan Society for the Promotion of Science under its 1992 Fellowship Program.
3. Institute of Scientific and Industrial Research, Osaka University, Osaka, Japan.
4. Graduate student from The University of Tennessee, Knoxville, Tenn.
5. Adjunct research and development participant from The University of Tennessee, Knoxville, Tenn.

ANISOTROPIC ELECTRICAL RESISTIVITY OF YBCO/PBCO SUPERLATTICE FILMS GROWN ON MISCUT SUBSTRATES[1]

H. R. Kerchner, C. E. Klabunde, D. K. Christen, J. D. Budai, D. H. Lowndes, D. P. Norton, and J. O. Thomson[2]

Anisotropic electrical resistivity was studied in epitaxial superlattice films of $YBa_2Cu_3O_{7-\delta}/PrBa_2Cu_3O_{7-\delta}$ grown in situ by laser ablation on $SrTiO_3$ substrates. These particular substrates had been miscut approximately 0.6° away from (001) planes toward an in-plane <110> direction. Overlapping tilted platelets were previously observed by scanning tunneling microscopy of $YBa_2Cu_3O_{7-x}$ films epitaxially grown on miscut $SrTiO_3$ and $LaAlO_3$

substrates.[3] Highly aligned platelets give rise to steps in the film surface. In addition, twin boundaries, universal in $YBa_2Cu_3O_{7-\delta}$ films, were observed to be highly aligned parallel to the surface steps.[4] Layer thicknesses of each compound range from two to eight atomic cells.

Shown in Fig. 3.9 is a temperature dependence of sheet resistance $R_{\square} = \rho/d$, where ρ is the bulk resistivity and d is the film thickness. The sheet resistance was deduced by Montgomery's[5] (anisotropic $R_{\square}$) and by van der Pauw's[6] (isotropy-assumed) techniques. The current-flow directions are cited as $\parallel$ or $\perp$ with respect to the parallel atomic-lattice steps and twin boundaries. The broad superconductive transition has been explained as a two-dimensional, Kosterlitz-Thouless (K-T) transition[7] or due to the absence of long-range phase coherence of the superconductive wave function above T_c.[8] The negative temperature derivative of resistivity at high temperatures arises from the presence of semiconductive $PrBa_2Cu_3O_{7-\varepsilon}$.

A steep decline in the resistivity ratio from $\rho_\perp/\rho_\parallel \sim 1$ to $\rho_\perp/\rho_\parallel \sim 0$ as T cools through the transition is a striking effect that is difficult to explain. If the crucial effect is the interactions between vortex-antivortex pairs of the K-T transition, then the pairs are more strongly bound in the direction parallel to the twins and step edges. Assuming the attractive interactions between vortices are only within individual $YBa_2Cu_3O_{7-\delta}$ platelets leads naturally to the observed low-temperature anisotropy.

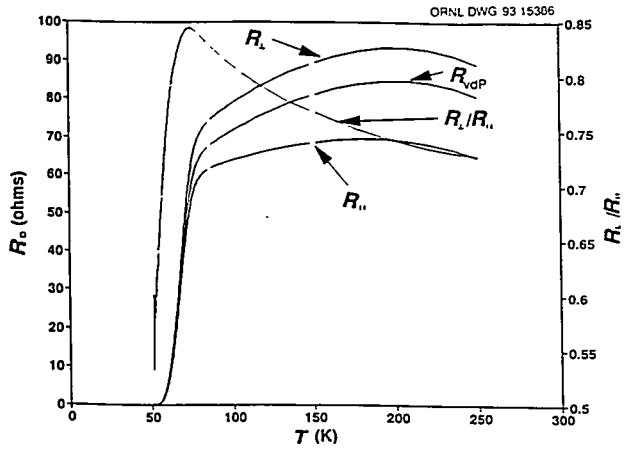

Fig. 3.9. Electrical sheet resistance $R_{\square}$ in a film of 20 layers of 2-cell-thick $YBa_2Cu_3O_7$ and 8-cell-thick $PrBa_2Cu_3O_7$ for current flow perpendicular ($R_\perp$) or parallel ($R_\parallel$) to the film surface steps and the twin boundaries aligned parallel to the step edges. R_{vdP} is the mean sheet resistance deduced assuming isotropic material.

---

1. Summary of paper: *Mat. Res. Soc. Symp. Proc.* **275**, 353 (1992).
2. Consultant from The University of Tennessee, Knoxville, Tenn.
3. D. H. Lowndes et al., *Appl. Phys. Lett.* **61**, 852 (1992).
4. J. D. Budai et al., *Appl. Phys. Lett.* **58**, 2174 (1991).
5. H. C. Montgomery, *J. Appl. Phys.* **42**, 2971 (1971).
6. L. J. van der Pauw, *Philips Res. Rep.* **13**, 1 (1958).
7. Mark Rasolt et al., *Phys. Rev. Lett.* **66**, 2927 (1991); H. R. Kerchner et al., *Physica C* **198**, 75 (1992).
8. D. P. Norton et al., *Phys. Rev. Lett.* **67**, 1358 (1991).

THIN-FILM BATTERIES AND SOLID ELECTROLYTES

RECHARGEABLE THIN-FILM LITHIUM BATTERIES[1]

J. B. Bates, G. R. Gruzalski, N. J. Dudney, C. F. Luck, and Xiaohua Yu[2]

Rechargeable thin-film batteries consisting of a lithium metal anode, amorphous inorganic electrolytes, and cathodes of a lithium intercalation compound have been fabricated and characterized. These include Li-TiS_2, Li-V_2O_5, and Li-$Li_xMn_2O_4$ cells with open-circuit voltages at full charges of about 2.5, 3.7, and 4.2 V, respectively. The components of the cells, which include metal cathode and anode current collectors, cathode, electrolyte, lithium anode, and protective coating, are deposited by sputtering or evaporation. Laboratory cells typically have an area of about 1 cm^2 with 1-μm-thick cathode and electrolyte films and a 3–5-μm-thick anode film.

Examples of discharge curves for Li-TiS_2, Li-V_2O_5, and Li-$LiMn_2O_4$ cells are shown in Fig. 3.10. The data are plotted as cell voltage vs the quantity of charge passed per volume of cathode. The Li-V_2O_5 and Li-TiS_2 cells are deposited in the fully charged state. The first deep discharge of these cells to 1.5 V for V_2O_5 and 1.8 V for TiS_2 is represented by

$$3\,Li + V_2O_5 = Li_3V_2O_5 \qquad (1)$$

and

$$Li + TiS_2 = LiTiS_2. \qquad (2)$$

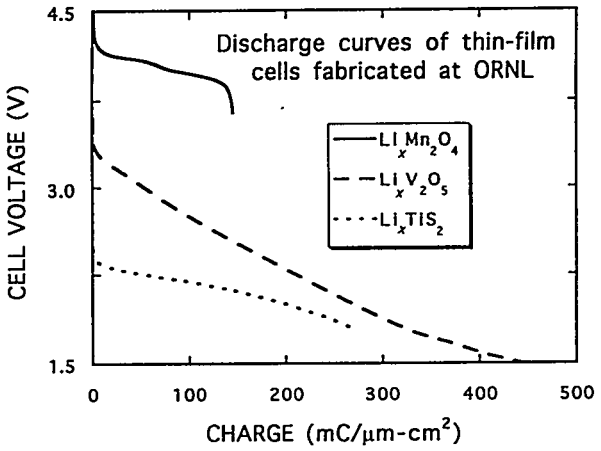

Fig. 3.10. Discharge curves for three types of rechargeable thin-film lithium batteries.

On the subsequent charge cycle, about 2.8 Li per V_2O_5 is extracted from the V_2O_5 cathode compared with the total mass of the cathode film. A similar effect is found for the Li-TiS_2 cells. For the Li-$Li_xMn_2O_4$ cell, the as-deposited cathode has a composition near $LiMn_2O_4$, which represents the discharged state for the cubic spinel phase. The battery is first charged to 4.5 V. Assuming that one Li per Mn_2O_4 is extracted from the cathode during this initial charge, the subsequent discharge-charge cycles, restricted to the voltage range shown in Fig. 3.10, are represented by

$$0.6Li + Mn_2O_4 = Li_{0.6}Mn_2O_4. \qquad (3)$$

The loss in capacity following the initial discharge or charge of these cells is not understood, but it is believed to be caused by a structural change in the cathodes. In subsequent deep cycling of each type of cell, the capacity decreases on the order of a few tenths of a percent per cycle. Except for this small capacity loss, the performance of the cells does not

degrade with cycling as a result of the electrochemical stability of the lithium phosphorous oxynitride electrolyte.[3] A limit on the practical current density of about 100 $\mu A/cm^2$ is due to slow lithium diffusion in the cathode as discussed elsewhere in this report.[4]

---

1. Summary of papers.
2. ORNL/ORISE postdoctoral research associate.
3. J. B. Bates et al., *J. Power Sources* **43–44**, 103 (1993).
4. J. B. Bates et al., "Impedance of Thin-Film Lithium Batteries," this report.

CYCLING A THIN-FILM SOLID STATE LITHIUM BATTERY: Li/Lipon/$LiMn_2O_4$

G. R. Gruzalski and J. B. Bates

A solid state thin-film voltaic cell fabricated with a lithium anode, an amorphous lithium phosphorous oxynitride electrolyte,[1] denoted as Lipon, and a $Li_xMn_2O_4$ cathode[2] was cycled at 30 $\mu A/cm^2$ between various voltage limits. At the end of each charge or discharge half cycle, the cell was kept at constant voltage until the current required to hold it at that voltage dropped to 0.9 $\mu A/cm^2$. An example of the cycling data is shown in Fig. 3.11. As can be seen, the charge-discharge loops did not coincide with one another from one cycle to the next; instead, they "spread" or evolved as suggested by the seven arrows in Fig. 3.11.

For the data shown, as well as for all other data obtained, the upper left-hand region of the charge-discharge loops (the region indicated with an A) moved very little if at all with

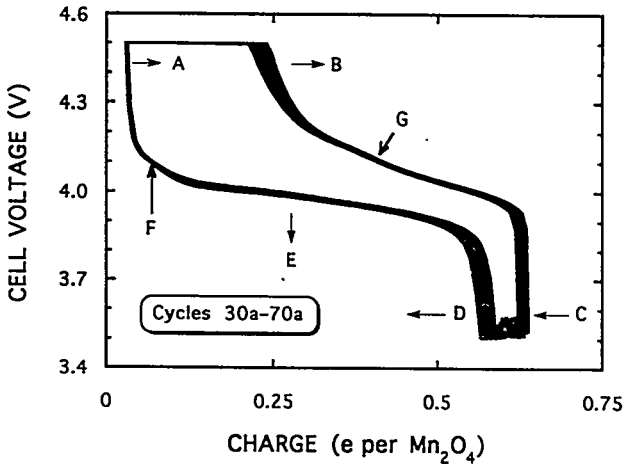

Fig. 3.11. Cell voltage vs charge for cycles 30–70a. The solid arrows indicate the direction in which the loop spreads or deforms with cycling. Note that point A moves very little compared with points B, C, or D. Lines from one loop to the next cross at points F and G.

cycling. As suggested by the arrow, the small movement of region A was to the right. This movement is consistent with less than 10^{-4} Li ions per unit of Mn_2O_4 being lost to the cathode per cycle. The lack of region A movement to the left suggests that no charge is "lost" because of a short or to electrolysis. The absence of electrolysis nicely demonstrates the viability of Lipon in the Li/$Li_xMn_2O_4$ environment.

Perhaps the most intriguing conclusion drawn from these data is that the cell's loss in capacity, which was about 0.1% per cycle (after the first cycle), was not due primarily to lithium becoming trapped in the cathode but rather to that portion of the cathode becoming inaccessible or inactive. Similar cycling behavior was observed for cells made with bulk $Li_xMn_2O_4$ cathodes.[3]

---

1. J. B. Bates et al., *J. Power Sources* **43–44**, 103 (1993).

2. The cathode material was supplied by F. Shokoohi of Bellcore, Red Bank, N.J.
3. J. M. Tarascon et al., *J. Electrochem. Soc.* 138, 2859 (1991).

AC IMPEDANCE OF THIN-FILM LITHIUM BATTERIES[1]

J. B. Bates and G. R. Gruzalski

Rechargeable thin-film batteries consisting of a lithium metal anode, an amorphous lithium phosphorus oxynitride electrolyte,[2] and a TiS_2, V_2O_5, or $Li_xMn_2O_4$ cathode have been fabricated and characterized. Presently, the current density of these batteries with 1-μm-thick cathode films is limited to about 100 $\mu A/cm^2$ without an excessive voltage drop due to internal resistance. To explore the source of this internal resistance, the impedance of these cells was measured at 25°C at frequencies from 0.01 Hz to 10 MHz.

The impedance of the Li-V_2O_5 cells was modeled using the equivalent circuit model shown below. The constant phase angle (CPA) elements Z in the circuit

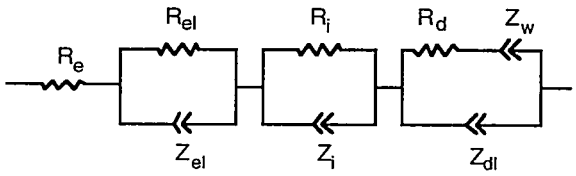

have the form $Z = A(j\omega)^{-n}$, where A and n are constants. Components 1, 2, and 4 represent the electronic resistance of the cathode, the impedance of the electrolyte film, and the impedance of the cathode, respectively. For the latter, Z_{dl} is the impedance of the double layer at the cathode-electrolyte interface, Z_w is the diffusion impedance, and R_d is the charge transfer resistance. Component 4 dominates the impedance of all the thin-film cells. The origin of component 3, though not well understood, is associated with the formation of the electrolyte-V_2O_5 interface.

The chemical diffusion coefficients $\tilde{D}_{Li}$ for the lithium ions in the three types of cathodes were calculated from the fitted values of the constant A_w of the diffusion impedance Z_w using the expression[3]

$$\tilde{D}_{Li} = \left(\frac{V_m \, dV/dx}{\sqrt{2}\, Fa} \cdot \frac{1}{A_w} \right)^2 \qquad (1)$$

Here dV/dx is the derivative of the cell potential with the change in the cation stoichiometry parameter (e.g., $Li_xV_2O_5$, V_m is the molar volume, F is Faraday's constant, and a is the area of the cathode. The diffusion coefficients (Table 3.1) for Li^+ in the thin-film cathodes are 3

Table 3.1. Chemical diffusion coefficients for Li^+ ions in thin-film cathodes.

Cathode	V_o	x	$\tilde{D}_{Li}(cm^2/s)$
$Li_xV_2O_5$ (119 A)	3.5	0.14	3×10^{-14}
$Li_xV_2O_5$ (119 A)	1.6	2.9	2×10^{-12}
$Li_xV_2O_5$ (76 A)	3.4	0.29	4×10^{-15}
$Li_xV_2O_5$ (76 A)	1.8	2.6	3×10^{-12}
$Li_xMn_2O_4$	4.0	0.3	3×10^{-12}
Li_xTiS_2	2.4	0.05	2×10^{-14}

V_o is the open circuit voltage, and x is the stoichiometry parameter.

to 4 orders of magnitude smaller than their respective values reported for bulk materials, which accounts for the low current density of the thin-film batteries. For the thin films, the measured diffusion coefficients include not only the effects of the ionic mobility and thermodynamic enhancement factors but also the film microstructure.

---

1. Summary of papers to be published.
2. J. B. Bates et al., *J. Power Sources* 43–44, 103 (1993).
3. C. Ho, I. D. Raistrick, and R. A. Huggins, *J. Electrochem. Soc.* **127**, 343 (1980).

SYNTHESIS, CRYSTAL STRUCTURE, AND IONIC CONDUCTIVITY OF A POLYCRYSTALLINE LITHIUM PHOSPHORUS OXYNITRIDE WITH THE γ-Li_3PO_4 STRUCTURE[1]

B. Wang,[2] B. C. Chakoumakos, B. C. Sales, B. S. Kwak,[2] and J. B. Bates

A crystalline lithium phosphorous oxynitride has been prepared for the first time by solid state reaction between Li_3N and $LiPO_3$ under a flowing N_2 atmosphere. From a thermogravimetric determination of the N content and based on the close similarity of the powder diffraction pattern to that of γ-Li_3PO_4, the composition of the material is $Li_3PO_{3.74}N_{0.17}$. The crystal structure of $Li_3PO_{3.74}N_{0.17}$ was obtained by Rietveld analysis of neutron powder diffraction data using the orthorhombic structure of γ-Li_3PO_4 (space group Pmnb). High-performance liquid chromatography and x-ray photoelectron spectroscopy measurements indicate the presence of PO_3N structural units and the linkage of phosphate anions by –N= and P–N$\langle^{P}_{P}$ bonding.

The ionic conductivity (Fig. 3.12) of $Li_3PO_{3.74}N_{0.17}$ ($\sigma_{25°C} \sim 10^{-13}$ S·cm^{-1}) is several orders of magnitude higher than that of γ-Li_3PO_4 ($\sigma_{25°C} \sim 10^{-18}$ S·cm^{-1}). A comparison of activation energy between $Li_3PO_{3.74}N_{0.17}$ and γ-Li_3PO_4 suggests that the higher conductivity of $Li_3PO_{3.74}N_{0.17}$ is due to an increase in lithium mobility as indicated by its lower activation energy. The defects created by N^{3-} ions substituting for the O^{2-} ions may facilitate lithium-ion conduction and, thus, decrease the activation energy. In addition, when the larger N^{3-} ions substitute for the smaller O^{2-} ions, the bottleneck size (i.e., the minimum opening in the structure that the mobile ions must pass through) is

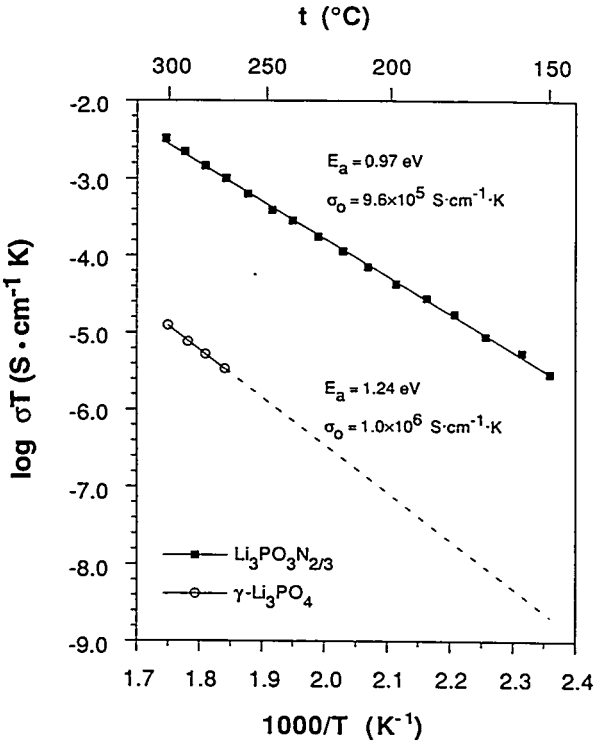

Fig. 3.12. Arrhenius plots of the ionic conductivity of γ-Li_3PO_4 and $Li_3PO_{3.74}N_{0.17}$.

increased as evidenced by the increase of *a* and *b* unit-cell parameters. This also lowers the activation energy.

1. Summary of paper to be published.
2. ORNL/ORISE postdoctoral research associate.

IONIC CONDUCTIVITIES AND STRUCTURE OF LITHIUM PHOSPHORUS OXYNITRIDE GLASSES[1]

B. Wang,[2] B. S. Kwak,[2] B. C. Sales, and J. B. Bates

Lithium phosphorus oxynitride glasses with different lithium contents have been prepared by melting two sets of base glasses at high temperatures in a flowing ammonia atmosphere. The compositions of these samples were determined by chemical analysis. The local structure around the oxygen and nitrogen in the glasses was studied by x-ray photoelectron spectroscopy. In the case of oxygen, three O ls components corresponding to P = 0, Li^+...-O-P, and P-O-P were observed. Two N ls peaks observed were attributed[3] to doubly coordinated nitrogen (P–N = P) and triply coordinated nitrogen (P–N$\langle^{P}_{P}$). The introduction of nitrogen into the base glasses and the formation of the P–N = P and P–N$\langle^{P}_{P}$ structures account for the decrease of average phosphate anion chain length observed in high-performance liquid chromatography measurements.

The results of ac impedance measurements show that nitrogen incorporation into the glass structure increases the ionic conductivity (Fig. 3.13). The highest conductivity, 3.0×10^{-7} $S \cdot cm^{-1}$ at 25°C, was found in $Li_{0.99}PO_{2.55}N_{0.30}$ glass. The increase in conductivity in the nitrided samples can be attributed to the increase of network disordering and structural cross-linking as the result of nitrogen incorporation.

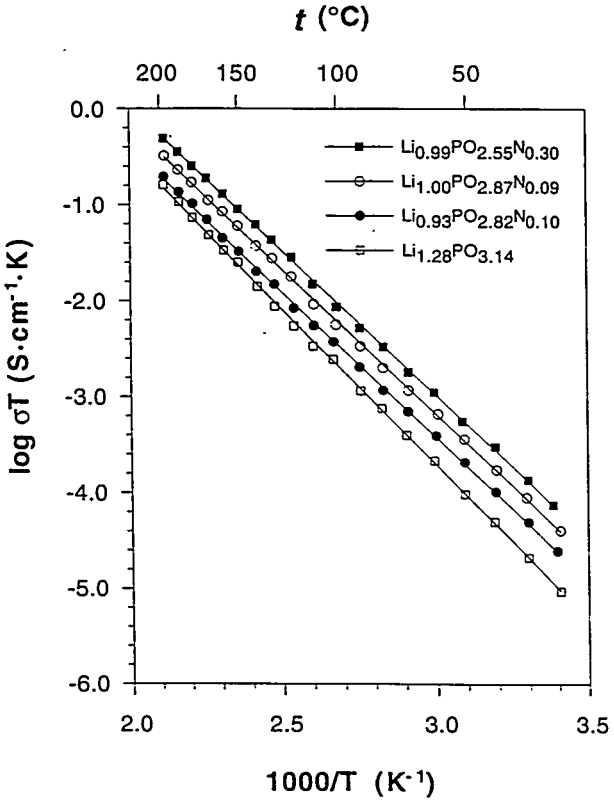

Fig. 3.13. Arrhenius plots of the ionic conductivity of high lithium content phosphorus oxynitride glasses.

1. Summary of paper to be published.
2. ORNL/ORISE postdoctoral research associate.
3. R. Marchand et al., *J. Non-Cryst. Solids* **103**, 35 (1988).

DEPOSITION OF ORGANIC-INORGANIC COMPOSITE THIN FILMS BY Li_3PO_4 SPUTTERING AND C_2H_4 PLASMA POLYMERIZATION[1]

B. S. Kwak,[2] R. A. Zuhr, and J. B. Bates

Results from the deposition of organic-inorganic composite macro-molecular thin films by combined rf magnetron sputtering and plasma-polymerization techniques are reported. Ethylene, C_2H_4, and lithium orthophosphate, Li_3PO_4, were used as the monomer and inorganic sources, respectively. The working gases were Ar, N_2, and Ar/O_2, of which only the Ar/O_2 mixture provided suitable control over the codeposition. It was found that the codeposition process requires a component in the gas mixture that can etch away the plasma-polymerized organic component from the inorganic target surface and, in so doing, preserve the sputtering of the inorganic species.

As-deposited films were characterized to determine the composition, structure, and ionic conductivity. The characterization techniques used included x-ray photoelectron spectroscopy (XPS), scanning electron microscopy, Fourier transform infrared spectroscopy (FTIR), Rutherford backscattering spectroscopy, x-ray diffraction, and ac-impedance measurements. The composite films were x-ray amorphous. The surface was featureless, smooth, and free of pinholes and voids. The compositions (i.e., relative variation with respect to parameter changes) were determined entirely with XPS. The spectra from ac-impedance measurements consisted of two features indicative of two distinct phases.[3] From the XPS and FTIR measurements, it appears that the inorganic phase is incorporated both as a separate phase and as a part of the polymeric backbone. The ionic conductivity of the composite thin films from this system was about 10^{-9} $(\Omega cm)^{-1}$ at room temperature and varied inversely with the amount of the organic phase in the sample. Unlike most polymer ionic conductors, the temperature behavior appeared to be purely Arrhenius rather than VTF which occurs because of a cooperative effect of the segmental motions in the polymeric backbone.[4]

---

1. Summary of paper to be published.
2. ORNL/ORISE postdoctoral research associate.
3. J. B. Bates et al., *Solid State Ionics* 55, 467 (1992).
4. M. A. Ratner and D. F. Shriver, *Chem. Rev.* 88, 109 (1988).

RADIO-FREQUENCY MAGNETRON SPUTTERING OF PURE AND MIXED TARGETS OF Li_4SiO_4, Li_3PO_4 AND Li_2O[1]

N. J. Dudney, J. B. Bates, and J. D. Robertson[2]

Sintered targets of Li_4SiO_4, Li_3PO_4, and Li_2O have been sputtered in argon and argon/oxygen atm. at 20-mTorr total pressure and 20–30 W rf power. The extent of lithium sputtering and the resulting film compositions varied greatly among the different compounds. Lithium orthophosphate sputtered normally yielding films with close to the stoichiometric target composition. Upon sputtering of lithium orthosilicate, however, much of the lithium was observed to segregate toward the center and rim

of the targets, away from the sputtered area, leaving large deposits of Li_2O on the target surface. This resulted in silicate films with a lithium concentration much less than that of the original Li_4SiO_4 target. A large redistribution of target material has also been observed for sputtered lithium oxide targets. For mixed silicate-phosphate targets, even a small amount of Li_4SiO_4 can facilitate the segregation of almost all the lithium in the target, including the lithium in the Li_3PO_4 phase.

A variety of experiments have indicated that the lithium segregation occurs by lithium migration along the surface of the target. An estimate of the magnitude of the lithium diffusivity required to compete with the observed sputter rate is much higher than the lithium diffusivity in the bulk crystalline compounds, but adequate lithium diffusivity could result if a thin layer of an amorphous silicate is formed on the surface of the sputtered target. The different behavior of Li_3PO_4 vs Li_4SiO_4 may be due to a difference in this tendency to form such a conductive phase. The silicate and phosphate materials may also differ in the direction of the lithium migration upon Ar^+ bombardment. Such a difference has been documented for Na migration in silicate vs phosphate glasses upon Ar^+ irradiation.

It was shown that the reproducible and homogeneous lithium phosphosilicate films can best be produced by codeposition with independently controlled sputter sources onto a rotating substrate.

---

1. Summary of paper: *J. Vac. Sci. and Technol. A* **11**, 377 (1993).
2. University of Kentucky, Lexington, Ky.

COMPOSITE THIN FILMS BY Li_3PO_4 SPUTTERING AND $Si(OC_2H_5)_4$ POLYMERIZATION

B. S. Kwak,[1] *R. A. Zuhr, and J. B. Bates*

Results from studies on the extended network structures based on C-O-Si chains are reported. The structures were synthesized by combined rf magnetron sputtering and plasma-polymerization techniques in off-axis geometry. Tetraethoxysilane (TEOS), $Si(OC_2H_5)_4$, and lithium orthophosphate (Li_3PO_4) were used as the monomer and inorganic sources, respectively. The working gases were Ar, N_2, and Ar/O_2.

The polymerization behavior of TEOS and codeposition process with Li_3PO_4 in Ar/O_2 were found to be very stable—in particular, for the codeposition where the deposition rate was stable in Ar without losing Li^+ intensity in the optical emission spectrum. Both the TEOS and codeposited thin films were x-ray amorphous. The TEOS and composite thin films grown in Ar/O_2 appear to consist entirely of Si-O-C, Si-O-Si, and O-H functional groups, whose relative ratios change with O_2 percent in the gas mixture. In the composite films, the modes related to Li_3PO_4 (and Li_2CO_3) could not be unambiguously identified. Without the O_2 flow, the C-H related modes appear. The films, however, were more disordered. The composite thin films exhibited rather low ionic conductivity, about 10^{-12} $(\Omega cm)^{-1}$ at room temperature. As with the Li_3PO_4/C_2H_4 system,[2] the impedance spectrum implied multiple phases. The films appeared to possess good mechanical properties.

Future experiments will attempt to improve the ionic conductivity by codeposition in N_2. Possibly, this will result in producing nitrogen cross-links in the system.[3]

---

1. ORNL/ORISE postdoctoral research associate.
2. B. S. Kwak, R. A. Zuhr, and J. B. Bates (to be published).
3. J. B. Bates et al., *J. Power Sources* **43–44**, 103 (1993).

COMPOSITE ELECTROLYTES[1]

N. J. Dudney

Recent research related to composite electrolytes has been reviewed. The term "composite electrolytes" refers to a class of crystalline electrolytes for which the ionic conductivity is enhanced greatly by the incorporation of fine particles or fibers of an insoluble rigid second phase. There are many examples of such composites; some of the more extensively studied composites include LiI, AgCl, AgI and CaF_2 containing dispersed submicron particles of alumina and other oxides (e.g., CeO_2 and SiO_2). The conductivities of these materials have been enhanced by 1 to 3 orders of magnitude in the composite compared with the pure matrix phase. This has generated much interest in these materials, both in research to identify the mechanisms responsible for the enhanced conduction and also as a new technique to fabricate useful electrolytic materials for batteries and other devices.

There is a growing body of evidence to demonstrate that the primary role of the second-phase particles is to stabilize a more conductive phase or a finer and more disordered microstructure than would exist in the pure electrolyte materials. The fine particles effectively inhibit both grain boundary migration and dislocation motion associated with the recrystallization or phase transformation. For example, a recent study of vapor-deposited CaF_2 films have shown an enhanced ionic conduction clearly related to the dislocation structure.[2] The dislocations were effectively stabilized by the addition of an alumina phase. Earlier work on composites of AgCl with alumina fibers, demonstrated that the presence of the fibers stabilized a fine-grain structure which can account for the enhanced conduction reported for the AgCl and AgBr composites.[3] X-ray examination of AgI alumina-fiber composites along with evidence in the literature have shown that the as-prepared composites are of a more highly conductive metastable AgI phase.[4] If this phase could be fully stabilized in the form of a composite electrolyte, it would have a conductivity comparable to the superionic Ag electrolyte materials.

---

1. Summary of paper to be published.
2. F. A. Modine, D. Lubben and J. B. Bates, *J. Appl. Phys.* 74, 2658 (1993); "Electrical Conduction in CaF_2 and CaF_2-Al_2O_3 Nanocomposite Films on Al_2O_3 Substrates," this report.
3. N. J. Dudney, *J. Am. Ceram. Soc.* **70**, 65 (1987).
4. N. J. Dudney, *J. Imag. Sci.* **34**, 104 (1990).

MAGNETRON SPUTTER DEPOSITION OF CaF_2 FILMS[1]

N. J. Dudney

Initial attempts to sputter deposit CaF_2 films with an rf-magnetron source in an argon process gas were unsuccessful because of a high resputtering rate for the film deposited on substrates positioned directly facing the surface of the target. This resputtering caused a near-zero or greatly reduced deposition rate and resulted in extremely fluorine-deficient films. Sputtering instead with a neon plasma leads to a much higher and more uniform film deposition rate, but the films are once again extremely fluorine deficient. Near-stoichiometric films were most readily achieved in either argon or neon by positioning the substrates well to the side of the target.

The near-stoichiometric films deposited with this off-axis geometry had a submicron grain or columnar microstructure which was both unstable and sensitive to exposure to moisture in the air. Subsequent annealing of the films in dry argon at relatively moderate temperatures (~100°C) stabilized the film structure and produced highly resistive, transparent films which were insensitive to air. This demonstrated that the off-axis sputtering technique may be promising for deposition of high-quality polycrystalline films of CaF_2 on near ambient temperature substrates or devices.

---

1. Summary of paper to be published.

ELECTRICAL CONDUCTION IN CaF_2 AND CaF_2-Al_2O_3 NANOCOMPOSITE FILMS ON Al_2O_3 SUBSTRATES[1]

F. A. Modine, D. Lubben, and J. B. Bates

In order to obtain an explanation of the enhanced ionic conduction in composite electrolytes, CaF_2 films and thin-film CaF_2-Al_2O_3 composites were deposited in vacuum onto Al_2O_3 substrates with interdigital electrodes, and in situ studies of the interfacial conductivity were made.

Measurements of the conductance of CaF_2 films grown on Al_2O_3 (0001) substrates disclosed an enhancement extending about 10 nm from the interface. The conductivity parallel to the substrate was 170 times the conductivity of bulk CaF_2 at 200°C. The enhancement was unstable and diminished as the logarithm of time at a thermally activated rate. However, the addition of about 10% Al_2O_3 to the films improved stability and enhanced the conductivity by a factor of 3600 over pure CaF_2 in bulk form and a factor of 7 over bulk composites.

In a space-charge interpretation, an interfacial layer of fluorine vacancies contributes a conductance given by:

$$G = 2\, e\, \lambda\, (w/l)\, U_V \sqrt{N_0 N_\infty}, \qquad (1)$$

where $\lambda = (\varepsilon\, \varepsilon_0\, kT/2\, e^2\, N_\infty)^{1/2}$ is the Debye length, U_V is the vacancy mobility, N_o and N_∞ are the vacancy concentrations at the interface and in the distant bulk, and the factor (w/l) is

contributed by the electrode geometry. The thickness of the enhancement (i.e., $2\lambda = 114$ nm) computed from Eq. (1) is an order of magnitude larger than the data suggest and gives little support for a space-charge interpretation.

The measurements suggest a microstructural interpretation. The log of time annealing behavior can be attributed to dislocation motion. If the conductance is proportional to the number of dislocations and the bulk contribution is neglected, a theory of dislocation motion suggests:

$$G = G_o\, n/n_o = G_0 \{1 - m \log [1 + (t - t_o)/\tau]\}, \quad (2)$$

$$m = (kT/n_o\, \gamma S b^3), \quad (3)$$

$$\tau = (kT/\nu \gamma S b^3) \exp (W_o/kT - 1/m), \quad (4)$$

where G_o, n_o, and t_o are initial values of conductance, dislocation number, and time, respectively; S is the yield stress; b is the interatomic distance; γ is a constant of order unity; ν is an attempt frequency; and W_o is an activation energy for dislocation climb. Equation (2) gives a good fit to the data for reasonable parameter values.

It is concluded that enhanced ionic conduction originates in microstructure. Dislocations provide paths for ionic conduction; the dislocations are mobile and anneal, but a dispersed second phase both creates and pins dislocations and, thereby, enhances the conductivity. It is demonstrated that composite materials with a record-high ionic conductivity can be fabricated as thin films.

---

1. Summary of paper: *J. Appl. Phys.* **74**, 2658 (1993).

FERROELECTRICS AND PEROVSKITE-STRUCTURE OXIDES

EPITAXIAL $YBa_2Cu_3O_7$ GROWTH ON $KTaO_3$ (001) SINGLE CRYSTALS[1]

W. Prusseit,[2] L. A. Boatner, and D. Rytz[3]

Epitaxial thin films of the high-T_c superconducting oxide $YBa_2Cu_3O_7$ have been deposited previously on a variety of single-crystal substrate materials ranging from dielectrics such as $SrTiO_3$, MgO, YSZ, Al_2O_3, and rare-earth gallates and aluminates to semiconducting materials such as silicon and GaAs. Because various device and research applications of epitaxial high-T_c films often impose stringent restrictive requirements on the film-substrate system, it is desirable to be able to select from as wide a range of substrate materials as possible.

The effects of substrate-surface preparation on the properties of epitaxial films of $YBa_2Cu_3O_7$, which were deposited by reactive thermal co-evaporation on (100) surfaces of the cubic-perovskite $KTaO_3$, have been investigated in order to develop an approach for growing consistently high-quality films on appropriately prepared potassium tantalate substrates.[4] The orientation of the $YBa_2Cu_3O_7$ crystallographic c axis in these films was perpendicular to the substrate surface throughout the complete range of deposition temperatures. Using substrates with appropriately prepared surfaces, $YBa_2Cu_3O_7$ films with a high degree of crystalline perfection which exhibited a minimum yield of 2 to 3% in the Rutherford

backscattering (RBS) channeling mode were obtained. Electronic properties which were comparable to those of films grown on $SrTiO_3$ substrates were consistently obtained, as illustrated in Fig. 3.14. The results were not affected by the presence of either Nb or Li dopants in the substrate, which indicate that it should be possible to effectively "tailor" the electro-optic properties, dielectric constant, and charge-carrier density of tantalate-based substrates over a wide range.

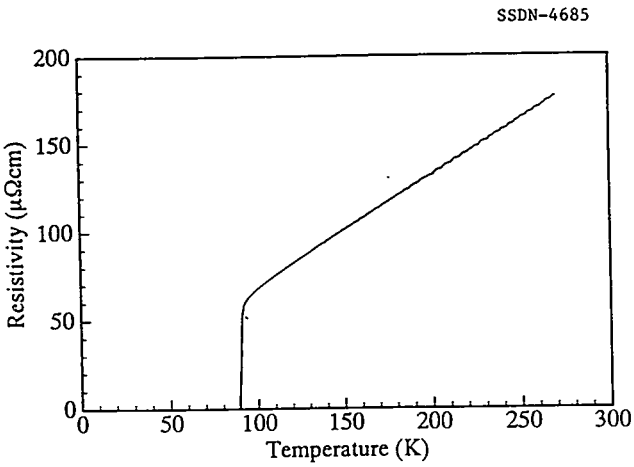

Fig. 3.14. Resistivity-vs-temperature plot illustrating the superconducting transition of a 110-nm-thick $YBa_2Cu_3O_7$ epitaxial film deposited on a $KTaO_3$ substrate.

The sensitivity of the $YBa_2Cu_3O_7$ growth to the presence of substrate-surface faults necessitates the use of carefully polished and prepared $KTaO_3$ surfaces. It may, however, be possible to make this sensitivity work to an advantage by forming artificial surface steps a few nanometers in height which could be sufficient to induce locally a-axis-oriented growth along the step edge in order to form grain-boundary Josephson junctions for SQUIL devices.

---

1. Summary of paper: *Applied Physics Letters* (in press).
2. Technical University München, Garching, Germany.
3. Centre de Recherche en Optoelectronique, Huningue, France.
4. R. Feenstra et al., *Appl. Phys. Lett.* **54**, 1063 (1989).

DOMAIN FORMATION AND STRAIN RELAXATION IN EPITAXIAL FERROELECTRIC HETEROSTRUCTURES[1]

B. S. Kwak,[2] A. Erbil,[2] J. D. Budai, M. F. Chisholm, L. A. Boatner, and W. J. Wilkens[3]

Heterostructures fabricated using a variety of semiconducting materials have been extensively investigated during the past two decades because of a high level of interest in the development of device applications for such systems. Heterostructures of materials other than semiconductors (e.g., ferroelectrics), on the other hand, have not been as extensively investigated—although the practical and fundamental potentials of such systems are high. While the study of heterostructures of metal oxides is still in the early stages of development, such systems have recently emerged as one of the most important classes of heterostructures. This emergence has been driven in part by the many novel and important physical phenomena recently observed in these systems, including high-T_c superconductivity. Progress in this area has been relatively slow, however, because of

difficulties in the growth of these materials with high crystalline quality and known defect structures.

In the present work, $PbTiO_3$ is employed as a prototype system because of its simple perovskite structure. Many compounds of this type undergo one or more structural phase transitions, and in fact, $PbTiO_3$ undergoes a cubic-to-tetragonal ferroelectric phase transition at around 770 K.

The growth of $PbTiO_3$ films by a metal-organic chemical-vapor-deposition technique has resulted in three-dimensional epitaxial heterostructures on various single-crystal substrates. These heterostructures consist of $PbTiO_3$ films on the (001) surface of the single crystals: potassium tantalate ($KTaO_3$), strontium titanate ($SrTiO_3$), and magnesium oxide (MgO). It was found that the presence of a structural (ferroelectric) phase transition in $PbTiO_3$ leads to a novel "strain-accommodating" mechanism in which a domain pattern forms as the system cools through the Curie temperature and limits the extension of interfacial strain in the heterostructure—thus minimizing the total energy of the heterostructure. For $PbTiO_3/KTaO_3$ (001), the interfacial strain is accommodated by the formation of a periodic-domain pattern in the overlayer. In $PbTiO_3/SrTiO_3$ (001), the film exists as a single c-domain. The $PbTiO_3$/MgO (001) system, having a poor lattice match for both the a and c axes, appears to find the energy minimum by locking into domains of two-dimensional superlattices with the greatest atomic coincidences. It is found that the nature of the domain pattern depends very strongly on both the film thickness and measuring temperature. A theoretical model of the domain-pattern formation has been developed using linear-elasticity theory and a Landau-Ginzburg-Devonshire-type phenomenological theory for the substrate and the overlayer, respectively.

---

1. Summary of paper: *Physical Review B* (in press).
2. Georgia Institute of Technology, Atlanta, Ga.
3. Bell Communications Research, Red Bank, N.J.

RAMAN DIFFERENCE SPECTRA OF $PbTiO_3$ THIN FILMS GROWN BY METALORGANIC CHEMICAL VAPOR DEPOSITION (MOCVD)[1]

Z. C. Feng,[2] B. S. Kwak,[3] A. Erbil,[3] and L. A. Boatner

Oxides based on the perovskite structure are characterized by a number of important physical, optical, and electronic properties, and this class of materials encompasses a number of important ferroelectric substances as well as the recently discovered high-temperature superconductors. Recent developments have shown that the MOCVD technique can be applied successfully to the growth of a number of perovskite and other types of oxide thin films, including $BaTiO_3$, $PbTiO_3$, textured MgO films, and thin films of the superconducting compound $Tl_2CaBa_2Cu_2O_y$. In the present work, the MOCVD technique has been applied to the formation of epitaxial thin films of $PbTiO_3$

that were grown on single-crystal $KTaO_3$ substrates and of polycrystalline lead titanate ($PbTiO_3$) thin films grown on fused quartz substrates.

$PbTiO_3$ is of considerable interest from both fundamental and practical points of view because it is characterized by a large spontaneous polarization, a small coercive field, and a high Curie temperature (~500°C), and therefore, it is a material with potential applications in both electronic and optical devices.

In the present case of thin $PbTiO_3$ films grown on another perovskite-structure oxide (e.g., $KTaO_3$), the separation of the Raman signals due to the substrate and film is particularly difficult because of the similarity and dominance of the substrate contribution. This difficulty has been surmounted in the present work by applying the technique of Raman difference spectroscopy. In this technique, Raman-scattering measurements are performed on both the film/substrate combination and the bare substrate; and by subtracting the contributions arising solely from the substrate, it is possible to obtain the Raman difference signal representing the Raman spectrum of the thin $PbTiO_3$ film. A comparison of the Raman spectra taken at 300 and 80 K for $PbTiO_3$ and $KTaO_3$ reveals two different types of temperature behavior, and these effects are accounted for by the soft-mode theory.

The present results represent the first report of Raman scattering from MOCVD-grown $PbTiO_3$ thin films on a perovskite substrate (e.g., $KTaO_3$), and additionally, the technique has been successfully applied to the Raman characterization of $PbTiO_3$ films grown on fused-quartz substrates.

---

1. Summary of paper: *Appl. Phys. Lett.* **62**, 349 (1993).
2. Emory University, Atlanta, Ga.
3. Georgia Institute of Technology, Atlanta, Ga.

RAMAN SCATTERING AND X-RAY DIFFRACTION INVESTIGATIONS OF HIGHLY TEXTURED $(Pb_{1-x}La_x)TiO_3$ THIN FILMS[1]

Z. C. Feng,[2] B. S. Kwak,[3] A. Erbil,[3] and L. A. Boatner

Lead lanthanum titanate $(Pb_{1-x}La_x)TiO_3$ (PLT), lanthanum-modified lead zirconate titanate $(Pb_{1-x}La_x)TiO_3$ (PLT), and lanthanum-modified lead zirconate titanate $(Pb_{1-x}La_x)(Zr_{1-y}Ti_y)O_3$ (PLZT) are ferroelectric ceramics that are characterized by a number of important physical and electronic properties, including piezoelectricity, pyroelectricity, the elasto-optic effect, and linear or quadratic electro-optic effects. Considering the existing and potential future applications of PLT and PLZT in either bulk or thin-film form, it is not surprising that a variety of film-growth techniques have been applied previously to the deposition of films of these materials on various substrates.

The thin films of PLT investigated here were deposited on (100) Si surfaces using an inverted vertical reactor.[4] X-ray diffraction (XRD), Raman spectroscopy, and energy-dispersive

x-ray analysis were used to characterize PLT films whose x values were ≤ 0.18. The XRD results established that the films had a polycrystalline structure with strong (100) texturing relative to the Si substrate. Additionally, the XRD results revealed a gradual change in the crystal structure with the system moving in the tetragonal-to-cubic sense with increasing values of x. Raman spectra, including the first spectra obtained at low temperature (i.e., 80 K), were obtained, and the results were compared with those reported previously.

The dependence of the mode frequencies on x is shown in Fig. 3.15 for the four different types of PLT films on Si substrates. As illustrated in Fig. 3.15, all the modes, with the exception of the so-called "silent mode," show some systematic change as a function of the film composition and sample temperature. The silent mode, which is neither Raman nor infrared active, exhibits a unique compositional and temperature dependence. The appearance of this feature may be attributed to the presence of disorder in the samples. Empirical trends were derived from the observed composition- and temperature-dependent behavior of the PLT Raman modes. In particular, the TO-like and LO-like modes were found to decrease and increase, respectively, with increasing x, and the silent mode did not depend on x over the range of variables investigated.

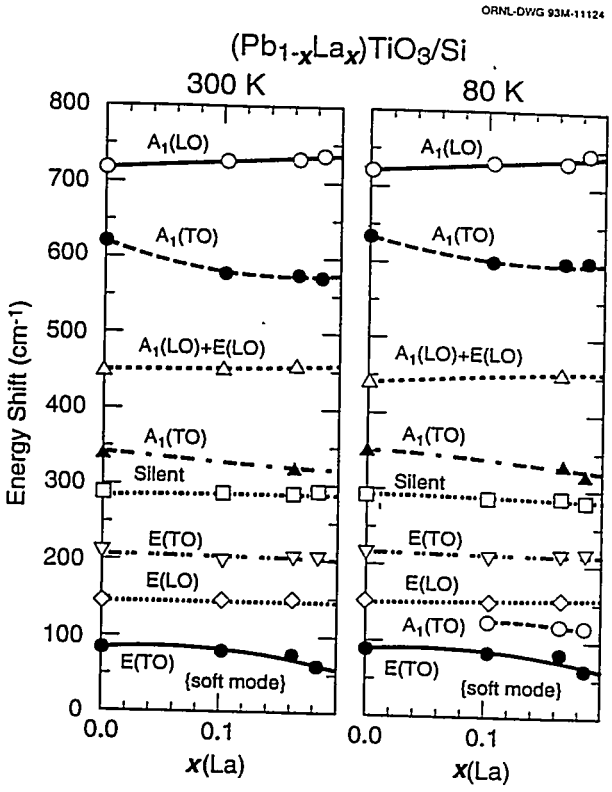

Fig. 3.15. Raman shift variations of various PLT modes with x varying from 0 to 0.18, at temperatures of 300 and 80 K.

---

1. Summary of paper: *Applied Physics Letters* (in press).
2. National University of Singapore, Singapore.
3. Georgia Institute of Technology, Atlanta, Ga.
4. Z. C. Feng et al., *Appl. Phys. Lett.* **62**, 349 (1993).

OXIDE FERROELECTRIC MATERIALS GROWN BY METALORGANIC CHEMICAL VAPOR DEPOSITION (MOCVD)[1]

A. Erbil,[2] W. Braun,[2]
B. S. Kwak,[2] B. J. Wilkens,[3]
L. A. Boatner, and J. D. Budai

The discovery of high-T_c superconductors in the layered perovskite oxides has stimulated a considerable amount of new research devoted to finding appropriate techniques for depositing perovskite-type compounds in thin-film form

for use in fundamental investigations and, ultimately, for possible microelectronics applications. Perovskite-type materials are also of interest for a variety of reasons other than high-temperature superconductivity, and many compounds of this type undergo one or more ferroelectric phase transitions. There are numerous potentially important applications of these ferroelectric oxides in the field of electronics and optoelectronics. The MOCVD technique has been established previously as a versatile thin-film growth method for compound semiconductors. Recent studies have also demonstrated its utility in the growth of perovskite oxide thin films with high-crystalline quality.

In the present investigations, various ferroelectric perovskite-type oxides were successfully grown using the MOCVD technique. Both horizontal and vertical-type reactors were used to deposit oxide thin films. However, the inverted vertical reactor had an advantage because it minimized the free-convection effects and, thereby, led to an enhanced laminar-flow pattern over the substrate. The metalorganic precursors used consisted of both solid and liquid compounds.

Results were obtained for the growth of $PbTiO_3$, $BaTiO_3$, and PZT. $PbTiO_3$ thin films grown on fused quartz and Si(100) were polycrystalline and were fully textured with the a- and c-axes perpendicular to the surface. Epitaxy was achieved on the (001) surfaces of the single crystals $KTaO_3$, $SrTiO_3$, and MgO. The prediction of thin-film properties was carried out using a Landau-Ginzburg-Devonshire-type free-energy functional. The ferroelectric properties and domain orientation of epitaxial $PbTiO_3$ thin films strongly depend on the substrate used and on film thickness in the range 200–8000 Å. The spontaneous polarization decreased with decreasing thickness for films grown on $KTaO_3$. The films grown on $KTaO_3$ were found to consist of periodic alternating a- and c-domains with 90° domain walls making an angle of about 45° with the surface.

---

1. Summary of paper: *J. Cryst. Growth* **124**, 684 (1992).
2. Georgia Institute of Technology, Atlanta, Ga.
3. Bell Communications Research, Red Bank, N.J.

POLAR FLUCTUATIONS AND FIRST-ORDER RAMAN SCATTERING IN HIGHLY POLARIZABLE $KTaO_3$ CRYSTALS WITH OFF-CENTER Li AND Nb IONS[1]

P. DiAntonio,[2] B. E. Vugmeister,[2] J. Toulouse,[2] and L. A. Boatner

Highly polarizable crystal lattices doped with ions that can occupy off-center positions offer particularly interesting opportunities for the study of collective effects associated with impurities in condensed matter. These collective effects can include impurity-induced fluctuations and phase transitions, as well as disorder and other effects. During the past 15 years, the study of highly polarizable crystalline materials such as $KTaO_3$ doped with off-center impurities has led to the observation of new types of interactions and effects.[3,4] In spite of these relatively extensive prior investigations,

the physical nature of the effects observed in systems of this type is still a subject of considerable controversy, and the experimental results have only provided partial answers to such fundamental questions as: (1) Does the system undergo a normal ferroelectric transition at low dopant concentrations or is some type of dipolar glass state formed? (2) What factors determine the critical concentration for the occurrence of a ferroelectric transition? (3) How does the physical nature of the transition evolve with increasing dopant concentration?

Accordingly, the two purposes of the present work were to contribute to a resolution of the controversy surrounding the problem of first-order Raman scattering that is observed in highly polarizable crystals doped with off-center ions and to provide new insights into the nature of the transitions observed for the KLT and KTN systems. To that effect, a detailed investigation of the Raman spectra of two of the hard modes, TO_2 and TO_3, observed in KLT and KTN crystals has been performed.

Relatively low concentrations of randomly substituted off-center ions are known to induce ferroelectric order in highly polarizable crystals. In the case of potassium tantalate ($KTaO_3$) doped with lithium or niobium, the results of first-order Raman scattering from two hard phonon modes (TO_2 and TO_3) show that polar microregions are formed at relatively high temperatures. At lower temperatures and above a certain critical dopant concentration, the Raman results are consistent with the occurrence of a structural phase transition. These results can be reasonably explained by using a random-molecular-field theory that takes into account the indirect dipolar interactions mediated by the soft lattice. This approach accounts for the characteristic asymmetry of the TO_2 Raman scattering detected at high temperatures and for the subsequent increase in the integrated scattering intensity with decreasing temperature. An analysis of the Raman results provides a means for determining the size of the polar microregions formed in the highly polarizable $KTaO_3$ lattice. The good agreement obtained between the theoretical and experimental results provides support to the physical concepts embodied in the theoretical approach developed here for describing the onset of order in these systems.

---

1. Summary of paper: *Phys. Rev. B* **47**, 5629 (1993).
2. Lehigh University, Bethlehem, Penn.
3. U. T. Höchli, H. E. Weibel, and L. A. Boatner, *Phys. Rev. Lett.* **41**, 1410 (1978).
4. R. L. Prater, L. L. Chase, and L. A. Boatner, *Phys. Rev. B* **23**, 221 (1981).

DETERMINATION OF THE A_1(TO) SOFT-MODE DAMPING RATE IN $KTa_{0.93}Nb_{0.07}O_3$[1]

P. Grenier,[2] S. Jandl,[2]
D. Houde,[2] and L. A. Boatner

The dynamical behavior associated with structural phase transitions in perovskite-structure materials is a subject of long-standing research interest and activity.[3,4] In particular, the relationship between the "relaxation-mode" vs "soft-mode" dynamics and the relative importance of "order-disorder" vs "displacive"

effects in driving the phase transition remain a subject of current controversy.[3] Recently, experiments were carried out using time-resolved third-order optical-susceptibility techniques (also called impulsive-stimulated Raman scattering or ISRS) with the goal of obtaining new insight into the dynamics of phase transitions in perovskites.[4] This previous work has shown that ISRS techniques are more appropriate for investigations of systems characterized by a highly damped vibrational mode mixed with a relaxation mode than are other optical methods.

In a previous report of the results of experiments performed on a $KTa_{0.93}Nb_{0.07}O_3$ (KTN) single crystal using the ISRS technique, it was noted that the observed damping rate of the soft-mode appears to be twice the value obtained by other techniques for similar crystals. In order to confirm this interesting observation, Raman scattering and infrared reflectivity experiments have been performed using the identical $KTa_{0.93}Nb_{0.07}O_3$ crystal investigated in Ref. 4 with a $T_c \approx 68$ K. The values obtained for the damping rate of the A_1(TO) soft-mode appear to be half those determined by impulsive-stimulated Raman scattering. Because the latter experiments probe the soft-mode in the polariton regime while the former probes outside this region, the observed discrepancy points toward some additional interaction for the polariton soft mode.

Similar behavior has been observed in other samples, and these results suggest the existence of important interactions between the polariton and low-frequency excitations. Currently, time-resolved third-order optical susceptibility measurements as a function of polariton wave vector and temperature are being performed to investigate these interactions further.

---

1. Summary of paper: *Canadian Journal of Physics* (in press).
2. Université de Sherbrooke, Sherbrooke, Canada.
3. E. Lee, L. L. Chase, and L. A. Boatner, *Phys. Rev. B* **31**, 1438 (1985).
4. P. Grenier et al., *Phys. Rev. B* **47**, 1 (1993).

POLARIZATION AND CRYSTAL-GEOMETRY DEPENDENCES OF THE NONLINEAR OPTICAL RESPONSES OF $KTa_{1-x}Nb_xO_3$ CRYSTALS AFTER PICOSECOND-PULSE LASER EXCITATION[1]

H. Liu,[2] R. J. Reeves,[2]
R. C. Powell,[2] and L. A. Boatner

The mixed-crystal system $KTa_{1-x}Nb_xO_3$ (KTN) is of particular interest among perovskite-structure ABO_3 materials[3,4] because at room temperature it undergoes a phase transition from the cubic paraelectric phase to tetragonal and orthorhombic ferroelectric phases as the niobium concentration x increases from 0 ($KTaO_3$) to 1 ($KNbO_3$). In recent years, research efforts have focused on understanding the mechanisms responsible for these structural changes. The soft-mode contributions to the linewidth of the central peak were determined in orthorhombic $KNbO_3$ from inelastic light scattering.[4] These components have the linewidths, line shapes, and thermal properties of relaxation modes and symmetry properties consistent with an eight-site order-disorder model for successive phase transitions. The

different structural phases are a consequence of the preferential occupation of a certain set of potential minima by the B ions. The dynamic aspects of this model predict relaxation modes in which the B ions (Nb or Ta) move from one equilibrium site to another in the multiwell potential. This movement of ions between potential minima manifests itself in the presence of hopping modes parallel and perpendicular to the polar axis.

In order to enhance our understanding of these polar ion hopping modes and other fast physical processes in this class of materials, degenerate four-wave-mixing (DFWM) studies of KTN crystals have been initiated using a picosecond-laser excitation source.

In the present investigations, the fast nonlinear optical signals on picosecond and nanosecond time scales have been studied in the mixed-crystal system $KTa_{1-x}Nb_xO_3$ using transient DFWM. The two distinct signal components, denoted as an instantaneous response and slow response in previous studies,[5] changed intensity as the niobium concentration was varied. The dependences of these signals on the crystal orientation and the polarization configuration of the optical pulses were characterized. The results were consistent with a lattice-relaxation model based on the laser-induced dynamic displacement of the Nb ion. In this model, the signal variations result from the competition between the dynamic displacement and intrinsic distortion associated with the spontaneous polarization along the optic axis.

---

1. Summary of paper: *Physical Review B* (in press).

2. Oklahoma State University, Stillwater, Okla.
3. J. Toulouse, X. M. Wong, and L. A. Boatner, *Solid State Commun.* **68**, 353 (1988).
4. J. P. Sokoloff, L. L. Chase, and L. A. Boatner, *Phys. Rev. B* **41**, 2398 (1990).
5. H. Liu, R. C. Powell, and L. A. Boatner, *Phys. Rev. B* **44**, 2461 (1991).

INFRARED ABSORPTION INVESTIGATIONS OF OH IMPURITIES IN DOPED $KTaO_3$ SINGLE CRYSTALS[1]

S. Jandl,[2] J. Rousseau[2] and L. A. Boatner

Hydrogen impurities are generally present in single crystals of the perovskite-structure oxides $KTaO_3$ and $SrTiO_3$ in the "as-grown" state.[3,4] Hydrogen impurities can also be intentionally introduced at higher concentrations by annealing these crystals at elevated temperatures in water-vapor-containing ambients. The presence of hydrogen in these materials is manifested in the observation of infrared-absorption bands that correspond to the OH-stretching mode and that occur in the vicinity of 3480 cm^{-1}. Usually these bands consist of a primary intense absorption plus one or more weaker "satellite" bands. The fundamental properties of hydrogen in $KTaO_3$ and $SrTiO_3$ have been the subject of a number of previous spectroscopic studies that have led to two different proposed crystallographic locations for the incorporation of hydrogen in the perovskite lattice.

The present work reports the results of infrared-absorption measurements as a function of temperature of hydroxyl radicals in pure $KTaO_3$ crystals doped with either Ni, Co, or Nb. The objectives of this work are, first, to

determine the effects of the different dopants on the OH-stretching mode (including the influence of the ferroelectric soft mode in the case of the Nb-doped material); second, to evaluate the validity of the cubic-face model vs the octahedron-edge model for the location of the hydrogen; and, third, to confirm the infrared-active character of the previously observed Raman-active OH stretching mode as affected by the ferroelectric soft mode.

Two distinct infrared-absorption bands associated with the stretching mode of OH radicals have been observed in pure $KTaO_3$ and in doped $KTaO_3$ single crystals. In the absence of the ferroelectric phase transition that occurs for the KTN case, the effects due to doping are restricted to band broadening without affecting the frequency. The identical three frequencies observed in Raman scattering are also detected in the splitting of band 1 that occurs at low temperatures. The relatively reduced intensity of the outer bands observed for pure $KTaO_3$ and for Ni- and Co-doped $KTaO_3$ indicates that the influence of the soft mode is greatly reduced in the nonferroelectric materials as compared with that characteristic of KTN below the ferroelectric transition temperature where the three infrared-absorption bands are of comparable intensity. Bands 1 and 2 are consistent with the occupation of site locations that are described by both the crystal-face and octahedron-edge models—both of which predict a triplet structure at low temperatures so that the hydrogen may be located either along the cube-face diagonals or along the oxygen-oxygen bonds.

---

1. Summary of paper: *Solid State Communications* (in press).
2. Universite de Sherbrooke, Sherbrooke, Quebec, Canada.
3. H. Engstrom, J. B. Bates, and L. A. Boatner, *J. Chem. Phys.* **73**, 1073 (1980).
4. R. Gonzalez et al., *J. Chem. Phys.* **78**, 660 (1983).

MATERIALS PROPERTIES

UNSTABLE NECK FORMATION DURING INITIAL-STAGE SINTERING[1]

J. Rankin[2] *and L. A. Boatner*

Previous fundamental investigations of the coalescence of particles during the initial stages of sintering have frequently employed idealized systems consisting of polycrystalline, micron-sized particles with approximately circular cross sections. The experimental approach used in these previous sintering studies usually consisted of ex situ microscopic observations of the particles subsequent to heat treatment to produce neck formation and coalescence through mass transport processes. In one of the more significant early sintering investigations[3] (whose results, in fact, provided the basis for the development of initial-stage sintering theory), polycrystalline copper cylinders were sintered onto flat copper plates by conventional furnace

heating and were then mechanically cross-sectioned. The neck morphologies were subsequently examined and analyzed ex situ using optical microscopy. Numerous intervening studies of the alterations in neck and pore morphologies that occur during the sintering of both ceramic and metal systems have been carried out,[4] but with one exception, these investigations have been based on ex situ observations. Such ex situ analytical methods are not capable of addressing a number of critical issues because these studies can only provide average measurements subsequent to the evolution of the neck morphology and particle size that are "averaged" over the total time of the heating cycle. In contrast to most of the previous work in this area, continuous transmission electron microscopy (TEM) observations of the particle size and neck morphology as they evolve during the initial-stage sintering of faceted particles heated in situ on a hot stage mounted in the microscope have been carried out. The present application of this experimental approach to the TEM/video observation of the initial-stage coalescence of cubic-faceted, single-crystal MgO particles has led to the discovery of a fundamental neck instability for certain particle-contact geometries.

These studies show that the initial-stage sintering behavior of cubic-faceted MgO particles is strongly dependent on the initial particle-contact geometry. Particle pairs in face-to-face contact form stable necks which continue to grow as the two particles coalesce into one nonfaceted particle. In contrast to this behavior, particle pairs with corner-to-corner or edge-to-edge contact form necks that initially grow, but subsequently shrink and abruptly break. These findings are quite general since they are potentially relevant in any system where small contact areas and large contact angles are found and where high-energy sources of material are present; they are not limited to systems of cubes or highly symmetric faceted particles.

---

1. Summary of paper: *Journal of the American Ceramic Society* (in press).
2. Consultant from Brown University, Providence, R.I.
3. G. C. Kuczynski, *J. Trans. AIME* **185**, 796 (1949).
4. *Sintering—Key Papers*, S. Somiya and Y. Moriyoshi, Eds., Elsevier Science Publishing Co., Inc., New York, 1989.

TEXTURED COATINGS FROM COLLOIDAL SUSPENSIONS OF FACETED OXIDE MICROCRYSTALS[1]

G. W. Steadman,[2] J. R. Brewster,[3] J. D. Budai, and L. A. Boatner

Achieving full control of the microstructural properties of ceramics both in the form of bulk materials and as coatings encompasses, in general, controlling not only the component grain sizes and shapes but also the relative orientations of these constituent microstructural grains as well. Until recently, most ceramic microstructural research has primarily emphasized the development of techniques for controlling the grain size and shape, and an additional level of control involving the development of preferred orientations or "texturing" in ceramic microstructures has

received relatively little attention. The present work investigates the potential for exploiting the morphological properties of faceted particles of MgO in order to form ceramic coatings with various degrees of crystallographic alignment. Coatings exhibiting a <100> "fiber" texture were formed by centrifugal sedimentation of colloidal suspensions onto a flat substrate. In each case, the substrate was a highly polished, single-crystal silicon wafer.

In order to deposit centrifugally the MgO coatings, colloidal suspensions of the faceted MgO particles were first prepared by ultrasonically dispersing the faceted MgO powder in isopropyl alcohol. By predetermining the weight of the powder relative to the volume of isopropanol, coatings with known thicknesses could be deposited.

X-ray powder diffraction was employed in investigating variations in the degree of texturing as a function of the thickness of the coatings formed using faceted MgO particles. A sequence of 5 θ–2θ x-ray powder diffraction patterns is shown in Fig. 3.16 for specimens with coverages in the range 0.1–5.0 μ. The relatively high degree of preferred fiber texture that is evident for coverage below 0.5 μ is gradually lost as direct contact between the faceted particles and the flat Si substrate is lost. Nevertheless, some degree of fiber texture can

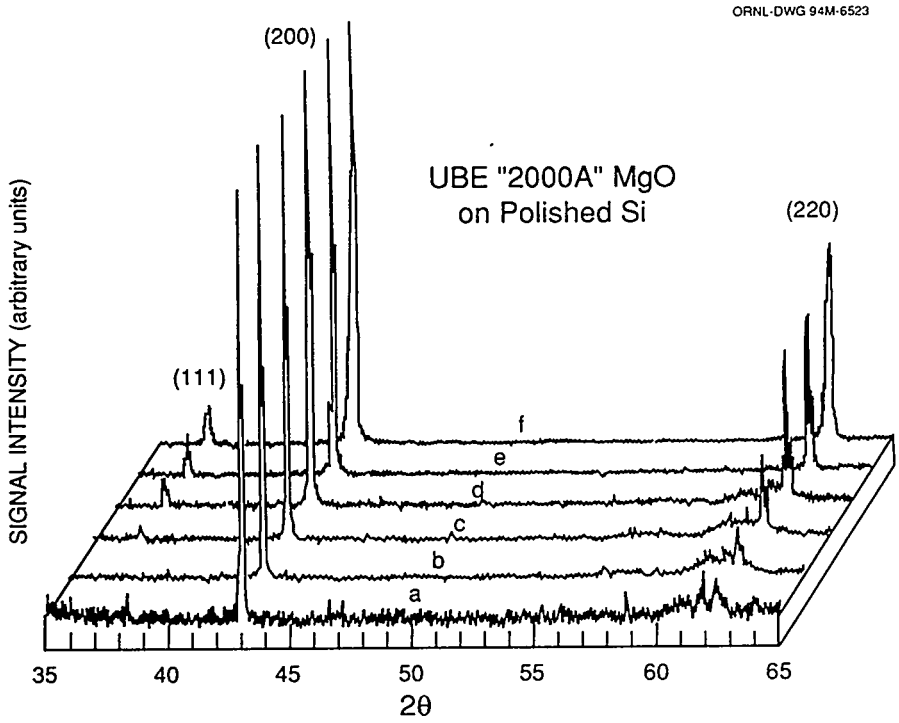

Fig. 3.16. X-ray diffraction patterns of various areal coverages for centrifugally deposited MgO: (a) 0.1, (b) 0.5,. (c) 1.0, (d) 3.0, (e) 5.0 mm, and (f) powder.

be maintained even for relatively thick centrifugal deposits.

These results show that the morphological properties of faceted MgO particles can be readily exploited in the formation of ceramic coatings that are characterized by a relatively high degree of fiber texture—even in the case of relatively thick deposits.

---

1. Summary of paper: *Mat. Res. Soc. Symp. Proc.* **286**, 33 (1993).
2. DOE Science and Engineering Research Semester student from the University of Southern Colorado, Colorado Springs, Colo.
3. ORNL/ORISE postdoctoral research associate.

STRUCTURAL PROPERTIES OF THE AMORPHOUS PHASES PRODUCED BY HEATING CRYSTALLINE $MgHPO_4 \cdot 3H_2O$[1]

B. C. Sales, B. C. Chakoumakos
L. A. Boatner, and J. O. Ramey

The crystalline phosphate $MgHPO_4 \cdot 3H_2O$ (newberyite) undergoes an unusual crystalline-to-amorphous transition when heated. The structural alterations associated with this transition have been investigated using high-performance liquid chromatography (HPLC) (Fig. 3.17), differential scanning calorimetry (DSC), thermogravimetric analysis, and x-ray diffraction (XRD). The dehydration of newberyite on heating results in amorphous XRD patterns that remain essentially unchanged over the interval between 150 and 600°C. Over the same temperature interval, however, HPLC results reveal a dramatic continuous evolution in

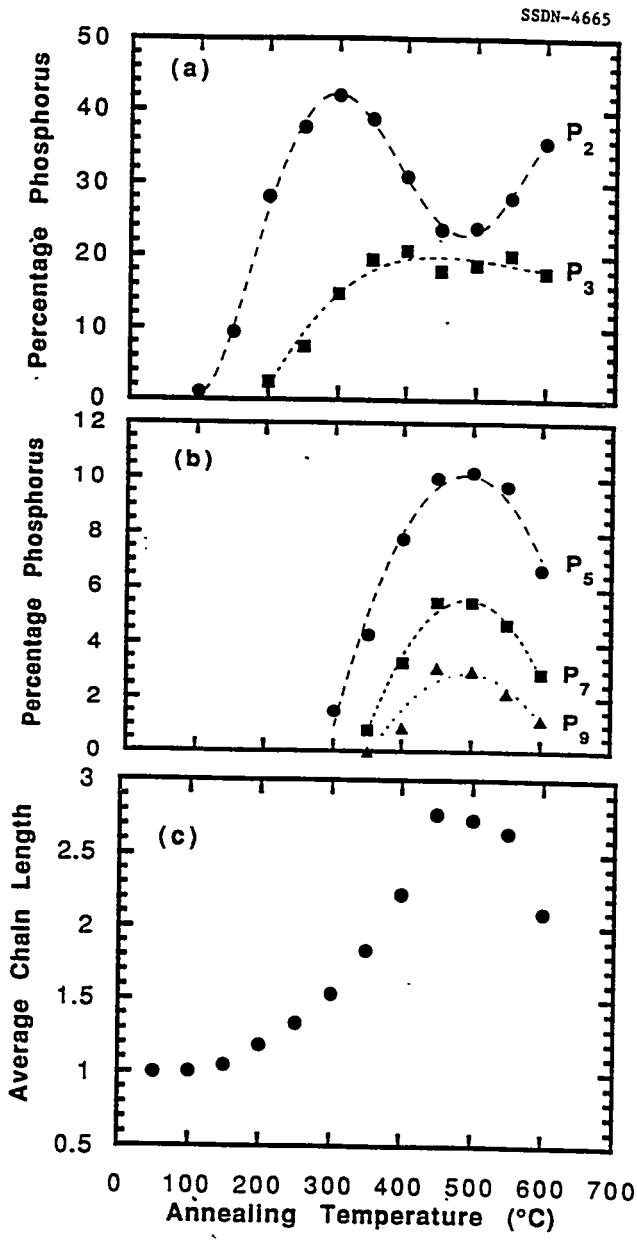

Fig. 3.17. Results from an analysis of the chromatograms for $MgHPO_4 \cdot 3H_2O$ samples annealed in flowing oxygen at temperatures between room temperature and 600°C. (a) Percentage of phosphorus present in the P_3 and P_2 phosphate anions as a function of annealing temperature. (b) Percentage of phosphorus present in the P_5, P_7, and P_9 anions. (c) Average phosphate chain length at each annealing temperature.

the distribution of phosphate chains of corner-linked PO_4 tetrahedra leading to the formation of chains up to 13 PO_4 tetrahedra in length. Above 600°C, crystalline $Mg_2P_2O_7$ is formed. At each annealing temperature in the interval from 150 to 600°C, the measured distribution of phosphate anions is in quantitative agreement with theory. During the dehydration-induced crystalline-to-amorphous transition, the original faceted crystal shape is preserved even though the crystals lose up to 36% of their original weight. High-pressure DSC experiments in which the waters of hydration were retained in the specimens during heating resulted in the formation of a unique new crystalline phosphate phase that contained equal amounts of orthophosphate and pyrophosphate anions. The results of HPLC, DSC, and XRD measurements on $CaHPO_4{\cdot}2H_2O$, $SrHPO_4$, and $BaHPO_4$ were also investigated.

---

1. Summary of paper: *J. Non-Cryst. Solids* 159, 121 (1993).

CHROMATOGRAPHIC DETERMINATION OF THE PHOSPHATE ANIONS IN CRYSTALLINE AND GLASSY $Na_4NbP_3O_z$[1]

B. C. Sales and B. C. Chakoumakos

Crystalline $Na_4NbP_3O_z$ was found by Jazouli et al.[2,3] to exhibit a reversible crystalline-to-glass phase change. On the basis of Raman and optical investigations, they concluded that the crystalline phase was an orthophosphate with a structure similar to the NASICON structure; hence, the crystalline composition was given as $Na_4Nb(PO_4)_3$. Very few orthophosphates convert to the glassy phase by conventional melt quenching, which made this material even more intriguing. This observation was also made by Prabakar and Rao,[4] who concluded on the basis of magic-angle spinning ^{31}P nuclear magnetic resonance (NMR) spectroscopy that the local phosphorus environments were quite different in the glassy and crystalline forms of $Na_4Nb(PO_4)_3$. They suggested that the crystalline material was actually a metaphosphate, which would account for the relative ease of glass formation as well as the change in local environments suggested by the NMR spectra. If single crystals of $Na_4NbP_3O_z$ could easily be produced, x-ray or neutron diffraction techniques could determine precisely the structure. For the glassy phase, however, diffraction techniques provide limited structural information.

High-performance liquid chromatography (HPLC) provides another approach to the resolution of some of the structural questions concerning crystalline and glassy $Na_4NbP_3O_z$. The HPLC technique is only sensitive to the distribution of phosphate anions present in the solid and is applicable to a large number of metal-phosphate materials. HPLC measurements on crystalline and glassy $Na_4NbP_3O_z$ (Fig. 3.18) prove that the crystalline phase is a pyrophosphate and that the glassy material contains a distribution of phosphate anions with anions up to five PO_4 tetrahedra in length. Powder x-ray diffraction data for a new trimetaphosphate crystalline

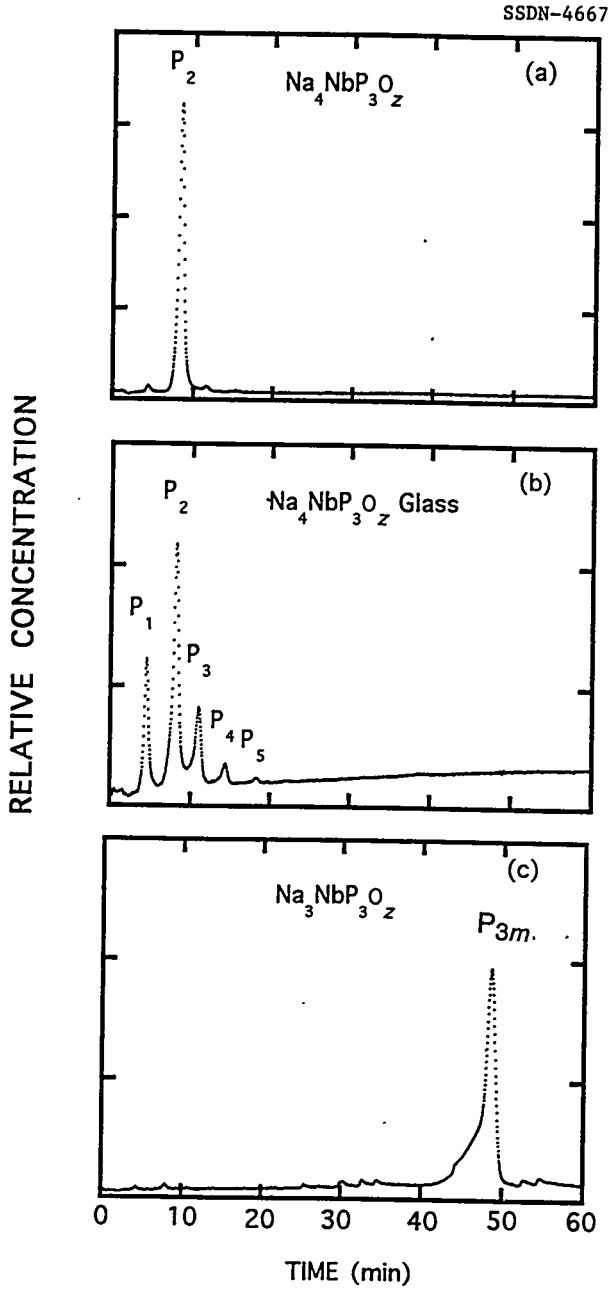

Fig. 3.18. Chromatograms from (a) crystalline $Na_4NbP_3O_z$, (b) $Na_4NbP_3O_z$ glass, and (c) crystalline $Na_3NbP_3O_z$. Phosphate anions consisting of 1, 2, 3, ..., n corner-linked PO_4 tetrahedra are labeled in the figure as P_1, P_2, P_3, ..., P_n. The cyclic phosphate anion, trimetaphosphate, is denoted by P_{3m}.

phase with the composition $Na_3NbP_3O_z$ are also reported.

---

1. Summary of paper: *J. Solid State Chem.* **105**, 406 (1993).
2. A. E. Jazouli et al., *C. R. Acad. Sci. Paris Ser.* 2 **303**, 1005 (1986).
3. A. E. Jazouli et al., *J. Solid State Chem.* **74**, 377 (1988).
4. S. Prabakar and K. J. Rao, *J. Solid State Chem.* **91**, 186 (1991).

MICROSTRUCTURAL FORMATION IN LONGITUDINAL BICRYSTAL WELDS[1]

M. Rappaz,[2] J. M. Vitek,[3] S. A. David,[3] and L. A. Boatner

In order to investigate the grain-selection mechanisms that are operative during the welding of polycrystalline metals, a number of investigations which employed welds of single crystals of austenitic stainless steel have recently been performed.[4,5] For these systems, it was found that epitaxial growth of dendrites from the unmelted substrate was the dominant mechanism in determining the microstructural features and that, in fact, the single-crystal nature of the base material was retained in the weld trace.

In the present work, the dendrite trunk-selection analysis that was developed previously for single-crystal welds is systematically applied to the more complex case of welds of two single crystals with different crystallographic

orientations. The formation and selection processes in dendritic microstructures that occur during the welding of two differently oriented Fe-15 wt. % Ni-15 wt. % Cr single-crystal pieces were analyzed. The specimens were oriented and cut along precise crystallographic orientations in order to weld specific surfaces in a manner that joined two predetermined crystallographic directions. Six orientation configurations were selected in the present investigation: a (001) surface with a [100] or [110] direction, a (011) surface with a [100], $[01\bar{1}]$, or $[2\bar{1}1]$, and a (111) surface with a $[2\bar{1}\bar{1}]$ direction. Using all the possible combinations, two crystal halves were welded along their boundary using an electron beam to form longitudinal bicrystal welds. Experimental and simulated metallographic sections have been directly compared for the bicrystal-weld configurations. The dendritic pattern observed in transverse-metallographic sections was analyzed for each single-crystal half on the basis of a selection criterion that had been developed previously for single-crystal welds [i.e., at a given location in the melt pool, the selected (100) dendrite trunk has a minimum undercooling or, equivalently, a minimum velocity]. In general, the bicrystal-weld microstructure is a simple composite of microstructures expected in each of the two single-crystal halves. However, near the weld center line, it was shown that grain competition between dendrites belonging to different single crystals also occurred according to this same minimum undercooling criterion. This competition is known to occur either by the disappearance of less favorably oriented dendrite trunks or by branching mechanisms giving rise to a new trunk from a tertiary arm. Accordingly, a full picture of this grain competition can only be given if the grain boundary is specified with respect to the heat-flow direction. Additional work is currently under way to analyze this competition in transverse bicrystal welds.

---

1. Summary of paper: *Metall. Trans. A* **24,** (1993).
2. Ecole Polytechnique Fédérale de Lausanne, Lausanne, Switzerland.
3. Metals and Ceramics Division, ORNL.
4. M. Rappaz et al., *Metall. Trans. A* **20,** 1125 (1989).
5. M. Rappaz et al., *Metall. Trans. A* **21,** 1767 (1990).

MODELING OF SINGLE-CRYSTAL LASER-WELD MICROSTRUCTURES[1]

J. M. Vitek,[2] T. Zacharia,[3] S. A. David,[2] M. Rappaz,[3] and L. A. Boatner

In recent years, numerous advances have been made in the field of heat and fluid-flow modeling in welds. These previous studies have provided much-needed insight as to what variables and conditions have a strong influence on the development of the weld pool and are valuable in and of themselves because they serve to predict the weld-pool shape and penetration. Heat and fluid-flow modeling can also be a valuable aid in attempting to understand and predict the development of the solidification microstructure in a weld. Accurate and reliable models can provide information that is often unavailable or extremely difficult to obtain

experimentally, but which plays a fundamental role in determining the nature of the solidification microstructure.

The purpose of the present investigation is to combine the two fields of heat and fluid-flow modeling and microstructural development in single-crystal welds in order to model and predict the solidification microstructure in laser-welded single crystals. The application of heat and fluid-flow modeling to the study of microstructural development in single crystals is an ideal case because the welded microstructure in single crystals is controlled almost exclusively by the weld-pool geometry, which can be readily calculated.[4,5]

A heat and fluid-flow model has been used to calculate the weld-pool size and shape for a high-speed, single-pass laser weld as a function of time. Based on the calculated weld-pool shape and with the use of a geometric model relating the dendrite growth to the weld-pool shape, a dendrite growth pattern was calculated for a single-crystal laser weld with a (001) surface that was welded along the [100] direction. The calculated results were compared with an actual experimental laser weld of an Fe-15Cr-15Ni alloy for the same orientation and weld direction. Agreement was obtained between the calculations and experimental observations, and an experimental dendritic growth pattern was accurately reproduced.

The following conclusions can be drawn: (1) The microstructure of single-crystal welds can be calculated from first principles. (2) Features that can be calculated include weld-pool size and shape, active dendritic growth directions, and the resultant dendritic growth pattern. (3) Reasonable agreement was found between the calculated and the observed microstructures. (4) Comparison of the calculated and observed microstructures in single-crystal welds provides an accurate means of evaluating the three-dimensional weld-pool-shape calculations.

---

1. Summary of paper: *Plasma and Laser Processing of Materials* (in press).
2. Metals and Ceramics Division, ORNL.
3. Guest scientist from the Ecole Polytechnique Fédérale de Lausanne, Lausanne, Switzerland.
4. M. Rappaz et al., *Metall. Trans. A* **21**, 1767 (1990).
5. M. Rappaz et al., *Metall. Trans. A* **20**, 1125 (1989).

OPTICAL CHARACTERIZATION OF MATERIALS

CERIUM-DOPED ORTHOPHOSPHATES: NEW PROMISING SCINTILLATORS[1]

A. Lempicki,[2] E. Berman,[2] A. J. Wojtowicz,[2] M. Balcerzyk,[2] and L. A. Boatner

There are at the present time two generic types of scintillators which use the Ce^{3+} ion as the light-emitting species. They fall into the category of "concentrated" or stoichiometric compounds in which Ce is a chemical constituent (e.g., CeF_3) and "diluted" or doped compounds [e.g., $Lu_2(SiO_4)O$ (LSO) and GSO, the latter being an analog of LSO, but incorporating Gd instead of Lu]. There is no question

that given the present state of knowledge, the doped compounds hold the lead as far as light output is concerned.

Lutetium orthophosphate ($LuPO_4$) doped with cerium and other rare earths is a material that has been the subject of extensive spectroscopic investigations concerned mostly with Raman scattering and various nonlinear effects. The luminescence of $LuPO_4$:Ce, however, has not been investigated in any detail. The effective Z number of this material is 63.7; the present studies are devoted to the delineation of the photoemission and scintillation aspects of this remarkable compound. To our knowledge, this is the second lutetium compound doped with cerium which exhibits superior scintillation properties. The first compound is Ce:$Lu_2(SiO_4)O$, which was discovered by Melcher and Schweitzer.[3] The two compounds share the properties of high density, a very fast decay time of a few tens of nanoseconds, and an efficiency higher than bismuth germanium oxide (BGO). These properties make these materials prime contenders for medical applications such as positron emission tomography. Because it is both fashionable and useful to abbreviate the names of these compounds, the Lu orthophosphate is referred to as LOP. A comparison of the basic characteristics of these scintillators is given in Table 3.2.

The results summarized in Table 3.2 show that Ce-doped $LuPO_4$ is a promising new scintillator, which under γ-excitation shows fast, single-exponential decay of 25 ns at room temperature, and a light output of 17,200 photons per 1 MeV. These features, combined with a reasonable density (6.53 g/cm^3), make it a strong contender for many applications.

---

1. Summary of paper: *IEEE Trans. Nucl. Sci.* **40**, 384 (1993).
2. Boston University, Boston, Mass.
3. C. L. Melcher and J. S. Schweitzer, *IEEE Trans. Nucl. Sci.* **39**, 502 (1992).

Table 3.2. Comparison of Ce-Doped Lutetium Compounds with BGO

	BGO	LOP	LSO
Relative light output	100	217	500
Emission wavelength (nm)	480	360	420
Decay constant (ns)	300	24	40
Density (g/cm^3)	7.13	6.53	7.4
Attenuation length (cm)	1.10	1.43	1.22
Index of refraction	2.15	1.7	1.82

TWO-PHOTON EXCITATION OF THE $4f^1 \rightarrow 5d^1$ TRANSITIONS OF Ce^{3+} IN $LuPO_4$ AND YPO_4[1]

J. Sytsma,[2] *D. Piehler,*[2] *N. M. Edelstein,*[2]
L. A. Boatner, and M. M. Abraham

The past decade has witnessed an increasing interest in the two-photon spectroscopy of lanthanide ions. This type of spectroscopy can be divided into two groups: (a) two-photon excitation (TPE), in which two photons are absorbed simultaneously by the lanthanide ion, and (b) electronic Raman scattering (ERS), in which a photon is inelastically scattered from an ion such that the ion is excited to a different electronic state. Both processes are parity-allowed for the $4f \rightarrow 4f$ transitions and are to be considered as complementary to single-photon spectroscopy.

ERS is especially suited to the study of low-lying energy levels. Despite a large amount of single-photon spectroscopic data for Ce^{3+} in the orthophosphates, only the first $5d^1$ level has been determined accurately. The goal of the present work, therefore, was to apply TPE to Ce^{3+} in $LuPO_4$ in order to obtain this information for the other $5d^1$ levels as well. One practical stimulus for the study of Ce^{3+} in orthophosphate hosts is their very promising scintillator characteristics, plus their potential as nuclear waste storage hosts and as a tunable UV-laser material. The $4f^1$ crystal-field components of Ce^{3+} have energies up to $\approx$2500 cm^{-1}. The positions of all seven crystal-field components were determined previously, and resonance-enhancement effects were studied.

In the present work, TPE spectra of the $4f^1 \rightarrow 5d^1$ transitions of Ce^{3+} in $LuPO_4$ and YPO_4 were observed as zero-phonon lines. The symmetry properties of the levels were obtained from the polarization dependence of the TPE signals. Measurements on Ce^{3+} in YPO_4 supported the assignments. Although a crystal-field fit yields a satisfactory rms energy deviation, an unrealistic value of the spin-orbit coupling parameter $\zeta(5d^1)$ was obtained. The vibronic coupling appears to be smaller than for the single-photon absorption spectra, and the vibronic bands show a rich structure. There are striking differences between the energies and the relative intensities of the vibronic lines and the associated zero-phonon lines. The vibronic coupling is also found to be strongly dependent on the Ce^{3+} concentration. Since the $5d^1$ configuration is not shielded from the crystal environment, as is the $4f^1$ configuration, this effect in itself is expected, but is surprisingly noticeable for small changes in the Ce^{3+} concentration.

In order to understand TPE of Ce^{3+}, it is essential to carry out a systematic study of these vibronic effects. A comparison should be made for Ce^{3+} in different host lattices in a manner similar to that used in the case of single-photon spectroscopic studies of Gd^{3+}.

---

1. Summary of paper: *Phys. Rev. B* **47**, 14786 (1993).
2. Lawrence Berkeley Laboratory, Berkeley, Calif.

ZERO-FIELD SPLITTING OF Cm^{3+} IN $LuPO_4$ SINGLE CRYSTALS[1]

W. K. Kot,[2] N. M. Edelstein,[2] M. M. Abraham, and L. A. Boatner

Because of the essentially spherical symmetry of the wave function associated with the predominantly $L = 0$ ground states of transition-series ions with half-filled shells (so-called S-state ions), only higher order interactions are possible with a surrounding crystalline environment. Such higher order interactions do, in fact, occur and result in splittings of S ground states that are observed experimentally. In the course of the past almost 60 years, various mechanisms or combinations of mechanisms have been proposed to account for the ground-state splittings of S-state ions as revealed in the relatively extensive experimental electron paramagnetic resonance (EPR) and magnetic susceptibility results for ions of this type.

Despite various prior theoretical attempts to account for the experimental findings, the nature of the interactions responsible for the ground-state splittings of S-state ions is, in general, still not well-understood. In the particular case of S-state ions associated with half-filled shells in the $4f$ and $5f$ transition series (i.e., $4f^7$ and $5f^7$ electronic configuration ions such as Eu^{2+}, Gd^{3+}, Tb^{4+} or Am^{2+}, Cm^{3+}, and Bk^{4+}) however, the significant differences that are found in the magnitude of the experimentally determined ground-state splittings can be qualitatively accounted for by a consideration of the effects of intermediate coupling.[3] The associated significantly larger admixture of non-($L = 0$) states results in a Cm^{3+} ground-state wave function that is only 79% pure $^8S_{7/2}$. These significant differences in the non-S-state character of the ground-state wave functions of Gd^{3+} and Cm^{3+} are directly manifested in differences in the effects that a crystalline environment has on ground-state splittings.

The present work represents an extension of our previous investigations[3] of crystal-field-induced splittings of the ground state of Cm^{3+} in the tetragonal-symmetry host single-crystal $LuPO_4$, where an excited-state EPR transition was observed.

This work reports the results of EPR, optical absorption, and fluorescence measurements for Cm^{3+} in $LuPO_4$. Here, the use of the isotope ^{248}Cm with its 3.4×10^5 year half-life and lower specific activity reduced the broadening of the absorption lines induced by internal radiation damage. Through the use of these higher quality samples, the EPR observation of an additional "interdoublet" transition was possible. Additionally, more accurate measurements of the "intradoublet" transitions were made using higher microwave frequencies (Q-band) rather than the X-band frequencies employed previously. The additional magnetic resonance and optical data obtained here have led to a more accurate determination of the Cm^{3+} energy-level structure. Finally, the room-temperature Cm^{3+} magnetic resonance spectrum reported represents the observation of an EPR transition at room temperature for an actinide ion.[4]

---

1. Summary of paper: *Phys. Rev. B* **48**, 12704 (1993).

2. Lawrence Berkeley Laboratory, University of California, Berkeley, Calif.
3. M. M. Abraham and L. A. Boatner, *Phys. Rev. B* **26**, 1434 (1982).
4. L. A. Boatner and M. M. Abraham, *Rep. Prog. Phys.* **41**, 87 (1978).

ELECTRON PARAMAGNETIC RESONANCE (EPR) OF Pu^{3+} AND Cf^{3+} IN SINGLE CRYSTALS OF $LuPO_4$[1]

W. K. Kot,[2] *N. M. Edelstein*[2]
M. M. Abraham, and L. A. Boatner

The EPR spectrum of the ion Pu^{3+} ($5f^5$ electronic configuration) in the form of a dilute impurity has been investigated previously for a number of host single crystals. For the hosts employed in these previous studies, the symmetry properties were such that the local crystal-field environment of the Pu^{3+} ion was characterized by cubic symmetry. The cumulative results emerging from these previous spectroscopic investigations have established that in contrast to the case of the $4f$ lanthanide ions, for the $5f$ actinide ions, intermediate-coupling effects play an important role in determining the properties of the electronic energy levels. In particular, in the case of Pu^{3+}, the $J = 5/2$ manifold ground state was found to contain only 66% of the pure $^6H_{5/2}$ state, with the remainder of the wave function consisting of other $J = 5/2$ states admixed by intermediate-coupling effects.

In the present study of actinide electronic properties, EPR spectroscopy has been used to investigate the ground-state properties of the actinide ions Pu^{3+} ($5f^5$) and Cf^{3+} ($5f^5$) incorporated as dilute impurities in single crystals of the tetragonal-symmetry host $LuPO_4$. The Pu^{3+} and Cf^{3+}-doped tetragonal single crystals of $LuPO_4$ employed in the present spectroscopic studies were grown in a glove-box-contained, platinum-wound furnace using a flux technique.[4]

As illustrated in Fig. 3.19, the g values of the electronic ground states were determined experimentally at a sample temperature of 4 K. These

SSDN-4687

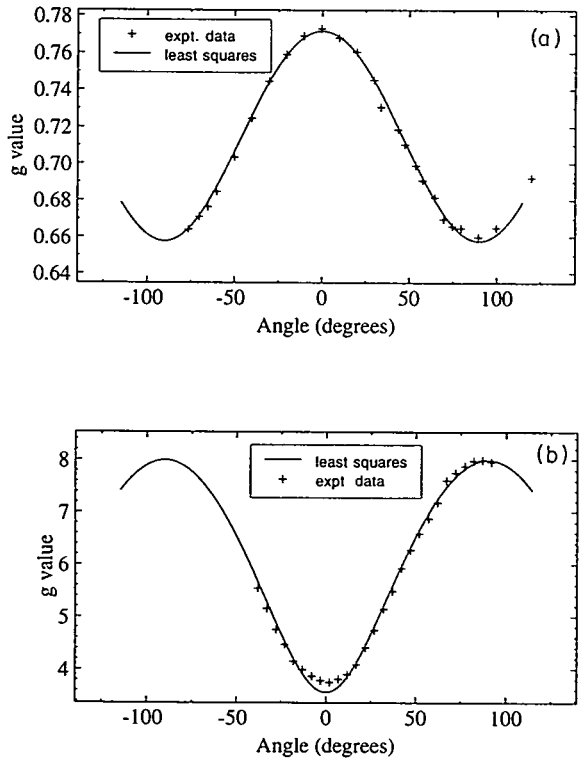

Fig. 3.19. Experimental EPR measurements as a function of the angle between the crystallographic c axis and magnetic field. The solid curves represent a least-squares fit of the data to the expression $g^2 = g_{\|}^2 \cos^2\theta + g_{\perp}^2 \sin^2\theta$. (a) $Pu^{3+}/LuPO_4$, microwave frequency of 9.223 GHz, $g_{\|} = 0.772(2)$, and $g_{\perp} = 0.658(2)$. (b) $Cf^3/LuPO_4$, microwave frequency of 9.217 GHz, $g_{\|} = 3.56(2)$, and $g_{\perp} = 7.79(3)$.

values were compared with those calculated using the free-ion parameters available from previous crystal-field analyses of Pu^{3+} and Cf^{3+} ions diluted in $LaCl_3$-host single crystals and a set of crystal-field parameters reported earlier for Cm^{3+} ($5f^7$) ions in $LuPO_4$. These crystal-field parameters were obtained from spin-Hamiltonian parameters using operator-equivalent factors and the assumption that the zero-field splitting of the ground state of the $5f^7$ ion is due primarily to intermediate-coupling effects. The relatively poor agreement between the experimental and calculated g values indicates that the crystal-field parameters obtained for Cm^{3+} in $LuPO_4$ cannot be used to predict the correct electronic ground-state properties of the other actinide ions Pu^{3+} and Cf^{3+} in the identical host single-crystal $LuPO_4$. Accordingly, in the case of actinide-impurity ions in single crystals, there is no simple correspondence between the spin-Hamiltonian parameters and the crystal-field parameters.

1. Summary of paper: *Phys. Rev. B* **47**, 3412 (1993).

2. Lawrence Berkeley Laboratory, Berkeley, Calif.

LUMINESCENCE PROPERTIES OF DEFORMED CaO CRYSTALS[1]

R. Gonzalez,[3] *Y. Chen, C. Ballesteros,*[3]
H. Liu,[4] *G. H. Rosenblatt,*[4]
R. T. Williams,[4] *and W. Gellerman*[4]

In deformed CaO crystals, the predominant optical absorption band at 270 nm and the corresponding luminescence band at 450 nm have been investigated. This emission has a quantum efficiency close to unity. Thermal annealing indicates that an appreciable decrease in the absorption begins at ~600 K. In contrast, the luminescence intensity diminishes rapidly at $T >$ 300 K, and by 650 K it is negligible—indicating that the defect had been converted to one which absorbs at 270 nm but does not emit at 450 nm. Therefore, the highest luminescence intensity was obtained with no thermal annealing. Time-resolved luminescence indicates that the 450-nm band is composed of two bands—a 475-nm band with lifetimes of <3 ns and ~10 μs and a 440-nm band with a lifetime of ~1 ms at room temperature.

Time-resolved luminescence experiments on a CaO crystal, deformed to 1.1%, were performed using the fourth harmonic (266 nm) of a Q-switched Nd:YAG (yttrium aluminum garnet) laser with a pulse width of 3 ns. The images taken with the streak camera were plotted in a three-dimensional form. Figures 3.20(a)–(d) show these overviews with the emission intensity plotted vs time and wavelength at temperatures of 289, 217, 131, and 18 K, respectively.

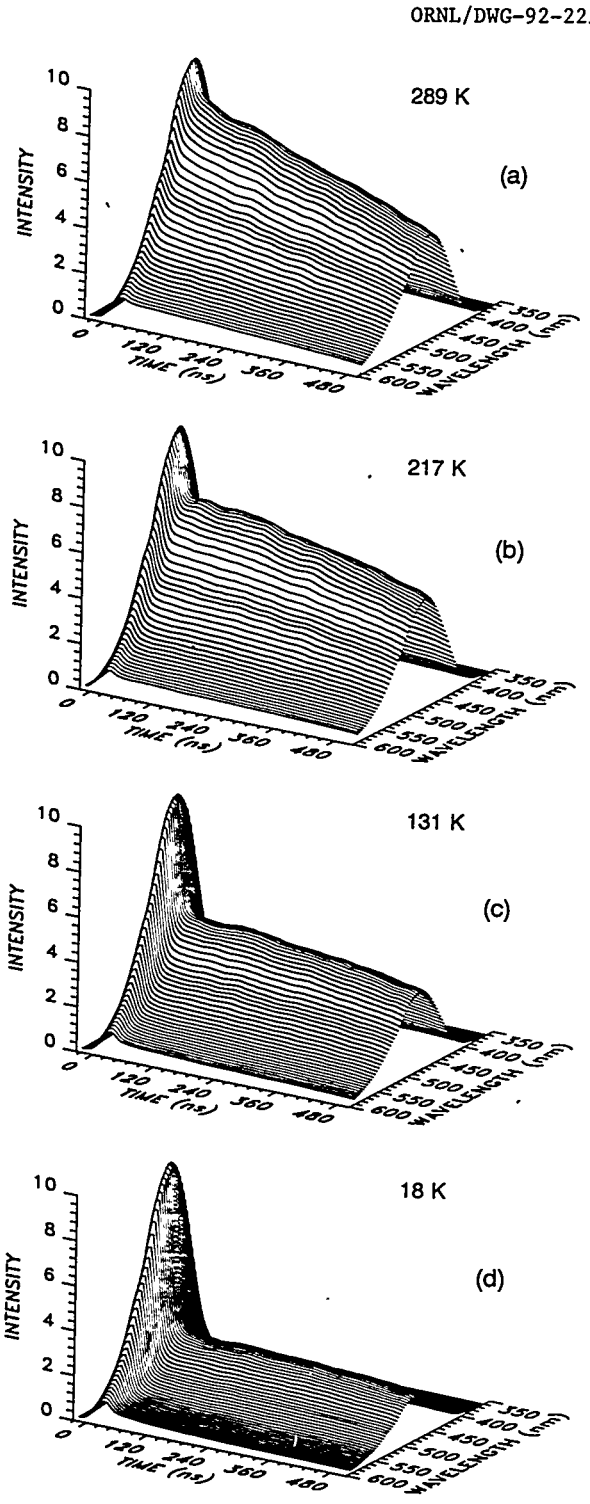

Fig. 3.20. Time-resolved emission spectra taken at temperatures of (a) 289, (b) 217, (c) 131, and (d) 18 K for a CaO sample deformed to 1.1%. The excitation was a 3-ns pulse of 266-nm light. The intensities are given in arbitrary units and are normalized to 10.

The optimum conditions for a deformed crystal to exhibit maximum luminescence intensity with minimum strain would be a 2-mm-thick unannealed sample with 1% deformation. Optical gain was tested using a pulsed excimer laser operating at 248 nm. No laser activity was observed at 77 and 300 K, with excitation powers up to the crystal-damage threshold.

---

1. Summary of paper: *Phys. Rev. B* **47**, 4910 (1993).
2. Guest scientist from Universidad Carlos III, Madrid, Spain.
3. Universidad Complutense, Madrid, Spain.
4. Wake Forest University, Winston-Salem, N.C.
5. University of Utah, Salt Lake City, Utah.
6. R. Gonzalez et al., *Phys. Rev. B* **43**, 5228 (1991).

ERRORS IN POLARIZATION MEASUREMENTS BECAUSE OF STATIC RETARDATION IN PHOTOELASTIC MODULATORS[1]

F. A. Modine and G. E. Jellison, Jr.

A photoelastic modulator (PEM) imparts a time-dependent phase retardation to a light beam. The device consists of a piece of crystalline quartz (-18° X cut) and a piece of fused quartz. The piezo-electric crystalline quartz is driven at its resonant frequency (~50 kHz) by an applied ac voltage. Mechanical coupling induces a strain in the fused quartz, which is tuned to the same resonance frequency. The oscillating strain results in a time-dependent retardation (photoelastic effect). The PEM is

used in a variety of optical measurements employing polarized light.

Errors in measurements made with a PEM were examined in the case in which a static retardation as well as a dynamic retardation is present. If the static and dynamic retardations are not colinear, the analysis is complicated by the fact that the Jones matrices that represent the retardations do not commute. However, a simple mathematical description of the PEM was obtained by adding the static and dynamic retardations according to the rules for adding the stress tensors from which they derive, thus avoiding the addition of Jones' matrices. The addition of retardations is simple because the hydrostatic components of the stresses contribute no net retardation. Hence, only the pure shear components of the stresses (i.e., traceless stress tensors) need to be retained, and their resulting retardations combine according to the rules for adding vectors at the angle 2ϕ, where ϕ is the angle between the retardations.

In ellipsometry with a PEM, the analysis disclosed the harmonic content for the light :

$$I_1 = -(\pm)_p\, 2I_o[(\pm)_A\ J_1(A)S - (\pm)_M\ \delta_o \cos(2\phi)$$
$$J_1(A)N - (\pm)_A\ (\pm)_M\ (\delta_o/A)\sin(2\phi)C] \qquad (1a)$$

$$I_2 = -(\pm)_p\, 2I_o[(\pm)_M\ J_2(A)N + (\pm)_A\ \delta_o$$
$$\cos(2\phi)J_2(A)S] \ . \qquad (1b)$$

The I_n denote harmonics of the modulation and the $J_n(A)$ denote the n^{th} order Bessel functions of the modulation amplitude. The notation $(\pm)_P$ indicates a sign change as a polarizer is rotated from +45° to -45° with respect to the PEM and the $(\pm)_M$ and $(\pm)_A$ indicate similar sign changes for the PEM and an analyzer. N, S, and C are Stokes parameters defined by $C = \sin(2\psi)\cos(\Delta)$, $S = \sin(2\psi)\sin(\Delta)$, and $N = \cos(2\psi)$, where the angles ψ and Δ are the usual ellipsometry angles. For zero static retardation (i.e., $\delta_o = 0$), Eqs. (1) simplify, and S and N are directly proportional to I_1 and I_2, respectively. The static retardation introduces errors proportional to δ_o. However, because of the sign changes indicated in Eqs. (1), the errors can be eliminated by averaging measurements made for the two equivalent orientations of the modulator. Similar results apply for a PEM used in a polarimeter or a dichrometer.

---

1. Summary of paper: *Appl. Phys. Commun.* **12**, 121 (1993).

POSITRON ANNIHILATION SPECTROSCOPY OF VACANCY AGGREGATES IN NEUTRON-IRRADIATED MgO CRYSTALS[1]

R. Pareja,[2] R. M. de la Cruz,[2] R. Gonzalez,[3] and Y. Chen

Neutron irradiation produces a variety of defects which change in concentration with thermal annealing as determined by optical, magnetic resonance, and positron-annihilation spectroscopy studies. In this study, neutron-irradiated crystals were isochronally annealed from 373 to 1523 K, in steps of 50 K for 15 min. Positron-annihilation lifetime and optical absorption measurements were made after each anneal.

All the lifetime spectra of these neutron-irradiated crystals were decomposed unambiguously into components. Figure 3.21 shows the annihilation parameters of these crystals as a function of the heating temperature; τ_1 (bottom) and τ_2 (middle) are the decay constants associated with the exponential terms; I_2 (top) is the relative intensity of the second component, and the average lifetime is $\tau = (1 - I_2)\tau_1 + I_2\tau_2$. The value of $\tau \cong 160$ ps remained approximately constant for $T \leq 673$ K and reached its maximum value of ~206 ps at 873 K. The second component lifetime, τ_2, increased from (187 ± 10) ps initially to a value of (295 ± 25) ps after annealing at ~1100 K. Simultaneously, the intensity of this second component, I_2, decreased from 83% to 12%. Annealing above 1100 K only induced a slight decrease in τ accompanied by a continuous reduction of the τ_1 value while I_2 remained practically constant.

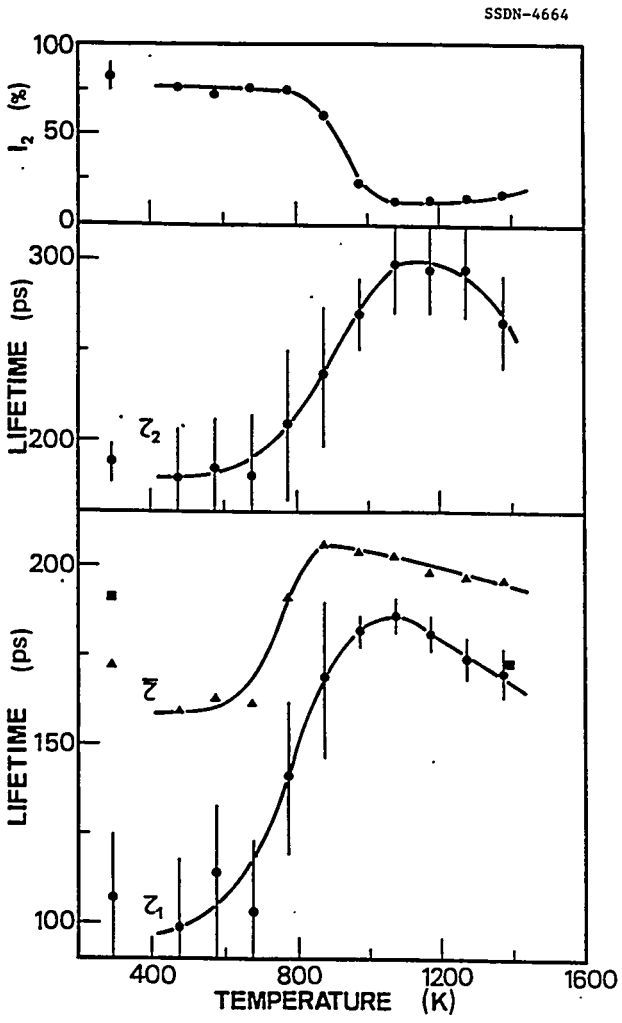

Fig. 3.21. Positron annihilation parameters vs temperature in H-doped MgO crystals.

Although the concentration of defects is very high, the positron average lifetime is noticeably shorter than in virgin crystals. Higher doses result in a higher defect concentration and a shorter positron lifetime. This suggests that the defects are positively charged.

---

1. Summary of paper: *Philos. Mag. A* 66, 597 (1992).
2. Universidad Complutense, Madrid, Spain.
3. Guest scientist from Universidad Carlos III, Madrid, Spain.

PROTONS IN NEUTRON-IRRADIATED AND THERMOCHEMICALLY REDUCED MgO CRYSTALS DOPED WITH LITHIUM IMPURITIES[1]

R. Gonzalez,[3] *R. Pareja,*[3] *and Y. Chen*

The present study focuses on protons in three types of lithium-doped MgO crystals—thermochemically reduced (TCR), neutron irradiated, and crystals which had previously been oxidized at high temperatures prior to neutron irradiation. TCR produces primarily anion vacancies and H^- ions. While three local modes are observed in undoped MgO crystals, only one of them (1024 cm^{-1}) is present in

significant quantities in lithium-doped crystals. The bands at 1032 and 1503 cm^{-1} are suppressed by the presence of lithium. The hydride ions in MgO:Li are thermally much less stable than those in undoped MgO.

Neutron irradiation produces H^- ions, as well as anion vacancies. In principle, the production of H^- ions in a fission reactor is not unexpected. The neutrons produce oxygen vacancies, and γ rays provide Compton electrons which displace protons from V_{OH}^- with a phenomenally large cross section—a process termed radiation-induced diffusion.[3] These H^- ions anneal between 600 and 650 K and are, therefore, much less stable than those produced by TCR. Unlike TCR crystals, neutron-irradiated crystals contain metastable oxygen interstitials which recombine with the oxygen vacancies at lower temperatures.

The existence of H^- ions raises a pertinent question regarding the issue of the suppression of radiation damage in MgO by lithium doping. Is it possible that in MgO:Li there is actually no suppression of anion-vacancy formation but that anion vacancies capture protons and are "camouflaged" as H^- ions! A quantitative analysis in which it was concluded that H^- ions are not present in sufficient quantities to camouflage the loss of anion vacancies was performed.

Changes are also observed in the OH^- regime. Prior to irradiation, only a broadband absorption at 3430 cm^{-1} is observed. This band is attributed to OH^- complexes associated with lithium since this band is observed only in lithium-doped MgO. After the irradiation, sharp bands are superimposed on the broadband. These sharp bands are observed in crystals which do not contain lithium and are, therefore, attributed to OH^- ions not associated with lithium impurities. The emergence of the sharp bands is attributed to the displacements of Li^+ ions by the highly efficient mechanism of radiation-induced diffusion,[3] leaving behind OH^- ions unassociated with lithium. Using experimental values in the present study, an estimate for the displacement cross section of lithium was obtained, and it was found to be consistent with a previous study which uses an entirely different approach.[4]

---

1. Summary of paper: *Phys. Rev. B* **45**, 12730 (1992).
2. Guest scientist from Universidad Carlos III, Madrid, Spain.
3. Y. Chen, M. M. Abraham, and H. T. Tohver, *Phys. Rev. Lett.* **37**, 1757 (1976).
4. Y. Chen et al., *Phys. Rev. B* **16**, 5535 (1977).

THERMOCHEMICAL REDUCTION OF YTTRIUM ALUMINUM GARNET (YAG) CRYSTALS[1]

R. Gonzalez,[3] C. Ballesteros,[3] Y.-J. Liu,[4] Yi Chen,[4] X.-F. Zong,[4] and Y. Chen

Colloidal particles with diameters in the range 1–200 nm in ionic crystals may modify the mechanical, optical, and electronic properties of YAG crystals. These colloids form by a nucleation and growth process. In general, cation impurities tend to form precipitates preferentially at strained regions in the oxides. Transition-metal impurities segregate and precipitate along dislocations and grain boundaries

to form metallic precipitates when oxide samples are heated in a reducing atmosphere, or an oxygen-free inert gas, a process referred to as decoration. These colloids are usually identified by transmission electron microscopy (TEM) and x-ray fluorescence and give rise to characteristically broad extinction bands, attributed to Mie scattering.

Strained regions were first identified in slabs of YAG single crystals via transmitted light viewed with crossed polarizers. The strained region had a symmetrical pattern and was situated at the center of the slabs. Because of the symmetry both in pattern and in location, it is believed that they were induced thermally during crystal growth.

TEM, x-ray microanalysis, and optical absorption were used to characterize the strained and unstrained regions in as-grown and subsequently thermochemically reduced (TCR) YAG crystals. As TCR takes place at increasing temperatures, a dark coloration emerges at the strained region. The strained region was always darker than the surrounding unstrained region, regardless of the temperature of reduction (Fig. 3.22). Optical measurements reveal that the coloration is due to a very broad band peaking at about 800 nm. There is no evidence from TEM and x-ray microanalysis to indicate the presence of precipitates in as-grown and TCR crystals, in contrast to oxides in which cation impurities form metallic precipitates preferentially at strained regions during TCR.

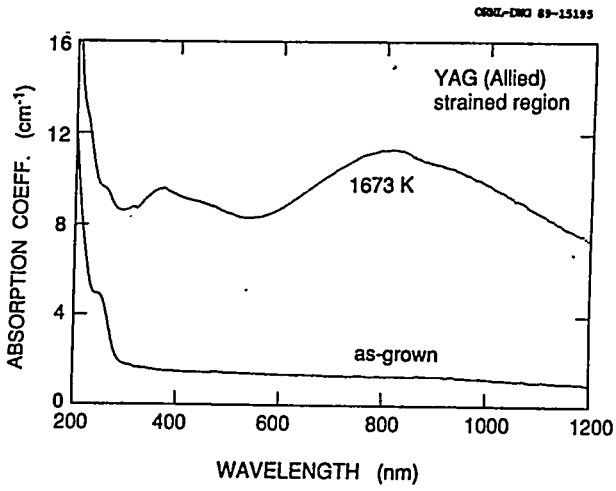

Fig. 3.22. Optical absorption spectra of an as-grown YAG single crystal and after TCR for 2 h at 1673 K.

1. Summary of paper: *Philos. Mag. A* **67**, 207 (1993).

2. Guest scientist from Universidad Carlos III, Madrid, Spain.

3. Universidad Complutense, Madrid, Spain.

4. Fudan University, Shanghai, P.R. China.

PRECIPITATION OF COPPER AND CHROMIUM IMPURITIES IN LANTHANUM MAGNESIUM ALUMINATE CRYSTALS DURING REDUCTION[1]

C. Ballesteros,[2] R. Gonzalez,[3] Y. Chen, and M. R. Kokta[4]

Thermochemical reduction (TCR) at high temperatures has been performed on chromium-doped lanthanum magnesium aluminate (LMA:Cr) crystals. Analytical transmission electron microscopy (TEM) and optical absorption techniques were used to characterize the crystals. There were two stages of impurity aggregation. In the first stage, copper impurities inherently present in the crystals began to aggregate and form Cu-rich particles at 1500 K near the surface region. Below 1870 K, there was

no evidence of chromium precipitates being formed. In the second stage, Cr-rich particles were formed at 2020 K. The distribution of the precipitates was very inhomogeneous, and the precipitates were concentrated near the surface region.

Optical absorption spectra before and after isochronal TCR are shown in Fig. 3.23. In the first-stage absorption, the 270-nm band increased monotonically with temperature, indicating that intrinsic defects were being formed. The spectra in the visible and infrared region remained the same, indicating that the concentration of Cr^{3+} ions remained constant.

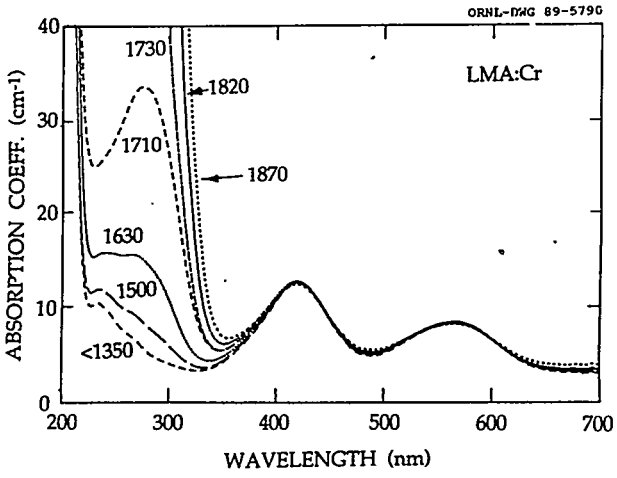

Fig. 3.23. Optical-absorption coefficient vs wavelength for a LMA:Cr crystal TCR up to a temperature of 1820 K.

Concomitant with the emergence of the 270-nm band at 1500 K was the appearance of a dark coloration at the surface region. TEM investigations showed that the dark regions were characterized by a dilute concentration of widely separated precipitates with an average size of 14 nm. X-ray fluorescence indicates that the precipitates were Cu-rich and are presumably Cu particles.

Aggregation of Cr impurities began to take place above 1870 K, and the two Cr^{3+} peaks (420 and 570 nm) diminished. In the near-infrared region, two extinction bands (1000 and 1400 nm) emerged. TEM revealed the presence of Cr precipitates, which had an average size of 800 nm and an inhomogeneous distribution. The parallel optical absorption and TEM measurements deduced that a large fraction of the Cr^{3+} ions had migrated to form Cr-rich precipitates.

---

1. Summary of paper: *Phys. Rev. B* **47**, 2460 (1993).
2. Universidad Complutense, Madrid, Spain.
3. Guest scientist from Universidad Carlos III, Madrid, Spain.
4. Union Carbide Corporation, Washougal, Wash.

4. *Ion Beam and Laser Processing*

Basic research in materials science using ion beams, molecular beams, and lasers are emphasized in this chapter. Progress in ion beam processing, ion implantation and analysis, and laser and molecular beam processing of thin films are reported. This research is performed at the Surface Modification and Characterization Research Center (SMAC RC) and the SSD pulsed-laser ablation and molecular-jet growth facilities.

The SMAC RC provides the scientific community with extensive capabilities for ion beam processing of the near-surface region of solids. The following are some recent examples included in this report. Formation of random or oriented nanocrystals of metals, semiconductors, and compounds in a variety of substrates has been achieved, and the structural, optical, and electrical properties of these nanoclusters are being investigated. A dislocation-free process for producing silicon-on-insulator by implantation, the kinetics of solid-phase-epitaxial crystallization in amorphous $Si_{1-x}Ge_x$ thin films following implantation, and the effects of implantation-induced damage on electrical carrier concentrations in tin-doped indium oxide and GaAs have been studied. A new lift-off technique for obtaining freestanding diamond films and the development of an electron cyclotron resonance plasma source for copper metallization have been demonstrated. Ion beams have been used to synthesize Ti-rich epitaxial buried layers in $LiNbO_3$, to modify the hardness of the surfaces of orthopedic alloys, and to provide oxygen needed to form a protective oxide coating on $NbAl_3$ and TiAl alloys. The adsorption of hydrogen on surfaces and its diffusion in the bulk have been studied by nuclear reaction and elastic recoil techniques.

The Semiconductor Physics and Thin Films Group has developed a pulsed-laser deposition (PLD) technique for depositing ternary semiconductor films with continuously variable composition and doping from a single target. PLD has facilitated electrical property investigations of the so-called "infinite-layer" parent structure of the high-temperature superconductors (HTSc) through the growth of very high quality thin films, and studies of the dimensionality and transport properties of high-temperature superconductivity have been carried out using superlattice and sandwich structures of YBCO. In addition, techniques are being developed for measuring Landau quantum oscillations in thin-film HTSc materials. Fast imaging has provided new information on the interaction of PLD ablation plumes with substrates and on the formation of fullerenes during ablation of graphite. Differential optical reflectivity has been used to characterize the kinetics of hydridic pulsed-jet chemical vapor deposition.

ION BEAM PROCESSING

FORMATION OF Au AND Ag NANOCLUSTERS IN FUSED SILICA BY ION IMPLANTATION

C. W. White, D. S. Zhou,[1] J. D. Budai, R. A. Zuhr, R. A. Magruder,[2] and R. F. Haglund[2]

One way to cause dramatic changes in the optical properties of fused silica is through the formation of metallic colloidal nanocluster precipitates. If the precipitate size is small enough (<500-Å diam), the precipitates will absorb light at the surface plasmon wavelength, thus altering the optical properties of the host medium. MeV implantation of Au or Ag ions into fused silica has been used to form a high density of colloidal precipitates in the near-surface region. One example is shown in the transmission electron microscopy (TEM) micrographs of Fig. 4.1(a) for the case of Au (2.75 MeV) implanted to a dose of $1.5 \times 10^{17}/\text{cm}^2$ into fused silica at an implantation temperature of 600°C. Near the end-of-range (~800 nm) of the ions, a high density of precipitates are observed [Fig. 4.1(a)]. The diffraction pattern identifies the precipitates as Au. Individual precipitates are spherical single crystals which are oriented at random relative to each other. The average size is ~130 Å. Figure 4.1(b) shows the optical absorption measurements for fused silica samples implanted at 600°C and at room temperature. Following implantation at elevated temperatures, a strong absorption band is measured at 2.34 eV, which is the surface plasmon resonance energy for Au particles in SiO_2. In the case of Ag implantation,

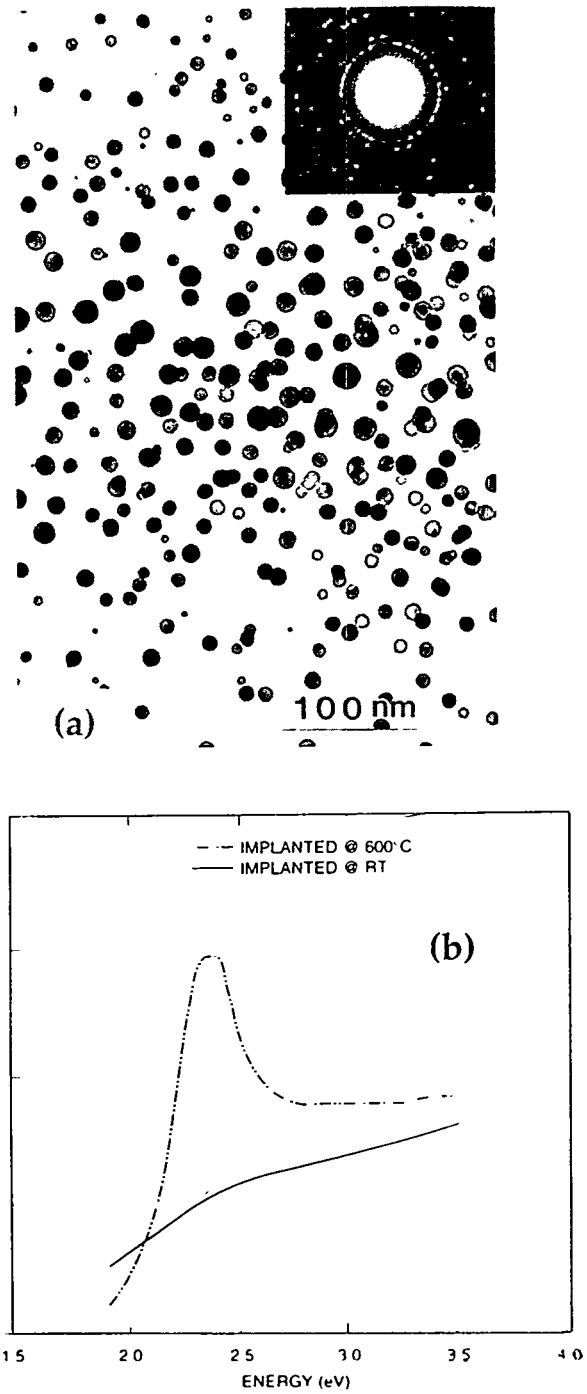

Fig. 4.1. (a) Cross-section TEM micrographs showing the microstructure in the near-surface region of Au-implanted fused silica. (b) Optical absorption measurements in fused silica implanted by Au at room temperature and 600°C.

strong absorption is observed at the surface plasmon energy for Ag in SiO_2 (3.1 eV).

Precipitate size and size distribution can be varied from ~30 to ~150 Å by an appropriate choice of implantation or annealing conditions. Precipitate volume fractions of several percent have been achieved in the near surface by ion implantation and annealing. This is much greater than that (~0.01% or less) which can be achieved by adding metal to the glass melt. The very high volume fraction and small precipitate size lead to very large nonlinear optical properties in the implanted materials as demonstrated in recent measurements.[3]

---

1. ORNL/ORISE postdoctoral research associate.
2. Vanderbilt University, Nashville, Tenn.
3. R. H. Magruder et al., *Appl. Phys. Lett.* **62**, 1730 (1993).

NANOSIZE METAL ALLOY PARTICLE FORMATION IN Ag AND Cu SEQUENTIALLY IMPLANTED SILICA[1]

R. A. Zuhr, R. H. Magruder III,[2]
T. A. Anderson,[2] *and J. E. Wittig*[2]

Recently, composites of nanosize metal particles (2–30 nm in diam) embedded in glass have been shown to exhibit third-order optical nonlinearities with a magnitude of 10^{-11} esu and a response time of less than 5 ps. The large nonlinear susceptibility is attributed to local-field enhancement for frequencies near the surface plasmon resonance of the metallic particles. As strong enhancements of the nonlinear response are expected to occur on or near the surface plasmon resonance, the ability to control the frequency of this resonance is of interest for possible wavelength tunability.

Figure 4.2 shows representative bright field images of the planar view of the implanted layer for Corning 7940 silica samples implanted with 6×10^{16} Cu ions/cm^2 at 160 keV and then sequentially with 2, 4, and 6×10^{16} Ag ions/cm^2 at 300 keV. The implantation energies were chosen using TRIM 89 calculations so that the depth distributions of the elements would overlap. The nanosize particles formed are uniform in shape and are spherical. The mean particle sizes for the three samples are 3.7 ± 3.2, 22.4 ± 6.0, 27.6 ± 9.7 nm, respectively. The volume fraction of the Ag-Cu alloy metal particles is ~5% in the center of the implanted region.

Sequentially implanted samples exhibit significantly different optical spectra than samples implanted with single elements. Shifts in both peak position and magnitude compared with single implantations are observed. These results indicate that the changes in the optical absorption are due to the presence of the two different metallic elements. The shift in the wavelength of the surface plasmon resonance with sequential implantation is attributed to alloying of the Cu-Ag ions during implantation, as observed by dispersive x-ray analysis. The difference in optical response with increasing Ag concentration is attributed to different degrees of alloying as well as to increasing particle size.

---

1. Summary of paper to be published.
2. Vanderbilt University, Nashville, Tenn.

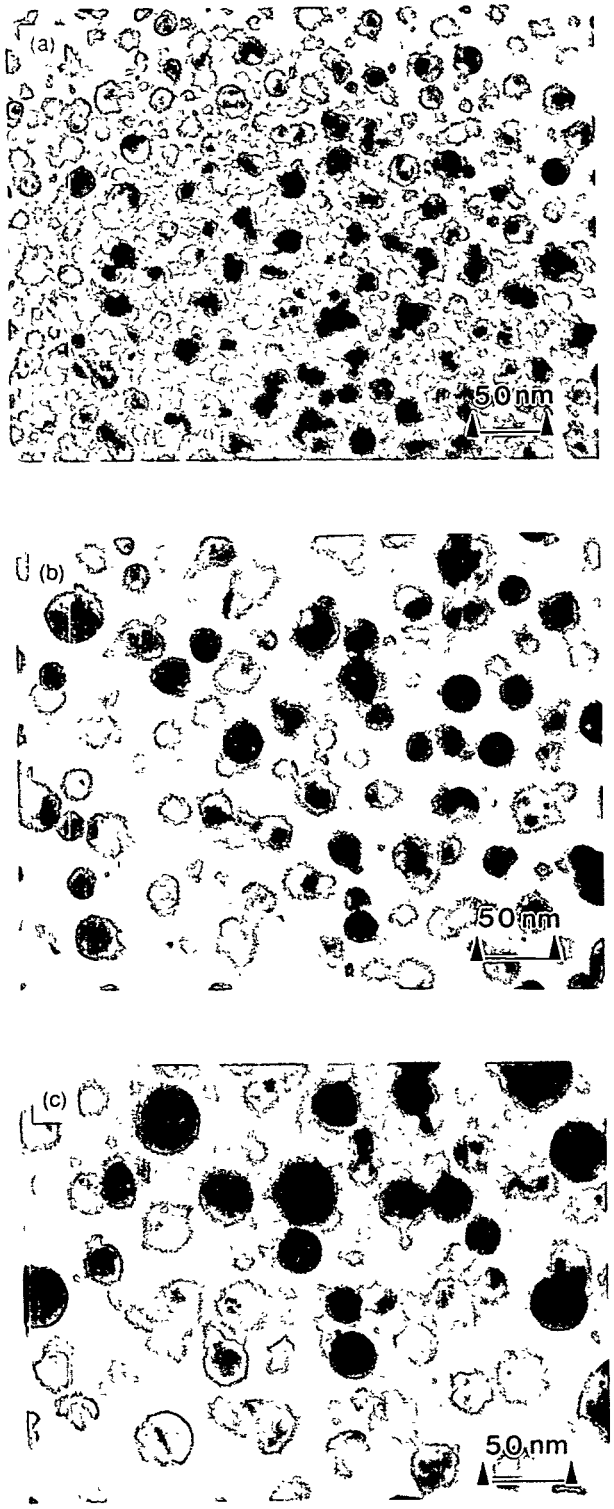

Fig. 4.2. Plan-view TEM micrographs of silica implanted at room temperature with 6×10^{16} Cu/cm^2 followed by (a) 2×10^{16}, (b) 4×10^{16}, and (c) 6×10^{16} Ag/cm^2.

FORMATION OF ORIENTED NANOCRYSTALS OF Si AND Ge IN Al_2O_3 BY ION IMPLANTATION

C. W. White, J. D. Budai, S. P Withrow, S. J. Pennycook, R. A. Magruder,[1] and D. M. Hembree[2]

Ion implantation followed by annealing in a reducing atmosphere has been used to create nanocrystals of Si and Ge in Al_2O_3. X-ray diffraction and transmission electron microscopy (TEM) show these nanocrystals to be oriented with respect to the Al_2O_3 matrix.[3]

Figure 4.3 shows x-ray diffraction results for a (0001)-oriented Al_2O_3 crystal implanted by Si (400 keV, 6×10^{17}/cm^2, 650°C). The scans along the c axis of Al_2O_3 show the expected diffraction peaks from the (0001) planes of Al_2O_3. In addition, there are strong diffraction peaks from (111) silicon planes, as well as (weaker) diffraction from (220) silicon planes. These results

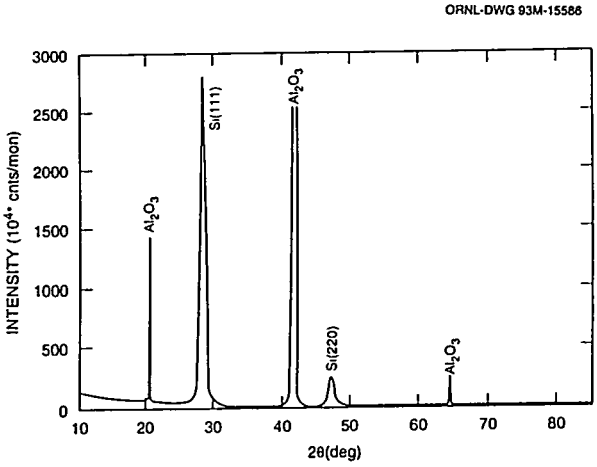

Fig. 4.3. θ–2θ scans along the (0001) axis of Al_2O_3 implanted by Si (400 keV, 6×10^{17}/cm^2, 650°C). Following implantation, the crystal was annealed at 1100°C for 2 h in a reducing environment.

show that the silicon nanocrystals are three-dimensionally aligned predominantly in the orientation Si(111) || Al_2O_3 (0001), Si [$1\bar{1}0$] || Al_2O_3 [$11\bar{2}0$]. To a much lesser extent, the orientation Si(110) || Al_2O_3(0001), Si [001] || Al_2O_3 [$10\bar{1}0$] is observed. Both domains exhibit sixfold rotational symmetry about the surface normal. The $\theta-2\theta$ width of the Si(111) diffraction peak is consistent with a nanocrystalline thickness of ~140 Å normal to the surface. Particle sizes depend on both the dose and the thermal treatment. Initial TEM results suggest that at high doses, the nanocrystals may have a pancake shape.

For Ge-implanted Al_2O_3, Ge nanocrystals oriented with (111) planes parallel to (0001) Al_2O_3 are observed. In addition, crystallites with (110) planes oriented approximately parallel to (0001) Al_2O_3 planes are observed with nearly equal x-ray intensity. However, the (110) domains have the Ge [110] axis tilted by ~3° away from the Al_2O_3 [0001] axis toward three symmetry-equivalent directions. In contrast to the Si observations, both types of Ge domains exhibit three-fold rotational symmetry about the surface normal. Sizes of Ge nanocrystals inferred from the width of the diffraction lines are in the range 50–100 Å (depending on dose and temperature), and initial TEM results show the shapes to be nearly spherical.

---

1. Vanderbilt University, Nashville, Tenn.
2. Oak Ridge Y-12 Plant, Oak Ridge, Tenn.
3. J. D. Budai et al., "Structure and Orientation of Si, Ge, and SiGe Nanocrystals Formed by Ion Implantation," this report.

FORMATION OF ORIENTED SiGe NANOCRYSTALS IN Al_2O_3 BY ION IMPLANTATION

C. W. White, J. D. Budai, S. P Withrow, S. J. Pennycook, R. A. Magruder,[1] and D. M. Hembree[2]

Ion implantation, followed by annealing, has been used to create nanocrystals of SiGe in Al_2O_3. The nanocrystals were formed by sequential implantation of Si and Ge at equal doses with the ion energy adjusted to give the same projected range. Following implantation, annealing was carried out in a reducing atmosphere at temperatures up to 1100°C for time periods of 1 h. Raman scattering and x-ray diffraction were used to confirm the existence of SiGe crystallites, and x-ray diffraction was used to determine the orientation of the SiGe nanocrystals with respect to the Al_2O_3 matrix.

Figure 4.4 gives Raman scattering results showing the presence of SiGe crystallites in Al_2O_3 following the implantation of Si and Ge and annealing for 1 h at 1100°C. Shown in Fig. 4.4 are Raman lines characteristic of Si-Si bonds (at 501 cm^{-1}), Ge-Ge bands (at 287 cm^{-1}), and Si-Ge bonds (at 409 cm^{-1}). Wavelengths characteristic of the individual bonds were determined from Raman spectra obtained from bulk SiGe alloys. X-ray diffraction results show that the SiGe nanocrystals are oriented with their (111) planes || to Al_2O_3 (0001) planes.[3] The observed x-ray diffraction peak position for the nanocrystalline (111) planes lies intermediate between the calculated bulk Si and bulk Ge positions and, hence, suggests the presence of mixed SiGe nanocrystals rather than separate Si

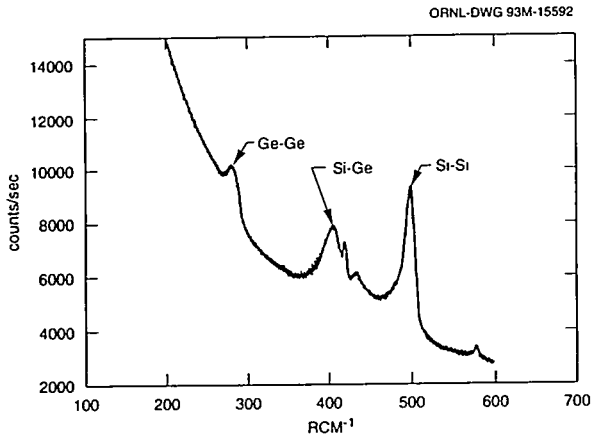

Fig. 4.4. Raman scattering from Al_2O_3 implanted by Ge (500 keV, $1.5 \times 10^{17}/cm^2$, room temperature) and Si (220 keV, $1.5 \times 10^{17}/cm^2$, 400°C) and annealed at 1100°C for 1 h. Spectral features assigned to Si-Si bonds, Ge-Ge bonds, and Si-Ge bonds are identified and were determined by comparison with similar spectra from bulk SiGe.

and Ge precipitates. In plane, the oriented SiGe nanocrystals exhibit sixfold rotational symmetry with SiGe $[1\bar{1}0]$ || Al_2O_3 $[10\bar{1}0]$. The Raman scattering results and the x-ray diffraction results provide strong evidence that SiGe nanocrystals are formed in Al_2O_3 by sequential implantation and annealing.

COLLOIDAL Au AND Ag NANOCRYSTALS FORMED IN Al_2O_3 BY ION IMPLANTATION AND ANNEALING[1]

C. W. White, J. D. Budai, D. K. Thomas, D. K. Hensley, R. A. Magruder,[2] R. F. Haglund,[2] L. Yang,[2] J. C. McCallum,[3] and A. Pogany[3]

Implantation of Au and Ag ions in Al_2O_3 followed by annealing results in the formation of a very high density of Au and Ag nanocrystals in the near-surface region. The presence of these nanocrystals in the near surface dramatically changes the optical properties of the host material. Figure 4.5 shows the optical absorption measured in Ag-implanted Al_2O_3 in the as-implanted state and after annealing. For Ag-implanted Al_2O_3, a strong absorption band develops at 2.75 eV after annealing, and for Au-implanted Al_2O_3, annealing causes a very strong band to develop at 2.25 eV. The development of these bands is correlated with the formation of

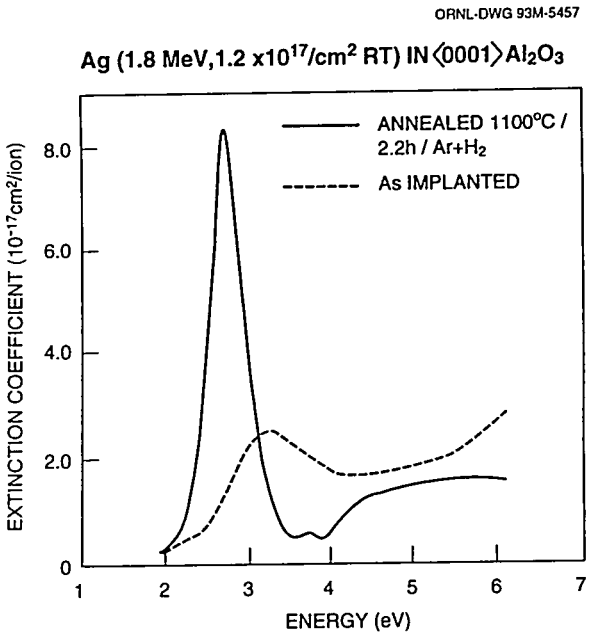

Fig. 4.5. Optical absorption measured in Ag-implanted (1.8 MeV, $1 \times 10^{17}/cm^2$) Al_2O_3.

1. Vanderbilt University, Nashville, Tenn.
2. Oak Ridge Y-12 Plant, Oak Ridge, Tenn.
3. J. D. Budai et al., "Structure and Orientation of Si, Ge, and SiGe Nanocrystals Formed by Ion Implantation," this report.

Au and Ag nanocrystals as a result of annealing the implanted materials. These nanocrystals absorb light at the surface plasmon resonance wavelength (2.25 eV for Au in Al_2O_3 and 2.75 eV for Ag in Al_2O_3).

The Au and Ag nanoclusters that form in Al_2O_3 as a result of implantation and annealing are crystalline and are oriented with respect to the Al_2O_3 matrix. For Au-implanted ($1 \times 10^{17}/cm^2$) Al_2O_3, the precipitate size varies from ~20 to ~200 Å, with the average diameter being ~80 Å. The Au precipitates are faceted, and both transmission electron microscopy and x-ray diffraction show that most of the precipitates are oriented with (111) planes of Au being parallel to (0001) planes of Al_2O_3.

The presence of a high density of Au nanocrystals in the near-surface region of Al_2O_3 gives rise to large optical nonlinearities. At 532 nm, the electronic component of the third-order susceptibility is measured to be $\sim 7 \times 10^{-10}$ esu for a sample implanted by Au to a dose of $2.2 \times 10^{16}/cm^2$. This value is about a factor of 3 larger than that measured for Au-implanted SiO_2 at the same wavelength; the nonlinear optical response time is measured to be in the picosecond time region.

KINETICS OF SOLID-PHASE EPITAXIAL CRYSTALLIZATION IN AMORPHOUS $Si_{1-x}Ge_x$ THIN FILMS[1]

T. E. Haynes, C. Lee, [2]and K. S. Jones[3]

Heterostructures of $Si_{1-x}Ge_x$ and Si provide new opportunities for integration of band-gap-engineered optical and electronic devices with silicon technology. During ion implantation doping of these heterostructures, $Si_{1-x}Ge_x$ layers are preferentially amorphized, so that recrystallization is required during postimplant annealing. $Si_{1-x}Ge_x$ layers, which are strained due to lattice mismatch, are known to recrystallize more slowly than pure Si, and defects often appear. In this study, the effect of strain on recrystallization in $Si_{1-x}Ge_x$ epilayers has been characterized more clearly by using time-resolved reflectivity (TRR) to measure recrystallization rates in situ in both strained and relaxed $Si_{1-x}Ge_x$ epilayers amorphized by ion implantation. Figure 4.6 shows a comparison of regrowth rates in different types of layers. A thick, relaxed $Si_{0.85}Ge_{0.15}$ layer regrows at a constant rate that is faster than in pure Si, and the regrown layer is defect-free. In the two MBE-grown samples, regrowth occurs through a SiGe-Si interface (2000 Å deep), where there is a lattice mismatch. In these samples, the regrowth rate is not constant, first gradually decreasing in the $Si_{1-x}Ge_x$ layer and then increasing again at a regrown thickness that decreases with increasing lattice mismatch. In situ TRR measurements permitted this transient to be observed for the first time. Cross-section transmission electron microscopy showed that strain-relieving defects

---

1. Summary of paper to be published.
2. Vanderbilt University, Nashville, Tenn.
3. Royal Melbourne Institute of Technology, Melbourne, Australia.

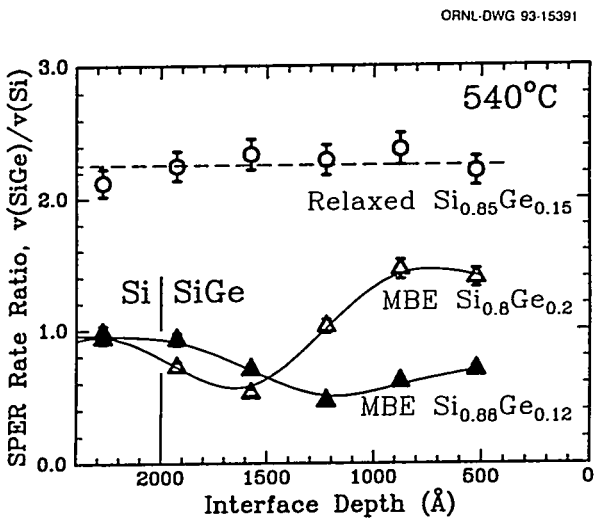

Fig. 4.6. The rate of solid-phase-epitaxial regrowth in various $Si_{1-x}Ge_x$ epilayers at 540°C is normalized to that in pure Si and shown as a function of the position of the amorphous-crystal interface. The original interface was ~3500 Å deep in all cases. The two MBE-grown $Si_{1-x}Ge_x$ layers were only 2000 Å thick, so that regrowth was initiated in the Si substrate, whereas the "relaxed" $Si_{0.85}Ge_{0.15}$ layer was 7 μm thick.

formed at the same depth where the regrowth rate began to increase. These results conclusively demonstrated that the regrowth rate in strained $Si_{1-x}Ge_x$ is not constant, as previously assumed, and that the transient retardation is due to compressive strain, disappearing when the strain is relieved by defects.

---

1. Summary of papers: *Appl. Phys. Lett.* **62**, 501 (1993); p. 479 in *Semiconductor Heterostructures for Photonic and Electronic Applications*, ed. by C. W. Tu, D. C. Houghton, and R. T. Tung, Materials Research Society, Pittsburgh, Pa., 1993.
2. SURA/ORNL Summer Cooperative Program student research participant from the University of Florida, Gainesville, Fla.
3. University of Florida, Gainesville, Fla.

FREESTANDING HOMOEPITAXIAL CHEMICAL VAPOR DEPOSITED (CVD) DIAMOND FILMS LIFTED OFF IMPLANTED SUBSTRATES[1]

J. D. Hunn,[2] S. P. Withrow, C. W. White, R. E. Clausing,[3] L. Heatherly,[3] J. Bentley,[3] D. M. Hembree, Jr.,[4] and N. R. Parikh[5]

A method has been developed by which thin (1-μm) plates can be lifted off a single-crystal diamond.[6] This technique involves implanting a diamond with high-energy (4–5-MeV) ions (usually carbon or oxygen) in order to create a buried amorphous layer at a depth of 1–2 μm. The buried amorphous region preferentially reacts with oxygen under the right conditions resulting in a gaseous residue. By controlling this reaction, the amorphous layer can be etched away without affecting the still crystalline surface plate.

A sample was implanted with 1.3×10^{18} C/cm^2 at 4 MeV. At this dose, the first two microns of the diamond are heavily damaged. A Raman spectrum from the implanted surface shows no evidence of the diamond peak at 1332 cm^{-1}. Rutherford backscattering (RBS)/channeling shows a large buried amorphous layer but a remarkably low channeling yield right at the surface [Fig. 4.7(a)]. A homoepitaxial film was grown on the implanted surface by hot-filament CVD. RBS/channeling shows this film to be of good crystalline quality [Fig. 4.7(b)]. Raman scattering shows only the peak at 1332 cm^{-1} as is observed in virgin single-crystal diamond. The full width half maximum of this peak was as good as the virgin material at 1.9 cm^{-1}.

SSD 4675

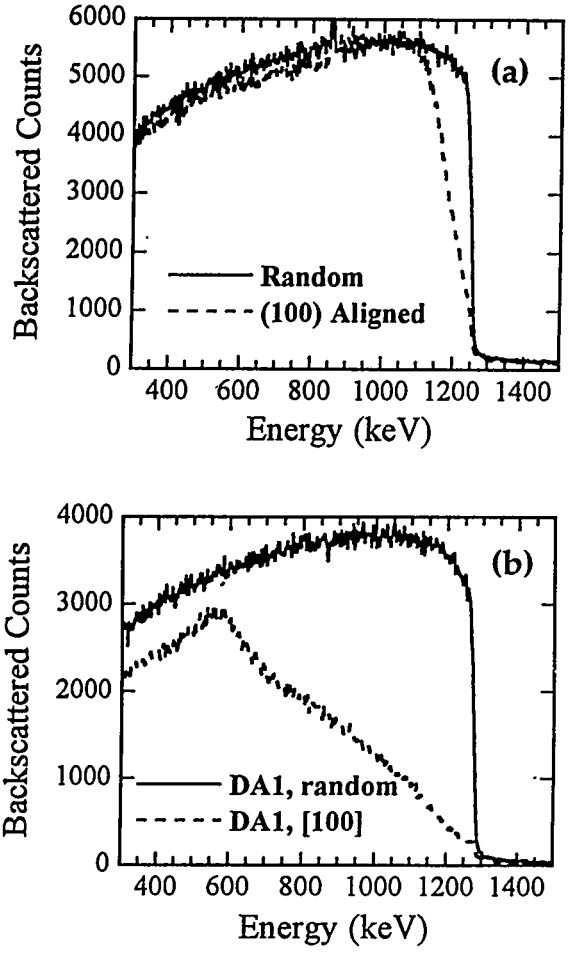

Fig. 4.7. RBS/channeling. (a) Diamond implanted with 1.3 × 10^{18} C/cm^2 at 4 MeV. (b) Homoepitaxial CVD film grown on implanted substrate.

The film was lifted off the substrate in one piece by an electrolytic etch. This involves immersing the sample in distilled water in which two platinum electrodes are placed. Because the buried amorphous region is conducting, a virtual anode is created at the side of the sample closest to the negative electrode. Anodic oxidations occur along this edge, among which is the conversion of carbon to gaseous carbon dioxide. Etching only occurs in the conductive buried damage layer resulting in the separation of the CVD film from the substrate.

---

1. Summary of paper to be published.
2. ORNL/ORISE postdoctoral research associate.
3. Metals and Ceramics Division, ORNL.
4. Oak Ridge Y-12 Plant, Oak Ridge, Tenn.
5. University of North Carolina at Chapel Hill, Chapel Hill, N. C.
6. N. R. Parikh et al., *Appl. Phys. Lett.* **61**, 3124 (1992).

ACCUMULATION OF IMPLANTATION DAMAGE IN MEV-IMPLANTED DIAMOND CRYSTALS[1]

J. D. Hunn,[2] S. P. Withrow, C. W. White, R. E. Clausing,[3] L. Heatherly,[3] J. Bentley,[3] D. M. Hembree, Jr.,[4] and N. R. Parikh[5]

Raman and Rutherford backscattering spectroscopies have been used to study the accumulation of implantation damage in single-crystal diamond from 4-MeV carbon ions. Previously unreported Raman peaks which are apparently unique to high-energy implantation have been observed. At high doses, the Raman spectrum is remarkably similar to the one-phonon density of states of amorphous carbon. Figure 4.8 shows the Raman spectrum from a [100]-oriented crystal implanted with 1.0 × 10^{16} C/cm^2 at 4 MeV. Five peaks generally observed in all the high-energy implanted specimens are labeled. The peak at 720 cm^{-1} only appeared with excitation at 488 nm and is due to photoluminescence. The remaining spectral features are due to Raman scattering. Furthermore, there is no evidence that the peaks are related to the

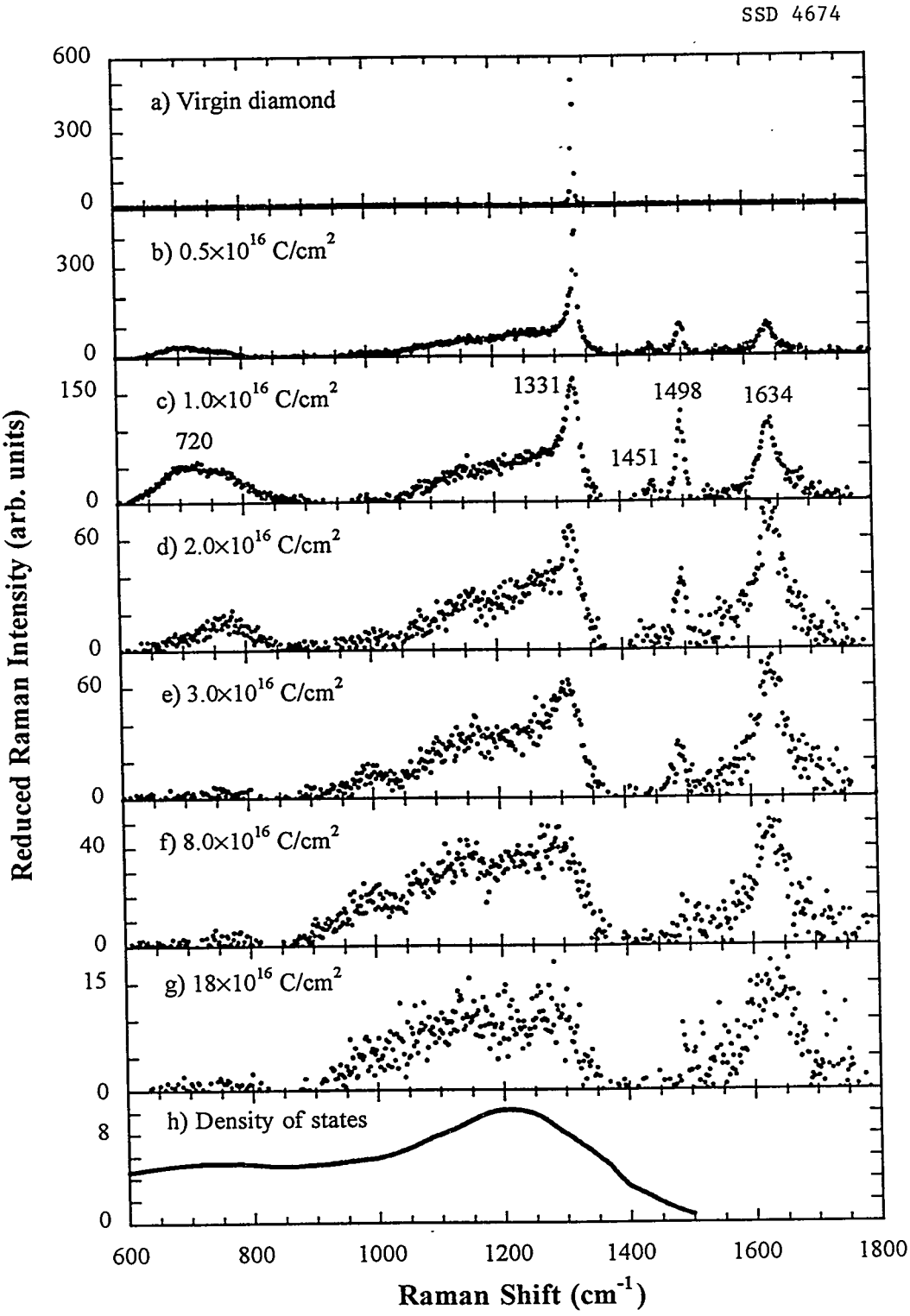

Fig. 4.8. (a–g) Reduced Raman spectra after subtracting background of a [100] diamond successively implanted to increasing doses with 4-MeV carbon ions. (h) The Gaussian-broadened one-phonon density of states for diamond.

implant species; oxygen and argon yield the same result. The peaks at 1451, 1498, and 1634 cm^{-1} have hitherto not been reported in the literature. These peaks are only observed for MeV-energy implants.

The 1332-cm^{-1} peak is the only allowed mode in single-crystal diamond [Fig. 4.8(a)]. The decrease in intensity of this peak is directly related to the ion implantation damage. As the ion dose is increased, the 1332-cm^{-1} peak can be seen to broaden and shift down in energy, finally approaching the one-phonon density of states. The reduced Raman spectrum of an amorphous material is expected to replicate the density of states. This Raman feature can, therefore, be interpreted as coming from an amorphous carbon network with fourfold coordinated (diamond-like) bonds. Furthermore, no sp^2 related Raman peaks are observed in the implanted material.

---

1. Summary of paper to be published.
2. ORNL/ORISE postdoctoral research associate.
3. Metals and Ceramics Division, ORNL.
4. Oak Ridge Y-12 Plant, Oak Ridge, Tenn.
5. University of North Carolina at Chapel Hill, Chapel Hill, N. C.

DEVELOPMENT OF AN ELECTRON CYCLOTRON RESONANCE (ECR) PLASMA SOURCE FOR COPPER METALLIZATION[1,2]

L. A. Berry,[3] S. M. Gorbatkin, G. H. Henkel,[3] and R. L. Rhoades[4]

The semiconductor industry's drive toward higher performance devices with shrinking feature sizes requires continuing efforts to develop new manufacturing tools and processes. Copper has been identified as a potential material for metallization because of its lower resistivity compared with aluminum, and there is a need for equipment capable of filling sub 0.25-micron features with aspect ratios in the 3–4 range.

This work, a Cooperative Research and Development Agreement between ORNL and IBM, is aimed at developing a metal ion plasma source capable of Cu metallization which is amenable to production implantation and processing of 200–250-mm-diam wafers. A permanent magnet is used for magnetic field production and is significantly more compact than ECR sources using electromagnetic coils, with a sputter target used as a simple, reliable source of neutrals.

Normally, to achieve arbitrarily high plasma densities, high-field injection, where the microwaves propagate parallel to the magnetic field, is used. This requires a dielectric microwave entrance window exposed to the processing plasma, which is unacceptable for metal deposition because the window becomes quickly coated, and microwaves cannot penetrate into the processing chamber. To get around this problem, a coupler has been designed which allows microwave injection initially perpendicular to the magnetic field while still maintaining the ability to avoid microwave cutoff. The window position in the system is out of the line of sight of the plasma and allows operation with Cu. The source has been successfully operated with Ar gas and Cu targets, yielding sputter target current densities above 30 mA/cm^2.

Use of a sputter target, however, results in a longer mean-free path for ionization compared with the use of a thermal evaporation source and reduces the ratio of metal ions/metal neutrals. Future efforts are aimed at increasing the total ion fraction, understanding trench and via filling in more detail, and developing specific Cu metallization processes.

---

1. Summary of paper to be published.
2. Work funded by Defense Programs Technology Commercialization Initiative.
3. Fusion Energy Division, ORNL.
4. ORNL/ORISE postdoctoral research associate.

BORON NITRIDE THIN-FILM DEPOSITION USING ELECTRON CYCLOTRON RESONANCE MICROWAVE PLASMAS[1]

S. M. Gorbatkin, R. F. Burgie,[2] W. C. Oliver,[3] J. C. Barbour,[4] T. M. Mayer,[4] and M. L. Thomas[4]

Electron cyclotron resonance (ECR) microwave plasma deposition has been used to deposit B_xN_{1-x} thin films from borazine ($B_3N_3H_6$)-based plasmas. Deposited films were analyzed using infrared absorption, x-ray diffraction, forward elastic recoil detection, and enhanced cross-section backscattering spectrometry, with precise quantitative measurements of low-mass elements (e.g., boron, nitrogen, and hydrogen) of particular interest. All three elements were detected using 24-MeV Si^{+5} for forward elastic recoil analysis at Sandia National Laboratories, with backscattering measurements used for additional determinations of B and N concentrations.

Mass spectrometry was used to identify ions bombarding the surface during film growth, and large concentrations of H^+, H_2^+, and H_3^+ were observed. In addition, a large fraction of the B and N incident on the growing film surface was tied up in hydrogen-containing precursors, which may be resputtered easily from the growing film surface.

Film hardness and modulus measurements were performed using an ultralow load indenter. For films deposited with pure borazine and NH_3-borazine mixtures, both hardness and modulus varied considerably from 1.4 to 10.5 GPa and 42 to 144 GPa, respectively, and were highest for films deposited at low substrate bias where the films were amorphous.

A wide range of stoichiometries were accessible, even with pure borazine as the source gas, with the ratio of B/N ranging from 0.54 to 4.4. The hydrogen atomic fraction varied from ~1 to 20 at. % and was typically 2–3 at. % for stoichiometric BN. No evidence of cubic phase formation was observed, and attempts at increasing the momentum transfer to the surface using Kr resulted in resputtering of the film well before the momentum transfer to the surface was 200 $(\text{eV amu})^{1/2}$, a value identified in recent ion beam deposition studies to be required for cubic phase formation.[5] There were, however, marked changes observed in infrared absorption and x-ray diffraction as a function of incident ion energy. Films deposited at lower ion energies were amorphous, while those deposited at higher ion energies, near the threshold for complete resputtering of the growing film,

exhibited decreased sp^2 absorption and were crystalline.

---

1. Summary of paper: *J. Vac. Sci. and Technol. A* **11**, 1863 (1993).
2. Science and Engineering Research Semester participant from Alfred University, Alfred, N.Y.
3. Metals and Ceramics Division, ORNL.
4. Sandia National Laboratories, Albuquerque, N. Mex.
5. D. J. Kester and R. Messier, *J. Appl. Phys.* **72**, 504 (1992).

SPATIAL PROFILING OF ION AND NEUTRAL EXCITATION IN NOBLE GAS ELECTRON CYCLOTRON RESONANCE (ECR) PLASMAS[1]

R. L. Rhoades[2] and S. M. Gorbatkin

Optical emission from the excited states of neutrals and ions of several noble gases has been profiled in an effort to characterize hollow mode formation in an ECR plasma. Under certain conditions, plasmas appear hollow when viewed down the axis of the system. One possible explanation is a mean-free path for ionization that is less than the distance from the edge to the center of the chamber. Under these circumstances, neutral atoms that are injected at the edge or that result from recombination at the walls have a high probability of being ionized before they reach the center of the chamber, thus leaving the center with a lower concentration of neutrals.

For pure argon plasmas with a net microwave power of 750 W, the neutral (696.5-nm) and ion (488-nm) emission profiles were slightly center peaked at 0.32 mTorr and gradually shifted to a hollow appearance at 2.5 mTorr as shown in Fig. 4.9. Neon profiles showed a similar trend from 2.5 to 10 mTorr. In general, ion profiles showed slightly stronger variations than neutral profiles, and the transition pressure scaled with the ionization potential of the gas, which is consistent with neutral

ORNL-DWG 93-15398

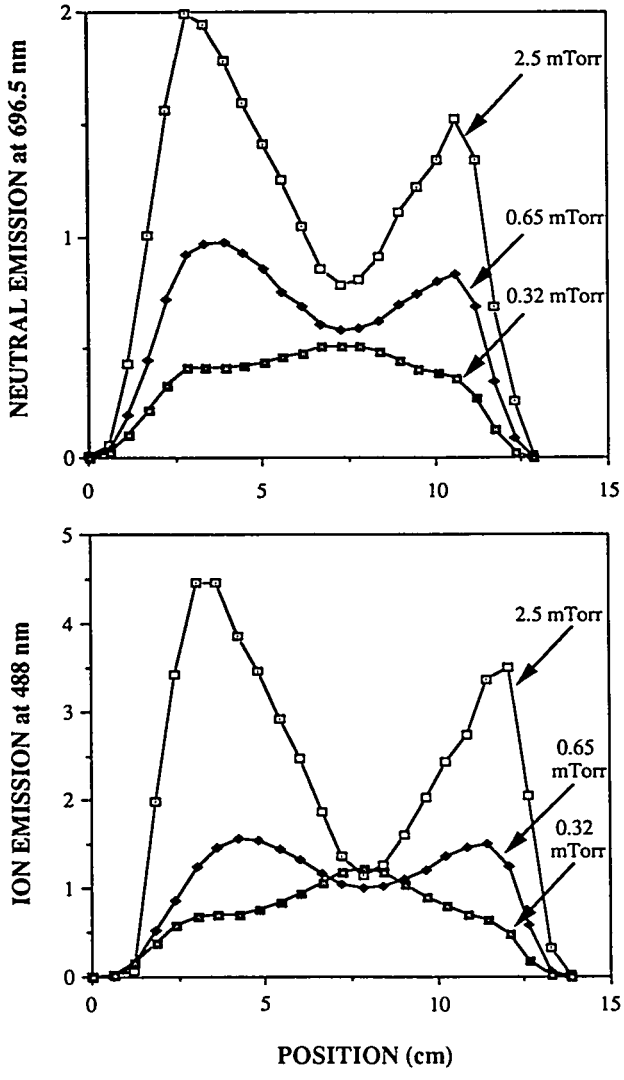

Fig. 4.9. Argon profiles taken in a mirror-field ECR source showing transition from center-peaked to hollow mode with increasing pressure and constant net microwave power of 750 W.

depletion. Studies of noble gas mixtures, however, indicated that neutral depletion is not always dominant in the formation of hollow profiles. For Kr/Ar, Ar/Ne, and Ne/He plasmas, the majority gas tended to set the overall shape of the profile. Profile trends also suggest that plasma density is more dominant than electron temperature in the formation of hollow profiles.

---

1. Summary of paper: *Applied Physics Letters* (in press).
2. ORNL/ORISE postdoctoral research associate.

DEUTERIUM-INDUCED RECONSTRUCTION OF Cu(100): CORRELATION OF SURFACE STRUCTURES WITH ABSOLUTE COVERAGE

C. F. Walters,[1] *D. B. Poker, D. M. Zehner, and E. W. Plummer*[2]

The Cu(100) surface undergoes reconstruction at low temperatures following exposure to atomic hydrogen. Several models, which predict different levels of hydrogen coverage for the saturated surface, have been proposed for the reconstruction. The $D(^3He,p)^4He$ nuclear reaction was used to determine the absolute coverage of both unsaturated and saturated atomic deuterium on the reconstructed Cu(100) surface. The sample was held at a temperature of 150 K during exposure to atomic deuterium and was then cooled to 80 K. As shown in Fig. 4.10, the saturation coverage is 1.0 ± 0.04 ML. Higher doses, up to 200 ML, show no change in the saturation coverage. Low-energy

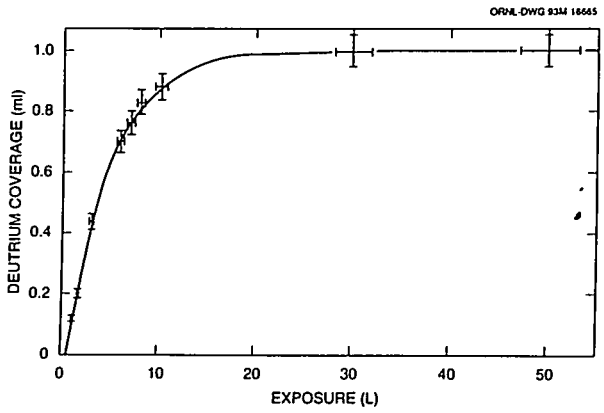

Fig. 4.10. Absolute coverage of deuterium on Cu(100) as a function of exposure, as determined by nuclear reaction analysis.

electron diffraction observations revealed no superlattice structures at deuterium coverages below ~0.45 ML and four different superlattice structures above this coverage, three of them never before reported. An unidentified superlattice structure is visible between 0.45 and 0.85 ML and is best developed at 0.65 ML. A $(2\sqrt{2} \times 2\sqrt{2})R45°$ structure is observed in a narrow range of coverages centered at 0.75 ML. Above coverages of 0.75 ML, a third pattern, the $p(2 \times 2)$-p4g structure, is observed, which has been reported previously. When the sample temperature is greater than 120 K, two domains of a $(2\sqrt{2} \times 4\sqrt{2})R45°$ structure are observed for the coverage range of 0.80 and 1.0 ML.

---

1. Graduate student from The University of Tennessee, Knoxville, Tenn.
2. ORNL/UT Distinguished Scientist.

PLASTIC FLOW INDUCED BY IONIZATION PROCESSES IN ION-DAMAGED MgO[1]

R. Brenier,[2] B. Canut,[2] L. Gea,[2]
S. M. M. Ramos,[2] P. Thevenard,[2] J. Rankin,[3]
L. Romana,[4] and L. A. Boatner

Recently, an intriguing new effect with a number of potentially important applications has been reported by Boatner et al.[5] It was found that K^+- or Kr^+-implanted MgO surfaces could be removed down to the implantation depth where the implanted MgO specimens were subjected to an ultrasonic-cavitation treatment in isopropanol. Additionally, a selected area of the K^+- or Kr^+-implanted surface could be stabilized by performing a second irradiation of the area with 2.0-MeV He^+ ions so that these He^+-irradiated areas were not removed by the subsequent ultrasonic-cavitation treatment. The goal of the present investigations is to contribute to a clarification of these implantation/ultrasonic cavitation results.

The change in mechanical properties induced by ionizing radiation in pre-implanted MgO single crystals has been investigated by surface-strain measurements and defect characterizations. Optically polished, oriented MgO substrates were implanted with 500-keV Xe^+ ions followed by 2-MeV He^+ ion bombardment at fluences up to 1.5×10^{16} He^+/cm^2. In order to use RBS to study the atomic migration accompanying the strain, some MgO samples were implanted with 150-keV Ca^+ "marker" ions and then irradiated with 2-MeV He^+ ions.

The Xe^+ and Ca^+ implantation characteristics in MgO are reported in Table 4.1. These implantations induce an out-of-plane strain of the MgO surface that is, respectively, $\Delta_1(Xe) = 12$ nm and $\Delta_1(Ca) = 30$ nm (step heights), which represent $\varepsilon_1^{out}(Xe) = 8\%$ and $\varepsilon_1^{out}(Ca) = 20\%$ of the ballistic-damage depth.

For the case of 2-MeV He^+ irradiation into unimplanted MgO, the He^+ ion energy is mainly lost by ionization processes (99%), and the number of dpa is negligible. The He^+-implanted region extends much deeper ($R_p = 4.1$ μm) than that of the Xe^+ or Ca^+ implantation, so that the measured out-of-plane strain $\Delta_1(He) = 18$ nm only represents $\varepsilon_1^{out}(He) = 0.5\%$ of the damage depth. The results of measurements of the strain induced by 2-MeV He^+ irradiation of the Xe^+ or Ca^+ pre-implanted MgO surfaces [respectively, $\Delta_2(Xe)$ and $\Delta_2(Ca)$] are reported in Fig. 4.11 as a function of He^+ fluence. In Fig. 4.11, the zero level is the unimplanted MgO surface, so that

Table 4.1. Characteristics of Single Ion Implantation into MgO

Ion	Energy	Energy Fraction in Ionization Process [%]	Fluence [10^{16} ion/cm^2]	dpa	Projected range [nm]	Induced strain [nm]
Xe^+	500	55	1	11	105	12
Ca^+	150	55	7	25	90	30
He^+	2000	99	1	~0	4100	18

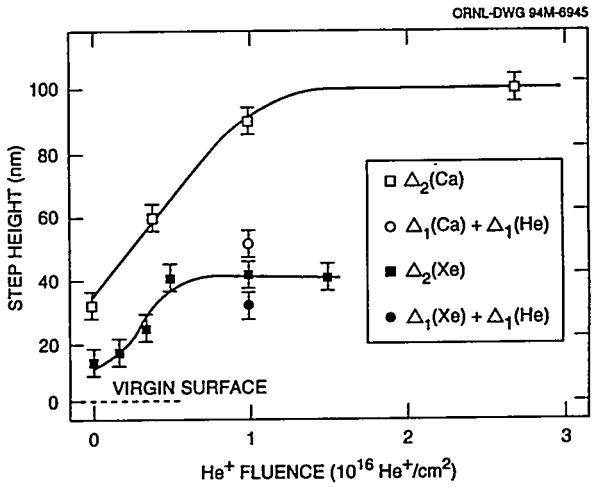

Fig. 4.11. Out-of-plane strains induced on MgO surfaces by ion implantation.

the strains due to the pre-implantations Δ_1(Xe) and Δ_1(Ca) are located at zero He^+ fluence. The strains Δ_1(He) and Δ_1(Xe) and Δ_1(He) and Δ_1(Ca) are also indicated at the fluence of 10^{16} He^+/cm^2.

It appears that the ionizing radiation induces an out-of-plane strain composed of a volume expansion and a plastic flow which relaxes the stress in the pre-implanted layer.

---

1. Summary of paper: *Nucl. Instrum. and Methods in Phys. Res. Sect. B* **80/81**, 1210 (1993).
2. Université Claude Bernard, Lyon I, Villeurbanne, France.
3. Brown University, Providence, R.I.
4. ORNL/ORISE postdoctoral research associate. Present address: Universite des Antilles et de La Guyane, Pourte a Pitre, French West Indies.
5. L. A. Boatner et al., American Ceramic Society Meeting, Minneapolis, Minn., 1992.; L. A. Boatner et al., Materials Research Society Spring Meeting, San Francisco, Calif., 1992.

ION IMPLANTATION AND ANALYSIS

ION IMPLANTATION EFFECTS IN TIN-DOPED INDIUM OXIDE THIN FILMS[1]

T. E. Haynes, Yuzo Shigesato,[2] and D. C. Paine[3]

Tin-doped indium oxide (ITO) is a degenerate semiconductor with very good optical transmission, making it a useful conductive coating material in displays, "smart" windows, and solar cells. Additional reduction of the resistivity of deposited ITO films is required to achieve faster switching speeds in thinner films. This study was initiated in order to quantify the dependence of electrical and structural properties of ITO on bombardment-induced damage, such as occurs during sputter deposition. A secondary motivation was to evaluate the prospect for reducing the resistivity by implantation of H^+, which has been argued to liberate chemically additional oxygen vacancies, important as electron donors. Figure 4.12 shows the resistivity of 2000-Å-thick, polycrystalline ITO films after implantation with various doses of either H_2^+ or O^+ at a depth of ~1000 Å. In Fig. 4.12, implant doses have been normalized by the number of displacements theoretically produced by each ion. The resistivity increased monotonically with dose for both ion species, because of reduction of both carrier concentration and mobility. The data for both H_2^+ and O^+ coincide within the dose range where they overlap, demonstrating that the effect of H_2^+ implantation is predominantly due

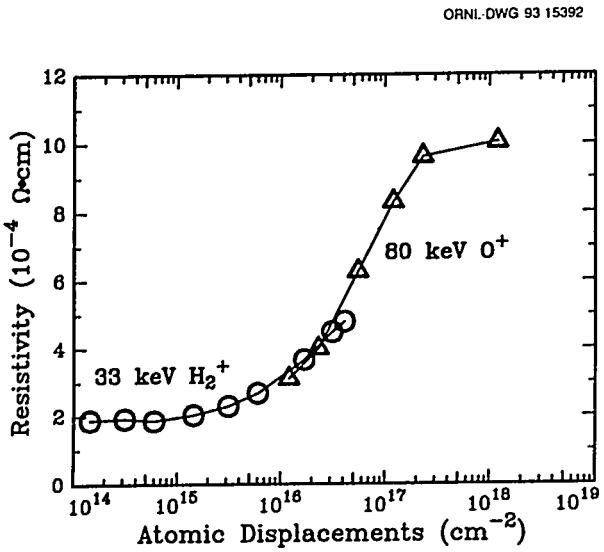

Fig. 4.12. Resistivity of ITO films implanted with either 33-keV H_2^+ or 80-keV O^+ as a function of the total number of atomic displacements induced in the film by the incident ions. Resistivity prior to implantation was 1.9×10^{-4} Ω-cm.

to damage rather than to a chemical interaction. Mobility degradation was shown to be controlled by production of neutral scattering centers during ion bombardment. Postimplant annealing at the deposition temperature recovered the initial resistivity. This evidence suggests that the mobility in sputter-deposited ITO is ultimately limited by carrier scattering at uncharged defects. Large point-defect aggregates imaged in transmission electron microscopy have been identified as candidate scatterers. It was also found that ITO is not amorphized up to very large O^+ doses, where the displacements far exceed the number of atoms in the film, implying that effective recombination of bombardment-induced defects occurs, even at 77 K.

---

1. Summary of paper: *J. Appl. Phys.* **73**, 3805 (1993); *Jpn. J. Appl. Phys.* **32**, L1352 (1993).
2. Asahi Glass Research Center, Yokohama, Japan.
3. Brown University, Providence, R.I.

IMPLANTATION DAMAGE AND ELECTRICAL ACTIVATION IN Si-IMPLANTED GaAs[1]

T. E. Haynes, R. Morton,[2] and S. S. Lau[2]

When Si is implanted into GaAs for *n*-type doping, the donor concentration becomes saturated at about $2 \times 10^{13}/cm^2$ as the implant dose is increased (illustrated by the solid curve in Fig. 1). Investigations in the Solid State Division had previously indicated that the damage induced in GaAs during ion implantation of Si is extremely sensitive to both implantation temperature and beam current near room temperature (RT). Multiple damage components were detected, indicating that the damage mechanism and microstructure undergo a critical transition as a function of temperature near RT. The proximity of this transition is likely to create problems for electrical activation following implantation at RT because of the necessity to anneal additional types of defects. A study was undertaken to investigate whether shifting the implant temperature slightly away from RT would be beneficial. Samples were implanted with 100-keV Si at

temperatures from RT to +90°C with various beam currents. Ion channeling was used to measure the damage prior to annealing, and Hall effect measurements were performed after annealing to determine the carrier activation. The results showed a strong inverse correlation between activation and implant damage. Consequently, electrical activation was improved significantly by a modest increase in implant temperature. As indicated in Fig. 4.13, the sheet carrier concentrations for 90°C implants exceeded the normal saturation level, suggesting that elevated-temperature implants may in fact be beneficial for device manufacturing. Alternatively, carrier activation was also improved by reducing the beam current by a factor of 20.

---

1. Summary of paper to be published.
2. University of California, San Diego, Calif.

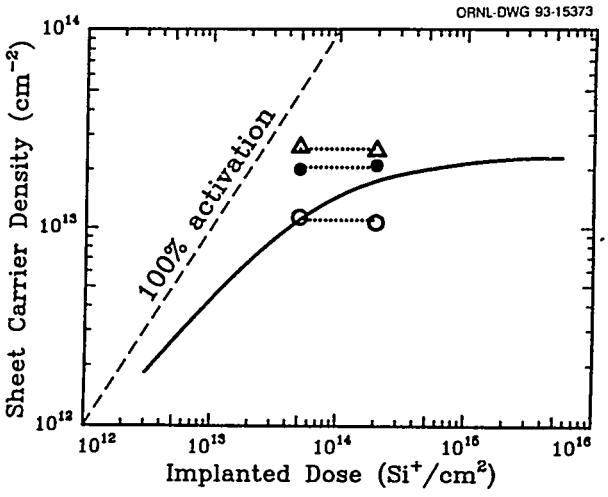

Fig. 4.13. Comparison of the electrical activation obtained in this study with typical reference data [solid curve, adapted from S. J. Pearton, *Solid State Phenom.* **1/2**, 247 (1988)]. Implant conditions were 21°C, 1.0 μA/cm^2 (open circles); 21°C, 0.05 μA/cm^2 (filled circles); and 90°C, 1.0 μA/cm^2 (triangles).

MICROVOIDING IN HIGH CURRENT DENSITY IRRADIATED Si

Ling Xie[1] *and O. W. Holland*

Ion-induced microstructure during implantation of Si(100) was investigated with a focus on the formation of microvoids, a unique morphology observed under extreme irradiation conditions such as high temperature and/or dose rate. In particular, the effect of ion chemistry on microvoiding was studied by comparing irradiations with dopant ions, As^+ and P^+, to irradiations with isoelectric ions, Ge^+ and Si^+, respectively. These combinations include ions with similar mass but different atomic number so that dopant effects can be separated from solely kinematical ones, as determined by the isoelectric ion implants. Microvoiding is clearly seen in the cross-sectional transmission electron microscopy (TEM) micrograph in Fig. 4.14(a) from a sample implanted with 80-keV P^+ ions. Two morphologically distinct layers are formed—a dislocation-free region at the surface extending over ~50 nm containing a dense distribution of microvoids, followed by an wide band of dislocation tangles. The importance of the ion-solid chemistry is demonstrated in the micrograph in Fig. 4.14(b) from a sample implanted under identical conditions but with Si^+ ions. While morphological similarities exist between the two samples, microvoids are clearly absent in the self-ion-implanted sample. Similar results were obtained from the As^+ and Ge^+ irradiations (i.e., voiding occurred only in the dopant-implanted sample). Therefore, while microvoiding is clearly dependent on the ion-solid chemistry, it does not appear to be strongly dependent of the nature of

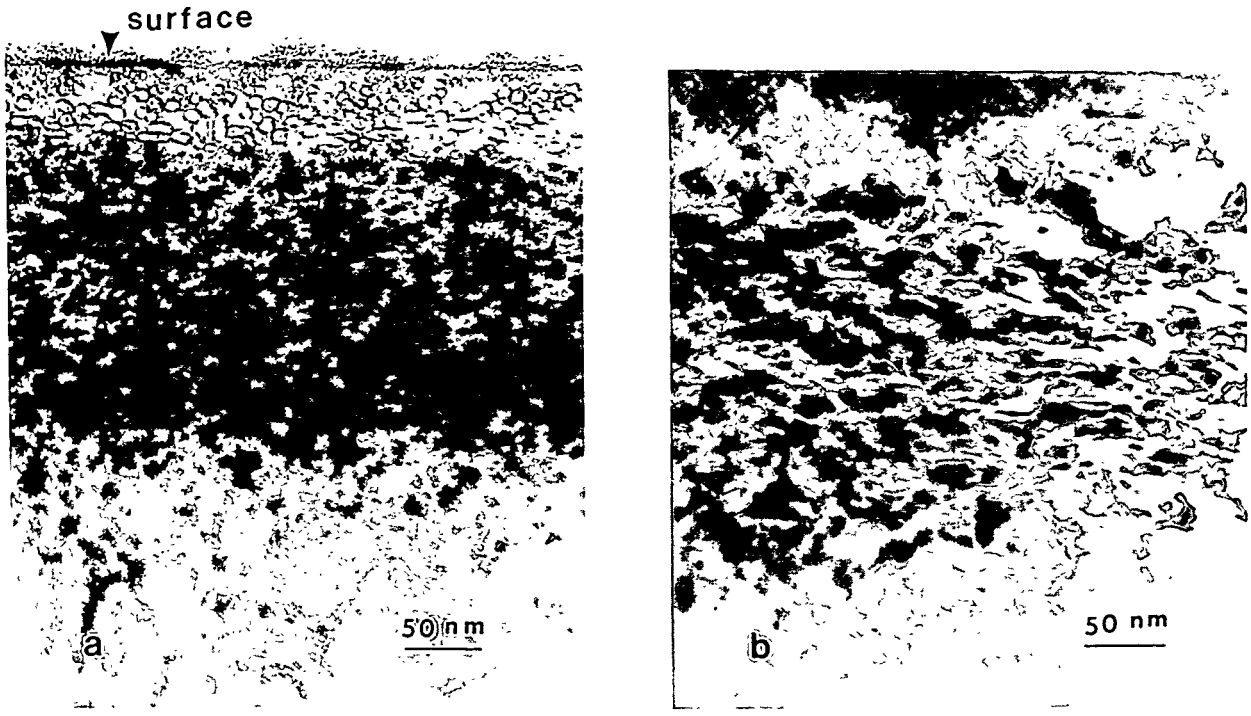

Fig. 4.14. XTEM micrographs of (a) P^+-and (b) Si^+-implanted Si (100) substrates at 80 keV with a dose of $2 \times 10^{16}/cm^2$ and a current density of 80 $\mu A/cm^2$. The initial sample temperature was 530°C but rose to 585°C because of beam heating during irradiation.

the dopant (i.e., *p*- or *n*-type). Rather, evidence suggests that chemical binding between the void embryo and the dopant stabilizes the former so that void formation becomes thermodynamically more favorable. A model has been developed to describe these results, one which can account for the microvoiding and also the differences in damage morphology in the Ge^+- and As^+-implanted samples (not shown).

A DISLOCATION-FREE PROCESS FOR PRODUCING SILICON-ON-INSULATOR BY IMPLANTATION[1,2]

O. W. Holland, D. S. Zhou,[3]
D. K. Thomas, and J. D. Budai

Ion beam synthesis of a silicon-on-insulator (SOI) material by high-dose, O^+ implantation has been studied. A buried oxide is formed during implantation near the end-of-range which electrically isolates the superficial Si layer at the surface from the bulk. The focus of this study was to understand the mechanism(s) for damage formation in the superficial layer ahead of the buried oxide during irradiation at 450°C, which ultimately limits the quality of the material. Damage growth in the Si overlayer was

1. Graduate student from the University of Wisconsin-Madison, Madison, Wis.

found to exhibit two distinctly different regimes—an initial one characterized by slow growth of vacancy-type clusters, followed by a transition to a faster growth regime marked by the onset of dislocation formation. This transition in the growth behavior was correlated with marked changes in the strain state in the superficial layer, as well as the damage morphology. These results established a causal relation between lattice strain and damage in which dislocations are formed when the buildup of negative strain arising from the vacancy-type defects in the superficial layer exceeds the yield point of the lattice. This suggested that it might be possible to intervene prior to the yield point to suppress dislocation formation by elimination or reduction of the lattice strain. This was, in fact, accomplished by a very simple but elegant method using Si^+, self-ion implantation. Prior to the yield point, O^+ implantation was interrupted so that Si^+ ions could be implanted into the strained layer. The self-ion implantation reduced the lattice strain presumably by providing excess Si atoms to occupy the vacant lattice sites. The strain relief provided by this technique delayed the onset of dislocation formation during subsequent O^+ implantation to a much higher fluence than observed in samples irradiated only with O^+ ions. Therefore, knowledge of the damage formation mechanism has led to the development of a processing technique to yield a higher quality SOI material by suppressing dislocation formation during high-dose O^+ implantation.

---

1. Summary of paper: *Appl. Phys. Lett.* **63**, 896 (1993).

2. D. S. Zhou, O. W. Holland, and J. D. Budai, *Applied Physics Letters* (in press).

3. ORNL/ORISE postdoctoral research associate.

ION BEAM SYNTHESIS OF $IrSi_3$ IN Si (111)

T. P. Sjoreen, H.-J. Hinneberg,[1] *and M. F. Chisholm*

Epitaxial metal silicides are of interest both for studies of the basic electronic properties of metal-semiconductor interfaces and for device applications. Of the metallic silicides, $IrSi_3$ has the highest measured Schottky barrier to *n*-type Si (0.94 eV) and, hence, the lowest to *p*-type, making it a possible material for use in long-wavelength infrared detectors. Because it is the stable phase of the iridium silicides and the most Si rich, it can be grown as a buried epitaxial layer in Si(111) by ion beam synthesis (i.e., high-dose Ir ion implantation followed by thermal annealing). Figure 4.15 shows a cross-sectional transmission electron microscope (TEM) image of a 90-nm thick $IrSi_3$ layer under 200 nm of Si that was produced by implanting 1-MeV Ir ions

Fig. 4.15. XTEM image of an epitaxial, buried $IrSi_3$ layer in Si(111), produced by implanting 1.6×10^{17} Ir/cm^2 at 1 MeV and 550°C and subsequent annealing at 1100°C for 5 h.

with a dose of 1.6×10^{17} Ir/cm^2 at a substrate temperature of 550°C and annealing for 5 h at 1100°C. Transmission electron diffraction results show that the epitaxial relationship of the silicide layer with the substrate is $[2\bar{1}\bar{1}0]$ $IrSi_3$ || [111]Si and $[01\bar{1}0]$ $IrSi_3$ || $[2\bar{2}0]$Si. In contrast to this single-epitaxial relationship, $IrSi_3$ films grown by interfacial reactions or by molecular beam epitaxy have two or three. Presently, experiments are in progress to find the ion implantation parameters which produce the best $Si/IrSi_3/Si$ structure. Recent Rutherford backscattering results seem to indicate that channeled ion implantation produces a superior structure, but additional characterization is needed.

---

1. Guest scientist from Technische Universität Chemnitz-Zwickau, Chemnitz, Germany.

ION BEAM SYNTHESIS OF Ti-RICH EPITAXIAL BURIED LAYERS IN $LiNbO_3$

D. B. Poker and D. S. Zhou[1]

Implantation of Ti into $LiNbO_3$ has been shown to be an effective technique for the fabrication of optical waveguides. The technique offers advantages in the control of the Ti concentration profile as well as the maximum attainable concentration. However, the need to perform solid-phase epitaxy and thermal annealing following implantation can result in significant migration of the implanted Ti. The stability of the implanted Ti (2.5×10^{17}/cm^2, 500°C) following high-temperature annealing (1000°C, 1–4 h) can be improved dramatically by an additional implant of oxygen before annealing, as measured by Rutherford backscattering (RBS)/channeling spectroscopy and secondary ion mass spectroscopy (SIMS). The improvement exhibits a threshold dependence upon the O/Ti ratio. Little effect is seen at ratios of 1.5 and below, while higher ratios produce significant improvements. At an O/Ti ratio of 3, the annealed samples showed evidence of the formation of a distinct buried layer, rich in Ti, which was epitaxially oriented with the $LiNbO_3$ substrate, as indicated by RBS analysis. SIMS analysis indicated that the concentration profile of the Ti narrowed significantly, and the concentration gradients on both sides of the peak became very sharp, as shown in Fig. 4.16(a). Without the extra oxygen implantation, the Ti migrates to the surface during solid-phase epitaxy and gradually diffuses deeper during annealing [Fig. 4.16(b)]. Cross sectional transmission electron microscopy indicated that the buried layer is distinct, with sharp interfaces, epitaxial with the $LiNbO_3$ matrix. Furthermore, the buried layer was shown to be continuous, which validated the RBS channeling analysis.

---

1. ORNL/ORISE postdoctoral research associate. Present address: Los Alamos National Laboratory, Los Alamos, N. Mex.

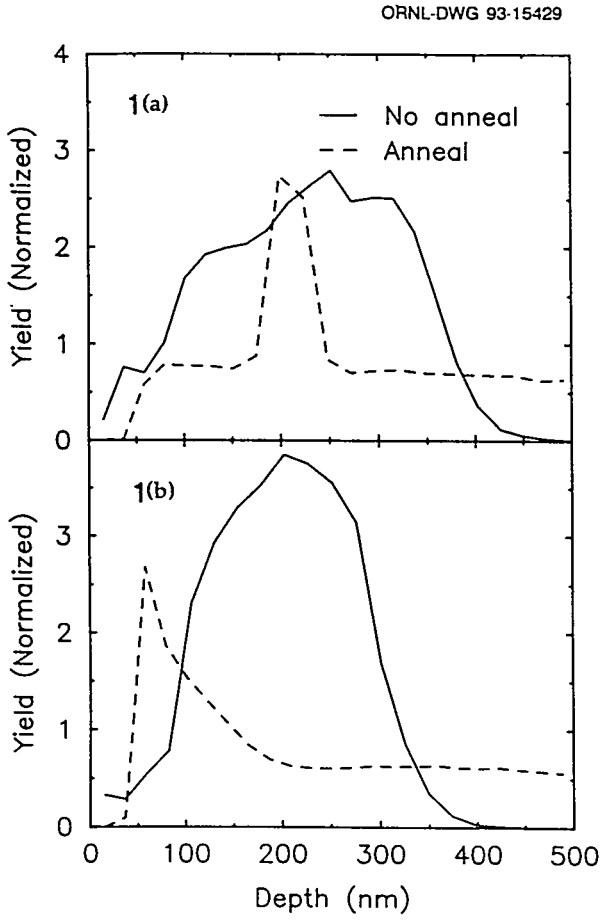

Fig. 4.16. SIMS analysis of Ti-implanted $LiNbO_3$ (a) with and (b) without additional O implantation. Lines indicate Ti concentration before (solid) and after (dashed) annealing.

ION IMPLANTATION OF ORTHOPEDIC ALLOYS

J. M. Williams and L. Riester[1]

Ion implantation of the orthopedic alloy, Ti-6Al-4V, is the accepted practice for wear prevention of the alloy in rubbing against the wear partner of ultrahigh molecular weight polyethylene (UHMWPE), but the complexity of reasons why the process works has not been established. A possibly important factor[2] is that the apparent threshold quality for prevention of severe wear results from a model in which the alloy surface is hardened to the point that it is harder than the abrasive wear agent. There is a strong basis for believing[3] that the abrasive wear agent is amorphous TiO_2 that has been wiped from the alloy surface and has become embedded in the UHMWPE surface. There are related issues, including wear of the UHMWPE surface in relation to surface properties of either Ti-6Al-4V or orthopedic CoCrMo alloys.

By use of the nanoindentation hardness technique, hardness vs fluence has been measured for Ti-6Al-4V alloys and CoCrMo following nitrogen implantation. Results (Fig. 4.17) have been compared with similar measurements

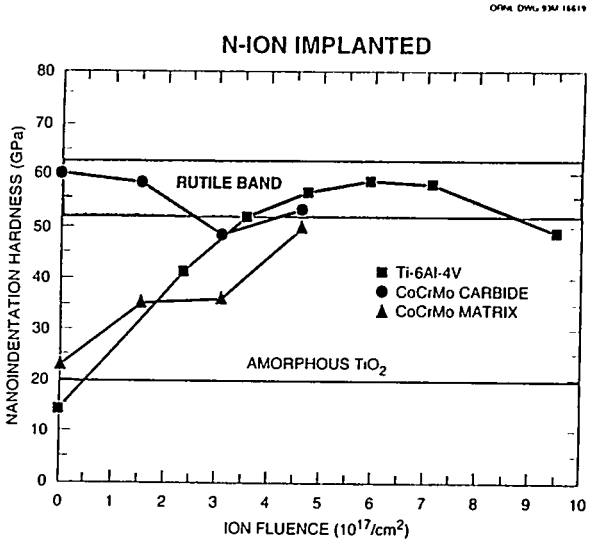

Fig. 4.17. Hardness vs nitrogen fluence for Ti-6Al-4V, CoCrMo matrix, and CoCrMo carbide. Energies for both alloys were designed to produce a treatment depth of about 0.12 μm. Hardnesses of rutile and amorphous TiO_2 (both unimplanted) by the same technique are indicated for reference.

for rutile and amorphous TiO_2, which was produced by ion implantation amorphization of rutile. Because of indenter geometry, absolute values are estimated to be too high by a factor of ~4, but intercomparisons from one material to the other are valid in principle.

For the Ti alloy, the hardness exceeds that of amorphous TiO_2 after a rather low fluence. Through the broad maximum, the hardness is about the same as that of rutile. Therefore, it is credible that the model mentioned above accounts for the wear improvement.

For the Co alloy, implantation markedly increases the hardness of the metal matrix, but the hardness of the carbide phase decreases or remains about the same. This improved uniformity of hardness due to implantation is a possible explanation of improved wear of the UHMWPE against ion-implanted CoCrMo.

---

1. Metals and Ceramics Division, ORNL.
2. M. A. Moore, *Int. J. Mater. Eng. Appl.* **1**, 97 (1978).
3. J. Lausmaaa et al., *Mat. Res. Soc. Symp. Proc.* **55**, 351 (1986).

ION BEAM MIXING STUDIES IN Pt/Ti AND Pt/Ni BILAYERED SAMPLES

J. M. Williams and D. B. Poker

Thermal spike energy deposition is considered to be the most important part of radiation damage in accounting for the kinetics of ion beam mixing.[1,2] Chemical dependency for ion mixing is regarded as an integral part of the thermal spike model.[1,2] However, the two aspects of mixing may not necessarily be connected.[3] The bilayered systems, Pt-Ti and Pt-Ni, were chosen for further careful investigations of these questions. These are examples of a highly exothermic system (Pt-Ti) vs a near-neutral system (Pt-Ni). Nuclear stopping is about the same for the two systems, so differences should be attributable to chemical effects.

For the Pt/Ti pair, samples were prepared by three methods. This procedure was done to help control against interfacial contamination for the reactive Ti layer. Ion mixing was done primarily with 1.0-MeV Xe ions. Irradiation temperatures were ~10 and ~80 K. Composition vs depth curves were deconvoluted from Rutherford backscattering data by use of the code SQUEAKIE. Effective interdiffusion was determined by use of the Matano analysis.

Figure 4.18 summarizes the data in comparison with the results of previous workers[2] for

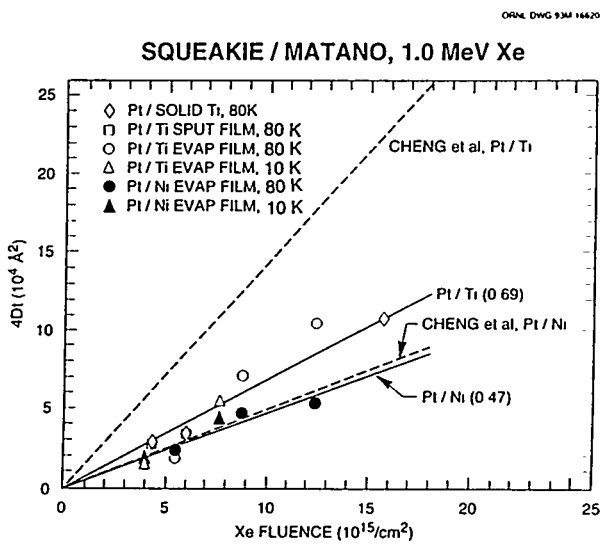

Fig. 4.18. $4Dt$ vs ion fluence for 1.0-MeV Xe ions on various bilayered films at ~10 and ~80 K. The data are compared with those of Cheng et al.[2] Slopes of the straight line fits are known as mixing efficiencies.

approximately equivalent parameter values. The data of the other workers do not span as large a dose range as the present data, but the curves have been extrapolated to facilitate comparison. The mixing efficiencies (slopes of the lines) are very nearly the same for the Pt/Ni layers, but present results for the Pt/Ti show considerably less efficiency than do those of previous workers, especially in the dose range below $7 \times 10^{15}/cm^2$.

The best explanation of the present data is that a thermal spike model is still required to account for absolute values of mixing efficiencies. Resolution of other questions may lie in the fact that chemical dependency is apparently much less than had been thought previously .

---

1. W. L. Johnson et al., *Nucl. Instrum. and Methods Phys. Res. Sect. B* **7/8**, 657 (1985).
2. Y.-T. Cheng, *Mater. Sci. Rep.* **5**, 45 (1990).
3. R. Kelly and A. Miotello, *Nucl. Instrum. and Methods Phys. Res. Sect. B* **59/60**, 517 (1991).

STUDY OF HYDROGEN DIFFUSION IN AlCu ALLOY

T. P. Sjoreen, C. W. White, O. W. Holland, and S. R.Wilson[1]

During very large scale integration fabrication, annealing in a forming gas is performed to passivate dangling bonds at the Si/SiO_2 gate interface by H absorption. However, there is an emerging concern that this step may also drive H into the Al interconnects, which may lead to voiding at the Al-oxide interface and loss of ohmic contact to *p*-type Si by neutralization of acceptors.

A study of the diffusion of H in 1.5%Cu/Al alloy was begun recently. In the initial experiments, $Si_3N_4/AlCu/SiO_2/Si$ and $AlCu/SiO_2/Si$ structures were exposed to 90% N_2 + 10% H_2 forming gas for 30 min at 450°C. The first structure was used to determine the diffusion of H through Si_3N_4, while the second structure exposed the AlCu layer directly to the forming gas. After annealing, the as-deposited and annealed samples were analyzed for hydrogen content by elastic recoil spectrometry (ERS) using 2.3-MeV He ions. As shown in Fig. 4.19, initial ERS analysis indicates that the concentrations of H in the Si_3N_4 layers are quite large: $\sim 2.5 \times 10^{22}$ H/cm^3. Nevertheless, comparison of the as-deposited and annealed samples shows that the H concentrations in aluminum are less than 10^{20} H/cm^3, either as a result of diffusion through the nitride (Fig. 4.19) or by direct uptake for the forming gas during annealing. If H plays a role in stress voiding, then it must be

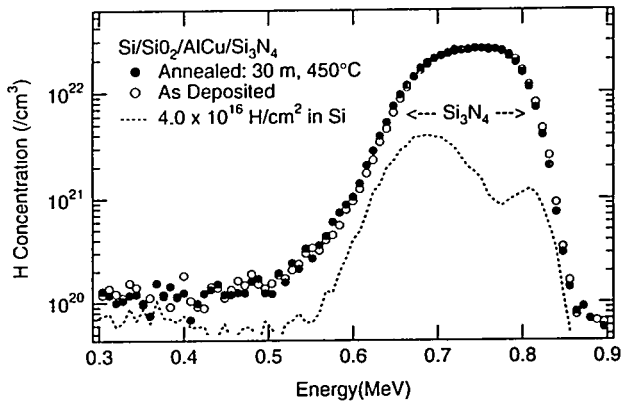

Fig. 4.19. Hydrogen concentration profiles obtained from as-deposited and annealed samples in which 110 nm of Si_3N_4, 700 nm of AlCu, and 200 nm of SiO_2 were deposited over a Si substrate. The yield from a Si substrate implanted with 25-keV H_2 ions to a dose of 4.0×10^{16} H/cm^2 is included for comparison.

at concentrations of less than 10^{20} H/cm^3, which seems unlikely. However, these initial measurements have a background limitation of about 0.5×10^{18} H/cm^3 per mC of ion beam charge (0.4–0.5 MeV in Fig. 4.19), which is believed to arise from H atoms knocked out of the mylar absorber. Studies are presently under way with different absorbing films in an attempt to lower the background.

---

1. Motorola, Inc., Mesa, Ariz.

PROTECTIVE OXIDE FORMATION ON $NbAl_3$ AND TiAl ALLOYS VIA ION IMPLANTATION

S. P. Withrow, R. J. Hanrahan, Jr.,[1] *E. D. Verink, Jr.,*[1] *and E. Ristolainen*[1]

High-temperature oxidation resistance in aluminide intermetallic compounds and related alloys can be achieved with the formation of a protective layer of alumina (Al_2O_3) by selective oxidation at high temperatures. The formation of alumina can be complicated, however, by the preferential reaction of the other elements to make nonprotective transient oxides at the onset of oxygen exposure. Surface modification by oxygen ion implantation to form a thin oxide layer just below the surface prior to annealing has been investigated as a technique for altering the high-temperature oxidation kinetics. Initial experiments have been made on the binary compounds $NbAl_3$ and TiAl.

Oxygen-18 was implanted at room temperature into $NbAl_3$ and TiAl samples at selected energies up to 168 keV to achieve both stoichiometric and substoichiometric alumina concentrations. The samples were subsequently annealed in oxygen at 1000°C for short times (up to 30 min). The oxides formed on both implanted and nonimplanted samples were characterized using secondary ion mass spectroscopy, Auger electron spectroscopy, and transmission electron microscopy.

For implantation of 1×10^{18} O/cm^2, an oxygen-saturated region is formed in both alloys. Auger depth profiles, which are sensitive to the bonding of the Al, indicated essentially all of the Al in this region is oxidized. The as-implanted region is amorphous or contains nanocrystalline precipitates. Annealing the $NbAl_3$ sample for 15 min produced a mixture of Nb metal and alumina. In contrast, the annealed TiAl sample contained both Ti and Al oxides at the surface. For lower dose, substoichiometric implantations (peak concentration ~20 at. %), the as-implanted results are similar to those seen at higher doses except that all the Al is not oxidized. Annealing induces an alumina (titania) layer to form on the $NbAl_3$ (TiAl) surface. The scale that forms over the implanted region is thinner, indicating that implantation slows the oxidation process.

---

1. University of Florida, Gainesville, Fla.

LASER AND MOLECULAR BEAM PROCESSING OF THIN FILMS

PULSED-LASER GROWTH OF EPITAXIAL COMPOUND SEMICONDUCTOR FILMS WITH CONTINUOUSLY VARIABLE COMPOSITION[1]

J. W. McCamy[2] and D. H. Lowndes

Pulsed-laser ablation (PLA) is a process in which a solid target (usually polycrystalline) is irradiated with a highly focused pulsed-laser beam. Each laser pulse produces a dense laser-generated plasma close to the target. Rapid expansion of the heated plasma causes an energetic beam containing electrons, ions, atoms, and very simple molecules in both ground and excited energy states to be ejected nearly perpendicular to the target surface. Thin-film growth occurs when this energetic beam is deposited on a heated substrate located nearby.

PLA has two outstanding advantages for film growth. First, because growth occurs from an energetic beam, epitaxial films can be grown at lower substrate temperatures than by most other film-growth methods. Second, deposition is stoichiometric—the deposited film has the same composition as the target, even for complex, multi-element materials. However, films with variable composition are needed to relieve lattice strain and to control electrical and optical properties by band-gap engineering.

A simple, new method to vary the composition and doping of PLA compound semiconductor films was recently developed; the method makes possible growth of unique epitaxial structures. Continuous variation of film composition is achieved by carrying out PLA in a low-pressure ambient gas atmosphere. By selecting an appropriate gas molecule, atoms produced by decomposition of the gas can be incorporated in the growing film, changing its composition. Many gas molecules can be used, the only requirement being that unwanted decomposition products be volatile so they are carried off in the gas phase. The low and continuously variable density of a gas makes possible very sensitive control of film composition, simply by varying the gas pressure. Large changes of film composition, ~>50%, can be achieved at quite low gas pressures so there is no interference with the PLA process. A high-purity, nonreactive gas (e.g., helium or argon) also can be added to moderate and "tune" the kinetic energy ablation beam (via gas-phase collisions). This makes possible film growth under constant plasma-energy conditions, but with variable film composition controlled by the partial pressure of the reactive gas component. It has been shown that low concentrations of dopant atoms also can be introduced in a similar way, so it should be possible to control the electrical properties of the semiconductor film.

This invention is significant because interest in PLA and its applications has grown "explosively" for about five years, but with virtually no use for compound semiconductors. This discovery overcomes the principal limitation of PLA for epitaxial semiconductor film

growth; namely, that film composition had been limited to that of the ablation target. A patent application has been filed with the U.S. Patent Office.[3]

---

1. Summary of paper: *Appl. Phys. Lett.* 63, 3008 (1993).
2. Graduate student from The University of Tennessee, Knoxville, Tenn.
3. J. W. McCamy and D. H. Lowndes, *Method for Continuous Control of Composition and Doping of Pulsed-Laser Deposited Films*, October 6, 1993.

SSDN-4662

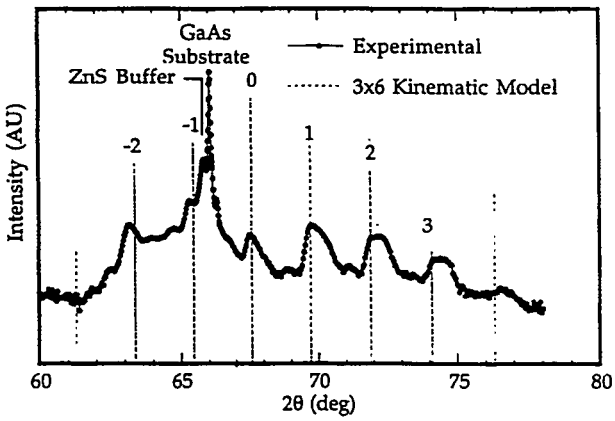

Fig. 4.20. XRD pattern ($\theta/2\theta$) for a 65-period ZnSe-ZnS superlattice grown on GaAs (001) at $T_g = 325°C$.

GROWTH OF ZnS-ZnSe STRAINED-LAYER SUPERLATTICES BY MULTITARGET PULSED-LASER ABLATION[1]

J. W. McCamy[2] and D. H. Lowndes

Recently, conventional multitarget pulsed-laser ablation (PLA) growth of wide band-gap Zn-based II-VI semiconductor strained-layer superlattices was investigated by growing structures of the form $(ZnSe)_m$ - $(ZnS)_n$, where m and n are the number of unit cells per epilayer. The epitaxial layers were formed by alternately ablating polycrystalline ZnS and ZnSe targets.

One structure consisted of 65 periods of compositional modulation of the form $(ZnSe)_6$ - $(ZnS)_3$, grown on a 370-nm-thick ZnSe buffer layer. The expected lattice constant along the surface normal for a superlattice with this 2:1 composition ratio is 0.556 nm ($2\theta = 67.3°$). Figure 4.20 shows a $\theta/2\theta$ x-ray diffraction (XRD) pattern in the vicinity of the (004) reflection. It reveals several orders of superlattice satellite peaks, with the position of the zero-order peak, $2\theta = 67.54°$, in good agreement with the calculated lattice constant. The compositional modulation period of the superlattice, determined from the separation of adjacent superlattice peaks, was $L = 4.8$ nm, only about 4% less than the $L = 5.0$-nm value that was expected based on the known deposition rate and number of laser shots per layer. The presence of several orders of satellite peaks shows that this $(ZnSe)_6$ - $(ZnS)_3$ structure has sharp compositional interfaces and is structurally comparable to strained-layer superlattices of these materials grown by other methods (e.g., molecular beam epitaxy).

---

1. Summary of papers: p. 471 in *Laser Ablation in Materials Processing: Fundamentals and Applications*, ed. by B. Braren, J. Dubowski, and D. Norton, Materials Research Society, Pittsburgh, Pa., 1993; p. 357 in *Wide Band-Gap Semiconductors*, ed. by Y. Hayashi et al., Tsukuba, Japan, 1992.
2. Graduate student from The University of Tennessee, Knoxville, Tenn.

GROWTH OF EPITAXIAL Zn-S-Se HETEROSTRUCTURES INCORPORATING BOTH CONTINUOUSLY GRADED AND ABRUPT, PERIODIC COMPOSITIONAL CHANGES[1]

J. W. McCamy,[2] D. H. Lowndes, and T. M. Rosseel[3]

As described previously,[4] it was recently discovered that compound semiconductor ternary alloy films can be grown by ablating a target of fixed composition into an appropriate ambient gas and controlling film composition via the gaseous partial pressure. In order to demonstrate and evaluate this method for spatial control of heterostructure composition, multilayered heteroepitaxial structures based on $ZnSe_{1-x}S_x$ that incorporate both abrupt, periodic, and continuously graded changes in composition have been fabricated.

A polycrystalline ZnSe target was ablated into an ambient atmosphere containing H_2S. Abrupt compositional changes were produced by interrupting laser ablation briefly, changing the H_2S partial pressure, and then resuming ablation. The thickness of each layer was controlled by the number of laser pulses, while its composition "x" was determined by ambient H_2S pressure. By periodically varying the gas pressure and number of laser shots, epitaxial layers with highly reproducible thickness and composition were grown. By changing the H_2S partial pressure gradually without interrupting growth, layers having continuously graded composition were grown.

Figure 4.21 shows a secondary ion mass spectrometry (SIMS) profile of the S^{32} content in an epitaxial $ZnSe_{1-x}S_x$ structure grown by depositing a $ZnSe_{0.94}S_{0.06}$ buffer layer in order to match lattice constants with the GaAs (001) substrate and then increasing x abruptly to 0.18 and holding constant while a rectangle-wave compositional modulation simultaneously was imposed. Next, the average sulfur content gradually was ramped down from $x = 0.18$ (at 165 nm) to $x = 0.06$ (at 600-nm thickness), still with the rectangle-wave compositional modulation present. Finally, a pure ZnSe cap layer was grown. Because the depth resolution of SIMS is only 5–10 nm, the compositional modulation actually achieved is considerably more abrupt than that shown in Fig. 4.21.

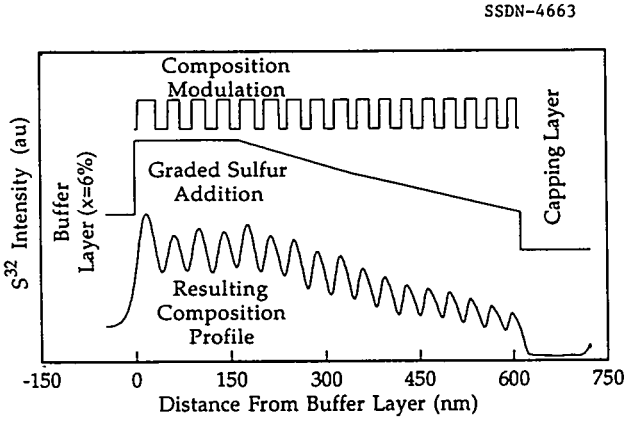

Fig. 4.21. Top two curves: Ideal periodically modulated and continuously graded sulfur compositional profiles. Bottom curve: Experimental SIMS profile of sulfur content vs depth.

The technological significance of this discovery is that it directly addresses the requirement for compound semiconductor films with continuously variable composition in semiconductor devices: (1) compositionally graded buffer layers are needed for strain relief between semiconductor layers with different lattice constants; (2) abrupt compositional transitions are

needed to form quantum well structures, to confine carriers, and to enhance their mobility ("band-gap engineering"); (3) dopant-atom concentrations must be varied precisely to control electrical properties of semiconductor films in unipolar devices; and (4) an ability to change dopant type abruptly (e.g., from *n*-type to *p*-type) is the key to fabrication of *p-n* junctions and bipolar devices. These examples also apply to thin-film photovoltaic cells used to convert solar energy to electricity, an application of direct interest to industry and the DOE.

---

1. Summary of paper: *Appl. Phys. Lett.* 63, 3008 (1993).
2. Graduate student from The University of Tennessee, Knoxville, Tenn.
3. Analytical Chemistry Division, ORNL.
4. J. W. McCamy and D. H. Lowndes, "Growth of ZnS-ZnSe Strained-Layer Superlattices by Multitarget Pulsed-Laser Ablation," this report.

GROWTH OF EPITAXIAL ZnSe FILMS BY PULSED-LASER ABLATION[1]

J. W. McCamy,[2] D. H. Lowndes, and G. E. Jellison, Jr.

ZnSe is an attractive optoelectronic material because of its wide direct band-gap (E_g = 2.7 eV, λ_g = 459 nm). Thin, epitaxial ZnSe films are needed for active device applications such as blue LEDs or laser diodes, as well as for passive structures such as optical waveguides and windows for solar cells.

Pulsed KrF (248 nm) laser ablation of a carbon-free polycrystalline ZnSe target was used to grow high-quality, epitaxial ZnSe thin films on GaAs (001), GaAs (111), and GaP (001). The films were grown at temperatures in the range 200–400°C, using a rotating substrate heater geometry that permitted growth of uniform-thickness films (~200 nm ± 1%) over an area ~75mm^2. The effects of film-substrate lattice-constant mismatch and of growth temperature on the defect structure of the films were determined by a combination of x-ray diffraction (XRD), Rutherford backscattering spectrometry, and electron microscopy measurements.

The optimal growth temperature, T_g, was found from the XRD linewidth to be 325 (± 25)°C, at which temperature the ZnSe (004) XRD rocking curve width for a 225-nm-thick film implied a misfit dislocation density $\rho_d \sim 1.6 \times 10^{14}$ cm^{-3}.

The electronic band structure of ZnSe films grown on (001) GaAs was investigated by using spectroscopic two-channel polarization modulation ellipsometry to determine the dielectric function. Transparency of the films below the band edge, as well as observation of a variety of optical transitions in the dielectric function spectrum, demonstrated that PLA-grown ZnSe films are of high optical quality.

Photoluminescence measurements for an 800-nm-thick film on GaAs (001) showed both donor-bound and acceptor-bound excitonic emissions, as well as emission from the free exciton. The free-exciton peak was split into heavy- and light-hole components because of strain present in the film. The observed splitting corresponded to a strain of 1.6×10^{-3}. This value

is in excellent agreement with the strain measured in the same manner for a comparable molecular beam epitaxial-grown ZnSe film.[3]

---

1. Summary of papers: p. 243 in *Wide Band-Gap Semiconductors*, ed. by T. D. Moustakas, J. I. Pankove, and Y. Hamakawa, Materials Research Society, Pittsburgh, Pa, 1992; *J. Appl. Phys.* **73**, 7818 (1993).
2. Graduate student from The University of Tennessee, Knoxville, Tenn.
3. D. J. Olego, *J. Vac. Sci. and Technol. B* **6**, 1193 (1988).

INVESTIGATION OF THE KINETICS OF DIGERMANE CHEMISORPTION AND REACTION PRODUCT DESORPTION IN THIN-FILM GROWTH OF GERMANIUM[1]

G. Eres and J. W. Sharp[2]

By entraining CVD growth molecules in pulsed supersonic-free jets, the process of thin-film epitaxial growth can be resolved into its successive chemisorption and surface-species decomposition stages. For Ge epitaxy from digermane, the dominant surface species is the Ge monohydride, which decomposes by H_2 desorption.[3] The surface kinetics of this film-growth process have been studied by combining pulsed gas delivery with high-resolution reflectance measurements.

Ge(001) homoepitaxy was performed in a high-vacuum growth chamber after the native oxide was desorbed by a 5-min bake at 700°C. Surface reaction kinetics were investigated for temperatures between 680 and 810 K. A home-built, water-cooled pulsed molecular beam valve delivered ~2 ML/pulse doses of digermane in a helium carrier. During growth, the beam of a low-power, ultrastable (0.02% rms noise) helium-neon (632.8-nm) laser beam was reflected from the sample onto a silicon photodiode. The diode output was amplified, digitized, and stored at sampling intervals as short as 0.1 ms.

Chemisorption of digermane causes a reflectance decrease; this is reversed as the surface monohydride desorbs. In Fig. 4.22, chemisorption data are plotted after multiplication by a negative constant in order to facilitate comparison with adsorption models. A similar

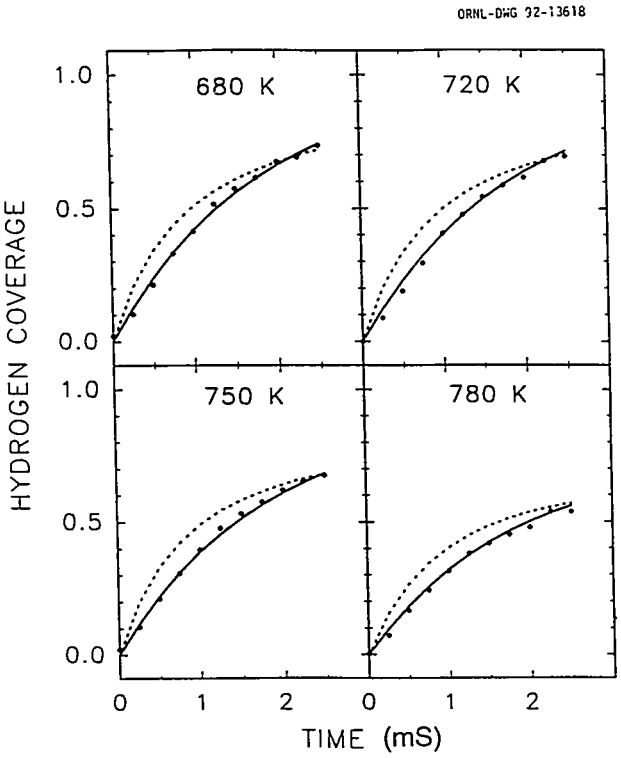

Fig. 4.22. The adsorption layer formation derived from the transient differential reflectance signal is given by the solid dots at four substrate temperatures. The solid line represents the fit given by a kinetic model for first-order chemisorption balanced by first-order desorption; the dashed line represents second-order chemisorption balanced by first-order desorption.

analysis was possible for the desorption data. Assuming that the adsorption-induced reflectance change is linearly proportional to the hydrogen coverage, it was possible to assign first-order kinetics to both Ge_2H_6 chemisorption and H_2 desorption. In addition, it was found that the chemisorption rate was independent of the substrate temperature, while H_2 desorption rates were consistent with a 1.7-eV thermal activation energy. It is believed that this first-order, recombinative H_2 desorption on Ge(001) results from the pre-pairing of H atoms on surface dimers.[4] First-order, temperature-independent digermane chemisorption suggests a direct sticking event involving a single dimer.

---

1. Summary of paper: *J. Vac. Sci. and Technol. A* **11**, 2463 (1993).
2. Graduate student from The University of Tennessee, Knoxville, Tenn.
3. J. A. Appelbaum et al., *Surf. Sci.* **70**, 654 (1978).
4. S. M. Cohen et al., *J. Vac. Sci. and Technol. A* **10**, 2166 (1992).

KINETICS OF HYDROGEN DESORPTION IN SURFACE-LIMITED THIN-FILM GROWTH OF SiGe ALLOYS[1]

J. W. Sharp[2] and G. Eres

Surface differential reflectance[3] was used to monitor hydrogen desorption during epitaxial growth of SiGe thin films from helium-seeded pulsed jets of digermane (Ge_2H_6) and disilane (Si_2H_6) mixtures. Two desorption components, which we associate with Si- and Ge-mediated desorption processes, were observed.

The alloy films were grown on Si(001) substrates in a load-locked chamber at temperatures between 670 and 830 K. At these temperatures, only the surface monohydrides are populated significantly. Disilane to digermane ratios of 1:1, 3:1, and 6:1 yielded films with Si fractions of 0.10, 0.39, and 0.54, respectively, indicating that digermane reacts 5–7 times more readily with the alloy surfaces. Following adsorption of the growth gas, isothermal measurements of hydrogen desorption rates were made by isolating the time-dependent surface layer contribution to the sample reflectance. An example of data for each hydrogen desorption component is given in Fig. 4.23, along with the

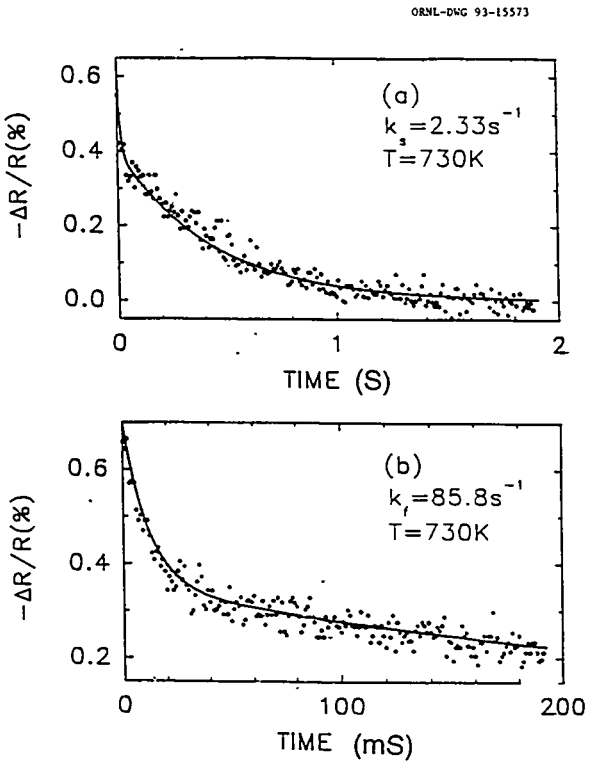

Fig. 4.23. Differential reflectance data for hydrogen desorption during SiGe alloy growth from a 3:1 disilane/digermane gas mixture are shown by the solid dots. The solid lines represent biexponential fits.

rate constants, k_f and k_s, for the fast and slow processes. The existence of two desorption components is consistent with the premise that the transition state consists of two H atoms interacting with a single Si or Ge atom.

The desorption rate constants have been studied as a function of film composition and surface temperature. For the 10% Si films, the rapid component is very similar to H_2 desorption from pure Ge. As the films become more Si-rich, both components become slower for a given temperature. Although both components are thermally activated for all compositions, the activation energies are between 0.4 and 1.3 eV, well below the activation energies of H_2 desorption from the monohydrides of Si (~2.5 eV) and Ge (~1.7 eV). This result is believed to reflect non-Arrhenius behavior, suggesting that a single mechanism is not rate-limiting over the studied temperature range.

---

1. Summary of paper: *Appl. Phys. Lett.* **62**, 2807 (1993).
2. Graduate student from The University of Tennessee, Knoxville, Tenn.
3. J. D. E. McIntyre and D. E. Aspnes, *Surf. Sci.* **24**, 417 (1971).

LASER ABLATION OF GRAPHITE INTO RARE GASES FOR FULLERENE PRODUCTION[1]

D. B. Geohegan, A. A. Puretzky,[2]
R. E. Haufler,[2] *R. L. Hettich,*[3]
X.-Y. Zheng, [4] *and R. N. Compton*[2]

The dynamics of KrF laser ablation (Φ = 20 J cm^{-2}) of graphite into 300 Torr of He, Ne, Ar, and Xe were investigated to understand how hot ablation plumes thermalize to form fullerenes and other clusters. Fast imaging of the visible plasma emission using a gated intensified charge-coupled device (ICCD) array camera revealed unexpected hydrodynamic phenomena, in which the plume was found to expand in stages governed by reflected shock waves within the plume.

Figure 4.24 illustrates the three common phases of plasma plume propagation: (1) forward motion, deceleration, and stopping of the leading edge of the plume at Δt = 300 ns; (2) a reflected shock within the plume which propagates backward and partially reflects from the rod surface at Δt = 1 μs, leaving "redeposited" material; and (3) a secondary forward propagation and coalescence of the material reflected from the rod surface, resulting in continued expansion and dissipation of the plasma and the appearance of glowing ultrafine particles at Δt = 500 μs. For argon, two sets of reflected shocks were observed, as seen at Δt = 10 μs.

The temporal and spatial behavior of both the "redeposition" of material on the target and the formation of hot nanoparticles from the hot plasma were discovered in these measurements and correlated with the presence of fullerenes in the deposited and redeposited material. For each gas, the soot redeposited on the graphite rod following ablation was highly fullerene-deficient compared with the material collected on a sample disk 1.5 cm from the rod, as determined by laser desorption Fourier transform mass spectrometry. The difference in fullerene content between the material deposited

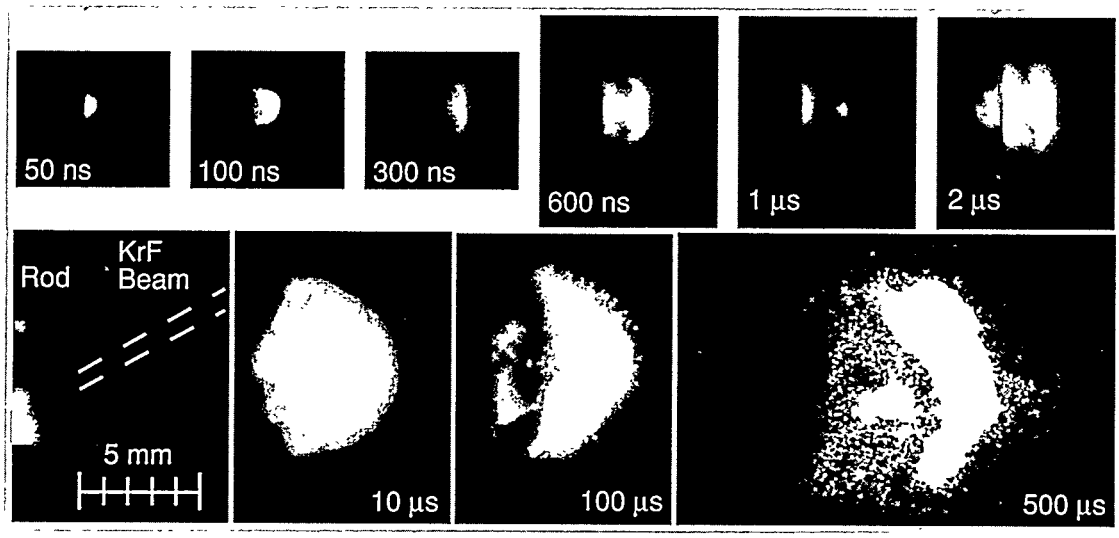

Fig. 4.24. Gated ICCD photographs of the visible plume following KrF laser (20 J cm^{-2}, 46 ns FWHM pulse) ablation of graphite into 300-Torr argon at the indicated time delays following the laser pulse. Exposures were varied from 5 to 200 ns. The side-on view of the graphite rod, scale, and band of redeposited soot is shown in the inset.

on the rod and on the disk may be rationalized if one takes into account that soot deposition on the disk occurs after 500–1000 μs (the third phase) when the ablated material has cooled and has mixed well with the buffer gas.

---

1. Summary of paper: in *Laser Ablation II—Mechanisms and Applications*, 288, ed. by D. B. Geohegan and J. C. Miller, American Institute of Physics, New York (in press).
2. Health Sciences Research Division, ORNL.
3. Analytical Chemistry Division, ORNL.
4. Postdoctoral research associate from The University of Tennessee, Knoxville, Tenn.

FAST INTENSIFIED CHARGE-COUPLED DEVICE (ICCD) PHOTOGRAPHY OF THE PULSED-LASER DEPOSITION PROCESS[1]

D. B. Geohegan

Sensitive imaging of visible light emission following excimer laser ablation has revealed several hydrodynamic phenomena that influence film growth during pulsed-laser deposition. These phenomena are observable in Fig. 4.25, which shows the propagation of a vaporized $YBa_2Cu_3O_{7-x}$ plasma plume, through 200-mTorr oxygen, toward a cold heater at a typical film-growth separation of 5 cm. The high-pressure plasma plume of vaporized target material expands unhindered during the first microsecond, then forms a contact front that undergoes noticeable slowing and eventually coalesces into a stable propagating shock front in the 200-mTorr oxygen background gas in Fig. 4.25(a–e). Observations of the plume by eye (or ordinary camera) appear to show that it stops short of the heater face. However, the photon-counting sensitivity of the ICCD camera system reveals that the plume does not stop, but continues to move slowly toward the heater [Fig. 4.25(g–h)]. The velocity of the plume boundary just before impact with the heater

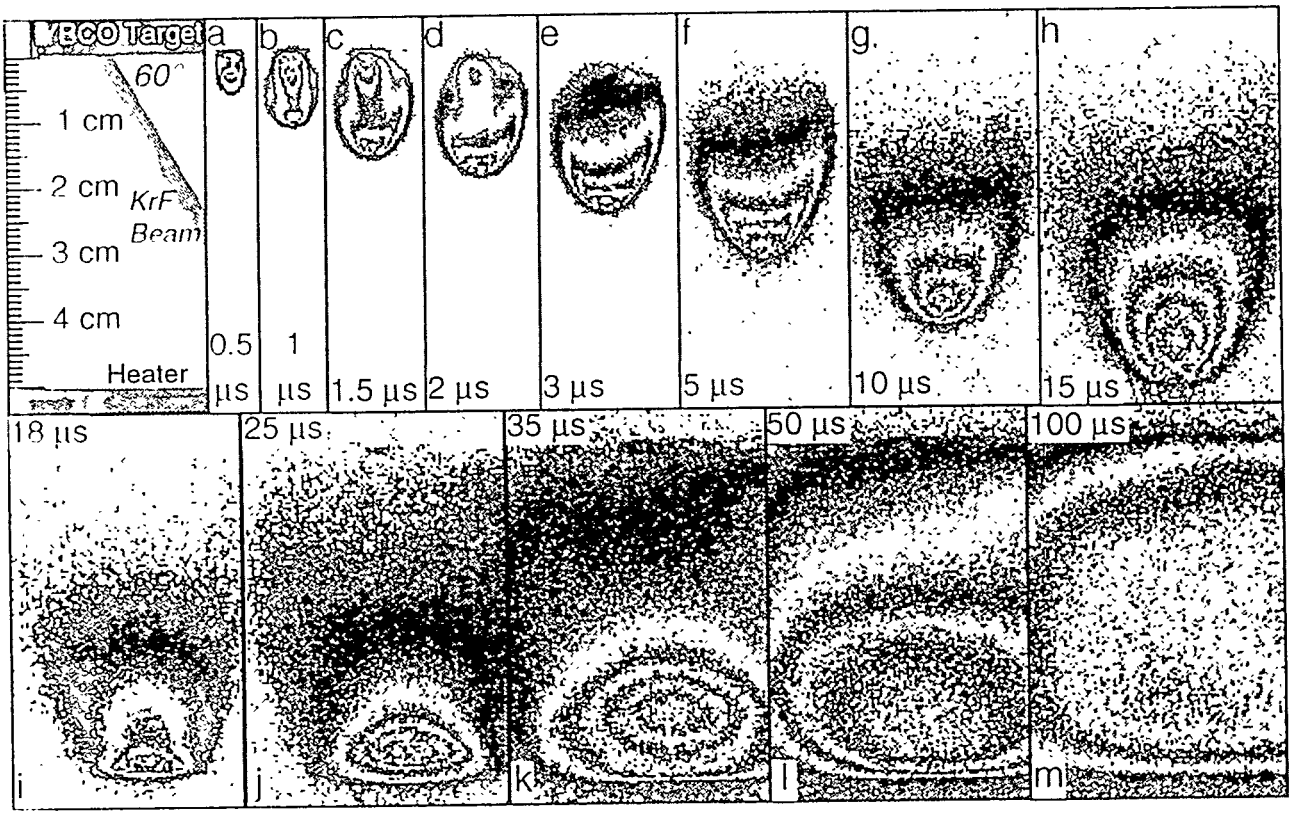

Fig. 4.25. Formation and propagation of the plasma plume generated by 2.5-J-cm^{-2} laser irradiation of YBCO in 200-mTorr oxygen, as recorded by a gated, ICCD-array camera. Exposure times were increased from 20 ns to 2 µs. A heater is located at d = 5 cm from the YBCO pellet. The digitized intensity data have been divided evenly into five contours to reveal the fainter regions of emission. The plume collides with a cold, stainless steel heater (h–m), partially rebounding to fill the space between the target and heater at Δt = 100 µs. Weak emission is just observable at the target surface (j–m) and is due to blackbody emission from slow-moving, hot particulates.

(from a distance-time plot using the images of Fig. 4.25) is 0.07 cm µs^{-1}, which yields arrival kinetic energies ≤ 0.25 eV, for atoms with m = 100 amu.

Figure 4.25(i–m) reveals that part of the vapor reflects from the heater face to form a nearly thermalized stagnation layer above the substrate surface. This layer is visible because of an increased fluorescence caused by collisions between the reflected vapor and the remainder of the incoming plume. This stagnation layer appears to move away from the heater, while diffusion occurs in an apparent afterglow, eventually filling the gap between target and heater as it continues to emit light for over 100 µs. Substrates on the heater surface are bathed in an excited stagnation layer for much longer than was realized previously.

Longer exposures and photon-counting emission spectroscopy are able to detect extremely weak emission at even longer times.

---

1. Summary of paper: in *Pulsed Laser Deposition of Thin Films*, ed. by D. B. Chrisey and

G. K. Hubler, Wiley-Interscience Publisher, New York (in press).

IMAGING AND TEMPERATURE MEASUREMENTS OF HOT PARTICULATES GENERATED DURING EXCIMER LASER ABLATION[1]

D. B. Geohegan

Macroscopic particles (usually spherical with diam < 1 μm) often are incorporated into thin films grown by pulsed-laser deposition. Two techniques have been developed to observe particulate generation and to measure their temperature and velocity following ejection from a laser-irradiated target.

The hot particles emit weak blackbody radiation that can be detected by a gated, intensified charge-coupled device (ICCD)-array camera system or by gated photon counting with a spectrometer and photomultiplier. Figure 4.26 presents the first images of hot particulates ejected from a YBCO target in vacuum at various time delays following a 50-ns duration KrF-laser pulse. The bright plasma in

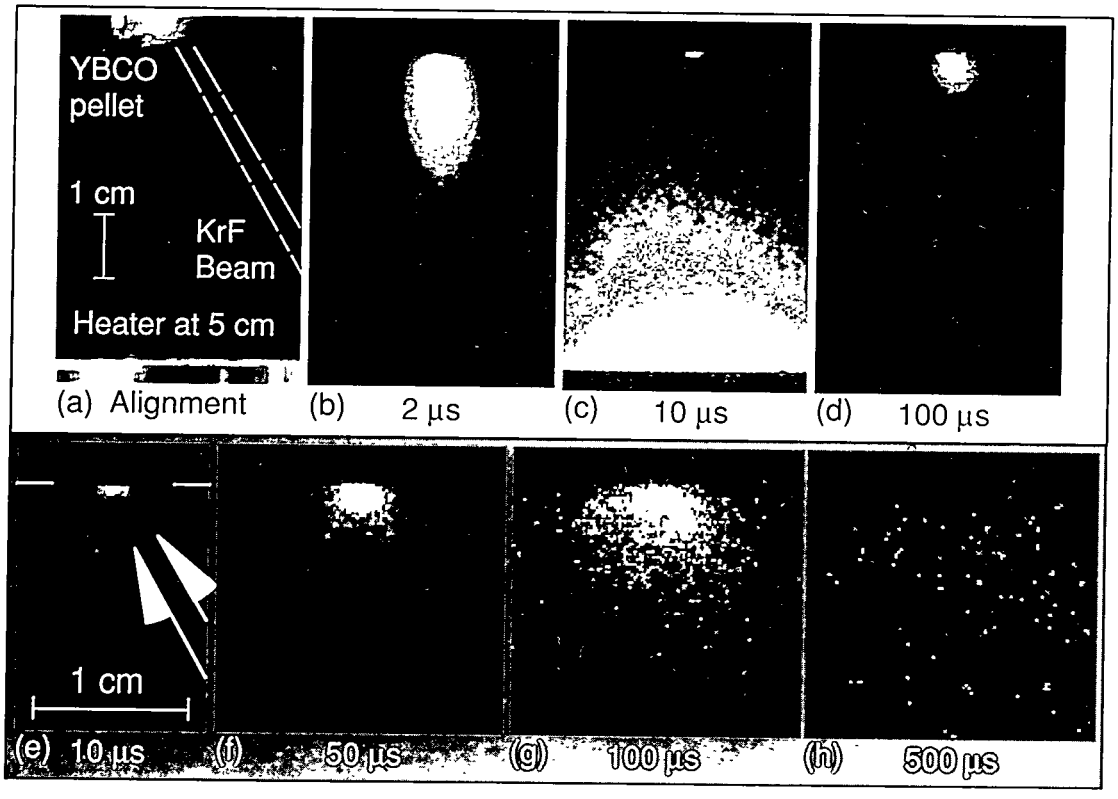

Fig. 4.26. (a–d) ICCD photographs tracing the appearance of glowing particulates at times much later than the plasma plume caused by 2.5-J cm^{-2} KrF laser ablation of YBCO in vacuum (1×10^{-6} Torr). Each photograph is a different laser shot; the exposures (lens f-stops/MCP gate widths) are: 2 μs [f/32, 20ns]; 10 μs [f/11, 200 ns]; 100 μs [f/4, 2.2 μs]. (e–h) Close-ups of the d = 0–1.5-cm region under the same conditions with time delays and exposures (lens f-stops/MCP gate width): 10 μs (f/5.6, 200 ns), 50 μs (f/4, 2 μs), 100 μs (f/4, 2 μs), 500 μs (f/4, 2 μs).

Fig. 4.26(b) travels at velocities $v \sim 1 \times 10^6$ cm/s and partially rebounds from the heater surface in Fig. 4.26(c) at $\Delta t = 10$ μs after the laser pulse. A small region of emission near the target surface in Fig. 4.26(c) was observed to expand spatially and diminish in intensity at later times, as in Fig. 4.26(d). Stop-action close-ups of this region [Figs. 4.26(e–h)] revealed the spatial dependence of this explosion of hot particles and enabled time-of-flight velocities to be estimated [$v \sim (0.45\text{–}1.2) \times 10^4$ cm s^{-1} for YBCO and BN targets].

Gated photon counting was employed to obtain temporally resolved spectra of this weak emission. The spectral shape is characteristic of blackbody emission and shifts to longer wavelengths as the particles cool during flight in vacuum. Estimates of the temperature of the particles were based on the emissivity of a perfect blackbody and range from 2200 to 3200 K for both BN ($\Phi_{248} = 3.5$ J cm^{-2}) and YBCO ($\Phi_{248} = 1.5$ J cm^{-2}). The measured temperature decrease of the particles in vacuum was compared with a radiative cooling model, which provided estimates of the initial surface temperature and radii of the particles. The particles appear to be superheated above the vaporization temperature during the ejection process and to cool both by evaporation and by radiation during flight.

TRANSPORT PROPERTIES OF ULTRATHIN $YBa_2Cu_3O_{7-\delta}$ LAYERS: EVIDENCE FOR TWO-DIMENSIONAL VORTEX FLUCTUATIONS[1]

D. P. Norton and D. H. Lowndes

High-temperature superconducting oxides are highly anisotropic because of their layered structure, with the superconducting CuO_2 planes being relatively weakly coupled. However, $YBa_2Cu_3O_{7-\delta}$ (YBCO) is one to two orders of magnitude less anisotropic than the Bi- and Tl-based superconducting cuprates, with significant c-axis coupling between CuO_2 bilayers in adjacent unit cells. Experiments on superlattice and sandwich structures containing YBCO layers as thin as a single c-axis unit cell show that the superconducting properties of YBCO are significantly altered as the CuO_2 bilayers are isolated from each other by interposing layers of other nearly lattice-matched materials with lower or zero T_c. A decrease in T_c, as well as a broadening of the resistive transition, is observed as the YBCO layer thickness approaches a single unit cell. Such observations suggest that YBCO may become quasi-two-dimensional (2D) in the limit of very thin isolated layers.

The transport properties of ultrathin YBCO layers have been studied, and the results were compared with predictions of the Ginzburg-Landau coulomb gas (GLCG) model for 2D vortex fluctuations. It was found that as predicted by the model, the normalized flux-flow resistances for several ultrathin YBCO structures collapse onto a single universal curve, as shown in Fig. 4.27. In addition, the values for the

1. Summary of paper: *Appl. Phys. Lett.* **62**, 1463 (1993).

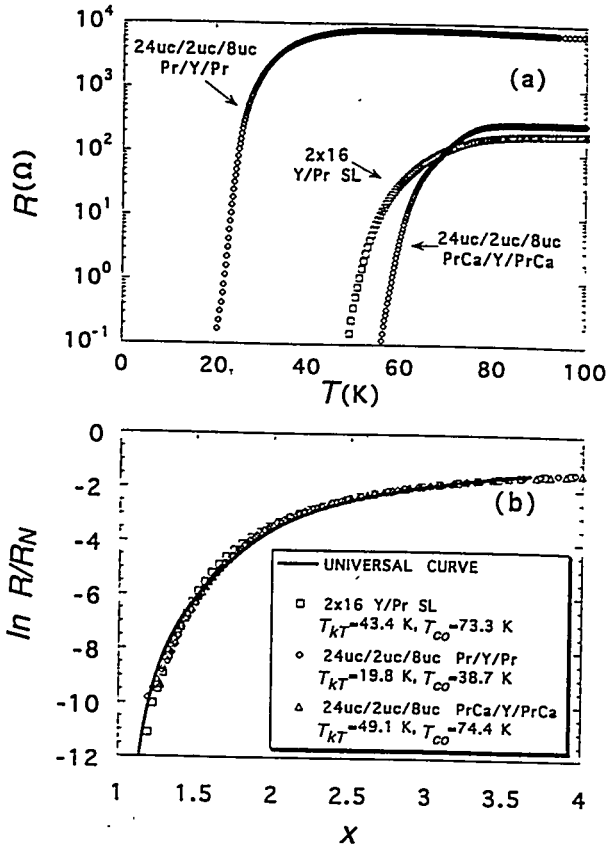

Fig. 4.27. GLCG analysis of the resistive transitions for three structures containing 2 unit cell-thick YBCO layers. Shown are (a) the resistance plotted against temperature and (b) the normalized resistance plotted against the scaling variable, X, for the three structures considered.

Kosterlitz-Thouless transition temperature, T_{KT}, and the Ginzburg-Landau temperature, T_{co}, obtained by separate analyses of I-V and resistance data within the context of the GLCG model, are in general agreement. Finally, it was found that the properties of a series of YBCO/$Pr_{0.5}Ca_{0.5}Ba_2Cu_3O_{7-\delta}$ superlattice structures are consistent with the GLCG treatment for anisotropic, three-dimensional layered superconductors.

---

1. Summary of paper: *Phys. Rev. B* **48**, 6460 (1993).

EPITAXIAL GROWTH OF $Ba_{1-x}K_xBiO_3$ THIN FILMS BY PULSED-LASER DEPOSITION[1]

D. P. Norton, J. D. Budai,
B. C. Chakoumakos, and R. Feenstra

Cubic bismuthate $Ba_{1-x}K_xBiO_3$ is an attractive candidate for superconducting electronic device applications. Although its superconducting transition temperature, $T_c \sim 30$ K, is not as high as for layered cuprates, its isotropic properties and especially its relatively long coherence length (~5 nm) may be advantageous for device fabrication. Epitaxial $Ba_{1-x}K_xBiO_3$ thin films have been grown by pulsed-laser deposition at temperatures as low as 400°C. Films have been grown on (100) MgO and $SrTiO_3$ with $T_c(R = 0) = 19.5$ K and transition widths less than 1 K. Four circle x-ray diffraction measurements show that these films are mostly (001)-oriented with good in-plane epitaxy.

Figure 4.28(a) shows the resistive transition for a $Ba_{1-x}K_xBiO_3$ thin film grown directly on (100) $SrTiO_3$ at 450°C. The normal state is non-metallic with the resistivity, $\rho(T)$, increasing by less than a factor of 2 as the temperature is decreased from room temperature to near the superconducting transition. This negative temperature coefficient of resistivity at high temperatures may be due to scattering at Ba/Bi antisite defects or grain boundaries. For the film shown, $T_c\,(R = 0) = 19.5$ K with a transition width of 0.6 K.

Although films grown directly on (100) $SrTiO_3$ show good superconducting properties, such was not the case for films grown directly on (001) MgO. This is somewhat surprising as

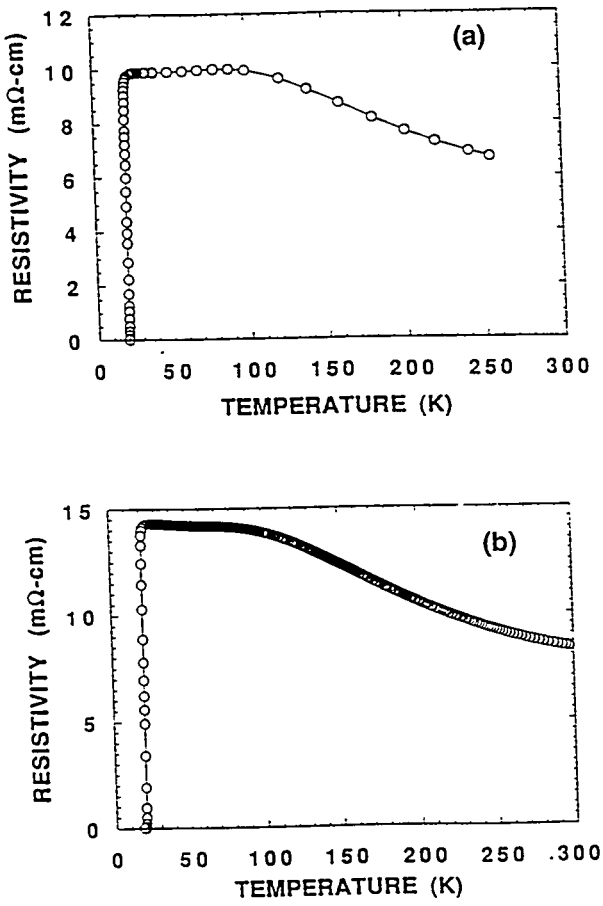

Fig. 4.28. Resistivity as a function of temperature for $Ba_{1-x}K_xBiO_3$ thin films grown on (a) (100) $SrTiO_3$ and (b) (100) MgO with a $BaBiO_3$ epitaxial buffer layer. In both cases, the $Ba_{1-x}K_xBiO_3$ films are ~1 μm thick.

the lattice constant for $Ba_{1-x}K_xBiO_3$ is closer to that of MgO than to $SrTiO_3$. Nevertheless, significant improvement was made in the quality of the $Ba_{1-x}K_xBiO_3$ films on (001) MgO by growing a $BaBiO_3$ buffer layer at 600°C before initiating $Ba_{1-x}K_xBiO_3$ film growth. Figure 4.28(b) shows the dc resistivity for a $Ba_{1-x}K_xBiO_3$ thin film grown at a heater block temperature of 400°C on (001) MgO with an initial $BaBiO_3$ layer grown at 600°C. For this film, T_c (R = 0) = 19.2 K with a transition width of ~1.0 K. Utilizing an epitaxial $BaBiO_3$ buffer layer, superconducting $Ba_{1-x}K_xBiO_3$ films were grown over the temperature range 350°–450°C.

---

1. Summary of paper: *Appl. Phys. Lett.* **62**, 414 (1993).

EPITAXIAL PULSED-LASER GROWTH AND PROPERTIES OF SINGLE-CRYSTAL $Ca_{1-x}Sr_xCuO_2$ THIN FILMS[1]

D. P. Norton, B. C. Chakoumakos, E. C. Jones,[2] J. D. Budai, D. K. Christen, and D. H. Lowndes

The parent compound of the copper oxide superconductors, $Ca_{1-x}Sr_xCuO_2$, has a simple layered structure consisting of CuO_2 planes separated by planes of alkaline-earth elements. It has been shown that this material can be made to superconduct either by electron doping (trivalent substitution on the alkaline-earth site) or by hole doping (vacancies on the alkaline-earth sites). However, bulk synthesis of $Ca_{1-x}Sr_xCuO_2$ with a tetragonal, infinite layer structure, in either the undoped, insulating phase or the doped, superconducting phase, has proven difficult. At ambient pressure, only $Ca_{1-x}Sr_xCuO_2$ with $x \sim 0.14$ can be synthesized in bulk; other compositions are possible only with high-pressure and high-temperature bulk processing techniques.

Very high quality epitaxial single-crystal $Ca_{1-x}Sr_xCuO_2$ thin films have been grown utilizing pulsed-laser deposition. In contrast to earlier work, these films were grown by codepositing from a single target for the entire compositional range $0.15 \leq x \leq 1.0$. X-ray

diffractometry has shown that these $Ca_{1-x}Sr_xCuO_2$ thin films were essentially single crystals with extremely narrow diffraction peaks, completely in-plane aligned with the (100) $SrTiO_3$ substrate, and contained virtually no impurity phases.

The transport and structural properties of $Sr_{1-x}CuO_{2-\delta}$ thin films grown by pulsed-laser deposition have also been studied.[3] Results support the contention that a tetragonal phase can accommodate alkaline-earth deficiencies up to $x \leq 0.3$. Resistivity measurements indicated a significant change in the carrier density in the CuO_2 planes as Sr vacancies were introduced. In addition, an enigmatic resistivity anomaly has been observed at 185 K for $Sr_{0.85}CuO_{2-\delta}$ thin films, as shown in Fig. 4.29. Magnetic measurements indicated that although a significant resistivity drop is observed at 185 K, it is not due to a superconducting transition. Hall measurements, as well as changes in resistivity with film-growth conditions, suggest that the majority carriers in these $Sr_{1-x}CuO_{2-\delta}$ thin films are electrons, even with the presence of Sr vacancies.

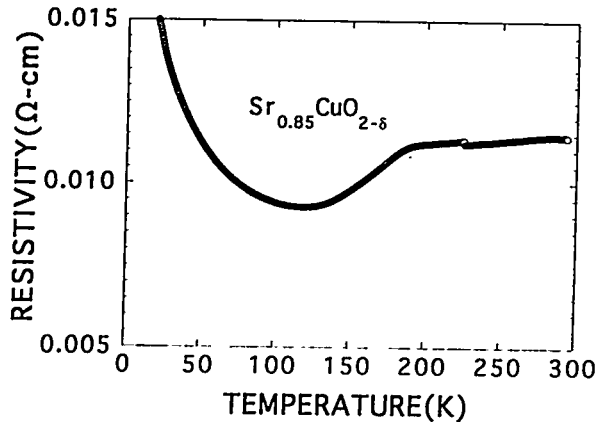

Fig. 4.29. Resistivity as a function of temperature for a $Sr_{0.85}CuO_{2-\delta}$ thin film grown at 550°C and 2-mTorr oxygen by pulsed-laser deposition highlighting the anomaly at ~185 K.

---

1. Summary of paper: *Appl. Phys. Lett.* **62**, 1679 (1993).
2. Graduate student from The University of Tennessee, Knoxville, Tenn.
3. D. P. Norton et al., *Physica C* (in press).

GROWTH MECHANISMS AND SUPERCONDUCTIVITY OF ULTRATHIN $YBa_2Cu_3O_{7-x}$ EPITAXIAL FILMS ON (001) MgO SUBSTRATES[1]

S. Zhu,[2] D. H. Lowndes, X. Y. Zheng,[3] B. C. Chakoumakos, S. J. Pennycook, and R. J. Warmack[4]

The T_c and J_c of YBCO films grown on MgO are almost as good as for YBCO grown on other substrates, regardless of lattice constant misfit (~1% misfit for YBCO on $SrTiO_3$ and $LaAlO_3$ and ~9% for YBCO on MgO). These properties create interest in the mechanism of YBCO film growth on MgO.

Scanning electron microscopy and scanning tunneling microscopy observations of the morphology of ultrathin films indicate a transition from terraced-island growth to spiral growth at ~4–5 unit-cell thickness in films grown at 720°C. The transition appears at greater thicknesses (~13–14 unit cells) in films grown at 800°C. There are larger variations of island thickness and less surface coverage in the films grown at higher temperatures compared with the films grown at lower temperatures.

Superconducting properties can be improved by achieving a relatively strain-free state. Figure 4.30 shows resistivity curves of four films

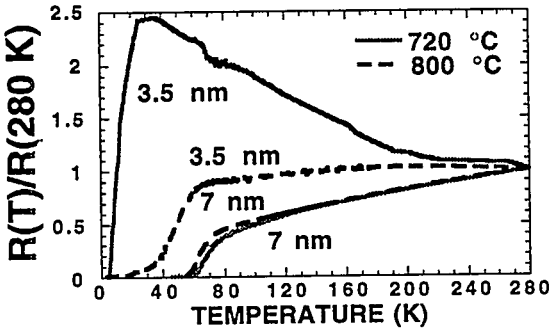

Fig. 4.30. Resistivity vs temperature curves of YBCO/MgO films.

grown at different temperatures and thicknesses. The two 3.5-nm films do not have zero resistance, probably because of a combination of weak links between grains and structural distortion. Insufficient film coverage does not interconnect all the islands in the 3.5-nm films, for which the average thickness at the center is several unit cells. Consequently, the thickest islands dominate the onset of the resistivity transition. Although the 3.5-nm/720°C film covers more area of the substrate, it lacks many thick islands. The high superconducting onset temperature implies that even a poor connection among the islands can achieve a continuous current path, perhaps even if the connecting film is only 1-unit-cell thick and distorted. The resistivity curves of 7-nm films grown at 720° and 800°C are alike, although their substrate coverage is different. As noted above, the 7-nm/720°C film has slightly higher zero resistance T_c, which could result either from reduced strain associated with the onset of spiral growth or (more likely) because the regions between islands are thicker on average and thickness variations are smaller, making the intergrain connections better.

---

1. Summary of paper: *Appl. Phys. Lett.* **62**, 3363 (1993).
2. Graduate student from The University of Tennessee, Knoxville, Tenn.
3. Postdoctoral research associate from The University of Tennessee, Knoxville, Tenn.
4. Health Sciences Research Division, ORNL.

IN SITU GROWTH OF EPITAXIAL $Bi_2Sr_2CaCu_2O_{8-x}$ AND $Bi_2Sr_2CuO_{6-x}$ FILMS BY PULSED-LASER ABLATION[1]

S. Zhu,[2] D. H. Lowndes, B. C. Chakoumakos, D. K. Christen, X.-Y. Zheng,[3] E. Jones,[2] J. D. Budai, and R. J.Warmack[4]

In the superconducting $Bi_2Sr_2Ca_{n-1}Cu_nO_{2n+4}$ (BSCCO) system, several competing stable phases coexist (n = 1, 2, 3), as well as meta-stable phases with higher n. To obtain phase purity, most epitaxial BSCCO films have been grown in two stages by post-deposition annealing. In contrast, single-step in situ growth of BSCCO epitaxial films on (001) MgO has been explored using pulsed-laser ablation of a single-phase polycrystalline Bi-2212 target.

The layer-stacking sequence, microstructure, and superconducting T_c of the epitaxial BSCCO films were found to be highly sensitive to the growth temperature and deposition rate. Table 4.2 shows that BSCCO films grown at different temperatures and deposition rates can have quite different major phases, even though

Table 4.2. Phase and T_c of films grown at different temperatures and deposition rates. The major phase, determined by XRD, is underlined. T_{co} is the zero-resistance transition temperature.

Rep. Rate	0.5 Hz		3.3 Hz	
Temperature	Phase	T_{co} (K)	Phase	T_{co} (K)
800°C	2201	—	2201 + 2212	—
770°C	2212	68	2212	52
740°C	2212	71	2212 + 2223	50
700°C	2212 + 2223	35	2223 + 2212	15

the ablation target composition (Bi-2212) is unchanged. Pure Bi-2212 films were found to exist over only a narrow temperature range, and pure Bi-2201 films were found at higher growth temperatures, while lower growth temperatures enhanced the Bi-2223 phase, though it was always mixed with Bi-2212.

The phase homogeneity, in-plane connections among grains, and superconducting T_c of Bi-2212 grown at a given temperature were found to be improved greatly by reducing the deposition rate. Epitaxial Bi-2212 films grown at 740°C and 0.5 Hz (~0.05 nm/s) have $J_c = 8 \times 10^5$ A/cm^2 at 50 K and 5×10^6 A/cm^2 at 4.2 K, which is almost one magnitude larger than some MOCVD films.[5,6]

---

1. Summary of paper: *Appl. Phys. Lett.* **62**, 3363 (1993).
2. Graduate student from The University of Tennessee, Knoxville, Tenn.
3. Postdoctoral research associate from The University of Tennessee, Knoxville, Tenn.
4. Health Sciences Research Division, ORNL.
5. T. Sugimoto et al., *Appl. Phys. Lett.* **57**, 928 (1990).
6. T. Sugimoto et al., *Physica C* **185–189**, 2045 (1991).

OPTICAL FUNCTIONS OF TRANSPARENT THIN FILMS OF SiO_3, $BaTiO_3$, AND SiO_x DETERMINED USING SPECTROSCOPIC ELLIPSOMETRY[1]

G. E. Jellison, Jr, L. A. Boatner, D. H. Lowndes, R. A. McKee,[2] and M. Godbole[3]

A procedure has been developed to determine accurately the thickness, optical functions, and surface roughness characteristics of thin-film insulators from two-channel spectroscopic polarization modulation ellipsometry data. For films with minimal surface roughness, the optical functions can be determined over the entire measured spectrum; for very rough films, analyses of spectroscopic ellipsometry data yield meaningful values of the optical functions only in the transparent region. In general, the films

must be transparent in a range of wavelengths sampled by the ellipsometer and sufficiently broad so that at least two interference oscillations can be observed.

Thin-film $SrTiO_3$ was grown on MgO using source-shuttering MBE techniques in ultrahigh vacuum. The films are adherent, single-phase epitaxial films. The first part of the data analysis determined that the film-substrate structure could be modeled using the model air/rough layer on $SrTiO_3$/MgO, where the thicknesses of the rough and $SrTiO_3$ layers were 3.0 and 510.8 nm, respectively. Figure 4.31 shows the resultant complex dielectric function ($\varepsilon = \varepsilon_1 + i\varepsilon_2$) and absorption coefficient (α) for bulk and thin-film $SrTiO_3$. As can be seen, the optical functions of the thin film and the bulk are nearly equal below the direct band edge (~3.7 eV), but differ slightly above this energy. Note that reasonable values of α can be obtained for $\alpha > 2 \times 10^3\ cm^{-1}$.

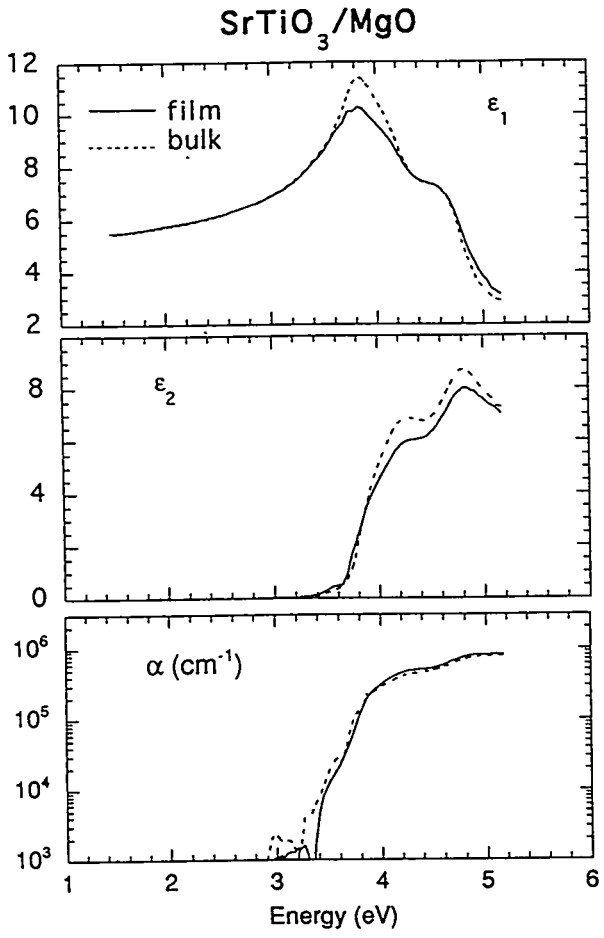

Fig. 4.31. Dielectric functions of thin-film and bulk $SrTiO_3$ corrected for interference effects and surface overlayers.

This procedure also was applied to $BaTiO_3$ thin films grown on MgO and to SiO_x films grown on Si. Because of the large surface roughness of the $BaTiO_3$ film, it was not possible to carry the calculations above the direct band edge (~3.4 eV); however, accurate values of the real part of the dielectric function could be obtained below that energy.

---

1. Summary of paper to be published.
2. Metals and Ceramics Division, ORNL.
3. Guest scientist from The University of Tennessee, Knoxville, Tenn.

OPTICAL FUNCTIONS OF GaAs, GaP, AND Ge DETERMINED BY TWO-CHANNEL POLARIZATION MODULATION ELLIPSOMETRY[1]

G. E. Jellison, Jr.

The optical functions of semiconductor materials in the visible, near infrared, and near ultraviolet are extremely important parameters for many diagnostic experiments. Because semiconductors are the active materials in solar cells and photodetectors, it is obvious that accurate knowledge of their absorptive and reflective properties is important for these device applications. In addition, in situ

spectroscopic ellipsometry (SE) is the best optical method to monitor film growth in real time, but interpretation of SE measurements also requires accurate values of the complex dielectric functions, both for the substrate and for the growing film.

Optical functions of GaAs, GaP, and Ge have been measured from 234 to 840 nm (1.47–5.3 eV) using two-channel spectroscopic polarization modulation ellipsometry.[2] Nulling ellipsometry measurements also were made at 1.152 μm to determine surface oxide layer thickness. Measurement of the surface overlayer allows the original ellipsometry data to be corrected for their optical effects, resulting in extremely accurate values of the bulk dielectric functions. The complex dielectric functions of GaAs, GaP, and Ge are shown in Fig. 4.32, where $\varepsilon = \varepsilon_1 + i\varepsilon_2 = \tilde{n}^2 = (n + ik)$,[2] and n and k are the refractive index and extinction coefficient of the materials, respectively. Tables of the data and a floppy disk containing the data in ASCII format (Mac compatible) are available from the author.

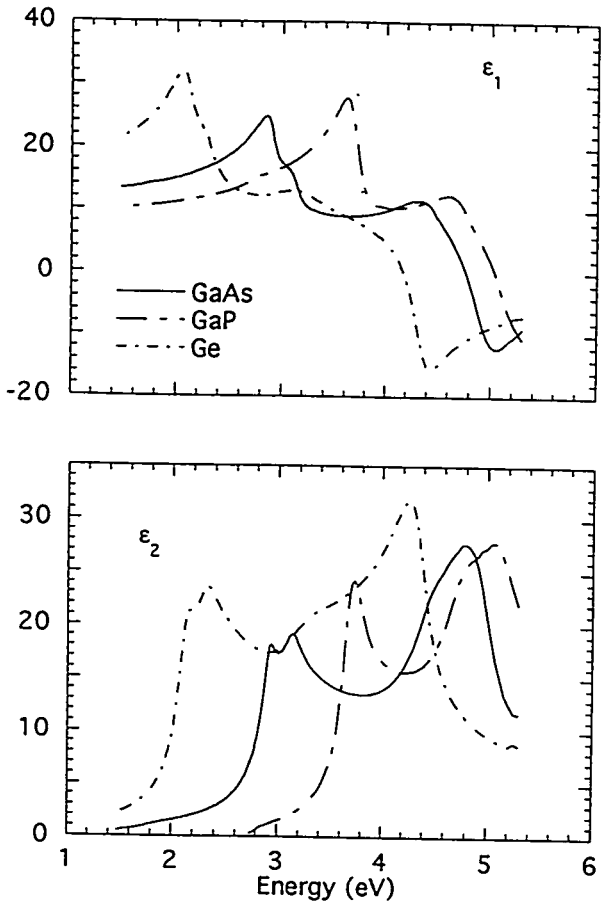

Fig. 4.32. Complex dielectric functions of GaAs, GaP, and Ge, determined using two-channel spectroscopic polarization modulation ellipsometry.

---

1. Summary of paper: *Opt. Mater.* **1**, 151 (1992).
2. G. E. Jellison, Jr. and F. A. Modine, *Appl. Opt.* **29**, 959 (1990).

OPTICAL FUNCTIONS OF CHEMICAL VAPOR DEPOSITED THIN-FILM SILICON DETERMINED BY SPECTROSCOPIC ELLIPSOMETRY[1]

G. E. Jellison, Jr., M. F. Chisholm, and S. M. Gorbatkin

Nondestructive diagnostics of thin films are essential in determining layer thicknesses, surface roughness, and their optical and electrical properties. At present, optical characterization techniques play a central role in these diagnostics, but interpretation of optical data requires either a detailed prior knowledge of the thin-film optical functions or a technique to simulate these optical functions. For thin-film silicon, this problem is compounded by the fact that the optical properties vary considerably, depending on microstructure. Amorphous Si (a-Si) or polycrystalline Si (p-Si) each can have large differences in their optical properties, depending on growth conditions.

Samples of thin-film silicon were grown on oxidized silicon (~100-nm SiO_2 grown on Si),

resulting in heavily As-doped, large-grained p-Si (p-Si:As); undoped, small-grained p-Si (p-Si:ud); and a-Si. The samples were measured by spectroscopic ellipsometry, from which the optical functions of the various forms of thin-film Si were determined, using a two-step process. In the first step, the thicknesses of the different layers were determined by restricting the fit to the interference region of the spectrum and by parameterizing the optical functions of a-Si and p-Si using the method of Forouhi and Bloomer.[2] In the second step, the optical functions were calculated, using the thicknesses of the various layers determined in the first step. The dielectric functions ($\varepsilon = \varepsilon_1 + i\varepsilon_2$), and the optical absorption coefficient (α) of the three forms of thin-film Si are shown in Fig. 4.33, along with crystalline Si as a reference. It must be remembered that the dielectric functions for p-Si:ud and a-Si are only representative and generally will depend on deposition conditions.

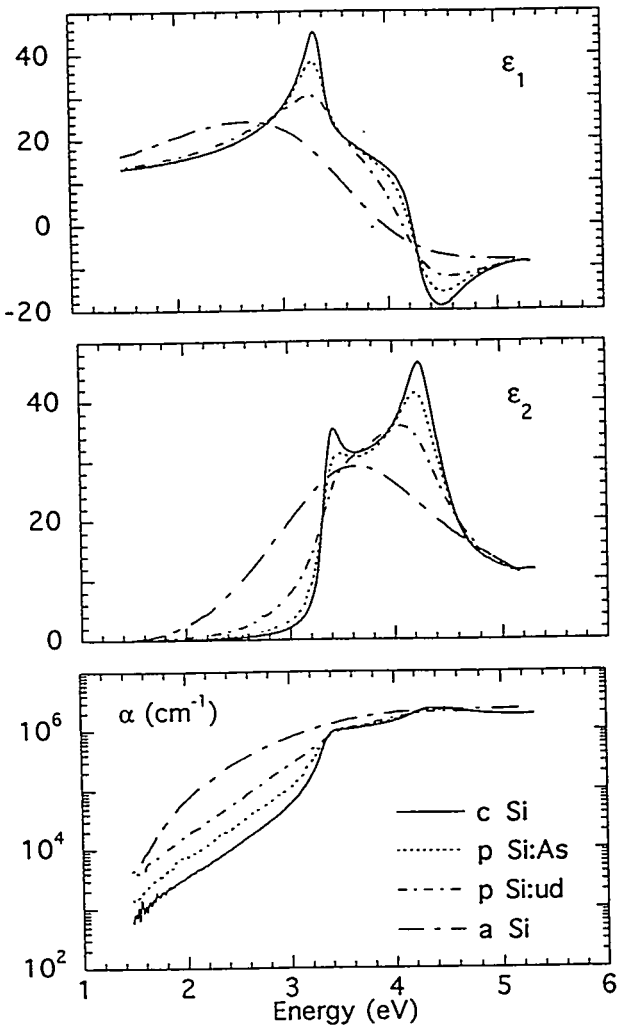

Fig. 4.33. Real and imaginary parts of the dielectric function (ε_1 and ε_2) and the optical absorption coefficient (α) for several forms of thin-film silicon.

1. Summary of paper: *Appl. Phys. Lett.* **62**, 3348 (1993).
2. A. R. Forouhi and I. Bloomer, *Phys. Rev. B* **34**, 7018 (1986).

OPTICAL FUNCTIONS OF SILICON-GERMANIUM ALLOYS DETERMINED USING SPECTROSCOPIC ELLIPSOMETRY[1]

G. E. Jellison, Jr., T. E. Haynes, and H. H. Burke[2]

High-quality crystalline alloys can be formed as single crystals or thin solid films over the entire composition range. Their optical, electrical, and structural properties vary with stoichiometry. This tunability of properties, as well as compatibility with existing silicon-based technology, has led to numerous applications of alloys in optical fiber communications, infrared detectors, solar cells, and band-gap engineering of Si-based microelectronic devices. However, for some applications it is essential to have very accurate values of their optical functions. For example, optical in situ control of $Si_{1-x}Ge_x$ alloy

thin-film growth requires very accurate values of the dielectric function, both as a function of wavelength and composition.

Several thin-film SiGe alloys were grown on single-crystal Si or Ge wafers by chemical vapor deposition, resulting in relatively unstrained 4–8-μm epitaxial films. Two-channel spectroscopic polarization modulation ellipsometry (2-C SPME) was used to measure their optical functions in the range 240–840 nm (5.16–1.47 eV). Very accurate values of the bulk dielectric functions were obtained because the 2-C SPME data were corrected for oxide and roughness overlayers. The complex dielectric function ($\varepsilon = \varepsilon_1 + i\varepsilon_2$) is shown in Fig. 4.34 for some of the spectra measured, including crystalline Si and Ge as references. Other compositions measured were 98 Si 2 Ge/Si, 48 Si 52 Ge/Ge, 28 Si 72 Ge/Ge, and 11 Si 89 Ge/Ge. Tables of the data and a floppy disk containing the data in ASCII format (Mac compatible) are available from the authors.

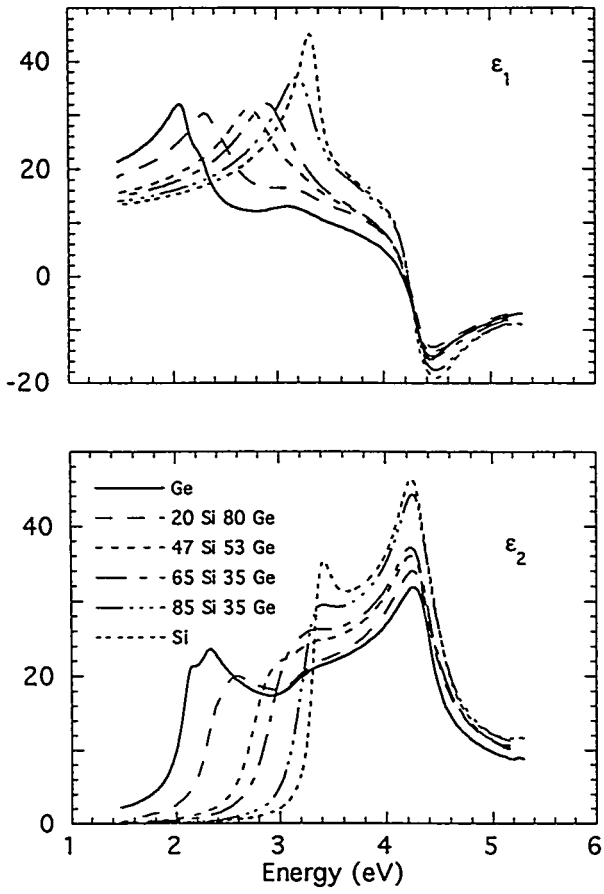

Fig. 4.34. Complex dielectric function for Si_xGe_{1-x} alloy films, determined using 2-C SPME. The Si-rich layers were grown on Si, and the Ge-rich layers were grown on Ge.

---

1. Summary of paper: *Opt. Mater.* 2, 105 (1993).
2. Graduate student from Columbia University, New York, N.Y.

SPECTROSCOPIC ELLIPSOMETRY AND INTERFERENCE REFLECTOMETRY MEASUREMENTS FOR CHEMICAL VAPOR DEPOSITED SILICON GROWN ON OXIDIZED SILICON[1]

G. E. Jellison, Jr., M. Keefer,[2] and L. Thornquist[2]

Several samples of thin-film Si grown on oxidized Si, both with and without a covering SiO_2 layer, have been examined using both spectroscopic ellipsometry (SE) and constant angle reflection interference spectroscopy (CARIS); the optical functions determined in ref. 3 were used for the fits.

Good fits to both the SE and CARIS data were obtained for thin films of amorphous Si and large-grain polycrystalline Si, and both techniques gave the same film thicknesses. However, the SE data for the small grain polycrystalline silicon samples required one or two additional surface layers to model the surface roughness of these films. CARIS thicknesses agreed

with SE thicknesses, if the total thickness of the thin-film Si plus any surface overlayers were used as the total SE thickness. Interpretation of the SE data for the oxided films required an additional interface layer between the top SiO_2 and the thin-film Si, which was not included in the CARIS interpretation; this resulted in minor differences between the thicknesses determined from SE and CARIS.

In summary, the SE technique and the CARIS technique determine very similar thicknesses, when the optical functions of all of the layers are known. Since CARIS measurements are faster than commercially available SE instruments, CARIS is the preferred technique if there are no layers with unknown optical functions. On the other hand, SE measures two or three quantities at each wavelength, compared with only one quantity from CARIS. This advantage, coupled with proper data interpretation, allows SE measurements to be interpreted even when the optical functions of a layer are not known, and SE should be used in these circumstances.

---

1. Summary of paper: *Mat. Res. Soc. Symp. Proc.* **283**, 561 (1993).
2. Prometrix Corporation, Santa Clara, Calif.
3. G. E. Jellison, Jr., M. F. Chisholm, and S. M. Gorbatkin, *Appl. Phys. Lett.* **62**, 3348 (1993), "Optical Functions of Chemical Vapor Deposited Thin-Film Silicon Determined by Spectroscopy Ellipsometry," this report.

DATA ANALYSIS FOR SPECTROSCOPIC ELLIPSOMETRY[1]

G. E. Jellison, Jr.

There are many applications for spectroscopic ellipsometry (SE) as a nondestructive diagnostic technique for thin-film characterization. SE is fast and very sensitive to changes in the film dielectric function in the direction perpendicular to the sample surface. However, SE data often require considerable mathematical analysis before they can be related directly to parameters of interest (e.g., thin-film morphology, film thickness, surface roughness, or the true dielectric functions of the film or substrate. In order to relate the SE-measured parameters with actual characteristics of the near-surface region, a model must be constructed in three phases.

The first phase involves a model of the near-surface region and selection of the technique used to calculate the Fresnel reflection coefficients (FRCs). Calculation of the FRCs for light reflected from a layered structure of known dielectric functions and thicknesses is well-known and straightforward if it is assumed that each layer is isotropic and uniform. Most modern techniques involve 2×2 Abelès matrices[2] or 2×2 transfer matrices.[3] If the medium is anisotropic, then a 4×4 matrix formalism must be used.[4]

The second phase involves the parameterization or selection of the spectroscopic optical functions used to describe the layers. For films

with well-defined structure and for many substrates, the dielectric functions of the bulk materials themselves can be used. However, the optical functions of thin films often are different from bulk values, so their film wavelength-dependent dielectric functions must be parameterized in some way. For insulators, the Lorentz oscillator model works reasonably well; while for semiconductors the parameterization of Forouhi and Bloomer[5] works well in restricted wavelength regions. For materials that consist of a mixture of phases, the Bruggeman effective medium approximation[6] often is used.

The third phase involves the determination of wavelength-independent parameters (e.g., film thicknesses) using an appropriate fitting procedure. Generally, one has to specify a figure of merit and minimize it by varying the fitting parameters. The choice of the figure of merit must result in a measure of the "goodness of fit," and both the correlated and uncorrelated errors of the fitted parameters must be calculated.[7]

---

1. Summary of paper: *Thin Solid Films* (in press).
2. F. Abelès, *Ann. Phys.* **5**, 596 (1950).
3. R. M. A. Azzam and N. M. Bashara, *Ellipsometry and Polarized Light*, North-Holland, Amsterdam, 1977.
4. D. W. Berreman, *J. Opt. Soc. Am.* **62**, 502 (1972).
5. A. R. Forouhi and I. Bloomer, *Phys. Rev. B* **34**, 7018 (1986).
6. D. A. G. Bruggeman, *Ann. Phys.* (Leipzig) **24**, 636 (1935).
7. G. E. Jellison, Jr., *Appl. Opt.* **30**, 3354 (1991).

ION CHANNELING AND SPECTROSCOPIC ELLIPSOMETRY EXAMINATIONS OF THIN-FILM SiO_2/epi-Si(001) STRUCTURES[1]

A. T. Fiory,[2] P. K. Roy,[3] and G. E. Jellison, Jr.

Structure-sensitive measurements are important in understanding and gaining control over the production of reliable thin oxides for MOS devices. The stacked-oxide method developed at AT&T is noted both for its compatibility with current manufacturing practice and for its marked improvement in reliability and yield of ultrathin films, compared with conventional oxidization.

The sample wafers for this study were taken from device development lots with 3–16-nm SiO_2 either after completion of the gate-oxide layer or after the first oxidation step in the stacked-oxide method. Samples for the Rutherford backscattering (RBS) and spectroscopic ellipsometry (SE) measurements were cut from adjacent areas near the centers of the wafers.

The RBS measurements were used to determine the areal densities of oxygen and silicon, N_O and N_{Si}, residing on the surface. The excess scattering for silicon, ΔN_{Si}, was determined from these results, subtracting off the theoretical surface peak. No systematic differences were observed for the three channeling directions. It was observed that ΔN_{Si} depended upon film thicknesses, being greater for thicker films than for thinner films, and ΔN_{Si} reached a minimum of 1–1.4 $\times 10^{15}$ atoms/cm^2 after complete oxide removal. The excess scattering indicates the existence of an extremely thin roughness layer (possibly SiO_x); even for zero oxide thickness, the nonzero ΔN_{Si} indicates that the surface does

not have bulk-like termination. Although the excess ΔN_{Si} for the stacked oxides is less than for conventional oxides of comparable thicknesses, the differences are not statistically significant.

SE measurements also were performed on these samples. The data were fitted using an air/SiO_2/c-Si model, in which the optical functions of the SiO_2 layer were parameterized using the single-term Sellmeier approximation $[n^2 = 1 + A\lambda^2/(\lambda^2 - \lambda_O^2)]$, with $\lambda_o = 92.3$ nm, and the optical functions of c-Si were taken from Ref. 4. Two parameters (A and d_{SiO2}, the thickness of the SiO_2 layer) were sufficient to obtain a good fit to the data.

The density of the film can be calculated from N_O (determined from RBS) and from d_{SiO2} (determined from SE). It was found that the densities of these films were independent of thickness and not significantly different from that of fused SiO_2, although the SE results indicated that the refractive index of the very thin films was considerably greater than the refractive index of fused SiO_2.

---

1. Summary of paper: *Mat. Res. Soc. Symp. Proc.* **259**, 131 (1992).
2. AT&T Bell Laboratories, Murray Hill, NJ
3. AT&T Bell Laboratories, Allentown, Pa.
4. G. E. Jellison, Jr., *Opt. Mater.* **1**, 41 (1992).

EXCIMER LASER ABLATION AND SURFACE ACTIVATION OF SiO_x AND SiO_x-CERAMIC COUPLES FOR SUBSEQUENT ELECTROLESS COPPER PLATING[1]

M. J. Godbole,[2] D. H. Lowndes, and G. E. Jellison, Jr.

Surface activation by pulsed-laser irradiation has been observed in polycrystalline Al_2O_3 and AlN. "Activation" in this context means that when the laser-treated ceramic is subsequently placed in an electroless copper plating bath, copper is autocatalytically deposited on the laser-irradiated part of the ceramic surface, leaving barren the non-irradiated regions. Such activation has significant technological potential, as it could eliminate several steps currently required to achieve selective deposition. Because the energy band gap for most ceramics (typically 8–12 eV) is much larger than the single-photon energies conveniently available from the 4.0–6.4-eV pulsed UV lasers, the possibility of surface activation of substoichiometric silicon oxide (SSO), SiO_x with $x \sim 1.0$, as a UV-absorbing surface coating, has been investigated.

A XeCl (4.0-eV photon energy) pulsed excimer laser was used to study the ablation behavior of SSO where the ablation threshold was found to be quite low (~0.3 J/cm^2) and amenable to pulsed-laser patterning without the use of deep-UV radiation. Surface activation, as illustrated by subsequent copper deposition in the electroless process, was observed along well-defined narrow (~10–20

μm) lines just beyond the edges of laser-ablated trenches in SSO films that were deposited on XeCl-transparent fused silica substrates. When a thin layer of SSO was deposited on polycrystalline Al_2O_3 or AlN substrates and subsequently laser treated, surface activation of these ceramics occurred on the laser-irradiated regions at much lower fluences and with fewer exposures than are required to activate the bare ceramic substrates. In both the SSO/SiO_2 and the SSO/Al_2O_3 or SSO/AlN experiments, activation is believed to result from redeposition of elemental silicon, which is produced by ablative etching of SSO. The important conclusion for metal deposition is that ceramic substrates such as alumina and aluminum nitride can be activated at much lower fluences and with far fewer exposures through the use of a thin, deposited SSO film.

---

1. Summary of paper: *Applied Physics Letters* (in press).
2. Guest scientist from The University of Tennessee, Knoxville, Tenn.
3. D. H. Lowndes et al., p. 321 in *Laser Ablation: Mechanisms and Applications–II*, ed. by J. C. Miller and D. B. Geohegan, American Institute of Physics, New York, 1993 (in press).

ABLATION, MELTING, AND SMOOTHING OF POLYCRYSTALLINE ALUMINA BY PULSED EXCIMER LASER RADIATION[1]

D. H. Lowndes, M. De Silva,[2] M. J. Godbole,[3] A. J. Pedraza,[3] and D. B. Geohegan

The use of pulsed UV radiation to etch, micromachine, or alter the near-surface chemical properties of ceramic materials is of strong technological interest. However, photonic mechanism(s) to produce these changes efficiently are not obvious, because a number of widely used ceramics have energy band gaps, E_g, that are much larger than the highest photon energies conveniently available (4.0, 5.0, or 6.4 eV) from pulsed excimer lasers. Consequently, a recent suggestion[4] that laser etching of wide band-gap ceramics might be accomplished using easily controlled single-photon processes—simply by introducing a sufficient concentration of mid-gap electronic energy levels associated with near-surface defects—is of great practical interest.

In order to understand better the phenomenon of ceramic etching by sub-band-gap radiation, a comparison of pulsed XeCl (308 nm, $h\nu$ = 4.0 eV) laser etching of the two technologically important forms of Al_2O_3 (E_g ~ 9 eV), polycrystalline alumina (99.6% pure) and single-crystal sapphire was made recently. Polycrystalline alumina contains a high concentration of "native defects" in the form of grain boundaries and irregular crystalline facets on the micrometer scale.

No XeCl laser etching of either alumina or sapphire was detected below a threshold fluence value. For instance, no ablation was observed for sapphire at 3 J/cm^2 even after 20 exposures, whereas etching was initiated for alumina after just 5 laser shots at 2 J/cm.^{2} Above their respective threshold fluences, laser etching of both alumina and sapphire was observed, but only after a number of incubation (induction) pulses. This incubation number also was much

larger for sapphire than for alumina, but decreased with fluence for both materials. Laser etching rates for both materials were similar at high fluences after their incubation periods.

Scanning electron micrographs showed that alumina melted and flowed under repeated irradiation at fluences ≥ 0.7 J/cm.[2] Atomic force microscopy and surface profilometry revealed significant smoothing of the polycrystalline alumina surface after multiple exposures to XeCl radiation at moderate fluences (1–3 J/cm^2), apparently due to the molten flow of alumina. At the relatively high fluences used in these studies, the laser energy couples into the Al_2O_3 surface after the first few nanoseconds of each laser pulse, primarily through the formation of a near-surface laser-generated plasma (Knudsen-layer formation). Ion probe measurements (carried out in vacuum for alumina) confirmed the incubation behavior and revealed that at a fixed fluence of 1.1 J/cm^2, the (positive) charge collected per pulse saturated after a sufficient number of pulses, as did the etch-plume velocity.

It is concluded that the mechanism for ablation in the high-fluence regime is primarily thermal, as suggested by the melting of alumina. These results reveal the importance of the "defect" absorption mechanism associated with grain boundaries, which drastically reduces both the ablation threshold and the incubation period for alumina relative to sapphire. However, it also is clear from our high-fluence results that these differences in ablation behavior are present only for the first few laser shots if the laser fluence is well above the etching thresholds for both materials. Consequently, these differences may totally disappear in the high-fluence regime (>>6 J/cm^2), as a high concentration of defects is generated in sapphire.

---

1. Summary of paper: *Mat. Res. Soc. Symp. Proc.* **285**, 191 (1993).
2. Graduate student from The University of Tennessee, Knoxville, Tenn.
3. Guest scientist from The University of Tennessee, Knoxville, Tenn.
4. P. A. Eschbach et al., *J. Vac. Sci. and Technol. A* **7**, 2943 (1989).

DESIGN AND MICROFABRICATION OF PLANAR PICKUP COILS FOR QUANTUM OSCILLATION MEASUREMENTS IN HTSc FILMS

D. H. Lowndes, M. J. Godbole,[1] *and R. G. Goodrich*[2]

A collaboration exists with an NSF-sponsored program[3] to develop facilities and methods for detection of Landau quantum oscillations (LQO) in epitaxial high-temperature superconductor (HTSc) films. A recent discovery[4] that magnetization [de Haas-van Alphen, (dHvA)] oscillations can be observed even in the mixed state ($H < H_{c2}$) of strong-coupling superconductors, combined with the existence of high-quality epitaxial HTSc film specimens, has created great interest in using HTSc films for LQO measurements. Measurements on HTSc Fermi surface dimensions, quasi-particle effective masses and scattering rates, and perhaps also the study of electron-vortex interactions in the mixed state will be possible. However, because techniques do not exist to observe

dHvA oscillations even in normal-metal thin films, a major experimental challenge has been to fabricate miniature planar pickup coils that couple efficiently to the dHvA magnetic flux oscillations. Because the dHvA oscillation amplitude increases exponentially with magnetic field, the pickup coil–HTSc film pairs must be small enough to fit in the bore of 30–100-T pulsed-field magnets.

Consideration of how to achieve maximum flux linkage between the pickup coil and thin film has led to the conclusion that the sample's perimeter-to-area ratio should be maximized. In these studies, the HTSc films have been patterned in a "comb" design, in which the "backbone" and each of 32 "teeth" are only 100 μm wide, separated by 100-μm spaces with the pickup coil following the sample's perimeter and placed as close as possible to the sample plane. Using photolithographic patterning, dry plasma etching in low-pressure CCl_4 and MgF_2 encapsulation, a successful fabrication of electrically continuous pickup coils consisting of 2-μm thick × 20-μm wide Al lines on transparent (001) MgO substrates has been completed. Al, which saturates at low magnetic field, was used because of its low magnetoresistance, while a transparent substrate was required in order to align the pickup coil/HTSc film pairs within a few μm. MgO was chosen because its thermal expansion coefficient closely matches that of $SrTiO_3$ and other ceramics on which the HTSc films were grown, so that alignment could be maintained down to temperatures below 1 K. LQO measurements are expected to commence early in 1994.

---

1. Guest scientist from The University of Tennessee, Knoxville, Tenn.
2. Louisiana State University, Baton Rouge, La.
3. R. G. Goodrich and D. H. Lowndes, *High-Precision Landau Quantum Oscillation Measurements in the Normal and Mixed States of High-Temperature Superconductors.*, NSF grant No. DMR-9115594.
4. F. M. Mueller et al., *Phys. Rev. Lett.* **68**, 3928 (1992).

5. *Structure of Solids and Surfaces*

This chapter focuses on the structural properties of surfaces and solids. These studies utilize a variety of techniques, including surface spectroscopies, electron diffraction, electron microscopy, electron energy loss spectroscopy (EELS), and both conventional and synchrotron x-ray diffraction.

Both static and dynamic properties of clean and adsorbate-modified surfaces continue to be investigated in the Surface Physics Program. The composition and arrangement of atoms on the (100) and (110) surfaces of the ordered alloy FeAl and the nitrogen-covered Cu(110) surface have been determined. Thermal roughness and faceting on Pt(001), the temperature dependence of interlayer spacings and surface vibrational amplitudes on Cu(110), the smoothing kinetics of a rough Cu(100) surface, and the faceted reconstruction of the TaC(310) surface have been studied with diffraction techniques. The effects of oxygen adsorption on the anharmonicity and vibrational relaxation on the Cu(110) surface and the surface dynamics of Be(0001) have been investigated using surface phonons. Adsorption sites as a function of coverage for S on W(001), CH_3SH and CH_3S on W(001) and Ru(0001), and the effect of H on the $Mo_{0.75}Re_{0.25}$(100) surface have been studied using synchrotron radiation.

Within the Electron Microscopy Program, delivery of a 300-kV Z-contrast scanning transmission electron microscope (STEM) with 1.4-Å resolution has facilitated imaging of GaAs dumbbells, and atomic plane resolution spatially resolved EELS has been demonstrated using a 2.3-Å resolution 100-kV STEM. This new EELS capability has been applied to investigations of hole doping at grain boundaries, cobalt silicide-silicon interfaces, and the structure of $SrTiO_3$ grain boundaries. Investigations of strained-layer molecular beam epitaxial growth of SiGe alloys on Si has provided new insights into the evolution of surface morphology and the mechanism of strain relaxation.

The X-Ray Diffraction Program has collaborated with the Electron Microscopy Program in the study of strained-layer SiGe alloy growth, identifying the chemical ordering structure and demonstrating that the ordered-domain populations are sensitive to miscuts of the Si substrate. The structure, size, and orientation of nanocrystalline Si, Ge, and SiGe particles have been investigated in sapphire and amorphous silica after ion implantation and annealing. Time-sliced synchrotron Doppler absorption measurements have demonstrated the quantum mechanical narrowing of the spectral energy width of resonant beams as a function of time, and detailed planning is in progress for a collaborative beam line at the Advanced Photon Source.

SURFACE PHYSICS

DETERMINATION OF THE TRUE RECONSTRUCTION OF Cu(110)-(2 × 3)-N WITH HIGH-ENERGY ION SCATTERING[1]

H. Dürr,[2] D. B. Poker, D. M. Zehner, and J. H. Barrett[3]

Subsequent to the adsorption of nitrogen, a (2 × 3) reconstructed structure is observed on the Cu(110) surface. Three uniquely different models have been proposed to explain this structure.[4] Two involve missing Cu rows in the outermost layer. The third model includes the addition of one [1$\bar{1}$0] row for every three substrate rows. This model involves lateral displacements of the first layer of Cu atoms, which permit discrimination among the three models using high-energy ion scattering (HEIS). An ion beam aligned normal to the surface results in shadowing of atoms in deeper layers, and only the topmost atoms contribute to the backscattering yield. Any lateral displacements of the top-layer atoms reduce this shadowing, and the scattering yield increases. Therefore, an increased scattering yield compared with the unreconstructed clean surface is expected for the additional-row model and relatively little, if any, increase is expected for the missing-row models.

In Fig. 5.1, typical HEIS spectra for the clean (open circles) and reconstructed (solid circles) surfaces are shown. The observed increase of 45% in the surface peak yield at 0.5 MeV for the reconstructed surface, relative to that of clean Cu(110), shows that more surface atoms are exposed to the incoming ions, which rules out any missing-row reconstruction of the surface. A quantitative evaluation shows that the measured increase in surface peak yield is higher than that expected for the additional-row model. This shows that subsurface Cu atoms are displaced laterally from their bulk-like positions. By comparing our measurements with Monte Carlo calculations, lateral shifts of 0.30 and 0.07 Å are obtained for 2/3 ML of second- and third-layer atoms, respectively.

ORNL DWG 93-16423

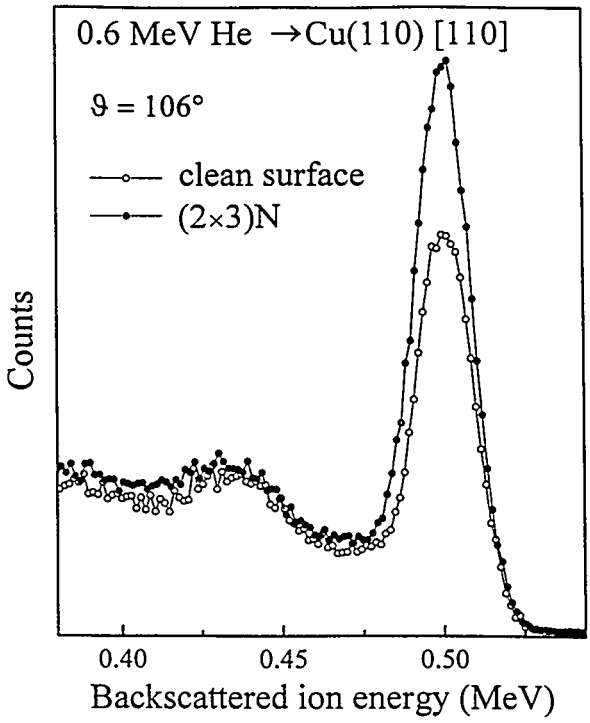

Fig. 5.1. Normal incidence HEIS spectra for the clean and reconstructed surface.

---

1. Summary of paper to be published.
2. Postdoctoral research associate from the University of Pennsylvania, Philadelphia, Penn.
3. Consultant representing self.
4. A. P. Baddorf et al., *Phys. Rev. B* **48**, 9013 (1993).

TERRACE-WIDTH AND STEP-HEIGHT ENLARGEMENT: RECONSTRUCTION OF THE TaC(310) SURFACE[1]

J.-K. Zuo[2] and D. M. Zehner

Because atoms in a surface might not be in a stable state when the surface is created, a reconstruction into a new energetically favored state differing from the bulk truncation frequently occurs. These new surface structures provide an opportunity for investigating and understanding the driving forces and their contributions to the surface-free energy, a rich testing ground for two-dimensional statistical models of collective phenomena and can serve as templates for epitaxial growth. Mechanisms for surface reconstructions of elemental materials can generally be grouped into atomic displacements, missing rows, facets, and their combinations. It has been shown that the TaC(110) surface exhibits a massive unidirectional reconstruction.[3] To determine if this reconstruction exists for other TaC surfaces, the (310) surface has been examined using high-resolution electron energy loss spectroscopy. The ideally truncated surface exhibits the staircase structure shown in Figs. 5.2(a) and 5.2(b). Instead of this arrangement, from the diffraction results a tripling of the terrace width and step height has been observed as shown in Fig. 5.2(c), maintaining the staircase geometry. On average, each unit of the reconstructed surface consists of a (100) terrace with nine row spacings and a (010) step wall with a step height of three row spacings. This structure is dramatically different from the ideal, bulk truncation for which each unit consists of a (100) terrace with three row spacings and a single-step height step. These are believed to be trapped during the reconstruction process. Also, the step edges are shown to be well-ordered through the angular profile analysis.

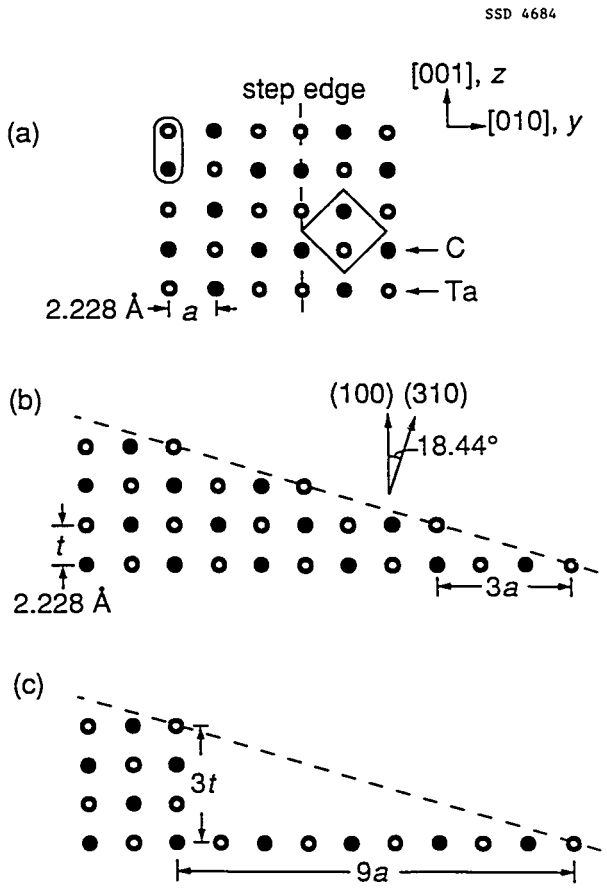

Fig. 5.2. (a) and (b) are the top view from the [100] direction and side view from the [00 $\bar{1}$] direction, respectively, for the ideally truncated TaC(310) surface, where the elongated circle indicates the Ta-C basis and the square is the surface unit mesh. (c) is the side view of the reconstructed TaC(310) surface.

---

1. Summary of paper: *Phys. Rev. B* **46**, 16122 (1992).
2. ORISE faculty research participant from Southwest Missouri State University, Springfield, Mo.
3. J.-K. Zuo et al., *Phys. Rev. B* **47**, 10743 (1993).

SEGREGATION AND OXIDATION BEHAVIOR OF THE $Fe_{0.53}Al_{0.47}$(110) SURFACE

H. Graupner,[1] *L. Hammer,*[2] *K. Müller,*[2] *and D. M. Zehner*

Transition-metal aluminides are very promising materials for high strength and medium- to high-temperature applications. The most widely studied systems in this respect are NiAl and FeAl. Both form ordered intermetallic alloys of the CsCl type. The surface structure of clean NiAl(110)[3] and its oxidation behavior[4] have been investigated in great detail. This surface shows a bulk-like termination with a large rippled reconstruction over a wide temperature range, whereas $Fe_{0.53}Al_{0.47}$(110) is characterized by several different surface structures, caused by Al segregation with increasing temperatures. Following sputtering at room temperature, the disordered surface is depleted in Al. Annealing this surface to ~400°C leads to a (2 × 1) superstructure in the low-energy electron diffraction pattern. Further annealing to ~600°C gives rise to an incommensurate superstructure, probably formed by a segregated monolayer of Al. Above ~600°C, the Al concentration on the surface does not increase further. The diffraction pattern in this temperature region shows severe streaking, which might result from the development of (100)-oriented facets, possibly terminated in Al like the (100) surface.[5] At temperatures higher than 800°C, Al sublimes resulting in the formation of the incommensurate surface. The differing behavior of the surface of these two alloys can be understood by considering their heats of formation. The FeAl alloy gains only 24 kJ/mol by forming the CsCl-like structure, compared with 59 kJ/mol for NiAl. It is, therefore, energetically more favorable for the FeAl system to lower its total energy by lowering the surface-free energy by Al segregation.

The composition of the oxide on $Fe_{0.53}Al_{0.47}$(110) is dependent on the oxidation rate. For low rates, such as in normal ultrahigh vacuum experiments, a film of pure Al_2O_3 is formed, passivating the surface against further oxidation. At very high oxidation rates, a thicker film develops, which contains FeO as well. This behavior is different with respect to the NiAl alloy, where only films of Al_2O_3 form. For FeAl, the film is amorphous up to ~500°C; while at higher temperatures, the structure of the film is related to a metastable modification of Al_2O_3. Between 500° and 700°C, γ-Al_2O_3 forms. Around 850°C, a well-ordered film of most probably δ-Al_2O_3 grows, which is a tetragonally distorted form of the γ modification. Even at very low exposures of oxygen, the sharp diffraction pattern of the film is already visible, indicating initial film growth by island formation. An oxide film with identical structure is observed on NiAl(110). On both alloys, the oxide layer decomposes with the upper boundary of the stability region for the *d* modification of the oxide.

---

1. Graduate student from the University of Erlangen-Nürnberg, Germany.
2. Guest scientist from the University of Erlangen-Nürnberg, Germany.
3. H. L. Davis and J. R. Noonan, *Phys. Rev. Lett.* **54**, 566 (1985).

4. D. M. Zehner and G. R. Gruzalski, *Mat. Res. Soc. Symp. Proc.* **83**, 199 (1987).
5. C. P. Wang et al.,*Surf. Sci.* **298**, 114 (1993).

X-RAY REFLECTIVITY OF THE Cu(110) SURFACE[1]

G. Helgesen,[2] Doon Gibbs,[2] A. P. Baddorf, D. M. Zehner, and S. G. J. Mochrie[3]

It is generally expected that the surface of a crystal will become more disordered as the temperature is raised toward the bulk melting point. In this work, structural disorder in the Cu(110) surface has been studied between 300 and 1000 K using x-ray specular reflectivity. Transverse scans (θ scans) were measured for a range of values of the surface-normal wave vector $Q_\perp$. The data were analyzed with two approaches: transverse line shapes identified long-range order parallel to the surface, and integrated intensities were modeled to determine unit cell structures normal to the surface. For small values of $Q_\perp$, line shapes exhibited two components, one sharp (resolution limited), the other broad. In our view, the simplest interpretation involves surface faceting. The narrow component originates from flat terraces with widths at 300 K greater than 2000 Å. The broad component results from surface regions with high step densities at 300 K on the order of 600 Å wide. Steps appear to be pinned at 300 K to limited regions of the surface, probably by defects. As the temperature is increased, the sharp component slowly disappears, while the broad component increases slightly in intensity and width. This suggests the steps are no longer pinned and proliferate across the formerly smooth (110) facets. No distinct phase transition is observed nor was it possible to characterize the long-range behavior of the height-height correlation function, as is necessary to distinguish rough and step-disordered surfaces.

Integrated peak intensities, or reflectivities, were compared with a model using simple calculations to determine atomic displacements and root-mean-square (rms) vibrational amplitudes normal to the surface. At 300 K, the outermost layer was found to be contracted 7.9% of the bulk layer spacing, and the second layer expanded 2%. These values agree with those of other surface techniques and are typical for fcc(110) metal surfaces. As T is increased, the outerlayer relaxation decreases to 4.5% at 950 K. This rate of thermal expansion is four times greater than that in the bulk. The expansion rate at the surface appears to be nonlinear, increasing at higher temperatures, particularly above 700 K. At the same time, rms vibrational amplitudes also increase. At 300 K, the rms of the outermost layer is about 50% greater than the bulk value, with second and lower levels essentially bulk-like. Above 700 K, the rms of the outermost layer increases to three times the bulk value, and second and third layer values are significantly increased. The increases in rms motion with temperature are also nonlinear. Both the greater thermal expansion and rms motion of the surface layers indicate enhanced anharmonicity of the Cu(110) surface.

---

1. Summary of paper: *Phys. Rev. B* **48**, 15320 (1993).

2. Brookhaven National Laboratory, Upton, N.Y.
3. Massachusetts Institute of Technology, Cambridge, Mass.

THERMAL ROUGHNESS OF A CLOSE-PACKED METAL SURFACE: Pt(001)[1]

D. L. Abernathy,[2] S. G. J. Mochrie,[2] D. M. Zehner, G. Grübel,[3] and D. Gibbs[3]

The equilibrium shape of a crystal of fixed volume is determined by the minimum of its surface-free energy. In many cases, the equilibrium shape involves facets. For example, the (001) and (111) orientations of fcc metals are believed to be faceted at room temperature. However, at high temperatures, orientations which appear rounded, reminiscent of a liquid droplet, may also occur. Crystal surfaces which correspond to rounded orientations are expected to support capillary modes in a manner similar to liquid surfaces. In both cases, liquid and solid, a surface with capillary modes is rough.

X-ray scattering was used to study the Pt(001) surface from room temperature to the bulk melting temperature. Because of the fine reciprocal space resolution possible with x-ray scattering techniques, it has been possible to investigate the surface morphology on length scales up to several thousand angstroms. Below 1820 K, the line shape of the specular reflectivity indicates that the clean hexagonally reconstructed surface is atomically smooth on length scales exceeding 5000 Å. However, above 1820 K, there is a dramatic change in the profile shape which indicates that the surface is rough. The results yield new insight into the microscopic structure of a rough metal surface. Specifically, the scattering near the specular condition is diffuse and may be modeled using a height-height correlation function which diverges logarithmically at large distances. In addition, it was found that the average separation between thermally generated steps is many lattice constraints.

---

1. Summary of paper: *Phys. Rev. Lett.* **69**, 941 (1993).
2. Massachusetts Institute of Technology, Cambridge, Mass.
3. Brookhaven National Laboratory, Upton, N.Y.

FACETING TRANSFORMATIONS OF THE STEPPED Pt(001) SURFACE[1]

G. M. Watson,[2] D. Gibbs,[2] D. M. Zehner, M. Yoon,[3] and S. G. J. Mochrie[3]

Equilibrium faceting is a remarkable phenomenon in which a crystal surface increases its area in order to decrease its free energy. It is accomplished through the rearrangement of surface steps so that their distribution across the surface is no longer uniform. Instead, the surface separates into regions of high and low step densities. Our present understanding of faceting is based on a description of the surface-free energy in which the surface orientation is a key thermodynamic variable. Thus, a faceting transformation is an example of thermodynamic phase separation in which a surface phase of uniform orientation is replaced by coexistence among phases with different orientations and separated by sharp edges.

To investigate this phenomenon, x-ray scattering and a Pt sample in which the surface normal was deliberately miscut by 1.4° away from the (001) direction and toward the (110) direction have been used. This corresponds to an average monatomic step separation of approximately 30 near-neighbor distances. For temperatures above T_0 = 1820 K, the surface reflectivity is aligned to the direction of the macroscopic miscut. Its line shape is diffuse and suggests that the miscut surface is rough as was found for the (001)-oriented surface at these temperatures. Below 1820 K, there is a faceting transformation which leads to coexistence among hexagonally reconstructed, step-free domains, called facets, aligned to the (001) direction, and stepped, unreconstructed domains. Between 1820 and 1620 K, the phase behavior of the (001) facets is similar to that of the Pt(001) surface. On the stepped domains, the surface normal is tilted at an angle α to the (001) direction. Remarkably, the data show that α follows a one-half power-law dependence on reduced temperature. This implies that the free energy of a rough, solid surface varies quadratically with misorientation, consistent with simple theoretical ideas.

At 1620 K, there is a second faceting transformation at which the rough domains disappear. Instead, the surface is populated by two new domain types with ordered step distributions, in addition to the step-free, hexagonally reconstructed (001) facets. The terraces of the stepped domains are reconstructed to form a buckled and rotated hexagonal structure. Surface buckling refers to the sinusoidal displacement of atoms along the surface normal direction and is a defining characteristic of the close-packed, hexagonal reconstructions of Pt and Au(001) surfaces. Finally, for temperatures below 1500 K, the step wave vector locks to the buckling wave vector with a periodicity four times smaller than the terrace width. This corresponds to the first experimental observation of the formation of a commensurate magic vicinal.

---

1. Summary of paper: *Phys. Rev. Lett.* 71, 3166 (1993).
2. Brookhaven National Laboratory, Upton, N.Y.
3. Massachusetts Institute of Technology, Cambridge, Mass.

EXPERIMENTAL STUDY OF SMOOTHING KINETICS ON A ROUGH SURFACE[1]

J.-K Zuo[2] *and J. F. Wendelken*

While a substantial body of theoretical work examines the mechanisms by which a smooth layer develops using molecular beam epitaxy, experimental work has been extremely limited. In this work, high-angular-resolution low-energy electron diffraction has been used to observe for the first time the smoothing kinetics of a rough surface prepared by the epitaxial deposition of Cu on Cu(100) to produce a multilayer terrace-type structure. Upon deposition of Cu on Cu(100) at room temperature on an initially smooth Cu(100) surface, square islands developed in the first atomic layer. But with the deposition equivalent of 100 atomic layers, the surface developed a multilevel terrace structure

with an average terrace width L of only 35 Å. Upon heating this surface quickly by 30° to 60°C, smoothing was observed to occur via observation of the changing line shape of a diffracted electron beam. Figure 5.3 shows a log-log plot of the measured values of 1/FWHM vs time t for a series of final temperatures. The scatter, which occurs in the first minute in the data points, is an experimental effect resulting from the finite times required to heat the sample to the chosen temperatures. With a correction for the initial roughness at t_0, the smoothing displayed a power-law dependence on time t, $L(t) \propto t^x$ with an initial rate exponent of $x = 1/3$, independent of smoothing temperature. This result provides the first experimental verification of a theory which predicts that the smoothing rate for this type of structure will be driven by an evaporation-condensation mechanism, which is a function of the atomic step-edge curvature and separation. Also as predicted by theory, scaling was observed during this smoothing (i.e., it was observed that the terrace-width size distribution function remained the same while the average length scale increased). After the average terrace widths grew to an average size of 200–250 Å, the smoothing slowed to be proportional to $t^{1/5}$, and the scaling behavior broke down. This change may reflect a diffusion-limited regime or a limit imposed by surface entropy.

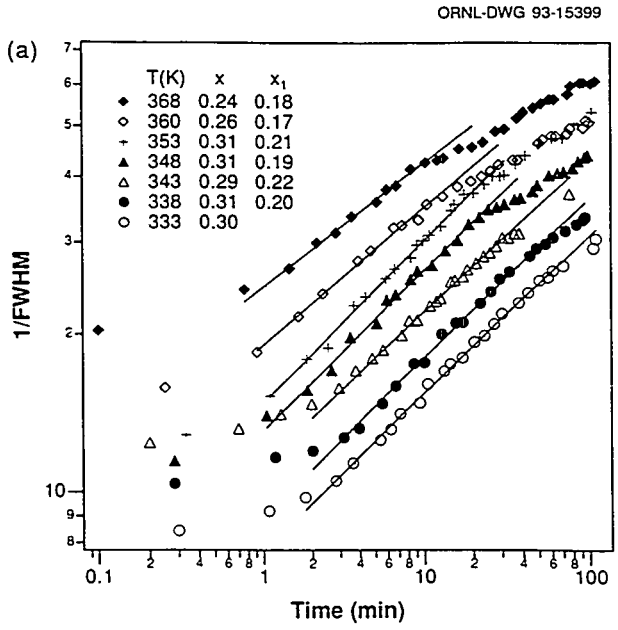

Fig. 5.3. Log-log plot of 1/FWHM vs t from the (00) beam with an out-of-phase scattering condition for different final temperatures. The average terrace width is proportional to 1/FWHM.

---

1. Summary of paper: *Phys Rev. Lett.* **70**, 1662 (1993).
2. ORISE faculty research participant from Southwest Missouri State University, Springfield, Mo.

ANHARMONICITY AND VIBRATIONAL RELAXATION ON THE Cu(110)-(2 × 1)-O SURFACE[1]

H. Dürr[2] *and A. P. Baddorf*

Reduced coordination at solid surfaces usually increases the anharmonicity of interatomic potentials because of the lower symmetry. This enhanced anharmonicity alters significantly the thermal atomic motion compared with that in the bulk; for example, amplitudes for vibrations normal to the surface are usually larger. Anharmonicity is also linked directly to the temperature-dependent energy shifts of phonons. If the interatomic bonds are harmonic, phonon energies remain independent of the

sample temperatures. Using high-resolution electron energy loss spectroscopy (HREELS) to measure the temperature dependence of surface phonons on Cu(110), a surface anharmonicity, 4–5 times larger than in the bulk,[3] was found.

The temperature-dependent energy shift (and broadening) of surface vibrations on the Cu(110)-(2 × 1)-O reconstructed surface have been studied between 100 and 600 K using HREELS. Typical HREELS spectra for 300 and 600 K are displayed in Fig. 5.4. Two prominent loss features are observed and can be assigned to a surface resonance at 24.3 meV and the oxygen vibration normal to the surface at 48.2 meV. The inserts show a side view of the atomic motion in the first three layers for the two modes. A much smaller energy shift than on the clean surface is observed. Comparison with bulk phonon measurements shows a bulk-like anharmonicity for the interatomic bonds at the surface. The temperature-dependent broadening observed in the oxygen-copper surface vibration can be explained by energy relaxation due to substrate anharmonicity.

These results show that oxygen adsorption reduces the strong anharmonicity in the copper-copper interatomic bonds present on the clean Cu(110) surface. The reason for this behavior is due to the formation of strong oxygen-copper bonds with negligible anharmonicity. The reconstruction of the surface also changes the bonding between Cu surface atoms, also making these bonds stronger and more harmonic.

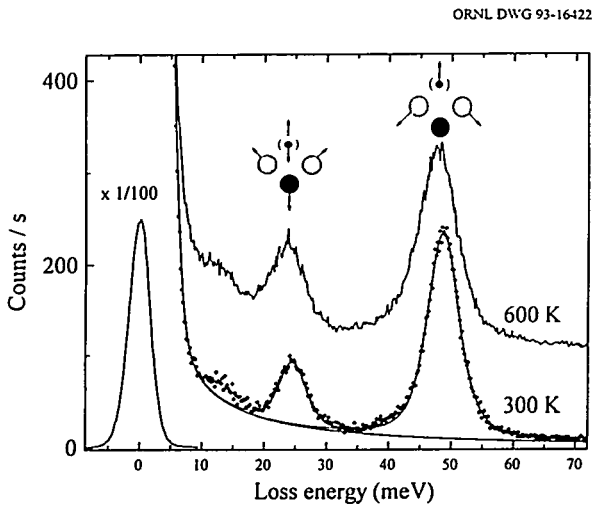

Fig. 5.4. HREELS spectra taken at 300 and 600 K. The 300-K spectrum is decomposed into smooth background and two loss peaks (atomic motion indicated in the insert).

---

1. Summary of paper: *Journal of Electron Spectroscopy and Related Phenomena* (in press); *Surface Science*, to be published.
2. Postdoctoral research associate from the University of Pennsylvania, Philadelphia, Pa.
3. A. P. Baddorf and E. W. Plummer, *Phys. Rev. Lett.* **66**, 2770 (1991).

SURFACE DYNAMICS OF BERYLLIUM[1]

J. B. Hannon,[2] *R. L. Sameth,*[2]
E. J. Mele,[2] *and E. W. Plummer*[3]

Beryllium is a challenging system to use as a test of our understanding of bonding in metals because the mechanism of bonding in Be depends dramatically upon the local atomic geometry. The electronic configuration of atomic Be is $1s^2 2s^2$. Bonding in the bulk is achieved via hybridization of atomic *s* and *p* states. Theoretical studies of Be in reduced dimensionality suggest that the energy gain associated with *s*-*p* hybridization is determined by coordination and local geometry. To develop a clearer picture of the bonding in Be, the dispersion of vibrational

modes at the Be(0001) surface has been measured. Surface phonon dispersion along the high-symmetry directions is shown in Fig. 5.5. Measurements of surface vibrations can be used to understand the effects of anharmonicity, stress, and inhomogeneous electronic screening at surfaces. The Be(0001) surface was chosen because our structural analysis indicates that the surface structure is anomalous—the first interplanar spacing is *expanded* by 6% from the bulk value.[4]

The unusual bonding mechanism gives rise to "three-body," or noncentral, forces between atoms in the bulk. Noncentral forces arise from an inhomogeneous distribution of screening electrons. A generalized tensor-force model has been used to calculate the dispersion of phonons at the Be(0001) surface. Although this model successfully reproduces bulk phonon dispersion, there are qualitative differences between the calculated and measured surface phonon dispersion. In fact, the data qualitatively agree with a

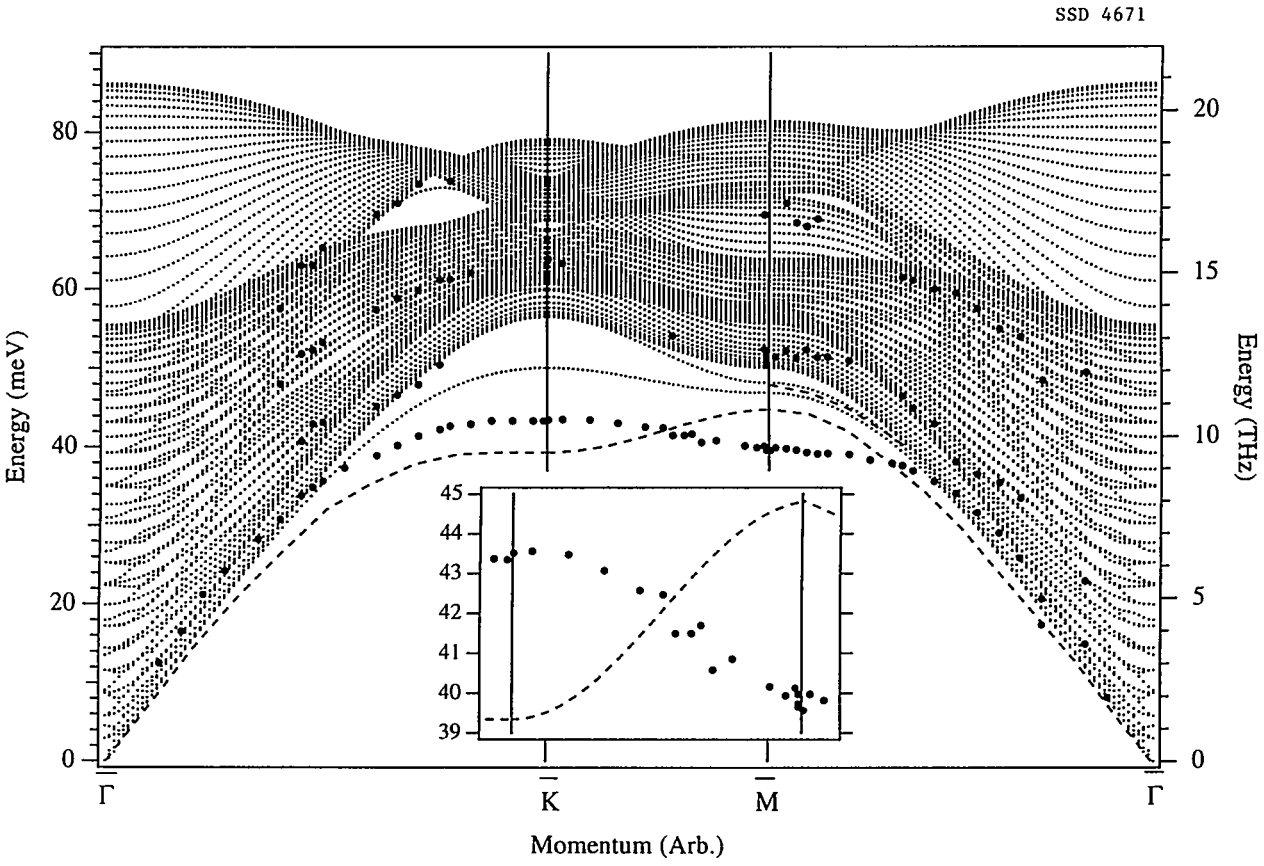

Fig. 5.5. Measured phonon dispersion (filled circles) superimposed on the dispersion of vibrational modes for a 30-layer Be(0001) slab calculated using a central-force model (dotted lines). Dashed lines are the surface modes calculated using a generalized tensor-force model. Model parameters were obtained from a fit to the dispersion of bulk phonons. The inset shows an expanded view of the dispersion from $\bar{K}$ to $\bar{M}$.

model which includes only *central* forces between atoms. Surface electronic states, which represent 80% of the surface density of states at the Fermi level,[5] make the bonding of surface atoms unlike that of bulk atoms. It is postulated that the added density of isotropic screening electrons at the surface reduces the effect of non-central forces, which dominate the dynamics of the bulk. The Be(0001) surface can be viewed as a new "form" of Be with unique structural and electronic properties.

---

1. Summary of paper to be published.
2. Graduate student from the University of Pennsylvania, Philadelphia, Pa.
3. ORNL/UT Distinguished Scientist.
4. H. L. Davis et al., *Phys. Rev. Lett.* **68**, 2632 (1992).
5. E. V. Chulkov, V. M. Silkin, and E. N. Shirykalov, *Surf. Sci.* **188**, 287 (1987).

NEW RESONANCES IN HIGH RESOLUTION ELECTRON ENERGY LOSS SPECTROSCOPY OF ADSORBED MOLECULES: ELECTRONIC EXCITATION OF PHYSISORBED O_2[1]

J. C. Barnard,[2] *K. M. Hock,*[2] *L. Siller,*[3]
M. R. C. Hunt,[2] *J. F. Wendelken, and R. E. Palmer*[2]

Resonance scattering is an important form of low-energy (1–30-eV) electron scattering from diatomic molecules in the gas phase and when adsorbed on surfaces. The mechanism arises from the formation of short-lived temporary negative ion states via trapping of the incident electron in an unoccupied orbital of the target molecule. Resonances have been seen in the cross section for vibrational and electronic excitation of gas phase and adsorbed O_2 and also in the yield of O^- ions in electron-stimulated desorption (ESD) experiments on adsorbed O_2. The negative ion state associated with resonance has been successfully identified in some cases through examination of the resonance energy and angular symmetry of the excitation. In a recent experiment, which provided the first report of a negative ion resonance from both the physisorbed and chemisorbed state of the same system,[4] the $^4\Sigma_u$ state was identified at 7.25 and 3.75 eV, respectively, in the vibrational excitations of physisorbed and chemisorbed O_2 on Pt(111). The $^2\Pi_u$ resonance was also observed at 4.5 eV for the physisorbed O_2 on Pt(111) but was quenched for the chemisorbed case.

In the present work, a new resonance in the $X^3\Sigma_g \rightarrow a^1\Delta_g$ electronic excitation was first observed with physisorbed O_2/Pt(111) at ORNL, as shown in Fig. 5.6. More detailed measurements were then made at Cambridge of the

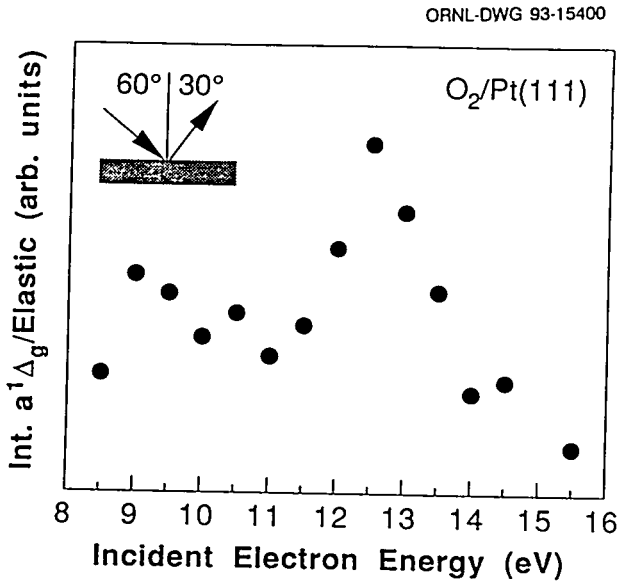

Fig. 5.6. Resonance energy profile of the $a^1\Delta_g$ intensity, normalized to the diffuse elastic intensity, from physisorbed O_2/Pt(111).

same resonance with physisorbed O_2/graphite. The energy of the new resonance is ~13 eV in both cases. The angular variation of the $a^1\Delta_g$ intensity at 13 eV shows that the intermediate state is most probably the $^2\Delta_u$ negative ion. This is a different state than the $^2\Sigma_u$ state to which a 13-eV resonance in ESD has been assigned and which is normally considered to be a forbidden state which could only be permitted through symmetry breaking. The present results suggest that the ESD assignment may be incorrect, and the degree to which the negative ion resonance symmetry is broken in the physisorbed state needs to be re-evaluated.

---

1. Summary of paper: *Surf. Sci.* **291**, 139 (1993).
2. Cavendish Laboratory, University of Cambridge, Cambridge, U.K.
3. Graduate student from University of Cambridge, Cambridge, U.K.
4. *Solid State Division Progress Report for Period Ending March 31, 1992*, ORNL 6722 (September 1992), p. 172; *Chem. Phys. Lett.* **210**, 15 (1993).

CORE-LEVEL SPECTROSCOPY INVESTIGATION OF THE $Mo_{0.75}Re_{0.25}(100)$ SURFACE[1]

P. F. Lyman[2] *and D. M. Zehner*

Using low-energy electron diffraction (LEED), the $Mo_{0.75}$ $Re_{0.25}(100)$ surface has been examined at a sample temperature of 100 K. From the analysis, it has been determined that the top layer consists of 95% Mo and 5% Re and that the second layer consists of ~50% of each. In addition, large interlayer relaxations are present in the surface region. Following the adsorption of hydrogen, it has been determined that the relative concentrations in the outermost layers are unchanged from the clean surface values but that the interlayer relaxations have been reduced to near zero.

These two surfaces have been examined using photoemission and synchrotron radiation. The investigations have been concerned with determining the Re 4*f* core-level binding energies and intensities. As shown at the top of Fig. 5.7, two core levels are present for the clean

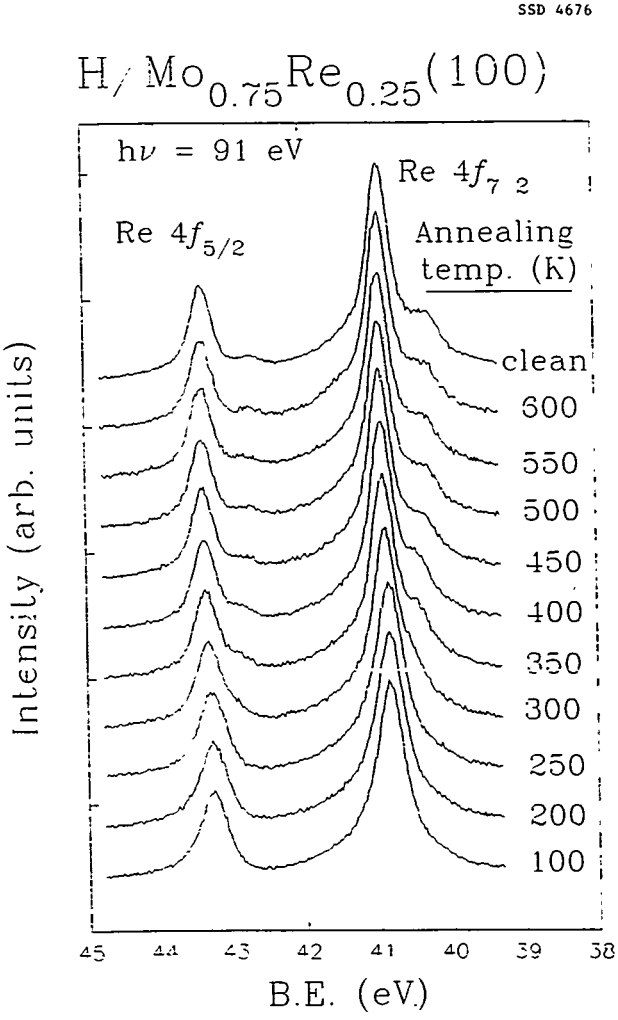

Fig. 5.7. Re 4*f* core-level spectra from a H-saturated $Mo_{0.75}Re_{0.25}(100)$ surface and after annealing to various temperatures. A clean surface spectrum is also shown for reference.

surface. The intense peak at 40.945 eV is associated with the Re atoms in the second and deeper layers, while the weaker peak at smaller binding energy is associated with the Re atoms in the outermost layer. The difference in binding energies is a consequence of the different environments for atoms in the outermost layer as compared with those in the bulk. Moreover, these assignments and the relative intensities are consistent with the LEED results with regard to the segregation gradient in the surface region. When hydrogen is adsorbed on the surface, the intensity of the peak associated with the surface Re atoms is quenched as shown in the bottom spectrum in Fig. 5.7. In addition, the binding energy of the peak associated with Re atoms in the deeper layers is decreased ~0.2 eV. This is a consequence of the change in the potential which results from both the adsorption of hydrogen and the changes in interlayer spacings which occur. As the sample is heated, hydrogen desorbs from the surface, and the peak intensities and energies shift as shown in the spectra in Fig. 5.7. When all of the hydrogen has been desorbed, the clean-surface spectrum is again obtained.

---

1. Summary of paper to be published.
2. ORNL/ORISE postdoctoral research associate.

THE ADSORPTION OF SULFUR ON W(001)[1]

D. R. Mullins,[2] P. F. Lyman,[3] and S. H. Overbury[2]

The adsorption of atomic sulfur on W(001) has been studied as a function of sulfur coverage and sample annealing temperature. Results from laboratory techniques such as work function changes, valence band photoemission, Auger electron spectroscopy, low-energy electron diffraction, and low-energy ion scattering indicate that the adsorption of sulfur on W(001) undergoes a distinct change at 0.5 ML of sulfur. Two distinct adsorption states are observed in the S 2*p* soft x-ray photoelectron spectra for sulfur on W(001), as shown in Fig. 5.8. A single adsorption state is observed for coverages up to 0.5 ML. A second adsorption state is populated as coverage increases from 0.5 to 1.0 ML. If the

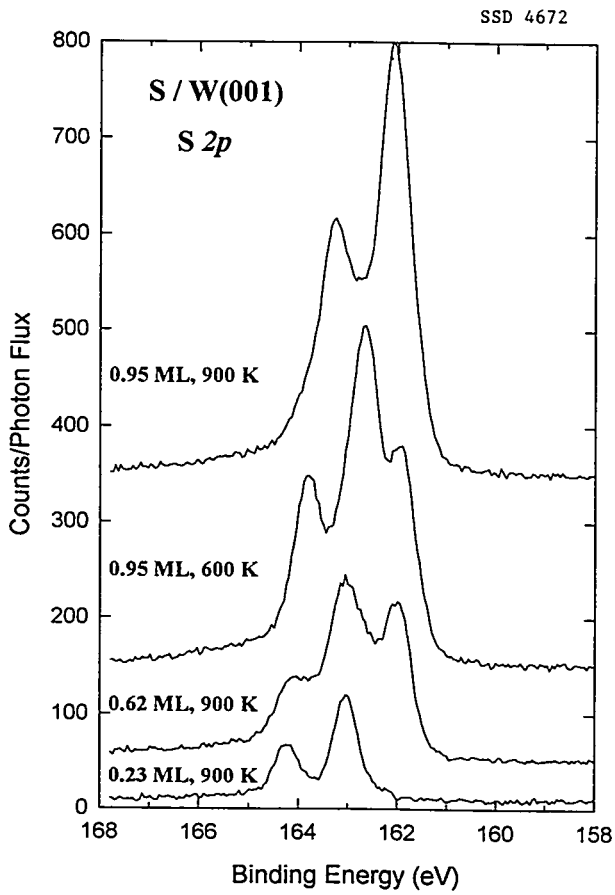

Fig. 5.8. S 2*p* core-level photoemission from several coverages of atomic sulfur adsorbed on W(001) and annealed as indicated. The excitation energy was 208 eV.

sample is annealed to 600 K, the two states are occupied by nearly equal amounts of sulfur at 1.0 ML. However, if the sample is annealed to 900 K, most of the sulfur which originally adsorbed in the low-coverage state is shifted to the new state.

The prevailing structural model for S/W(001) is that the sulfur adatoms occupy evenly dispersed fourfold sites up to a coverage of 0.5 ML. The low-coverage state observed in the S 2*p* spectra is consistent with this model. Crowding between the sulfur atoms makes continued adsorption in the fourfold sites unfavorable at higher coverage. The S 2*p* spectra indicate either that lower coordination sites are populated on an unperturbed surface or that the surface is reconstructed. Low-energy ion scattering experiments and high-resolution photoemission spectra from the W 4*f* level provide strong evidence that the substrate reconstructs, resulting in vacancy formation at high sulfur coverages and elevated temperatures.

---

1. Summary of paper: *Surf. Sci.* 277, 64 (1992).
2. Chemistry Division, ORNL.
3. ORNL/ORISE postdoctoral research associate. Present address: Northwestern University, Evanston, Ind.

METHANETHIOL ON W(001) AND Ru(0001)[1]

D. R. Mullins[2] *and P. F. Lyman*[3]

The adsorption and decomposition of methanethiol, CH_3SH, on W(001) and Ru(0001) have been studied as a function of coverage and temperature. As has been observed on other surfaces, CH_3SH follows two distinct reaction pathways on W(001) and Ru(0001)—total decomposition to adsorbed atomic sulfur and carbon with desorption of molecular hydrogen or partial decomposition to adsorbed sulfur and desorbed methane. Ru(0001) is more reactive in the sense that carbon-sulfur bond cleavage occurs at a lower temperature on Ru(0001) than on W(001). Methyl thiolate, CH_3S, is readily formed at 100 K on both surfaces. The adsorption and reaction of CH_3SH were followed by temperature-programmed desorption, soft x-ray photoelectron spectroscopy (SXPS), Auger electron spectroscopy, and valence band photoelectron spectroscopy.

As shown in Fig. 5.9, numerous adsorption states can be differentiated in the SXPS spectra of the S 2*p* core level. Molecular CH_3SH, which is seen at the highest binding energy, is only observed at very high exposures at 100 K. Experiments at coverages up to saturation indicate that all of the chemisorbed CH_3SH partially decomposes at 100 K into two distinct states. The two states are believed to result from the same nominal species, CH_3S, adsorbed in different adsorption sites. By analogy with atomic sulfur on W(001), the higher binding energy state results from CH_3S in either a fourfold or threefold site on W(001) or Ru(001), respectively. The lower binding energy state results from adsorption in a twofold or a top site.

---

1. Summary of papers: *J. Phys. Chem.* 97, 9226 (1993); *Journal of Physical Chemistry* (in press).
2. Chemistry Division, ORNL.

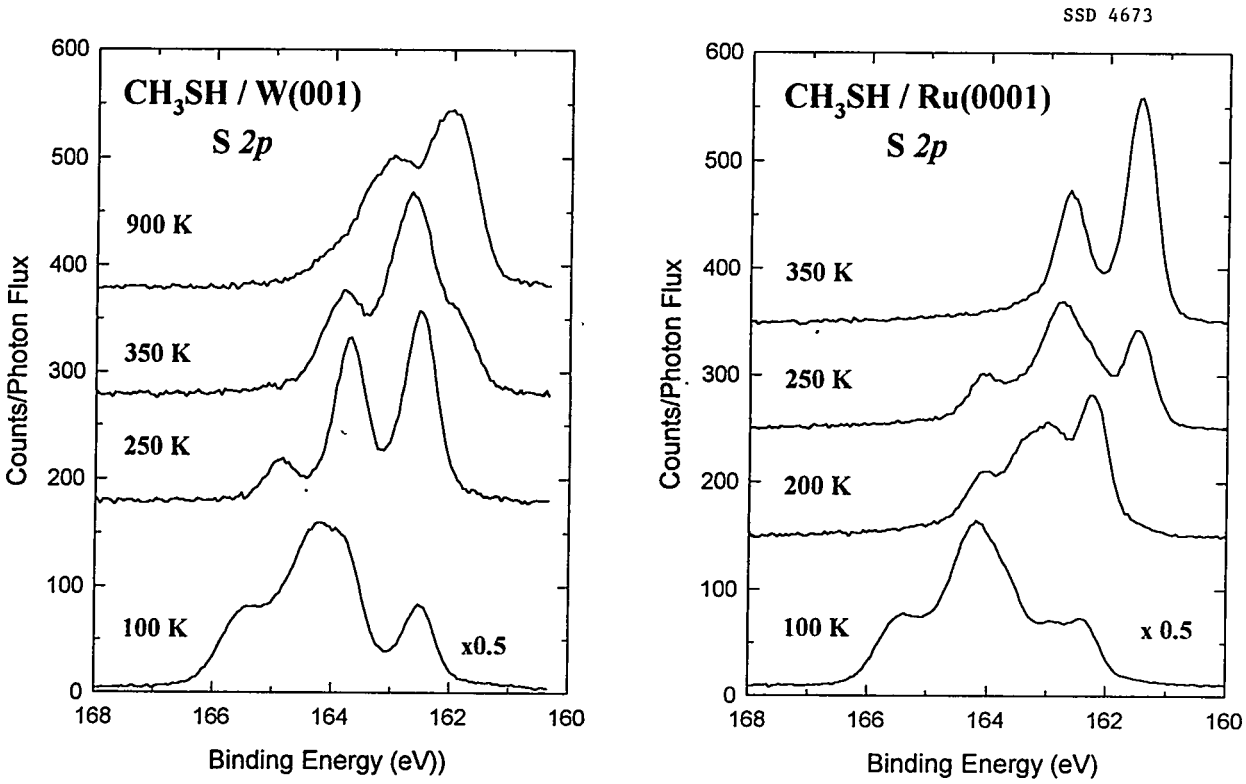

Fig. 5.9. S 2*p* core-level photoemission from multilayers of methanethiol adsorbed on W(001) and Ru(0001) and annealed as indicated. The excitation energy was 208 eV.

3. ORNL/ORISE postdoctoral research associate.

ATOMIC LAYER-BY-LAYER SURFACE REMOVAL BY FORCE MICROSCOPY[1]

B. C. Sales, T. Thundat,[2]
B. C. Chakoumakos, L. A. Boatner,
D. P. Allison,[2] *and R. J. Warmack*[2]

Using an atomic force microscope (AFM) operating under ambient conditions (Fig. 5.10), the first atomic-resolution AFM images of atomic-scale defects have been obtained, and observations of the scanning-induced removal of atoms from lead pyrophosphate cleavage faces have been made. Repeated scanning of the same surface area revealed cyclic changes in the $Pb_2P_2O_7$ atomic structure consistent with a layer-by-layer removal of atoms. Subsequent large area imaging of a region that had been subjected to repeated scanning revealed a depression several nanometers deep, indicating that this technique may be applicable to patterning the surfaces of materials on an atomic scale. Excellent agreement was also found between the calculated and observed AFM images of a cleaved $Pb_2P_2O_7$ surface.

---

1. Summary of paper: *Surf. Sci. Lett.* **293**, L863 (1993).
2. Health Sciences Research Division, ORNL.

SSDN-4666

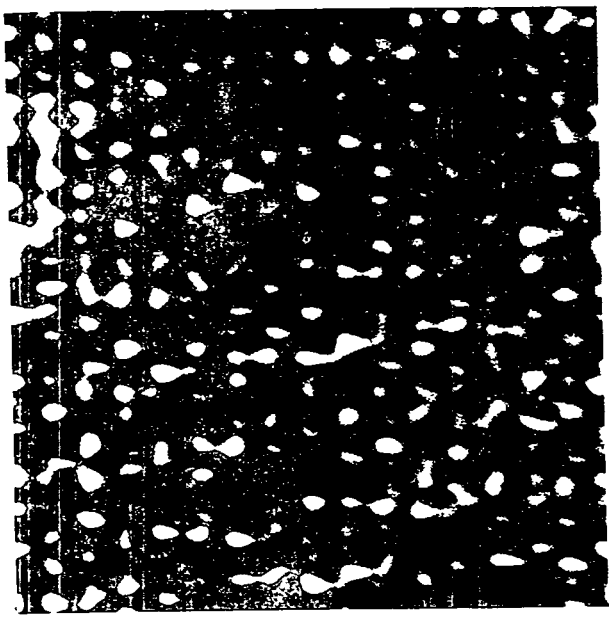

Fig. 5.10. Atomic-resolution AFM image (8 × 8 nm) of a freshly cleaved lead pyrophosphate surface showing the presence of atomic-scale defects. These defects are most likely oxygen atoms that are "pulled" from the upper cleavage surface to the lower as a result of the cleavage process. The "oxygen atom" defects correspond to the bright (higher) circular spots about 0.2 nm in diam.

ELECTRON MICROSCOPY

ATOMIC-RESOLUTION COMPOSITIONAL IMAGING OF THE SUB-LATTICE IN III–V SEMICONDUCTORS[1]

A. J. McGibbon,[2] *S. J. Pennycook, and Z. Wasilewski*[3]

It is now possible to examine directly crystalline structures possessing atomic separations in the range 1–2 Å with both spatial and atomic number sensitivity. This is achieved by employing Z-contrast imaging[4] on a 300-kV, 1.3-Å resolution, VG HB603U scanning transmission electron microscope (STEM). Here, the benefit of combining increased spatial resolution with atomic number sensitivity is demonstrated by reporting the first direct observations of structural polarity (the alternate ordering of group III and group V sites) in samples of GaAs grown by molecular beam epitaxy (MBE). A consequence of this development in the analysis of III–V semiconductors is that it is now possible to provide direct and unambiguous information on atomic ordering at interfaces and phase boundaries.

III–V semiconductor heterostructures possess a zinc-blende crystal structure consisting of two interpenetrating face-centered-cubic sublattices of group III and group V atoms displaced with respect to each other by $a/4\langle 111\rangle$, where a is the lattice parameter. When examining a specimen oriented along a zone axis direction using Z-contrast imaging in a STEM, the resultant image is a map of the columnar scattering intensity, the resolution of which is primarily limited by the size of the electron probe. In the HB603U STEM, the electron probe full-width half-maximum (FWHM) at optimum defocus conditions is 1.3 Å; therefore, it becomes possible to observe directly atomic separations (including all $\langle 110\rangle$ projections of III–V semiconductors), hitherto unattainable by any other experimental technique. Furthermore, variations in image intensity approach that of the Z^2 dependence of unscreened Rutherford scattering; therefore, elements as close in atomic number as Ga (Z = 31) and As (Z = 33) will exhibit >10% difference in image intensity. A

schematic diagram of GaAs oriented in the ⟨110⟩ direction is shown in Fig. 5.11(a), with an as-acquired Z-contrast image shown in Fig. 5.11(b). By applying the simple image processing technique of median filtering, Fig. 5.11(c) clearly

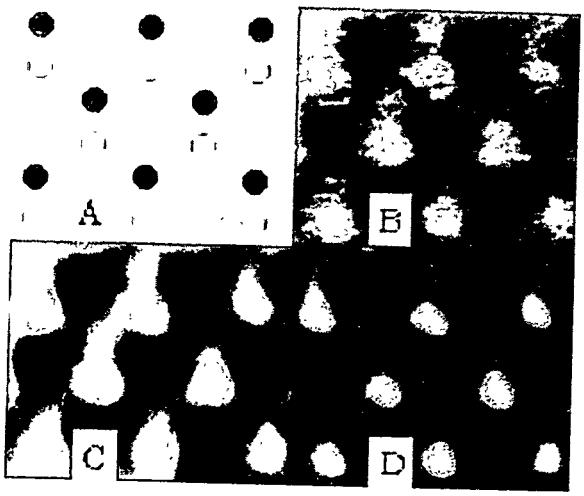

Fig. 5.11. (a) A schematic diagram of GaAs oriented in the ⟨110⟩ direction. Columns of Ga are represented by black circles, whereas columns of As are represented by white circles. (b) An as-acquired 300-kV Z-contrast image of this material. (c) Median-filtered image of (b). (d) Maximum entropy image of (b).

demonstrates that the required atomic resolution and atomic number sensitivity have been achieved to produce a direct, compositionally sensitive image of ⟨110⟩ GaAs. Furthermore, by employing a maximum entropy[5] approach to image processing (in which a "most likely" image is obtained given a particular probe function), the resultant image [Fig. 5.11(d)] clearly demonstrates the potential of these imaging techniques for analyses of III–V semiconductor heterostructures.

---

1. Summary of paper to be published.

2. ORNL/ORISE postdoctoral research associate.

3. National Research Council of Canada, Ottawa, Canada.

4. S. J. Pennycook and D. E. Jesson, *Phys. Rev. Lett.* **64**, 938 (1990).

5. S. F. Gull and J. Skilling, *IEEE Proc.* **131F**, 646 (1984)

NEW INTERFACE STRUCTURE FOR A-TYPE $CoSi_2$/Si(111)[1]

M. F. Chisholm, S. J. Pennycook, R. Jebasinski,[2] and S. Mantl[2]

Because of their small lattice mismatch and similar structures, single-crystal cobalt and nickel-disilicide films can be grown with relative ease in contact with Si. These well-defined couples have attracted much interest because of their technological importance and because they appear to be model systems for studies of a range of interface properties, including the correlation between atomic structure and Schottky barrier height (SBH). However, even in this well-matched system, the actual interface structure remains controversial.[3–5]

In this study, the atomic structure of $CoSi_2$/Si interfaces of buried layers formed by Co implantation was characterized by high-resolution Z-contrast imaging. In this imaging mode, each atomic column can be imaged independently with high compositional sensitivity.[6] These images clearly reveal a new structure for the $CoSi_2$/Si(111) interface that does not appear to have been considered in previous investigations. A Z-contrast image of the [110] projection of the $CoSi_2$/Si(111) interface is presented in Fig. 5.12.

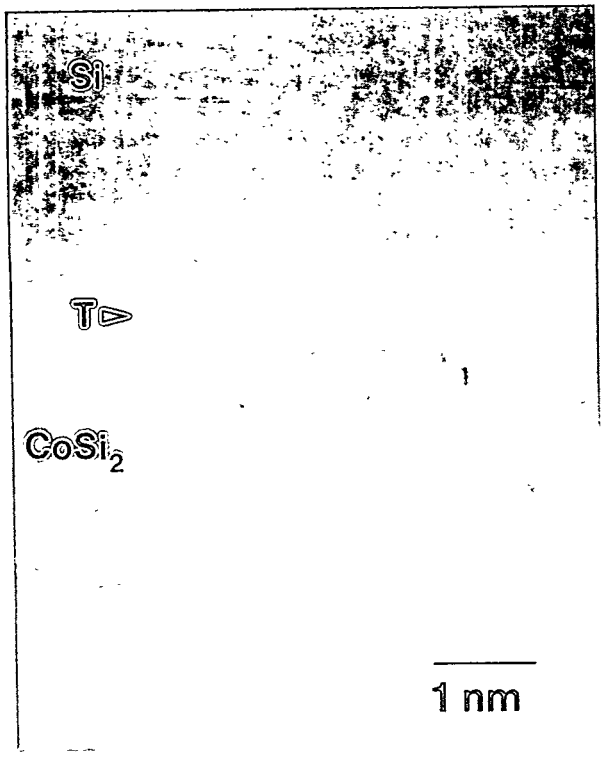

Fig. 5.12. Z-contrast image of a section of $CoSi_2$/Si(111) interface projected along the ⟨0-11⟩ direction showing a twinned interfacial layer of Si.

The $CoSi_2$ and Si lattices are observed to have the same orientation, as indicated by the parallel {111} and {110} planes on the two sides of the interface, and the shifts of the {111} planes across the interface are consistent with the interface model where the Co at the boundary has sevenfold coordination. However, this direct image shows that there is a stacking fault in the Si crystal at the interface. The interfacial Si layer is rotated 180° around the [111] surface normal so that Si atoms in contact with the disilicide have a twinned orientation. From the position of this twinned layer of Si relative to the interfacial Co layer, it has been determined that the Co coordination is eightfold at this interface, as it is in the bulk.

These results indicate that type-A buried $CoSi_2$ layers in Si(111) have the same combination of two different atomic structures at the top and bottom interfaces. Both interface structures have eightfold coordinated Co atoms. The preference for this interface over the sevenfold type-A structure is in agreement with theoretical predictions.[4] Additionally, very similar Schottky barrier heights for top and bottom diodes have been measured on similarly prepared samples.[7] It is expected that further work will lead to new levels of insight into the important and controversial relationship between the atomic structure and electronic properties.

---

1. Summary of paper: *Applied Physics Letters* (submitted for publication).
2. Institut für Schicht- und Ionentechnik, Jülich, Germany.
3. D. Cherns et al., *Philos. Mag. A* **46**, 849 (1982).
4. P. J. van den Hoek et al., *Phys. Rev. Lett.* **60**, 1743 (1988).
5. C. W. T. Bulle-Lieuwma et al., *Appl. Phys. Lett.* **55**, 648 (1989).
6. S. J. Pennycook and D. E. Jesson, *Acta Metall. Mater.* **40**, S149 (1992).
7. R. Jebasinski, Thesis, University Cologne (1993); *KFA Report* Juel-2738 (1993), D52428 Jülich, Germany.

THE ORDERED ATOMIC INTERFACE OF $CoSi_2$/Si(001)[1]

M. F. Chisholm, N. D. Browning,[2] S. J. Pennycook, R. Jebasinski,[3] and S. Mantl[3]

The most straightforward structure models of the $CoSi_2$/Si(001) interface connect bulk-terminated single crystals at a planar interface.[4]

The so-called "sixfold" model was originally found to provide a reasonable match with high-resolution phase contrast microscopy images from the $CoSi_2$/Si(001) interface[5] and from interfaces of a similar $NiSi_2$/Si(001) system.[4] However, Z-contrast images [Fig. 5.13(a)] of the $CoSi_2$/Si(001) interface show that the structure of this interface involves a 2×1 ordering of the interfacial Co atoms. It appears the planar {001} interface prefers to transform to atomic-sized {111} facets. The atomic structure derived from the Z-contrast images [Fig. 5.13(b)] shows the observed interfacial ordering can reduce by half the number of sixfold-coordinated Co atoms present at the interface when compared with a flat, bulk-terminated boundary. Evidence for a doubling of the periodicity at this interface has been seen in some recent phase contrast and medium-energy ion scattering studies for both ion-implanted and MBE-grown samples of $CoSi_2$ and $NiSi_2$ in contact with Si(001). However, all models that were proposed to provide the best fit to observations involved modulations of interfacial Si atoms.[6–8] Unfortunately, these methods rely on preconceived models of the structure being studied for data interpretation and, necessarily, have reduced sensitivity to unforeseen structures. From our studies, it seems likely that these observations are actually due to the same stable $2 \times 1/1 \times 2$ ordered structure.

It is expected that higher resolution images from the new SSD 300-kV Z-contrast scanning transmission electron microscope (in which individual Si columns can be resolved) combined with theoretical calculations of the energy of various interface configurations will provide further insights into the atomic and electronic

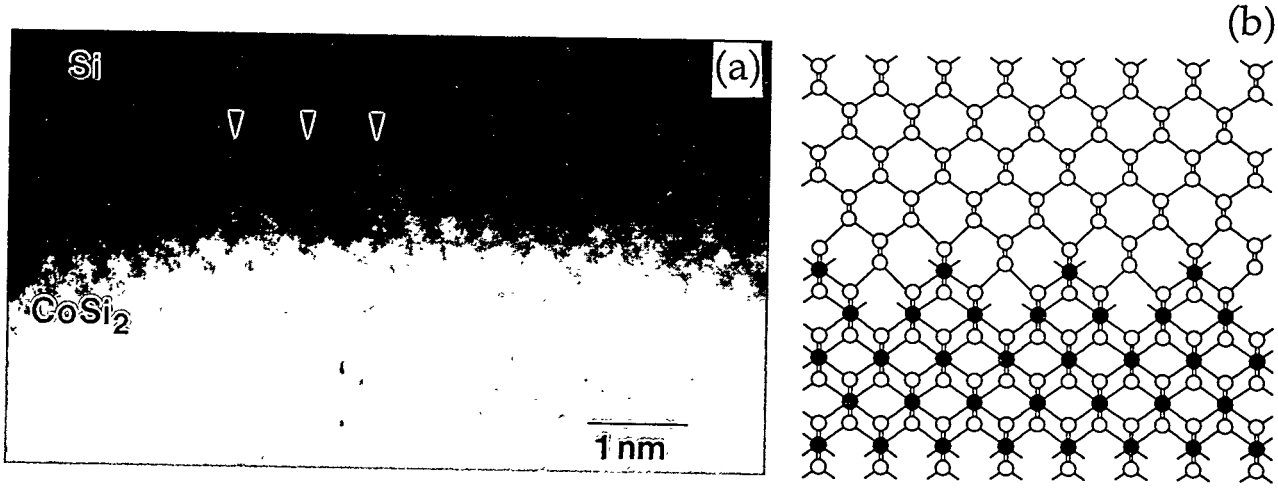

Fig. 5.13. (a). High-resolution Z-contrast image of the ⟨110⟩ projection of the $CoSi_2$/Si(001) interface, which reveals a doubling of the periodicity of the interfacial Co atoms. (b) Atomic model of the ordered 2×1 interface structure deduced from the images. This model includes an observed rigid-body translation of the $CoSi_2$ film relative to the Si lattice of 0.05 nm perpendicular to the interface plane. Si atom columns are represented by unfilled circles and Co columns by filled circles.

structure of this technologically important interface.

---

1. Summary of paper: *Applied Physics Letters* (submitted for publication).
2. ORNL/ORISE postdoctoral research associate.
3. Institüt für Schicht- und Ionentechnik, Jülich, Germany.
4. D. Cherns et al., *Philos. Mag. A* **49**, 165 (1984).
5. J. M. Gibson et al., *Appl. Phys. Lett.* **41**, 818 (1982).
6. C. W. T. Bulle-Lieuwma et al., *Philos. Mag. A* **64**, 255 (1991).
7. D. Loretto et al., *Phys. Rev. Lett.* **63**, 298 (1989).
8. M. Copel and J. Falta, *Phys. Rev. B* **36**, 4769 (1993).

ATOMIC-RESOLUTION CHEMICAL ANALYSIS[1]

N. D. Browning,[2] M. F. Chisholm, and S. J. Pennycook

In the SSD scanning transmission electron microscope (STEM), changes in atomic structure and composition can be observed directly by the high-resolution Z-contrast imaging technique.[3] Additionally, as the image requires only high-angle scattering, it can be used to position the probe for simultaneous electron energy loss spectroscopy with atomic precision. For the core loss region of the spectrum (>300 eV), the energy loss signal is sufficiently localized that the spatial resolution is limited only by the probe.[4] The electronic structure of the material can thus be determined on the same scale as changes in composition and atomic structure can be observed in the image, allowing the structure and chemical bonding at interfaces and boundaries to be characterized at the atomic level.

This high spatial resolution has been demonstrated by studying epitaxial $CoSi_2$-Si interfaces produced by high-dose implantation of Co^+ ions in a heated Si(001) substrate. A Z-contrast image of a {111} facet produced by this method is shown in Fig. 5.14(a), with the brighter region corresponding to the increased scattering power of the heavier cobalt atoms in the silicide. A stacking fault is visible at the interface, which leads to a separation of the planes across the boundary of 2.7 Å rather than the 3.1-Å planar spacing of the bulk. Cobalt $L_{2,3}$ edges obtained from individual planes across the interface are shown in Fig. 5.14(b), where an intensity variation dropping from 86% to 7% is observed on moving a single atomic plane across the interface. This is in good agreement with the image and predicted spatial resolution. The slight reduction in the contrast at the two planes on either side of the interface is most likely due to an amorphous surface layer broadening the probe or possibly elastic scattering of the probe out of the channeling condition.

The energy loss profile in Fig. 5.14(b) clearly demonstrates atomic resolution in one dimension. Since the Z-contrast image shows two-dimensional resolution, this result demonstrates that atomic-resolution microanalysis from a single column is possible, in principle. This method overcomes problems caused by beam broadening and uncertainties in the interface structure that occur in microanalysis without the benefit of a high-resolution reference image. Therefore, column-by-column compositional

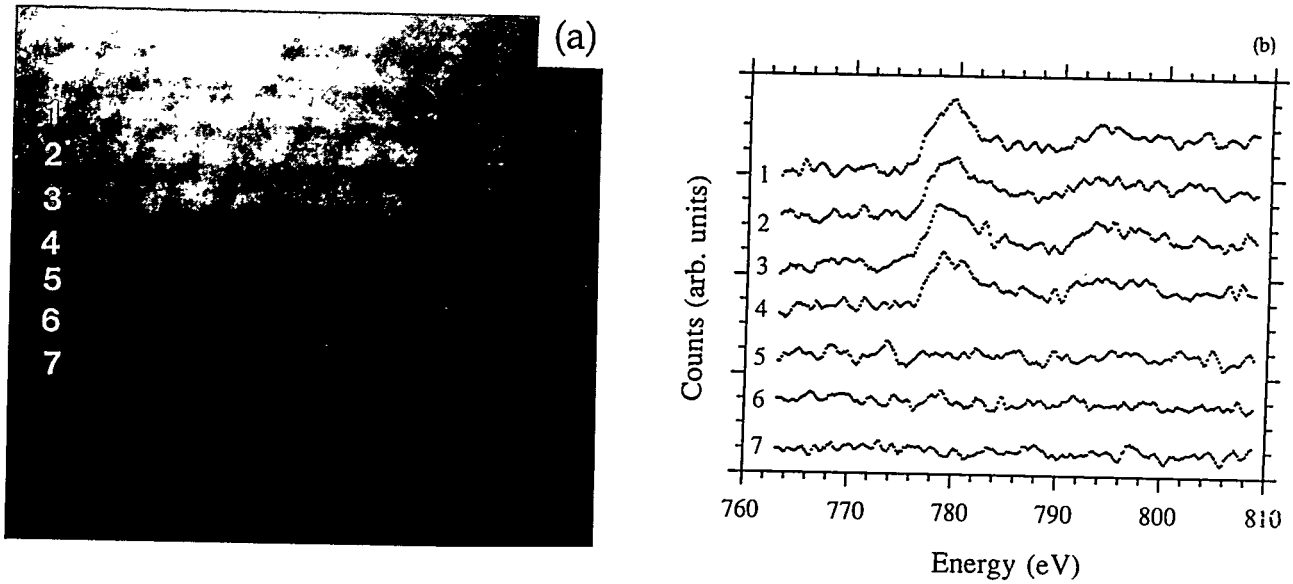

Fig. 5.14 (a) Z-contrast image of a {111} facet in a $CoSi_2$-Si interface. (b) Background stripped cobalt $L_{2,3}$ spectra obtained plane by plane across the interface.

and bonding information can be directly related to the interface structure seen in the image. This ability to correlate structure and chemistry with atomic resolution offers an opportunity to examine the role of defects and interfaces in determining the bulk properties of materials.

CELL-BY-CELL MAPPING OF CARRIER CONCENTRATIONS IN HIGH-TEMPERATURE SUPERCONDUCTORS[1]

N. D. Browning,[2] M. F. Chisholm, and S. J. Pennycook

The correlation between grain boundary structure and hole depletion in the high-temperature superconductor $YBa_2Cu_3O_{7-\delta}$ can be studied on the scale of the coherence length in the SSD scanning transmission electron microscope (STEM). The Z-contrast image can be used to position the probe for electron energy loss spectroscopy (EELS) with atomic precision,[3] and the oxygen K-absorption edge pre-edge feature can be utilized to measure changes in hole doping to an accuracy of ±5%.[4] This combination of imaging and spectroscopy provides both structural and electronic characterizations of the boundary on the atomic scale. In addition, the Z-contrast image allows areas to be

1. Summary of paper: *Nature* **366**, 143 (1993).
2. ORNL/ORISE postdoctoral research associate.
3. S. J. Pennycook and D. E. Jesson, *Phys. Rev. Lett.* **64**, 938 (1990).
4. N. D. Browning and S. J. Pennycook, *Microbeam Analysis* **2**, 81 (1993).

selected that are free from specimen preparation damage, while the ability for time-resolved EELS allows the effects of electron beam irradiation to be observed. The resulting measurements are thus free from experimentally induced effects and are representative of the original material.

Oxygen K-edge spectra have been recorded 8 Å apart, across a 29° [near Σ17 (001) 28.1°] asymmetric tilt boundary and a 36° [near Σ5 (001) 36.9°] symmetric tilt boundary in polycrystalline $YBa_2Cu_3O_{7-\delta}$. The film was prepared by laser ablation and used to quantify the hole depletion (Fig. 5.15). As both boundaries are high-angle grain boundaries, the results of Dimos et al.[5] would suggest both boundaries have a reduced critical current and are the source of weak links. Results on the asymmetric boundary are in agreement with this model, with a significant hole depletion zone extending over a range 50–60 Å on either side of the boundary. This hole depletion, combined with the disordered region seen in the image, makes a reduction in critical current seem likely. The symmetric boundary, however, shows no evidence of any hole depletion zone or disordered region (within ±0.05 in local hole concentration and ±2 Å of the boundary plane), strongly suggesting that this symmetric boundary is not a weak link and that the properties of the boundary may not be reduced from that of the bulk. There appears to be a direct correlation between the grain boundary structure and the hole depletion in the boundary region. This provides the first clear microscopic evidence that not all high-angle boundaries act as weak links, as proposed by Babcock et al.[6]

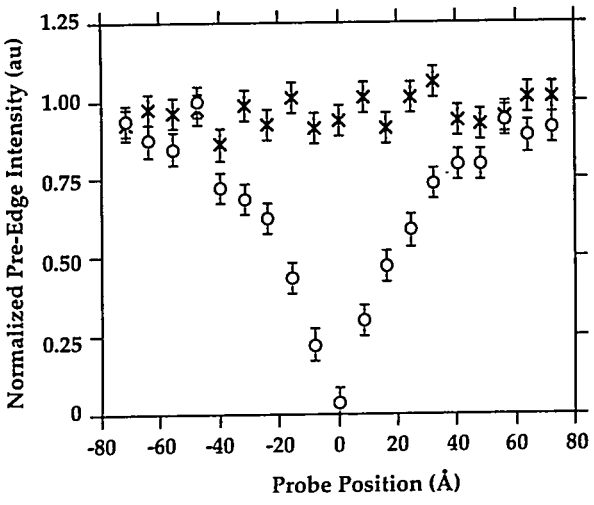

Fig. 5.15. There is no hole depletion around the symmetric boundary (x), whereas the asymmetric boundary shows a hole depletion zone extending 50–60 Å either side of the boundary (o).

The combination of Z-contrast and EELS also has a number of potential applications in the field of high-temperature superconductivity (e.g., the study of hole-doping effects at interfaces between electron and hole-doped superconductors and the study of ultrathin films and multilayers). An ability to make these observations on the scale of the coherence length has major implications for the study of boundaries and interfaces used in device applications.

---

1. Summary of paper: *Physica C* **212**, 185 (1993).
2. ORNL/ORISE postdoctoral research associate.
3. N. D. Browning, M. F. Chisholm and S. J. Pennycook, "Atomic-Resolution Chemical Analysis," this report.
4. N. D. Browning, J. Yuan, and L. M. Brown, *Physica C* **202**, 12 (1992).
5. D. Dimos et al., *Phys. Rev. Lett.* **61**, 219 (1988).

6. S. E. Babcock et al., *Nature* 347, 167 (1990).

ATOMIC-SCALE ANALYSIS OF A $SrTiO_3$ GRAIN BOUNDARY BY COMBINED Z-CONTRAST IMAGING AND ENERGY LOSS SPECTROSCOPY IN THE SSD STEM[1]

M. M. McGibbon,[2] N. D. Browning,[2] M. F. Chisholm, and S. J. Pennycook

The macroscopic properties in materials (e.g., $SrTiO_3$) are controlled by the atomic structure and chemistry at the grain boundaries. A basic understanding of the structure-property relationship requires a technique which probes both composition and chemical bonding on an atomic scale. The high-resolution *Z*-contrast technique in the SSD scanning transmission electron microscope (STEM) forms an incoherent image in which changes in atomic structure and composition can be interpreted intuitively. This direct image allows the electron probe to be positioned over individual atomic columns for parallel detection electron energy loss spectroscopy (EELS) at a spatial resolution approaching 0.22 nm. The bonding information that can be obtained from the fine structure within the parallel detection EELS edges can then be used in conjunction with the *Z*-contrast images to determine in detail the structure at the grain boundary.

Figure 5.16(a) shows a *Z*-contrast image from a 25° tilt boundary in a $SrTiO_3$ bicrystal. The brighter regions correspond to the increased scattering power of the heavier Sr columns in the $SrTiO_3$. The lighter Ti columns are barely visible in the image and so contribute to the uniform bright background seen between those of Sr. The *Z*-contrast image, therefore, allows us to establish the position of the Sr columns and to a lesser degree Ti columns at the grain boundary. However, the lighter O atoms are not visible in the *Z*-contrast image; therefore, it is not possible to determine the O structure at the grain boundary from the image alone. Sequences of Ti and O parallel detection EEL spectra were collected at 4-Å intervals across the grain boundary. The Ti spectra are shown in Fig. 5.16(b), where the first peak in the Ti L_{23} edge (which corresponds to a π^* transition) is significantly reduced at the grain boundary. This corresponds to a disruption of the linear Ti-O coordination at the grain boundary. The corresponding O spectra acquired across a grain boundary are shown in Fig. 5.16(c). Again, the chemical changes at the grain boundary can be seen by the increase in intensity of the σ^* peak relative to that of the π^* peak as the linear coordination is disrupted. In addition to the observation of individual transitions, the ratio of intensities in the L_2 and L_3 edges can be used to measure the valency of transition metals such as Ti.[3] The L_2:L_3 ratio for the Ti spectra shown in Fig. 5.16(b) confirms that within experimental limits, the valency of Ti remains constant at 4^+ across the grain boundary. Although disruption of the linear coordination of the Ti-O bonds at the grain boundary in $SrTiO_3$ is perhaps not surprising, the fact that this result can be directly observed on an atomic scale presents new and exciting possibilities for the study of grain boundaries.

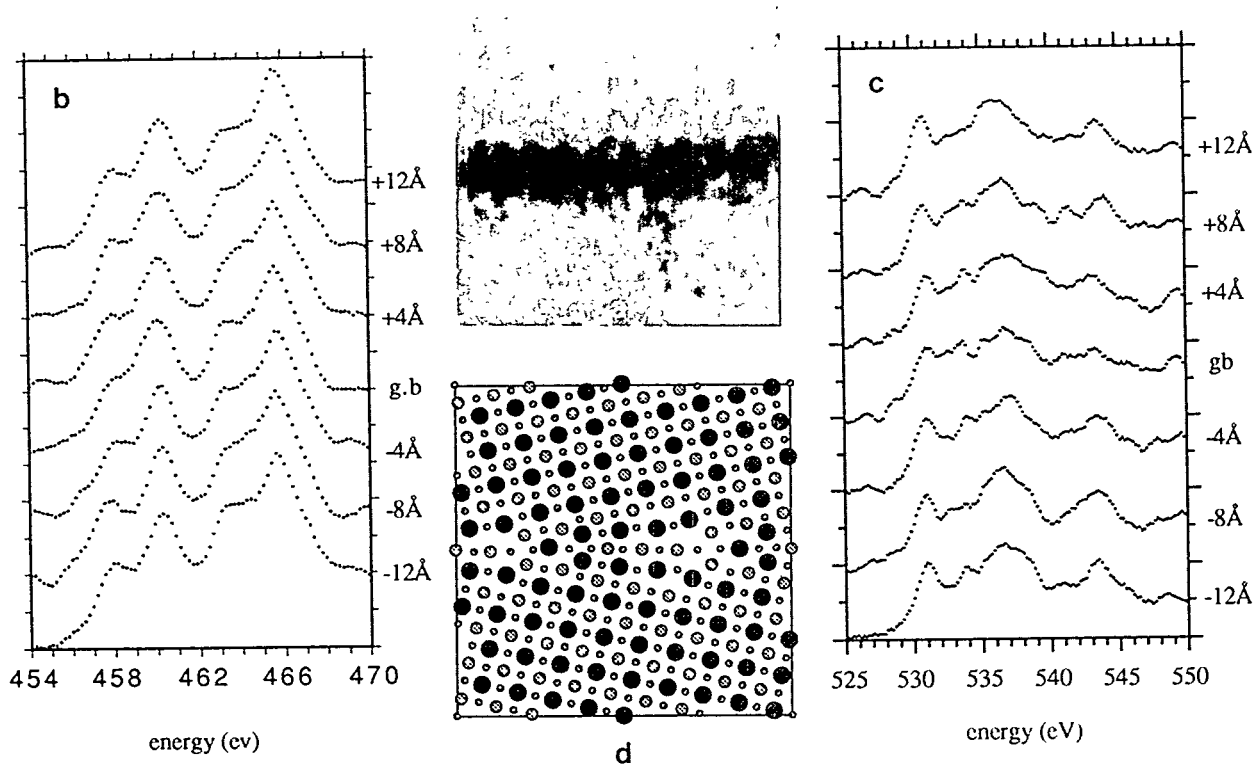

Fig. 5.16. (a) Z-contrast image of a $SrTiO_3$ grain boundary. (b) Ti L_{23}-edge intensity profile across the grain boundary. (c) O K-edge intensity profile across the grain boundary. (d) $SrTiO_3$ grain boundary reconstruction calculated from the Z-contrast image and parallel detection EELS. The large, dark circles represent Sr atoms, medium sized circles are Ti atoms, and the smallest circles represent the O atoms.

Using a combination of the structural information obtained from the Z-contrast image and the bonding information obtained from the parallel detection EELS, it is possible to determine the likely structure at the grain boundary, purely from experimental data. The boundary structure calculated for this 25° tilt boundary is shown in Fig. 5.16(d).

---

1. Summary of paper to be published.
2. ORNL/ORISE postdoctoral research associate.
3. M. De Crescenzi et al. *Phys. Rev. B* **39**, 5520 (1989).

ATOMIC STRUCTURE OF GRAIN BOUNDARIES IN $YBa_2Cu_3O_{7-\delta}$ AS OBSERVED BY Z-CONTRAST IMAGING[1]

M. F. Chisholm, S. J. Pennycook, D. P. Norton, and N. D. Browning[2]

Determination of the atomic structure of grain boundaries is the key to fundamental understanding of the critical-current density in polycrystalline superconductors. High-resolution images with incoherent characteristics, obtained using a high-angle annular detector on an atomic-resolution scanning transmission electron microscope, have been

used to study the structural units of these technologically important boundaries. These boundaries were formed in a laser-ablated $YBa_2Cu_3O_{7-\delta}$ film grown on polycrystalline yttrium-stabilized zirconia. The grains share a common [001] surface normal but are randomly rotated in the surface plane, producing both low- and high-angle ⟨001⟩ tilt boundaries. The low-angle boundaries consist of arrays of dislocations (b = 0.39 nm) to accommodate the misorientation of the adjacent grains. The low-angle boundaries are found to be parallel to the {100} plane of one grain and rotated by the entire misorientation angle from the {100} plane of the adjacent grain. The high-angle grain boundary in Fig. 5.17 is seen to consist of {100}-faceted sections of adjacent grains.

The atomic structures at grain boundaries in $YBa_2Cu_3O_{7-\delta}$ are strongly influenced by the tendency of this compound to exist only as complete unit cells terminated at {001} and {100} planes. The weak-link behavior associated with high-angle grain boundaries may follow from this structure in which there is no apparent connection between grains. Another, but less prevalent, boundary type is the symmetric grain boundary where the adjacent grains share a common boundary plane. In these boundaries, partial coupling of the grains is maintained. There is evidence that these two boundary forms produce junctions with very different superconducting properties.[3]

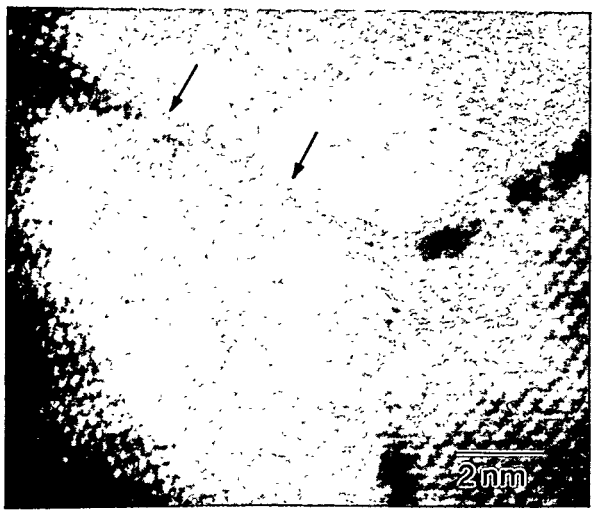

Fig. 5.17. Z-contrast image of a grain-boundary junction in which three asymmetric $YBa_2Cu_3O_{7-\delta}$ ⟨001⟩ tilt boundaries separate {100}-faceted sections of adjacent grains.

---

1. Summary of paper: *Interface Science* (in press).
2. ORNL/ORISE postdoctoral research associate.
3. N. D. Browning et al., *Physica C* **212**, 185 (1993).

INCOHERENT IMAGING OF THIN SPECIMENS USING COHERENTLY SCATTERED ELECTRONS[1]

D. E. Jesson and S. J. Pennycook

It is now over 30 years since the first images of single atoms and atom clusters were obtained in a scanning transmission electron microscope (STEM). Such images were formed from coherent elastically scattered electrons integrated over an annular detector with a relatively low inner angle (~30 mrad). Since that time, considerable controversy has raged as to the degree to which the images could be interpreted using incoherent imaging theory. It has been demonstrated clearly in the SSD that for the range of detector angles used in forming the early images, interpretation based on incoherent scattering theory

was justified, but with the important proviso that atoms need to be separated in a plane perpendicular to the optic axis. It has also been shown that interference effects between atoms possessing identical projected coordinates must be considered explicitly, which has led to a re-evaluation of the early images of atomic columns.

Figure 5.18 illustrates the important physics underlying the use of incoherent imaging theory to interpret images from two point scatterers separated by 1.5 Å in the transverse plane. Increasing the inner detector angle from 10.3 to 50 mrad samples more fringes in the detector plane intensity distribution, and the integrated signal approaches the incoherent scattering limit. A useful condition for the minimum detector angle required for incoherent imaging is

$$\theta_i^{inc} = \frac{1.22\,\lambda}{\Delta R},$$

where ΔR is the atomic separation and λ is the incident electron wavelength. This result should allow the extension of scanning transmission electron microscopy incoherent imaging methods to a number of scientifically and technologically important samples, including heavy atom stained biological materials and catalysts.

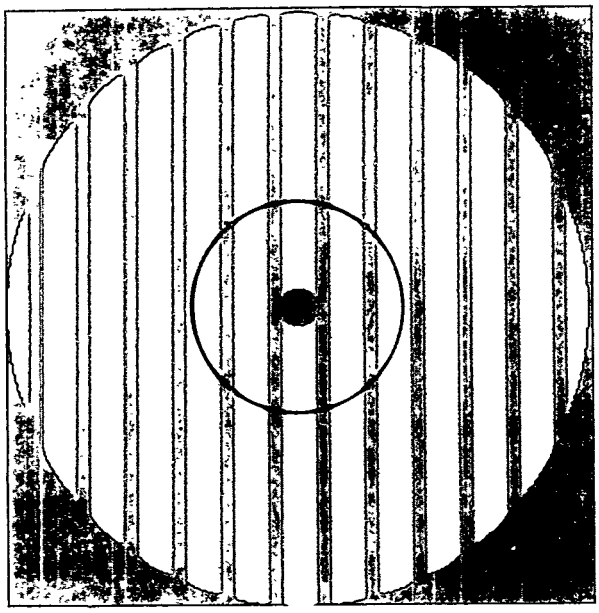

Fig. 5.18. Detector plane intensity distribution resulting from two point scatterers separated by 1.5 Å. The solid circle represents an increase of the 10.3-mrad inner detector angle to 50 mrad.

---

1. Summary of paper: *Proc. R. Soc. Lond. A* 441, 261 (1993).

INCOHERENT IMAGING OF CRYSTALS USING THERMALLY SCATTERED ELECTRONS[1]

D. E. Jesson and S. J. Pennycook

Z-contrast scanning transmission electron microscopy images are usually formed from thermally scattered electrons. From a simplified Einstein picture of atoms acting as independent oscillators, it can be expected that coherence effects, even along an atomic column, will be destroyed as long as Bragg reflections do not make a significant contribution to the high-angle signal. However, unlike a full phonon thermal diffuse scattering (TDS) description involving correlated displacements, the Einstein model assumes incoherent scattering from each atom in the vibrating column and, therefore, does not properly describe the interference effects present in large-angle TDS. Such residual interference is

particularly important for the quantification of column intensities, since the simple dependence on columnar cross sections could be appreciably complicated.

This problem has been studied in the SSD in the context of a phonon model based on the Warren approximation of x-ray diffraction.[2] This correctly takes into account atom correlations and shows that scattering from an individual atomic column can be visualized in terms of an assembly of independent packets of atoms [Fig. 5.19(a)]. Within a packet, the scattering is partially coherent, as shown by the correlation function in Fig. 5.19(b). Under typical conditions, this partial coherence leads to deviations from the predictions of the Einstein model of less than 20%. This result justifies the use of an independent oscillator model for many cases, but indicates that the partial coherence of the atomic vibrations should be considered when accurate quantitative calculations are required.

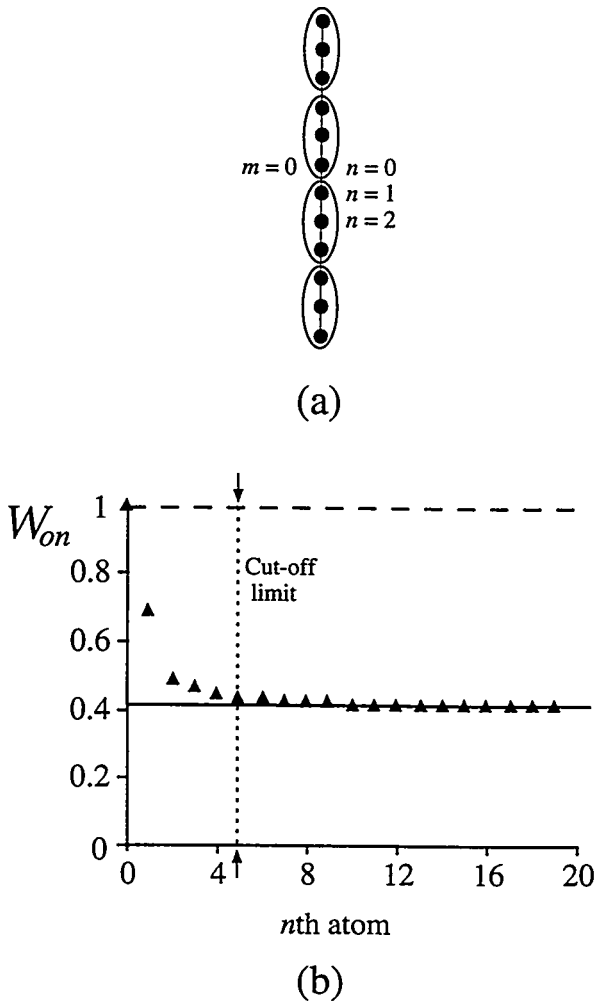

Fig. 5.19. (a) Representation of an atomic column scattering as individual packets. (b) Values of the correlation function W_{on} (triangles), which expresses the correlation between the zeroth atom ($m = 0, n = 0$) and the n-th atom along the column. The Einstein (solid line) and coherent (dashed line) limits of W_{on} are shown for an inner detector angle of 75 mrad and Debye Waller factor of 0.45. The arrowed vertical line defines the boundary of the packet.

---

1. Summary of paper to be published.
2. B. E. Warren, *X-Ray Diffraction*, Dover Publishing, New York, 1990.

DIRECT IMAGING OF SURFACE CUSP EVOLUTION DURING STRAINED-LAYER EPITAXY[1]

D. E. Jesson, S. J. Pennycook, J.-M. Baribeau,[2] and D. C. Houghton[2]

The morphological evolution of a thin overlayer film subjected to substrate-induced misfit strain remains a central issue in strained-layer epitaxy. Although it is understood that flat surfaces are unstable to the formation of surface waves, little is known about the detailed shape or time evolution of surface features. Utilizing the deposition of two-monolayer-thick Ge marker layers at selected intervals during the molecular beam epitaxial growth of a $Si_{0.5}Ge_{0.5}$ alloy [Fig. 5.20(a)], it has been demonstrated that

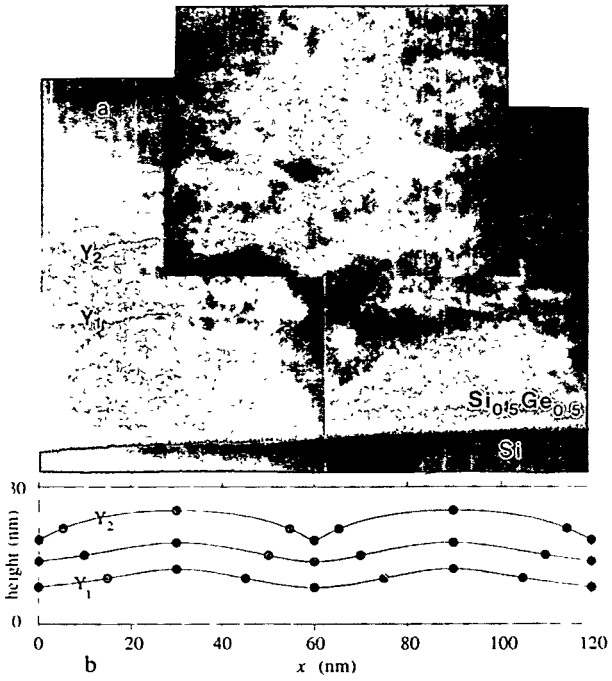

Fig. 5.20. (a) [110] Z-contrast image of a $Si_{0.5}Ge_{0.5}$ alloy grown by molecular beam epitaxy with 0.25-nm Ge marker layers deposited at selected intervals. The profile simulations in (b) correspond to the period of cusp formation in (a) between vertical ordinates Y_1 and Y_2.

the strained overlayer is unstable to the formation of a surface cusp-like morphology. The cusps arise naturally as a consequence of gradients in the surface chemical potential, and they can be predicted utilizing a model based on the surface evolution equation [Fig. 5.20(b)].

An important feature of cusp formation is the high stress concentration at the cusp tip. It has been demonstrated that the concentration is sufficient to inject dislocations into the strained layer, providing a very plausible solution to the 30-yr-old dislocation nucleation problem in these systems. It is believed that the discovery of surface cusps is as significant in thin-film growth as the discovery of the crack was for materials science and engineering. It is likely to be a general phenomenon in strained-layer epitaxy.

---

1. Summary of paper: *Phys. Rev. Lett.* **71**, 1744 (1993).
2. National Research Council of Canada, Ottawa, Canada.

INTERPLAY BETWEEN EVOLVING SURFACE MORPHOLOGY, ATOMIC-SCALE GROWTH MODES, AND ORDERING DURING Si_xGe_{1-x} EPITAXY[1]

D. E. Jesson, S. J. Pennycook, J. Z. Tischler, J. D. Budai, J.-M. Baribeau,[2] and D. C. Houghton[2]

One of the most intriguing issues in strained-layer epitaxy is the relationship between atomistic growth mechanisms and evolving surface morphology. Using specially designed growth experiments combined with Z-contrast imaging, it has been possible to map directly evolving surface morphology during MBE growth of SiGe alloys, revealing the true nonequilibrium shape of coherent islands. Cross-sectional and plan-view transmission electron microscopy (TEM) was then used to image atomic-scale ordered domains (Fig. 5.21), providing a direct correlation with the islands occurring during growth. This linkage has provided dramatic new insight into atomic-scale growth mechanisms. The locally vicinal surfaces associated with the coherent islands is believed to establish bilayer step-flow conditions, and a growth mechanism in which the ordering occurs during the flow of kinks along such bilayer steps has been proposed. The determination of the structure of the chemically ordered phase (RS3,

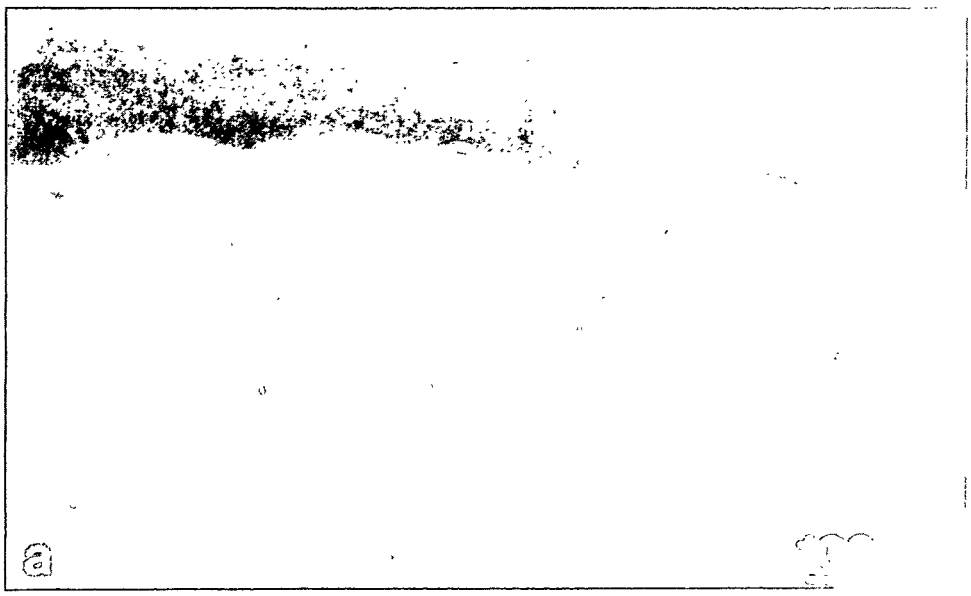

Fig. 5.21. [110] TEM cross-sectional dark-field image obtained from a 1/2(111) ordered superlattice reflection. The size of the ordered domains (bright patches) correlates well with the coherent island size of 60 nm.

space group R3m) by x-ray diffraction is precisely consistent with this model.

---

1. Summary of paper: *Phys. Rev. Lett.* **70**, 2293 (1993).
2. National Research Council of Canada, Ottawa, Canada.

MORPHOLOGICAL INSTABILITIES IN STRAINED FILMS[1]

K. M. Chen,[2] D. E. Jesson, S. J. Pennycook, T. C. Estes, T. Thundat,[3] and R. J. Warmack[3]

Strain-induced morphological instability has recently received considerable attention.[4,5] Morphological instability tends to roughen the film surface by mass diffusion during film growth or annealing. Initial perturbations or undulations can be expected to develop into cusp-like structures under certain growth conditions because of stress-induced surface chemical potential gradients. Using atomic force microscopy (AFM), the surface morphology of Ge_xSi_{1-x} films that were epitaxially grown on a Si(100) substrate has been measured. A three-dimensional cusp-like structure is clearly identified in coherently strained films whose thicknesses are larger than the critical thickness for dislocation introduction.

Epitaxial growth of Ge_xSi_{1-x} films was performed in a recently developed molecular beam epitaxy system, which consists of a growth chamber and a load-lock chamber. The base pressure of the growth chamber was below 3×10^{-10} Torr. The Si(100) wafers were loaded after chemical etching in a 10% HF solution for 15 min. The resultant H-terminated Si surface showed a streaky (1 × 1) reflection high-energy electron diffraction (RHEED) pattern. The hydrogen was desorbed from the surface upon

heating the substrates to 700°C and left behind a weak reconstructed (2 × 1) surface. A Si buffer layer was then grown at 550°C before cooling to the alloy growth temperature of 400°C. A sharp, strong (2 × 1) RHEED pattern obtained after the buffer layer growth indicated a smooth and clean surface. The Ge_xSi_{1-x} alloy layer growth was commenced by codeposition of Si and Ge fluxes onto the substrate surface. The sample was immediately cooled down to room temperature after growth (to quench the surface structure) and removed from the chamber for AFM in air.

The AFM measurements, shown in Fig. 5.22(a), revealed a cusp-like structure on a 45-nm-thick $Ge_{0.43}Si_{0.57}$ alloy surface, where the structure appears as a rectangular hole with edges parallel to ⟨110⟩ directions. A line-trace profile, shown in Fig. 5.22(b), revealed that the lateral size of the structure is about $100 \times 100\,nm^2$, with a depth between 5 and 20 nm. The concentration of such cusp-like holes was observed to be $\sim 10^7\ cm^{-2}$, and the fact that no holes were observed on homoepitaxial films [e.g., Si on Si(100) and Ge on Ge(100)] indicates that this cusp-like structure is directly related to the strain effect.

The formation of cusp-like holes seems surprising but may be understandable in terms of the biaxial film stress. Further investigations are needed to clarify the question of whether the cusp-like structure is a nucleation site of misfit dislocation because of high-stress concentration at the tip or actually is a natural resultant of dislocation development under high stress.

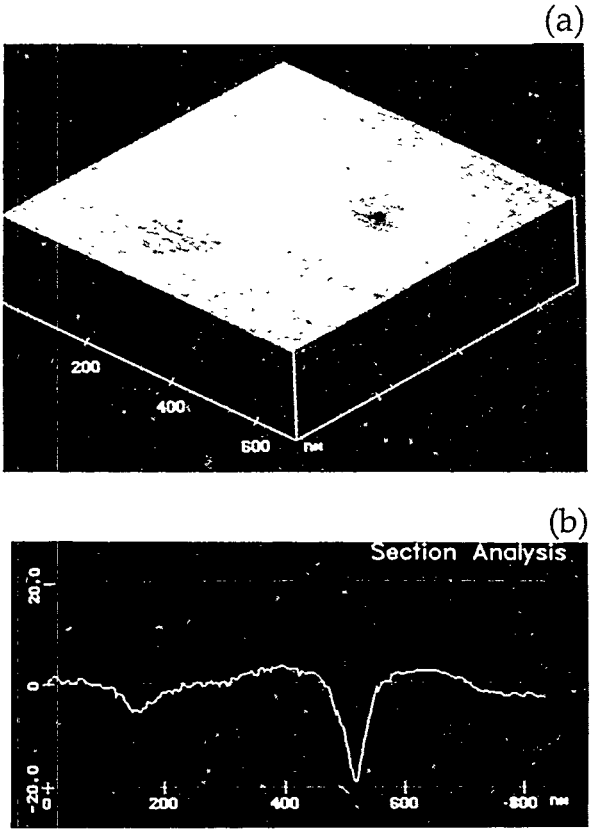

Fig. 5.22. (a) AFM image of the surface morphology of a $Ge_{0.43}Si_{0.57}$ alloy grown on Si(100) substrate. (b) Line-trace profile.

---

1. Summary of paper to be published.
2. ORNL/ORISE postdoctoral research associate.
3. Health Sciences Research Division, ORNL.
4. D. E. Jesson et al., *Phys. Rev. Lett.* **71**, 1744 (1993).
5. J. Berréhar et al., *Phys. Rev. B* **46**, 13487 (1992).

X-RAY DIFFRACTION

STRUCTURE AND ORIENTATION OF Si, Ge, AND SiGe NANOCRYSTALS FORMED BY ION IMPLANTATION

J. D. Budai, C. W. White, S. P. Withrow, S. J. Pennycook, D. C. Paine,[1] and D. M. Hembree[2]

Recent observations of the emission of visible light from nanometer-sized indirect band-gap semiconductors such as Si and Ge have generated considerable interest in both fundamental and applied research on the structure and properties of nanocrystals. In our collaborative work, nanocrystalline precipitates of Si, Ge, and SiGe have been formed in the near-surface region of (0001) α-Al_2O_3 (sapphire) and SiO_2 (amorphous silica) substrates by a process of ion implantation and annealing.[3] Ions have been implanted at doses up to $6 \times 10^{17}/cm^2$ into substrates held at temperatures up to 650°C, and subsequent annealing was carried out at temperatures up to 1100°C.

X-ray diffraction measurements, using both conventional and synchrotron sources, show: (1) the precipitates have a diamond cubic structure, (2) the nanocrystals are three dimensionally oriented within the Al_2O_3 matrix and randomly oriented in SiO_2, (3) the particle dimensions are in the nanometer range, and (4) the size and strain in the nanocrystals can be controlled by varying dose and thermal treatment. The observed dimensions are such that quantum confinement can be expected to affect the optical properties and that visible photoluminescence from these samples has, in fact, been observed in preliminary measurements.

The orientation of the nanocrystals with respect to the Al_2O_3 lattice has been found to depend strongly on the implanted species. In all cases, θ–2θ scans reveal the presence of nanocrystals oriented such that the (111) or (110) planes are aligned with the substrate (0001) planes. Si and SiGe nanocrystals are primarily (111)-aligned, while Ge nanocrystals have a greater tendency toward (110) alignment. The in-plane orientational dependence on composition is also striking. Fig. 5.23 shows ϕ scans for (111)-aligned nanocrystals, illustrating that the Si and SiGe (111)-aligned precipitates possess sixfold symmetry (two orientations), while the

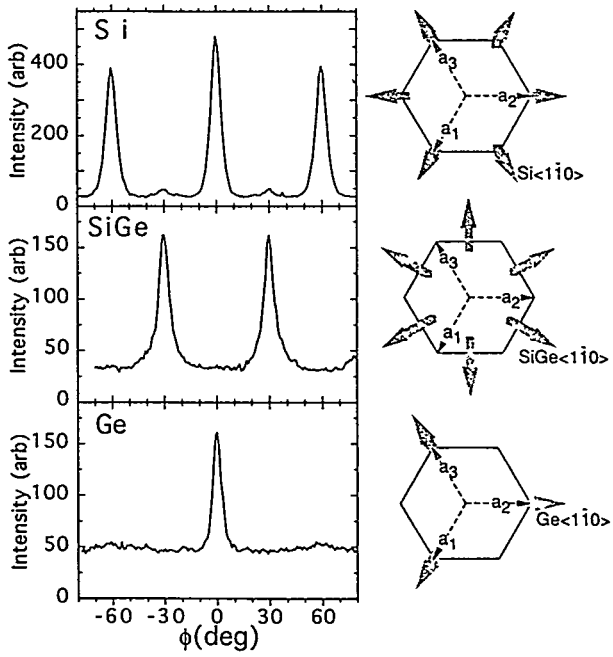

Fig. 5.23. In-plane orientations for Si, SiGe, and Ge (111)-aligned nanocrystals in (0001) Al_2O_3. The left side shows x-ray ϕ scans through the nanocrystalline {220} reflections. In the schematic on the right, the dashed lines represent the in-plane Al_2O_3 hexagonal unit cell and the thick arrows depict in-plane $\langle 1\,\bar{1}0 \rangle$ directions.

Ge (111)-aligned nanocrystals possess threefold symmetry (a single orientation). Surprisingly, the orientation observed for SiGe nanocrystals is not intermediate between those seen for Si or Ge nanocrystals, but instead is rotated by 30°. The origin of this strong orientational dependence on composition is currently being investigated.

---

1. Brown University, Providence, R.I.
2. Y-12 Plant, Oak Ridge, Tenn.
3. C. W. White et al., "Formation of Oriented Nanocrystals of Si and Ge in Al_2O_3 by Ion Implantation," this report.

STRUCTURE OF ORDERED SiGe EPITAXIAL LAYERS[1]

J. Z. Tischler, J. D. Budai, P. Zschack,[2] D. E. Jesson, J.-M. Baribeau,[3] and D. C. Houghton[3]

$Si_{0.5}Ge_{0.5}$ alloy films grown on (001)-oriented Si substrates show compositional ordering of the SiGe epitaxial layer when grown by either metal-organic chemical vapor deposition or molecular beam epitaxy near 400°C. This ordering is believed to occur because of the kinetics of growth on the (001) surface, as it is not seen in growth on other crystallographic faces nor in bulk grown alloys. This ordering is of interest because of the current use of SiGe alloys for fabrication of strained-layer superlattices, as well as the insight that the ordering provides into the surface kinetics of film growth.

Previous studies using electron diffraction have observed half-integral superlattice reflections, which have led to the proposal of a number of epitaxial growth models where the conventional cubic unit cell is doubled by chemical ordering.

The X-14 synchrotron beam line at the National Synchrotron Light Source has been used to make absolute measurements of the integrated intensity from superlattice reflections to determine the ordered structure. In both relaxed and coherently strained alloy films, it was found that the RS3 structure (described in Ref. 4) accurately describes the ordered phase as shown in Fig. 5.24. The RS3 structure has chemical ordering on one of the four {111}-type planes, and it is the only proposed structure with a nonzero value for the (002) reflection. The (002) reflection not only singles out the RS3 structure, but also its relative strength provides information on the growth kinetics in the bilayer step-flow model.[4]

In addition to the observed half-order reflections, the first observations of integral ($hk\ell$)

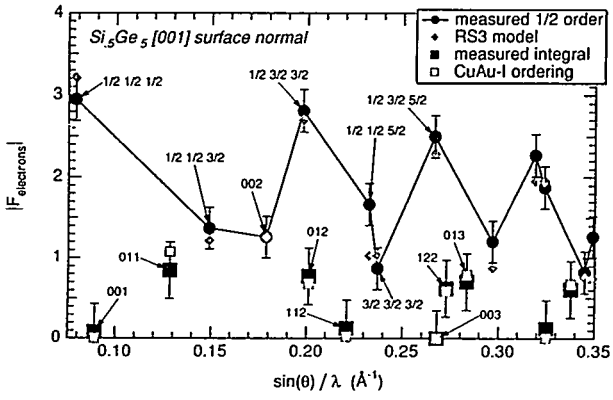

Fig. 5.24. Measured and computed structure factors for an ordered SiGe film. The solid circles and squares denote measurements, and the gray diamonds and squares denote calculations for the RS3 and CuAu-I structures. Note that both models are needed to account for all the measurements.

superlattice reflections, which indicate the presence of a second phase with CuAu-I type ordering in a direction perpendicular to the surface normal, were made. From the absolute intensities, the order parameter for the RS3 structure is 14%, and for the CuAu-I ordering it is a factor of 2.5 smaller. The observation of the CuAu-I phase is the first evidence for a second type of ordering in this system, and its structure and mode of growth are currently being investigated.

---

1. Summary of paper to be published.
2. Oak Ridge Associated Universities, Oak Ridge, Tennessee.
3. National Research Council of Canada, Ottawa, Canada.
4. D. E. Jesson et al., *Phys. Rev. Lett.* 71, 1744 (1993).

PREFERENTIAL DOMAIN GROWTH OF ORDERED SiGe FILMS[1]

J. Z. Tischler, J. D. Budai, P. Zschack,[2]
D. E. Jesson, J.-M. Baribeau,[3] *and D. C. Houghton*[3]

$Si_{0.5}Ge_{0.5}$ alloy films grown on (001)-oriented Si substrates show compositional ordering on {111} planes. However, because of the symmetry of the surface, the ordering occurs equally in the four available ⟨111⟩ directions, which gives four distinct ordered domains. Because optimal use of the properties of an ordered film for device applications would require growth of only one domain, the use of substrate miscuts have been investigated to influence domain growth. By growing the ordered alloy film on substrates miscut 4° from the [001] direction toward the [010] and [110] directions, the enhanced growth of a single domain at the expense of the other three has been demonstrated.

X-ray diffraction integrated intensity measurements of the (*h*/2, *k*/2, *ℓ*/2)-type superlattice reflections, made on the X-14 synchrotron beam line at the National Synchrotron Light Source at Brookhaven National Laboratory, were used to determine the population of each of the four orientational domain types. The results of these measurements are shown in Fig. 5.25, where the length of the arrows corresponds to the relative volume of each domain type, and the direction of the arrow is the normal to the ordered {111}-type plane for that domain. These results show a strong sensitivity of the domain formation to the direction of the miscut. Even a small twist of the miscut from the [110] direction in Fig. 5.28(b) favors the growth of *D*- over *A*-type domains. This behavior is understood in terms of the

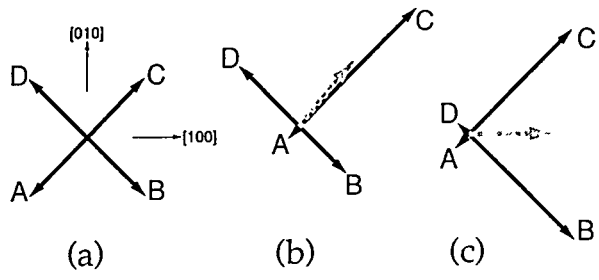

Fig. 5.25. Projection onto the (001) plane of the relative ordered domain populations for growth on samples with three different miscuts: (a) symmetrically cut sample, surface normal is [001], (b) sample is miscut 4° toward the [110] (with a 5° twist), and (c) sample miscut 4° toward the [100]. The dashed line is the projection of the surface normal showing the direction of miscut. The letters *A*–*D* are used to label the four domain orientations.

bilayer step flow model for growth discussed elsewhere in this report.[4,5] This work is continuing with variations in the miscut (direction and magnitude) and the film-growth procedure to investigate the degree to which single-ordered domains may be grown and to investigate the mechanisms responsible for the ordering.

---

1. Summary of paper to be published.
2. Oak Ridge Institute for Science and Education, Oak Ridge, Tenn.
3. National Research Council of Canada, Ottawa, Canada.
4. J. Z. Tischler et al., "Structure of Ordered SiGe Epitaxial Layers," this report.
5. D. E. Jesson et al., "Direct Imaging of Surface Cusp Evolution During Strained-Layer Epitaxy," this report.

ENERGY TIME CORRELATIONS IN RESONANT NUCLEAR BRAGG SCATTERING[1]

J. Z. Tischler, B. C. Larson, and E. E. Alp[2]

The spectral energy widths of resonant x-ray beams from nuclear Bragg reflections are much greater than those from radioactive Mössbauer sources as a result of the collective excitation of the resonant nuclei. In this study, the time-structure of synchrotron radiation has been used to make time-sliced Doppler absorption measurements on the resonant beam from a mosaic $^{57}Fe_2O_3$ resonant monochromator. These time-resolved measurements have demonstrated the increased width of the time-integrated energy spectrum and the quantum mechanical narrowing of the spectral width as a function of time. In addition, comparison of the computed Doppler absorption widths of nuclear Bragg resonant beams for thick and thin absorbers has been made in order to assess their performance for elastic/inelastic and quasi-elastic x-ray scattering spectroscopy measurements.

The time-resolved Doppler absorption measurements were carried out at the Cornell High Energy Synchrotron Source (CHESS) using a resonant beam from the (777) reflection of a mosaic $^{57}Fe_2O_3$ crystal and a 9.6-mg/cm^2 $^{57}Fe_2O_3$ absorber. As shown in Fig. 5.26(a, b, and c), measurements were made for the time interval [40–294 ns] and for time slices at the beginning and end of this interval. The energy width of the long interval is ~35 neV, while the widths for the [40–70-ns] and [100–294-ns] time intervals are ~60 and 20 neV. Both the shape and the widths of the absorption spectra are in agreement with numerical, dynamical diffraction calculations, including details such as the shoulders on the side of the absorption dip in Fig. 5.26(c).

The 9.6-mg/cm^2 $^{57}Fe_2O_3$ absorber used in these measurements is much thicker than the ~0.5-mg/cm^2 absorbers that are normally used in radioactive source Mössbauer measurements. However, the wider energy widths associated with collective excitation of a resonant nuclear reflection encourages the use of a thicker absorber. This is demonstrated in Fig. 5.26(a), which shows calculated absorption spectra for a 0.5-mg/cm^2 $^{57}Fe_2O_3$ absorber (with the magnitude of the dip normalized to that of the thick absorber). Although decreasing the absorber thickness has a small effect upon the width, the thin absorber produced only a 3% dip before

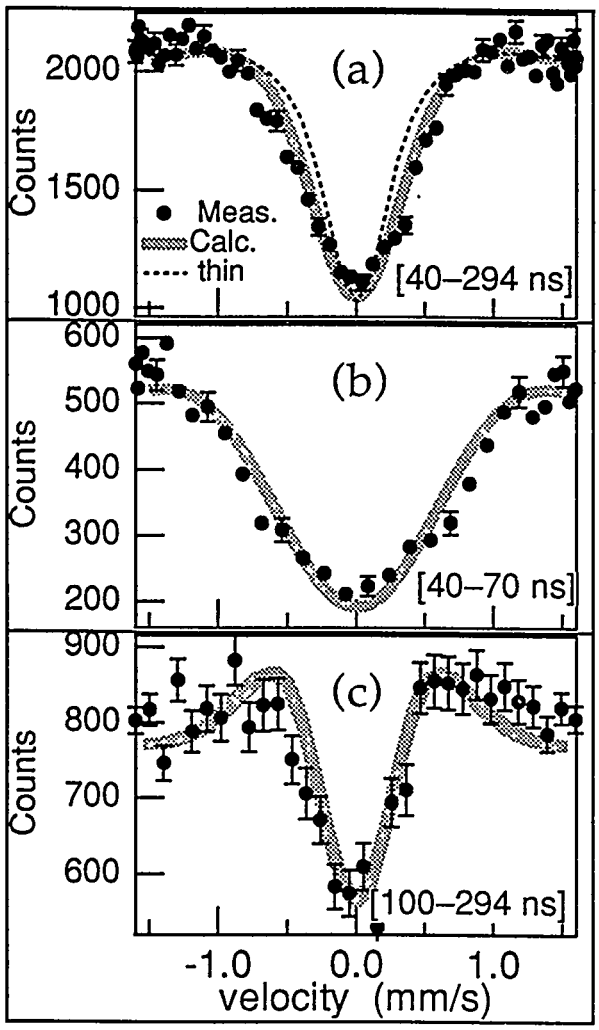

Fig. 5.26. (a) Measured Doppler absorption spectrum with calculated absorption spectra for three different time intervals. (a) [40–294 ns] with calculated curves for 9.6-mg/cm^2 and 0.5-mg/cm^2 thick absorbers. (b) [40–70 ns] with calculated curve for 9.6-mg/cm^2. (c) [100–294 ns] with calculated curve for 9.6-mg/cm^2.

normalization to the ~50% dip of the thick absorber.

---

1. Summary of paper to be published.
2. Argonne National Laboratory, Argonne, Ill.

ORIENTED HIGH-T_c SUPERCONDUCTING FILMS ON ARBITRARY SUBSTRATES

J. D. Budai, D. P. Norton, D. K. Christen, B. C. Chakoumakos, R. Feenstra, and E. C. Jones[1]

The electrical transport properties of high-T_c superconductors such as $YBa_2Cu_3O_{7-x}$ (YBCO) are critically dependent on crystal microstructures. In particular, thin-film superconductors consisting of misoriented grains typically exhibit values for the critical current density, J_c, which are orders of magnitude less than for epitaxial films. In previous studies,[2] it was established that in-plane epitaxy can be achieved for YBCO films grown by laser ablation on Ag and Pt single-crystal surfaces. This work has been extended, and a technique for producing epitaxial high-T_c superconductors on arbitrary substrates has been developed.

The technique consists of growing epitaxial Ag films on cleaved or polished NaCl substrates and then dissolving the NaCl substrates so that the oriented metal foil can be mounted on an arbitrary substrate (e.g., a polycrystalline metal foil). Essentially, single-crystal Ag films between 2-μm and 20-μm thick in both the (100) and (110) epitaxial orientations have been produced at growth temperatures of ~300°C. After depositing epitaxial YBCO films on these metal substrates, four-circle x-ray diffraction measurements have revealed three-dimensional epitaxial, c⊥ YBCO films with bulk-like orthorhombic lattice parameters and mosaic spreads of ≤4°. Four-probe resistance data have shown $T_c(R = 0)$ as high as 85–89 K for these films, and critical-current density measurements are now

in progress. These samples should provide quantitative upper limits for transport properties of long-length, superconducting wires on highly textured metal substrates.

---

1. Graduate student from The University of Tennessee, Knoxville, Tenn.
2. J. D. Budai et al., *Appl. Phys. Lett.* **62**, 1836 (1993).

STRUCTURE OF INFINITE-LAYER $Sr_{1-x}Ca_xCuO_2$ THIN FILMS

J. D. Budai, D. P. Norton, R. Feenstra, B. C. Chakoumakos, E. C. Jones,[1] *D. K. Christen, and T. Kawai*[2]

The relatively simple structure of the so-called "infinite layer" superconducting compounds [e.g., $(Sr_{1-x}Ca_x)CuO_2$] suggests that these compounds provide ideal model systems for fundamental investigations of doping mechanisms in copper oxide superconductors. X-ray diffraction was used to characterize the structure and the defect content of $(Sr_{1-x}Ca_x)CuO_2$ films that were grown by single-target laser ablation (at ORNL) and by multiple-target ablation (at Osaka University, Japan), and these results have been correlated with transport measurements.

$Sr_{1-x}Ca_xCuO_2$ films were grown on $SrTiO_3$ substrates over the composition range $0.0 \le x \le 0.85$; and four-circle x-ray diffraction measurements, made using synchrotron and conventional x-ray sources, showed these tetragonal films to be high-quality single crystals. The log-scale x-ray intensity scans in Fig. 5.27 illustrate large coherence lengths and

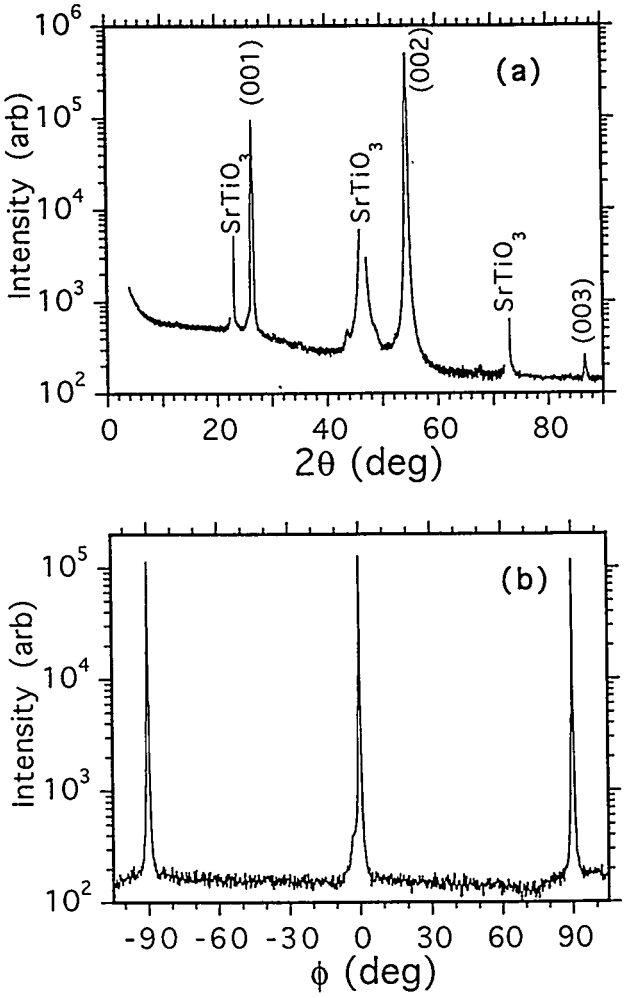

Fig. 5.27. X-ray diffraction intensities for an epitaxial $Sr_{0.7}Ca_{0.3}CuO_2$ thin film grown by single-target laser ablation showing (a) a θ-2θ scan near the surface normal and (b) a φ scan for the (202) peak.

excellent in-plane epitaxy as well as the absence of secondary phases. Mosaic spreads were found to be ≤0.2°. Because resistance measurements performed on these highly perfect films showed semiconducting behavior and no evidence for superconductivity, it does not appear that structural perfection will lead to superconductivity, and the emphasis has now shifted

toward the introduction of structural defects for providing carriers to the CuO_2 planes.

Comparisons of measured (001) and (002) x-ray integrated intensities with calculated values have shown that $Sr_{1-x}CuO_{2-\delta}$ films can be grown with a substantial density of stable Sr vacancies, using either single- or multiple-target sources. Distinct planar defects have been intentionally incorporated into thin films as well, and characterization of these samples after a series of reversible oxygen anneals showed that hole doping can be achieved by the insertion of defect layers, even though $Sr_{1-x}CuO_{2-\delta}$ films have a natural tendency toward electron doping.

---

1. Graduate student from The University of Tennessee, Knoxville, Tenn.
2. Osaka University, Osaka, Japan.

IN-PLANE EPITAXIAL ALIGNMENT OF $YBa_2Cu_3O_{7-x}$ FILMS GROWN ON SILVER CRYSTALS AND BUFFER LAYERS[1]

J. D. Budai, R. T. Young,[2] D. P. Norton, D. K. Christen, R. Feenstra, and B. S. Chao[2]

In contrast to the tremendous amount of research involving the growth of epitaxial high-T_c films on oxide crystals such as $SrTiO_3$ and $LaAlO_3$, very little is known about oriented film growth on metal substrates. Interactions between superconducting films and metal substrates are particularly important in determining physical properties of metal-sheathed superconducting wires where high critical currents and mechanical flexibility are required. In this study, it has been established that specific epitaxial relationships exist between high-T_c superconducting films and metal substrates; and further, it has been demonstrated that near-coincidence site lattice (NCSL) models can provide a basis for understanding the nature of the epitaxy and the atomic structure of the metal-oxide interface.

$YBa_2Cu_3O_{7-x}$ (YBCO) films were grown by in situ pulsed-laser ablation on Ag(001), Ag(110), and Ag(111) bulk single-crystal surfaces. Four-circle x-ray diffraction measurements made on ~200-nm-thick YBCO films showed that in all cases, the films were aligned with specific in-plane epitaxial relationships with respect to the crystallographic axes of the substrate. This technique for achieving three-dimensional film alignment was extended to include a Ag(111) epitaxial buffer layer on mica and a Pt(001) buffer layer on $KTaO_3$ in place of bulk single crystals. YBCO-metal interfacial structures as a function of rotation angle, ϕ, were geometrically modeled using a NCSL analysis. As summarized in Table 5.1, observed orientations were found to correspond to boundaries possessing high atomic coincidences (i.e., low σ) and small lattice mismatches (small ε). These epitaxial growth properties are presently being applied to the development of processing techniques that eliminate weak-link grain boundary effects and, hence, greatly enhance critical-current densities.

---

1. Summary of paper: *Appl. Phys. Lett.* **62**, 1836 (1993).
2. Energy Conversion Devices, Inc., Troy, Mich.

Table 5.1. Summary of NCSL orientations for c⊥ YBCO on metal surfaces. O: Observed, NO: Not Observed.

Ag(001)	ϕ	$\Delta\phi$	σ_{Ag}	σ_Y	ε_1(%)	ε_2(%)
O	0°		2	1	-6.0	
NO	18.4°		9	5	-0.8	
NO	26.6 °		8	5	+5.1	
O	45°		16	9	-0.1	
Ag(110)						
O	0°	0°	4	3	-0.1	-6.0
NO	18.4°	0°	12	10	-0.8	+5.1
O	26.6°	0°	6	5	+5.1	-0.8
O	45°	0°	4	3	-0.1	-6.0
Ag(111)						
O	0°	0°	24	12	-0.1	+2.5
NO	4.3°	1.7°	15	7	-1.4	-0.8
O	15°±4°	0°	4	2	-6.0	+8.3
Pt(001)						
O	0°		2	1	-1.3	

EPITAXIAL LEAD ZIRCONATE-TITANATE THIN FILMS ON SAPPHIRE[1]

W. Braun,[2] B. S. Kwak,[2] A. Erbil,[2] J. D. Budai, and B. J. Wilkens[3]

$Pb(Zr_{1-x}Ti_x)O_3$ (PZT) thin films covering the compositional range $x = 0$ to $x = 1$ have been grown on a sapphire $(1\bar{1}02)$ plane for the first time using metalorganic chemical vapor deposition. Four-circle x-ray diffraction measurements have shown that the films are three dimensionally epitaxial with PZT(110) ∥ $Al_2O_3(1\bar{1}02)$ and PZT[001] ∥ $Al_2O_3[11\bar{2}0]$. The structural transitions examined by x-ray diffraction were found to be shifted slightly from the bulk single-crystal values. Ferroelectric hysteresis curves and the dielectric constant of the films were investigated using interdigitated electrodes fabricated by photolithography.

---

1. Summary of paper: *Appl. Phys. Lett.* **63**, 467 (1993).
2. Georgia Institute of Technology, Atlanta, Ga.
3. Bell Communications Research, Red Bank, N.J.

REFINEMENT OF OXIDE CRYSTAL STRUCTURES BY RIETVELD ANALYSIS OF NEUTRON POWDER DIFFRACTION DATA[1]

B. C. Chakoumakos, J. A. Fernandez-Baca, M. M. Abraham, and L. A. Boatner

It has been confirmed by Pabst,[2] who made an early refinement of the M = Ca structure by film methods, that the compounds $MCuSi_4O_{10}$ (M = Ca, Sr, Ba) are isostructural with gillespite ($BaFeSi_4O_{10}$). These compounds are an intense blue color, and the Ca analog ("Egyptian blue") has been used as a pigment since ancient times. The $MCuSi_4O_{10}$ structure is tetragonal, with space group symmetry $P4/ncc$. For M = Ca, a = 7.3017 (3) Å, c = 15.1303 (6) Å, R_{wp} = 0.0515, for 487 reflections. For M = Sr, a = 7.3707 (2) Å, c = 15.5904 (6) Å, R_{wp} = 0.0489, for 521 reflections. For M = Ba, a = 7.4409 (3) Å, c = 16.1367 (8) Å, R_{wp} = 0.0522, for 546 reflections. The structure contains an unusual, unbranched single-silicate layer, which can be viewed as a tessellation of corner-linked Si_4O_{10} rings. The Cu is in square-planar coordination with the nonbridging

oxygens of the corrugations of the silicate layer. The alkaline-earth atom, in distorted cubic coordination, joins together adjacent $[CuSi_4O_{10}]^{2-}$ slabs. Increasing the size of the alkaline-earth atom increases the cell dimensions anisotropically (i.e., $\Delta c > \Delta a$) because of the inflexibility of the silicate anion. The lattice mismatch between the $[CuSi_4O_{10}]^{2-}$ slabs of the gillespite-structure type and the square-planar CuO_2 layers of the cuprate superconductors is small, which suggests possible applications of these materials as exotic thin-film substrates for the high-T_c cuprates or other novel structures having cuprate and silicate layers.

Improved precision of the structural parameters of the zircon-type MVO_4 vanadates (including also YVO_4 and $ScVO_4$ and new results for $PrVO_4$, $TmVO_4$, and the $LuVO_4$ end members) has been achieved. These compounds are of interest for their luminescence and magnetic properties. High-quality powders were prepared by homogeneous coprecipitation in molten urea. The zircon structure has space group symmetry *I4₁/amd*. In all, 22 parameters were refined with final agreement values of R_{wp} = 0.0361–0.0511 and *G-of-F* = 1.210–1.962. The average V-O bond length for all of the MVO_4 samples is 1.7088 Å, and the V-O distance exhibits a small systematic shortening with decreasing *M*-atom size. The oxygen positional parameters, cell dimensions, and *M*-O distances vary systematically with the metal-ion atomic number. The oxygen displacement about its mean position is highly anisotropic, with the largest amplitude normal to the shared polyhedral edge between the VO_4 tetrahedron and MO_8 bisdisphenoid. Empirical relations are given for the cell dimensions and oxygen-atom position as a function of the size of the lanthanide ion which can be used to estimate structural parameters for other zircon-type lanthanide-vanadate end members and vanadate solid solutions.

---

1. Summary of papers: *J. Solid State Chem.* **103**, 105 (1993); *Journal of Solid State Chemistry* (in press).
2. A. Pabst, *Am. Mineral.* **28**, 372 (1943).

ANOMALOUS DISPERSION AND THERMAL EXPANSION IN LIGHTLY DOPED $KTa_{1-z}Nb_zO_3$[1]

P. M. Gehring,[2] H. Chou,[2] S. M. Shapiro,[2] J. A. Hriljac,[2] D. H. Chen,[2] J. Toulouse,[3] D. Rytz,[4] and L. A. Boatner

It is widely accepted that concentrated $KTa_{1-z}Nb_zO_3$ (KTN) undergoes the same sequence of three structural phase transitions as the pure-niobate compound—but at progressively lower temperatures as the concentration of Nb is reduced. There is, however, considerable debate about what happens at very low impurity levels. For $x \leq 0.060$, the dielectric constant shows only a single peak as a function of temperature, implying a single-phase transition.[5] The issue, then, is whether this peak still signals the occurrence of a static structural phase transition with long-range ferroelectric order or a freezing of dipolar impurities in analogy to a spin-glass phase and, thus, no change in symmetry.

In an effort to shed new light on this subject, high-resolution x-ray diffraction experiments have been performed to look for changes in symmetry between 300 and 10 K in a series of single-crystal specimens of KTN in the limit $x \leq 0.060$.

The temperature dependences of the lattice constant and TA phonon dispersion in dilute single crystals of KTN with $0.012 \leq x \leq 0.09$ have been studied using x-ray diffraction and neutron scattering techniques, respectively. For $x \leq 0.06$, an anomalous low-temperature expansion of the cubic lattice parameter is observed at a temperature T_{min} that increases monotonically with Nb concentration, with no measurable change in symmetry down to 10 K (i.e., there is no deviation from cubic symmetry at any temperature for $0.012 \leq x \leq 0.06$ within experimental uncertainty). Upper bounds are established for the size of any structural distortion which might be present, but too small to be detected, given the finite resolution of the x-ray spectrometer. Inelastic neutron scattering measurements reveal that the coupling between TA and TO modes, first observed in pure $KTaO_3$, is both wave vector and concentration dependent. In addition, a characteristic temperature T_o is observed above and below which both TA and TO branches harden and which coincide with T_{min}.

The observed behavior, along with the lack of evidence of any structural phase transition seen by the x-ray diffraction experiments argues in favor of a dipolar-glass description for the low-temperature polar phase and against the presence of a long-range-ordered ferroelectric phase in dilute KTN. Instead, it is likely that small, ordered clusters of dipoles form below the freezing temperature (T_{min}) in dilute KTN, thereby producing a strain in the crystal. Such a scenario would also explain the observation of diffuse x-ray scattering observed in a single crystal of KTN.

---

1. Summary of paper: *Ferroelectrics* (in press).
2. Brookhaven National Laboratory, Upton, N.Y.
3. Lehigh University, Bethlehem, Pa.
4. Centre de Recherche en Opto-electronique, Huningue, France.
5. U. T. Höchli, H. E. Weibel, and L. A. Boatner, *Phys. Rev. Lett.* **39**, 1158 (1977).

X-RAY ABSORPTION SPECTROSCOPY OF THE RARE-EARTH ORTHOPHOSPHATES[1]

D. K. Shuh,[2] L. J. Terminello,[3] L. A. Boatner, and M. M. Abraham

The electronic structures of the rare-earth (*RE*) ions in the orthophosphates (La, Ce, Nd...)PO_4 are of particular interest because these materials are geological standards[4] and actinide material substitutes/prototypes. *RE* orthophosphates are also analogs of the corresponding actinide orthophosphates, which have been considered as materials for primary nuclear waste containment and disposal.[5] *RE* orthophosphates are suitable materials for the characterization of transitions originating from trivalent cores, and they provide useful information for studies of mixed-valence systems. The *RE* ions are also ideal from a spectroscopic perspective, because the $M_{4,5}$ cross sections are large. In addition,

several of the lightly doped *RE* orthophosphates have recently been shown to be of interest as new scintillator materials.[6]

X-ray absorption spectroscopy (XAS) of the *RE* $M_{4,5}$ edges ($3d$ levels) exhibits sharp peaks near the edges as a result of strong quasi-atomic $3d^{10}4f^n \rightarrow 3d^9 4f^{n+1}$ transitions, which contain a wealth of spectroscopic features. These exitonic transitions appear a few electron volts below the true edges as a consequence of the strong core-hole/$4f$ Coulomb interaction that lowers the $4f^{n+1}$ final state by ~10 eV with respect to the Fermi level (E_F). The $M_{4,5}$ spectra consist of two well-separated lines since the spin-orbit (Δ_{SO}) interaction of the $3d^9$ hole is larger than the $3d^9 4f^{n+1}$ exchange interaction. Although the purpose of XAS experiments is to obtain information on the *RE* ground state, the technique also probes the excited electronic final states. The total $3d^9 4f^{n+1}$ multiplets of the *RE*'s are quite complex and, even with dipole selection rules limiting the allowed transitions from the ground state, give rise to a large number of possible final states. XAS measurements of single-crystal $REPO_4$ *RE* = La, Ce, Pr, Nd, Sm, Eu Gd, Tb, Dy, Er) at the $3d$ edge were performed in a total-yield mode at beam line 8-2 at the Stanford Synchrotron Radiation Laboratory.

Figure 5.28 shows the XAS spectra of the $M_{4,5}$ edges of the *RE* orthophosphates, $LaPO_4$, $CePO_4$, $PrPO_4$, $NdPO_4$, and $SmPO_4$. The Ce $3d$ spectrum of $CePO_4$ shown in Fig. 5.28 was collected with second-order light and is representative of the total-electron-yield spectra of $REPO_4$'s. The spin-orbit-split Ce $3d_{5/2}$ and $3d_{3/2}$ peaks are the predominant features of the

SSDN-4686

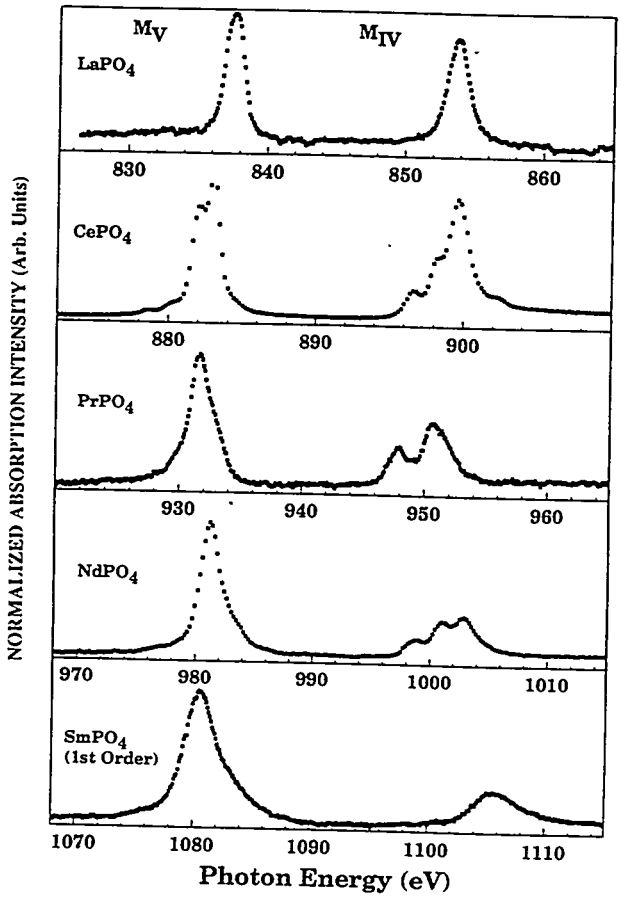

Fig. 5.28. XAS spectra of the *RE* (La, Ce, Pr, Nd, Sm) orthophosphates $M_{4,5}$ edges collected with monochromator diffraction grating satisfying a second-order Bragg condition to improve spectral resolution, except for Sm. The spectra have been normalized to the largest respective feature.

spectrum, whereas the exchange interaction provides an observed fine structure. The XAS spectra of the *RE* ions in the orthophosphate matrix generally resemble the XAS of the corresponding *RE* metal. This is not unexpected and emphasizes a major contribution of the trivalent state to the electronic transitions at the *RE* $3d$ edges. These spectra unequivocally

identify the transitions originating from well-characterized *RE* cores and correlate well with previous theoretical investigations.

---

1. Summary of paper: *Materials Research Society Symposium Proceedings*, Vol. 307, in press.
2. Lawrence Berkeley Laboratory, Berkeley, Calif.
3. Lawrence Livermore National Laboratory, Livermore, Calif.
4. E. Jarosewich and L. A. Boatner, *Geostandards Newsletter* **15**, 397 (1991).
5. L. A. Boatner and B. C. Sales, p. 495 in *Radioactive Waste Forms for the Future*, ed. by W. Lutze and R. C. Ewing, Elsevier Science Publishers, New York, 1988.
6. A. Lempicki et al., *IEEE Trans. Nucl. Sci.* **40**, 384 (1993).

COLLABORATIVE SYNCHROTRON BEAM LINE FOR THE ADVANCED PHOTON SOURCE

B. C. Larson, G. E. Ice,[1] *J. Z. Tischler, J. D. Budai, C. J. Sparks,*[1] *and E. Specht*[1]

A high-brightness synchrotron beam line is under development in collaboration with the University of Illinois Materials Research Laboratory and UOP Research and Development, Inc., for construction as an x-ray scattering user facility at the Advanced Photon Source (APS). Detailed planning and engineering are in progress on beam line hardware and optical components, and APS approval has been received for the beam line conceptual design and management plan. Engineering design has been completed, and fabrication has been initiated on an inclined geometry, high heat load focusing monochromator for an undulator insertion device as part of a research and development agreement with the APS Experimental Facilities Division. The results of this development will be available for general use at the APS as well as by the UNI-CAT beam line consortium. Construction progress by the APS on the synchrotron storage ring facility indicates that initial photon beams will be available for test purposes by mid-1995, and UNI-CAT plans are to complete the undulator beam line so that testing, alignment, and final beam line component development can begin at that time.

Discussions are in progress with personnel from the National Institute for Standards and Technology (NIST) as an additional collaborator. In addition to general x-ray scattering, the proposed NIST scientific program includes extended x-ray absorption fine structure, topography, and small-angle scattering capabilities which are largely complementary to the programs of the present collaborators and would strengthen the consortium.

---

1. Metals and Ceramics Division, ORNL.

Publications and Papers

(April 1, 1992–September 30, 1993)

JOURNAL ARTICLES

D. L. Abernathy, S. G. J. Mochrie, D. M. Zehner, G. Grübel, and D. Gibbs, "Orientational Epitaxy and Lateral Structure of the Hexagonally Reconstructed Pt(001) Surfaces," *Phys. Rev. B* **45**, 9272 (1992).

D. L. Abernathy, S. G. J. Mochrie, D. M. Zehner, G. Grübel, and D. Gibbs, "Thermal Roughness of a Close-Packed Metal Surface: Pt(001)," *Phys. Rev. Lett.* **69**, 941 (1992).

D. L. Abernathy, D. Gibbs, G. Grübel, K. G. Huang, S. G. J. Mochrie, A. R. Sandy, and D. M. Zehner, "Reconstruction of the (111) and (001) Surfaces of Au and Pt: Thermal Behavior," *Surf. Sci.* **283**, 260 (1993).

G. Aeppli, Z. Fisk, S. M. Hayden, M. F. Hundley, H. Mook, and D. Rytz, "The Marginal Fermi Liquid Hypothesis and Magnetic Fluctuations in $La_{1.95}Ba_{0.05}CuO_4$," *J. Magn. Magn. Mater.* **104–107**, 507 (1992).

A. P. Baddorf, D. M. Zehner, G. Helgesen, D. Gibbs, A. R. Sandy, and S. G. J. Mochrie, "X-Ray Scattering Determination of the Cu(110)-(2 × 3)N Structure," *Phys. Rev. B* **48**, 9013 (1993).

C. Ballesteros, R. Gonzalez, Y. Chen, and M. R. Kokta, "Precipitation of Matrix Cations in Fusion Ionic Insulators During Reduction at High Temperatures," *Electron Microsc.* **2**, 377 (1992).

C. Ballesteros, R. Gonzalez, Y. Chen, and M. R. Kokta, "Precipitation of Copper and Chromium Impurities in Lanthanum Magnesium Aluminate Crystals During Thermochemical Reduction," *Phys. Rev. B* **47**, 2460 (1993).

J. C. Barnard, K. M. Hock, L. Siller, M. R. C. Hunt, J. F. Wendelken, and R. E. Palmer, "New Resonances in High-Resolution EELS of Adsorbed Molecules: Electronic Excitation of Physisorbed O_2," *Surf. Sci.* **291**, 139 (1993).

C. W. Bartges and J. S. Lin, "Effect of Sn Additions on GP Zone Formation in Al-Cu Alloys," *Scr. Metall. Mater.* **28**, 1283 (1993).

R. A. Bartynski, S. Yang, S. L. Hulbert, C.-C. Kao, M. Weinert, and D. M. Zehner, "Surface Electronic Structure and Off-Site Auger Transitions on TaC(111) Observed with Auger-Photoelectron Coincidence Spectroscopy," *Phys. Rev. Lett.* **68**, 2247 (1992).

J. B. Bates and Y. T. Chu, "Electrode-Electrolyte Interface Impedance: Experiments and Model," *Ann. Biomed. Eng.* **20**, 349 (1992).

J. B. Bates, N. J. Dudney, G. R. Gruzalski, R. A. Zuhr, A. Choudhury, C. F. Luck, and J. D. Robertson, "Electrical Properties of Amorphous Lithium Electrolyte Thin Films," *Solid State Ionics* **53–56**, 647 (1992).

J. B. Bates, N. J. Dudney, G. R. Gruzalski, R. A. Zuhr, A. Choudhury, C. F. Luck, and J. D. Robertson, "Fabrication and Characterization of Amorphous Lithium Electrolyte Thin Films and Rechargeable Thin-Film Batteries" *J. Power Sources* **43–44**, 103 (1993).

J. B. Bates, N. J. Dudney, C. F. Luck, B. C. Sales, R. A. Zuhr, and J. D. Robertson, "Deposition and Characterization of Li_2O-SiO_2-P_2O_5 Thin Films," *J. Am. Ceram. Soc.* **76**, 929 (1993).

J. B. Bates, G. R. Gruzalski, N. J. Dudney, C. F. Luck, X.-H. Yu, and S. D. Jones, "Rechargeable Thin-Film Lithium Microbatteries," *Solid State Technology* **36**, 59 (1993).

R. Berliner, H. G. Smith, J. R. D. Copley, and J. Trivisonno, "Structures of Sodium Metal," *Phys. Rev. B* **46**, 14436 (1992).

P. Böni, G. Shirane, J. L. Martinez, and H. A. Mook, "Spin Fluctuations in Ni Above T_c: Comparison with RG," *Physica B* **180 & 181**, 219 (1992).

P. Böni, H. A. Mook, J. L. Martinez, and G. Shirane, "Comparison of the Paramagnetic Spin Fluctuations in Nickel with Asymptotic Renormalization-Group Theory," *Phys. Rev. B* **47**, 3171 (1993).

A. T. Boothroyd, T. G. Perring, A. D. Taylor, D. M. Paul, and H. A. Mook, "High-Energy Spin Waves in Iron Measured by Neutron Scattering," *J. Magn. Magn. Mater.* **104–107**, 113 (1992).

W. Braun, B. S. Kwak, A. Erbil, J. D. Budai, and B. J. Wilkens, "Epitaxial Lead Zirconate-Titanate Thin Films on Sapphire," *Appl. Phys. Lett.* **63**, 467 (1993).

N. D. Browning and S. J. Pennycook, "Atomic Resolution Spectroscopy for the Microanalysis of Materials," *Microbeam Analysis* **2**, 81 (1993).

N. D. Browning, M. F. Chisholm, and S. J. Pennycook, "Atomic-Resolution Electron Energy Loss Spectroscopy in the Scanning Transmission Electron Microscope," *Microbeam Analysis* **2**, S270 (1993).

N. D. Browning, M. F. Chisholm, S. J. Pennycook, D. P. Norton, and D. H. Lowndes, "Correlation Between Hole Depletion and Atomic Structure at High-Angle Grain Boundaries in $YBa_2Cu_3O_{7-\delta}$," *Physica C* **212**, 185 (1993).

J. D. Budai, R. T. Young, and B. S. Chao, "In-Plane Epitaxial Alignment of $YBa_2Cu_3O_{7-x}$ Films Grown on Silver Crystals and Buffer Layers," *Appl. Phys. Lett.* **62**, 1836 (1993).

W. J. L. Buyers, Z. Tun, A. Harrison, J. A. Rayne, and R. M. Nicklow, "Haldane Gap in $RbNiCl_3$," *Physica B* **180 & 181**, 222 (1992).

J. W. Cable and Y. Tsunoda, "Spin Density Waves in Dilute CuMn Alloys," *J. Appl. Phys.* **73**, 5454 (1993).

J. W. Cable, N. Wakabayashi, and P. Radhakrishna, "Magnetic Excitations in the Triangular Antiferromagnets Mn_3Sn and Mn_3Ge," *Phys. Rev. B* **48**, 6159 (1993).

G. S. Canright and A. G. Rojo, "Ellipsometry and Broken T Symmetry in the High-Temperature Superconductors," *Phys. Rev. B* **46**, 14078 (1992).

G. S. Canright and A. G. Rojo, "Reply to Comment on 'Some Consequences of PT Symmetry for Optical Rotation Experiments,'" *Phys. Rev. Lett.* **69**, 3132 (1992); *Phys. Rev. Lett.* **69**, 3133 (1992).

B. C. Chakoumakos, J. A. Fernandez-Baca, and L. A. Boatner, "Refinement of the Structures of the Layer Silicates $M\mathrm{CuSi_4O_{10}}$ (M = Ca, Sr, Ba) by Rietveld Analysis of Neutron Powder Diffraction Data," *J. Solid State Chem.* **103**, 105 (1993).

X. M. Chen and J. J. Quinn, "Numerical Study of Fractional Quantum Hall Electron-Hole Systems: Evidence of Stable Anyonic Ions," *Phys. Rev. Lett.* **70**, 2130 (1993).

Y. W. Cheung, R. S. Stein, J. S. Lin, and G. D. Wignall, "Small-Angle Scattering Investigations of Poly(ε-caprolactone)/Polycarbonate Blends. 2. Small-Angle X-Ray and Light Scattering Study of Semicrystalline/Semicrystalline and Semicrystalline/Amorphous Blend Morphology," *Macromol.* **26**, 5365 (1993).

J. T. Cheung, P. E. D. Morgan, D. H. Lowndes, X.-Y. Zheng, and J. Breen, "Structural and Electrical Properties of $\mathrm{La_{0.5}Sr_{0.5}CoO_3}$ Epitaxial Films," *Appl. Phys. Lett.* **62**, 2045 (1993).

M. H. Cho, T. Kyu, J. S. Lin, K. Saijo, and T. Hashimoto, "Time-Resolved Small-Angle X-Ray Scattering and Wide-Angle X-Ray Scattering Studies on Premelting During Annealing of Gelation Crystallized Ultrahigh Molecular Weight Polyethylene Films," *Polymer* **33**, 4152 (1992).

D. K. Christen, R. C. Dynes, V. J. Emery, C. M. Falco, D. U. Gubser, S. Jin, H. Kroger, and D. T. Shaw, "New Research Opportunities in Superconductivity III," *Cryogenics* **32**, 337 (1992).

D. K. Christen and J. R. Thompson, "Current Problems at High T_c," *Nature* **364**, 98 (1993).

Y. T. Chu, "Determination of the Optical Dielectric Functions of Thin Absorbing Films from IR Reflectivity Measurements," *Thin Solid Films* **229**, 119 (1993).

L. Civale, T. K. Worthington, L. Krusin-Elbaum, A. D. Marwick, F. Holtzberg, J. R. Thompson, M. A. Kirk, and R. A. Wheeler, "Irradiation-Enhanced Pinning in $\mathrm{YBa_2Cu_3O_{7-x}}$ Crystals" *J. Metals* **44**, 60 (1992).

R. Cubitt, E. M. Forgan, D. McK. Paul, S. L. Lee, J. S. Abell, H. A. Mook, and P. Timmins, "Neutron Diffraction by the Flux Lattice in High-T_c Superconductors," *Physica B* **180**, 377 (1992).

R. Cubitt, E. M. Forgan, G. Yang, S. L. Lee, D. McK. Paul, H. A. Mook, M. Yethiraj, P. H. Kes, T. W. Li, A. A. Menovsky, Z. Tarnawski, and K. Mortensen, "Direct Observation of Magnetic Flux Lattice Melting and Decomposition in the High-T_c Superconductor $\mathrm{Bi_{2.15}Sr_{1.95}CaCu_2O_{8+x}}$," *Nature* **365**, 407 (1993).

H. L. Davis, J. B. Hannon, K. B. Ray, and E. W. Plummer, "Anomalous Interplanar Expansion at the (0001) Surface of Be," *Phys. Rev. Lett.* **68**, 2632 (1992).

R. M. de la Cruz, R. Pareja, R. Gonzalez, L. A. Boatner, and Y. Chen, "Effect of Thermochemical Reduction in the Electrical, Optical-Absorption, and Positron-Annihilation Characteristics of ZnO Crystals," *Phys. Rev. B* **45**, 6581 (1992).

P. DiAntonio, X. M. Wang, J. Toulouse, and L. A. Boatner, "Dielectric and Raman Study of Short- and Long-Range Order in KTN," *Ferroelectrics* **120**, 107 (1991).

N. J. Dudney, J. B. Bates, R. A. Zuhr, C. F. Luck, and J. D. Robertson, "Sputtering of Lithium Compounds for Preparation of Electrolyte Thin Films," *Solid State Ionics* **53–56**, 655 (1992).

N. J. Dudney, J. B. Bates, and J. D. Robertson, "Radio-Frequency Magnetron Sputtering of Pure and Mixed Targets of Li_4SiO_4, Li_3PO_4, and Li_2O," *J. Vac. Sci. and Technol. A* **11**, 377 (1993).

A. Erbil, W. Braun, B. S. Kwak, B. J. Wilkens, L. A. Boatner, and J. D. Budai, "Oxide Ferroelectric Materials Grown by Metalorganic Chemical Vapor Deposition," *J. Cryst. Growth* **124**, 684 (1992).

D. Eres and J. W. Sharp, "Real-Time Monitoring and Control of a Surface Reaction in Germanium Film Growth," *Appl. Phys. Lett.* **60**, 2764 (1992).

G. Eres and J. W. Sharp, "Investigation of the Kinetics of Digermane Chemisorption and Reaction Product Desorption in Thin-Film Growth of Germanium," *J. Vac. Sci. Technol. A* **11**, 2463 (1993).

R. Feenstra, D. K. Christen, C. E. Klabunde, and J. D. Budai, "Role of Oxygen Vacancies in the Flux Pinning Mechanism, and Hole-Doping Lattice Disorder in High-Current Density $YBa_2Cu_3O_{7-x}$ Films," *Phys. Rev. B* **45**, 7555 (1992).

Z. C. Feng, B. S. Kwak, A. Erbil, and L. A. Boatner, "Difference Raman Spectra of $PbTiO_3$ Thin Films Grown by Metalorganic Chemical Vapor Deposition," *Appl. Phys. Lett.* **62**, 349 (1993).

J. A. Fernandez-Baca, M. E. Hagen, R. M. Nicklow, T. G. Perring, and Y. Tsunoda, "High-Energy Magnetic Excitations in $Mn_{90}Cu_{10}$," *J. Appl. Phys.* **73**, 6548 (1993).

J. B. Field, C. Toprakcioglu, R. C. Ball, H. B. Stanley, L. Dai, W. Barford, J. Penfold, G. Smith, and W. Hamilton, "Determination of End-Adsorbed Polymer Density Problems by Neutron Reflectometry," *Macromolecules* **25**, 434 (1992).

J. B. Field, C. Toprakcioglu, L. Dai, G. Hadziioannou, G. Smith, and W. Hamilton, "Neutron Reflectivity Study of End-Adsorbed Diblock Copolymers: Cross-Over from Mushrooms to Brushes," *J. Phys. II France* **2**, 2221 (1992).

B. N. Figgis, P. A. Reynolds, and J. W. Cable, "Extreme Covalence in the T_c-Cl Bond from Polarized Neutron Diffraction," *J. Chem. Phys.* **98**, 7743 (1993).

R. S. Fishman and S. H. Liu, "Effect of Impurities on the Magnetic Ordering in Chromium," *Phys. Rev. B* **45**, 12306 (1992).

R. S. Fishman and S. H. Liu, "Impurity Effects on the Magnetic Ordering in Chromium," *Int. J. Mod. Phys. B* **7**, 620 (1993).

R. S. Fishman and S. H. Liu, "Magnetic Structure and Paramagnetic Dynamics of Chromium and Its Alloys," *Phys. Rev. B* **47**, 11870 (1993).

R. S. Fishman and S. H. Liu, "Phase Diagram of Chromium Alloys," *J. Magn. Magn. Mater.* **125**, L1 (1993).

R. S. Fishman and S. H. Liu, "Free Energy and Phase Diagram of Chromium Alloys," *Phys. Rev. B* **48**, 3820 (1993).

K. Flensberg, S. M. Girvin, M. Johnson, D. R. Penn, and M. D. Stiles, "Quantum Mechanics of the Electromagnetic Environment in the Single-Junction Coulomb Blockade," *Physica Scripta* **T42**, 189 (1992).

J. Forster, C. C. Klepper, L. A. Berry, and S. M. Gorbatkin, "Doppler Shift Measurements of Ion Energy Distribution Widths in an Electron Cyclotron Resonance/ Multipole Hybrid Reactor," *J. Vac. Sci. and Technol. A* **10**, 3114 (1992).

H. O. Frota and Karsten Flensberg, "Renormlization-Group Calculations of Ground State and Transport Properties of Ultrasmall Tunnel Junctions," *Phys. Rev. B* **46**, 15207 (1992).

D. B. Geohegan, "Fast-Intensified CCD Photography of $YBa_2Cu_3O_{7-x}$ Laser Ablation in Vacuum and Ambient Oxygen," *Appl. Phys. Lett.* **60**, 2732 (1992).

D. B. Geohegan, "Physics and Diagnostics of Laser Ablation Plume Propagation for High-T_c Superconductor Film Growth," *Thin Solid Films* **220**, 138 (1992).

D. B. Geohegan, "Imaging and Blackbody Emission Spectra of Particulates Generated in the KrF-Laser Ablation of BN and $YB_2Cu_3O_{7-x}$," *Appl. Phys. Lett.* **62**, 1463 (1993).

P. M. Gehring, H. Chou, S. M. Shapiro, J. A. Hriljac, D. H. Chen, J. Toulouse, D. Rytz, and L. A. Boatner, "Dipole-Glass Behavior of Lightly Doped $KTa_{1-x}Nb_xO_3$," *Phys. Rev. B* **46**, 5116 (1992).

T. M. Giebultowicz, J. A. Fernandez-Baca, R. M. Nicklow, J. K. Furdyna, and U. Debska, "Spin Dynamics in a Diluted Heisenberg NN Antiferromagnet on a HCP Lattice: $Zn_{1-x}Mn_xSe$" *J. Appl. Phys.* **73**, 5660 (1993).

M. J. Godbole, A. J. Pedraza, D. H. Lowndes, and J. R. Thompson, Jr., "Role of Interfacial Thermal Resistance and Laser Energy Density During Laser Processing of Copper-Sapphire Couples," *J. Mater. Res.* **7**, 1004 (1992).

R. Gonzalez, Y. Chen, C. Ballesteros, H. Liu, G. P. Williams, Jr., G. H. Rosenblatt, R. T. Williams, and W. Gellermann, "Luminescence Properties of Deformed CaO Crystals," *Phys. Rev. B* **47**, 4910 (1993).

R. Gonzalez, C. Ballesteros, Y. J. Liu, Yi Chen, X. F. Zong, and Y. Chen, "Thermochemical Reduction of Yttrium Aluminum Garnet Crystals," *Philos. Mag. A* **67**, 207 (1993).

R. Gonzalez, R. Pareja, and Y. Chen, "Protons in Neutron-Irradiated and Thermochemically Reduced MgO Crystals Doped with Lithium Impurities," *Phys. Rev. B* **45**, 12730 (1992).

S. M. Gorbatkin and L. A. Berry, "Contamination by Sputtering in Mirror-Field Electron Cyclotron Resonance Microwave Plasma Sources," *J. Vac. Sci. and Technol. A* **10**, 3104 (1992).

S. M. Gorbatkin, L. A. Berry, and J. Swyers, "Poly-Si Etching Using an Electron Cyclotron Resonance Microwave Plasma Source with Multipole Confinement," *J. Vac. Sci. and Technol. A* **10**, 1295 (1992).

S. M. Gorbatkin, R. F. Burgie, W. C. Oliver, J. C. Barbour, T. M. Mayer, and M. L. Thomas, "Boron Nitride Thin-Film Deposition Using Electron Cyclotron Resonance Microwave Plasmas," *J. Vac. Sci. and Technol. A* **11**, 1863 (1993).

P. Grenier, S. Jandl, M. Blouin, and L. A. Boatner, "Study of Ferroelectric Microdomains Due to Oxygen Vacancies in $KTaO_3$," *Ferroelectrics* **137**, 105 (1992).

P. Grenier, D. Houde, S. Jandl, and L. A. Boatner, "Soft Mode Studies in $KTa_{0.93}Nb_{0.07}O_3$ with Use of the Time-Resolved Third-Order Optical Susceptibility χ^3," *Phys. Rev. B* **47**, 1 (1993).

G. Grübel, D. Gibbs, D. M. Zehner, D. L. Abernathy, A. R. Sandy, and S. G. J. Mochrie, "Phase Behavior of Au and Pt Surfaces," *Surf. Sci.* **287/288**, 842 (1993).

V. A. Hackley, M. A. Anderson, and S. Spooner, "A Small-Angle X-Ray Scattering Study of Microstructure Evolution During Sintering of Sol-Gel Derived Porous Nanophase Titania," *J. Mater. Res.* **7**, 2555 (1992).

M. Hagen, H. R. Child, J. A. Fernandez-Baca, and J. L. Zarestky, "A Study of the Magnetic Critical Scattering from the Longitudinally Modulated Antiferromagnets Thulium and Erbium," *J. Phys.: Condens. Matter* **4**, 8879 (1992).

R. F. Haglund, Jr., R. H. Magruder III, S. H. Morgan, D. O. Henderson, R. A. Weller, L. Yang, and R. A. Zuhr, "Nonlinear Index of Refraction of Cu- and Pb-Implanted Fused Silica," *Nucl. Instrum. and Methods Phys. Res. Sect. B* **365**, 405 (1992).

R. F. Haglund, Jr., L. Yang, R. H. Magruder III, J. E. Wittig, K. Becker, and R. A. Zuhr, "Picosecond Nonlinear Optical Response of a Cu:Silica Nanocluster Composite," *Opt. Lett.* **18**, 373 (1993).

T. E. Haynes and O. W. Holland, "Damage Accumulation During Ion Implantation of Unstrained $Si_{1-x}Ge_x$ Alloy Layers," *Appl. Phys. Lett.* **61**, 61 (1992).

T. E. Haynes and O. W. Holland, "Lattice Damage in Ion-Implanted Silicon-Germanium Alloys," *Nucl. Instrum. and Methods Phys. Res. Sect. B* **80/81**, 901 (1993).

O. W. Holland and T. E. Haynes, "Damage Saturation During High-Energy, Ion Implantation of $Si_{1-x}Ge_x$," *Appl. Phys. Lett.* **61**, 3148 (1992).

O. W. Holland, D. S. Zhou, and D. K. Thomas, "Damage Accumulation During High-Dose, O^+ Implantation in Si," *Appl. Phys. Lett.* **63**, 896 (1993).

H. Hosono, H. Fukushima, Y. Abe, R. A. Weeks, and R. A. Zuhr, "Cross-Sectional TEM Observation of Copper-Implanted SiO_2 Glass," *J. Non-Cryst. Solids* **143**, 157 (1992).

M. Hou, W. Eckstein, and M. T. Robinson, "Computer Simulation of Temporal Aspects of the Copper Single-Crystal Sputtering," *Nucl. Instrum. and Methods Phys. Res. Sect. B* **82**, 234 (1993).

I. G. Hughes, J. Burgdörfer, L. Folkerts, C. C. Havener, S. H. Overbury, M. T. Robinson, D. M. Zehner, P. A. Zeijlmans van Emmichoven, and F. W. Meyer, "Separation of Kinetic and Potential Electron Emission Arising from Slow Multicharged Ion-Surface Interactions," *Phys. Rev. Lett.* **71**, 291 (1993).

J. D. Hunn, N. R. Parikh, M. L. Swanson, and R. A. Zuhr, "Conduction in Ion-Implanted Single-Crystal Diamond," *Diamond and Related Materials* **2**, 847 (1993).

G. E. Jellison, Jr., and J. W. McCamy, "Sample Deplorization Effects from Thin Films of ZnS on GaAs as Measured by Spectroscopic Ellipsometry," *Appl. Phys. Lett.* **61**, 512 (1992).

G. E. Jellison, Jr., "Optical Functions of GaAs, GaP, and Ge Determined by Two-Channel Polarization Modulation Ellipsometry," *Opt. Mater.* **1**, 151 (1992).

G. E. Jellison, Jr., T. E. Haynes, and H. H. Burke, "Optical Functions of Silicon-Germanium Alloys Determined Using Spectroscopic Ellipsometry," *Opt. Mater.* **2**, 105 (1993).

G. E. Jellison, Jr., M. F. Chisholm, and S. M. Gorbatkin, "Optical Functions of Chemical Vapor Deposited Thin-Film Silicon Determined by Spectroscopic Ellipsometry," *Appl. Phys. Lett.* **62**, 3348 (1993).

D. E. Jesson, S. J. Pennycook, J.-M. Baribeau, and D. C. Houghton, "Atomistic Processes of Surface Segregation During Si-Ge MBE Growth," *Thin Solid Films* **222**, 98 (1992).

D. E. Jesson and S. J. Pennycook, "Incoherent Imaging of Thin Specimens Using Coherently Scattered Electrons," *Proc. R. Soc. London A* **441**, 261 (1993).

D. E. Jesson, S. J. Pennycook, J. Z. Tischler, J. D. Budai, J.-M. Baribeau, and D. C. Houghton, "Interplay Between Evolving Surface Morphology, Atomic-Scale Growth Modes, and Ordering During Si_xGe_{1-x} Epitaxy," *Phys. Rev. Lett.* **70**, 2293 (1993).

D. E. Jesson, S. J. Pennycook, J.-M. Baribeau, and D. C. Houghton, "Direct Imaging of Surface Cusp Evolution During Strained-Layer Epitaxy and Implications for Strain Relaxation," *Phys. Rev. Lett.* **71**, 1744 (1993).

Q. T. Jiang, T. Gustafsson, P. Häberle, and D. M. Zehner, "Missing-Row Surface Reconstruction of Au(113) Induced by Adsorbed Calcium Atoms," *Phys. Rev. B* **45**, 14256 (1992).

Q. T. Jiang, P. Statiris, T. Gustafsson, P. Häberel, and D. M. Zehner, "Ion Scattering Study of the Adatom Induced Missing-Row Reconstructions of Ni(110) and Au(113)," *J. Vac. Sci. and Technol. A* **10**, 2197 (1992).

E. C. Jones, D. K. Christen, J. R. Thompson, R. Feenstra, S. Zhu, D. H. Lowndes, J. M. Phillips, M. P. Siegal, and J. D. Budai, "Correlations Between the Hall Coefficient and the Superconducting Transport Properties of Oxygen-Deficient $YBa_2Cu_3O_{7-\delta}$ Epitaxial Thin Films," *Phys. Rev. B* **47**, 8986 (1993).

T. Kanaya, M. Ohkura, K. Kaji, M. Furusaka, M. Misawa, H. Yamaoka, and G. D. Wignall, "Small-Angle Neutron Scattering From Poly(vinyl Alcohol) Gels," *Physica B* **180 & 181**, 549 (1992).

T. Kaplan, M. Rasolt, M. Karimi, and M. Mostoller, "Numerical Simulation of He^+ and Li^+ Collisions with C_{60}," *J. Phys. Chem.* **97**, 6124 (1993).

M. Karimi, T. Kaplan, M. Mostoller, and D. E. Jesson, "Ge Segregation at Si-Ge (001) Stepped Surfaces," *Phys. Rev. B* **47**, 9931 (1993).

S. Katano, S. Funahashi, N. Môri, Y. Ueda, and J. A. Fernandez-Baca, "Pressure Effects on the Structural Phase Transitions and Superconductivity of $La_{2-x}Ba_xCuO_4$ ($x = 0.125$)," *Phys. Rev. B* **48**, 6569 (1993).

S. Katano, J. A. Fernandez-Baca, S. Funahashi, N. Môri, Y. Ueda, and K. Koga, "Crystal Structure and Superconductivity of $La_{2-x}Ba_xCuO_4$ ($0.03 \leq x \leq 0.24$)," *Physica C* **214**, 64 (1993).

H. R. Kerchner, D. K. Christen, C. E. Klabunde, J. O. Thomson, Y. R. Sun, and J. R. Thompson, "Evidence of Kosterlitz-Thouless Transition in $YBa_2Cu_3O_7/PrBa_2Cu_3O_7$ Superlattice Films," *Physica C* **198**, 75 (1992).

W. K. Kot, M. Edelstein, M. M. Abraham, and L. A. Boatner, "The EPR of Pu^{3+} and Cf^{3+} in Single Crystals of $LuPO_4$," *Phys. Rev. B* **47**, 3412 (1993).

M. N. Kunchur, D. K. Christen, and J. M. Phillips, "Observation of Free Flux Flow at High Dissipation Levels in $YBa_2Cu_3O_{7-\delta}$ Epitaxial Films," *Phys. Rev. Lett.* **70**, 998 (1993).

B. S. Kwak, A. Erbil, B. J. Wilkens, J. D. Budai, M. F. Chisholm, and L. A. Boatner, "Strain Relaxation by Domain Formation in Epitaxial Ferroelectric Thin Films," *Phys. Rev. Lett.* **68**, 3733 (1992).

B. S. Kwak, P. N. First, A. Erbil, B. J. Wilkens, J. D. Budai, M. F. Chisholm, and L. A. Boatner, "Study of Epitaxial Platinum Thin Films Grown by Metalorganic Chemical Vapor Deposition," *J. Appl. Phys.* **72**, 3735 (1992).

C. Lee, T. E. Haynes, and K. S. Jones, "Kinetics of Solid Phase Epitaxial Regrowth in Amorphized $Si_{0.88}Ge_{0.12}$ Measured by Time-Resolved Reflectivity," *Appl. Phys. Lett.* **62**, 501 (1993).

M. F. Lin and K. W.-K. Shung, "Magnetoplasmons and Persistent Currents in Cylindrical Tubules," *Phys. Rev. B* **48**, 5567 (1993).

S. H. Liu, "Formation and Anomalous Properties of Fractals," *Eng. Med. and Biology* **11**, 28 (1992).

S. H. Liu, "Electronic Polaron Effects in Mixed Valence and Heavy Fermion Materials," *Int. J. Mod. Phys. B* **7**, 9 (1993).

S. H. Liu and R. A. Klemm, "Intra- Versus Interlayer Pairing in Copper Oxide Superconductors: Response to Magnetic Field," *Phys. Rev. B* **48**, 4080 (1993).

S. H. Liu and R. A. Klemm, "Energy Gap Structure and Tunneling Characteristics of Layered Superconductors," *Physica C* **216**, 293 (1993).

J. D. Londono, V. M. Shah, G. D. Wignall, H. D. Cochran, and P. R. Bienkowski, "Small-Angle Neutron Scattering Studies of Dilute Supercritical Neon," *J. Chem. Phys.* **99**, 466 (1993).

C.-K. Loong, L. Soderholm, M. M. Abraham, L. A. Boatner, and N. M. Edelstein, "Crystal-Field Excitations and Magnetic Properties of $TmPO_4$," *J. Chem. Phys.* **98**, 4214 (1993).

D. H. Lowndes, X.-Y. Zheng, S. Zhu, J. D. Budai, and R. J. Warmack, "Suppression of the Spiral-Growth Mechanism in Epitaxial $YBa_2Cu_3O_{7-x}$ Films Grown on Miscut Substrates," *Appl. Phys. Lett.* **61**, 852 (1992).

R. H. Magruder III, D. O. Henderson, S. H. Morgan, and R. A. Zuhr, "Optical Spectra of Pb-Implanted Fused Silica," *J. Non-Cryst. Solids* **152**, 258 (1993).

R. H. Magruder III, L. Yang, R. F. Haglund, Jr., C. W. White, L. Yang, R. Dorsinville, and R. R. Alfano, "Optical Properties of Gold Nanocluster Composites Formed by Deep Ion Implantation in Silica," *Appl. Phys. Lett.* **62**, 1730 (1993).

R. H. Magruder III, D. O. Henderson, C. W. White, and R. A. Zuhr, "Formation of Photosensitive Materials by Ion Implantation of Oxygen Ions in Silica," *J. Non-Cryst. Solids* **159**, 269 (1993).

G. D. Mahan, "Ionic Polarization," *Ferroelectrics* **136**, 57 (1992).

G. D. Mahan, "Electron-Electron Interactions: Ward Identities," *Int. J. Mod. Phys.* **6**, 3381 (1992).

G. D. Mahan, "Fractal Vertex for Electron-Electron Interactions," *Mod. Phys. Lett. B* **7**, 13 (1993).

G. D. Mahan and J. O. Sofo, "Resistivity and Superconductivity from Anharmonic Phonons," *Phys. Rev. B* **47**, 8050 (1993).

A. G. Mal'shukov and G. D. Mahan, "Magnon Renormalization of a Localized Hole," *Phys. Rev. Lett.* **68**, 2200 (1992).

J. M. Martin, R. K. Nadella, J. Vellanki, M. V. Rao, and O. W. Holland, "Thermally Stable Buried High Resistance Layers in *P*-Type InP Obtained by MeV-Energy Ti Implantation," *J. Appl. Phys.* **73**, 7238 (1993).

A. D. Marwick, L. Civale, L. Krusin-Elbaum, R. Wheeler, J. R. Thompson, T. K. Worthington, M. A. Kirk, Y. R. Sun, H. R. Kerchner, and F. Holtzberg, "Processing High-T_c Superconductors with GeV Heavy Ions," *Nucl. Instrum. and Methods Phys. Res. Sect. B* **80/81**, 1143 (1993).

T. E. Mason, G. Aeppli, S. M. Hayden, A. P. Ramirez, and H. A. Mook, "Low Energy Excitations in Superconducting $La_{1.86}Sr_{0.14}CuO_4$," *Phys. Rev. Lett.* **71**, 919 (1993).

J. W. McCamy, D. H. Lowndes, J. D. Budai, R. A. Zuhr, and X. Zhang, "Epitaxial ZnS Films Grown on GaAs (001) and (111) by Pulsed-Laser Ablation," *J. Appl. Phys.* **73**, 7818 (1993).

C. J. McHargue and J. M. Williams, "Ion Implantation Effects in Silicon Carbide," *Nucl. Instrum. and Methods Phys. Res. Sect. B* **80/81**, 889 (1993).

A. D. Migone, M. T. Alkhafaji, G. Vidali, and M. Karimi, "Thermodynamic Study of Argon Films Adsorbed on Boron Nitride," *Phys. Rev. B* **47**, 6685 (1993).

F. A. Modine and G. E. Jellison, Jr., "Errors in Polarization Measurements Due to Static Retardation in Photoelastic Modulators," *Appl. Phys. Commun.* **12**, 121 (1993).

F. A. Modine, D. C. Lubben, and J. B. Bates, "Electrical Conduction in CaF_2 and CaF_2-Al_2O_3 Nanocomposite Films on Al_2O_3 Substrates," *J. Appl. Phys.* **74**, 2658 (1993).

H. A. Mook, B. C. Chakoumakos, M. Mostoller, A. T. Boothroyd, and D. McK. Paul, "Phonons and Superconductivity in $Bi_2Sr_2CaCu_2O_8$," *Phys. Rev. Lett.* **69**, 2272 (1992).

H. A. Mook, M. Yethiraj, G. Aeppli, T. E. Mason, and T. Armstrong, "Polarized Neutron Determination of the Magnetic Excitations in $YBa_2Cu_3O_7$," *Phys. Rev. Lett.* **70**, 3490 (1993).

H. A. Mook, M. Yethiraj, G. D. Wignall, E. M. Forgan, S. L. Lee, R. Cubitt, D. McK. Paul, and T. Armstrong, "Neutron Measurements of the Vortex Lattice in $YBa_2Cu_3O_7$," *J. Appl. Phys.* **73**, 5855 (1993).

H. A. Mook, C. L. Seaman, M. B. Maple, M. A. Lopez de la Torre, D. L. Cox, and M. Makivic, "Neutron Scattering Study of the Quadrupolar Kondo Alloy $Y_{0.8}U_{0.2}Pd_3$," *Physica B* **186–188**, 341 (1993).

T. Motooka and O. W. Holland, "Amorphization Processes in Ion-Implanted Si: Ion Species Effects," *Appl. Phys. Lett.* **61**, 3005 (1992).

F. M. Mueller, D. H. Lowndes, Y. K. Chang, A. J. Arko, and R. S. List, "De Haas-van Alphen Effect on Superconducting V_3Si," *Phys. Rev. Lett.* **68**, 3928 (1992).

D. F. Mullica, E. L. Sappenfield, and L. A. Boatner, "Single-Crystal Analysis of Mixed ($Ln/TbPO_4$) Orthophosphates," *J. Solid State Chem.* **99**, 313 (1992).

D. R. Mullins, P. F. Lyman, and S. H. Overbury, "Interaction of S with W(001)," *Surf. Sci.* **227**, 64 (1992).

D. R. Mullins and P. F. Lyman, "Sulfur-Induced Changes in the W(001) Surface Core Level Shift," *Surf. Sci. Lett.* **285**, L473 (1993).

D. R. Mullins and P. F. Lyman, "The Adsorption and Reaction of Methanethinol on W(001)," *J. Phys. Chem.* **97**, 9226 (1993).

R. K. Nadella, J. Vellanki, M. V. Rao, and O. W. Holland, "MeV B Compensation Implants into *n*-Type GaAs and InP," *J. Appl. Phys.* **72**, 2179 (1992).

D. P. Norton, J. D. Budai, B. C. Chakoumakos, and R. Feenstra, "Epitaxial Growth of $Ba_{1-x}K_xBiO_3$ Thin Films by Pulsed-Laser Deposition," *Appl. Phys. Lett.* **62**, 414 (1993).

D. P. Norton, B. C. Chakoumakos, J. D. Budai, and D. H. Lowndes, "Epitaxial Growth of Single-Crystal $Ca_{1-x}Sr_xCuO_2$ Thin Films by Pulsed-Laser Deposition," *Appl. Phys. Lett.* **62**, 1679 (1993).

D. P. Norton and D. H. Lowndes, "Transport Properties of Ultrathin $YBa_2Cu_3O_{7-\delta}$ Layers: Evidence for Two-Dimensional Vortex Fluctuations," *Phys. Rev. B* **48**, 6460 (1993).

D. P. Norton and D. H. Lowndes, "Enhanced Superconducting Properties in Ultrathin $YBa_2Cu_3O_{7-\delta}$ Layers," *Appl. Phys. Lett.* **63**, 1432 (1993).

M. E. O'Hern, L. J. Romana, C. J. McHargue, J. C. McCallum, and C. W. White, "The Effect of Crystal Orientation on Damage Accumulation in Chromium-Implanted Al_2O_3," *Standard Technical Publication* **1125**, 740 (1992).

L. E. Oliveira and G. D. Mahan, "Donor-Photoluminescence Line Shapes from GaAs-(Ga,Al)As Quantum Wells," *Phys. Rev. B* **47**, 2406 (1993).

T. P. Ong, F. Xiong, R. P. H. Chang, and C. W. White, "Nucleation and Growth of Diamond on Carbon-Implanted Single-Crystal Copper Surfaces," *J. Mater. Res.* **7**, 2429 (1992).

T. P. Ong, F. Xiong, R. P. H. Chang, and C. W. White, "A Mechanism for Diamond Nucleation and Growth on Single-Crystal Copper Surfaces Implanted with Carbon," *Appl. Phys. Lett.* **60**, 2083 (1992).

J. G. Ossandon, J. R. Thompson, D. K. Christen, B. C. Sales, H. R. Kerchner, J. O. Thomson, Y. R. Sun, K. W. Lay, and J. E. Tkaczyk, "Influence of Oxygen Deficiency on the Superconductive Properties of Grain-Aligned $YBa_2Cu_3O_{7-\delta}$," *Phys. Rev. B* **45**, 12534 (1992).

J. G. Ossandon, J. R. Thompson, D. K. Christen, B. C. Sales, Y. Sun, and K. W. Lay, "Flux Creep Studies of Vortex Pinning in Aligned $YBa_2Cu_3O_{7-\delta}$ Superconductor with Oxygen Deficiencies $\delta \leq 0.2$," *Phys. Rev. B* **46**, 3050 (1992).

J. G. Ossandon, J. R. Thompson, D. K. Christen, Y. R. Sun, B. C. Sales, H. R. Kerchner, J. E. Tkaczyk, and K. W. Lay, "Properties of Aligned $YBa_2Cu_3O_{7-\delta}$ Superconductor as a Function of Oxygen Deficiency δ" *Appl. Superconductivity* **1**, 371 (1993).

S. H. Overbury, R. J. A. van den Oetelaar, and D. M Zehner, "Surface Segregation in $Mo_{0.75}Re_{0.25}(001)$ Studied by Low-Energy Alkali-Ion Scattering," *Phys. Rev. B* **48**, 1718 (1993).

R. Pareja, R. M. de la Cruz, R. Gonzalez, and Y. Chen, "Positron Annihilation Spectroscopy of Vacancy Aggregates in Neutron-Irradiated MgO Crystals," *Philos. Mag. A* **66**, 597 (1992).

N. R. Parikh, J. D. Hunn, E. McGucken, M. L. Swanson, C. W. White, R. A. Rudder, D. P. Malta, J. B. Posthill, and R. J. Markunas, "Single-Crystal Diamond Plate Liftoff Achieved by Ion Implantation and Subsequent Annealing," *Appl. Phys. Lett.* **61**, 3124 (1992).

D. McK. Paul, E. M. Forgan, R. Cubitt, S. L. Lee, H. A. Mook, and P. Timmins, "Neutron Scattering from the Flux Lattice in High-Temperature Superconductors," *J. Magn. Magn. Mater.* **104**, 591 (1992).

M. Paranthaman, J. R. Thompson, Y. R. Sun, and J. Brynstad, "Synthesis and Magnetic Characterization of the High-T_C Compound $HgBa_2CuO_{4+\delta}$," *Physica C* **213**, 271 (1993).

S. J. Pennycook and D. E. Jesson, "Atomic Resolution Z-Contrast Imaging of Interfaces," *Acta. Metall. Mater.* **40**, S149 (1992).

S. J. Pennycook, M. F. Chisholm, D. E. Jesson, R. Feenstra, S. Zhu, X. Y. Zheng, and D. H. Lowndes, "Growth and Relaxation Mechanisms of $YBa_2Cu_3O_{7-x}$ Films," *Physica C* **202**, 1 (1992).

S. J. Pennycook, R. Feenstra, M. F. Chisholm, and D. P. Norton, "Amorphization and Recrystallization of $YBa_2Cu_3O_{7-x}$ by Ion Implantation and Annealing," *Nucl. Instrum. and Methods Phys. Res. Sect. B* **79**, 641 (1993).

S. J. Pennycook and D. E. Jesson, "Z-Contrast Imaging with a 300-kV STEM," *Microbeam Analysis* **2**, S208 (1993).

R. S. Pfeiffer and G. D. Mahan, "Mean-Field Theory of Elastic Dipoles on a Face-Centered-Cubic Lattice," *Phys. Rev. B* **48**, 669 (1993).

E. W. Plummer and P. A. Dowben, "When are Thin Films of Metals Metallic?" *Prog. Surf. Sci.* **42**, 201 (1993).

J. Rankin, P. Thevenard, L. J. Romana, L. A. Boatner, C. W. White, C. J. McHargue, and L. L. Horton, "Ion Bombardment, Ultrasonic, and Pulsed-Laser Beam Effects on Small Metallic Clusters of Potassium in MgO," *Surf. and Coat. Technol.* **51**, 471 (1992).

M. V. Rao, S. M. Gulwadi, S. Mulpuri, D. S Simons, P. H. Chi, O. W. Holland, and H. B. Dietrich," *J. Electron. Mater.* **21**, 923 (1992).

M. Rasolt and Z. Tesanovic, "Theoretical Aspects of Superconductivity in Very High Magnetic Fields," *Rev. Mod. Phys.* **64**, 709 (1992).

M. Rasolt and F. Perrot, "Spontaneously Symmetry-Broken-Current-Carrying States in a Strongly Inhomogeneous Interacting Two-Dimensional Fermi Liquid," *Phys. Rev. Lett.* **69**, 2563 (1992).

M. Rasolt, "Fluctuations in High-Ranking Tensor Order Parameters: Implication for the Orientational Transition of C_{60}," *Phys. Rev. B* **46**, 1944 (1992).

M. Rasolt, G. Vignale, and F. Perrot, "Current Density Functional Theory in a Continuum and Lattice Lagrangians: Application to Spontaneously Broken Chiral Ground States," *J. Quantum Chem.* **26**, 359 (1992).

M. Rasolt and F. Perrot, "Spontaneously Symmetry-Broken Current-Carrying States in Nanostructures," *Australian J. Phys.* **46**, 381 (1993).

J. A. Rice and J. S. Lin, "Fractal Nature of Humic Materials," *Environ. Sci. and Tech.* **27**, 413 (1993).

M. T. Robinson, "Review of 'Computer Simulation of Ion-Solid Interactions,' by Wolfgang Eckstein, *Springer Series in Materials Science*, Vol. 10 (Springer-Verlag, Berlin, 1991)," *Nucl. Instrum. and Methods Phys. Res. Sect. B* **71**, 354 (1992).

R. B. Rogge, Y. S. Yang, Z. Tun, B. D. Gaulin, J. A. Fernandez-Baca, R. M. Nicklow, and A. Harrison, "A Neutron Scattering Study of the Quasi-One-Dimensional, Dilute Ising-Like Antiferromagnet $CsCo_{0.83}Mg_{0.17}Br_3$," *J. Appl. Phys.* **73**, 6451 (1993).

A. G. Rojo, G. Kotliar, and G. S. Canright, "Sign of Equilibrium Hall Conductivity in Strongly Correlated Systems," *Phys. Rev. B* **47**, 9140 (1993).

A. G. Rojo and G. D. Mahan, "Nonlinear Polarizability of Correlated One-Dimensional Systems," *Phys. Rev. B* **47**, 1794 (1993).

L. J. Romana, P. S. Sklad, C. W. White, J. C. McCallum, A. Choudhury, L. L. Horton, and C. J. McHargue, "Formation and Annealing Behavior of an Amorphous Layer Induced by Tin Implantation Into Sapphire," *Surf. and Coat. Technol.* **51**, 415 (1992).

P. Saalfrank, J. Ladik, R. F. Wood, M. A. Abdel-Raouf, and C.-M. Liegener, "Ab Initio Cluster and Band Structure Calculations on Systems Modeling La_2CuO_4: Effects of Interplane Charge Transfer and Madelung Potentials," *Physica C* **196**, 340 (1992).

B. C. Sales, B. C. Chakoumakos, L. A. Boatner, and J. O. Ramey, "Structural Evolution of the Amorphous Solids Produced by Heating Crystalline $MgHPO_4 \bullet 3H_2O$," *J. Mater. Res.* **7**, 2646 (1992).

B. C. Sales, R. A. Zuhr, J. C. McCallum, and L. A. Boatner, "Electronic Damage in the Ion Beam Amorphization of $Pb_2P_2O_7$," *Phys. Rev. B* **46**, 3215 (1992).

B. C. Sales, B. C. Chakoumakos, L. A. Boatner, and J. O. Ramey, "Structural Properties of the Amorphous Phases Produced by Heating Crystalline $MgHPO_4 \bullet 3H_2O$," *J. Non.-Cryst. Solids* **159**, 121 (1993).

B. A. Sanborn, P. B. Allen, and G. D. Mahan, "Theory of Screening and Electron Mobility: Applications to *n*-Type Silicon," *Phys. Rev. B* **46**, 15123 (1992).

A. R. Sandy, S. G. J. Mochrie, D. M. Zehner, G. Grübel, K. G. Huang, and D. Gibbs, "Reconstruction of the Pt(111) Surface," *Phys. Rev. Lett.* **68**, 2192 (1992).

A. R. Sandy, S. G. J. Mochrie, D. M. Zehner, G. Grübel, K. G. Huang, and D. Gibbs, "Au(111) and Pt(111) Surface Phase Behavior," *Surf. Sci.* **287/288**, 321 (1993).

T. Scherban, A. S. Nowick, L. A. Boatner, and M. M. Abraham, "Protons and Other Defects in Fe-Doped $KTaO_3$," *Appl. Phys. A* **55**, 324 (1992).

R. P. Setna, J. M. Hyde, A. Cerezo, G. D. W. Smith, and M. F. Chisholm, "Position-Sensitive Atom Probe Study of the Decomposition of a Cu-2.6 at.% Co Alloy," *Appl. Surf. Sci.* **67**, 368 (1993).

J. W. Sharp and D. Eres, "In Situ Observation of Surface-Limited Ge Growth Processes by Transient Optical Reflectometry," *J. Cryst. Growth* **125**, 553 (1992).

J. W. Sharp and G. Eres, "Kinetics of Hydrogen Desorption in Surface-Limited Thin-Film Growth of SiGe Alloys," *Appl. Phys. Lett.* **62**, 2807 (1993).

Y. Shigesato, D. C. Paine, and T. E. Haynes, "Study of the Effect of Ion Implantation on the Electrical and Microstructural Properties of Tin-Doped Indium Oxide Thin Films," *J. Appl. Phys.* **73**, 3805 (1993).

Y. Shigesato, D. C. Paine, and T. E. Haynes, "Lattice Defects in O^+-Implanted Tin-Doped Indium Oxide Films," *Jpn. J. Appl. Phys.* **32**, L1352 (1993).

L. Siller, K. M. Hock, R. E. Palmer, and J. F. Wendelken, "Resonance Electron Scattering by Adsorbed Molecules: σ^* Resonance Energy Versus Bond Length," *Surf. Sci.* **287/288**, 165 (1993).

L. Siller, R. E. Palmer, and J. F. Wendelken, "Resonant Excitation of Low-Frequency Modes in Electron Scattering by Physisorbed O_2 on Pt(111)," *J. Chem. Phys.* **99**, 7175 (1993).

P. S. Sklad, C. J. McHargue, C. W. White, and G. C. Farlow, "Analytical Electron Microscopy of Al_2O_3 Implanted with Iron Ions," *J. Mater. Sci.* **27**, 5895 (1992).

S. D. Smith, R. J. Spontak, M. M. Satkowski, A. Ashraf, and J. S. Lin, "Microdomain Contraction in Microphase-Separated Multiblock Copolymers," *Phys. Rev. B* **47**, 14555 (1993).

S. Spooner, "Using Federal X-Ray, Electron, and Neutron Facilities," *J. Min. Met. Mater. Soc.* **3**, 72 (1992).

Y. R. Sun, J. R. Thompson, D. K. Christen, F. Holtzberg, A. D. Marwick, and J. G. Ossandon, "The Temperature- and Field-Dependent Activation Energy of a Proton-Irradiated YBCO Single Crystal," *Physica C* **194**, 403 (1992).

Y. R. Sun, J. R. Thompson, D. K. Christen, J. G. Ossandon, Y. J. Chen, and A. Goyal, "Effects of Field-Sweep Rate on the Magnetization of Melt-Textured $YBa_2Cu_3O_{7-\delta}$," *Phys. Rev. B* **46**, 8480 (1992).

Y. R. Sun, J. R. Thompson, Y. J. Chen, D. K. Christen, and A. Goyal, "Strong Evidence for Vortex-Glass—Collective-Pinning Theory in $YBa_2Cu_3O_7$ Superconductors," *Phys. Rev. B* **47**, 14481 (1993).

G. Sundar, J. J. Hoyt, and S. Spooner, "Nucleation and Growth in Al-Zn: A Test of the Langer-Schwartz Model," *Phys. Rev. B* **46**, 14266 (1992).

E. Takasuka, K. Asai, K. Fujita, M. F. Chisholm, and S. J. Pennycook, "High-Resolution Z-Contrast Observation of GaAs/Si Hetero-Interfaces Through Scanning Transmission Electron Microscope," *Jpn. J. Appl. Phys. (Part 2)* **31**, L1788 (1992).

J. R. Thompson, J. G. Ossandon, D. K. Christen, Y. R. Sun, B. C. Sales, H. R. Kerchner, J. E. Tkaczyk, and K. W. Lay, "Systematics of Flux Pinning Versus Oxygen Deficiency δ in Aligned $YBa_2Cu_3O_{7-\delta}$ Materials," *Cryogenics* **32**, 982 (1992).

J. R. Thompson, Y. R. Sun, L. Civale, A. P. Malozemoff, M. W. McElfresh, A. D. Marwick, and F. Holtzberg, "Effect of Flux Creep on the Temperature Dependence of the Current Density in Y-Ba-Cu-O Crystals," *Phys. Rev. B* **47**, 14440 (1993).

J. R. Thompson, Y. R. Sun, H. R. Kerchner, D. K. Christen, B. C. Sales, B. C. Chakoumakos, A. D. Marwick, L. Civale, and J. O. Thomson, "Enhanced Current Density J_C and Extended Irreversibility in Single-Crystal $Bi_2Sr_2CaCu_2O_8$ via Linear Defects from Heavy Ion Irradiation," *Appl. Phys. Lett.* **60**, 2306 (1992).

T. Thundat, B. C. Sales, B. C. Chakoumakos, L. A. Boatner, D. P. Allison, and R. J. Warmack, "Atomic Layer-by-Layer Surface Removal by Force Microscopy," *Surf. Sci. Lett.* **293**, L863 (1993).

J. Z. Tischler, B. C. Larson, G. E. Ice, and P. Zschack, "Time-Structure and Mössbauer Filtering of Nuclear Bragg Scattering from a Mosaic $^{57}Fe_2O_3$ Crystal," *Phys. Rev. B* **47**, 552 (1993).

J. E. Tkaczyk, J. A. DeLuca, P. L. Karas, P. J. Bednarczyk, D. K. Christen, C. E. Klabunde, and H. R. Kerchner, "Enhanced Transport Critical Current at High Fields After Heavy Ion Irradiation of Textured $TlBa_2Ca_2Cu_3O_z$ Thick Films," *Appl. Phys. Lett.* **62**, 3031 (1993).

Y. Tsunoda and J. W. Cable, "Cu-Mn: Atomic Short-Range Order, Spin-Density Wave, and Spin Glass," *Phys. Rev. B* **46**, 930 (1992).

C. E. Vallet, A. Choudhury, P. E. Sobol, and C. W. White, "XPS Characterization of Anodic Layers Grown on Ir- and Rh-Implanted Titanium," *Electrochimica Acta* **38**, 1313 (1993).

J. Vellanki, R. K. Nadella, M. V. Rao, O. W. Holland, D. S. Simons, and P. H. Chi, "MeV-Energy Fe and Co Implants to Obtain Buried Insulating Layers and to Compensate Donor Implant Tails in InP," *J. Appl. Phys.* **73**, 1126 (1993).

J. M. Williams, I.-S. Lee, and R. A. Buchanan, "Charge Injection Properties of Iridium Oxide Films Produced on Ti-Y-Al-4V Alloy Substrates by Ion-Beam Mixing Techniques," *Surf. and Coat. Technol.* **51**, 385 (1992).

S. P. Withrow, C. W. White, R. A. Zuhr, J. W. McCamy, S. J. Pennycook, and D. M. Hembree, Jr., "Analysis of C Films Formed on Single-Crystal Cu by Ion Implantation and Laser Annealing," *J. Appl. Phys.* **72**, 3485 (1992).

J. Y. C. Wong, L. Zhang, G. Kakarantzas, P. D. Townsend, P. J. Chandler, and L. A. Boatner, "Ion-Implanted Optical Waveguides in $KTaO_3$," *J. Appl. Phys.* **71**, 49 (1992).

W. Wu, G. D. Wignall, and L. Mandelkern, "A SANS Study of the Plastic Deformation Mechanism in Polyethylene," *Polymer* **33**, 4137 (1992).

Y. S. Yang, B. D. Gaulin, J. A. Fernandez-Baca, N. Ali, and G. D. Wignall, "Small-Angle Neutron Scattering Studies of $Ce(Fe_{1-x}Al_x)_2$," *J. Appl. Phys.* **73**, 6066 (1993).

M. Yethiraj, H. A. Mook, G. D. Wignall, R. Cubitt, E. M. Forgan, D. M. Paul, and T. Armstrong, "Small-Angle Neutron Scattering Study of Flux-Line Lattices in Twinned $YBa_2Cu_3O_7$," *Phys. Rev. Lett.* **70**, 857 (1993).

J. Yi and G. S. Canright, "Spontaneous Magnetization of Anyons with Long-Range Repulsion," *Phys. Rev. B* **47**, 273 (1993).

R. T. Young, K. H. Young, M. D. Muller, S. R. Ovshinsky, J. D. Budai, C. W. White, and J. S. Martens, "High-Quality Epitaxial YBCO(F) Films Directly Deposited on Sapphire," *Physica C* **200**, 437 (1992).

P. A. Zeijlmans van Emmichoven, C. C. Havener, I. G. Hughes, D. M. Zehner, and F. W. Meyer, "Emission of Low-Energy Electrons from Multicharged Ions Interacting with Metal Surfaces," *Phys. Rev. A* **47**, 3998 (1993).

L. Zhang and X.-W. Wang, "Critical Exponents for the Three-Dimensional Superfluid—Bose-Glass Phase Transition," *Phys. Rev. B* **47**, 11518 (1993).

X.-Y. Zheng, D. H. Lowndes, S. Zhu, J. D. Budai, and R. J. Warmack, "Early Stages of $YBa_2Cu_3O_{7-\delta}$ Epitaxial Growth on MgO and $SrTiO_3$," *Phys. Rev. B* **45**, 7584 (1992).

S. Zhu, D. K. Christen, C. E. Klabunde, J. R. Thompson, E. C. Jones, R. Feenstra, D. H. Lowndes, and D. P. Norton, "Superconducting Transport Properties of Epitaxial $YBa_2Cu_3O_{7-\delta}$ Thin Films: A Consistent Description Based on Thermally Activated Flux Motion," *Phys. Rev. B* **46**, 5576 (1992).

S. Zhu, D. H. Lowndes, B. C. Chakoumakos, J. D. Budai, D. K. Christen, X.-Y. Zheng, E. C. Jones, and B. Warmack, "In Situ Growth of Epitaxial $Bi_2Sr_2CaCu_2O_{8-x}$ and $Bi_2Sr_2CuO_{6-x}$ Films by Pulsed-Laser Ablation," *Appl. Phys. Lett.* **63**, 409 (1993).

S. Zhu, D. H. Lowndes, B. C. Chakoumakos, S. J. Pennycook, X.-Y. Zheng, and R. J. Warmack, "Growth Mechanisms and Superconductivity of Ultrathin $YBa_2Cu_3O_{7-x}$ Epitaxial Films on (001) MgO Substrates," *Appl. Phys. Lett.* **62**, 3363 (1993).

J.-K. Zuo and D. M. Zehner, "Terrace Width and Step-Height Enlargement: Reconstruction of the TaC(310) Surface," *Phys. Rev. B* **46**, 16122 (1992).

J.-K. Zuo, R. J. Warmack, D. M. Zehner, and J. F. Wendelken, "Periodic Faceting on TaC(110): Observations Using High-Resolution Low-Energy Electron Diffraction and Scanning Tunneling Microscopy," *Phys. Rev. B* **47**, 10743 (1993).

J.-K. Zuo and J. F. Wendelken, "Experimental Study of Smoothing Kinetics on a Rough Surface," *Phys. Rev. Lett.* **70**, 1662 (1993).

BOOKS AND PROCEEDINGS

J. B. Bates, G. R. Gruzalski, N. J. Dudney, and C. F. Luck, "New Amorphous Thin-Film Lithium Electrolyte and Rechargeable Microbattery," p. 337 in *Proceedings of 35th International Power Sources Symposium*, Institute of Electrical and Electronics Engineers, Piscataway, New Jersey, 1993.

J. B. Bates, G. R. Gruzalski, and C. F. Luck, "Rechargeable Solid State Lithium Microbatteries," p. 82 in *Proceedings of IEEE Workshop on Micro Electro Mechanical Systems*, Institute of Electrical and Electronics Engineers, Piscataway, New Jersey, 1993.

N. D. Browning and S. J. Pennycook, "Application of Z-Contrast Imaging to Obtain Column-by-Column Spectroscopic Analysis of Materials," p. 279 in *Atomic-Scale Imaging of Surfaces and Interfaces*, ed. by D. K. Biegelsen, D. J. Smith, and S. Y. Tong, Materials Research Society, Pittsburgh, Pennsylvania, 1993.

N. D. Browning, M. M. McGibbon, M. F. Chisholm, and S. J. Pennycook, "Atomic-Resolution Characterization of Interface Structures by Electron Energy Loss Spectroscopy," p. 576 in *Proceedings of the 51st Annual Meeting of the Microscopy Society of America*, ed. by G. W. Bailey and C. L. Rieder, San Francisco Press, Inc., San Francisco, California, 1993.

J. W. Cable and Y. Tsunoda, "Atomic Short-Range Order and Spin Density Wave Propagation in CuMn," p. 663 in *International Conference on the Physics of Transition Metals*, Vol. II, ed. by P. M. Oppeneer and J. Kübler, World Scientific, Singapore, New Jersey, London, Hong Kong, 1993.

G. S. Canright, "From Path Integrals to Anyons," p. 174 in *Lectures on Path Integration: Trieste 1991*, World Scientific, Singapore, New Jersey, London, Hong Kong, 1993.

M. F. Chisholm, D. E. Jesson, S. J. Pennycook, and S. Mantl, "Z-Contrast Imaging of an Ordered Interface Structure in the $Si/CoSi_2/Si$ System," p. 802 in *Proceedings of the 51st Annual Meeting of the Electron Microscopy Society of America*, ed. by G. W. Bailey and C. L. Rieder, San Francisco Press, Inc., San Francisco, California, 1993.

D. K. Christen, J. R. Thompson, H. R. Kerchner, B. C. Sales, B. C. Chakoumakos, L. Civale, A. D. Marwick, and F. Holtzberg, "Limits to Critical Currents in High-Temperature Superconductors: What We Can Learn From Tailored Defects," p. 24 in *Superconductivity and Its Applications*, Vol. 273, ed. by H. S. Kwok, D. T. Shaw, and M. J. Naughton, American Institute of Physics, New York, 1993.

D. Eres and J. W. Sharp, "Temperature-Dependent Evolution of Chemisorbed Digermane in Ge Thin-Film Growth," p. 243 in *Interface Dynamics and Growth*, ed. by K. S. Liang, M. P. Anderson, R. F. Bruinsma, and G. Scoles, Materials Research Society, Pittsburgh, Pennsylvania, 1992.

Y. N. Erokin, B. K. Patnaik, S. Pramanick, F. Hong, C. W. White, and G. A. Rozgony, "Thin Ni Silicon Formation by Low-Temperature-Induced Metal Atom Reaction with Ion-Implanted Amorphous Silicon," p. 237 in *Beam Solid Interactions*, ed. by M. A. Nastasi, N. Herbots, L. R. Harriott, and R. S. Averback, Materials Research Society, Pittsburgh, Pennsylvania, 1993.

R. Feenstra, D. K. Christen, C. E. Klabunde, J. D. Budai, M. D. Galloway, S. J. Pennycook, D. P. Norton, and D. H. Lowndes," Properties of Low-Temperature, Low Oxygen Pressure Postannealed $YBa_2Cu_3O_{7-x}$ Thin Films," p. 331 in *High-T_c Superconductor Thin Films*, ed. by L. Correra, North-Holland Elsevier Science Publishers B.V., Amsterdam, the Netherlands, 1992.

R. Feenstra, D. P. Norton, J. D. Budai, D. K. Christen, D. H. Lowndes, V. C. Matijasevic, C.-B. Eom, T. H. Geballe, E. S. Hellman, and E. H. Hartford, "T_c-δ Relations in $YBa_2Cu_3O_{7-\delta}$ Thin Films: Effects of Oxygen Pressure During Growth," p. 101 in *Layered Superconductors: Fabrication, Properties, and Applications*, ed. by D. T. Shaw, C. C. Tsuei, T. R. Schneider, and Y. Shiohara, Materials Research Society, Pittsburgh, Pennsylvania, 1992.

A. T. Fiory, P. K. Roy, and G. E. Jellison, Jr., "Ion Channeling and Spectroscopic Ellipsometry Examinations of Thin-Film SiO_2/EPI-Si (001) Structures," p. 131 in *Chemical Surface Preparation, Passivation, and Cleaning for Semicondutor Growth and Processing*, ed. by R. J. Nemanich, C. R. Helms, M. Hirose, and G. W. Rubloff, Materials Research Society, Pittsburgh, Pennsylvania, 1992.

R. S. Fishman and S. H. Liu, "Impurity Effects on the Magnetic Ordering in Chromium," p. 620 in *International Conference on the Physics of Transition Metals*, Vol. II, ed. by P. M. Oppeneer and J. Kübler, World Scientific, Singapore, New Jersey, London, Hong Kong, 1993.

D. J. W. Geldart and M. Rasolt, "Energy Functionals for Inhomogeneous Many-Electron Systems," p. 123 in *Strongly Correlated Electron Systems*, ed. by M. P. Das and D. Nelson, Nova Science Publishers, Inc., Commack, New York, 1992.

D. B. Geohegan, "Spectroscopic and Ion Probe Characterization of Laser Produced Plasmas Used for Thin-Film Growth," p. 28 in *Laser Ablation—Mechanisms and Applications Proceedings*, ed. by J. C. Miller and R. F. Haglund, Jr., Springer-Verlag, Berlin, Germany, 1992.

D. B. Geohegan, "Effects of Ambient Background Gases on YBCO Plume Propagation Under Film Growth Conditions: Spectroscopic, Ion Probe, and Fast Photographic Studies," p. 73 in *Laser Ablation of Electronic Materials: Basic Mechanisms and Applications*, ed. by E. Fogarassy and S. Lazare, Elsevier Science Publishers, Amsterdam, the Netherlands, 1992.

D. B. Geohegan, "Fast-ICCD Photography and Gated Photon Counting Measurements of Blackbody Emission from Particulates Generated in the KrF-Laser Ablation of BN and YBCO," p. 27 in *Laser Ablation in Materials Processing: Fundamentals and Applications*, ed. by B. Braren, J. Dubowski, and D. P. Norton, Materials Research Society, Pittsburgh, Pennsylvania, 1993.

B. L. Giammara, J. M. Williams, D. J. Birch, and J. J. Dobbins, "Quantitative Ruthenium Method for Analysis of Nitrogen Ion-Implanted Titanium Alloy (Ti-6Al-4V) and the Effect on Bacterial Adherence," p. 247 in *Tissue-Inducing Biomaterials*, ed. by L. G. Cima, M. Flanagan, and E. Ron, Materials Research Society, Pittsburgh, Pennsylvania, 1992.

R. F. Haglund, R. H. Magruder, L. Yang, J. E. Wittig, and R. A. Zuhr, "Optical Characteristics of Cu-Nanocluster Layers Assembled by Ion Implantation," p. 1239 in *Proceedings of Conference on Physics and Chemistry of Finite Systems*, ed. by P. Jena, S. N. Khasma, and B. K. Rao, Kluwer Academic Publishers, Amsterdam, the Netherlands, 1992.

R. F. Haglund, Jr., L. Yang, R. H. Magruder III, K. Becker, J. E. Wittig, C. W. White, R. A. Zuhr, L. Yang, R. Dorsinville, and R. R. Alfano, "Metal-Nanocluster Composites Made by Ion Implantation: A Novel Third-Order Nonlinear Material," p. 113 in *Nonlinear Optical Properties of Advanced Materials*, ed. by S. Etemad, International Society for Optical Engineering, Bellingham, Washington, 1993.

T. E. Haynes, O. W. Holland, and U. V. Desnica, "Damage Accumulation in Gallium Arsenide During Silicon Implantation Near Room Temperature," p. 823 in *Advanced III–V Compound Semiconductor Growth, Processing, and Devices*, ed. by S. J. Pearton, D. K. Sadana, and J. M. Zavada, Materials Research Society, Pittsburgh, Pennsylvania, 1992.

T. E. Haynes, R. Morton, and S. S. Lau, "Lattice Damage in Ion-Implanted Compound Semiconductors and Its Effect on Electrical Activation," p. 311 in *III–V Electronic and Photonic Device Fabrication and Performance*, ed. by K. S. Jones, H. Kanber, and S. J. Pearton, Materials Research Society, Pittsburgh, Pennsylvania, 1993.

T. E. Haynes, C. Lee, and K. S. Jones, "Time-Resolved Reflectivity Study of Solid-Phase-Epitaxial Regrowth in Relaxed and Strained $Si_{1-x}Ge_x$ Epilayers," p. 479 in *Semiconductor Heterostructures for Photonic and Electronic Applications*, ed. by D. C. Houghton, C. W. Tu, and R. T. Tung, Materials Research Society, Pittsburgh, Pennsylvania, 1993.

D. M. Hembree, Jr., D. F. Pedraza, G. R. Romanoski, S. P. Withrow, and B. K. Annis, "Raman Spectroscopy of C-Irradiated Graphite," p. 351 in *Beam-Solid Interactions*, ed. by M. A. Nastasi, N. Herbots, L. R. Harriott, and R. S. Averback, Materials Research Society, Pittsburgh, Pennsylvania, 1993.

D. O. Henderson, S. H. Morgan, R. Mu, N. Chen, R. H. Magruder III, C. W. White, and R. A. Zuhr, "A Vibrational Analysis of Au-Implanted Al_2O_3 Single Crystals: Ion and Thermal Annealing Effects," p. 439 in *Beam-Solid Interactions*, ed. by M. A. Nastasi, N. Herbots, L. R. Harriott, and R. S. Averback, Materials Research Society, Pittsburgh, Pennsylvania, 1993.

D. O. Henderson, S. H. Morgan, R. Mu, R. H. Magruder, III T. S. Anderson, J. E. Wittig, and R. A. Zuhr, "Optical and Infrared Spectra of Thermally Annealed Pb-Implanted SiO_2 Glasses," p. 190 in *Proceedings of Properties and Characteristics of Optical Glass III*, ed. by A. J. Marker III, International Society for Optical Engineering, Bellingham, Washington, 1992.

B. J. Heuser, S. Spooner, C. J. Glinka, D. L. Gilliam, N. A. Winslow, and M. S. Boley, "Structural Investigation of Electrochemically Etched Silicon," p. 209 in *Nanophase and Nanocomposite Materials*, ed. by Sridhar Komarren, John C. Parker, and George J. Thomas, Materials Research Society, Pittsburgh, Pennsylvania, 1993.

T. M. Holden, K. Mikke, E. Fawcett, and J. A. Fernandez-Baca, "The Magnetism of Metallic Manganese Alloys," p. 644 in *International Conference on the Physics of Transition Metals*, Vol. II, ed. by P. M. Oppeneer and J. Kübler, World Scientific, Singapore, New Jersey, London, Hong Kong, 1993.

I. G. Hughes, C. C. Havener, S. H. Overbury, M. T. Robinson, D. M. Zehner, P. A. Zeijlmans van Emmichoven, and F. W. Meyer, "Incident Ion Charge State Dependence of Electron Emission During Slow Multicharged Ion-Surface Interactions," p. 610 in *Proceedings of VIth International Conference on the Physics of Highly-Charged Ions*, Vol. 274, ed. by P. Richard, M. Stökei, C. L. Cooke, and C. D. Lin, American Institute of Physics, New York, 1993.

G. E. Jellison, Jr., M. Keefer, and L. Thornquist, "Spectroscopic Ellipsometry and Interference Reflectometry Measurements of CVD Silicon Grown on Oxidized Silicon," p. 561 in *Microcrystalline Semiconductors—Materials Science and Devices*, ed. by Y. Aoyagi, L. T. Canham, P. M. Fauchet, and I. Shimizu, Materials Research Society, Pittsburgh, Pennsylvania, 1993.

G. E. Jellison, Jr., D. H. Lowndes, and R. F. Wood, "The Optical Functions of Silicon at Elevated Temperatures and Their Application to Pulsed Laser Annealing," p. 344 in *Proceedings of the Conference on Rapid Thermal Processing '93*, ed. by R. B. Fair and B. Lojek, Scottsdale, Arizona, 1993.

D. E. Jesson, S. J. Pennycook, J.-M. Baribeau, and D. C. Houghton, "Step-Driven Surface Segregation and Ordering During Si-Ge MBE Growth," p. 9 in *Mechanisms of Heteroepitaxial Growth*, ed. by M. F. Chisholm, R. Hull, L. J. Schowalter, and B. J. Garrison, Materials Research Society, Pittsburgh, Pennsylvania, 1992.

D. E. Jesson and S. J. Pennycook, "Incoherence in Atomic-Resolution Z-Contrast Imaging," p. 978 in *Proceedings of the 51st Annual Meeting of the Electron Microscopy Society of America*, ed. by G. W. Bailey and C. L. Rieder, San Francisco Press, Inc., San Francisco, California, 1993.

D. E. Jesson, S. J. Pennycook, J.-M. Baribeau, and D. C. Houghton, "Evolving Surface Cusps During Strained-Layer Epitaxy," p. 47 in *Common Themes and Mechanisms of Epitaxial Growth*, ed. by P. Fuoss, J. Tsao, D. W. Kisker, A. Zangwill, and T. Kuech, Materials Research Society, Pittsburgh, Pennsylvania, 1993.

K. S. Jones, H. G. Robinson, T. E. Haynes, M. D. Deal, C. C. Lee, and E. L. Allen, "Defects and Diffusion in Si^+-Implanted GaAs," p. 323 in *III–V Electronic and Photonic Device Fabrication and Performance*, ed. by K. S. Jones, H. Kanber, and S. J. Pearton, Materials Research Society, Pittsburgh, Pennsylvania, 1993.

D. L. Joslin, L. J. Romana, C. W. White, C. J. McHargue, P. A. Thévenard, and L. L. Horton, "Temperature Effects in Ion Beam Mixing of Oxide-Oxide Interfaces," p. 351 in *Phase Formation and Modification by Beam-Solid Interactions*, ed. by G. S. Was, L. E. Rehn, and D. M. Follstaedt, Materials Research Society, Pittsburgh, Pennsylvania, 1992.

H. R. Kerchner, C. E. Klabunde, D. K. Christen, J. D. Budai, D. H. Lowndes, D. P. Norton, and J. O. Thomson, "Anisotropic Electrical Resistivity of YBCO/PBCO Superlattice Films Grown on Miscut Substrates," p. 353 in *Layered Superconductors: Fabrication, Properties, and Applications*, ed. by D. T. Shaw, C. C. Tsuei, T. R. Schneider, and Y. Shiohara, Materials Research Society, Pittsburgh, Pennsylvania, 1992.

B. S. Kwak, K. Zhang, A. Erbil, B. J. Wilkens, J. D. Budai, M. F. Chisholm, and L. A. Boatner, "MOCVD of Epitaxial Ferroelectric Lead Titanate Thin Films," p. 203 in *Ceramic Transactions, Vol. 25: Symposium on Ferroelectric Films*, ed. by A. F. Bhalla and A. S. Nair, American Ceramic Society, Westerville, Ohio, 1992.

S. H. Liu, "Fractals," p. 416 in *McGraw-Hill Encyclopedia of Science and Technology*, McGraw-Hill Publishing Company, New York, 1992.

S. H. Liu, "Electronic Polaron Effects in Mixed Valence and Heavy Fermion Materials," p. 9 in *International Conference on the Physics of Transition Metals*, Vol. I, ed. by P. M. Oppeneer and J. Kübler, World Scientific, Singapore, New Jersey, London, Hong Kong, 1993.

D. H. Lowndes, D. P. Norton, S. Zhu, and X.-Y. Zheng, "Laser Ablation Synthesis and Properties of Epitaxial $YBa_2Cu_3O_{7-\delta}/PrBa_2Cu_3O_{7-\delta}$ Superconductor Superlattices," p. 265 in *Laser Ablation of Electronic Materials: Basic Mechanisms and Applications*, ed. by E. Fogarassy, and S. Lazare, Elsevier Science Publishers, Amsterdam, the Netherlands, 1992.

D. H. Lowndes, D. P. Norton, S. Zhu, and X.-Y. Zheng, "Superconducting Properties and Microstructure of Epitaxial $YBa_2Cu_3O_{7-\delta}/PrBa_2Cu_3O_{7-\delta}$ Superlattices," p. 29 in *Advances in Superconductivity IV*, ed. by H. Hayakawa and N. Koshizuka, Springer-Verlag, Tokyo, Japan, 1992.

D. H. Lowndes and D. P. Norton, "Kosterlitz-Thouless-Like Behavior Over Extended Ranges of Temperature and Layer Thickness in Crystalline $YBa_2Cu_3O_{7-x}/PrBa_2Cu_3O_{7-x}$ Superlattices," p. 377 in *High-Temperature Superconductivity*, ed. by J. Ashkenazi, S. E. Barnes, F. Zuo, G. C. Vezzoli, and B. M. Klein, Plenum Publishing Corporation, New York, 1992.

D. H. Lowndes, M. DeSilva, M. J. Godbole, A. J. Pedraza, and D. B. Geohegan, "Ablation, Melting, and Smoothing of Polycrystalline Alumina by Pulsed Excimer Laser Radiation," p. 191 in *Laser Ablation in Materials Processing*, ed. by B. Braren, J. J. Dubowski, and D. P. Norton, Materials Research Society, Pittsburgh, Pennsylvania, 1993.

R. H. Magruder III, D. O. Henderson, S. H. Morgan, and R. A. Zuhr, "Optical and Infrared Spectroscopy of Laser-Irradiated Bi-Implanted SiO_2 Glasses," p. 383 in *Phase Formation and Modification by Beam-Solid Interactions*, ed. by G. S. Was, D. M. Follstaedt, and L. E. Rehn, Materials Research Society, Pittsburgh, Pennsylvania, 1992.

R. H. Magruder III, R. F. Haglund, L. Yang, J. E. Wittig, K. Becker, and R. A. Zuhr, "Picosecond Nonlinear Optical Response of Copper Clusters Created by Ion Implantation in Fused Silica," p. 369 in *Optical Waveguide Materials*, ed. by M. M. Broder, G. H. Siegel, R. Th. Karsten, and H. Kawazoe, Materials Research Society, Pittsburgh, Pennsylvania, 1992.

R. H. Magruder III, D. L. Kinser, J. E. Wittig, and R. A. Zuhr, "Structure Property Relationships of Nanometer-Size Metal Clusters in Glasses," p. 180 in *Proceedings of Properties and Characteristics of Optical Glass III*, ed. by A. J. Marker III, International Society for Optical Engineering, Bellingham, Washington, 1992.

G. D. Mahan, B. A. Sanborn, and P. B. Allen, "Mobility of Electrons and Holes in Semiconductors," p. 76 in *Physics and Simulation of Optoelectronic Devices*, ed. by David Yevick, International Society for Optical Engineering, Bellingham, Washington, 1992.

V. C. Matijasevic, R. H. Hammond, P. Rosenthal, K. Shinohara, A. F. Marshall, M. R. Beasley, and R. Feenstra, "Evidence for Cation Disorder in In-Situ Grown YBaCuO Superconducting Films," p. 353 in *High-T_c Superconductor Thin Films*, ed. by L. Correra, North-Holland Elsevier Science Publishers B.V., Amsterdam, the Netherlands, 1992.

J. C. McCallum, T. W. Simpson, I. V. Mitchell, J. Rankin, and L. A. Boatner, "Annealing of Pb-Implanted $SrTiO_3$ in the Presence of Water Vapor: A Study Using $D_2{}^{18}O$ Labeling," p. 419 in *Phase Formation and Modification by Beam-Solid Interactions*, ed. by G. S. Was, L. E. Rehn, and D. M. Follstaedt, Materials Research Society, Pittsburgh, Pennsylvania, 1992.

J. W. McCamy, D. H. Lowndes, J. D. Budai, B. C. Chakoumakos, and R. A. Zuhr, "Growth of Epitaxial ZnS Films by Pulsed-Laser Ablation," p. 243 in *Wide Band-Gap Semiconductors*, ed. by T. D. Moustakas, J. I. Pankove, and Y. Hamakawa, Materials Research Society, Pittsburgh, Pennsylvania, 1992.

J. W. McCamy, D. H. Lowndes, and J. D. Budai, "Growth of Epitaxial ZnS, ZnSe, and ZnS-ZnSe Multilayers on GaAs by Pulsed-Laser Ablation," p. 357 in *Extended Absracts of the 1992 International Conference on Solid State Devices and Materials*, ed. by Y. Hayashi, C. Hamaguchi, E. Takeda, and M. Yamaguchi, The Japanese Society of Applied Physics, Tokyo, Japan, 1992.

J. W. McCamy, D. H. Lowndes, J. D. Budai, G. E. Jellison, Jr., I. P. Herman, and S. Kim, "Epitaxial ZnS, ZnSe, and ZnS/ZnSe Superlattices Grown on (001)GaAs by Pulsed-Laser Ablation," p. 471 in *Laser Ablation in Materials Processing: Fundamentals and Applications*," ed. by B. Braren, J. J. Dubowski, and D. P. Norton, Materials Research Society, Pittsburgh, Pennsylvania, 1993.

K. Mikke, T. M. Holden, J. A. Fernandez-Baca, E. Fawcett, and J. Jankowska-Kisielinska, "High-Energy Magnetic Excitations in Single-Domain Homogeneous Antiferromagnetic γ-Mn(18%Cu) Alloy at 10 K," p. 659 in *International Conference on the Physics of Transition Metals*, Vol. II, ed. by P. M. Oppeneer and J. Kübler, World Scientific, Singapore, New Jersey, London, Hong Kong, 1993.

S. G. J. Mochrie, D. Gibbs, and D. M. Zehner, "Phase Behavior of Monolayers," p. 336 in *Materials Interfaces: Atomic-Level Structure and Properties*, ed. by D. Wolf and S. Yip, Chapman and Hall, London, 1992.

S. H. Morgan, D. O. Henderson, Z. Pan, R. H. Magruder III, and R. A. Zuhr, "Characterization of Thermal-Annealed Bi-Implanted Silica," p. 327 in *Beam-Solid Interactions*, ed. by M. A. Nastasi, N. Herbots, L. R. Harriott, and R. S. Averback, Materials Research Society, Pittsburgh, Pennsylvania, 1993.

D. R. Mullins and P. F. Lyman, "Methanethinol on W(001) and Ru(0001)," p. 99 in *Proceedings of the 25th SRC Users Group Meeting*, University of Wisconsin, Stoughton, Wisconsin, 1992.

D. R. Mullins, S. H. Overbury, and P. F. Lyman, "The Adsorption of Sulfur on W(001)," p. 101 in *Proceedings of the 25th SRC Users Group Meeting*, University of Wisconsin, Stoughton, Wisconsin, 1992.

D. P. Norton, D. H. Lowndes, Z.-Y. Zheng, R. Feenstra, and S. Zhu, "Properties of Epitaxial $YBa_2Cu_3O_{7-\delta}$-Based Superconducting Superlattices," p. 33 in *Proceedings of the Fifth Annual Conference on Superconductivity and Applications*, ed. by Y. H. Kao, A. E. Kaloyeros, and H. S. Kwok, American Institute of Physics, New York, 1992.

D. P. Norton and D. H. Lowndes, "Growth and Properties of Ultrathin $YBa_2Cu_3O_{7-\delta}$ Layers Grown by Pulsed Laser Ablation," p. 73 in *Superconductivity and Its Applications*, Vol. 273, ed. by H. S. Kwok, D. T. Shaw, and M. J. Naughton, American Institute of Physics, New York, 1993.

M. E. O'Hern, L. J. Romana, C. J. McHargue, J. C. McCallum, and C. W. White, "The Effect of Crystal Orientation on Damage Accumulation in Chromium-Implanted Al_2O_3," p. 740 in *Effects of Radiation on Materials: 15th International Symposium*, ed. by R. Stoller, A. S. Kumar, and D. S. Gelles, American Society for Testing and Materials, Philadelphia, Pennsylvania, 1992.

S. Y. Park, R. H. Magruder,III, R. A. Weeks, and R. A. Zuhr, "Optical Bleaching of Bismuth-Implanted Silica Glass: A Threshold Effect," p. 291 in *Beam-Solid Interactions*, ed. by M. A. Nastasi, N. Herbots, L. R. Harriott, and R. S. Averback, Materials Research Society, Pittsburgh, Pennsylvania, 1993.

A. J. Pedraza, M. J. Godbole, M. J. DeSilva, and D. H. Lowndes, "Laser-Induced Surface Activation of Aluminum Oxide for Electroless Deposition," p. 203 in *Laser Ablation in Materials Processing: Fundamentals and Applications*, ed. by B. Braren, J. J. Dubowski, and D. P. Norton, Materials Research Society, Pittsburgh, Pennsylvania, 1993.

S. J. Pennycook, "Z-Contrast Transmission Electron Microscopy," p. 171 in *Annual Reviews of Materials Science*, Vol. 22, Annual Reviews, Inc., Palo Alto, California, 1992.

S. J. Pennycook and D. E. Jesson, "High-Resolution Imaging in the Scanning Transmission Electron Microscope," p. 333 in *Proceedings of the International School on Electron Microscopy in Materials Science*, World Scientific, Singapore, New Jersey, London, Hong Kong, 1992.

S. J. Pennycook, D. E. Jesson, and M. F. Chisholm, "Column-By-Column Compositional Imaging by Z-Contrast STEM," p. 1470 in *Proceedings of the 50th Meeting of the Electron Microscopy Society of America*, ed. by G. W. Bailey, J. Bentley, and J. A. Small, San Francisco Press, San Francisco, California, 1992.

S. J. Pennycook, D. E. Jesson, M. F. Chisholm, and N. D. Browning, "Atomic Resolution Imaging and Analysis with the STEM," p. 217 in *Proceedings of the XIII International Congress on X-Ray Optics and Microanalysis*, Conference Series No. 130, Institute of Physics, Bristol, United Kingdom, 1992.

S. J. Pennycook, D. E. Jesson, M. F. Chisholm, and N. D. Browning, "Insights into Semiconducting Materials and Growth Phenomena Through Z-Contrast STEM," p. 22 in *Proceedings of the 20th Annual Meeting of the Microscopical Society of Canada*, ed. by F. W. Doane, Microscopical Society of Canada, Toronto, Ontario, Canada, 1993.

S. J. Pennycook, N. D. Browning, M. F. Chisholm, S. Zhu, R. Feenstra, D. P. Norton, and D. H. Lowndes, "High-Resolution Z-Contrast Imaging and Hole Concentration Mapping of YBCO Thin Films," p. 103 in *Proceedings of the 1993 International Workshop in Superconductivity*, International Superconductivity Technology Center, Hakodate, Japan, 1993.

S. J. Pennycook, N. D. Browning, D. E. Jesson, and M. F. Chisholm, "Probing Interface Structure and Bonding at Atomic Resolution by STEM," p. 105 in *Proceedings of Multinational Congress on Electron Microscopy*, University of Parma, Parma, Italy, 1993.

M. Rasolt, "Thermodynamic and Transport Properties of Superconductors in Very High Magnetic Fields," p. 292 in *Physical Phenomena at High Magnetic Fields*, ed. by E. Manousakis, P. Schlottmann, P. Kumar, K. S. Bedell, and F. M. Mueller, Addison-Wesley Publishing Company, Redwood City, California, 1992.

M. Rasolt, "Comtemporary Topics in Band Theory," p. 1 in *Basic Properties of Semiconductors*, ed. by P. T. Landsberg, Elsevier Science Publishers B.V, Amsterdam, the Netherlands, 1992.

M. Rasolt, "Superconductivity Induced by Very High Magnetic Fields: Thermodynamic and Transport Properties," p. 223 in *Strongly Correlated Electron Systems*, Nova Publications, New York, 1992.

M. Ree, T. L. Nunes, and J. S. Lin, "X-Ray Scattering Studies of Polyimide Thin Films From Poly(amic acid)s Functionalized with a Methacrylate," p. 415 in *Advances in Polyimide Surface and Technology*, Technomics Publishing, Inc., Lancaster, Pennsylvania, 1992.

W. Rhine, R. Gottschall, and Y. Chen, eds., *Synthesis and Processing of Ceramics: Scientific Issues, and Defect Properties and Processing of High-Technology Nonmetallic Material*, North-Holland, New York, 1992.

M. T. Robinson, "Computer Simulation of Atomic-Collision Processes in Solids," p. 3 in *Beam-Solid Interactions*, ed. by M. A. Nastasi, N. Herbots, L. R. Harriott, and R. S. Averback, Materials Research Society, Pittsburgh, Pennsylvania, 1993.

J. H. Root, T. M. Holden, J. Schröder, S. Spooner, C. A. Hubbard, T. A. Dodson, and S. A. David, "Residual Stresses in a Multipass Ferritic Weldment," p. 99 in *International Trends in Welding Science and Technology*, ed. by S. A. David and J. M. Vitek, ASM International, Materials Park, Ohio, 1993.

J. W. Sharp and G. Eres, "Investigation of the Kinetics in Surface-Limited Thin-Film Growth of SiGe Alloys by CVD of Si_2H_6/Ge_2H_6 Mixtures," p. 433 in *Mechanisms of Epitaxial Growth*, ed. by M. F. Chisholm, R. Hull, L. J. Showalter, and B. J. Garrison, Materials Research Society, Pittsburgh, Pennsylvania, 1993.

E. Y. Sheu, M. M. De Tar, K. Kotlarchyk, J. S. Lin, M. Capel, and D. A. Storm, "Structural Evolution and Transition of a Three Component Dense Microemulsion System," p. 419 in *Supramolecular Aggregates in Solution and Structure Dynamics of Strongly Interacting Colloids*, ed. by S. H. Chen and J. S. Huang, The NATO Advanced Study Institute, Kluwer Publishers, Dordrecht, the Netherlands, 1992.

D. K. Shuh, L. J. Terminello, L. A. Boatner, and M. M. Abraham, "X-Ray Absorption Spectroscopy of the Rare-Earth Orthophosphates," p. 95 in *Applications of Synchrotron Radiation Techniques to Materials Science*, ed. by D. L. Perry, N. D. Shinn, R. L. Stockbauer, K. L. Damico, and L. J. Terminello, Materials Research Society, Pittsburgh, Pennsylvania, 1993.

T. P. Sjoreen, H.-J. Hinneberg, and M. F. Chisholm, "Ion Beam Synthesis of $IrSi_3$ by Implantation of 2-MeV Ir Ions," p. 243 in *Beam-Solid Interactions*, ed. by M. A. Nastasi, N. Herbots, L. R. Harriott, and R. S. Averback, Materials Research Society, Pittsburgh, Pennsylvania, 1993.

G. S. Smith, W. Hamilton, M. Fitzsimmons, S. M. Baker, K. M. Hubbard, M. Nastasi, J-P. Hirvonen, and T. G. Zocco, "Neutron Reflectometry Study of Thermally Induced Boron Diffusion in Amorphous Elemental Boron," p. 246 in *Proceedings of The Society of Photo-Optical InstrumentationEngineers*, International Society for Optical Engineering, Bellingham, Washington, 1993.

S. Spooner, S. A. David, J. H. Root, T. M. Holden, M. A. M. Bourke, and J. Goldstone, "Residual Stress and Strain Measurements in an Austenitic Steel Plate Containing a Multipass Weld," p. 139 in *International Trends in Welding Science and Technology*, ed. by S. A. David and J. M. Vitek, ASM International, Materials Park, Ohio, 1993.

G. W. Steadman, J. R. Brewster, J. D. Budai, and L. A. Boatner, "Textured Coatings from Colloidal Suspensions of Cubic-Faceted Nanophase MgO Particles," p. 33 in *Nanophase and Nanocomposite Materials*, ed. by S. Komarneni, I. C. Parker, and G. J. Thomas, Materials Research Society, Pittsburgh, Pennsylvania, 1993.

J. R. Thompson, C. Politis, and Y. C. Kim, "Properties of Materials with a Fine Length Scale: Mechanically Alloyed Metals and the High-Temperature Superconductor $YBa_2Cu_3O_7$," p. 545 in *Mechanical Alloying, Materials Sciences Forum 88–90*, ed. by P. H. Shingu, Transtech Publishers, Zürich, Switzerland, 1992.

J. R. Thompson, D. K. Christen, H. R. Kerchner, L. A. Boatner, B. C. Sales, B. Chakoumakos, H. Hsu, J. Brynestad, D. M. Kroeger, R. K. Williams, Y. Sun, Y. C. Kim, J. G. Ossandon, A. P. Malozemoff, L. Civale, A. D. Marwick, T. K. Worthington, and F. Holtzberg, "Studies of Non-Ideal Superconductors Using DC Magnetic Methods," p. 157 in *Magnetic Susceptibility of Superconductors and Other Spin Systems*, ed. by T. Francavilla, R. A. Hein, and D. Liebenburg, Plenum Press, New York, 1992.

J. R. Thompson, Y. R. Sun, D. K. Christen, H. R. Kerchner, A. P. Malozemoff, L. Civale, A. D. Marwick, T. K. Worthington, L. Krusin-Elbaum, M. W. McElfresh, and F. Holtzberg, "Magnetization Studies of Irradiation Modified Single-Crystal $YBa_2Cu_3O_7$ Superconductors: Flux Creep and Annealing Effects," p. 573 in *Physics and Materials Science of High-Temperature Superconductors–II*, ed. by R. Kossowski, B. Raveau, D. Wohllebin, and S. K. Patapis, Kluwer, Dordrecht, the Netherlands, 1992.

J. R. Thompson, "What Can We Learn From Magnetization Experiments on High-T_c Superconductors? An Overview," p. 23 in *Layered Superconductors: Fabrication, Properties, and Applications*, ed. by D. T. Shaw, C. C. Tsuei, T. R. Schneider, and Y. Shiohara, Materials Research Society, Pittsburgh, Pennsylvania, 1992.

J. R. Thompson, Y. R. Sun, J. G. Ossandon, D. K. Christen, H. R. Kerchner, B. C. Sales, B. C. Chakoumakos, L. Civale, A. D. Marwick, and F. Holtzberg, "Magnetic Studies of Current Conduction and Flux Pinning in High-T_c Cuprates: Virgin, Irradiated, and Oxygen-Deficient Materials," p. 179 in *Superconductivity and Its Applications*, Vol. 273, ed. by H. S. Kwok, D. T. Shaw, and M. J. Naughton, American Institute of Physics, New York, 1993.

J. R. Thompson, Y. R. Sun, J. G. Ossandon, D. K. Christen, H. R. Kerchner, B. C. Sales, B. C. Chakoumakos, L. Civale, A. D. Marwick, and F. Holtzberg, "Magnetization and Flux Pinning in High-T_c Cuprates: Virgin, Irradiated, and Oxygen-Deficient Materials," p. 232 in *Proceedings of Fifth US/Japan Workshop on High-T_c Superconductors*, Society of Non-Traditional Technology, Tokyo, Japan, 1993.

H. S. von Harrach, D. E. Jesson, and S. J. Pennycook, "Towards 1 Angstrom Resolution STEM," p. 996 in *Proceedings of the 51st Annual Meeting of the Electron Microscopy Society of America*, ed. by G. W. Bailey and C. L. Rieder, San Francisco Press, Inc., San Francisco, California, 1993.

C. W. White, D. K. Thomas, R. A. Zuhr, J. C. McCallum, A. Pogany, R. F. Haglund, R. H. Magruder, and L. Yang, "Modification of the Optical Properties of Al_2O_3 by Ion Implantation," p. 331 in *Materials Modification by Energetic Atoms and Ions*, ed. by K. S. Grabowski, S. A. Barnett, S. M. Rossnagel, and K. Wasa, Materials Research Society, Pittsburgh, Pennsylvania, 1992.

G. D. Wignall, "Combined Small-Angle Neutron and X-Ray Scattering Studies of Polymers," p. 355 in *Advances in X-Ray Analysis*, ed. by J. V. Gilfrich, T. C. Huang, C. R. Hubbard, M. R. James, R. Jenkins, G. R. Lachance, D. K. Smith, and P. K. Predecki, Plenum Press, New York, 1993.

J. M. Williams, "High-Energy Ion Implantation of Materials," p. 151 in *Current Status, Research Needs, and Opportunities in Applications of Surface Processing to Transportation and Utilities Technologies*, ed. by A. W. Czanderna and A. R. Landgrebe, NREL, Golden, Colorado, 1992.

J. M. Williams, "High-Energy Ion Implantation of Materials," p. 151 in *Critical Reviews in Surface Chemistry*, ed. by P. M. A. Sherwood and guest ed. by A. W. Czanderna and A. R. Landgrebe, CRC Press, Inc., Boca Raton, Florida, 1993.

F. Xiong, R. P. H. Chang, and C. W. White, "Structure and Properties of a-C:N Films Prepared by Pulsed Excimer Laser Deposition," p. 587 in *Laser Ablation in Materials Processing: Fundamentals and Applications*, ed. by B. Braren, J. Dubowski, and D. P. Norton, Materials Research Society, Pittsburgh, Pennsylvania, 1993.

P. A. Zeijlmans van Emmichoven, C. C. Havener, I. G. Huges, D. M. Zehner, and F. W. Meyer, "Analysis of Low-Energy Electron Emission Arising During Slow Multicharged Ion-Surface Interactions," p. 606 in *Proceedings of VIth International Conference on the Physics of Highly Charged Ions*, Vol. 274, ed. by P. Richard, M. Stöckei, C. L. Cooke, and C. D. Lin, American Institute of Physics, New York, 1993.

X. Y. Zheng, D. H. Lowndes, S. Zhu, and R. J. Warmack, "Scanning Tunneling Microscope Studies of Initial Epitaxial Growth of $YBa_2Cu_3O_{7-\delta}$ Thin Films," p. 41 in *Mechanisms of Epitaxial Growth*, ed. by M. F. Chisholm, R. Hull, L. J. Showalter, and B. J. Garrison, Materials Research Society, Pittsburgh, Pennsylvania, 1993.

S. Zhu, D. H. Lowndes, X.-Y. Zheng, D. P. Norton, and R. J. Warmack, "Epitaxial $YBa_2Cu_3O_{7-x}$ Thin Films: Scanning Tunneling Microscopy Study of the Initial Stages of Epitaxial Growth, Growth Mechanisms, and Effects of Substrate Temperature," p. 541 in *Interface Dynamics and Growth*, ed. by K. S. Liang, M. P. Anderson, R. F. Bruinsma, and G. Scoles, Materials Research Society, Pittsburgh, Pennsylvania, 1992.

REPORTS ISSUED

D. L. Abernathy, S. G. J. Mochrie, D. M. Zehner, G. Grübel, and D. Gibbs, "Capillary Modes on a Close-Packed Metal Surface: Pt(001)," p. 256 in *National Synchrotron Light Source Annual Report 1991, Volume II*, BNL-52317, Brookhaven National Laboratory, Upton, New York (1992).

Y. Chen and L. D. Hulett, *Proceedings of the DOE Workshop Meeting on the Application of Positron Spectroscopy to Materials Sciences*, Oak Ridge National Laboratory, CONF-9209221 (1993).

R. W. Dull and H. R. Kerchner, *A Teacher's Guide to Superconductivity for High School Students*, ORNL/M-3063 (October 1993).

R. Feenstra, "Atomic Layer Control in High-T_c Superconductors," *Research Report to the Japan Society for the Promotion of Science, October 6, 1992–April 8, 1993* (May 8, 1993).

J. A. Fernandez-Baca, M. E. Hagen, R. M. Nicklow, T. G. Perring, and Y. Tsunoda, "High-Energy Magnetic Excitations in $Mn_{90}Cu_{10}$," p. A257 in *ISIS Experimental Reports*, Rutherford Appleton Laboratory, Didcot, England (July 1993).

G. R. Gruzalski, S.-C. Lui, D. Heskett, X. Shi, and D. M. Zehner, "Core-Level Spectroscopy from Low-Index Surfaces of HfC Exposed to Oxygen," p. 63 in *National Synchrotron Light Source Annual Report 1991, Volume II*, BNL-52317, Brookhaven National Laboratory, Upton, New York (1992).

B. S. Itchkawitz, P. F. Lyman, E. W. Plummer, and D. M. Zehner, "Photoemission Spectroscopy from Monolayer Graphite on TaC(111)," p. 163 in *National Synchrotron Light Source Annual Report*, BNL-52371, Brookhaven National Laboratory, Upton, New York (1993).

S.-C. Lui, G. R. Gruzalski, D. Heskett, X. Shi, and D. M. Zehner, "Core-Level Spectroscopy from Low-Index Surfaces of TaC," p. 64 in *National Synchrotron Light Source Annual Report 1991, Volume II*, BNL-52317, Brookhaven National Laboratory, Upton, New York (1992).

R. M. Moon and R. M. Nicklow, *General User Training for HFIR Access*, (April 22, 1993).

D. R. Mullins and P. F. Lyman, "W(100) Surface Core Level Shifts Induced by S Adsorption," p. 165 in *National Synchrotron Light Source Annual Report*, BNL-52371, Brookhaven National Laboratory, Upton, New York (1993).

A. R. Sandy, D. L. Abernathy, S. G. J. Mochrie, D. M. Zehner, and L. D. Gibbs, "Au(113) Surface Studies," p. 259 in *National Synchrotron Light Source Annual Report 1991, Volume II*, BNL-52317, Brookhaven National Laboratory, Upton, New York (1992).

G. M. Watson, D. Gibbs, S. Song, S. G. J. Mochrie, and D. M. Zehner, "Temperature-Dependent Surface Morphology of Vicinal Au(111)," p. 349 in *National Synchrotron Light Source Annual Report*, BNL-52371, Brookhaven National Laboratory, Upton, New York (1993).

G. M. Watson, D. Gibbs, S. Song, S. G. J. Mochrie, and D. M. Zehner, "High-Temperature Structure of Vicinal Au(111)," p. 355 in *National Synchrotron Light Source Annual Report*, BNL-52371, Brookhaven National Laboratory, Upton, New York (1993).

S. P. Withrow, *Surface Modification and Characterization Research Center at Oak Ridge National Laboratory*, Oak Ridge National Laboratory (June 1993).

P. A. Zeijlmans van Emmichoven, C. C. Havener, I. G. Hughes, S. H. Overbury, M. T. Robinson, D. M. Zehner, and F. W. Meyer, "Electron Emission During Multicharged Ion-Metal Surface Interactions," p. 150 in *Proceedings of the 14th Werner Brandt Workshop on Charged Particle Penetration Phenomena*, Oak Ridge National Laboratory, CONF-9204144 (1992).

PATENTS GRANTED

D. Eres and D. H. Lowndes, *Method and Apparatus for Rapidly Growing Films on Substrates Using Pulsed Supersonic Jets*, U.S. Patent No. 5,164,040 (November 17, 1992).

R. Feenstra and L. A. Boatner, *Superconducting Thin Films on Potassium Tantalate Substrates*, U.S. Patent No. 5,110,790 (May 5, 1992).

R. Feenstra and L. A. Boatner, *Substrates Suitable for Deposition of Superconducting Thin Films*, U.S. Patent No. 5,188,906 (February 23, 1993).

THESES

E. C. Jones, "Electrical Transport Properties of Epitaxial and Granular-Oriented $YBa_2Cu_3O_{7-\delta}$ Thin Films," Ph.D. Thesis, The University of Tennessee, Knoxville, Tennessee, 1992.

J. W. McCamy, "Growth of Epitaxial ZnS, ZnSe, and $ZnSe_{1-x}S_x$ Alloy Thin Films, Multilayers, and Superlattices by Pulsed-Laser Ablation," Ph.D. Thesis, The University of Tennessee, Knoxville, Tennessee, 1993.

J. W. Sharp, "An In Situ Investigation of Si_xGe_{1-x} Chemical Vapor Deposition by Differential Reflectance," Ph.D. Thesis, The University of Tennessee, Knoxville, Tennessee, 1993.

Y. R. Sun, "Flux-Creep Studies in $YBa_2Cu_3O_{7-\delta}$ Superconductors," Ph.D. Thesis, The University of Tennessee, Knoxville, Tennessee, 1993.

S. Zhu, "Growth Mechanism and Electrical Transport Properties of Superconducting $YBa_2Cu_3O_{7-x}$ Thin Films Grown by Pulsed-Laser Ablation," Ph.D. Thesis, The University of Tennessee, Knoxville, Tennessee, 1993.

PAPERS PRESENTED AT TECHNICAL MEETINGS

Condensed Matter Physics Seminar, West Lafayette, Indiana, April 1–3, 1992:

J. R. Thompson, D. K. Christen, H. R. Kerchner, Y. R. Sun, J. G. Ossandon, J. O. Thomson, Y. J. Chen, A. P. Malozemoff, L. Civale, A. D. Marwick, and F. Holtzberg, "Better High-T_c Superconducting Materials Through Ion-Induced Defects" (invited paper)

Division of Environmental Chemistry, American Chemical Society, San Francisco, California, April 5–10, 1992:

J. A. Rice and J. S. Lin, "Fractal Nature of Humic Materials"

International Conference on Metallurgical Coatings and Thin Films, San Diego, California, April 6–10, 1992:

D. B. Geohegan, "Physics and Diagnostics of Laser Ablation Plume Propagation for High-T_c Superconductor Film Growth" (invited paper)

American Ceramic Society Meeting, Minneapolis, Minnesota, April 12–16, 1992:

J. B. Bates, N. J. Dudney, G. R. Gruzalski, A. Choudhury, R. A. Zuhr, C. F. Luck, and J. D. Robertson, "Amorphous Lithium Phosphorus Oxynitride Electrolyte Thin Films"

L. A. Boatner, J. Rankin, L. J. Romana, P. Thevenard, and D. J. Gilmore, "Ion Implantation and Ultrasonic Cavitation Etching of Ceramics"

J. R. Brewster, M. M. Abraham, L. A. Boatner, and R. W. Rice, "Texturing in Hot-Pressed or Extruded MgO as Evaluated by an EPR Method"

N. J. Dudney, J. B. Bates, and J. D. Robertson, "Preparation of Thin-Film Lithium Electrolytes"

S. J. Pennycook, M. F. Chisholm, and D. E. Jesson, "Z-Contrast Imaging of Interfaces" (invited paper)

J. Rankin, Q.-R. Fan, T. A. Nguyen, and L. A. Boatner, "In Situ TEM Study of the Coarsening of Nanophase MgO Particles"

Critical Currents in High-T_c Superconductors, Austria, April 22–24, 1992:

J. G. Ossandon, J. R. Thompson, D. K. Christen, Y. R. Sun, B. C. Sales, H. R. Kerchner, J. E. Tkaczyk, and K. W. Lay, "Systematics of Flux Pinning Versus Oxygen Deficiency δ in Aligned $YBa_2Cu_3O_{7-\delta}$ Materials"

Materials Research Society Spring Meeting, San Francisco, California, April 27–May 1, 1992:

L. A. Boatner, J. Rankin, L. J. Romana, P. Thevenard, and D. J. Gilmore, "A New Method for Etching Ceramic Materials Using Ion Implantation and Ultrasonic Cavitation"

M. F. Chisholm, T. Kaplan, M. E. Mostoller, and S. J. Pennycook, "Atomic Structure of Interfacial Misfit Dislocations in Si_xGe_{1-x}/Si(001)"

D. Eres and J. W. Sharp, "Thin-Film Growth from a Heterogeneous Surface Reaction"

R. Feenstra, D. P. Norton, J. D. Budai, D. K. Christen, D. H. Lowndes, V. C. Matijasevic, C.-B. Eom, T. H. Geballe, E. S. Hellman, and E. H. Hartford, "T_c-δ Relations in $YBa_2Cu_3O_{7-\delta}$ Thin Films: Oxygen Pressure During Growth"

A. T. Fiory, P. K. Roy, and G. E. Jellison, Jr., "Ion Channeling and Spectroscopic Ellipsometry Examinations of Thin-Film SiO_2/EPI-Si(001) Structures"

H. R. Kerchner, C. E. Klabunde, D. K. Christen, J. D. Budai, D. H. Lowndes, D. P. Norton, and J. O. Thomson, "Anisotropic Electrical Resistivity of YBCO/PBCO Superlattice Films Grown on Miscut Substrates"

D. E. Jesson, S. J. Pennycook, J.-M. Baribeau, and D. C. Houghton, "Step-Driven Surface Segregation and Ordering During Si-Ge MBE Growth" (invited paper)

S. J. Pennycook, M. F. Chisholm, D. E. Jesson, R. Feenstra, S. Zhu, and D. H. Lowndes, "Growth Mechanisms of Layered Superconductors" (invited paper)

B. C. Sales, R. A. Zuhr, J. C. McCallum, and L. A. Boatner, "Dominant Role of Electronic Energy Losses in the Ion Beam Amorphization of $Pb_2P_2O_7$"

J. R. Thompson, "What Can We Learn From Magnetization Experiments on High-T_c Superconductors? An Overview" (invited paper)

C. W. White, D. K. Thomas, R. A. Zuhr, J. C. McCallum, A. Pogany, R. F. Haglund, R. H. Magruder, and L. Yang, "Modification of the Optical Properties of Al_2O_3 by Ion Implantation"

X.-Y. Zheng, D. H. Lowndes, S. Zhu, and R. J. Warmack, "Scanning Tunneling Microscope Studies of Epitaxial Growth of $YBa_2Cu_3O_{7-\delta}$ Thin Films"

Spring College on Superconductivity, Trieste, Italy, April 27–June 30, 1992:

G. D. Mahan, "Theory of Normal Metals" (invited paper)

Joint TMS-Australian IMM Rare Earth Symposium: Sources, Science, Technology, and Applications, San Diego, California, May 2–5, 1992:

R. M. Moon, "Neutron Scattering from Rare-Earth Materials" (invited paper)

AIME Annual Meeting, San Diego, California, May 2–5, 1992:

G. Sundar, J. J. Hoyt, and S. Spooner, "A Test of the Langer-Schwartz Model of Nucleation and Growth"

Workshop on Neutron and Synchrotron Radiation Studies of Materials, Upton, New York, May 4–8, 1992:

R. M. Nicklow, "Neutron Inelastic Scattering" (invited paper)

Proceedings of Phase Separation in Cuprate Superconductors, Erice, Italy, May 6–12, 1992:

S. M. Hayden, T. E. Mason, G. Aeppli, H. A. Mook, S.-W. Cheong, and Z. Fisk, "Neutron Scattering Studies of the Spin Dynamics in $La_{2-x}Sr_xCuO_4$"

CLEO/QELS 1992 Conference on Lasers and Electro-Optics and Quantum Electronics and Laser Science, Anaheim, California, May 10–15, 1992:

S. W. Allison, M. A. Abraham, L. A. Boatner, M. R. Cates, D. L. Beshears, K. W. Tobin, B. W. Noel, and W. D. Turley, "High-Temperature Spectroscopy of Fluorescent Materials for Thermometry Applications"

D. B. Geohegan, "Fast Imaging of Ablation Plume Propagation Through Background Gases Used for Pulsed-Laser Deposition"

6th International Meeting on Lithium Batteries, Münster, Germany, May 10–15, 1992:

J. B. Bates, N. J. Dudney, G. R. Gruzalski, R. A. Zuhr, A. Choudhury, C. F. Luck, and J. D. Robertson, "Fabrication and Characterization of Amorphous Lithium Electrolyte Thin Films and Rechargeable Thin-Film Batteries" (invited paper)

Joint Meeting of the American Geophysical Union, Canadian Geophysical Union, and the Mineralogical Society of America, Montreal, Canada, May 12–15, 1992:

B. C. Chakoumakos, J. A. Fernandez-Baca, and L. A. Boatner, "Crystal Growth and Structure Refinements of the Gillespite-Type Layer Silicates $M\mathrm{CuSi_4O_{10}}$ (M = Ca, Sr, Ba)"

181st Meeting of the Electrochemical Society, Inc., St. Louis, Missouri, May 17–22, 1992:

S. H. Liu, "Theory of Interfacial Constant Phase Element in Electrode-Electolyte Systems" (invited paper)

National Synchrotron Light Source Workshop on Small-Angle Scattering for Materials Science, Upton, New York, May 18, 1992:

B. C. Larson, "Small-Angle X-Ray Scattering Around Bragg Peaks; Diffuse Scattering From Clusters" (invited paper)

SAS Studies of Synthetic Polymers, With Particular Reference to Polyolefin Blends, Bartlesville, Oklahoma, May 18, 1993:

G. D. Wignall, "Small-Angle Scattering Studies of Synthetic Polymers" (invited paper)

Near-Edge X-Ray Adsorption Fine Structure (NEXAFS), Stockholm, Sweden, May 18–20, 1992:

L. Siller, K. M. Hock, R. E. Palmer, and J. F. Wendelken, "Negative Ion Resonances in EELS of Adsorbed Molecules: Physisorbed and Chemisorbed Oxygen on Pt(111)"

Small-Angle X-Ray and Neutron Scattering from Polymers, Summit, New Jersey, May 20, 1993:

G. D. Wignall, "Small-Angle Scattering Studies of Synthetic Polymers" (invited paper)

Joint Annual Meeting–Geological Association of Canada/Mineralogical Association of Canada, Wolfville, Nova Scotia, Canada, May 25–27, 1992:

R. K. Eby, J. Janeczek, R. C. Ewing, B. C. Chakoumakos, T. S. Ercit, L. A. Groat, B. C. Can, and F. C. Hawthorne, "Metamictization and Alternation of Vesuvianite"

Beijing International Conference on High-T_c Superconductivity, Beijing, China, May 25–29, 1992:

Y. R. Sun, J. R. Thompson, D. K. Christen, Y. J. Chen, J. G. Ossandon, F. Holtzberg, A. D. Marwick, and A. Goyal, "Flux Creep Studies in $YBa_2Cu_3O_{7-\delta}$"

Accuracy in Powder Diffraction II, Gaithersburg, Maryland, May 26–29, 1992:

B. C. Chakoumakos, J. A. Fernandez-Baca, and G. A. Lager, "Crystal Structure Refinements of $M_3Al_2O_6$ (M = Ca, Sr, Ba) Using Neutron Powder Diffraction Data—An Example Study from the New HB-4 Diffractometer at the HFIR, Oak Ridge"

J. A. Fernandez-Baca, H. A. Mook, H. S. White, B. S. Hoffheins, and B. C. Chakoumakos, "Neutron Powder Diffraction at the High-Flux Isotope Reactor at Oak Ridge"

3rd International Conference on Advances in Welding Research, Gatlinburg, Tennessee, June 1–5, 1992:

J. H. Root, T. M. Holden, J. Schroder, S. Spooner, C. A. Hubbard, T. A. Dodson, and S. A. David, "Residual Stresses in a Multipass Ferritic Weldment"

S. Spooner, S. A. David, J. H. Root, T. M. Holden, M. A. M. Bourke, and J. Goldstone, "Residual Stress and Strain Measurements in an Austenitic Steel Plate Containing a Multipass Weld"

J. M. Vitek, M. Rappaz, S. A. David, and L. A. Boatner, "Grain Competition in Bicrystal Welds"

Spring Meeting of the European Materials Research Society, Strasbourg, France, June 2–5, 1992:

D. E. Jesson, S. J. Pennycook, J.-M. Baribeau, and D. C. Houghton, "Atomistic Processes of Surface Segregation During Si-Ge MBE Growth" (invited paper)

6th International Conference on Metalorganic Vapor Phase Epitaxy, Cambridge, Massachusetts, June 8–11, 1992:

A. Erbil, W. Braun, B. S. Kwak, L. A. Boatner, and J. D. Budai, "Oxide Ferroelectric Materials Grown by Metalorganic Chemical Vapor Deposition".

International Seminar on High-Resolution STEM, Osaka, Japan, June 10, 1992:

S. J. Pennycook, "Atomic Resolution Incoherent Imaging with the STEM: Applications to Superconductors and Semiconductors" (invited paper)

35th International Power Sources Symposium, Cherry Hill, New Jersey, June 22–25, 1992:

J. B. Bates, G. R. Gruzalski, N. J. Dudney, A. Choudhury, and C. F. Luck, "New Amorphous Thin-Film Lithium Electrolyte and Rechargeable Microbattery"

International Workshop on Superconductivity, Honolulu, Hawaii, June 23–26, 1992:

D. K. Christen, C. E. Klabunde, D. B. Chandler, M. J. Neal, M. V. Parish, B. C. Chakoumakos, A. Goyal, and D. M. Kroeger, "The Production and Properties of Melt-Zone-Textured $YBa_2Cu_3O_{7-\delta}$ Filaments" (invited paper)

J. R. Thompson, Y. R. Sun, H. R. Kerchner, D. K. Christen, B. C. Sales, B. C. Chakoumakos, A. D. Marwick, L. Civale, and J. O. Thomson, "Enhanced Current Density J_C and Extended Irreversibility in Single-Crystal $Bi_2Sr_2CaCu_2O_8$ via Linear Defects from Heavy Ion Irradiation"

1992 Electronic Materials Conference, Cambridge, Massachusetts, June 24–26, 1992:

T. E. Haynes and O. W. Holland, "Production of Lattice Damage During Ion Implantation of Si-Ge Alloys"

Gordon Research Conference on Ion-Solid Interactions, Plymouth, New Hampshire, July 6–10, 1992:

D. B. Geohegan, "Laser Plasma Formation and Propagation in Vacuum and Background Gases Used for Pulsed-Laser Deposition" (invited paper)

M. T. Robinson, "Theory of Displacement Cascades" (invited paper)

10th European Congress on Electron Microscopy, Granada, Spain, July 13–17, 1992:

C. Ballesteros, R. Gonzalez, Y. Chen, and M. R. Kokta, "Precipitation of Matrix Cations in Fusion Ionic Insulators During Reduction at High Temperatures"

Property and Characteristics of Optical Glass III, San Diego, California, July 19–22, 1992:

D. O. Henderson, S. H. Morgan, R. Mu, R. H. Magruder III, T. S. Anderson, J. E. Wittig, and R. A. Zuhr, "Optical and Infrared Spectra of Thermally Annealed Pb-Implanted SiO_2 Glasses"

R. H. Magruder III, D. L. Kinser, J. Wittig, and R. A. Zuhr, "Structure Property Relationships of Nanometer-Size Metal Clusters in Glasses"

Workshop on Recent Advances in Two-Dimensional and Nanostructure Electron Systems, Sydney, Australia, July 20–21, 1992:

M. Rasolt and F. Perrot, "Spontaneously Symmetry-Broken Current-Carrying States in Nanostructures" (invited paper)

International Conference on Martensitic Transformation (ICOMAT) 1992, Monterey, California, July 20–24, 1992:

H. G. Smith, R. Berliner, and J. Trivisonno, "Neutron Scattering Studies of the Structures and Lattice Dynamics of the Alkali Metals"

International Conference on the Physics of Transition Metals, Darmstadt, Germany, July 20–24, 1992:

J. W. Cable and Y. Tsunoda, "Atomic Short-Range Order and Spin-Density Wave Propagation in CuMn"

R. S. Fishman and S. H. Liu, "Impurity Effects on the Magnetic Ordering in Chromium"

T. M. Holden, K. Mikke, E. Fawcett, and J. A. Fernandez-Baca, "The Magnetism of Metallic Manganese Alloys" (invited paper)

S. H. Liu, "Electronic Polaron Effects in Mixed-Valence and Heavy Fermion Materials" (invited paper)

K. Mikke, T. M. Holden, J. A. Fernandez-Baca, E. Fawcett, and J. Jankowska-Kisielinska, "High-Energy Magnetic Excitations in Single-Domain Homogeneous Antiferromagnetic γ-Mn(18%Cu) Alloy at 10 K"

10th International Conference on Vacuum Ultraviolet Radiation Physics, Paris, France, July 27–31, 1992:

L. Siller, J. F. Wendelken, and R. E. Palmer, "Resonance EELS Study of Physisorbed and Chemisorbed O_2 on Pt(111): Comparison with NEXAFS"

41st Annual Denver X-Ray Conference, Colorado Spring, Colorado, August 3–7, 1992:

X-L. Wang, C. R. Hubbard, K. B. Alexander, P. F. Becher, J. A. Fernandez-Baca, and S. Spooner, "Neutron Diffraction Study of the Pseudo-Macro Residual Stresses in ZrO_2 (CeO_2)/Al_2O_3 Ceramic Composites"

G. D. Wignall, "Combined Small-Angle Neutron and X-Ray Scattering Studies of Polymers" (invited paper)

G. D. Wignall, "Introduction to Small-Angle X-Ray Neutron Scattering"

Gordon Conference on Polymer Physics, Newport, Rhode Island, August 3–7, 1992:

J. D. Londono, G. D. Wignall, H. D. Cochran, and A. H. Narten, "The Single-Chain Structure of C_{36} Chains in the Intermediate-Angle Region"

American Crystallographic Association 1992 Annual Meeting, Pittsburgh, Pennsylvania, August 9–14, 1992:

J. W. Cable, "The Discovery of Antiferromagnetic Structures" (invited paper)

B. C. Larson, "X-Ray Diffraction with Nanosecond Time-Resolution and Nanovolt Energy Resolution Using the Pulsed Nature of Synchrotron Sources" (invited paper)

B. C. Sales, "Structural Analysis of Amorphous Phosphates Using High-Performance Liquid Chromatography" (invited paper)

11th Pfefferkorn Conference on Physics of Generation and Detection of Signals Used for Microcharacterization, Amherst, Massachusetts, August 9–14, 1992:

S. J. Pennycook, D. E. Jesson, and N. D. Browning, "Electron Channeling with a Coherent STEM Probe: Column-by-Column Imaging and Analysis" (invited paper)

39th International Field Emission Symposium, Halifax, Nova Scotia, August 9–14, 1992:

R. P. Setna, J. M. Hyde, A. Cerezo, G. D. W. Smith, and M. F. Chisholm, "Position-Sensitive Atom Probe Study of the Decomposition of a Cu-2.6 at. % Co Alloy"

8th International Summer School on Crystal Growth (ISSCG-8), Palm Springs, California, August 9–15, 1992:

D. H. Lowndes, "Growth of Epitaxial Thin Films by Pulsed-Laser Ablation" (invited paper)

International Conference on Defects in Insulating Materials (ICDM), Nord Kirchen, Germany, August 15–19, 1992:

B. D. Evans, G. J. Pogatshnik, and Y. Chen, "Aggregate Color Centers in α-Al_2O_3"

M. L. Sanjuan, V. M. Orera, M. Jouanne, and Y. Chen, "Resonant Raman Scattering of the Metastable H^{2-} Defect in CaO"

50th Meeting of the Electron Society of America, Boston, Massachusetts, August 16–21, 1992:

S. J. Pennycook, D. E. Jesson, and M. F. Chisholm, "Column-By-Column Compositional Imaging by Z-Contrast STEM" (invited paper)

Tenth International Conference on Crystal Growth, San Diego, California, August 16–21, 1992:

B. C. Sales, B. C. Chakoumakos, L. A. Boatner, and J. O. Ramey, "Crystal Growth and Characterization of $MgHPO_4 \cdot 3H_2O$"

S. Zhu, D. H. Lowndes, B. Chakoumakos, R. Feenstra, and X.-Y. Zheng, "Growth of Epitaxial $Bi_2Sr_2Ca_{n-1}Cu_nO_{2n+4}$ Films by Pulsed-Laser Ablation"

International Conference on Anomalous Scattering, Malente/Hamburg, Germany, August 17–21, 1992:

J. Z. Tischler, B. C. Larson, E. E. Alp, T. Mooney, and Q. Shen, "Development of Nuclear Bragg Scattering Applications" (invited paper)

1992 Applied Superconductivity Conference, Chicago, Illinois, August 23–28, 1992:

H. R. Kerchner, D. K. Christen, C. E. Klabunde, D. H. Lowndes, D. P. Norton, J. O. Thomson, Y. R. Sun, and J. R. Thompson, "Transport-Current Resistivity and Inductive Impedance of $YBa_2Cu_3O_7/PrBa_2Cu_3O_7$ Superlattice Films"

D. P. Norton, D. H. Lowndes, J. D. Budai, and S. J. Pennycook, "Superconductivity and Reduced Dimensionality in Ultrathin $YBa_2Cu_3O_x$ Films and $YBa_2Cu_3O_x$-Based Superlattice Structures"

K. H. Young, M. D. Muller, R. T. Young, S. R. Ovshinsky, J. S. Martens, J. D. Budai, and C. W. White, "Structural and Microwave Properties of YBCOF Thin Films on Sapphire Substrate Without Buffer Layer"

American Chemical Society National Meeting, Washington, D.C., August 23–28, 1992:

S. Kulkarni, S. Krause, and G. D. Wignall, "Small-Angle Neutron Scattering from Synthethic Membranes"

International Conference on Computer Simulation of Radiation Effects in Solids, Berlin, Germany, August 23–28, 1992:

M. T. Robinson, "The Binary Collision Approximation: Background and Introduction" (invited paper)

1992 International Conference on Solid State Devices and Materials (SSDM '92), Tsukuba Science City, Japan, August 26–28, 1992:

J. W. McCamy, D. H. Lowndes, and J. D. Budai, "Growth of Epitaxial ZnS, ZnSe, and ZnS-ZnSe Multilayers on GaAs by Pulsed-Laser Ablation"

Workshop on Grain Boundaries in High-T_c Superconductors, Madison, Wisconsin, August 30–September 1, 1992:

N. D. Browning, M. F. Chisholm, and S. J. Pennycook, "Direct Atomic Scale Imaging and Analysis of $YBa_2Cu_3O_{7-\delta}$ Grain Boundaries by STEM" (invited paper)

Symposium on Sputtering, Copenhaven, Denmark, August 31–September 4, 1992:

M. Hou, W. Eckstein, and M. T. Robinson, "The Kinetics of the Copper Single-Crystal Sputtering Studied by Computer Simulation,"

M. T. Robinson, "Computer Simulation of Sputtering: A Review" (invited paper)

XIII International Congress on X-Ray Optics and Microanalysis, Manchester, United Kingdom, August 31–September 4, 1992:

S. J. Pennycook, D. E. Jesson, M. F. Chisholm, and N. D. Browning, "Atomic Resolution Imaging and Analysis with the STEM" (invited paper)

3rd International Conference on New Diamond Science and Technology, Heidelberg, Germany, August 31–September 4 ,1992:

J. D. Hunn, N. R. Parikh, M. L. Swanson, and R. A. Zuhr, "Conduction in Ion-Implanted Single-Crystal Diamond"

8th International Conference on Ion Beam Modification of Materials, Heidelberg, Germany, September 7–11, 1992:

R. Brenier, B. Canut, L. Gea, S. M. M. Ramos, P. Thévenard, J. Rankin, L. Romana, and L. A. Boatner, "Surface Expansion of Ion-Damaged MgO Induced by Ionization Processes"

T. E. Haynes and O. W. Holland, "Lattice Damage in Ion-Implanted Silicon-Germanium Alloys"

A. D. Marwick, L. Civale, L. Krusin-Elbaum, R. Wheeler, J. R. Thompson, T. K. Worthington, M. A. Kirk, Y. R. Sun, H. R. Kerchner, and F. Holtzberg, "Processing High-T_c Superconductors with GeV Heavy Ions" (invited paper)

J. M. Williams and C. J. McHargue, "Ion Implantation Effects in Silicon Carbide" (invited paper)

N. R. Parikh, J. D. Hunn, M. L. Swanson, C. W. White, J. B. Posthill, R. A. Rudder, and R. J. Markunas, "Ion Beam Applications for Diamond Growth and Lift-Off"

Conceptual Design Review, Argonne, Illinois, September 9–10, 1992:

B. C. Larson and J. Z. Tischler, "Conceptual Design Report for the UNI-CAT Beam Line Proposal"

International Workshop on the Determination of Partial Structure Factors of Disordered Matter by Neutron and Anomalous X-Ray Diffraction, Grenoble, France, September 10–11, 1992:

C. Lamers, D. Richter, W. Schweika, J. Batoulis, K. Sommer, J. W. Cable, and S. M. Shapiro, "Short-Range Order in Amorphous Polycondensates"

3rd International Conference and Exhibition, World Congress on Superconductivity, Münich, Germany, September 14–18, 1992:

J. G. Ossandon, J. R. Thompson, D. K. Christen, Y. R. Sun, B. C. Sales, H. R. Kerchner, J. E. Tkaczyk, and K. W. Lay, "Properties of Aligned $YBa_2Cu_3O_{7-\delta}$ Superconductor as a Function of Oxygen Deficiency δ"

Sixth Annual Conference on Superconductivity and Applications, Buffalo, New York, September 15–17, 1992:

D. K. Christen, J. R. Thompson, H. R. Kerchner, B. C. Sales, B. C. Chakoumakos, L. Civale, A. D. Marwick, and F. Holtzberg, "Limits to Critical Currents in High-Temperature Superconductors: What We Can Learn From Tailored Defects" (invited paper)

D. P. Norton and D. H. Lowndes, "Growth and Properties of Ultrathin $YBa_2Cu_3O_{7-\delta}$ Layers" (invited paper)

J. R. Thompson, Y. R. Sun, J. G. Ossandon, D. K. Christen, H. R. Kerchner, B. C. Sales, B. C. Chakoumakos, L. Civale, A. D. Marwick, and F. Holtzberg, "Magnetic Studies of Current Conduction and Flux Pinning in High-T_c Cuprates: Virgin, Irradiated, and Oxygen-Deficient Materials" (invited paper)

Annual Meeting of the Norwegian Physical Society, Graftavalen, Norway, September 19, 1992:

G. D. Mahan, "Current Drag in Semiconductors" (invited paper)

2nd National Congress on the Science of Materials, Mexican Academy on the Science of Materials, Cancun, Mexico, September 20–25, 1992:

J. L. Bóldú, L. A. Boatner, and M. M. Abraham, "Characterization of Textured Ceramics by Electron Paramagnetic Resonance Spectroscopy"

First International Conference on Nanostructure Materials, Cancun, Mexico, September 22–26, 1992:

C. W. White, D. K. Thomas, D. K. Hensley, R. A. Zuhr, J. C. McCallum, A. Pogany, R. F. Haglund, R. H. Magruder, and L. Yang, "Colloidal Au and Ag Precipitates Formed in Al_2O_3 by Ion Implantation and Annealing" (invited paper)

Sixth International Humic Substances Society Meeting, Bari, Italy, September 23–27, 1992:

J. A. Rice and J. S. Lin, "Fractal Dimension of Humic Materials"

VIth International Conference on the Physics of Highly Charged Ions, Manhattan, Kansas, September 28–October 2, 1992:

I. G. Hughes, C. C. Havener, S. H. Overbury, M. T. Robinson, D. M. Zehner, P. A. Zeijlmans van Emmichoven, and F. W. Meyer, "Incident Ion Charge State Dependence of Electron Emission During Slow Multicharged Ion-Surface Interactions"

F. W. Meyer, J. Burgdörfer, I. G. Hughes, S. H. Overbury, D. M. Zehner, and P. M. Zeijlmans van Emmichoven, "Neutralization of Slow Multicharged Ions Above a Cesiated Au Surface"

P. A. Zeijlmans van Emmichoven, C. C. Havener, I. G. Hughes, D. M. Zehner, and F. W. Meyer, "Analysis of Low-Energy Electron Emission Arising During Slow Multicharged Ion-Surface Interactions"

Midwest Solid State Conference, Champaign, Illinois, October 2–3, 1992:

D. H. Lowndes, "Superconductivity in Epitaxial High-T_c Superconductor Multilayers" (invited paper)

XVIth International Congress on Glass, Madrid, Spain, October 4–9, 1992:

R. H. Magruder, R. A. Weeks, S.-Y. Park, R. F. Haglund, Jr., L. Lang, and R. A. Zuhr, "Bi-Implanted SiO_2: A Potential Optical Device Material"

25th SRC Users Group Meeting, Stoughton, Wisconsin, October 5–6, 1992:

D. R. Mullins, S. H. Overbury, and P. F. Lyman, "The Adsorption of Sulfur on W(001)"

D. R. Mullins and P. F. Lyman, "Methanethiol on W(001) and Ru(0001)"

16th International Seminar on Surface Physics, Kudowa, Poland, October 5–10, 1992:

E. W. Plummer and P. A. Dowben, "When Are Thin Films of Metals Metallic?"

Eighth International Conference on Solid Surfaces, Utrecht, Netherlands, October 12–16, 1992:

G. Grübel, D. Gibbs, D. M. Zehner, D. L. Abernathy, A. Sandy, and S. G. J. Mochrie, "Phase Behavior of Au and Pt Surfaces"

J.-K. Zuo, D. M. Zehner, J. F. Wendelken, and R. J. Warmack, "A High-Resolution LEED and STM Study of Reconstructed TaC(110)"

12th International Vacuum Congress/Eighth International Conference on Solid Surfaces, Hague, the Netherlands, October 12–16, 1992:

B. Dötsch, A. Schmidt, L. Hammer, M. Kottcke, R. Döll, K. Heinz, K. Müller, H. L. Davis, and D. M. Zehner, "The Structure of the Clean and H-Covered Alloy $Mo_{1-x}Re_x(100)$"

D. C. Lubben, R. Tsu, T. R. Bramblett, and J. E. Greene, "Mechanisms and Kinetics of Photo-Stimulated Si Atomic-Layer Epitaxy on Si(001)2 × 1 and Ge(001)2 × 1" (invited paper)

A. R. Sandy, S. G. J. Mochrie, D. M. Zehner, G. Grübel, K. G. Huang, and D. Gibbs, "Au and Pt(111) Surface Phase Behavior"

L. Siller, R. E. Palmer, and J. F. Wendelken, "Negative Ion Resonance in Electron Scattering by Physisorbed and Chemisorbed O_2 on Pt(111)"

L. Siller, K. M. Hock, R. E. Palmer, and J. F. Wendelken, "Resonance Electron Scattering by Adsorbed Molecules: σ^* Resonance Energy Versus Bond Length"

J.-K. Zuo, D. M. Zehner, J. F. Wendelken, and R. J. Warmack, "A High-Resolution LEED and STM Study of Reconstructed TaC(110)"

TMS Fall Meeting, Chicago, Illinois, November 1–5, 1992:

M. F. Chisholm and S. J. Pennycook, "Direct Atomic-Scale Imaging of Heterophase Boundaries by Z-Contrast STEM" (invited paper)

12th International Conference on the Application of Accelerators in Research and Industry, Denton, Texas, November 2–5, 1992:

T. E. Haynes, "Growth of Lattice Damage During Ion Implantation of Compound Semiconductors" (invited paper)

D. Joslin and O. W. Holland, "Ion Beam Synthesis of Buried Insulating Layers in Single-Crystal Si and SiC" (invited paper)

S. J. Pennycook, R. Feenstra, D. P. Norton, D. H. Lowndes, and M. F. Chisholm, "Amorphization, Recrystallization, and Growth Mechanisms of $YBa_2Cu_3O_{7-x}$ Films and Superlattices" (invited paper)

Analytical Laboratory Equipment Exposition and Conference, San Francisco, California, November 3–4, 1992:

S. J. Pennycook, "Z-Contrast Scanning Transmission Electron Microscopy" (invited paper)

Fifth US/Japan Workshop on High-T_c Superconductors, Tsukuba, Japan, November 9–10, 1992:

J. R. Thompson, Y. R. Sun, J. G. Ossandon, D. K. Christen, H. R. Kerchner, B. C. Sales, B. C. Chakoumakos, L. Civale, A. D. Marwick, and F. Holtzberg, "Magnetization and Flux Pinning in High-T_c Cuprates: Irradiated and Oxygen-Deficient Materials" (invited paper)

39th Annual AVS Symposium and Topical Conference, Chicago, Illinois, November 9–13, 1992:

A. P. Baddorf, G. Helgesen, D. Gibbs, A. R. Sandy, and S. G. J. Mochrie, "X-Ray Scattering for Surface Structure Determination"

S. M. Gorbatkin, W. C. Oliver, J. C. Barbour, and T. M. Mayer, "Electron Cyclotron Resonance Microwave Plasma Deposition of BN Thin Films"

P. F. Lyman and D. R. Mullins, "Core Level Spectrosopy of S on W(0001)"

D. R. Mullins and P. F. Lyman, "Reactions of Sulfur-Containing Species on Metal Surfaces Characterized by Synchrotron Radiation"

L. Siller, J. F. Wendelken, and R. E. Palmer, "Observation of Negative Ion Resonances in Physisorbed and Chemisorbed O_2 on Pt(111)"

J.-K. Zuo, R. J. Warmack, D. M. Zehner, and J. F. Wendelken, "A Direct Observation of Periodic (100) Faceting on TaC(110) by STM"

Fifty-Ninth Meeting of the Southeastern Section of the American Physical Society, Oak Ridge, Tennessee, November 12–14, 1992:

N. D. Browning, M. F. Chisholm, and S. J. Pennycook, "Atomic-Scale Imaging and Analysis of Grain Boundaries in $YBa_2Cu_3O_{7-\delta}$ by Scanning Transmission Electron Microscopy" [*Bull. Am. Phys. Soc*. **37**, 1665 (1992)]

Y. J. Chen, J. R. Thompson, S. K. Patapis, D. K. Christen, Y. R. Sun, H. R. Kerchner, and B. C. Sales, "Enhanced Supercurrent Density in Single-Crystal $Bi_{2-x}Pb_xSr_2CaCu_2O_z$ by Heavy Ion Irradiation" [*Bull. Am. Phys. Soc.* **37**, 1666 (1992)]

D. K. Christen, "Electrical Transport Properties of High-Temperature Superconductors" [*Bull. Am. Phys. Soc.* **37**, 1665 (1992)] (invited paper)

Z. C. Feng, B. S. Kwak, A. Erbil, and L. A. Boatner, "Raman Spectra of $PbTiO_3$ Thin Films on Various Substrates Grown by Metalorganic Chemical Vapor Deposition" [*Bull. Am. Phys. Soc.* **37**, 1657 (1992)]

T. R. Finlayson, H. G. Smith, and N. Wakabayashi, "Neutron Diffraction Study of the Martensitic Phase Transformation in In-Tl Alloys" [*Bull. Am. Phys. Soc.* **37**, 1651 (1992)]

E. C. Jones, D. K. Christen, J. R. Thompson, and S. Zhu, "Effect of Inhomogeneities on the Hall Effect in $YBa_2Cu_3O_{7-\delta}$ Thin Films Near the Superconducting Transition" [*Bull. Am. Phys. Soc.* **37**, 1666 (1992)]

M. N. Kunchur, D. K. Christen, C. E. Klabunde, and J. M. Phillips, "Free-Flux Flow at High Dissipation Levels in $YBa_2Cu_3O_{7-\delta}$ Films" [*Bull. Am. Phys. Soc.* **37**, 1666 (1992)]

S. J. Pennycook, "Direct Atomic Imaging of Materials by Z-Contrast STEM" [*Bull. Am. Phys. Soc.* **37**, 1679 (1992)] (invited paper)

J. O. Sofo and G. D. Mahan, "Resistivity and Superconductivity from Anharmonic Phonons" [*Bull. Am. Phys. Soc.* **37**, 1646 (1992)]

Y. R. Sun, J. R. Thompson, D. K. Christen, Y. J. Chen, and A. Goyal, "Measuring Critical Current Density in High-T_c Superconductors" [*Bull. Am. Phys. Soc.* **37**, 1665 (1992)]

J. Z. Tischler, B. C. Larson, and Q. Shen, "The Effect of Crystal Mosaic on the Nanovolt-Range Energy Resolution of a $^{57}Fe_2O_3$ Mössbauer Resonant Bragg Monochromator" [*Bull. Am. Phys. Soc.* **37**, 1649 (1992)]

C. N. Yeh, L. E. McNeil, and T. E. Haynes, "Raman Scattering Study of Ion-Implanted Silicon Germanium Alloys" [*Bull. Am. Phys. Soc.* **37**, 1657 (1992)]

S. Zhu, D. K. Christen, C. E. Klabunde, J. R. Thompson, R. Feenstra, D. H. Lowndes, and D. P. Norton, "Flux Pinning Force Analysis of Epitaxial $YBa_2Cu_3O_7$ Thin Films" [*Bull. Am. Phys. Soc.* **37**, 1665 (1992)]

Fall Meeting of the Materials Research Society, Boston, Massachusetts, November 30–December 4, 1992:

N. D. Browning and S. J. Pennycook, "Application of Z-Contrast Imaging to Obtain Column-by-Column Spectroscopic Analysis of Materials"

N. D. Browning, J. Yuan, and L. M. Brown, "Determination of Oxygen Deficiency in $YBa_2Cu_3O_{7-\delta}$ with Nanometer Spatial Resolution by Electron Energy Loss Spectroscopy"

B. C. Chakoumakos, L. A. Boatner, J. O. Ramey, D. P. Norton, and M. Petek, "Textured Superconducting $YBa_2Cu_3O_{7-\delta}$ Films by Electrodeposition on Semiconducting Oxide Substrates"

D. K. Christen, S. Zhu, C. E. Klabunde, R. Feenstra, J. R. Thompson, H. R. Kerchner, L. Civale, and A. D. Marwick, "Effects of Columnar Defects on the Superconducting Transport Properties of Epitaxial $YBa_2Cu_3O_7$ Thin Films"

Y. N. Erokin, S. Pramanick, F. Hong, G. A. Rozgony, B. K. Patnaik, and C. W. White, "Thin Ni Silicon Formation by Low-Temperature-Induced Metal Atom Reaction with Ion-Implanted Amorphous Silicon,"

D. B. Geohegan, "Fast-ICCD Photography and Gated Photon Counting Measurements of Blackbody Emission from Particulates Generated in the KrF-Laser Ablation of BN and YBCO" (invited paper)

T. E. Haynes, C. Lee, and K. S. Jones, "Time-Resolved Reflectivity Study of Solid-Phase-Epitaxial Regrowth in Relaxed and Strained $Si_{1-x}Ge_x$ Epilayers"

D. M. Hembree, Jr., D. F. Pedraza, G. R. Romanoski, S. P. Withrow, and B. K. Annis, "Raman Spectroscopy of C-Irradiated Graphite"

D. O. Henderson, S. H. Morgan, R. Mu, N. Chen, R. H. Magruder III, C. W. White, and R. A. Zuhr, "A Vibrational Analysis of Au-Implanted Al_2O_3 Single Crystals: Ion and Thermal Annealing Effects"

B. J. Heuser, S. Spooner, C. J. Glinka, D. L. Gilliam, N. A. Winslow, and M. S. Boley, "Structural Investigation of Electrochemically Etched Silicon"

G. E. Jellison, Jr., M. Keefer, and L. Thornquist, "Spectroscopic Ellipsometry and Interference Reflectometry Measurements of CVD Silicon Grown on Oxidized Silicon" (invited paper)

D. E. Jesson, S. J. Pennycook, J. Z. Tischler, J. D. Budai, J.-M. Baribeau, and D. C. Houghton, "The Relationship Between Compositional Ordering and Surface Morphology During Si_xGe_{1-x} Alloy Growth"

D. L. Joslin, C. W. White, L. L. Horton, L. J. Romana, C. J. McHargue, and P. A. Thévenard, "Ion Beam Mixing of Oxide Films on Sapphire"

H. R. Kerchner, J. R. Thompson, Y. R. Sun, D. K. Christen, J. O. Thomson, B. C. Sales, B. C. Chakoumakos, L. Civale, and A. D. Marwick, "Enhanced Critical Current Density and Magnetic Irreversibility Line in Single-Crystal $Bi_2Sr_2CaCu_3O_8$ via Columnar Defects from Heavy Ion Irradiation"

D. H. Lowndes, M. DeSilva, M. J. Godbole, A. J. Pedraza, and D. B. Geohegan, "Ablation, Melting, and Smoothing of Polycrystalline Alumina by Pulsed Excimer Laser Irradiation"

J. W. McCamy, D. H. Lowndes, J. D. Budai, G. E. Jellison, Jr., I. P. Herman, and S. Kim, "Epitaxial ZnS, ZnSe, and ZnS/ZnSe Superlattices Grown on (001) GaAs by Pulsed-Laser Ablation"

S. H. Morgan, D. O. Henderson, Z. Pan, R. H. Magruder III, and R. A. Zuhr, "Characterization of Thermal-Annealed Bi-Implanted Silica"

D. P. Norton, B. C. Chakoumakos, J. D. Budai, and D. H. Lowndes, "Epitaxial Growth and Properties of $Ca_{1-x}Sr_xCuO_2$ Thin Films Grown by Pulsed-Laser Deposition"

S. Y. Park, R. H. Magruder III, R. A. Weeks, and R. A. Zuhr, "Optical Bleaching of Bismuth-Implanted Silica Glass: Threshold Effects"

S. J. Pennycook, "Direct Atomic Imaging of Materials by Z-Contrast STEM" (invited paper)

M. T. Robinson, "Computer Simulation of Atomic-Collision Processes in Solids" (invited paper)

J. W. Sharp and D. Eres, "Investigation of the Kinetics in Surface-Limited Thin-Film Growth of SiGe Alloys by CVD of Si_2H_6/Ge_2H_6 Mixtures"

T. P. Sjoreen, "Ion Beam Synthesis of $IrSi_3$ by Implantation of 2-MeV Ir $Ions^+$"

G. W. Steadman, J. R. Brewster, J. D. Budai, and L. A. Boatner, "Textured Coatings from Colloidal Suspensions of Cubic-Faceted Nanophase MgO Particles"

J. R. Thompson, "Vortex Pinning by Line- and Point-Like Defects in High-Temperature Superconductors" (invited paper)

J. M. Williams and D. B. Poker, "Ion Beam Mixing Studies in Pt/Ti and Pt/Ni Bilayered Samples"

S. P. Withrow, S. J. Pennycook, N. Browning, J. D. Budai, and D. M. Hembree, Jr., "Epitaxial Regrowth of Highly Doped Si Using Ion Beams"

F. Xiong, R. P. H. Chang, and C. W. White, "Structure and Properties of a-C:N Films Prepared by Pulsed Excimer Laser Deposition"

J.-K. Zuo and J. F. Wendelken, "Experimental Study of Smoothing Kinetics on a Crystal Surface: Cu/Cu(100)"

37th Annual Conference on Magnetism and Magnetic Materials, Houston, Texas, December 1–4, 1992:

J. W. Cable and Y. Tsunoda, "Spin Density Waves in Dilute CuMn Alloys"

C.-K. Loong, L. Soderholm, J. P. Hammonds, M. M. Abraham, L. A. Boatner, and N. M. Edelstein," Neutron Scattering Study of Crystal-Field Transitions in $ErPO_4$"

J. A. Fernandez-Baca and H. A. Mook, "Search for the Breakdown of the Spin-Wave Approximation in EuO"

J. A. Fernandez-Baca, M. E. Hagen, R. M. Nicklow, T. G. Perring, and Y. Tsunoda, "High-Energy Magnetic Excitations in $Mn_{90}Cu_{10}$"

T. M. Giebultowicz, J. A. Fernandez-Baca, R. M. Nicklow, J. K. Furdyna, and U. Debska, "Spin Dynamics in a Diluted Heisenberg NN Antiferromagnet on a HCP Lattice: $Zn_{1-x}Mn_xSe$"

H. A. Mook, M. Yethiraj, G. D. Wignall, E. M. Forgan, S. L. Lee, R. Cubitt, D. McK. Paul, and T. Armstrong, "Neutron Measurements of the Vortex Lattice in $YBa_2Cu_3O_7$" (invited paper)

R. B. Rooge, Y. S. Yang, Z. Tun, B. D. Gaulin, J. A. Fernandez-Baca, R. M. Nicklow, and A. Harrison, "A Neutron Scattering Study of the Quasi-One-Dimensional Dilute Ising-Like Antiferromagnet $CsCo_{0.83}Mg_{0.17}Br_3$"

Y. S. Yang, B. D. Gaulin, J. A. Fernandez-Baca, N. Ali, and G. D. Wignall, "Small-Angle Neutron Scattering Studies of $Ce(Fe_{1-x}Al_x)_2$"

23rd Winter Colloquium on Quantum Electronics, Snowbird, Utah, January 1–5, 1993:

R. C. Powell, H. Liu, R. J. Reeves, I. Floldvari, and L. A. Boatner, "Nonlinear Optical Responses of Photorefractive Crystals after Picosecond Pulse Excitation"

Gordon Conference on Superconductivity, Oxnard, California, January 4–8, 1993:

M. N. Kunchur, D. K. Christen, C. E. Klabunde, and J. M. Phillips, "Free-Flux Flow at High Dissipation Levels in $YBa_2Cu_3O_{7-\delta}$ Epitaxial Films" (invited paper)

First International Conference on Spectroscopic Ellipsometry, Paris, France, January 11–14, 1993:

G. E. Jellison, Jr., "Data Analysis for Spectroscopic Ellipsometry" (invited paper)

1993 Los Angeles O-E Laser Program of the Society of Photo-Optical Instrumentational Engineers, Los Angeles, California, January 16, 1993:

R. F. Haglund, Jr., L. Yang, R. H. Magruder III, K. Becker, J. E. Wittig, C. W. White, R. A. Zuhr, L. Yang, R. Dorsinville, and R. R. Alfano, "Metal-Nanocluster Composites Made by Ion Implantation: A Novel Third-Order Nonlinear Material"

IEEE Workshop on Micro Electro Mechanical Systems, Ft. Lauderdale, Florida, February 7–10, 1993:

J. B. Bates, G. R. Gruzalski, and C. F. Luck, "Rechargeable Solid State Lithium Microbatteries" (invited paper)

Naval Special Warfare Command R&D Conference, Panama City, Florida, February 9–11, 1993:

J. B. Bates and G. R. Gruzalski, "A Thin-Film Rechargeable Lithium Battery" (invited paper)

18th American Institute of Physics Condensed Matter Physics Meeting, Wagga Wagga, Australia, February 10–12, 1993:

A. P. Radlinski, C. J. Boreham, G. D. Wignall, and J. S. Lin, "Small-Angle Scattering Study of Structural Evolution of Organic Macerals in Hydrocarbon Source Rocks"

A. P. Radlinski, G. D. Wignall, and J. S. Lin, "Application of SANS and SAXS to Structural Studies of Hydrocarbon-Bearing Rocks"

WATTec '93, Knoxville, Tennessee, February 16–19, 1993:

D. P. Norton, "Laser Ablation Film Growth of High-Temperature Superconductors"

AIME Annual Meeting, Symposium on Nanocrystalline Materials, Denver, Colorado, February 21–25, 1993:

S. Spooner and G. E. Ice, "On the Structure of Nanocrystalline Materials Seen by X-Ray and Neutron Diffraction" (invited paper)

122nd TMS Annual Meeting, Denver, Colorado, February 21–25, 1993:

D. H. Lowndes and D. P. Norton, "Experimental Investigations of Superconductivity in Quasi-Two-Dimensional Epitaxial Copper Oxide Superlattice and Trilayers" (invited paper)

J. M. Vitek, T. Zacharia, S. A. David, M. Rappaz, and L. A. Boatner, "Modeling of Single-Crystal Laser-Weld Microstructures"

Workshop on Recent Developments in Computer Simulation Studies in Condensed Matter Physics, Athens, Georgia, February 22–26, 1993:

L. Zhang, G. Canright, and T. Barnes, "Quantum Monte Carlo with Complex Weights"

Sixth International Symposium on Advanced Nuclear Energy Research, Mito Ibaraki, Japan, March 10–12, 1993:

S. Katano, S. Funahashi, J. A. Fernandez-Baca, N. Mori, C. Murayama, and Y. Ueda, "Structural Phase Transition and Superconductivity in $La_{2-x}Ba_xCuO_4$"

Bar-Ilan International Conference on Frontiers of Condensed Matter Physics, Tel Aviv, Israel, March 15–18, 1993:

J. R. Thompson, "Vortex Depinning Processes in Ion-Irradiated $YBa_2Cu_3O_7$ Crystals" (invited paper)

1993 Gordon Conference on Crystal Growth, Oxnard, California, March 15–19, 1993:

L. A. Boatner, S. A. David, J. B. Sipf, J. Vitek, and M. Rappaz, "The Growth of Single Crystals of Stainless Steel and Their Application to the Study of Solidification Phenomena" (invited paper)

March Meeting of the American Physical Society, Seattle, Washington, March 22–26, 1993:

A. Biswas, R. Barton, A. Dhere, and J. S. Lin, "SAXS Investigations of Aramid Fiber Morphology" [*Bull. Am. Phys. Soc.* **38**, 92 (1993)]

N. D. Browning, M. F. Chisholm, S. J. Pennycook, D. P. Norton, and D. H. Lowndes, "Atomic-Resolution Mapping of Hole Concentrations Around $YBa_2Cu_3O_{7-\delta}$ Grain Boundaries" [*Bull. Am. Phys. Soc.* **38**, 111 (1993)]

J. D. Budai, D. P. Norton, B. C. Chakoumakos, E. C. Jones, R. Feenstra, D. K. Christen, D. H. Lowndes, and R. T. Young, "Epitaxial YBaCuO Films on Metal Substrates and Buffer Layers" [*Bull. Am. Phys. Soc.* **38**, 260 (1993)]

D. K. Christen, C. E. Klabunde, H. R. Kerchner, S. Zhu, R. Feenstra, J. R. Thompson, J. E. Tkaczyk, and J. M. Phillips, "Electrical Transport Dissipation and Flux Pinning in Superconducting Films with Columnar Defects" [*Bull. Am. Phys. Soc.* **38**, 802 (1993)]

J. F. Cooke, J. M. Bass, and J. A. Blackman, "Electronic Screening, Magnetic Moment, and the Magnetic Susceptibility of Itinerant Electron Systems" [*Bull. Am. Phys. Soc.* **38**, 82 (1993)]

H. Dürr and A. P. Baddorf, "Anharmonicity on the Cu(110)-(2 × 1)-O Surface" [*Bull. Am. Phys. Soc.* **38**, 730 (1993)]

J. A. Fernandez-Baca, R. M. Nicklow, M. E. Hagen, T. G. Perring, and Y. Tsunoda, "High-Energy Magnetic Excitations in $Mn_{90}Cu_{10}$" [*Bull. Am. Phys. Soc.* **38**, 534 (1993)]

P. M. Gehring, H. Chou, S. M. Shapiro, D. Rytz, and L. A. Boatner, "Anomalous Dispersion in Lightly Doped $KT_xNb_{1-x}O_3$" [*Bull. Am. Phys. Soc.* **38**, 406 (1993)]

D. B. Geohegan, "Fast Diagnostics of the Pulsed Laser Ablation Process" [*Bull. Am. Phys. Soc.* **38**, 669 (1993)] (invited paper)

D. E. Jesson, S. J. Pennycook, J.-M. Baribeau, and D. C. Houghton, "Interplay Between Atomic-Scale Growth Modes and Evolving Surface Morphology During Si_xGe_{1-x} MBE Growth" [*Bull. Am. Phys. Soc.* **38**, 678 (1993)]

E. C. Jones, D. K. Christen, J. R. Thompson, R. Feenstra, and S. Zhu, "Electrical Transport Properties of Oxygen-Deficient Epitaxial $YBa_2Cu_3O_{7-\delta}$ Thin Films" [*Bull. Am. Phys. Soc.* **38**, 272 (1993)]

M. N. Kunchur, "Free-Flux Flow in $YBa_2Cu_3O_{7-\delta}$ Films" [*Bull. Am. Phys. Soc.* **38**, 459 (1993)] (invited paper)

B. C. Larson, J. Z. Tischler, L. A. Boatner, E. E. Alp, and T. Mooney, "Mössbauer Resonant X-Ray Beams from Synchrotrons for Performing High-Resolution X-Ray Scattering Spectroscopy". [*Bull. Am. Phys. Soc.* **38**, 113 (1993)]

S. H. Liu, "Static and Dynamic Properties of Cr Alloys" [*Bull. Am. Phys. Soc.* **38**, 83 (1993)] (invited paper)

C.-K. Loong, L. Soderholm, M. A. Abraham, L. A. Boatner, and N. M. Edelstein, "Crystal-Field Splittings and Magnetic Properties of RPO_4 (R = Tb-Yb)" [*Bull. Am. Phys. Soc.* **38**, 532 (1993)]

D. P. Norton, B. C. Chakoumakos, J. D. Budai, and D. H. Lowndes, "Structural and Transport Properties of $Ca_{1-x}Sr_xCuO_2$ Thin Films Grown by Pulsed-Laser Deposition" [*Bull. Am. Phys. Soc.* **38**, 259 (1993)]

B. C. Sales, T. Thundat, B. C. Chakoumakos, L. A. Boatner, and B. Warmack, "Direct AFM Observations of Surface Defects and Scanning-Induced Atom Removal on $Pb_2P_2O_7$" [*Bull. Am. Phys. Soc.* **38**, 280 (1993)]

P. W. Schmidt, D. Avnir, H. B. Neumann, A. Hohr, M. Steiner, J. S. Lin, D. Levy, and V. R. Kaufman, "Small-Angle X-Ray Scattering Study of Some Xerogels Similar to Precursor Gels for Sol-Gel Glass Processing" [*Bull. Am. Phys. Soc.* **38**, 544 (1993)]

K. W.-K. Shung and S. K. Ma, "Calculated Photoemission Spectra from the Al(100) Surface" [*Bull. Am. Phys. Soc.* **38**, 698 (1993)]

H. G. Smith, J. A. Fernandez-Baca, M. Wuttig, and T. R. Finlayson, "Study of the Martensitic Phase Transformation in In-Tl Alloys by Neutron Powder Diffraction" [*Bull. Am. Phys. Soc.* **38**, 307 (1993)]

J. O. Sofo and G. D. Mahan, "Resistivity and Superconductivity from Anharmonic Phonons" [*Bull. Am. Phys. Soc.* **38**, 273 (1993)]

Y. Sun, R. L. Cone, M. J. M. Leask, and M. M. Abraham, "Angle-Dependent ODNMR on the Defects in $EuVO_4$" [*Bull. Am. Phys. Soc.* **38**, 469 (1993)]

Y. R. Sun, J. R. Thompson, D. K. Christen, H. R. Kerchner, Y. J. Chen, C. E. Klabunde, B. C. Sales, B. C. Chakoumakos, L. Civale, A. D. Marwick, and F. Holtzberg, "DC Magnetization Studies of Anisotropy in Heavy Ion-Irradiated $Bi_2Sr_2CaCu_2O_8$ and $YBa_2Cu_3O_{7-\delta}$ Single Crystals" [*Bull. Am. Phys. Soc.* **38**, 802 (1993)]

J. R. Thompson, Y. R. Sun, L. Civale, D. K. Christen, H. R. Kerchner, Y. J. Chen, B. C. Sales, B. C. Chakoumakos, A. D. Marwick, and F. Holtzberg, "Effective Vortex Pinning Energy $U_{eff}(L,T)$ in High-T_c Superconductors with Point- and Line-Like Defects" [*Bull. Am. Phys. Soc.* **38**, 835 (1993)]

J. Z. Tischler, J. D. Budai, D. E. Jesson, D. Eres, P. Zschack, J.-M. Baribeau, and D. C. Houghton, "Structure of the Ordering in $Si_{0.5}Ge_{0.5}$ Using X-Ray Diffraction" [*Bull. Am. Phys. Soc.* **38**, 678 (1993)]

J. E. Tkaczyk, J. A. Deluca, P. L. Karas, P. J. Bednarzyk, and D. K. Christen, "Enhanced Transport Critical Current at High Fields after Ag Ion Irradiation of Polycrystalline T1(1223) Films" [*Bull. Am. Phys. Soc.* **38**, 830 (1993)]

C. F. Walters, D. B. Poker, D. M. Zehner, and E. W. Plummer, "Correlation of the H-Induced Reconstructions of Cu(100) with an Absolute Determination of the Coverage" [*Bull. Am. Phys. Soc.* **38**, 286 (1993)]

G. M. Watson, D. Gibbs, S. H. Song, S. G. J. Mochrie, and D. M. Zehner, "High-Temperature Faceting and Reconstruction of Vicinal Au(111)" [*Bull. Am. Phys. Soc.* **38**, 437 (1993)]

J. F. Wendelken and J. K. Zuo, "A High-Resolution LEED Study of the Monoepitaxial Growth and Smoothing Kinetics of Cu/Cu(100)" [*Bull. Am. Phys. Soc.* **38**, 670 (1993)]

R. F. Wood, "Charge Transfer and Dimensionality Effects in YBCO Superlattices" [*Bull. Am. Phys. Soc.* **38**, 520 (1993)]

M. Yethiraj, H. A. Mook, G. D. Wignall, E. M. Forgan, S. L. Lee, R. Cubitt, and D. Mck. Paul, "Small-Angle Neutron Scattering Measurements of the Anisotropic Flux Lattice in $YBa_2Cu_3O_7$" [*Bull. Am. Phys. Soc.* **38**, 579 (1993)]

D. M. Zehner, "Temperature-Dependent Surface Structures" (invited paper) [*Bull. Am. Phys. Soc.* **38**, 436 (1993)]

L. Zhang, G. Canright, and T. Barnes, "Quantum Monte Carlo Simulations of 2D Systems with External Magnetic Field" [*Bull. Am. Phys. Soc.* **38**, 166 (1993)]

S. Zhu, D. K. Christen, C. E. Klabunde, J. R. Thompson, E. C. Jones, R. Feenstra, D. H. Lowndes, and D. P. Norton, "Superconductive Transport Properties of Heavy Ion-Irradiated Epitaxial $YBa_2Cu_3O_7$ Thin Films" [*Bull. Am. Phys. Soc.* 38, 802 (1993)]

Metropolitan Microscopy Society Meeting, Paramus, New Jersey, March 31, 1993:

S. J. Pennycook, "Direct Atomic Imaging of Materials by Z-Contrast STEM" (invited paper)

Spring Meeting of the Japan Institute of Metals, Yokohama, Japan, March 31–April 2, 1993:

E. Takasuka, S. J. Pennycook, and M. F. Chisholm, "Z-Contrast Observation of GaAs/Si Through STEM"

International Symposium on High-T_c Superconductivity and Its Applications, Cairo, Egypt, April 4–16, 1993:

R. F. Wood, "Spin-Polaron Theory of High-T_c Superconductivity. I. Spin Polarons and High-T_c Pairing" (invited paper)

R. F. Wood, "Spin-Polaron Theory of High-T_c Superconductivity. II. Electronic Structure of the CuO_2 Planes" (invited paper)

R. F. Wood, "Spin-Polaron Theory of High-T_c Superconductivity. III. Gap Function and Critical Temperature" (invited paper)

R. F. Wood, "High-T_c Superconducting Superlattices" (invited paper)

Spring Meeting of the Materials Research Society, San Francisco, California, April 12–16, 1993:

N. D. Browning, M. F. Chisholm, S. J. Pennycook, D. P. Norton, and D. H. Lowndes, "Determination of $YBa_2Cu_3O_{7-\delta}$ Grain Boundary Structure and Electronic Properties by Z-Contrast Imaging and Energy Loss Spectroscopy in STEM"

G. Eres and J. W. Sharp, "Investigation of the Hydrogen Desorption Kinetics in Surface-Limited Thin-Film Growth of SiGe Alloys From Binary Mixtures of Silanes and Germanes"

T. E. Haynes, R. Morton, and S. S. Lau, "Lattice Damage in Ion-Implanted Compound Semiconductors and Its Effect on Electrical Activation" (invited paper)

D. E. Jesson, S. J. Pennycook, J.-M Baribeau, and D. C. Houghton, "Evolving Surface Cusps During Strained-Layer Epitaxy"

K. S. Jones, H. G. Robinson, T. E. Haynes, M. D. Deal, C. C. Lee, and E. L. Allen, "Defects and Diffusion in Si^+-Implanted GaAs"

D. Lederman, D. P. Belanger, J. Wang, S-J. Han, C. P. Paduani, C. A. Ramos, and R. M. Nicklow, "Neutron and X-Ray Scattering Studies of $(FeF_2)_m(CoF_2)_n$ Multilayers"

D. K. Shuh, L. J. Terminello, L. A. Boatner, and M. M. Abraham, "X-Ray Absorption Spectroscopy of the Rare-Earth Orthophosphates"

X.-L. Wang, J. A. Fernandez-Baca, C. R. Hubbard, K. B. Alexander, and P. F. Becher, "Transformation Behavior in $ZrO_2(CeO_2)/Al_2O_3$ Ceramic Composites"

L. Xie, O. W. Holland, and C. W. White, "Microvoiding in High-Current Density-Irradiated Si"

1993 Annual Meeting of the American Ceramic Society, Cincinnati, Ohio, April 18–22, 1993:

J. R. Brewster, G. W. Steadman, and L. A. Boatner, "Fiber-Textured and In-Plane-Aligned Coatings from Colloidal Suspensions of Faceted Cubic MgO Microcrystals"

J. B. Fanselow, R. F. Cooper, and D. B. Poker, "Redox Reactions, Chemical Diffusion, and Nucleation in Fe^{2+}-Bearing Calcium-Magnesium Aluminosilicate Glasses"

X.-L. Wang, J. A. Fernandez-Baca, K. B. Alexander, P. F. Becher, and C. R. Hubbard, "Residual Microstresses and the $t \rightarrow m$ Phase Transition in $ZrO_2(CeO_2)/Al_2O_3$ Ceramic Composites"

Second International Conference on Laser Ablation, Knoxville, Tennessee, April 19–22, 1993:

D. B. Geohegan, "Imaging and Blackbody Emission Spectra of Hot Particulates Generated During Laser Ablation" (invited paper)

D. H. Lowndes, M. J. Godbole, G. E. Jellison, Jr., and A. J. Pedraza, "Ablation, Surface Activation, and Electroless Metallization of Insulating Materials by Pulsed Excimer Laser Irradiation"

J. W. McCamy and D. H. Lowndes, "Growth of Semiconductor Alloys and Superlattices with Continuously Variable Composition by Pulsed-Laser Ablation"

D. P. Norton, B. C. Chakoumakos, J. D. Budai, and D. H. Lowndes, "Pulsed-Laser Deposition of Metastable $Ca_{1-x}Sr_xCuO_2$ Thin Films"

S. Zhu, D. H. Lowndes, B. C. Chakoumakos, D. K. Christen, E. C. Jones, J. D Budai, X.-Y. Zheng, and R. J. Warmack, "Effects of Deposition Rate on $Bi_2Sr_2CaCu_2O_{8+x}$ and $Bi_2Sr_{1.6}La_{0.4}CuO_{6+x}$ Epitaxial Thin-Film Growth by Pulsed-Laser Ablation"

X.-Y. Zheng, D. H. Lowndes, S. Zhu, and R. J. Warmack, "Particles on Surfaces of Laser-Ablated $YBa_2Cu_3O_{7-\delta}$ Films"

American Vacuum Society, New Mexico Chapter Meeting, Santa Fe, New Mexico, April 27–30, 1993:

J. M. Williams, R. A. Buchanan, and C. J. McHargue, "Ion Implantation for Corrosion and Wear Inhibition in Materials" (invited paper)

D. M. Zehner, "Atomic Structure and Composition of Ordered and Random Alloy Surfaces" (invited paper)

IXth International Congress on Small-Angle Scattering, Saclay, France, April 27–30, 1993:

S.-L. Chang, C.-Y. Ku, S.-H. Chen, and J. S. Lin, "Measurement and Interpretation of Counterion Distributions Around Cylindrical Micelles" (invited paper)

Conference on Lasers and Electro-Optics (CLEO '93), Baltimore, Maryland, May 2–7, 1993:

D. B. Geohegan, "Fast Diagnostics of Laser Ablation Used in Pulsed-Laser Deposition"

High Aspect Ratio Micro-Electro-Magnetic-Mechanical Systems Conference, Detroit, Michigan, May 17–18, 1993:

S. M. Gorbatkin, G. T. Alley, J. B. Bates, L. A. Berry, S. C. Jacobson, and J. M. Ramsey, "Selected Oak Ridge National Laboratory Programs Relevant to Micro-Systems Development" (invited paper)

Annual Meeting of the American Crystallographic Association, Albuquerque, New Mexico, May 23–28, 1993:

B. C. Chakoumakos, J. D. Budai, and D. P. Norton, "Structural Systematics of Alkaline-Earth Copper Oxide Films Grown by Pulsed-Laser Deposition on Single-Crystal Perovskites"

American Association for Information Science (ASIS) 1993 Mid-Year Meeting, Knoxville, Tennessee, May 24–27, 1993:

S. J. Pennycook, "Direct Atomic Imaging of Materials Through Z-Contrast Electron Microscopy" (invited paper)

6th Symposium on Surface Physics, Czechoslovakia, May 24–29, 1993:

E. W. Plummer, "Beryllium Surfaces" (invited paper)

Electronic Properties of Two-Dimensional Systems Conference, Newport, Rhode Island, May 31–June 4, 1993:

X. M. Chen and J. J. Quinn, "Numerical Studies of the Photoluminescence Spectrum of Quantum Hall Systems"

5th European Workshop on Metal-Organic Vapor Phase Epitaxy and Related Growth Techniques, Malmo, Sweden, June 2–4, 1993:

A. Erbil, W. Braun, B. S. Kwak, L. A. Boatner, and J. D. Budai, "Oxide Ferroelectric Materials Grown by Metalorganic Chemical Vapor Deposition"

Workshop on High-Temperature Superconductor Phase Diagrams, Santa Fe, New Mexico, June 2–4, 1993:

M. Paranthaman, J. R. Thompson, Y. R. Sun, J. Brynestad, and D. M. Kroeger, "Evidence for Phase Stability and Weak Links in Polycrystalline $HgBa_2CuO_{4+\delta}$" (invited paper)

20th Annual Meeting of the Microscopical Society of Canada, Toronto, Canada, June 2–5, 1993:

S. J. Pennycook, D. E. Jesson, M. F. Chisholm, and N. D. Browning, "Insights into Semiconducting Materials and Growth Phenomena Through Z-Contrast STEM" (invited paper)

National Research Council Workshop on Quantum Dots and Mesoscopic Systems, Ontario, Canada, June 6–11, 1993:

X. Chen and J. J. Quinn, "Numerical Studies of the Photoluminescence of Quantum Hall Systems," (invited paper)

13th Annual Tennessee Valley Chapter of the American Vacuum Society Symposium and Equipment Exhibit, Oak Ridge, Tennessee, June 9–10, 1993:

J. B. Bates, "Rechargeable Thin-Film Lithium Batteries" (invited paper)

S. M. Gorbatkin, R. F. Burgie, W. C. Oliver, J. C. Barbour, T. M. Mayer, and M. L. Thomas, "Electron Cyclotron Resonance Microwave Plasma Processing of BN Thin Films" (invited paper)

Vibrations at Surfaces VII, Genova, Italy, June 14–17, 1993:

H. Dürr and A. P. Baddorf, "Anharmonicity on the Cu(110)-(2 × 1)-O Surface"

J. B. Hannon and E. W. Plummer, "Shear Horizontal Vibrations at the (0001) Surface of Beryllium"

70th Birthday Symposium for Professor Bernard Goodman, Cincinnati, Ohio, June 19, 1993:

Ordean S. Oen, "Discovery of Ion Channeling"

L. Zhang, "From Fermion Sign to Fermion Phase: Quantum Monte Carlo Simulations with Anyons"

53rd Physical Electronics Conference, Troy, New York, June 21–23, 1993:

P. F. Lyman and D. M. Zehner, "Core Level Spectroscopy Investigation of the BCC Random Alloy $Mo_{0.75}Re_{0.25}$"

1993 International Workshop on Superconductivity, Hakodate, Japan, June 28–July 1, 1993:

S. J. Pennycook, N. D. Browning, M. F. Chisholm, S. Zhu, R. Feenstra, D. P. Norton, and D. H. Lowndes, "High-Resolution Z-Contrast Imaging and Hole Concentration Mapping of YBCO Thin Films" (invited paper)

6th Analytical Electron Microscopy (AEM) Workshop, Los Angeles, California, July 11–16, 1993:

N. D. Browning, M. F. Chisholm, and S. J. Pennycook, "Atomic-Resolution Electron Energy Loss Spectroscopy in the Scanning Transmission Electron Microscope"

S. J. Pennycook and D. E. Jesson, "Z-Contrast Imaging with a 300-kV STEM"

NATO Advanced Research Workshop, Boca Raton, Florida, July 16–21, 1993:

P. F. Lyman and D. M. Zehner, "Core-Level Spectroscopy Investigation of the $Mo_{0.75}Re_{0.25}(100)$ Surface" (invited paper)

34th Annual Meeting of the Institute of Nuclear Materials Management, Scottscale, Arizona, July 18–21, 1993:

L. A. Boatner and A. Lempicki, "Portable Nuclear Weapons and Fissile Materials Identification System"

M. L. Simpson, L. A. Boatner, D. E. Holcomb, S. A. McElhaney, J. T. Mihalczo, J. D. Muhs, M. R. Roberts, and N. W. Hill, "Passive Sensor Systems for Nuclear Material Monitoring"

1993 International Conference on Defects in Semiconductors, Gmünden, Austria, July 18–23, 1993:

M. Ivanda, U. V. Desnica, and T. E. Haynes, "Raman Study of 'Boson Peak' in Ion-Implanted GaAs: Dependence on Ion Dose and Dose Rate"

XVIIIth International Conference on the Physics of Electronic and Atomic Collisions, Aarhus, Denmark, July 21–27, 1993:

I. G. Hughes, J. Burgdörfer, L. Folkerts, C. C. Havener, S. H. Overbury, M. T. Robinson, D. M. Zehner, P. A. Zeijlmans van Emmichoven, and F. W. Meyer, "The Role of Below-Surface Secondary Cascade Processes in Potential Electron Emission During Multicharged Ion-Surface Interactions"

F. W. Meyer, L. Folkerts, C. C. Havener, I. G. Hughes, S. H. Overbury, D. M. Zehner, and P. A. Zeijlmans van Emmichoven, "Electron Spectroscopic Studies of the Neutralization of Slow Muticharged Ions During Interactions with a Metal Surface" (invited paper)

The Society of Photo-Optical Instrumentational Engineers (SPIE) Neutron Optical Devices and Applications, San Diego, California, July 22–24, 1993:

G. S. Smith, W. Hamilton, M. Fitzsimmons, S. M. Baker, K. M. Hubbard, M. Nastasi, J-P. Hirvonen, and T. G. Zocco, "Neutron Reflectometry Study of Thermally Induced Boron Diffusion in Amorphous Elemental Boron"

15th International Conference on Atomic Collisions in Solids, London, Ontario, Canada, July 26–30, 1993:

M. T. Robinson, "The Statistics of Sputtering"

Workshop on the Statics and Dynamics of Vortices in Superconductors, Eugene, Oregon, August 1–3, 1993:

E. C. Jones, "Intrinsic and Extrinsic Effects Observed in the Superconducting Hall Transitions of Epitaxial Thin Films of $YBa_2Cu_3O_{7-\delta}$ and Polycrystalline $TlCa_2Ba_2Cu_3O_{-8}$" (invited paper)

M. N. Kunchur, "Mixed State Transport at High Current Densities" (invited paper)

International Summer School on the Fundamentals of Radiation Damage, Urbana, Illinois, August 1–5, 1993:

M. T. Robinson, "Basic Physics of Radiation Damage Production" (invited paper)

51st Annual Meeting of the Microscopy Society of America, Cincinnati, Ohio, August 1–6, 1993:

M. F. Chisholm, D. E. Jesson, S. J. Pennycook, and S. Mantl, "Z-Contrast Imaging of an Ordered Interface Structure in the $Si/CoSi_2/Si$ System"

N. D. Browning, M. M. McGibbon, M. F. Chisholm, and S. J. Pennycook, "Atomic-Resolution Characterization of Interface Structures by Electron Energy Loss Spectroscopy"

D. E. Jesson and S. J. Pennycook, "Incoherence in Atomic-Resolution Z-Contrast Imaging"

H. S. von Harrach, D. E. Jesson, and S. J. Pennycook, "Toward 1-Angstrom Resolution STEM"

International Workshop on Plasma-Based Ion Implantation, Madison, Wisconsin, August 4–6, 1993:

J. M. Williams, C. C. Tsai, W. L. Stirling, and J. H. Whealton, "Potential Applications of Fusion Neutral Beam Facilities for Advanced Material Processing"

XXth International Conference on Low-Temperature Physics, Eugene, Ohio, August 4–11, 1993:

D. K. Christen, S. Zhu, C. E. Klabunde, H. R. Kerchner, J. R. Thompson, R. Feenstra, L. Civale, and J. M. Phillips, "Effects of Columnar Defects on the Superconducting Properties of $YBa_2Cu_3O_{7-\delta}$: Limits to the Irreversibility Line"

H. R. Kerchner, J. R. Thompson, Y. R. Sun, D. K. Christen, J. O. Thomson, B. C. Sales, B. C. Chakoumakos, L. Civale, and A. D. Marwick, "Enhanced Vortex-Pinning Strength and Magnetic-Irreversibility Line Via Columnar Defects in Single-Crystal $Bi_2Sr_2CaCu_2O_8$"

S. H. Liu and R. A. Klemm, "Density of States and Tunneling Characteristics of Layered Superconductors"

J. R. Thompson, D. K. Christen, and J. G. Ossandon, "Equilibrium Magnetization of the High-T_c Superconductor $Tl_2Ca_2Ba_2Cu_3O_{10+\delta}$ and Fluctuation Effects"

International Conference on Applications of the Mössbauer Effect, Vancouver, Canada, August 8–13, 1993:

J. Z. Tischler, B. C. Larson, and E. E. Alp, "Resonantly Scattered Beams from Synchrotrons for High-Resolution X-Ray Scattering Spectroscopy" (invited paper)

International Conference on Luminescence, Storrs, Connecticut, August 9–13, 1993:

G. Chen, R. G. Haire, J. R. Peterson, and M. M. Abraham, "A Luminescence Study of $EuVO_4$ at High Pressure"

A. J. Wojtowicz, M. Balcerzyk, A. Lempicki, and L. A. Boatner, "Rare-Earth Orthophosphate Scintillators"

Y. Sun, R. L. Cone, M. J. M. Leask, and M. M. Abraham, "Defect Structure and Dynamics in $EuVO_4$"

Workshop on Frontiers of Surface Diffraction and Imaging, Hong Kong, China, August 10–13, 1993:

H. L. Davis, "LEED Investigation of Both the Multilayer Relaxation and the Layer-by-Layer Constituent Segregation in Surfaces of Substitutionally Random Binary Alloys" (invited paper)

Fourth International Conference on the Structure of Surfaces, Shanghai, China, August 16–19, 1993:

H. L. Davis and J. R. Noonan, "Layer-by-Layer Segregation and Multilayer Relaxation of the Random Alloy $Au_{62}Ag_{38}$(111) Surface"

Workshop on Copper Interconnect Technology, Rensselaer Polytechnic Institute, Troy, New York, August 17–18, 1993:

L. A. Berry and S. M. Gorbatkin, "Permanent Magnet ECR Plasma Source With Remote Window"

XVIth International Congress and General Assembly International Union of Crystallography, Beijing, China, August 21–29, 1993:

H. G. Smith and J. B. Davidson, "A Neutron-Sensitive TV-Image Intensifier System"

206th American Chemical Society National Meeting, Chicago, Illinois, August 22–27, 1993:

J. D. Londono, G. D. Wignall, A. H. Narten, K. G. Honnell, A. Yethiraj, and K. S. Schweizer, "Asymmetries in the Flory-Huggins Interaction Parameter in Isotropic Polymer Blends"

D. R. Mullins and P. F. Lyman, "The Adsorption and Reaction of Methanethiol on Clean and Modified W(001) and Ru(0001)"

3rd Annual International Conference and Exposition on Surface Mount Technology, San Jose, California, August 29–September 2, 1993:

J. B. Bates, G. R. Gruzalski, N. J. Dudney, C. F. Luck, and X. Yu, "Rechargeable Thin-Film Lithium Batteries" (invited paper)

13th European Conference on Surface Science, Warwick, United Kingdom, August 30–September 4, 1993:

R. Döll, M. Kottoke, K. Heinz, L. Hammer, K. Müller, and D. M. Zehner, "Chemical Tensor LEED and Its Application to $Mo_xRe_{1-x}(100)$ Surfaces"

8th Electronic Materials and Processing Conference, San Jose, California, August 31–September 3, 1993:

J. B. Bates, "Rechargeable Thin-Film Lithium Batteries" (invited paper)

3rd International Union of the Materials Research Society International Conference on Advanced Materials, Tokyo, Japan, August 31–September 4, 1993:

Y. Chen and R. Gonzalez, "Low-Temperature Diffusion of Hydrogenic Species in Oxide Crystals: Radiation-Induced Diffusion" (invited paper)

D. B. Geohegan, A. A. Purezky, R. L. Hettich, X.-Y. Zheng, R. E. Haufler, and R. N. Compton, "Gated ICCD Photography of the KrF-Laser Ablation of Graphite into Background Gases" (invited paper)

D. B. Geohegan, "Physics and Diagnostics of Pulsed-Laser Deposition Laser Plasmas" (invited paper)

T. E. Haynes, "Lattice Damage During Ion Implantation of Semiconductors" (invited paper)

C. J. McHargue, D. L. Joslin, J. M. Williams, and M. E. O'Hern, "Surface Modification of Sapphire for Enhanced Infrared Window Performance" (invited paper)

N. Parikh, E. McGucken, M. L. Swanson, J. D. Hunn, C. W. White, and R. A. Zuhr, "Ion Implantation of Diamond: Doping, Damage, and Lift-Off" (invited paper)

Y. Shigesato, D. C. Paine, and T. E. Haynes, "Ion Implantation and Dynamic Recovery of Tin-Doped Indium Oxide Thin Films"

C. W. White, D. S. Zhou, R. A. Zuhr, and R. A. Magruder, "Formation of Colloidal Ag Precipitates in Fused Silica by MeV Implantation" (invited paper)

Seventh International Conference on Radiation Effects in Insulators, Nagoya, Japan, September 6–10, 1993:

R. F. Haglund, L. Yang, R. H. Magruder, C. W. White, R. A. Zuhr, L. Yang, R. Dorsinville, and R. R. Alfano, "Nonlinear Optical Properties of Metal-Quantum-Dot Composites Synthesized by Ion Implantation" (invited paper)

D. L. Joslin, C. J. McHargue, and C. W. White, "Ion Mixing in Oxide-Sapphire Systems"

D. L. Joslin, C. J. McHargue, C. W. White, and N. D. Evans, "Amorphization of Sapphire During Ion Beam Mixing"

9th International Conference on Thin Films, Vienna, Austria, September 6–10, 1993:

S. J. Pennycook, N. D. Browning, M. F. Chisholm, S. Zhu, R. Feenstra, D. P. Norton, and D. H. Lowndes, "Electron Microscopy of Layered Oxide Superconducting Thin Films" (invited paper)

NATOASI Conference, Elounda (Crete), Greece, September 6–17, 1993:

D. B. Geohegan, "Time-Resolved Diagnostics of Excimer Laser-Generated Abaltion Plasmas Used for Pulsed-Laser Deposition" (invited paper)

Conference on Rapid Thermal Processing '93, Scottsdale, Arizona, September 8–10, 1993:

G. E. Jellison, Jr., D. H. Lowndes, and R. F. Wood, "The Optical Functions of Silicon at Elevated Temperatures and Their Application to Pulsed-Laser Annealing" (invited paper)

Surfaces in Biomaterials '93, Cambridge, Massachusetts, September 12–15, 1993:

J. M. Williams, "Ion Implantation of Orthopedic Alloys" (invited paper)

9th International Conference on Solid State Ionics, The Hague, The Netherlands, September 12–17, 1993:

J. B. Bates, G. R. Gruzalski, N. J. Dudney, and X. Yu, "Rechargeable Thin-Film Lithium Batteries" (invited paper)

20th Rare Earth Research Conference, Monterey, California, September 12–17, 1993:

C.-K. Loong, L. Soderholm, J. S. Xue, M. M. Abraham, and L. A. Boatner, "Rare-Earth Energy Levels and Magnetic Properties of $DyPO_4$"

Multinational Congress on Electron Microscopy, Parma, Italy, September 13–17, 1993:

S. J. Pennycook, N. D. Browning, D. E. Jesson, and M. F. Chisholm, "Probing Interface Structure and Bonding at Atomic-Resolution STEM" (invited paper)

European Research Conference on Electronic Structure of Surfaces, Interfaces, and Localized Defects, Porto Carras, Greece, September 18–23, 1993:

G. D. Mahan, "Electron-Electron Interactions in Metals" (invited paper)

V. Milman, D. E. Jesson, S. J. Pennycook, M. C. Payne, and I. Stich, "*Ab Initio* Study of Ge Adsorption and Diffusion on the Si(100) Surface" (invited paper)

7th Alabama Materials Research Conference, Huntsville, Alabama, September 21–22, 1993:

L. A. Boatner, B. C. Sales, and B. C. Chakoumakos, "Recent Advances in the Modification and Characterization of Surfaces and Disordered Materials" (invited paper)

Y. Powell-Friend, D. Ila, L. A. Boatner, and J. Brewster, "Ultrasonic Cavitation Effects on the Physical Properties of Magnesium Oxide and Stainless Steel"

L. J. Romana, J. B. Brewster, and L. A. Boatner, "Ultrasonic Cavitation Effects on Ion-Implanted MgO Surfaces: A New Method for Mechnically Etching Ceramics"

T. P. Sjoreen, "Ion Beam Synthesis of Mesotaxial Transition-Metal Silicides"

J. M. Williams, "Ion Implantation of Biomedical Materials" (invited paper)

Symposium of North Eastern Accelerator Personnel, Rochester, New York, September 22–26, 1993:

D. K. Hensley, "1993 Laboratory Report to SNEAP for the Surface Modification and Characterization Research Center at Oak Ridge National Laboratory"

Second Interamerican Congress on Electron Microscopy, Cancun, Mexico, September 26–October 2, 1993:

N. D. Browning, M. F. Chisholm, and S. J. Pennycook, "Atomic Scale Microanalysis in the STEM"

54th Autumn Meeting of the Japan Society of Applied Physics, Hokkaido, Japan, September 27–30, 1993:

E. Takasuka, S. J. Pennycook, and M. F. Chisholm, "Z-Contrast and Conventional HRTEM Observation of GaAs/Si Interfaces"

Seminars

SOLID STATE DIVISION SEMINARS AT ORNL

During the periodcovered by this report, S. J. Pennycook served as Seminar Chairman. The following seminars were held:

"Molecular Dynamics Analyses of Low-Energy Atom-Surface Interactions," C. Gilmore, George Washington University, Washington, D.C.

"Magic Strains, Magic Numbers, Magic Angles: Applications and Limitations of Density Functional Theory," T. Kaxiras, Harvard University, Boston, Mass.

"Compositional Disordering of Superlattices," W. Xia, University of California–San Diego, San Diego, Calif.

"Ultrasonic Studies on Martensitic Phase Transitions in Metals," J. Trivisonno, John Carroll University, Cleveland, Ohio

"Great Balls of Carbon! What's All the Fuss About Buckyballs?" P. Heiney, University of Pennsylvania, Philadelphia, Pa.

"Atomistic Simulation of Materials: Empirical and *Ab Initio* Investigations," A. Antonelli, Virginia Commonwealth University, Richmond, Va.

"TEM Investigations of the Damage Produced by Ion Implantation of GaAs and Other Semiconductors," M. W. Bench, University of Illinois, Urbana, Ill.

"Applications of Resonant Nuclear Bragg Scattering," J. Z. Tischler, Solid State Division, ORNL

"Toward a First-Principles Implementation of Density-Functional Theory at a Metal Surface," A. G. Eguiluz, Montana State University, Bozeman, Mont.

"Electron Cyclotron Resonance Microwave Plasmas for Thin-Film Processing," S. M. Gorbatkin, Solid State Division, ORNL

"Are High-T_c Cuprates Conventional Superconductors? A Van Hove Scenario for High-Temperature Superconductivity," C. C. Tseui, IBM T. J. Watson Research Center, Yorktown Heights, N.Y.

"Crystal Defects in Tetrahedrally, Closed-Packed Faces in Metals and Crystallography of Austenite Decomposition in Steels," D. Zhou, University of Virginia, Charlottesville, Va.

"Thermoelectrics: Materials, Modeling, and Physical Limits," G. D. Mahan, ORNL-UT Distinguished Scientist, Solid State Division, ORNL

"Tight-Binding Molecular Dynamics: Some Subtleties and Generalizations," K. R. Subbaswamy, University of Kentucky, Lexington, Ky.

"Relations Between Structure and T_c in Oxide Superconductors," A. Hewat, Institut Laue Langevin, Grenoble, France

"Properties of a Layered SN Model for Superconducting Cuprates," A. A. Abrikosov, Argonne National Laboratory, Argonne, Ill.

"In Situ and Ex Situ Annealing Studies of Metal/Gas Interfacial Reactions Using HRTEM," D.-H. Ko, Stanford University, Stanford, Calif.

"Studies of Chemical Bonding and Transport Processes in Oxygen-Implanted SiGe Alloys," H. Liu, University of Surrey, Surrey, United Kingdom

"Barrierless Misfit Dislocation Nucleation in Strained-Layer Heteroepitaxy," D. D. Perovic, University of Toronto, Toronto, Canada

"Microstructural and Interfacial Stability of Nanometer X-Ray Multilayers," T. D. Nguyen, Lawrence Berekley Laboratory, Berkeley, Calif.

"Sputter Deposition Ceramics," C. R. Aita, University of Wisconsin, Milwaukee, Wis.

"Doping of Diamond by Ion Implantation," J. D. Hunn, University of North Carolina, Chapel Hill, N.C.

"Chemical and Atomic Displacement Pair Correlations in a BCC $Fe^{53}Cr^{47}$ Single Crystal," L. Robertson, National Institute of Standards and Technology, Washington, D.C.

"Features of Microstrip Proportional Counters," P. Geltenbort, Institut Laue Langevin, Grenoble, France

"Those Little Drops of Light: Raman and Brillouin Spectroscopy in Condensed Matter," L. E. McNeil, University of North Carolina, Chapel Hill, N.C.

"Update on High-Flux Pulsed Reactor IBR-2 and Research Programs at this Facility," V. Akesenov, Joint Institute for Nuclear Research, Dubna, Russia

"Polarized Neutron Reflectivity Studies of Superconductors," D. Korneev, Joint Institute for Nuclear Research, Dubna, Russia

"Transport and Relaxational Properties of Heavy Metal Fluoride Systems," W. C. Hasz, Rensselaer Polytechnic Institute, Troy, N.Y.

"Layer-by-Layer Growth and Stability of $BaTiO_3$ on MgO," R. A. McKee, Metals and Ceramics Division, ORNL

"Crystal Structure Systematics of the Cuprate Superconductors," B. C. Chakoumakos, Solid State Division, ORNL

"Electron Beam-Pumped Recombination Lasers," R. L. Rhoades, McKechnie Packaging, Campaign, Ill.

"The Transition from the Thermal to Plasma Mechanism During the Excimer Ablation of Copper Metal," R. Dreyfus, IBM T. J. Watson Research Center, Yorktown Heights, N.Y.

"Materials Science in the Electron Microscope," F. M. Ross, Lawrence Berkeley Laboratory, Berkeley, Calif.

"Neutron Scattering Studies of the Magnetic Excitations of Itinerant-Electron Antiferromagnets: The Case of γ-Mn Alloys," J. A. Fernandez-Baca, Solid State Division, ORNL

"Scanning Tunneling Microscope Studies of Surface and Subsurface Electronic Properties of Semiconductors," R. J. Hamers, University of Wisconsin, Madison, Wis.

"Two-Dimensional Model of a Magnetized Glow-Discharge Plasma," D. Graves, University of California, Berkeley, Calif.

"Spectroscopic Ellipsometry: A Technique for Thin-Film and Bulk Material Analysis," G. E. Jellison, Jr., Solid State Division, ORNL

"Ambient Temperature Solid State Batteries," B. B. Owens, University of Minnesota, Minneapolis, Minn.

"Epitaxy on GaAs {111}B: Physical Properties, Growth, and Devices," K. Yang, Rensselaer Polytechnic Institute, Troy, N.Y.

"Laser-Induced Site-Specific Reactions in Precursors for Materials Growth," S. Deshmukh, Tulane University, New Orleans, La.

"Strain Relief in Heteroepitaxial Systems: Where Did All the Threads Go?" L. J. Schowalter, Rensselaer Polytechnic Institute, Troy, N.Y.

"Structure and Atomistic Behavior of Silicate Glasses and Crystalline Alumina Surfaces," S. H. Garofalini, Rutgers University, Piscataway, N.J.

"Prospects for Atomic-Resolution Spectroscopy: Applications to High-T_c Superconductivity," N. D. Browning, Solid State Division, ORNL

"Molecular-Beam-Epitaxial Growth of Si/Ge and III/V Compound Semiconductors," K. Chen, University of Minnesota, Minneapolis, Minn.

"Ellipsometric Studies of Charge Transport in Conducting Polymer Films—Diffusion vs Migration," L. J. Kepley, University of New Mexico, Albuquerque, N. Mex.

"Photon Scattering by Magnetic Materials," S. W. Lovesey, Rutherford Appleton Laboratory, Oxfordshire, United Kingdom

[1]"Experiments and Interpretation of Stopping Slow Highly Charged Ions in Insulators," J. P. Biersack, Hahn-Meitner Institut, Berlin, Germany

"Studies of Diffusion Mechanisms at Metal Surfaces Using the Embedded Atom Method," C.-L. Liu, University of Illinois, Urbana, Champaign, Ill.

"Core Level Spectroscopy at Surfaces," M. Riffe, University of Texas, Austin, Tex.

"Dynamics of Gas-Surface Reactions in Heterogeneous Catalysis," P. Saalfrank, University of California, Berkeley, Calif.

"Gap Engineering in Alternating Layer and Interlayer Substituted BNC Compounds," P. Saalfrank, University of California, Berkeley, Calif.

"X-Ray Standing Wave Studies of Semiconductor Surfaces and Metal Semiconductor Interfaces," J. Woicik, Brookhaven National Laboratory, Upton, N.Y.

2"A Tale of Two Topics: Epitaxial Growth and Atomistic Calculations of Large Systems," M. S. Daw, Sandia National Laboratories, Livermore, Calif.

"Inner-Shell Excitation by X-Ray Photons: A Probe of Structural and Electronic Information in Molecules and Solids," T. A. Tyson, Instituto Nazionale di Fisica Nucleare, Rome, Italy

"X-Ray Resonant Inelastic Scattering," Y. Ma, Brookhaven National Laboratory, Upton, N.Y.

"Structural- and Electronic-Phase Behavior in High-T_c Cuprates," J. Tallon, New Zealand Institute for Industrial Research and Development, Lower Hutt, New Zealand

"Structure, Metallization, and Electrical Transport at Metal-Semiconductor Interfaces," H. Weitering, University of Pennsylvania, Philadelphia, Penn.

"$Sr_{1-x}Ca_xRuO_3$ ($0 \leq x \leq 1$) for Device Applications," C.-B. Eom, AT&T Bell Laboratories, Murray Hill, N.J.

"Free-Electron Lasers at CEBAF and Their Applications to Material Science Research," H. F. Dylla, Continuous Electron Beam Accelerator Facility, Newport News, Va.

"Charge Carriers and Internal Interfaces in Oxides," V. P. Dravid, Northwestern University, Evanston, Ill.

"Thin-Film Fabrication of High-Temperature Superconductors," Y. K. Park, Korean Research Institute of Standards and Science, Taejon, Korea

"Magnetic Properties of Dilute Alloys of Chromium," S. H. Liu, Solid State Division, ORNL

"Vortex Motion in High-Temperature Superconductors," V. Guechkenbein, Weizmann Institute of Science, Rehovot, Israel

"Comparative Study of Ion Implantation Damage in III–V Compound Semiconductors," W. Wesch, Friedrich-Schiller-Universität, Jena, Germany

"Characterization of Ordered Nickel Oxide Films Grown on Single-Crystal Metal Substrates," C. Ventrice, Tennessee Technology University, Cookeville, Tenn.

"*Ab Initio* Pseudopotential Simulations in Materials Physics: Theory and Applications," V. Y. Milman, Oak Ridge Institute for Science and Education and Solid State Division, ORNL

"Electron Scattering at Surfaces: Crystallography, Resonant States, and Dynamics," P. Rous, University of Maryland, College Park, Md.

"Crystal Surface According to Helium Atom Scattering," J. G. Skofronic, Florida State University, Tallahassee, Fla.

"Electronic Many-Body Effects in Metals," A. Eguiluz, Montana State University, Bozeman, Mont.

"Recent Advances in High-Resolution Soft X-Ray Spectroscopy," C.-T. Chen, AT&T Bell Laboratories, Murray Hill, N.J.

"Computer Simulations of Critical Behavior in the 3D Classical Heisenberg Ferromagnet," K. Chen, University of Georgia, Athens, Ga.

"*Ab Initio* Calculation of the Phonon Dispersion of Silicon and Germanium," S. Wei, Georgia Institute of Technology, Atlanta, Ga.

"Chiral Melting of Si(113)(3 × 1) Reconstruction," D. Abernathy, Massachusetts Institute of Technology, Cambridge, Mass.

"Excitonic Transitions at the Mott-Hubbard Gap of the Insulating Parent States of the Cuprate Superconductors: A Raman Scattering Study," M. Klein, University of Illinois, Urbana, Ill.

"Structure and Growth of Xe on Ag(111)," P. Dai, University of Missouri, Columbia, Mo.

"Structure and Dynamics for Low-Dimensional Systems," W. Zhong, Michigan State University, East Lansing, Mich.

"First-Principles Studies on Structural Properties of Beta-Cristobatlite SiO_2," F. Liu, Rutgers University, Piscataway, N.J.

"First Principles MD Simulations of the Clean and Alkali-Covered Si(100) Surface," K. Terakura, University of Tokyo, Tokyo, Japan

"Elementary Excitations and Neutron Scattering in Liquid ^{4}He," H. R. Glyde, University of Delaware, Newark, Del.

"Spin Ordering on a NiO(100) Surface Measured by Elastic Metastable He Scattering," A. K. Swan, Boston University, Boston, Mass.

"Photon Matter Interaction at Solid Surfaces—Material Processing and Optical Detection," C. Ying, University of Pennsylvania, Philadelphia, Pa.

"Characterization of Submonolayer Growth of Cu Islands on Cu(001)," G. Vidali, Syracuse University, Syracause, N.Y.

"Neutron Reflectivity Studies of Magnetic Coupling in Transition-Metal Multilayers," J. F. Ackner, National Institute of Standards and Technology, Gaithersburg, Md.

"Vortex Motion and Pinning in High-Temperature Superconductors," L. Civale, Centro Atomico Bariloche, Bariloche, Argentina

"The JEOL JSTM 4500-VT Variable Temperature Scanning Tunneling Microscope," M. Iwatsuki, JEOL USA, Inc., Peabody, Mass.

"Toward the Prediction of a New Class of Surface Alloys," S. Blugel, Festkörperforschung der Forschungszentrum, Jülich, Germany

"Growth and Structural Characterization of Semiconductor Heterostructures," J. G. Zhu, National Renewable Energy Laboratory, Golden, Col.

"Surface Contributions to the Irreversible Magnetization of High-T_c Superconductors," L. Burlachkov, Bar Ilan University, Ramat Gat, Israel

---

[1]Joint Physics and Solid State divisions seminar.

[2]Joint Solid State and Metals and Ceramics divisions seminar.

[3]Joint Solid State and Health Sciences Research divisions seminar.

Lectures and Seminars by Division Members

J. B. Bates—The University of Tennessee, Knoxville, Tennessee, "Ceramic Lithium Electrolyte Thin Films and Rechargeable Thin-Film Lithium Batteries"

L. A. Boatner—Longview High School, Longview, Texas, "The Structure and Growth of Single Crystals"; Longview Independent School District, Longview Texas, "Response to Recognition as Distinguished Aluminus"

G. S. Canright—University of Hyderabad, India, "Ordering Disorder: Prospects and Retrospects in Condensed Matter Physics"; Matscience Institute, Madras, India, "Introduction to the Fractional Quantum Hall Effect," "Search for Broken Time-Reversal Symmetry in the HTSC," and "Haldane Fractional Statistics and the Fractional Quantum Hall Effect"; Georgia Institute of Technology, Atlanta, Georgia, "Fractional Statistics, Versions I and II," "From Sunflowers to Superconductors: A Novel Application of Chaos to Equilibrium Statistical Physics"; ICTP, Trieste, Italy, "Course on Geometric Phases in Physics" (3 lectures)

Y. Chen—Gordon Conference on Hydrogen-Metal Systems, Tilton, New Hampshire, "Radiation-Induced Diffusion of Hydrogenic Species in Refractory Oxides"; International Materials Research Society on Frontiers of Science, Sunshine City, Tokyo, Japan, "Low-Temperature Diffusion of Hydrogenic Species in Crystalline Oxides"; Los Alamos National Laboratory, Los Alamos, New Mexico, "Radiation-Enhanced Electrical Degradation: Neutrons or Gamma Rays?"; Fudan University, Shanghai, China, "Radiation-Induced Diffusion of Light Impurity Ions in Ceramic Oxides" and "Materials Sciences in the United States of America"; Idaho National Engineering Laboratory, Shanghai, China, "Radiation-Enhanced Electrical Breakdown of Insulating Ceramics"

D. K. Christen—University of Louisville, Louisville, Kentucky, "Limits to Critical Currents in High-Temperature Superconductors"

J. F. Cooke—The University of Tennessee, Knoxville, Tennessee, "Theory of Magnetism in Solids"

H. L. Davis—University of Alabama, Tuscaloosa, Alabama, "Low-Energy Electron Diffraction Investigation of Metallic Surface Relaxation—From Cu(110) to NiAl(110) and Beyond"; University of Alabama, Birmingham, Alabama, "The Why, The How, and the What of Low-Energy Electron Diffraction for the Investigation of Surface Atomic Structure"; Rutgers University, Piscataway, New Jersey, "Oak Ridge LEED Studies of Metallic Surface Relaxation"; Johns Hopkins University, Baltimore, Maryland, "Precision LEED Studies of Multilayer Relaxation in Monatomic Metallic Surfaces and Layer-by-Layer Segregation in Surface Regions of Binary Random Alloys"; University of Tokyo, Tokyo, Japan, "The Interaction of Hydrogen with $Mo_xRe_{1-x}(100)$ Surfaces"

R. Feenstra—Osaka University, Osaka, Japan, Kyoto University, Kyoto, Japan, Institute of Physical and Chemical Research, Tokyo, Japan, Tokyo Institute of Technology, Yokohama, Japan, University of Tokyo, Tokyo Japan, and Stanford University, Stanford, California, "Oxygen Vacancies in $YBa_2Cu_3O_{7-\delta}$ Thin Films: Growth Properties, Lattice Disorder, and Flux Pinning"

J. A. Fernandez-Baca—University of Missouri, Kansas City, Missouri, "Neutron Scattering Studies of the Spin Dynamics of Itinerant Electron Antiferromagnets"

T. E. Haynes—FOM Institute for Atomic and Molecular Physics, Amsterdam, Netherlands, Forschungszentrum Jülich, Jülich, Germany, Daimler-Benz Research Center, Ulm, Germany, and Universität Augsburg, Augsburg, Germany, "Production of Lattice Damage During Ion Implantation of Semiconductors"; Motorola, Inc., Mesa, Arizona, Texas Instruments, Inc., Dallas, Texas, Kyushu University, Fukuoka, Japan, Hitachi Research Laboratory, Hitachi-shi, Japan, and Asahi Glass Co., Ltd., Yokohama, Japan, "Lattice Damage During Ion Implantation of Semiconductors"

O. W. Holland—Motorola, Inc., Mesa, Arizona, and Texas Instruments, Inc., Dallas, Texas, "Formation of SOI by SIMOX: Mechanism for Dislocation Growth in the Superficial Si Layer"

G. E. Jellison, Jr.—Laboratory PHASE, Strasbourg, France, Max-Planck-Institut für Festkorperforschung, Stuttgart, Germany, Ecole Polytechnique, Lausanne, Switzerland, Kopin Corporation, Stanton, Massachusetts, and Motorola Corporation, Mesa, Arizona, "Spectroscopic Ellipsometry: A Technique for Thin-Film and Bulk Materials Analysis"; Rudolph Research Inc., Flanders, New Jersey, "Two-Channel Spectroscopic Polarization Modulation Ellipsometry and Applications"

H. R. Kerchner—The University of Tennessee, Knoxville, Tennessee, "Superconductivity—The Phenomenon and Its Applications"

M. N. Kunchur—University of Maryland, College Park, Maryland, "Investigation of Superconducting Transport Behavior at High Dissipation Levels"

S. H. Liu—North Dakota State University, Fargo, North Dakota, "Fractals in Condensed Matter Physics"; Argonne National Laboratory, Argonne, Illinois, "Electronic Polaron Effects in Heavy Fermion Materials"; Iowa State University, Ames, Iowa, "Magnetic Properties of Dilute Chromium Alloys"; The University of Tennessee, Knoxville, Tennessee, "Deterministic Sand Pile, Route to Chaos in Large Systems"; University of Missouri, Columbia, Missouri, "The Chromium Story"

D. H. Lowndes—Department of Energy, Basic Energy Sciences/Materials Sciences Information Meeting, Oak Ridge, Tennessee, "Synthesis of Tailored Materials and Superconducting Superlattices by Pulsed-Laser Ablation"; Department of Energy Review of Research Projects, Bethesda, Maryland, "Superconductors with High Critical Temperatures"; University of Toronto, Toronto, Canada, "Epitaxial Growth of Films and Superlattices by Pulsed-Laser Ablation"

G. D. Mahan—Pennsylvania State University, University Park, Pennsylvania, Ohio State U iversity, Columbus, Ohio, "Current Drag in Semiconductors"; Norwegian Institute of Technology, Trondheim, Norway, "Thermoelectrics"; Centre Europeen de Calcul Atomique et Moleculaire, Paris, France, "Electron-Electron Interactions in Metals"; International Centre Theoretical Physics, Trieste, Italy, "Theory of Metals" (8 lectures); Ohio State University, Columbus, Ohio, and Pennsylvania State University, University Park, Pennsylvania, "Coulomb Drag in Semiconductors"; Norwegian Institute of Technology, Trondheim, Norway, "Electron-Electron Interactions in Metals"

V. Milman—University of Cambridge, Cambridge, United Kingdom, "*Ab Initio* Study of Ge Adsorption and Diffusion on the Si(100) Surface"

H. A. Mook—McMaster University, Hamilton, Ontario, Canada, "Neutron Scattering Studies of High-Temperature Superconductors"

D. P. Norton—IBM T. J. Watson Research Center, Yorktown Heights, New York, "Epitaxial Growth of Properties of the 'Infinite Layer' $Ca_{1-x}Sr_xCuO_2$ Compound"

S. J. Pennycook—Sumitomo Metal Industries, Osaka, Japan, "Atomic-Resolution Incoherent Imaging with the STEM: Applications to Superconductors and Semiconductors"; Osaka University, Osaka, Japan, "Growth Mechanisms of Layered Superconductors Visualized Through Z-Contrast Imaging"; University of Toronto, Toronto, Canada, "Atomic-Resolution Imaging and Analysis of Materials Based on Z-Contrast STEM"; Georgia Institute of Technology, Atlanta, Georgia, "Insights into Materials Through Z-Contrast Electron Microscopy"

D. B. Poker—Ohio University, Athens, Ohio, "Ion Scattering for Materials Analysis"

J. B. Roberto—Forschungszentrum (KFA), Jülich, Germany, and Max Planck Institut für Plasma Physik, Garching, Germany, "Deposition and Characterization of Thin Films"

M. T. Robinson—ORNL 50th Anniversary Seminar—50 Years of Ion Beam Research, Oak Ridge, Tennessee, "Radiation Damage and the Birth of Channeling"

J. R. Thompson—Japan Atomic Energy Research Agency, Tokai, Japan, "Intragrain Current Density and Vortex Pinning in High-T_c Superconductors"; The University of Tennessee, Knoxville, Tennessee (2 lectures) and University of Mississippi, University, Mississippi, "Improving Mother Nature's Gift: Processing High-Temperature Superconductors for High Current Conduction"

J. Z. Tischler—University of Hamburg, Hamburg, Germany, "Development of Nuclear Bragg Scattering Applications"

J. F. Wendelken—IBM Almaden Research Center, San Jose, California, "Surface Morphology and Thin-Film Growth Studies with High-Resolution LEED"

C. W. White—Motorola, Inc., Mesa, Arizona and Texas Instruments, Inc., Dallas, Texas, "Materials Modification and Materials Characterization Using Ion Beams"

G. D. Wignall—Sandia National Laboratories, Albuquerque, New Mexico, "Molecular Weight Scaling in Blends and Blockcopolymers by SANS"; Phillips Petroleum Company Research Laboratories, Bartlesville, Oklahoma, and Hoechst-Celanese Research Laboratories, Summit, New Jersey, "Small-Angle Scattering Studies of Synthetic Polymers"

Scientific Activities, Awards, & Honors

M. M. Abraham

- Member, ORNL-Universidad Nacional Autonoma de Mexico Joint Steering Committee, 1992–1993
- Adjunct Professor, Instituto de Fisica, Universidad Nacional Autonoma de Mexico, 1992–1993
- Advisor, Superconducting Super Collider GEM BaF_2 Panel, Dallas, Texas, 1992

A. P. Baddorf

- Past-President, Tennessee Valley Chapter, American Vacuum Society, 1992–1993

J. B. Bates

- Recipient, Martin Marietta Energy Systems Technical Achievement Award for Invention, 1993

L. A. Boatner

- Recipient, Martin Marietta Corporate Fellowship, 1993
- Executive Secretary, Materials Research Society, 1992–1993
- Associate Editor, *Optical Materials*, 1990–1993
- Co-Chairman, Eighth International Summer School on Crystal Growth, Palm Springs, California, 1992
- Member, Executive Committee, American Association for Crystal Growth, 1993
- Böhmische Physical Society, Scientific Member, 1992
- Recipient, First in Class Award, International Metallographic Contest, New and Unique Techniques, 1992
- Recipient, Second in Class Award, American Ceramic Society, Ceramographic Competition, Optical Microscopy, 1992
- Recipient, Second Place Award, Tenth International Conference on Crystal Growth, Crystal Photograph Competition, 1993
- Recipient, Second Place Award, Ninth American Conference on Crystal Growth, Crystal Photograph Competition, 1993
- Member, William Hunt Eisenman Rare Book Committee of ASM International, 1992–1993
- Member, Fellowship Selection Committee, ASM International, 1992–1993
- Vice-Chairman, Awards Committee, American Association for Crystal Growth, 1992–1993
- Member, Vitality Committee of the Glass and Optical Materials Division, The American Ceramic Society, 1992–1993
- Recipient, Distinguished Alumnus Award, Longview Independent School District, Longview, Texas, 1993
- Member, Showcase Talk Selection Committee, ORNL, 1990–1993
- Chairman, ORNL-Universidad Nacional Autonoma de Mexico Joint Steering Committee, 1991–1993
- Special Graduate Faculty Member, Alabama A&M University, 1991–1993

	Thesis Advisor, ORINS Graduate Research Program 1992–1993 Thesis Advisor, SSD/University of Tennessee Research Activity Research Advisor, ORNL/SERS Program, 1992–1993 Research Advisor, ORNL/GLCA Program, 1993 Member, Program Committee, 26th International Symposium on Automotive Technology and Automation, Aachen, Germany, 1993
J. D. Budai	Member, ORNL X-Ray Safety Review Committee, 1992–1993
B. C. Chakoumakos	Recipient, First in Class Award, International Metallographic Contest, New and Unique Techniques, 1992 Recipient, Second in Class Award, American Ceramic Society, Ceramographic Competition, Optical Microscopy, 1992 Recipient, Martin Marietta Energy Systems Technical Achievement Award for Publications, 1992
Y. Chen	Chairman, DOE Workshop on the Application of Positron Spectroscopy to Materials Sciences, Rancho Mirage, California, 1992 Advisor, Superconducting Super Collider GEM BaF_2 Panel, Dallas, Texas, 1992 Co-Organizer, TMS Symposium on Defects at Heterointerfaces, San Francisco, California, 1994 Detailee, Division of Materials Sciences, Office of Basic Energy Sciences, Department of Energy, Washington, D.C., 1992–1993
M. F. Chisholm	Co-Chairman, Symposium on Mechanisms of Heteroepitaxial Growth, San Francisco, California, 1992 Session Chairman, Materials Research Society Fall Meeting, Boston, Massachusetts, 1993 Traveling Lecturer, Oak Ridge Institute for Science and Education, 1992–1993
D. K. Christen	Session Chairman, American Physical Society Meeting, March 1992 Session Chairman, Materials Research Society, November 1992 Member, Review Panel on High-Temperature Superconductivity Program for Space Applications, 1992 Member, Review Panel for National Science Foundation Proposals on Material Synthesis and Processing, 1993 Co-Chairman, Symposium on Superconductivity: Materials and Properties, Materials Research Society Fall Meeting, 1993
J. F. Cooke	Member, Advisory Committee, *Journal of Physics, Condensed Matter*
H. L. Davis	Traveling Lecturer, Oak Ridge Associated Universities, 1992–1993 Detailee, Division of Materials Sciences, Office of Basic Energy Sciences, Department of Energy, Germantown, Maryland; Full-Time 10/1/91–3/31/93, Part-Time 4/1/93–9/30/94 Participant, Research Assistance Task Force on Photovoltaic Materials, Vail, Colorado, 1992 Member, Organizing and Program Committees, Fourth International Conference on the Structure of Surfaces, Shanghai, China, 1993

Session Chairman, Symposium on Application of Multiple Scattering Theory to LEED, Materials Research Society Fall Meeting, Boston, Massachusetts, 1992
Session Chairman, Symposium on New Materials, Fourth International Conference on the Structure of Surfaces, Shanghai, China, 1993

N. J. Dudney

Recipient, Martin Marietta Energy Systems Technical Achievement Award for Invention, 1993

D. B. Geohegan

Co-Chairman, Second International Conference on Laser Ablation, Knoxville, Tennessee, 1993
Member, Advisory Committee, LASERION '93, Munich, Germany, 1993

S. M. Gorbatkin

Member, Plasma Science and Technology Program Committee, 40th Annual American Vacuum Society Symposium, 1993
Session Chairman, Second Workshop on High Density Plasmas and Applications, American Vacuum Society Topical Conference, San Francisco, California, 1993
Secretary, Plasma Science and Technology Division, American Vacuum Society, 1992–1993
Member, Executive Board, Tennessee Valley Chapter, American Vacuum Society, 1993
Member, Plasma Science and Technology Division Student Award Committee, American Vacuum Society, 1993
Research Advisor, ORISE/SERS Program, 1992
Research Advisor, ORISE/GLCA Program, 1993
Instructor, Introduction to Electrodynamics, Oak Ridge Science Semester Program, 1993
Recipient, Martin Marietta Energy Systems Significant Event Award, 1993

G. R. Gruzalski

Recipient, Martin Marietta Energy Systems Technical Achievement Award for Invention, 1993

W. A. Hamilton

Traveling Lecturer, Oak Ridge Institute for Science and Education, 1992–1993
Participant, Workshop on Scientific Opportunities at Future Spallation Neutron Sources, Argonne, Illinois, 1993

T. E. Haynes

Co-Chairman, Symposium on Crystallization and Related Phenomena in Amorphous Materials, Materials Research Society Fall Meeting, Boston, Massachusetts, 1993
Member, Executive Board, Tennessee Valley Chapter, American Vacuum Society, 1992–1993
Member, Symposium Organizing Committee, Third International Conference on Advanced Materials, 1993

O. W. Holland	Co-Chairman, Symposium on Materials Synthesis and Processing Using Ion Beams, Materials Research Society, Boston, Massachusetts, 1993 Member, Publications Committee, Materials Research Society Session Organizer, Conference on Industrial Applications of Small Accelerators, Denton, Texas, 1992
G. E. Jellison, Jr.	Member, Editorial Board, *Applied Physics Communications* Referee, Nebraska Engineering Research Initiative
D. E. Jesson	Co-Chairman, Symposium on Si Epitaxy, American Physical Society, Seattle, Washington, 1993 Session Chairman, Microscopy Society of America, Cincinnati, Ohio, 1993
T. Kaplan	Traveling Lecturer, Oak Ridge Institute for Science and Education, 1992–1993
H. R. Kerchner	Session Chairman, Materials Research Society Spring Meeting, San Francisco, California, 1992 Session Chairman, Materials Research Society Fall Meeting, Boston, Massachusetts, 1992 and 1993 Co-Chairman, Symposium on Superconductivity, Materials Research Society Fall Meeting, Boston, Massachusetts, 1993 Mini-Workshop Presenter, National Educators Workshop, Hampton, Virginia, 1993
B. C. Larson	Chairman, Cornell High-Energy Synchrotron Source Policy and Advisory Board, 1992–1993 Member, ORNL Total Quality Management Benchmarking Committee, 1993
J. S. Lin	Research Advisor, ORISE/SERS Program, 1993–1994 Adjunct Professor, The University of Tennessee, Knoxville, Tennessee Consultant, NASA High-Temperature Project Summitec Corporation, Oak Ridge, Tennessee, 1992–1993
S. H. Liu	Member, Physics and Astronomy Council, Iowa State University Managing Editor, *International Journal of Modern Physics B*
D. H. Lowndes	Adjunct Professor, Department of Materials Science and Engineering, The University of Tennessee, Knoxville, Tennessee Ph.D. Thesis Advisor, The University of Tennessee, Knoxville, Tennessee Adjunct Professor, Department of Physics and Astronomy, Louisiana State University, Baton Rouge, Louisiana Co-Director, Adriatico Research Conference on Vortex Fluctuations in Superconductors, Trieste, Italy, 1993 Judge, Graduate Student Research Awards, Materials Research Society Fall Meeting, Boston, Massachusetts, 1993 Member, International Program Committee, Third IUMRS-ICAM Conference, Tokyo, Japan, 1993

Member, International Program Committee, Second International Conference on Laser Ablation, Knoxville, Tennessee, 1993
Member, Program Committee, Conference on Superconducting Superlattices and Multilayers, Los Angeles, California, 1993

D. C. Lubben

Equipment Exhibit Organizer, 14th Tennessee Valley Chapter, American Vacuum Society Symposium on Innovative Technologies for Materials Processing and Analysis, Oak Ridge, Tennessee (to be held in 1994)

C. F. Luck

Recipient, Martin Marietta Energy Systems Technical Achievement Award for Invention, 1993

G. D. Mahan

Member, Scandinavian Committee to choose Professorships for:
- Experimental Solid State, Chalmers Technical University, Sweden, Spring, 1992
- Theoretical and Experimental Solid State (2 positions), Norwegian Institute of Technology, Trondheim, Norway, 1993

Judge, International Science and Engineering Fair, Nashville, Tennessee, 1992
Chairman, Scientific Committee, International Center of Condensed Matter Physics, Brasilia, 1989–1993
Member, Executive Committee, Division of Condensed Matter Physics, American Physical Society, 1989–1992
Co-Chairman, Conference on "Vortex Fluctuations in Superconductors," International Centre of Theoretical Physics, Trieste, Italy, 1993
Co-Editor, Plenum Publishing Company Book Series

H. A. Mook

Chairman, Corporate Fellows Council, ORNL
Co-Chairman, First Advanced Neutron Source User Meeting, Oak Ridge, Tennessee, 1993
Recipient, Martin Marietta Energy Systems Technical Achievement Award for Publications, 1992
Member, LANSCE II External Advisory Committee, Los Alamos National Laboratory
Member, National Steering Committee for the Advanced Neutron Source
Member, Steering Committee for the U.S.–Japan Cooperative Program on Neutron Scattering
Member, ORNL Awards Committee
Member, Brochures Development Task Force, ORNL
Member, Nomination Committee, Sigma Xi
Session Chairman, Magnetism and Magnetic Materials Conference, Houston, Texas, 1993

R. M. Moon

Co-Chairman, First Advanced Neutron Source User Meeting, Oak Ridge, Tennessee, 1993
Recipient, American Association for the Advancement of Science Fellowship, 1994
Acting Division Director, Solid State Division, 1993
Member, Advisory Panel for Reactor Radiation Division, National Institute for Standards and Technology

	Member, Advisory Committee, International Conference on Neutron Scattering, Sendai, Japan (to be held in 1994) Executive Secretary, National Steering Committee for the Advanced Neutron Source
R. M. Nicklow	Member, IPNS Program Advisory Committee, Argonne National Laboratory Member, Research Committee, U.S.–Japan Cooperative Program on Neutron Scattering
S. J. Pennycook	Recipient, MRS Medal, 1992 Kurt F. Heinrich Outstanding Young Scientist Award, Microbeam Analysis Society, 1992 Martin Marietta Energy Systems Author of the Year, 1992 Recipient, Martin Marietta Energy Systems Technical Achievement Award for Publication, 1992 Meeting Co-Chairman, Materials Research Society Fall Meeting, Boston, Massachusetts, 1992 Member, National Science Foundation Panel on Atomic Resolution Microscopy, 1992 ORNL Showcase Lecturer, 1993 Member, Editorial Board, *Journal of Microscopy* Member, Program Committee and Awards Committee, Materials Research Society Lecturer, Saturday Academy, Oak Ridge Institute for Science and Education, 1993
D. B. Poker	Meeting Chair, Materials Research Society Fall Meeting, Boston, Massachusetts, 1993 Member, *Nuclear Instruments and Methods in Physics Research Section B* Member, Materials Research Society Publication Committee, Program Committee, and Corporate Participation Committee
J. B. Roberto	Acting Associate Director for Physical Sciences and Advanced Materials, ORNL, 1993 Member, Solid State Sciences Committee, National Research Council, 1993–1995 Member, Committee on Free-Electron Lasers and Other Coherent Light Sources, National Research Council, 1993–1994 Chairman, Advisory Review Board, *Journal of Materials Research* Past President, Materials Research Society, 1992 Focus Area Coordinator, Advanced Ceramics and Ceramic Thin Films, DOE-BES Synthesis and Processing Center, 1993–1994 Member, Technology Area Coordination Team, Microelectronics and Photonics, DOE Technology Commercialization Initiative (1992–1993) Member, Organizing Committee, Second HBCU Conference on the Physics of Materials, Washington, D.C. (to be held in 1994) Co-Organizer, Symposium on Surface Evolution and Epitaxy in Thin Film Growth, American Physical Society, Pittsburgh, Pennsylvania (to be held in 1994)

	Chairman, BES Center of Excellence Workshop on Surface Hardness, Dallas, Texas, 1994
	Participant, Milliken Pursuit of Excellence Seminar, Milliken Corporation, 1993
	Member, Nominating Committee, Materials Research Society
	Member, ORNL Strategic Planning Committee, 1992–1993
	Member, ORNL Fix-It Committee, 1993
	Member, ORNL General Plant Projects Committee
	Member, Advisory Committee, Environmental, Safety, and Health Compliance Directorate, ORNL
M. T. Robinson	*Proceedings of the International Conference on Computer Simulations of Radiation Effects in Solids, Berlin, Germany, August 23–28, 1992*, Dedicated to Mark T. Robinson
	Recipient, Martin Marietta Energy Systems Technical Achievement Award, 1993
	Member, International Committee for the International Conference on Computer Simulation of Radiation Effects in Solids, 1992–1994
	Member, International Committee for a Symposium in Sputtering, a 250th Anniversary Symposium of the Royal Danish Academy of Sciences and Letters, 1990–1992
B. C. Sales	Member, Editorial Advisory Board, *Journal of the Physics and Chemistry of Solids*
	Recipient, Martin Marietta Energy Systems Technical Achievement Award for Publications, 1992
	Recipient, First in Class Award, International Metallographic Contest, New and Unique Techniques, 1992
	Recipient, Second in Class Award, American Ceramic Society, Ceramographic Competition, Optical Microscopy, 1992
T. P. Sjoreen	Member, ORNL Accelerator Safety Review Committee
S. Spooner	Advisor, *Journal of Metals*, TMS-AIME, 1989–1993
	Past Chairman, Physics and Chemistry of Materials Committee, TMS-AIME, 1991–1992
	Co-Organizer and Session Chairman, Symposium on Nanocrystalline Materials, TMS-AIME Annual Meeting, Denver, Colorado, 1993
	Member, Structures Activity, ASM-MSD
	Member, Shaping and Forming Committee, TMS-AIME
	Recipient, Martin Marietta Energy Systems Significant Event Award, 1993
Y. R. Sun	First Place–Graduate Student Paper Competition (Mathematical and Physical Sciences), Sigma Xi, the Scientific Research Society, 1993
J. R. Thompson	Recipient, American Physical Society Fellowship, 1992
	Recipient, The University of Tennessee Chancellor's Award for Research and Creativity, 1992

	Co-Chairman, Critical Currents—92 Conference, Vienna, Austria, 1992
	Invited Member, Official U.S. Delegation for Japan-U.S. Workshop on Superconductivity, Tsukuba, Japan, 1992
	Chairman, Pinning Via Irradiation Induced Defects Symposium, March Meeting of the American Physical Society, 1993
	Professor of Physics, The University of Tennessee, Knoxville, Tennessee
	Member, The University of Tennessee Science Alliance Faculty Review Committee
	Visiting Scholar Lecturer, Oak Ridge Institute for Science and Education, 1993
J. F. Wendelken	Co-Chairman, 14th Tennessee Valley Chapter, American Vacuum Society Symposium on Innovative Technologies for Materials Processing and Analysis, Oak Ridge, Tennessee (to be held in 1994)
C. W. White	Co-Chairman, Symposium on Ion Beam Processing of Materials, International Conference on Advanced Materials, Tokyo, Japan, 1993
	Member, Advisory Review Board, *Journal of Materials Research*, 1992–1993
	Chairman, International Relations Subcommittee, Materials Research Society, 1991, 1993
	Member, External Affairs, Publications, and Long-Range Planning Committees, Materials Research Society, 1992–1993
	Member, International Committee, Ion Beam Modification of Materials Conference, 1994
G. D. Wignall	Contributing Editor, *Chemtracts*
	Organizer, Workshop on "Polymer Diffraction: Small-Angle X-Ray Scattering," Denver X-Ray Conference, Denver, Colorado, 1992
	Session Chairman, Denver X-Ray Conference, Denver, Colorado, 1992
	Recipient, Martin Marietta Energy Systems Technical Achievement Award for Publications, 1993
R. A. Zuhr	Treasurer, East Tennessee Section of the Materials Research Society, 1993–1994
	Member, Organizing Committee, First Annual Symposium and Short Course Presentation of the East Tennessee Materials Research Society, 1993
	Recipient, Martin Marietta Energy Systems Technical Achievement Award for Invention, 1993

Personnel Changes

New Staff Members

A. *Administrative and Technical Support Staff*

S. J. Cox, Secretary
R. B. Maples, Senior Laboratory Technician
N. F. Delene, Secretary

Staff Transfers and Terminations

A. *Scientific Staff*

H. R. Child (retirement)
M. Rasolt (deceased)
H. G. Smith (retirement)

B. *Administrative and Technical Support Staff*

S. B. Hannon (voluntary resignation)
S. L. Davis (transferred to MMES Central Staff Offices)

Guest Assignments

A. *Scientific Staff*

J. H. Barrett, Oak Ridge National Laboratory Retiree
G. S. Canwright, The University of Tennessee, Knoxville, Tennessee
S. S. Chandavakar, The University of Tennessee, Knoxville, Tennessee
H. Durr, The University of Tennessee, Knoxville, Tennessee
A. Eguiliuz, The University of Tennessee, Knoxville, Tennessee
H. O. Frota, The University of Tennessee, Knoxville, Tennessee
K. Fukutani, University of Tokyo, Tokyo, Japan
H.-J. Hinneberg, Forschungszentrum Jülich, Jülich, Germany
M. Karimi, Alabama A&M University, Normal, Alabama
H. Khan, Forschung Institüt für Edelmetalle, Gmuend, Germany
G. D. Mahan*, The University of Tennessee, Knoxville, Tennessee
Y. Morii, Japan Atomic Energy Research Institute, Tokai, Japan
M. Okada, University of Tokyo, Tokyo, Japan
E. W. Plummer*, The University of Tennessee, Knoxville, Tennessee
A. Rojo, The University of Tennessee, Knoxville, Tennessee
B. Sernelius, The University of Tennessee, Knoxville, Tennessee

*ORNL/UT Distinguished Scientist

K. W. K. Shung, The University of Tennessee, Knoxville, Tennessee
J. Sofo, The University of Tennessee, Knoxville, Tennessee
J. I. Suzuki, Japan Atomic Energy Research Institute, Tokai, Japan
E. Takasuka, Sumitomo Metal Industries, Ltd., Amagasaki, Japan
R. Triolo, University of Palermo, Palermo, Italy
N. Wakabayashi, Keio University, Yokohama, Japan
G. Watson, The University of Tennessee, Knoxville, Tennessee
H. H. Weitering, The University of Tennessee, Knoxville, Tennessee
M. K. Wilkinson, Oak Ridge National Laboratory Retiree
F. W. Young, Jr., Oak Ridge National Laboratory Retiree
J. L. Zarestky, Ames Laboratory/Iowa State University, Ames, Iowa

B. *Postgraduate Research Participation Program*

M. Bartiowiak, A. Michiewicz University, Poznan, Poland
J. R. Brewster, The University of Tennessee, Knoxville, Tennessee
N. Browning, University of Cambridge, Cambridge, United Kingdom
Keming Chen, Fudan University, Shanghai, China
Kun Chen, University of Georgia, Athens, Georgia
J. D. Hunn, University of North Carolina, Chapel Hill, North Carolina
E. C. Jones, The University of Tennessee, Knoxville, Tennessee
B. S. L. Kwak, Georgia Institute of Technology, Atlanta, Georgia
M. N. Kunchur, Rutgers University, Piscataway, New Jersey
C. L. Liu, University of Illinois, Urbana, Illinois
P. F. Lyman, University of Pennsylvania, Philadelphia, Pennsylvania
A. J. McGibbon, Glasgow University, Glasgow, United Kingdom
M. M. McGibbon, University of Cambridge, Cambridge, United Kingdom
V. Milman, Institute of Metal Physics, Kiev
R. L. Rhoades, University of Illinois, Urbana, Illinois
J. L. Robertson, University of Houston, Houston, Texas
J. W. Sharp, The University of Tennessee, Knoxville, Tennessee
J. Sofo, Instituto Balseiro, Balseiro, Argentina
B. Wang, Rutgers University, Piscataway, New Jersey
M. Yethiraj, University of Missouri, Columbia, Missouri
X. Yu, Universityof Minnesota, Minneapolis, Minnesota
X. Y. Zheng, The University of Tennessee, Knoxville, Tennessee
D. Zhou, University of Virginia, Charlottesville, Virginia
J. K. Zuo, Renssealear Polytechnic Institute, Troy, New York

C. *Graduate Students*

S. Ackleh, The University of Tennessee, Knoxville, Tennessee
H. H. Burke, Columbia University, New York, New York
J. M. Carpinelli, The University of Tennessee, Knoxville, Tennessee
Y. J. Chen, The University of Tennessee, Knoxville, Tennessee
H. Graupner, University of Erlangen, Erlangen, Germany
A. T. Hanbicki, The University of Tennessee, Knoxville, Tennessee
J. B. Hannon, The University of Tennessee, Knoxville, Tennessee
Q. He, The University of Tennessee, Knoxville, Tennessee
S. Hong, The University of Tennessee, Knoxville, Tennessee
E. C. Jones, The University of Tennessee, Knoxville, Tennessee
B. C. Kim, University of Pennsylvania, Philadelphia, Pennsylvania

C. *Graduate Students (cont'd)*

R. A. Kumar, The University of Tennessee, Knoxville, Tennessee
A. Lee, The University of Tennessee, Knoxville, Tennessee
G. Lee, The University of Tennessee, Knoxville, Tennessee
X. Y. Liu, University of Pennsylvania, Philadelphia, Pennsylvania
J. W. McCamy, The University of Tennessee, Knoxville, Tennessee
K. Pohl, The University of Tennessee, Knoxville, Tennessee
C. Richardson, The University of Tennessee, Knoxville, Tennessee
J. Sharp, The University of Tennessee, Knoxville, Tennessee
J. P. Sipf, The University of Tennessee, Knoxville, Tennessee
Y. R. Sun, The University of Tennessee, Knoxville, Tennessee
C. Walters, University of Pennsylvania, Philadelphia, Pennsylvania
G. E. Wang, The University of Tennessee, Knoxville, Tennessee
L. Xie, University of Wisconsin, Madison, Wisconsin
S. Zhu, The University of Tennessee, Knoxville, Tennessee

D. *Undergraduate Students*

R. Burgie, Alfred University, Alfred, New York
D. L. Demarest, Grinnell College, Grinnell, Iowa
N. L. Miles, DePauw University, Greencastle, Indiana
Y. Powell, Alabama A&M University, Normal, Alabama
G. Steadman, University of Southern Colorado, Pueblo, Colorado
M. L. Stricklin, The University of Tennessee, Knoxville, Tennessee

Summer Assignments (1992)

A. *Scientific Staff*

M. J. Aziz, Harvard University, Cambridge, Massachusetts
L. Civale, IBM Corporation, Yorktown Heights, New York
H. Ikeda, National Laboratory for High-Energy Physics, Oho, Japan
S. Kawarazaki, Osaka University, Osaka, Japan
S. Patapis, University of Athens, Athens, Greece
E. W. Plummer, University of Pennsylvania, Philadelphia, Pennsylvania
L. J. Romana, University Claude-Bernard, Lyon, France
R. Triolo, University of Palermo, Palermo, Italy

B. *Students*

T. C. Burwell, The University of Tennessee, Knoxville, Tennessee
K. Boyd, University of Houston, Houston, Texas
L. J. Carson, Lincoln Univesity, Jefferson City, Tennessee
D. A. Harris, Middle Tennessee State University, Murfreesboro, Tennessee
K. M. Hogan, Pennsylvania State University, University Park, Pennsylvania
C. Lee, University of Florida, Gainesville, Florida
J. J. Senkevich, California Poly State University, San Luis Obispo, California
K. M. Severance, University of South Carolina, Columbia, South Carolina
G. Steadman, Southern Colorado University, Pueblo, Colorado
M. C. Stricklin, The University of Tennessee, Knoxville, Tennessee
A. Von Zomeren, Delft University, Delft, the Netherlands

Summer Assignments (1993)

A. *Scientific Staff*

R. Dull, Largo High School, Clearwater, Florida
O. Biham, Syracuse University, Syracuse, New York
R. Gonzalez, Universite Carlos III, Madrid, Spain
R. Fishman, North Dakota State University, Fargo, South Dakota
J. Ossandon, Universidad de Talca, Talca, Chile
J. J. Quinn, The University of Tennessee, Knoxville, Tennessee
J. Rankin, Brown University, Providence, Rhode Island
L. J. Romana, Universite des Antilles et de la Guyana, French West Indies
J. Roth, Max-Planck-Institut für Plasmaphysik, Garching, Germany
R. Wunstorf, The University of Tennessee, Knoxville, Tennessee
J.-K. Zuo, Southwest Missouri State University, Springfield, Missouri

A. *Students*

D. Corrigan, Rensselaer Polytechnic Institute, Troy, New York
J. J. Hernandez, Florida State University, Tallahassee, Florida
M. Antonell, University of Florida, Gainesville, Florida

SOLID STATE DIVISION

October 1, 1993

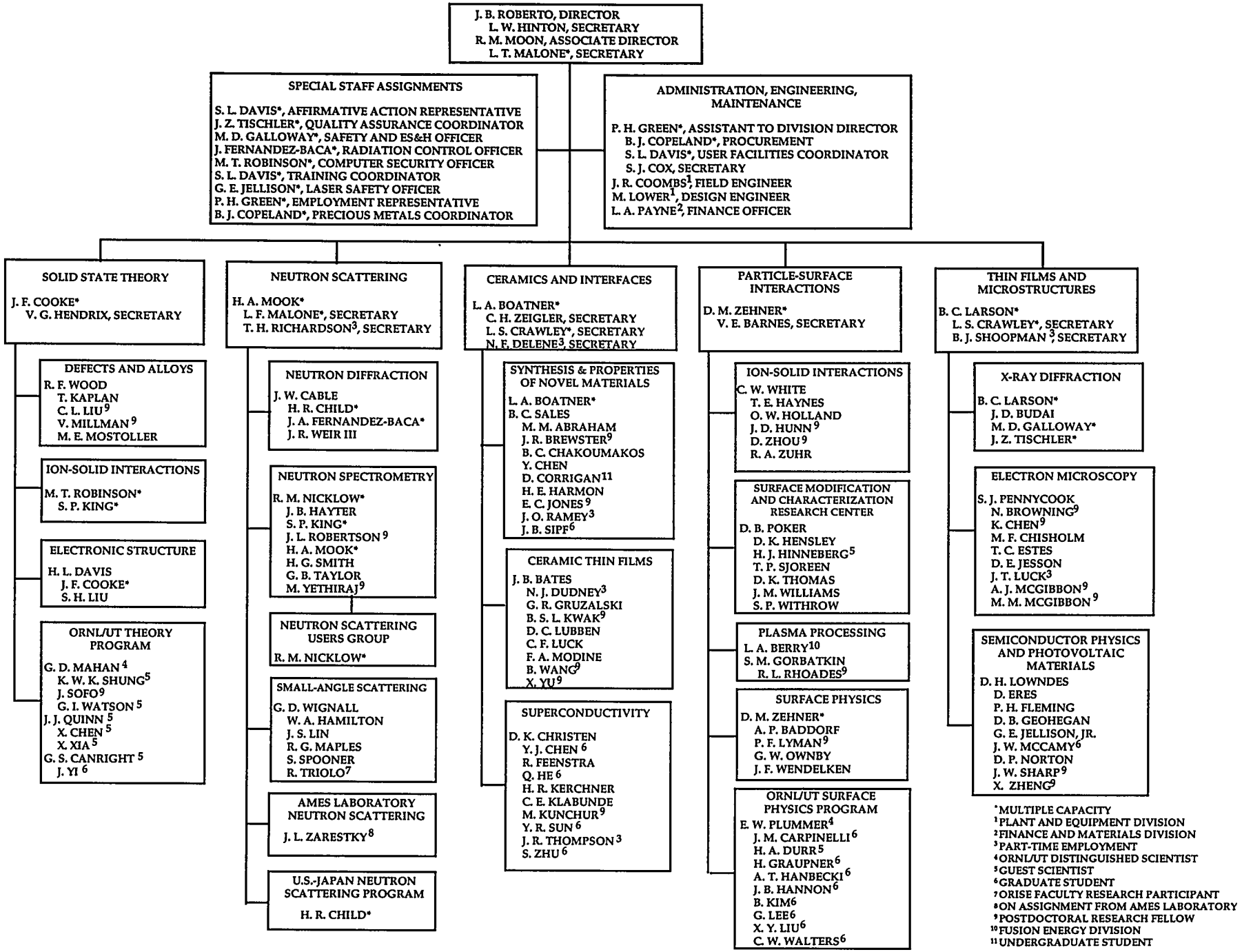

Author Index

ORNL-6816
Distribution Category UC-404

Internal Distribution

1. M. Abdel-Raouf
2. M. M. Abraham
3. K. Affholter
4. B. R. Appleton
5. A. P. Baddorf
6. J. B. Ball
7. V. E. Barnes
8. J. B. Bates
9. P. F. Becher
10. B. A. Berven
11. L. E. Berry
12. T. M. Besmann
13. E. E. Bloom
14. P. J. Blau

15–19. L. A. Boatner

20. N. Browning
21. J. D. Budai
22. G. J. Bunick
23. W. H. Butler
24. J. W. Cable
25. J. Canright
26. J. M. Carpinelli
27. R. S. Carlsmith
28. B. C. Chakoumakos
29. S. S. Chandavarkar
30. Keming Chen
31. Kun Chen
32. Y. Chen
33. Y-J. Chen
34. M. F. Chisholm
35. D. K. Christen

36–40. J. F. Cooke

41. B. J. Copeland

42–46. S. J. Cox

47. D. F. Craig
48. L. S. Crawley
49. S. A. David
50. H. L. Davis
51. N. F. Delene
52. E. R. DuBose
53. N. J. Dudney
54. L. B. Dunlap
55. A. Eguiluz
56. D. Eres
57. T. C. Estes
58. G. G. Fee
59. R. Feenstra
60. R. E. Fenstermaker
61. J. A. Fernandez-Baca
62. P. H. Fleming
63. W. Fulkerson
64. M. D. Galloway
65. L. Gea
66. R. K. Genung
67. D. B. Geohegan
68. H. A. Glovier
69. S. M. Gorbatkin
70. C. A. Grametbauer
71. H. Graupner

72–76. P. H. Green

77. G. R. Gruzalski
78. W. A. Hamilton
79. A. T. Hanbicki
80. J. B. Hannon
81. H. E. Harmon
82. F. C. Hartman
83. T. E. Haynes
84. J. B. Hayter
85. Q. He
86. V. G. Hendrix
87. D. K. Hensley
88. J. N. Herndon

89–93. L. W. Hinton

94. O. W. Holland
95. R. B. Honea
96. S. Hong
97. J. Hunn
98. L. L. Horton
99. D. W. Jared
100. G. E. Jellison, Jr.
101. D. E. Jesson
102. E. Jones
103. J. E. Jones, Jr.
104. T. Kaplan
105. H. R. Kerchner
106. B. Kim
107. Y. Kim
108. S. P. King
109. P. W. King
110. C. E. Klabunde

111. F. C. Kornegay
112. E. H. Krieg
113. M. N. Kunchur
114. B. S. Kwak
115–119. B. C. Larson
120. G. Lee
122. R. P. Leinius
123. J. S. Lin
124. F. Liu
125. S. H. Liu
126. X.-Y. Liu
127. D. H. Lowndes
128. D. C. Lubben
129. C. F. Luck
130. J. T. Luck
131. G. D. Mahan
132. L. F. Malone
133. L. K. Mansur
134. R. G. Maples
135. F. A. Modine
136–140. H. A. Mook, Jr.
141–145. R. M. Moon, Jr.
146. M. E. Mostoller
147. R. M. Nicklow
148. D. P. Norton
149. G. E. Oliphant
150. C. E. Oliver
151. C. C. Overbey
152. S. H. Overbury
153. G. W. Ownby
154. S. J. Pennycook
155. E. W. Plummer
156. K. Pohl
157. D. B. Poker
158. M. L. Poutsma
159. J. J. Quinn
160. J. O. Ramey
161. D. E. Reichle
162. R. L. Rhoades
163. J. B. Richard
164. T. H. Richardson
165. C. R. Richmond
166–205. J. B. Roberto
206. J. L. Robertson
207. M. T. Robinson
208. T. H. Row
209. B. C. Sales
210. M. J. Saltmarsh
211. A. C. Schaffhauser
212. J. W. Sharp
213. J. Sheffield
214. R. B. Shelton
215. B. J. Shoopman
216. W. D. Shults
217. W. D. Siemens
218. T. P. Sjoreen
219. E. J. Soderstrom
220. S. Spooner
221. J. O. Stiegler
222. A. K. Swan
223. J. H. Swanks
224. G. B. Taylor
225. V. J. Tennery
226. D. K. Thomas
227. J. R. Thompson
228. J. Z. Tischler
229. A. W. Trivelpiece
230. R. I. Van Hook
231. A. Van Zomeron
232. C. Walters
233. B. Wang
234. R. C. Ward
235. D. A. Waters
236. G. I. Watson
237. J. R. Weir III
238. H. Weitering
239. J. F. Wendelken
240. C. D. West
241. C. W. White
242. G. E. Whitesides
243. G. D. Wignall
244. M. K. Wilkinson
245. J. M. Williams
246. S. P. Withrow
247. R. F. Wood
248. M. Yethiraj
249. X. Yu
250. J. L. Zarestky
251–255. D. M. Zehner
256. C. H. Zeigler
257. S. Zhu
258. R. A. Zuhr
259. Biology Library
260–264. Central Research Library
265. ORNL Y-12 Technical Library
266. Document Reference Section
267–268. Laboratory Records Department
269. Laboratory Records, ORNL–RC

External Distribution

270. Dr. A.A.Z. Ahmad, Chief Scientific Officer, Institute of Nuclear Science and Technology, Atomic Energy Research Establishment, Ganakbari, Savar, Dhaka, G.P.O. Box 3787, Dhaka, Bangladesh

271. Dr. Craig Allison, Department of Physics, Oklahoma State University, Stillwater, OK 74078

272. Dr. S. Amelinckx, SCK/CEN, B 2400-Mol, Belgium

273. Dr. Rosalia N. Andrews, School of Engineering, University of Alabama at Birmingham, University Station, Birmingham, AL 35294

274. Dr. R. R. Arons, Institut für Festkörperforschung, Forschungszentrum, Postfach 1913, D-5170, Jülich, Germany

275. Dr. Neil W. Ashcroft, Laboratory of Atomic and Solid State Physics, Clark Hall, Cornell University, Ithaca, NY 14853-2501

276. Prof. Frank Avignone, Chairman, Department of Physics, University of South Carolina, Columbia, SC 29208

277. Dr. John Axe, Associate Director, Brookhaven National Laboratory, Upton, NY 11973

278. Dr. Michael J. Aziz, Department of Applied Science, Harvard University, Cambridge, MA 02138

279. Dr. K. J. Bachmann, Department of Chemistry, North Carolina State University, Box 5247, Raleigh, NC 27650

280. Dr. R. W. Balluffi, Department of Materials Science and Engineering, Massachusetts Institute of Technology, 77 Massachusetts Avenue, Cambridge, MA 02139

281. Dr. J. H. Barrett, 827 W. Outer Drive, Oak Ridge, TN 37830

282. Dr. F. S. Bates, 151 Amundson Hall, Department of Chemical Engineering, University of Minnesota, Minneapolis, MN 55455

283. Prof. Boris W. Batterman, Applied and Engineering Physics, 227 Clark Hall, Cornell University, Ithaca, NY 14853

284. Dr. Walter Bauer, Physical Research Division, Department 8340, Sandia National Laboratories, P.O. Box 969, Livermore, CA 94550

285. Dr. Rainer Behrisch, Max-Planck-Institut für Plasmaphysik, D-8046 Garching bei München, Germany

286. Dr. Ronald R. Berliner, Dept. of Physics, University of Missouri, Research Reactor Facility, Columbia, MO 65211

287. Bibliotheque, Institut Max von Laue–Paul Langevin, 156 X 38042 Grenoble, Cedex, France

288. Dr. A. I. Bienenstock, Stanford Synchrotron Radiation Laboratory, Stanford University, P.O. Box 4349, Bin 69, Stanford, CA 94305

289. Prof. H. Birnbaum, University of Illinois, Materials Research Laboratory, 104 South Goodwin, Urbana, IL 61801

290. Dr. N. Bloembergen, Gordon McKay Laboratory, 9 Oxford Street, Cambridge, MA 02138

291. Dr. M. Blume, Brookhaven National Laboratory, Upton, NY 11973

292. Dr. Dawn Bonnell, Department of Materials Science, University of Pennsylvania, 3231 Walnut Street, Philadelphia, PA 19104

293. Dr. J. L. Bóldú O., Instituto de Física, Universidad Nacional Autonoma de Mexico, Apartado Postal 20-364, 01000 Mexico, D.F.

294. Dr. William F. Brinkman, Room 1C-224, AT&T Bell Laboratories, 600 Mountain Avenue, Murray Hill, NJ 07974

295. Dr. Bruce Brown, PNS-372, Argonne National Laboratory, 9700 South Cass Avenue, Argonne, IL 60439

296. Dr. F. C. Brown, Department of Physics, University of Illinois, Urbana, IL 61801

297. Dr. Walter Brown, Room IE-452, AT&T Bell Laboratories, 600 Mountain Avenue, Murray Hill, NJ 07974

298. Dr. Christoph J. Buchal, Kernforschungsanlage, Postfach 1913, 5170 Jülich 1, Germany

299. Dr. R. Bullough, Atomic Energy Research Establishment, Harwell, Didcot, Oxon OX11 ORA, United Kingdom

300. Dr. John L. Burnett, Division of Chemical Sciences, ER-142, Office of Basic Energy Sciences, Office of Energy Research, Department of Energy, Washington, DC 20585

301. Prof. W.J.L. Buyers, Atomic Energy of Canada Limited, Chalk River Nuclear Laboratories, Chalk River, Ontario KOJ 1JO, Canada

302. Prof. Nicolas Cabrera, Departamento de Fisica Fundamental, Facultad de Ciencias, Universidad Autonoma de Madrid, Canto-Blanco, Madrid 34, Spain

303. Prof. Robert W. Cahn, Department of Materials Science and Metallurgy, Cambridge University, Pembroke Street, Cambridge CB2 3Q2, United Kingdom

304. Dr. J. M. Carpenter, Argonne National Laboratory, 9700 South Cass Avenue, Argonne, IL 60439

305. Prof. Ray W. Carpenter, Center for Solid State Science, Arizona State University, Tempe, AZ 85287

306. Prof. Bruce H. T. Chai, University of Central Florida, CREOL, 12424 Research Parkway, Suite 400, Orlando, FL 32826

307. Dr. R. L. Chaplin, Department of Physics, Clemson University, Clemson, SC 29631

308. Prof. Girish Chandra, Tata Institute of Fundamental Research, National Centre of the Government of India for Nuclear Science and Mathematics, Homi Bhabha Road, Colaba, Bombay 400 005, India

309. Dr. Lloyd Chase, MS L-490, Lawrence Livermore National Laboratory, P.O. Box 808, Livermore, CA 94550

310. Dr. Andre Chatelain, Lab. Phys. Exp., Federal Institute of Technology, PH Ecublens, 1015 Lausanne, Switerland

311. Dr. D. S. Chemla, Lawrence Berkeley Laboratory, MS-66, 1 Cyclotron Road, Berkeley, CA 94720

312. Dr. W. J. Choyke, Westinghouse R&D Center, 1310 Beulah Road, Pittsburgh, PA 15235

313. Dr. Wei-Kan Chu, Texas Center for Superconductivity, University of Houston, Science and Research 1, Houston, TX 77204-5506

314. Dr. C. B. Clark, Department of Physics, University of North Carolina, Greensboro, NC 27412

315. Francisco H. Claro, Catholic University of Chile, Casilla 6177, Santiago, Chile

316. Dr. Frank Clinard, MS-546, Los Alamos National Laboratory, Los Alamos, NM 87545

317. Prof. Marvin Cohen, Department of Physics, University of California, Berkeley, CA 94720

318. Dr. Morrel H. Cohen, Corporate Research Science Laboratories, Exxon Research and Engineering Company, Clinton Township, Route 22 East, Annandale, NJ 08801

319. Mr. Ralph R. Coltman, Jr., 7905 Wiebelo Drive, Knoxville, TN 37931

320. Prof. James W. Corbett, Department of Physics, State University of New York at Albany, Albany, NY 12222

321. Dr. Roger A. Cowley, Department of Physics, Clarendon Laboratory, University of Oxford, Parks Road, Oxford, OX1 3PU, United Kingdom

322. Dr. Juan C. Crespi, Comision Nacional de Energía Atómica, Gerencia Desarrollo-Dto. Materiales, Avenida del Libertador 8250, 1429 Buenos Aires, Argentina

323. Dr. Peter A. Curreri, NASA, Mail Code ES74, Space Science Laboratory, George C. Marshall Space Flight Center, AL 35806

324. Dr. Gordon Czjzek, Kernforschungszentrum Karlsruhe, INFP, Postfach 3640, D-7500 Karlsruhe 1, Germany

325. Dr. L. S. Darken, Tennelec, Inc., 601 Oak Ridge Turnpike, Oak Ridge, TN 37830

326. Dr. Lubomir David, Director, Centro de Física, Instituto Venezolano de Investigaciones Cientificas (IVIC), Apartado 1827, Caracas 1010-A, Venezuela

327. Dr. Robert F. Davis, Department of Materials Science & Engineering, North Carolina State University, Box 7907, Raleigh, NC 27695

328. Prof. Dr. P. H. Dederichs, Institut für Festkörperforschung der Forschungszentrum Jülich GmbH, Postfach 1913, 5170 Jülich 1, Germany

329. Dr. Adriaan M. de Graaf, Division of Materials Research, National Science Foundation, 1800 G Street NW, Washington, DC 20550

330. Dr. J. Diehl, Max-Planck-Institut für Metallforschung, Institut für Werkstoffwissen–schaften, Sestrasse 92/BRD, D-7000 Stuttgart 1, Germany

331. Dr. J. Dienes, Department of Physics 510B, Brookhaven National Laboratory, Upton, NY 11973

332. Prof. Dr. H.-D. Dietze, Institut fur Theoretische Physik C, RWTH Aachen, 5100 Aachen, Germany

333. Dr. Sam Divita, U.S. Army Communications, Electronics Command, AMSEL-COM-RM1, Fiber Optics Team, Ft. Monmouth, NJ 07703

334. Dr. G. Dolling, Atomic Energy of Canada Limited, Chalk River Nuclear Laboratories, Chalk River, Ontario KOJ 1JO, Canada

335. Dr. Mildred Dresselhaus, Rm. 13-2090, Massachusetts Institute of Technology, Cambridge, MA 02139

336. Dr. C. B. Duke, Xerox Webster Research Center, 800 Phillips Rd 0114-38D, Webster, NY 14850

337. Dr. B. D. Dunlap, Argonne National Laboratory, MSD-212, 9700 South Cass Avenue, Argonne, IL 60439

338. Dr. Robert C. Dynes, Department of Physics, 0319, University of California–San Diego, La Jolla, CA 92093

339. Dr. Dean E. Eastman, Vice-President of Logic, Memory, and Packaging, International Business Machines Corporation, P.O. Box 218, Yorktown Heights, NY 10598

340. Dr. Norman Edelstein, MMRD/Bldg. 70A/Room 1115, Lawrence Berkeley Laboratory, Berkeley, CA 94720

341. Prof. Henry Ehrenreich, Division of Engineering and Applied Physics, Pierce Hall 205A, Harvard University, Cambridge, MA 02138

342. Dr. Vic Emery, Department of Physics, Brookhaven National Laboratory, Upton, NY 11973

343. Dr. Ahmet Erbil, School of Physics, Georgia Institute of Technology, 225 North Avenue, Atlanta, GA 30332-0430

344. Prof. T. L. Estle, Physics Department, Rice University, Houston, TX 77001

345. Dr. Peder J. Estrup, Department of Physics, Brown University, Providence, RI 02912

346. Dr. R. C. Ewing, Department of Geology, University of New Mexico, Albuquerque, NM 87131

347. Ms. Harriet L. Fadem, Librarian, National Synchrotron Light Source, Brookhaven National Laboratory, Upton, Long Island, NY 11973

348. Dr. G. C. Farlow, Physics Department, Wright State University, Dayton, OH 45435

349. Dr. G. C. Farrington, Department of Materials Science and Engineering, University of Pennsylvania, 3231 Walnut Street, LSRM Building K-1, Philadelphia, PA 19104

350. Prof. Robert S. Feigelson, Center for Materials Research, Stanford University, 105 McCullough Building, Stanford, CA 94305

351. Dr. Jack Feinberg, Department of Physics, SSC-421, University of Southern California, Los Angeles, CA 90089-0484

252. Dr. Martin M. Fejer, Ginzton Laboratory, Stanford University, Stanford, CA 94305

353. Dr. G. P. Felcher, Argonne National Laboratory, 9700 South Cass Avenue, Argonne, IL 60439

354. Dr. Trevor R. Finlayson, Department of Physics, Monash University, Clayton, Victoria, 3168, Australia

355. Mr. David Fitzgerald, President, Tennessee Innovation Center, Inc., 120 Badger Avenue, P.O. Box 607, Oak Ridge, TN 37830

356. Dr. Robert Fleischer, General Electric Research & Development Center, P. O. Box 8, Schenectady, NY 12301

357. Dr. M. Fluss, Lawrence Livermore National Laboratory, L-326, P. O. Box 808, Livermore, CA 94550

358. Dr. C. Peter Flynn, Materials Research Laboratory, University of Illinois, 104 S. Goodwin, Urbana, IL 61801

359. Dr. F. Y. Fradin, Associate Laboratory Director for Physical Sciences, Argonne National Laboratory, Building 221, 9700 South Cass Avenue, Argonne, IL 60439

360. Prof. Dr. Werner Frank, Max-Planck-Institut für Metallforschung, Institut für Physik, Heisenbergstrasse 1, D-7000, Stuttgart 80, Germany

361. Dr. Larry Franks, EG&G/EM Santa Barbara Operations, 130 Robin Hill Road, Goleta, CA 93117

362. Dr. Roger Frech, Department of Chemistry, University of Oklahoma, Norman, OK 73019

363. Prof. Arthur Freeman, Physics Department, Northwestern University, Evanston, IL 60201

364. Dr. Roger H. French, Central Research & Development Department, E.I. du Pont de Nemours & Co., Experimental Station, E356-323, Wilmington, DE 19898

365. Dr. J. Friedel, Physique des Solides, Universite Paris Sud, 91405 Orsay, France

366. Dr. A. T. Fromhold, Department of Physics, Auburn University, Auburn, AL 36849

367. Dr. Noboru Fukuoka, Division of Science, Naruto University of Teacher Education, Naruto, Tokushima 772, Japan

668. Dr. Y. Fujii, Institute of Solid State Physics, University of Tokyo, Roppongi Minato-ku, Tokyo 106, Japan

369. Dr. S. Funahashi, Japan Atomic Energy Research Institute, Tokai-mura, Naka-gun, Ibaraki-ken, Japan

370. Dr. B. Gaulin, McMaster University, Dept. of Physics, 1280 Main Street West, Hamilton, Ontario, L8S 4M1, Canada

371. Dr. J. F. Gibbons, Stanford Electronics Laboratories, McCullough 220, Stanford University, Stanford, CA 94305

372. Dr. Doon Gibbs, Brookhaven National Laboratory, Upton, NY 11973

373. Dr. Jill Glass, Sandia National Laboratories, Dept. 1845, P. O. Box 5800, Albuquerque, NM 87185-5800

374. Prof. Martin Glicksman, Rensselaer Polytechnic Institute, Materials Research Center, Troy, NY 12181

375. Dr. A. N. Goland, Associate Chairman for Energy Sciences, Department of Applied Sciences, Bldg. 179A, Brookhaven National Laboratory, Upton, NY 11973

376. Dr. A. Golanski, C.N.E.T.-R.P.T., B.P. 98, 38240 Meylan, France

377. Prof. Roberto Gonzalez, Dept. de Fisica del Estado Solido, Facultad de Ciencias Fisica, Universidad Compulutense 28040, Madrid, Spain

378. Dr. R. Gotthardt, Ecole Polytechnique Federale de Lausanne, Dept. de Physique, CH-1015 Lausanne, Switzerland

379. Dr. R. J. Gottschall, Metallurgy & Ceramics Branch, Division of Materials Sciences, Office of Basic Energy Sciences, ER-131, Washington, D.C. 20585

380. Dr. M. Guinan, Lawrence Livermore National Laboratory, P.O. Box 808, Livermore, CA 94550

381. Dr. Mark Hagen, Neutron Division, Rutherford Appleton Laboratory, Chilton, Didcot OXON OX11 OQX, United Kingdom

382. Prof. Richard F. Haglund, Jr., Dept. of Phys. & Astronomy, Vanderbilt University, Nashville, TN 37235

383. Dr. Carol A. Handwerker, Metallurgical Processing Group, Metallurgy Division, National Bureau of Standards, Gaithersburg, MD 20899

384. Dr. B. N. Harmon, Ames Laboratory, Iowa State University, Ames, IA 50011

385. Dr. Craig S. Hartley, Department of Materials Engineering, University of Alabama at Birmingham, Birmingham, AL 35294

386. Dr. Werner Heiland, Fachbereich Physik, Universität Osnabrück, Postfach 4469, D-4500 Osnabrück, Germany

387. Prof. Larry Hench, University of Florida, Advanced Materials Research Ctr., One Progress Blvd., #14, Alachua, FL 32615

388. Dr. Jim Herrington, Science & Technology, 11845 Forestgate Drive, Dallas, TX 75243

389. Dr. T. J. Hicks, Department of Physics, Monash University, Clayton, Victoria, Australia 3168

390. Dr. W. O. Hofer, Forschungszentrum, Postfach 1913, D-5170, Jülich, Germany

391–395. Dr. William A. Hoffman, Jr., Director, Oak Ridge Science Semester, GLCA, Denison University, Main Street, Granville, OH 43023

396. Dr. P. H. Holloway, Department of Materials Sciences and Engineering, University of Florida, Gainesville, FL 32601

397. Dr. Marc Hou, Physique des Surfaces, Faculté des Sciences, Université Libre de Bruxelles, Campus de la Plaine (C.P. 234), Boulevard de Triomphe, B-1050 Bruxelles, Belgium

398. Dr. John J. Hren, North Carolina State University, Raleigh, NC 27607

399. Dr. A. E. Hughes, Materials Development Division B552, Atomic Energy Research Establishment, Harwell, Didcot, Oxon OX11 ORA, United Kingdom

400. Dr. Tom Hutchinson, A114 Thornton Hall, University of Virginia, Charlottesville, VA 22901

401. Prof. Daryush Ila, Dept. of Physics, Alabama A&M University, 4900 Meridian St., Normal, AL 35762

402. Dr. M. Iizumi, Deputy Director General, Tokai Research Establishment, Japan Atomic Energy Research Institute, Tokai-mura, Naka-gun, Ibaraki-ken, Japan

403. Dr. Tadao Iwata, Division of Physics, Japan Atomic Energy Research Institute, Tokai-mura, Naka-gun, Ibaraki-ken 319-ll, Japan

404. Dr. Vincent Jaccarino, Department of Physics, University of California, Santa Barbara, CA 93106

405. Dr. Leslie H. Jenkins, 817 Whirlaway Circle, Knoxville, TN 37923

406. Ms. Beth Jinkerson, University Programs Division, Oak Ridge Associated Universities, P.O. Box 117, Oak Ridge, TN 37830

407. Dr. A. Wayne Johnson, Division 5126, Sandia National Laboratories, Albuquerque, NM 87185

408. Dr. R. H. Jones, P8-15, Pacific Northwest Laboratory, P. O. Box 999, Richland, WA 99352

409. Dr. Pierre H. Jourde, Charge du Centre d'Information sur les Déchets Nucléaires, CEA/DCAEA/CIDN, CEN/CADARACHE, B.P. 1, F 13115 Saint Paul lez Durance, France

410. Dr. W. A. Kamitakahara, Division of Materials Sciences, Office of Basic Energy Sciences, Office of Energy Research, ER-132, Department of Energy, Washington, DC 20585

411. Dr. Takuji Kaneda, Research Laboratories, Ashigara, Fuji Photo Film Company, Ltd., Minami-Ashigara, Kanagawa, 250-01 Japan

412. Dr. S. Katano, Japan Atomic Energy Research Institute, Tokai-mura, Naka-gun, Iboraki-ken, Japan

413. Dr. Elton N. Kaufmann, Building 207 (TTC), Argonne National Laboratory, 9700 South Cass Avenue, Argonne, IL 60439

414. Dr. Shinji Katano, Research Reactor Institute, Kyoto University, Kumatori, Sennan, Osaka 590-04, Japan

415. Dr. Fred Keller, Department of Physics, Clemson University, Clemson, SC 29631

416. Dr. Richard D. Kelley, Division of Materials Sciences, Office of Basic Energy Sciences, Office of Energy Research, ER-132, Department of Energy, Washington, DC 20585

417. Dr. Q. H. Khan, N.P.D., PINSTECH, P.O. Nilore, Rawalpindi, Pakistan

418. Prof. Angus Kingon, North Carolina State University, Dept. of Mats. Sci. & Engrg., P. O. Box 7919, Raleigh, NC 27695-7919
419. Dr. Donald L. Kinser, Vanderbilt University, 610 Olin Hall, Box 1689-B, Nashville, TN 37235
420. Dr. J. K. Kjems, Risø National Laboratory, DK-4000 Roskilde, Denmark
421. Dr. J. S. Koehler, Physics Department, University of Illinois, Urbana, IL 61801
422. Prof. Walter Kohn, Physics Department, University of California, Santa Barbara, CA 93106
423. Dr. Daniel E. Koshland, Jr., Editor, *Science*, 1515 Massachusetts Avenue N.W., Washington, DC 20005
424. Prof. Eckhard Krätzig, Universitat Osnabrück, Fachbereich Physik, Postfach 4469, 4500 Osnabrück, Germany
425. Prof. J. Kübler, Theoretische Physik, Institut für Festkörperphysik, Technische Hochschule Darmstadt, Hochschulstrasse 2, 6100 Darmstadt, Germany
426. Prof. Stewart K. Kurtz, Materials Research Laboratory, The University of Pennsylvania, University Park, PA 16802
427. Dr. Gerard H. Lander, Tu-Euratom, Postfach 2340, D7500, Karlsruhe, Germany
428. Dr. S. S. Lau, Department of EECS, C-014, University of California at San Diego, La Jolla, CA 92093
429. Dr. R. A. Laudise, Director, Materials and Processing Research Laboratory, AT&T Bell Laboratories, 600 Mountain Avenue, Murray Hill, NJ 07974
430. Prof. H. J. Leamy, Director, C. C. Cameron Applied Research Center, Univ. of North Carolina, Charlotte, NC 28223
431. Dr. Hassel Ledbetter, NIST, Materials Reliability Division, 325 Broadway, Boulder, CO 80303
432. Prof. F. Levy, Lab. de Physique des Materiaux Electroniques, Ecole Polytechnique Federal de Lausanne, PHG Ecublens, CH-1015 Lausanne, Switzerland
433. Prof. Alex Leyderman, Physics Department, University of Puerto Rico, Mayaquez, PR 00680
434. Library, Building 465, Atomic Energy Research Establishment, Harwell, Didcot, Oxon OX11 ORB, United Kingdom
435. Library, Department of Physics, Quaid-I-Azam, University Islamabad, Pakistan
436. Dr. A. B. Lidiard, Theoretical Physics Division, Building 424.4, Atomic Energy Research Establishment, Harwell, Didcot, Oxon OX11 ORA, United Kingdom
437. Prof. Per-Anker Lindgård, Physics Department, Risø National Laboratory, DK-4000 Roskilde, Denmark
438. Dr. Huimin Liu, Department of Physics, University of Puerto Rico, Mayaguez, Puerto Rico 00680
439. Dr. W. M. Lomer, Director, UKAEA Culham Laboratory, Abingdon, Oxon OX14 3DB, United Kingdom
440. Dr. C.-K. Loong, Bldg. 360, Argonne National Laboratory, 9700 S. Cass Avenue, Argonne, IL 60439
441. Dr. Stephen W. Lovesey, Rutherford Appleton Laboratory, Chilton, Didcot, Oxon OX11 OQX, United Kingdom
442. Dr. G. Lucovsky, Department of Physics, North Carolina State University, Raleigh, NC 27650
443. Dr. Siu-Ching Lui, 2403 Merrywood Drive, Edison, NJ 08817
444. Dr. Paul Lyman, Brookhaven National Laboratory, Upton, L.I., NY 11973
445. Dr. D. W. Lynch, Department of Physics, Iowa State University, Ames, IA 50011
446. Dr. J. W. Lynn, Reactor Radiation Division, NIST, Gaithersburg, MD 20899
447. Prof. Allan R. Mackintosh, Physics Laboratory, H. C. Oersted Institute, Universitetsparken 5, DK 2100 Copenhagen, Denmark
448. Dr. R. W. Major, Department of Physics, University of Richmond, Richmond, VA 23173

449. Dr. W. C. Mallard, Department of Physics and Astronomy, Georgia State University, Atlanta, GA 30303

450. Dr. J. D. Mannhart, IBM Research Division, Zurich Research Laboratory, Saumerstrasse 4, CH-8803 Ruschikon, Switzerland

451. Professor M. Brian Maple, Department of Physics–0319, University of California-San Diego, 9500 Gilman Drive, La Jolla, CA 92093-0319

452. Dr. P. M. Marcus, T. J. Watson Research Center, International Business Machines Corporation, P.O. Box 218, Yorktown Heights, NY 10598

453. Prof. Egon Matijevic, Dept. of Chemistry, Clarkson University, Potsdam, NY 13676

454. Dr. J. W. Mayer, Department of Materials Sciences, Cornell University, Ithaca, NY 14853

455. Dr. G. L. McVay, Battelle-Pacific Northwest Laboratories, P. O. Box 999, Richland, WA 99352

456. Dr. Alfonso E. Merlini, Milano 13, 21027 Ispra (Va), Italy

457. Dr. James L. Merz, Electrical and Computer Engineering Department, University of California, Santa Barbara, CA 93106

458. Dr. Pat Morris, DuPont Corporation, P. O. Box 80306, E356/317A, Wilmington, DE 19880-0306

459. Prof. Charles Myles, Chairman, Department of Physics, Texas Technology University, Box 4180, Lubbock, TX 79409-1051

460. Dr. I. V. Mitchell, Department of Physics, Physics and Astronomy Building, University of Western Ontario, London, Ontario N6A 3K7, Canada

461. Dr. Y. Morii, Japan Atomic Energy Research Institute, Tokai-mura, Naka-gun, Ibaraki-ken 319-11, Japan

462. Prof. K. A. Müller, Manager, Physics Department, International Business Machines Corporation, Forschungslaboratorium Zurich, CH-8803 Rüschlikon, Saumerstrasse 4, Switzerland

463. Prof. Klaus E. Müller, University of Erlangen–Nürnberg, Institut für Angewandt Physik, Lehrstuhl für Festkörperphysik, Erwin-Rommel-Str 1, D-8520 Erlangen, Germany

464. Dr. R. B. Murray, Office of Graduate Studies, University of Delaware, Newark, DE 19711

465. Dr. H. Naramoto, Department of Physics, Japan Atomic Energy Research Institute, Tokai, Ibaraki, Japan

466. Dr. Jagdish Narayan, Division of Materials Research, National Science Foundation, 1800 G Street NW, Washington, DC 20550

467. Dr. Stuart Nelson, Director, Northern Research Laboratories, UK Atomic Energy Authority, Risley, Warrington, Cheshire WA3 6AT, United Kingdom

468. Dr. M.-A. Nicolet, Department of Electrical Engineering, 116–81, California Institute of Technology, Pasadena, CA 91125

469. Dr. C. J. Northrup, Jr., Sandia National Laboratories, Building 805, Albuquerque, NM 87185

470. Oak Ridge Institute for Science and Education (ORISE), DOE/Oak Ridge Associated Universities, ATTN: H. T. Burn, Librarian, Information Center/EES, P. O. Box 117, Oak Ridge, TN 37831-0117

471. Office of Assistant Manager for Energy Research and Development, Department of Energy, Oak Ridge Operations Office, Oak Ridge, TN 37831

472. Dr. O. S. Oen, 119 Lehigh Lane, Oak Ridge, TN 37830

473. Dr. D. N. Olson, Department of Physics, St. Olaf College, Northfield, MN 55057

474. Dr. W. T. Oosterhuis, Chief, Solid State Sciences Branch, Division of Materials Sciences, Office of Basic Energy Sciences, ER-132, Washington, D.C. 20585

475. Dr. V. M. Orera, Departamento de Optica, Facultad de Ciencias, Universidad de Zaragoza, Zaragoza, Spain

476. Dr. A. W. Overhauser, Department of Physics, Purdue University, West Lafayette, IN 47907

477. Dr. Robert L. Park, Director, Center for Materials Research, University of Maryland, College Park, MD 20742

478. Dr. D. Parkin, Los Alamos National Laboratory, MS-K765, P. O. Box 1663, Los Alamos, NM 87545

479. Dr. P. S. Peercy, Division 5112, Sandia National Laboratories, Albuquerque, NM 87115
480. Dr. Hans Peisl, Sektion Physik, Universitat München, Geschwister-Scholl-Platz 1, 8000 München 22, Germany
481. Dr. Norman E. Phillips, Lawrence Berkeley Laboratory, Cyclotron Road, Berkeley, CA 94720
482. Physics/Optics/Astronomy Library, 374 Bausch and Lomb Building, University of Rochester, Rochester, NY 14627
483. Dr. Lothar A. R. Pintschovius, Kernforschungszentrum Karlsruhe GmbH, Postfach 3640, D-7500 Karlsruhe 1, Germany
484. Dr. J. M. Poate, AT&T Bell Laboratories, 600 Mountain Avenue, Murray Hill, NJ 07974
485. Dr. C. P. Poole, Department of Physics, University of South Carolina, Columbia, SC 29208
486. Dr. Richard C. Powell, Director, Optical Sciences Center, University of Arizona, Tucson, AZ 85721
487. Dr. Rene Pretorius, Head, Ion-Solid Interaction Division, National Accelerator Centre, P.O. Box 72, Faure 7131, South Africa
488. Dr. P. P. Pronko, Universal Energy Systems, 3195 Plainfield Road, Dayton, OH 45432
489. Dr. L. David Pye, Inst. of Glass & Engrg., New York State College of Ceramics, Alfred, NY 14802
490. Dr. Roger Pynn, LANSCE, MS H805, Los Alamos National Laboratory, Los Alamos, NM 87545
491. Dr. Y. Quéré, Centre d'Études Nucléaires de Fontenay-aux-Roses, B.P. No. 6, 92260 Fontenay-aux-Roses (Seine), France
492. Dr. V. R. Ramakrishnan, Biology Department, Brookhaven National Laboratory, Upton, NY 11973
493. Dr. Michel Rappaz, Ecole Polytechnique Fédérale de Lausanne, Department des Matériaux, 34 ch. de Bellerive, CH-1007, Lausanne, Switzerland
494. Dr. W. Reichardt, Kernforschungszentrum Karlsruhe GmbH, Institut für Angewandte Kernphysik 1, Postfach 3640, D-7500 Karlsruhe, Germany
495. Dr. Robert C. Rhome, Director, Microgravity Science & Appl. Div., NASA, Washington, DC 20546-0001
496. Dr. James Rhyne, Research Reactor Facility, University of Missouri, Columbia, MO 65211
497. Dr. James R. Rice, Division of Applied Sciences, Rm 224, Pierce Hall, Harvard University, 29 Oxford Street, Cambridge, MA 02138
498. Dr. E. Rimini, Istituto di Struttura della Materia, Dell Universita, 57 Corso Italia, I95129 Catania, Italy
499. Dr. T. Riste, Institute for Energy Technology, P.O. Box 40, 2007 Kjeller, Norway
500. Dr. J. E. Rives, Department of Physics, University of Georgia, Athens, GA 30602
501. Dr. H. E. Rorschach, Physics Department, Rice University, Houston, TX 77251
502. Dr. Franz Rosenberger, Director, Center for Microgravity Research, University of Alabama-Huntsville, Huntsville, AL 35899
503. Prof. G. R. Rossman, Division of Earth & Planetary Sciences, California Institute of Technology, Pasadena, CA 01125
504. Dr. Joachim Roth, Max-Planck-Institut für Plasmaphysik, 8046 Garching bei München, Germany
505. Dr. Marvin L. Roush, Chemical and Nuclear Engineering, University of Maryland, College Park, MD 20742
506. Dr. J. M. Rowe, Reactor Radiation Division, National Institute of Standards and Technology, Washington, DC 20234
507. Dr. J. J. Rush, Reactor Radiation Division, National Institute of Standards and Technology, Washington, DC 20234
508. Dr. Daniel Rytz, Sandoz Produkte (Schweiz) AG Optoelectronics Research, BAU 88/301 CH-4002, Basel, Switzerland

509. Dr. George Samara, Dept. 1150, P. O. Box 5800, Sandia National Laboratories, Albuquerque, NM 87115

510. Dr. F. W. Saris, FOM-Institute for Atomic and Molecular Physics, P.O. Box 41883, 1009 DB Amsterdam, the Netherlands

511. Dr. H. Sato, School of Materials Engineering, Purdue University, West Lafayette, IN 47907

512. Dr. D. W. Schaeffer, Division 1152, Sandia National Laboratories, Albuquerque, NM 87185

513. Dr. Kurt Scharnberg, Institut für Angewandte Physik, Universität Hamburg, Jungiusstrasse 11, D-2000 Hamburg 36, Germany

514. Dr. W. Schilling, Institut für Festkörperforschung der Forschungszentrum Jülich GmbH, Postfach 1913, 5170 Jülich 1, Germany

515. Prof. R. Schuttler, I.N.S.A. Service Informatique, Avenue de Rangueil, F-31077 Toulouse, Cedex, France

516. Dr. H.-B. Schweer, Institut für Plasmaphysik der Forschungszentrum Jülich GmbH, Postfach 1913, 5170 Jülich 1, Germany

517. Prof. Dr. A. Seeger, Max-Planck-Institut für Metallforschung, Institut für Physik, Heisenbergstrasse 1, Postfach 80 06 65, 7000 Stuttgart 80, Germany

518. Dr. David N. Seidman, Northwestern University, Evanston, IL 60201

519. Prof. David Sherrington, Department of Theoretical Physics, Oxford University, 1 Keble Road, Oxford OX1 3NP, United Kingdom

520. Prof. G. Graham Shipley, Professor of Biochemistry, Boston University Medical Center, 80 East Concord Street, Boston, MA 02118

521. Dr. G. Shirane, Department of Physics, Bldg. 510B, Brookhaven National Laboratory, Upton, NY 11973

522. Dr. W. A. Sibley, Vice-President for Academic Affairs, University of Alabama-Birmingham, UAB Station, Birmingham, AL 35294

523. Dr. R. H. Silsbee, Clark Hall, Physics Department, Cornell University, Ithaca, NY 14853

524. Prof. Joseph H. Simmons, Department of Materials Science & Engineering, University of Florida, Gainesville, FL 32611

525. Dr. S. Sinha, Corporate Research Laboratory, Exxon Research & Engineering Co., Route 22 East, Annandale, NJ 08801

526. Dr. Jerry J. Smith, Division of Materials Sciences, Office of Basic Energy Sciences, Office of Energy Research, Department of Energy, ER-132, Washington, DC 20585

527. Prof. Dr. T. Springer, Institut für Festkörperforschung der Forschungszentrum Jülich GmbH, Postfach 1913, D-5170 Jülich 1, Germany

528. Dr. C. Stassis, Physics Department, Iowa State University, Ames, IA 50011

529. Dr. J. R. Stevenson, Ionic Atlanta Inc., 1347 Spring Street, Atlanta, GA 30309

530. Prof. R. Street, Vice-Chancellor, The University of Western Australia, Nedlands, Western Australia 6009, Australia

531. Prof. B. W. Stritzker, Universität Augsburg, Institüt für Physik, Memminger Strasse 6, Augsburg D-8900, Germany

532. Dr. M. Strongin, Brookhaven National Laboratory, Dept. of Phys., Bldg. 510B, Upton, L.I., NY 11973

533. Dr. T. T. Sugihara, L-353, Lawrence Livermore National Laboratory, P.O. Box 808, Livermore, CA 94550

534. Prof. S. Sundaram, Head, Department of Physics, University of South Florida, Tampa, FL 33620

535. Dr. Thomas Surek, Photovoltaic Program Office, Solar Energy Research Institute, 1617 Cole Boulevard, Golden, CO 80401

536. Dr. M. L. Swanson, Department of Physics and Astronomy, University of North Carolina, Chapel Hill, NC 27599-3255

537. Dr. Frank R. Szofran, ES75, Marshall Space Flight Center, Huntsville, AL 35812

538. Dr. E. H. Taheri, Department of Solid State Physics, NRC Atomic Energy Organization of Iran, Tehran, Iran

539. Dr. F. J. E. Tasset, Institut Max Von Laue–Paul Langevin, BP 156X, 38042 Grenoble Cedex, France

540. Dr. Paul Thevenard, Dept. de Physique des Materiaux, Université Claude Bernard-Lyon 1, Unite de Recherche Associee au C.N.R.S., 43, Boulevard du 11 Novembre 1918, F 69622 Villeaurbanne Cedex, France

541. Dr. Iran L. Thomas, Acting Associate Director, Office of Basic Energy Sciences, Office of Energy Research, ER-10, Department of Energy, Washington, DC 20585

542. Dr. D. O. Thompson, Ames Laboratory, Iowa State University, Ames, IA 50010

543. Dr. M. W. Thompson, Vice-Chancellor, University of East Anglia, Norwich, Norfolk, NR4 7TJ, United Kingdom

544. Dr. R. B. Thompson, Ames Laboratory, Iowa State University, Ames, IA 50011

545. Dr. J. O. Thomson, Department of Physics, The University of Tennessee, Knoxville, TN 37996-1200

546. Dr. R. M. Thomson, Institute for Materials Science and Engineering, National Institute of Standards and Technology, Gaithersburg, MD 20899

547. Dr. H. T. Tohver, Department of Physics, University of Alabama, Birmingham, AL 35233

548. Prof. Peter Townsend, School of Mathematical and Physical Science, University of Sussex, Brighton, BN1 9QH United Kingdom

549. Dr. G. T. Trammell, Physics Department, Rice University, P.O. Box 1892, Houston, TX 77251

550. Dr. J. G. Traylor, Buena Vista College, Storm Lake, IA 50588

551. Dr. B. Y. Tsaur, MIT Lincoln Laboratory, Lexington, MA 02173

552. Dr. K. N. Tu, T. J. Watson Research Center, International Business Machines Corporation, P.O. Box 218, Yorktown Heights, NY 10598

553. Prof. Harry Tuller, Dept. of Mats. Sci. & Engrg., MIT, 13-3126, Metallurgy Bldg., 60 Vassar St. Underpass, Cambridge, MA 02139

554. Prof. David Turnbull, Division of Applied Sciences, Harvard University, Cambridge, MA 02138

555. Dr. Robert Ullman, Department of Nuclear Engineering, University of Michigan, Ann Arbor, MI 48109-2104

556. Dr. Bob Uhrin, Deltronics Crystals, 60 Harding Avenue, Dover, NJ 07801

557. Universidade Federal de Minas Gerais, ICEx-Cx.P. 702-Depto. de Física (Instituto de Ciencias Exatas), Serviço de Documentação, 30.000–Belo Horizonte–MG–Brasil

558. Dr. Jon Veigel, President, Oak Ridge Associated Universities, Oak Ridge, TN 37831

559. Dr. H. Verbeek, Max-Planck-Institut für Plasmaphysik, 8046 Garching bei München, Germany

600. Dr. P. R. Vijayaraghavan, Nuclear Physics Division, Bhabha Atomic Research Centre, Trombay, Bombay 400 085, India

601. Dr. F. L. Vook, Solid State Sciences, Org. 1100, Sandia National Laboratories, Albuquerque, NM 87185

602. Dr. N. Wakabayashi, Keio University, Yokohama, Japan

603. Dr. Scott Walck, Department of Materials Engineering, University of Alabama–Birmingham, University Station, Birmingham, AL 35294

604. Prof. Gwo-Ching Wang, Department of Physics, Rensselaer Polytechnic Institute, Troy, NY 12180-3590

605. Prof. Zhonglie Wang, Director, Institute for Low Energy Physics, Beijing Normal University, Beijing, China

606. Prof. George D. Watkins, Sherman Fairchild Laboratory 161, Department of Physics, Lehigh University, Bethlehem, PA 18015

607. Dr. Harlan L. Watson, Deputy Staff Director, Subcommittee on Energy Development & Applications, Committee on Science & Technology, U.S. House of Representatives, B374 Rayburn House Office Building, Washington, DC 20515

608. Dr. Marvin J. Weber, L-326, Lawrence Livermore National Laboratory, P.O. Box 808, Livermore, CA 94550

609. Dr. William J. Weber, Battelle Pacific Northwest Lab., P. O. Box 999, MSIN K2-44, Richland, WA 99352

610. Dr. R. A. Weeks, P.O. Box 1687, Vanderbilt University, Nashville, TN 37235

611. Dr. Julia R. Weertman, Department of Materials Science and Engineering, Northwest University, Evanston, IL 60201-9990

612. Prof. Dr. H. F. Wenzl, Institut für Festkörperforschung der Forschungszentrum Jülich GmbH, Postfach 1913, 5170 Jülich 1, Germany

613. Prof. S. Werner, Department of Physics, University of Missouri, Columbia, MO 65211

614. Dr. C. A. Wert, Department of Metallurgy and Mining Engineering, University of Illinois, Urbana, IL 61801

615. Mr. Tom E. Wessels, Manager, Ames Laboratory Energy and Mineral Resources Research Institute, 52 Spedding Hall, Iowa State University, Ames, IA 50011

616. Mr. R. D. Westbrook, 1038 W. Outer Drive, Oak Ridge, TN 37830

617. Dr. Thomas Wichert, Fakultat für Physik, Universitat Konstanz, D-7750 Konstanz, Germany

618. Prof. William R. Wilcox, Center for Advanced Materials Processing, Clarkson University, Potsdam, NY 13676

619. Dr. A. R. Williams, T. J. Watson Research Center, International Business Machines Corporation, P.O. Box 218, Yorktown Heights, NY 10598

620. Dr. S. R. Wilson, Semiconductor Group, Motorola, Inc., Mail Drop B-132, 5006 East McDowell, Phoenix, AZ 85008

621. Dr. T. M. Wilson, Department of Physics, Oklahoma State University, Stillwater, OK 74078

622. Dr. James C. Withers, KeraMont Corporation, 4233 South Freemont Avenue, Tucson, AZ 85714

623. Prof. Dr. H. Wollenberger, Hahn-Meitner-Institut für Kernforschung Berlin GmbH, Glienicker Strasse 100, D-1000 Berlin 39, Germany

624. Dr. Gary L. Workman, Materials Processing Lab., University of Alabama, 201 South Loop Road, Huntsville, AL 35899

625. Dr. F. W. Young, Jr., 2900 W. Gallaher Ferry Road, Knoxville, TN 37932

626. Dr. R. T. Young, Energy Conversion Devices, Inc., 1675 West Maple Road, Troy, MI 48084

627. Prof. Richard Zallen, Physics Department, Virginia Institute of Technology, Blacksburg, VA 24061

628. Prof. Z.-K. Zuo, Physics & Astronomy Department, Southwest Missouri State University, 901 South National Avenue, Springfield, MO 65804

629–633. Office of Scientific and Technical Information, Department of Energy, P. O. Box 62, Oak Ridge, TN 37831

*U.S. GOVERNMENT PRINTING OFFICE: 1994-550-165/00001